Order-Disorder Enantiotropy, Monotropy, and Isostructurality in a Tetroxoprim-Sulfametrole 1:1 Molecular Complex: Crystallographic and Thermal Studies

MINO R. CAIRA,[1] GIAMPIERO BETTINETTI,[2] MILENA SORRENTI,[2] LAURA CATENACCI[2]

[1]Department of Chemistry, University of Cape Town, Rondebosch 7701, South Africa

[2]Dipartimento di Chimica Farmaceutica, Università di Pavia, Viale Taramelli 12, I-27100 PV, Italy

Received 21 November 2002; revised 26 February 2003; accepted 14 March 2003

Published online 21 August 2003 in Wiley InterScience (www.interscience.wiley.com). DOI 10.1002/jps.10435

ABSTRACT: Two enantiotropic polymorphs of a tetroxoprim (TXP)-sulfametrole (SMTR) 1:1 molecular complex monohydrate and two isostructural TXP-SMTR 1:1 molecular complex solvates with methanol and ethanol were grown and studied by X-ray diffraction and thermal methods (thermogravimetric analysis and differential scanning calorimetry). Interconversion of the polymorphic hydrates is essentially an order/disorder transition involving a substituent on the TXP molecule. These hydrated phases may be described as "nearly isostructural" with the methanol and ethanol solvates. Thermal data for decomposition of the solvates were rationalized on the basis of the location and topologies of solvent crystallographic sites. Solid-state properties of two monotropic polymorphs of the unsolvated TXP-SMTR 1:1 molecular complex were also investigated and the theoretical and experimental phase diagrams of the individual components were assessed. The existence of polymorphic and pseudopolymorphic forms is determined by conformational flexibility of the TXP-SMTR bimolecular complex components, a tendency for molecular disorder in TXP, the ability of the drug complex to form intricate, highly stabilized hydrogen-bonded frameworks, and the competition between nonspecific van der Waals and specific hydrogen bond interactions. © 2003 Wiley-Liss, Inc. and the American Pharmacists Association J Pharm Sci 92:2164–2176, 2003

Keywords: polymorphism; solvates; tetroxoprim; sulfametrole; complex

INTRODUCTION

Polymorphism and pseudopolymorphism of the antibiotic antagonist of folic acid tetroxoprim [5-[[3,5-dimethoxy-4-(2-methoxyethoxy)phenyl]-methyl]-2,4-pyrimidinediamine (TXP)] have recently been assessed.[1] The binary system of TXP with sulfadiazine, a sulfa drug used in association with TXP in tablet formulations (co-tetroxazine), was also investigated and the occurrence of a single eutectic V-type phase diagram was demonstrated.[2] Analogous phase diagrams were obtained for the TXP-sulfamethoxazole and TXP-sulfadimidine binary systems, whereas a congruently melting ($T_f = 172.4$°C, $\Delta H_f = 158.1$ J g^{-1}) equimolar complex between TXP and sulfamethoxypyridazine (SMPD) was isolated and characterized through the X-ray powder diffraction pattern and the phase diagram.[2]

Our attempts to obtain crystals of this complex suitable for a crystallographic study to explain the way in which SMPD and TXP are linked in TXP·SMPD were unsuccessful. In our investigations on the binary system of TXP with sulfametrole

Correspondence to: Mino R. Caira (Telephone: 27-21-650-3071; Fax: 27-21-689-749; E-mail: xraymino@science.uct.ac.za)

Journal of Pharmaceutical Sciences, Vol. 92, 2164–2176 (2003)
© 2003 Wiley-Liss, Inc. and the American Pharmacists Association

UM00013078

NOVARTIS EXHIBIT 1517
Novartis v. Regents, IPR2023-01347
Page 1824 of 4460

[4-amino-*N*-(4-methoxy-1,2,5-thiadiazol-3-yl) benzenesulfonamide (SMTR)], a sulfa drug already tested in this respect with a structural analog of TXP, trimethoprim,[3,4] SMTR proved to be a good complex-forming partner for TXP (see Fig. 1). Herein, we report the structural [single crystal and powder X-ray diffraction (PXRD)] and thermal [thermogravimetric analysis (TGA); differential scanning calorimetry (DSC)] characterization of solvated (*viz.*; hydrate, ethanolate, methanolate) and anhydrous crystalline forms of the TXP · SMTR 1:1 molecular complex prepared respectively by recrystallization of the TXP-SMTR equimolar mixture from the solvation solvent and thermal desolvation of the TXP · SMTR solvates. The structural features (crystal packing, hydrogen bonding, solvent inclusion modes) of two polymorphic hydrates and isostructural ethanol and methanol solvates of the TXP · SMTR complex are described, and possible relationships between thermal behavior and solid-state phase transitions are discussed.

EXPERIMENTAL SECTION

Sample Preparations and Thermal Characterization

TXP (Istituto Biologico Chemioterapico, Divisione ABC Farmaceutici, Turin, Italy) and SMTR (Menarini, Florence, Italy), recrystallized following published procedures,[1,3] were sieved and the respective 125–180 μm granulometric fractions were mixed in equimolar amounts and thoroughly ground by hand in an agate mortar with a pestle. Clear, needle-shaped crystals of TXP · SMTR · H_2O (*Anal.* Calcd $C_{25}H_{34}N_8O_8S_2$: C, 47.01; H, 5.37; N, 17.54%. Found: C, 46.89; H, 5.31; N, 17.91%) were obtained by spontaneous cooling to room temperature of a hot aqueous solution (35 mL/g physical mixture). Similarly, triclinic prisms of TXP · SMTR · C_2H_5OH (*Anal.* Calcd $C_{27}H_{38}N_8O_8S_2$: C, 48.64; H, 5.74; N, 16.81%. Found: C, 48.64; H, 5.69; N, 17.04%) were isolated from ethanol (24 mL/g physical mixture). Very similar triclinic prisms of TXP · SMTR · CH_3OH (*Anal.* Calcd $C_{26}H_{36}N_8O_8S_2$: C, 47.84; H, 5.56; N, 17.17%. Found: C, 47.16; H, 5.52; N, 17.73%) were obtained from methanol (18 mL/g physical mixture). The stoichiometry of the bound solvents was confirmed by TGA (Mettler TA 4000: heating rate 10 K min^{-1}; 7–10 mg samples in open alumina crucibles; temperature range 30°–200°C; static air atmosphere; triplicate measurements) performed on samples screened through a 180-μm sieve, with mass losses of $2.83 \pm 0.03\%$ for the hydrate (calcd 2.82%), $6.2 \pm 0.7\%$ for the ethanolate (calcd 6.91%), and $5.2 \pm 0.3\%$ for the methanolate (calcd 4.91%) (Fig. 2).

Thermal behavior of TXP · SMTR · H_2O, TXP · SMTR · C_2H_5OH and TXP · SMTR · CH_3OH, the respective desolvation products (by heating in a hot air oven at 130°C for 2 h) and the TXP-SMTR equimolar mixture as prepared and heated at 140°C for 2 h was investigated by DSC (METTLER

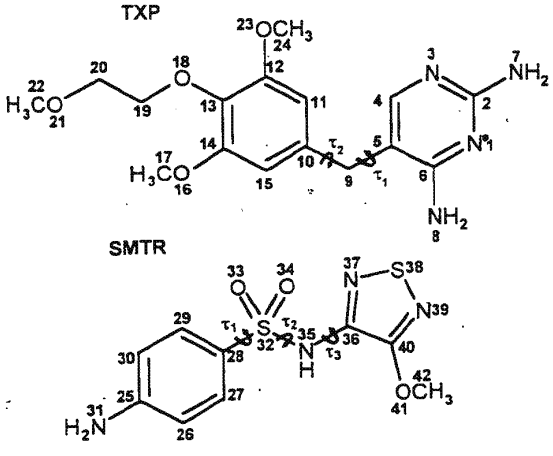


Figure 1. Chemical structures of TXP and SMTR. Crystallographic numbering and principal torsion angles are indicated.

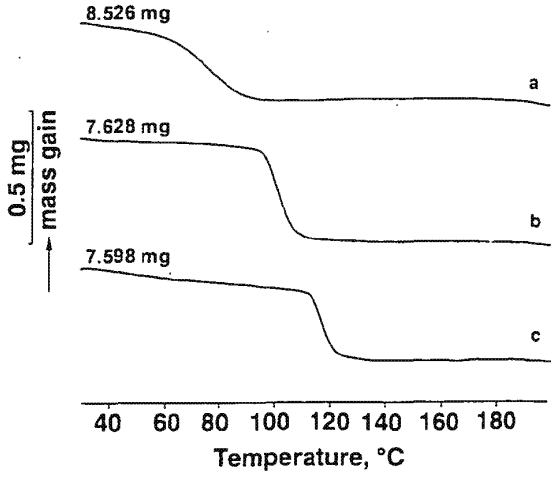


Figure 2. TGA curves of TXP · SMTR solvates. Key: TXP · SMTR · H_2O: (a); TXP · SMTR · C_2H_5OH: (b); TXP · SMTR · CH_3OH: (c) (initial mass of the sample on the curves).

UM00013079
NOVARTIS EXHIBIT 1517
Novartis v. Regents, IPR2023-01347
Page 1825 of 4460

STAR[e] with a DSC821[e] Module and IntraCooler: heating rate 10 K min^{-1}; 3–5 mg samples in standard open aluminum pans; temperature range 30°–200°C; static air atmosphere; triplicate measurements) performed on samples screened through a 180-μm sieve (Fig. 3). Thermal cycling, i.e., cooling from 30° to −60°C and heating from −60° to 200°C, were also performed on solvated samples.

X-ray Diffraction Studies

All the solvates afforded colorless crystals suitable for X-ray analysis. Preliminary surveys of the X-ray diffraction patterns collected on a Nonius Kappa CCD diffractometer revealed Laue symmetry $\bar{1}$ for all three solvates, indicating the triclinic crystal system. Intensity data were subsequently collected using MoKα radiation (λ = 0.71073 Å) with the crystal specimens coated in Paratone oil (Exxon Chemical Co., Houston, TX) and cooled to 173 K in a stream of N_2 vapor. The crystal data and refinement parameters in Table 1 for these low-temperature analyses are headed TXP · SMTR · H_2O, TXP · SMTR · CH_3OH and TXP · SMTR · C_2H_5OH. On returning the crystals to room temperature, the unit cell dimensions for the methanolate and ethanolate were substantially unchanged within the experimental error, whereas a lattice change involving a halving of one unit cell dimension was observed for the hydrate. A fresh specimen was subsequently mounted and intensity data were collected at 297 K. Crystal data for this species are headed TXP · SMTR · H_2O (RT) in Table 1. The data-collection strategy indicated by the program COLLECT[5] involved suitable combinations of 1° φ- and ω-scans. Program DENZO-SMN[6] was used for cell refinement and data reduction. Centric distributions for the intensity data indicated the space group $P\bar{1}$ for all species. From the crystal

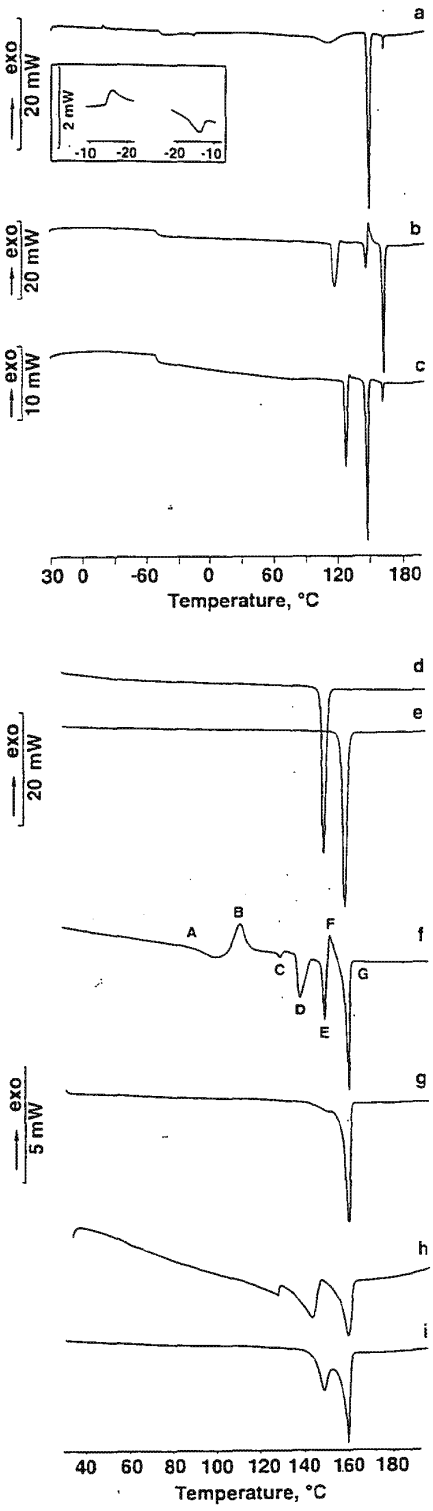


Figure 3. DSC curves of TXP · SMTR solvates, TXP · SMTR anhydrous polymorphs, TXP-SMTR equimolar mixture, and mixtures of TXP · SMTR form I with either SMTR or TXP. Key: TXP · SMTR · H_2O: (a); TXP · SMTR · C_2H_5OH: (b); TXP · SMTR · CH_3OH: (c); TXP · SMTR · H_2O, freshly filtered crystals: (d); TXP · SMTR form I by desolvation of TXP · SMTR · C_2H_5OH at 130°C: (e); TXP-SMTR equimolar mixture as prepared: (f); TXP-SMTR equimolar mixture heated at 140°C for 2 h: (g); TXP · SMTR form I-SMTR mixture at 0.40 mole fraction of TXP: (h); TXP · SMTR form I-TXP mixture at 0.60 mole fraction of TXP: (i).

UM00013080
NOVARTIS EXHIBIT 1517
Novartis v. Regents, IPR2023-01347
Page 1826 of 4460

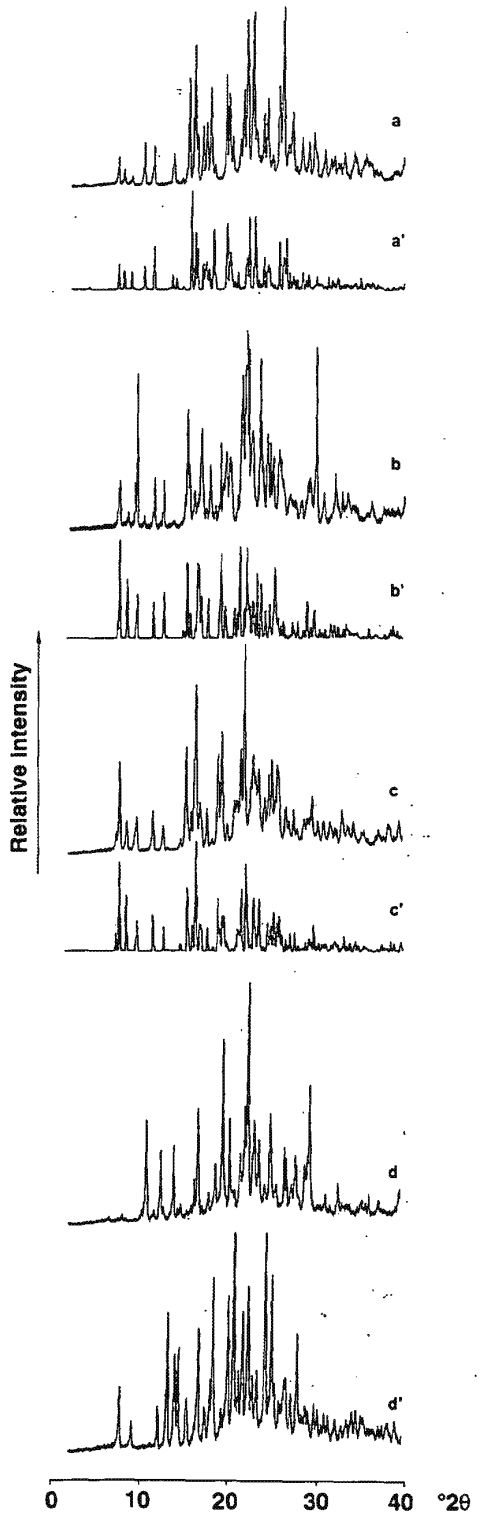
Table 1. Crystal Data and Details of Refinement

Parameter	TXP · SMTR · H_2O	TXP · SMTR · CH_3OH	TXP · SMTR · C_2H_5OH	TXP · SMTR · H_2O (RT)
Chemical	$C_{25}H_{34}N_8O_8S_2$	$C_{26}H_{36}N_8O_8S_2$	$C_{27}H_{38}N_8O_8S_2$	$C_{25}H_{34}N_8O_8S_2$
Formula weight	638.73	652.75	666.77	638.73
Crystal system	Triclinic	Triclinic	Triclinic	Triclinic
Space group	$P\bar{1}$	$P\bar{1}$	$P\bar{1}$	$P\bar{1}$
a (Å)	12.9952 (2)	11.3343 (4)	11.3152 (2)	11.3184 (2)
b (Å)	11.2526 (2)	12.6839 (5)	12.5991 (2)	13.2486 (3)
c (Å)	22.9867 (5)	12.0041 (4)	12.3148 (2)	11.5355 (3)
α (°)	74.236 (1)	94.802 (1)	95.968 (1)	89.203 (1)
β (°)	89.528 (1)	73.699 (1)	74.019 (1)	74.423 (1)
γ (°)	68.214 (1)	74.879 (1)	76.497 (1)	66.938 (1)
V (Å^3)	2987.7 (1)	1575.9 (1)	1613.28 (5)	1524.93 (6)
Formula units, Z	4	2	2	2
T (K)	173 (2)	173 (2)	173 (2)	297 (2)
R (on F)	0.054	0.072	0.038	0.055
Goodness-of fit, S	0.943	1.089	1.023	1.068

densities (measured by flotation in PhBr/PhCl solutions) and unit cell volumes, it was deduced that the asymmetric units comprised one complex unit (TXP · SMTR) and one solvent molecule for each of the phases TXP · SMTR · CH_3OH, TXP · SMTR · C_2H_5OH, and TXP · SMTR · H_2O (RT), but two complex units and two water molecules for TXP · SMTR · H_2O. Furthermore, the close similarity of the unit cell data for TXP · SMTR · C_2H_5OH and TXP · SMTR · CH_3OH suggested their isostructurality. The structure of the ethanol solvate was determined by direct methods using the program SHELXS86.[7] The same set of non-hydrogen atom coordinates for the complex unit in the ethanol solvate was successfully used as the trial model for the methanol solvate structure, thus confirming the isostructurality of these phases. The structures of the hydrate phases were determined independently using SHELXS86.[7]

Solvent molecules and all hydrogen atoms were located in difference electron-density maps in all four structures. The two terminal atoms of the TXP methoxyethoxy substituent in both TXP · SMTR · CH_3OH and TXP · SMTR · C_2H_5OH were found to be disordered analogously over two sites each and were modeled accordingly. In one of the crystallographically independent TXP molecules in TXP · SMTR · H_2O, the three central atoms (C–C–O) of the methoxyethoxy chain were found to be disordered over two sites each and were modeled as such. Analogous disorder appeared in the methoxyethoxy chain in the asymmetric unit of TXP · SMTR · H_2O (RT). Appropriate distance restraints were applied to maintain reasonable geometries for the observed chain conformers. Hydrogen atoms were added in idealized positions in a riding model except for those of the solvent –OH groups, where free refinement with a distance constraint of O–H 1.000 Å, $\sigma = 0.005$ Å was imposed. The structures were refined on F^2 with SHELXL97[8] with non-H atoms modeled anisotropically and H atoms assigned isotropic thermal parameters equal to 1.2 times those of their parent atoms. In the final cycles of refinement, least-squares weights of the form $w = 1/[\sigma^2(F_o)^2 + (aP)^2 + bP]$, $P = [\max(F_o^2, 0) + 2F_c^2]/3$ were used. Molecular parameters were calculated with PLATON.[9] Programs ZORTEP[10] and WebLab ViewerPro 3.7[11] were used for illustrations. The program SECTION[12] was used to probe the nature of voids in the crystals of the solvates. In this routine, bitmapped images of selected cross-sections through the crystal unit cell are generated with atoms represented as spheres with their van der Waals radii. The unit cell data, atomic positions, thermal parameters, and space group data for all four of the above phases were used as input to the program LAZY PULVERIX[13] to generate their idealized PXRD patterns for CuK_α radiation (1.5418 Å). The idealized patterns were compared with the experimental PXRD patterns (Philips PW 1800/10 apparatus; powdered samples in Al holders; $CuK_{\alpha,1} = 1.54060$ Å, $CuK_{\alpha,2} = 1.54439$ Å; 2–50° 2θ scan range; 0.02° 2θ s^{-1} scan speed; monochromator: graphite crystal) of each solvate in Figure 4, where those taken on the common desolvation product and the TXP-SMTR equimolar mixture are also presented.

UM00013081
NOVARTIS EXHIBIT 1517
Novartis v. Regents, IPR2023-01347
Page 1827 of 4460



RESULTS AND DISCUSSION

Thermal Analysis of Molecular Complexes

The small exothermal effect ($\Delta H_{exo} = 1.96 \pm 0.25$ J g^{-1}, corresponding to 1.25 ± 0.16 kJ mol^{-1}) recorded in the cooling segment of the DSC curve and mirrored by the endotherm ($\Delta H_{endo} = 1.82 \pm 0.28$ J g^{-1}, corresponding to 1.16 ± 0.18 kJ mol^{-1}) between $-20.4° \pm 0.8°C$ and $-11.3° \pm 0.4°C$ in the heating segment (Fig. 3) signified the enantiotropic dimorphism of TXP · SMTR · H_2O, according to the Heat of Transition Rule.[14] The structural implications of the solid-state phase transition will be discussed later (see Single Crystal X-Ray Diffraction). The TGA (Fig. 2) and DSC (Fig. 3) traces showed that water was liberated over a wide temperature range at varying onset temperatures in contrast to the narrower ranges for ethanol and methanol. By relating the percent mass loss measured over the TGA desolvation step ($\Delta m_S\%$) to the enthalpy change calculated over the corresponding DSC desolvation endotherm ($\Delta H_{S,exp}$, in J g^{-1}) as in eq. 1,[1]

$$\Delta H_S = [(\Delta H_{S,exp} \times 100)/\Delta m_S\%] \times M_S \quad (1)$$

where ΔH_S (in J mol^{-1}) is the heat of vaporization of the TXP · SMTR-bound solvent and M_S its molecular weight, data presented in Table 2 were obtained. In the hydrate crystals, whose onset temperature of dehydration is lower than the normal boiling point of water, the TXP · SMTR-water interactions appear ~20% stronger than those in liquid water.[15] The presence of tightly bound solvent in the ethanolate and methanolate complexes can be inferred not only from the ΔH_S values for ethanol and methanol, which indicate ~50% and ~20% stronger interactions with the TXP · SMTR host than in the respective pure liquids,[15] but also from the desolvation temperatures, which are higher than the normal boiling points of the respective pure solvents. From these data it was thus inferred that the strength of binding between the TXP · SMTR framework and

Figure 4. PXRD patterns for TXP · SMTR solvates and TXP-SMTR equimolar mixture. Key: TXP · SMTR · H_2O: expt. (a), compt. (a'); TXP · SMTR · C_2H_5OH: expt. (b), compt. (b'); TXP · SMTR · CH_3OH: expt. (c), compt. (c'); TXP-SMTR equimolar mixture: (d); TXP-SMTR equimolar mixture heated at 140°C for 2 h, in exact agreement with the common desolvation product by heating each TXP · SMTR solvate at 130°C for 2 h: (d').

UM00013082
NOVARTIS EXHIBIT 1517
Novartis v. Regents, IPR2023-01347
Page 1828 of 4460

Table 2. Thermogravimetric and Calorimetric Data for TXP Solvates[a]

Solvate	Desolvation Onset Temperature (°C)	Desolvation Enthalpy Change, $\Delta H_{S,exp}$ (J g^{-1})	Percent Mass Loss, Δm_S%	Heat of Vaporization of the Bound Solvent, ΔH_S (kJ mol^{-1})	Heat of Vaporization of the Pure Solvent, ΔH_{PS} (kJ mol^{-1})
TXP · SMTR · H_2O	85 (5)	59 (6)	2.2 (4)	48 (5)	40.7
TXP · SMTR · C_2H_5OH	115 (3)	80 (6)	5.9 (5)	59 (5)	40.5
TXP · SMTR · CH_3OH	126.3 (4)	67 (3)	4.5 (3)	48 (2)	39.2

[a]Standard deviations in parentheses refer to last decimal digit.

the respective solvent molecules is in the order EtOH > MeOH ~ H_2O, with the latter having greater mobility as indicated by the considerably lower onset temperatures for dehydration.

As shown in Figure 3, the pure lower-melting polymorph of anhydrous TXP · SMTR, form II ($T_{f,II} = 147.9 \pm 0.7$°C, $\Delta H_{f,II} = 96 \pm 6$ J g^{-1}), can be isolated by dehydration of freshly filtered TXP · SMTR · H_2O crystals. Instead, the pure higher-melting polymorph of anhydrous TXP · SMTR, form I ($T_{f,I} = 161.6 \pm 0.4$°C, $\Delta H_{f,I} = 117 \pm 7$ J g^{-1}), can be prepared by heating the solvates to a temperature slightly higher than that marking the end of the desolvation process (e.g., 130°C for 2 h in a hot air oven), as shown for TXP · SMTR · C_2H_5OH as representative. Both anhydrous polymorphs were obtained by desolvation under the DSC thermal cycling conditions, mostly form II from both TXP · SMTR · H_2O and TXP · SMTR · CH_3OH, and mostly form I from TXP · SMTR · C_2H_5OH. Form II, the thermodynamically metastable polymorph due to its monotropic relationship with form I according to the Heat of Fusion Rule,[14] rapidly reverted to TXP · SMTR · H_2O by exposure to ambient conditions of relative humidity (~40%) and temperature (~22°C). Instead, anhydrous TXP · SMTR form I was stable under the same atmospheric conditions. TXP · SMTR · C_2H_5OH was also stable by exposure to ambient atmosphere, whereas under similar conditions TXP · SMTR · CH_3OH could exchange methanol with water, to an extent that depended on relative humidity percent.

Phase Diagrams of the TXP-SMTR Binary System

From thermal and calorimetric data of a molecular complex and its individual components, the theoretical phase diagram can be drawn from eq. (2)[16]:

$$T_f = \Delta H_f / [\Delta S_f - R \ln(a/a*)] \qquad (2)$$

where T_f is the solid-liquid equilibrium temperature (in K), i.e., the final fusion temperature of the mixture; R is the gas constant; a is the activity of the component in the melt; a^* is the activity of pure molten component; ΔH_f is the enthalpy of fusion of the component (assumed independent of temperature); ΔS_f is the molar fusion entropy of the component at its fusion temperature (T_c), i.e., $\Delta H_f/T_c$. The solid-liquid equilibrium curves for TXP and SMTR were calculated by introducing into the above equation the respective enthalpic and entropic parameters[1,3] and different values of a ($0 < a < 1$), which represents the mole fraction of the component (the activity term a^* equals unity). The solid-liquid equilibrium curve for the TXP · SMTR complex was obtained considering that the activity term of the complex ($a_{TXP \cdot SMTR}/a^*_{TXP \cdot SMTR}$) is $x_{TXP} \cdot x_{SMTR}/(0.5 \times 0.5)$, i.e., 4 $x_{TXP} \cdot x_{SMTR}$. The symmetrical bell-shaped equilibrium curve of the complex is obtained by inserting the enthalpic and entropic parameters for the stable TXP · SMTR higher-melting polymorph I and different mole fraction values in equation (2). The intersection points of the bell-shaped curve with the curves for pure TXP and SMTR assuming complete dissociation of the complex in the melt[16] gave eutectic fusion temperatures of 141.7° and 150.5°C and the corresponding eutectic compositions of 0.18 and 0.75 mole fractions of TXP (Fig. 5, continuous curve). The eutectic fusion temperatures of 135.6° and 144.5°C and the corresponding eutectic compositions of 0.26 and 0.63 mole fractions of TXP for the metastable TXP · SMTR lower-melting polymorph II are also indicated (Fig. 5, dashed curve).

As can be seen from the phase diagram (Fig. 5) and the DSC curve of the equimolar mixture (Fig. 3), the triplet of endotherms at ~131°C (C), ~140°C (D), and ~149°C (E) which follow the fusion of a metastable eutectic between TXP and SMTR (A) and the formation of the molecular complex TXP · SMTR form II (B),[16] can be assigned

UM00013083
NOVARTIS EXHIBIT 1517
Novartis v. Regents, IPR2023-01347
Page 1829 of 4460

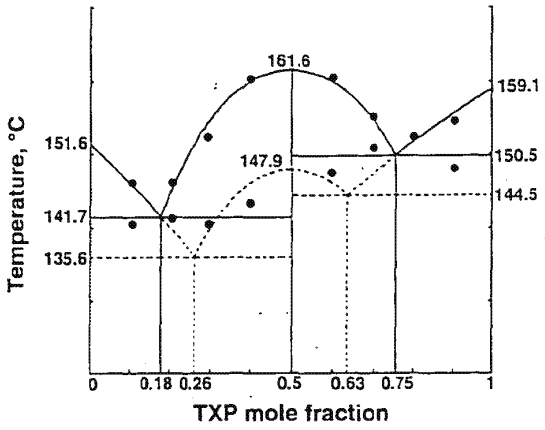


Figure 5. Phase diagram of the TXP-SMTR binary system assuming complete dissociation in the melt of the TXP · SMTR higher-melting polymorph I ($T_{f,I} = 161.6°C$, $\Delta H_{f,I} = 117\ J\ g^{-1}$) (continuous curve). Dots represent the experimental DSC peak temperatures of eutectic halts and final melting recorded for physical mixtures of TXP · SMTR form I with either SMTR or TXP (see text and Fig. 3). The phase diagram for the metastable TXP · SMTR lower-melting polymorph II ($T_{f,II} = 147.9°C$, $\Delta H_{f,II} = 96\ J\ g^{-1}$) is also drawn (dashed curve).

respectively to the eutectic between TXP · SMTR form II and SMTR, the eutectic between TXP · SMTR form II and TXP, and melting of TXP · SMTR form II. The last exotherm at ~152°C (E) represents the crystallization of TXP · SMTR form I and the following endotherm at ~161°C (G) its melting. In the DSC run of the equimolar mixture kept at 140°C for 2 h, only melting of TXP · SMTR form I was recorded (Fig. 3, curve g). DSC runs of mixtures of TXP · SMTR form I and either SMTR or TXP show eutectic halts and final melting temperatures in agreement with the theoretical phase diagram. Typical DSC traces of mixtures with excess SMTR (0.40 TXP mole fraction, curve h) or excess TXP (0.60 TXP mole fraction, curve i) are presented in Figure 3. The peak temperatures of the couple of endotherms recorded for these and other (not shown) mixtures are reported as dots in the phase diagram of TXP · SMTR form I (Fig. 5).

Powder XRD

As shown in Figure 4, TXP · SMTR · H_2O and TXP · SMTR · C_2H_5OH are readily distinguishable from their PXRD patterns, which matched the computed ones from single-crystal X-ray analysis. The distinct PXRD patterns give evidence for different structural arrangements in the hydrate and ethanolate phases. Superposition of both experimental and computed patterns of TXP · SMTR · C_2H_5OH and TXP · SMTR · CH_3OH confirms that the angular positions for the majority of the peaks are in close correspondence, leading to the conclusion that these phases are isostructural, just as the ethanol and methanol solvates of free TXP.[1] Specifically, this implies that the three-dimensional arrangement of the host TXP · SMTR molecules is a common structural motif in both solvated crystals and that the included ethanol and methanol molecules occupy common crystallographic sites.

The PXRD pattern of the untreated equimolar physical mixture of TXP and SMTR corresponds to the weighted average of those taken on pure components, indicating that no apparent interaction between the components was induced by grinding. Discernible differences were instead evident in the PXRD pattern of the mixture heated in a hot air oven at 140°C for 2 h, which is substantially superimposable on that of the common desolvation product of TXP · SMTR solvates by heating at 130°C for 2 h. Thus, the stable polymorph of anhydrous TXP · SMTR can be obtained by heating the equimolar mixture of the components via metastable eutectic and metastable polymorph or the crystalline solvates via a desolvation product which crystallizes into the metastable polymorph (see Figs. 3 and 4).

Single Crystal X-Ray Diffraction

Crystals of TXP · SMTR · CH_3OH and TXP · SMTR · C_2H_5OH are isostructural, whereas those of TXP · SMTR · H_2O (RT) have a unit cell and crystal packing arrangement very similar to the former pair. In view of the close structural relationships among these phases, they are discussed as a group. The structural relationship between TXP · SMTR · H_2O (RT) and TXP · SMTR · H_2O, the low-temperature hydrate phase, is discussed separately below. The solvated complexes are all based on a 1:1 hydrogen-bonded cyclic heterodimer of TXP and SMTR. The crystallographic asymmetric unit in TXP · SMTR · CH_3OH, TXP · SMTR · C_2H_5OH, and TXP · SMTR · H_2O (RT) consists of one complex formula unit TXP · SMTR and a molecule of the corresponding solvent (Fig. 6). Complexation between TXP and SMTR is invariably accompanied by proton transfer from SMTR to TXP. Each complex unit TXP · SMTR comprises a molecule of TXP protonated at N3 and a molecule of SMTR deprotonated at N35, and in

UM00013084
NOVARTIS EXHIBIT 1517
Novartis v. Regents, IPR2023-01347
Page 1830 of 4460

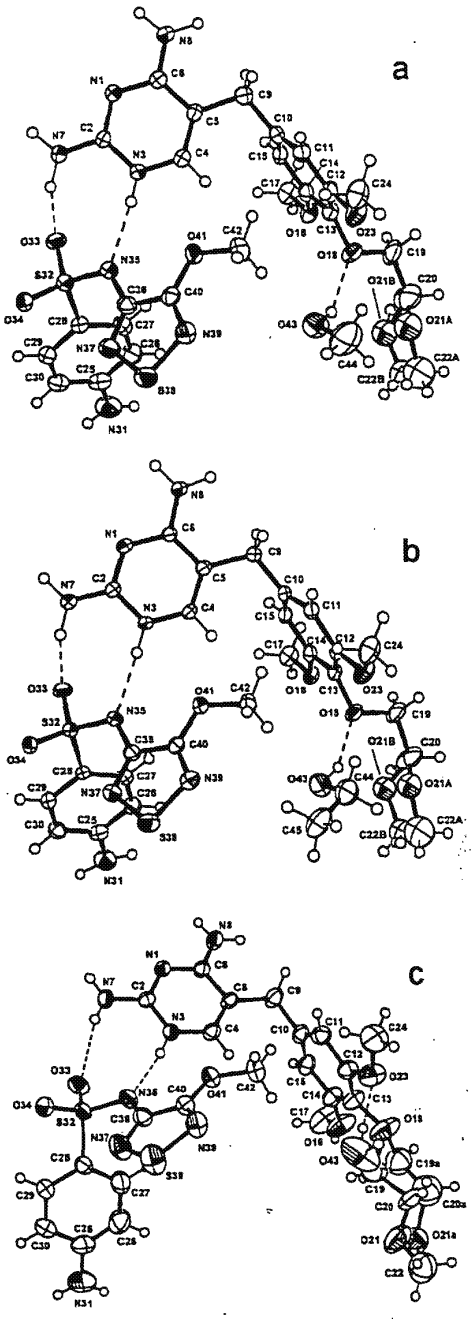


Figure 6. The asymmetric units in the solvates of TXP·SMTR with CH_3OH (a), C_2H_5OH (b), H_2O (c). Thermal ellipsoids are drawn at the 50% probability level. In all structures, label O43 designates the guest oxygen atom. Suffix "a" on atom labels denotes disordered components.

all cases, complex formation is effected by one $N^+-H\cdots N^-$ hydrogen bond and one $N-H\cdots O$ hydrogen bond (Table 3), yielding an $R_2^2(8)$ system[17] in which TXP is the donor and SMTR is the acceptor. Analogous proton transfer and the formation of the same $R_2^2(8)$ system was previously reported for complexation between trimethoprim and SMTR,[4] where it was noted that a sulfonyl oxygen atom of SMTR rather than a nitrogen atom of the thiadiazole ring is involved in the molecular association. Deprotonation of the free molecule SMTR results in significant shortening of the bond S32–N35 from 1.642(5) Å[18] to values in the range 1.576(4)–1.585(1) Å in the TXP·SMTR solvates.

The isostructurality of TXP·SMTR·CH_3OH and TXP·SMTR·C_2H_5OH, evident from Figure 6, is remarkable, extending not only to equivalent disorder of the methoxyethoxy substituents of the TXP molecule, but also to the positions of common atoms of the included EtOH and MeOH molecules. Crystal isostructurality for the solvates of TXP with water, ethanol, and methanol, as well as disorder in the methoxyethoxy chain in polymorphic form I of TXP featured prominently in a recent account[1] of the solid-state properties of various modifications of this drug. In the present series, molecular conformations are defined by the torsion angles (Fig. 1) C6–C5–C9–C10 ($\tau_{1,TXP}$) and C5–C9–C10–C15 ($\tau_{2,TXP}$) for TXP (as previously defined[1]) and C27–C28–S32–N35 ($\tau_{1,SMTR}$), C28–S32–N35–C36 ($\tau_{2,SMTR}$), and S32–N35–C36–N37 ($\tau_{3,SMTR}$) for SMTR (as previously defined[4]). The values of these parameters for the MeOH and EtOH solvates correspond within 3° (Table 4).

Replacement of MeOH and EtOH molecules by water molecules within the TXP·SMTR host framework to form TXP·SMTR·H_2O (RT) results in a structural deformation, as indicated by significant changes in unit cell edges (up to ~0.6 Å) and interaxial angles (up to ~10°) (Table 1). Although these changes in lattice dimensions are sufficient to lead to a PXRD pattern that permits easy distinction of the hydrate from the isostructural pair TXP·SMTR·CH_3OH and TXP·SMTR·C_2H_5OH (Fig. 4), the overall structure of the hydrate is nevertheless closely related to those of the former pair. This is evident both from crystal packing diagrams (Figs. 7 and 8) and from the six hydrogen bonds that are common to all three phases (Table 3).

Of primary interest in this study is the nature of the hydrogen bonding and the topology of inclusion

UM00013085
NOVARTIS EXHIBIT 1517
Novartis v. Regents, IPR2023-01347
Page 1831 of 4460

Table 3. Data for Principal Hydrogen Bonds

D–H···A	D···A/Å	H···A/Å	D–H···A/(°)
TXP · SMTR · CH_3OH			
N3–H3···N35	2.936 (3)	2.063 (2)	171.1 (2)
N7–H7A···O34^{i}	2.959 (4)	1.98 (2)	165 (4)
N8–H8A···N1^{ii}	3.107 (4)	2.15 (2)	161 (3)
N7–H7B···O33	2.832 (4)	1.89 (3)	156 (3)
N8–H8B···O34^{iii}	2.838 (4)	2.12 (5)	126 (3)
O43–H43···O18	2.872 (4)	2.115 (2)	149.8 (3)
N31–H31A···O43^{iv}	2.942 (5)	1.96 (5)	167 (3)
TXP · SMTR · C_2H_5OH			
N3–H3···N35	2.930 (2)	2.05 (2)	172 (2)
N7–H7B···O33	2.823 (2)	2.05 (2)	158 (2)
N7–H7A···O34^{i}	2.947 (2)	1.97 (1)	168 (2)
N8–H8A···N1^{ii}	3.126 (2)	2.15 (1)	167 (2)
N8–H82···O34^{iii}	2.822 (2)	2.02 (2)	136 (2)
O43–H43···O18	2.941 (2)	2.19 (2)	156 (2)
N31–H31B···O43^{iv}	3.017 (2)	2.04 (2)	169 (2)
TXP · SMTR · H_2O (RT)			
N3–H3···N35	2.945 (3)	2.09 (2)	173 (2)
N7–H7B···O33	2.855 (3)	2.21 (2)	132 (2)
N7–H7A···O34^{i}	3.085 (3)	2.26 (2)	161 (2)
N8–H8A···N1^{ii}	3.040 (3)	2.24 (2)	154 (2)
N8–H8B···O34^{iii}	2.851 (3)	2.13 (2)	141 (2)
N31–H31B···O43^{iv}	2.944 (5)	2.09 (2)	174 (2)
O43–H43A···O33^{v}	3.010 (4)	2.03 (4)	156 (2)
O43–H43B···O23	2.882 (4)	1.90 (3)	168 (3)
N31–H31A···N39^{iv}	3.279 (4)	2.48 (2)	154 (3)
TXP · SMTR · H_2O			
N3–H3···N35	2.945 (2)	2.071 (2)	172.4 (1)
N7–H7B···O33	2.861 (2)	2.153 (2)	137.1 (1)
N45–H45···N77	2.913 (3)	2.036 (2)	173.8 (1)
N49-H49B···O75	2.868 (2)	2.246 (2)	127.5 (1)
N7–H7A···O76^{vi}	3.074 (3)	2.214 (2)	165.7 (1)
N49–H49A···O34^{vii}	3.075 (3)	2.246 (2)	156.8 (1)
N8–H8A···N43	3.044 (3)	2.233 (2)	153.2 (1)
N50–H50A···N1	2.987 (3)	2.166 (2)	155.0 (1)
N8–H8B···O34^{vii}	2.845 (2)	2.126 (2)	138.3 (1)
N50–H50B···O76^{vi}	2.857 (2)	2.103 (2)	143.2 (1)
N31–H31B···N39^{viii}	3.275 (3)	2.445 (2)	157.7 (1)
N73–H73A···N81^{ix}	3.242 (3)	2.432 (2)	153.4 (2)
O85–H85A···O33	2.956 (3)	1.98 (3)	164 (2)
O85–H85B···O65^{x}	2.854 (3)	1.86 (2)	176 (2)
N73–H73B···O85^{xi}	2.966 (3)	2.089 (2)	173.4 (2)
O86–H86A···O75	3.088 (3)	2.10 (2)	177 (4)
O86–H86B···O18^{xii}	3.139 (3)	2.31 (5)	139 (4)
O86–H86B···O23^{xii}	2.927 (3)	2.044 (2)	142 (2)
N31–H31B···O86^{xiii}	2.918 (3)	2.039 (2)	172 (2)

Symmetry operations: (i) $1-x, 2-y, 2-z$; (ii) $-x, 2-y, 2-z$; (iii) $-1+x, y, z$; (iv) $2-x, 1-y, 1-z$; (v) $x, y, -1+z$; (vi) $x, 1+y, z$; (vii) $x, -1+y, z$; (viii) $-1-x, 4-y, 1-z$; (ix) $1-x, -y, 2-z$; (x) $-x, 2-y, 2-z$; (xi) $1+x, -2+y, z$; (xii) $-x, 2-y, 1-z$; (xiii) $-1+x, 2+y, z$.

of the solvent molecules in the respective solvate crystal structures, because these features should correlate with the behavior recorded by thermal analysis. The common hydrogen bonding network occurring in the isostructural solvates TXP · SMTR · CH_3OH and TXP · SMTR · C_2H_5OH is illustrated in Figure 9 for TXP · SMTR · CH_3OH as representative. Complexation between TXP and

UM00013086
NOVARTIS EXHIBIT 1517
Novartis v. Regents, IPR2023-01347
Page 1832 of 4460

Table 4. Principal Torsion Angles (°) for TXP and SMTR Molecules

Complex	$\tau_{1,TXP}$	$\tau_{2,TXP}$	$\tau_{1,SMTR}$	$\tau_{2,SMTR}$	$\tau_{3,SMTR}$
TXP · SMTR · CH_3OH	−173.4 (3)	78.0 (4)	−34.5 (3)	−66.3 (3)	−2.8 (5)
TXP · SMTR · C_2H_5OH	−172.9 (1)	75.0 (2)	−34.2 (2)	−65.5 (1)	−3.9 (2)
TXP · SMTR · H_2O (RT)	−174.0 (2)	94.8 (3)	−35.2 (3)	−69.6 (2)	1.5 (3)
TXP · SMTR · H_2O[a]	170.2 (2)	−80.1 (3)	30.0 (2)	70.3 (2)	−10.0 (3)
	−178.2 (2)	100.7 (3)	−37.9 (2)	−69.0 (2)	−0.7 (4)
Average magnitudes	174	86	34	68	4

[a]Two independent units.

SMTR and the association of the resulting units TXP · SMTR give rise to a variety of hydrogen-bonded ring formations (1–4). The repeating pattern of hydrogen-bonded rings propagates indefinitely through the crystal parallel to the *a*-axis, thus yielding a highly stabilized TXP · SMTR framework. Figure 9 also shows the mode of attachment of the MeOH molecule to the host TXP · SMTR array.

The solvent molecule has a bridging role by hydrogen bonding as donor to the ethereal oxygen atom of a TXP molecule (O43–H43 ··· O18) and as acceptor of a hydrogen bond from an amino group of a symmetry related TXP molecule (N31–H31A ··· $O43^{iv}$). MeOH molecules occupy distinct, isolated sites forming a zigzag array parallel to the crystal *a*-axis with alternating O(solvent) ··· O(solvent) distances of 6.5 and 8.5 Å. X-ray analysis confirmed that the mode of attachment of EtOH molecules in TXP · SMTR · C_2H_5OH is identical to that described above for the MeOH molecules. Notably, however, the hydrogen bond lengths involving the solvent molecules are significantly different in the two structures, those of O43 ··· O18 and N31 ··· $O43^{iv}$ both being shorter in TXP · SMTR · CH_3OH (by 15 and 12 σ_c, respectively, σ_c = combined esd). The MeOH molecule is thus initially significantly more tightly bound

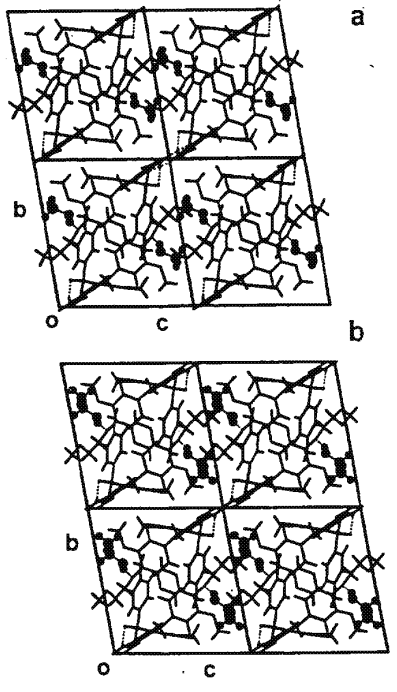


Figure 7. [100] Projections of the crystal structures of TXP · SMTR · CH_3OH (a), TXP · SMTR · C_2H_5OH (b). Solvent molecules are drawn in ball-and-stick mode. Four unit cells are shown and labels *b*, *c* refer to the projected lengths of these axes.

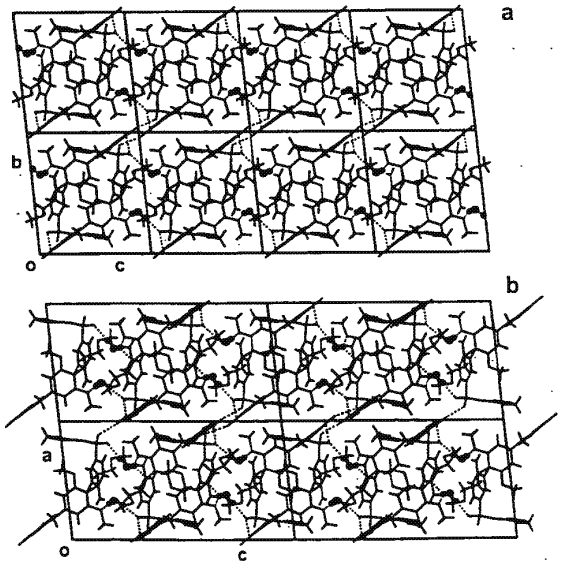


Figure 8. Common projections of the crystal structures of TXP · SMTR · H_2O (RT) (a); TXP · SMTR · H_2O (low-temperature phase) (b). Eight and four unit cells are shown for (a) and (b), respectively. Labels *a*, *b*, *c* refer to the projected lengths of these axes.

UM00013087
NOVARTIS EXHIBIT 1517
Novartis v. Regents, IPR2023-01347
Page 1833 of 4460

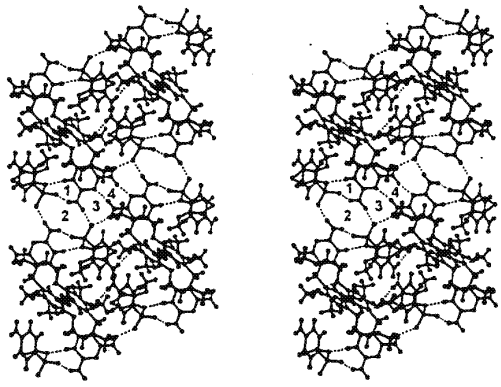


Figure 9. Stereoview of the hydrogen bonding pattern in TXP · SMTR · CH_3OH.

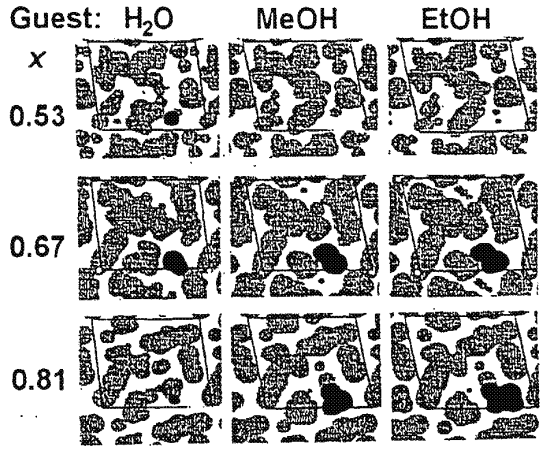


Figure 10. Corresponding sections drawn through the unit cells of the solvates of TXP · SMTR. Lighter shaded regions represent the common TXP · SMTR framework and black regions the solvent molecule cross-sections. The section at $x = 0.67$ passes through the center of the water oxygen atom.

than the EtOH molecule, a result that correlates with the higher temperature of onset of desolvation for TXP · SMTR · CH_3OH compared with that for TXP · SMTR · C_2H_5OH (Fig. 3). After solvent molecular loosening and fracture of the host-guest hydrogen bonds upon heating, diffusion of the more sterically bulky EtOH molecule through the common host framework accounts for the larger ΔH_S value (Table 2) required for complete desolvation of TXP · SMTR · C_2H_5OH.[1] For both solvates, the sharpness of the endotherms for desolvation is consistent with their location in isolated sites.

A very similar TXP · SMTR hydrogen-bonded framework occurs in TXP · SMTR · H_2O (RT) and water molecules are again located in isolated sites, analogous to those accommodating MeOH and EtOH molecules in their respective solvates (Figs. 7 and 8). Each water molecule engages in two hydrogen bonds as donor and in one hydrogen bond as acceptor (Table 3). It was therefore surprising to note the anomalous DSC behavior for TXP · SMTR · H_2O (RT), namely dehydration at a relatively low (and variable) onset temperature and over a broad temperature range (see Fig. 3). To explain this anomaly, appropriate sections through the respective unit cells were examined. Figure 10 shows three sections drawn at 1.6-Å intervals which practically span the range of the water molecule in TXP · SMTR · H_2O (RT), together with the corresponding sections in the MeOH and EtOH solvates. The existence of narrow, constricted channels (Fig. 10, unshaded areas) in the solvent regions is evident in all three structures. Furthermore, the close isostructurality of TXP · SMTR · CH_3OH and TXP · SMTR · C_2H_5OH, and their close relationship with TXP · SMTR · H_2O (RT) is reflected in very similar host frameworks and channel topologies on each corresponding section, despite the differences in guest molecular sizes. We propose that a reasonable explanation for the relative ease of dehydration is that the smaller water molecule is able to migrate through such channels much more readily than the sterically more bulky MeOH and EtOH molecules, particularly upon heating, when small conformational changes in the host framework can widen the channels sufficiently to facilitate diffusion of H_2O molecules through the crystal. The observed variability in onset temperature for dehydration is presumed to be attributable to differences in crystal defect concentrations in various crystal batches.

Cooling a single crystal of the hydrate TXP · SMTR · H_2O (RT) on the diffractometer from 297 to 173 K led to a change in the lattice parameters without a change in the space group. Comparison of the unit cell data (Table 1) shows that there is an effective doubling of the unit cell dimension c at low temperature. (This is more obvious if the unit cell parameters a and b, as well as α and β, for one of the phases are interchanged. The altered crystal setting for the low-temperature phase was necessitated by a change of handedness accompanying the use of different crystal specimens for full X-ray analyses at 297 and 173 K and subsequent matrix transformations to cells with common axial directions.) Programmed warming (10 K min^{-1}) from 173 to 297 K led to reappearance of the smaller

UM00013088
NOVARTIS EXHIBIT 1517
Novartis v. Regents, IPR2023-01347
Page 1834 of 4460

unit cell, thus confirming the reversibility of the transformation (see below). The structural relationship between the hydrate phases is subtle, involving primarily an order/disorder transition of the methoxyethoxy chain of a TXP molecule. Figure 11, a comparison of the motifs undergoing transformation, shows that at 297 K the motif comprises a pair of inversion-related asymmetric units TXP · SMTR · H_2O linked by the base-paired pyrimidine rings (unique hydrogen bond N8–H8A ··· $N1^{ii}$). Inversion symmetry requires the two methoxyethoxy chains to be identically disordered. At 173 K, disorder in one of the two methoxyethoxy chains persists, but disorder in the other chain (atoms C19, C20, O21) is "frozen out." The resulting dimeric base-paired motif (hydrogen bonds N8–H8A ··· N43 and N50–H50A ··· N1) has a pseudo-inversion center only, thus becoming the asymmetric unit at low temperature. Because the space group $P\bar{1}$ is retained, the unit cell contains two base-paired dimers and hence a unit cell volume double that of the phase at 297 K. The packing diagrams comparing the hydrate structures (Fig. 8) show the doubling of the crystal *c*-axis accompanying the transition.

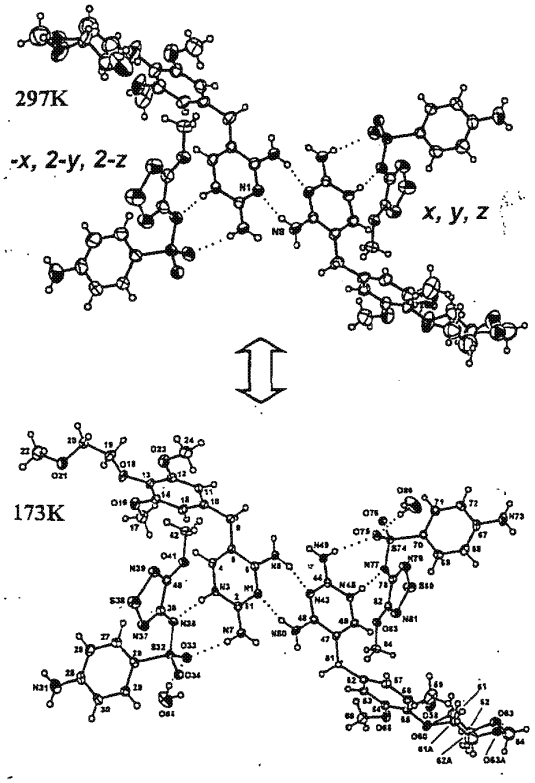


Figure 11. Structural motifs in the crystals of the room-temperature and low-temperature polymorphs of TXP · SMTR · H_2O showing disorder of both methoxyethoxy chains at 297 K and disorder in only one chain at 173 K.

Molecular parameters for the low-temperature phase are included in the relevant tables. Significant differences are evident between the magnitudes of corresponding torsion angles for the two pseudo-inversion-related TXP · SMTR units in the hydrate (maximum ~20° for $\tau_{2,TXP}$) and the values of the torsion angles tend to straddle those observed in the other solvates (Table 4). Because the two independent water molecules (O85, O86) are related by a pseudo-inversion center only, the sets of hydrogen bonds in which they engage are not identical. In particular, the single hydrogen bond O85–H85B ··· $O65^{x}$ (involving acceptor methoxyl oxygen atom O65 of TXP) is replaced by bifurcated hydrogen bonds O86–H86B ··· $O18^{xii}$ and O86–H86B ··· $O23^{xii}$, the latter involving an oxygen atom of the methoxyethoxy chain of TXP). The phase transition, as well as its reversibility, initially observed and characterized by DSC, were thus confirmed by temperature cycling of the single crystal on the diffractometer. The nature of the transition, involving subtle structural changes, is consistent with the small magnitude of the enthalpy change (~1 kJ mol^{-1}) measured in DSC. The subtlety of the transition is also reflected in the nearly identical PXRD patterns computed from the single crystal X-ray results at the two temperatures. That shown in Figure 4 represents the room-temperature phase.

CONCLUSIONS

Crystalline solvated drug species (or pseudopolymorphs) are of interest because entrapment of the solvent molecules in cavities formed by the host drug framework can yield very stable clathrates. Desolvation of such species can be exploited in the preparation of pure polymorphic forms of the parent drug. For the solvates of TXP · SMTR reported herein, the physical conditions for isolating two distinct polymorphic forms of the bimolecular complex via desolvation have been established. These polymorphs have been characterized and their thermodynamic relationship has also been determined. In addition, the experimental and theoretical phase diagrams for the TXP-SMTR binary system have been elucidated.

The system comprising the polymorphs and solvates of TXP · SMTR is remarkable and, to our

UM00013089
NOVARTIS EXHIBIT 1517
Novartis v. Regents, IPR2023-01347
Page 1835 of 4460

knowledge, unique in manifesting a variety of structural and thermodynamic relationships. Thus, TXP · SMTR displays enantiotropic dimorphism in its hydrated form TXP · SMTR.H_2O, monotropic dimorphism in the unsolvated state, and isostructurality in the solvated states containing methanol and ethanol. Structural resolution of the two hydrated forms has revealed subtle differences between them, associated with an unusual order/disorder transition. The persistence of a common TXP · SMTR framework in the series of solvates is associated with formation of an intricate, well-defined network of hydrogen-bonded ring systems which has been completely characterized. Location of solvent molecules in isolated sites within essentially the same framework of TXP · SMTR has been demonstrated for all three solvates. These structural features have been successfully reconciled with thermodynamic data derived by TGA and DSC techniques. Finally, we draw attention to the dominant role of TXP in the behavior of the solvates of TXP · SMTR, as reflected in parallel thermal properties of the solvates of TXP alone.[1]

SUPPORTING INFORMATION

X-ray crystallographic data for all four solvates in CIF format are available from the authors. The structures have been deposited at the Cambridge Crystallographic Data Centre (CCDC 188491–188494).

ACKNOWLEDGMENTS

MRC thanks the NRF (Pretoria) and the University of Cape Town for financial assistance. Technical assistance from Vincent J. Smith and Hong Su is gratefully acknowledged.

REFERENCES

1. Caira MR, Bettinetti GP, Sorrenti M. 2002. Structural relationships, thermal properties and physicochemical characterization of anhydrous and solvated crystalline forms of tetroxoprim. J Pharm Sci 91:467–481.
2. Bettinetti GP, Sorrenti M, Caira MR. Proceedings of the 4th World Meeting ADRITELF/APGI/APV, Florence, April 8–11, 2002, pp 355–356.
3. Bettinetti GP, Giordano F. 1988. Interaction between trimethoprim and some sulfa drugs. Drug Dev Ind Farm 14:431–449.
4. Giuseppetti G, Tadini C, Bettinetti GP. 1994. 1:1 Molecular complex of trimethoprim and sulfametrole. Acta Crystallogr C50:1289–1291.
5. COLLECT. 2000. Nonius. Delft The Netherlands: Nonius BV.
6. Otwinowski Z, Minor W. 1997. Processing of X-ray diffraction data collected in oscillation mode. In: Carter CW, Sweet RM, editors. Methods in enzymology. New York: Academic Press. pp 307–326.
7. Sheldrick GM. 1985. SHELXS86. In: Kruger GM, Goddard R, editors. Crystallographic computing 3. Oxford, UK: Oxford University Press. pp 175–178.
8. Sheldrick GM. 1997. SHEXL97: Program for the refinement of crystal structures. Göttingen, Germany: University of Göttingen.
9. Spek AL. 1990. PLATON: A multipurpose crystallographic tool. Acta Crystallogr A46:C34.
10. Zsolnai L, Pritzkow H. 1994. ZORTEP: ORTEP program for personal computer. Heidelberg, Germany: University of Heidelberg.
11. WebLab ViewerPro 3.7. 2000. San Diego, CA: Molecular Simulations, Inc.
12. Barbour LJ. 1999. J Appl Crystallogr 32:353–354. Program SECTION.
13. Yvon K, Jeitschko W, Parthe E. 1977. LAZY PULVERIX: A computer program for calculating X-ray and neutron diffraction powder patterns. J Appl Crystallogr 10:73–74.
14. Burger A, Ramberger R. 1979. On the polymorphism of pharmaceuticals and other molecular crystals. Mikrochim Acta [Wien] II:259–271.
15. CRC handbook of chemistry and physics, 66a ed. 1985. Boca Raton, FL: CRC Press.
16. Giordano F, Bettinetti GP. 1988. An experimental and theoretical approach to the analysis of pharmaceutical binary systems. J Pharm Biomed Anal 6:951–955.
17. Etter MC. 1990. Encoding and decoding hydrogen bond patterns of organic compounds. Acc Chem Res 12:120–126.
18. Koo CH, Chung YJ, Shin HS, Suh JS. 1982. The crystal and molecular structures of sulfametrole. Bull Korean Chem Soc 3:9–13.

UM00013090
NOVARTIS EXHIBIT 1517
Novartis v. Regents, IPR2023-01347
Page 1836 of 4460

This Page is Inserted by IFW Indexing and Scanning Operations and is not part of the Official Record

BEST AVAILABLE IMAGES

Defective images within this document are accurate representations of the original documents submitted by the applicant.

Defects in the images include but are not limited to the items checked:

- ☐ BLACK BORDERS
- ☐ IMAGE CUT OFF AT TOP, BOTTOM OR SIDES
- ☐ FADED TEXT OR DRAWING
- ☐ BLURRED OR ILLEGIBLE TEXT OR DRAWING
- ☐ SKEWED/SLANTED IMAGES
- ☐ COLOR OR BLACK AND WHITE PHOTOGRAPHS
- ☐ GRAY SCALE DOCUMENTS
- ☐ LINES OR MARKS ON ORIGINAL DOCUMENT
- ☐ REFERENCE(S) OR EXHIBIT(S) SUBMITTED ARE POOR QUALITY
- ☐ OTHER: _____

IMAGES ARE BEST AVAILABLE COPY.
As rescanning these documents will not correct the image problems checked, please do not report these problems to the IFW Image Problem Mailbox.

Selective formation of hydrogen bonded cocrystals between a sulfonamide and aromatic carboxylic acids in the solid state

Mino R. Caira,* Luigi R. Nassimbeni and Alexander F. Wildervanck
Department of Chemistry, University of Cape Town, Rondebosch 7700, South Africa

Co-grinding sulfadimidine [4-amino-*N*-(4,6-dimethylpyrimidin-2-yl)benzenesulfonamide] with several aromatic carboxylic acids in the solid state produces 1 : 1 hydrogen bonded cocrystals which are identical to those obtained from reaction between the components in solution. The kinetics of solid state formation of selected cocrystals have been measured using X-ray powder diffraction. Sulfadimidine selectively cocrystallizes with 2-aminobenzoic acid when the latter is present in binary mixtures of acids. Solid state reaction of the cocrystal sulfadimidine·2-hydroxybenzoic acid with 2-aminobenzoic acid results in elimination of 2-hydroxybenzoic acid and formation of the cocrystal sulfadimidine·2-aminobenzoic acid.

Introduction

There is growing interest in the hydrogen bond directed molecular recognition properties of organic molecules. Many systems of this type have been studied by X-ray analysis to determine the structures of molecular assemblies after association has occurred while cocrystallization studies have been useful in monitoring competitive interactions that determine the selectivity of recognition processes.[1–7]

The terms 'cocrystal' and 'molecular complex' are used widely and interchangeably to describe hydrogen bonded structures of the type discussed in this paper.

The carboxylic acids referred to in this study, together with their abbreviated designations, are: benzoic acid (BA), 2-aminobenzoic acid (anthranilic acid, AA), 2-hydroxybenzoic acid (salicylic acid, SA), 2-acetoxybenzoic acid (acetylsalicylic acid, AC), benzene-1,2-dicarboxylic acid (*o*-phthalic acid, PHA), 4-chlorobenzoic acid (*p*-chlorobenzoic acid, PCL), 4-aminobenzoic acid (*p*-aminobenzoic acid, PAB) and 4-amino-2-hydroxybenzoic acid (*p*-aminosalicylic acid, PAS).

The first X-ray crystal structure of a 1 : 1 molecular complex between the sulfa drug sulfadimidine, {[4-amino-*N*-(4,6-dimethylpyrimidin-2-yl)benzenesulfonamide], hereinafter SD} and an aromatic carboxylic acid, namely 2-hydroxybenzoic acid, was reported by Patel *et al.*[8] We subsequently extended the study of compounds of this type and reported the preparation and X-ray crystal structures of the 1 : 1 cocrystals SD·2-aminobenzoic acid[9] (SD·AA), SD·4-aminobenzoic acid[9] (SD·PAB), SD·*p*-aminosalicylic acid[10] (SD·PAS) and SD·acetylsalicylic acid[10] (SD·AC). We have also prepared and elucidated the crystal structures of SD·*p*-chlorobenzoic acid (SD·PCL) and SD·*o*-phthalic acid[11] (SD·PHA). Fig. 1 shows the structure of a representative example, the 1 : 1 sulfadimidine·benzoic acid (SD·BA) complex unit in its cocrystal,[11] the most recent addition to the series. Molecular association between SD and BA is effected by two intermolecular hydrogen bonds, namely N–H · · · O=C and N · · · H–O, involving the N atom of the sulfonamide group, one pyrimidine N atom and the carboxylic group of the acid. The same hydrogen bonding pattern occurs in all of the cocrystals listed above. The complex motif has a graph set $R_2^2(8)$ in the notation of Etter,[12] indicating that the hydrogen bonds result in the formation of an eight-membered ring and that two donors and two acceptors are used in assembling the motif.

Hitherto, each of the cocrystals in this series was obtained by crystallization from a solution containing the two components in equimolar ratio using solvents such as EtOH, Me_2CO and MeCN. We now report the facile formation of the cocrystals SD·BA, SD·AA, SD·SA, SD·AC, SD·PHA and SD·PCL, by co-grinding SD with the respective acid in the solid state and we demonstrate their structural identity with the cocrystals obtained by crystallization from solution. The results of a study of the kinetics of formation of two selected cocrystals (SD·SA and SD·AA) by X-ray powder diffraction (XRD) are also described. Finally, we present novel results from competition experiments involving, on the one hand, co-grinding SD with an equimolar mixture of carboxylic acids to investigate the possibility of selective cocrystallization, and on the other, co-grinding a 1 : 1 SD–aromatic carboxylic acid cocrystal with a different acid from that contained in the cocrystal, to ascertain whether an exchange of the complexing partners is possible.

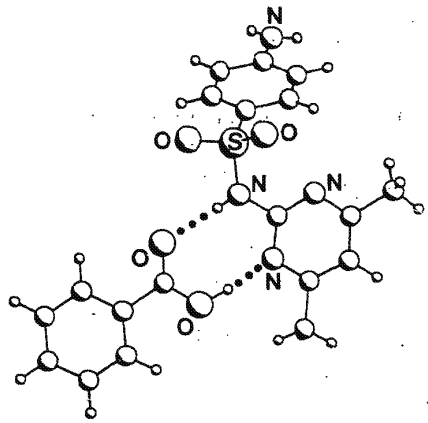


Fig. 1 Hydrogen bonded motif in the complex SD·BA

The products of co-grinding were analysed by IR spectroscopy, differential scanning calorimetry and X-ray powder diffraction. Unambiguous identification of the solid phases produced by co-grinding experiments relied on the availability of the single crystal X-ray data for the cocrystals. The latter were used to compute XRD patterns for comparison with the experimental patterns of co-ground materials. The single crystal X-ray analyses[8–11] have revealed different unit cell dimensions and space groups for the co-crystals described here, so that each has a unique XRD pattern.

UM00013092
NOVARTIS EXHIBIT 1517
Novartis v. Regents, IPR2023-01347
Page 1838 of 4460

Experimental

SD was co-ground with an equimolar amount of each of the acids BA, AA, SA, AC, PHA and PCL. In a typical experiment, 140 mg SD (0.5 mmol) and 61 mg BA (0.5 mmol) were mixed and ground manually in a mortar and pestle for 4 min. The mixture was then ground for 3 min in a Grindex ball grinder using a 12 mm iron ball (8.34 g) in a stainless steel cylinder of internal diameter 14 mm and length 35 mm. The products of co-grinding were analysed by differential scanning calorimetry (DSC) using a Perkin-Elmer PC7 Series thermal analysis system, by IR spectroscopy (hexachlorobutadiene mulls, CsI plates) on a Perkin Elmer model 983 IR spectrophotometer and by X-ray powder diffraction (XRD) on a Philips PW1050/80 goniometer using Ni-filtered Cu-Kα radiation (λ = 1.5418 Å).

The program Lazy Pulverix[13] was used to generate XRD patterns for cocrystals whose single crystal X-ray structures have been determined.[8-11] Input data comprised space group information, unit cell parameters, atomic coordinates and thermal parameters.

The kinetics of cocrystallization formation were followed by measuring the intensities of non-overlapping reflections of SD and the product cocrystal (SD·SA or SD·AA) as a function of grinding time. Manual grinding in a mortar and pestle at a constant rate was used since the reactions proceeded too rapidly in the ball grinder. Grinding for up to 60 min was required for complete reaction.

Competition experiments involved co-grinding SD and two acids in a 1:1:1 molar ratio using the apparatus described above and analysing the product phases by XRD.

Prior to the co-grinding experiments, the XRD patterns of the individual components were recorded before and after 10 min grinding to ascertain whether polymorphic changes occurred. No changes were observed.

Results and discussion

Cocrystal formation

Representative results are given for the pair SD and BA. The DSC trace of the co-ground material yielded a melting endotherm at 215 °C which differs from the melting point of either SD (197 °C) or BA (122 °C). This was the first indication of the formation of a new phase. The N–H stretching frequencies in SD occurring at 3436, 3337 and 3236 cm^{-1} appeared in the product at 3464, 3375 and 3259 cm^{-1}. Finally, as shown in Fig. 2, for the product of co-grinding, XRD yielded a pattern which was identical to that calculated using the single crystal X-ray data for the 1:1 SD–benzoic acid cocrystal, SD·BA.[11]

Analogous and equally convincing results were obtained with the acids AA, SA, AC, PHA and PCL. Table 1 lists the measured melting points and N–H stretching frequencies in the cocrystals. In all cases, the products were obtained in under 5 min grinding time at room temperature and in a pure state as gauged from the absence of DSC fusion endotherms or XRD peaks corresponding to the reactants. Control of the temperature during mechanical grinding was not feasible and temperatures as high as 40 °C were registered in the stainless steel vial.

Kinetics of cocrystallization

To obtain meaningful kinetic results, manual grinding at room temperature (25 °C) was employed to minimize localized heating effects. Fig. 3 shows successive traces of the (1 2 0) reflection of SD and the (0 4 1) reflection of SD·SA as co-grinding of SD and SA proceeded. The integrated intensities (areas under the curves) decreased and increased respectively for these reflections. That representing the formation of SD·SA

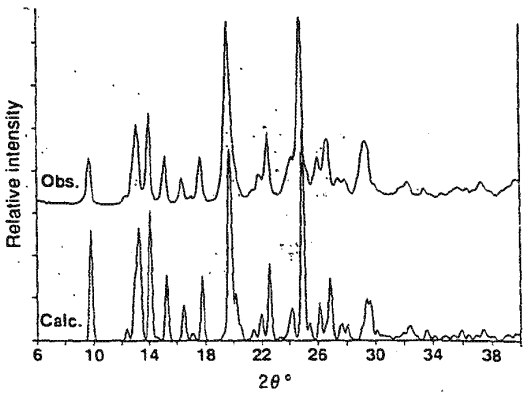


Fig. 2 Comparison between the experimental XRD pattern of the product of co-grinding SD and BA (obs.) with the XRD pattern of the cocrystal SD·BA calculated from its crystal structure (calc.)

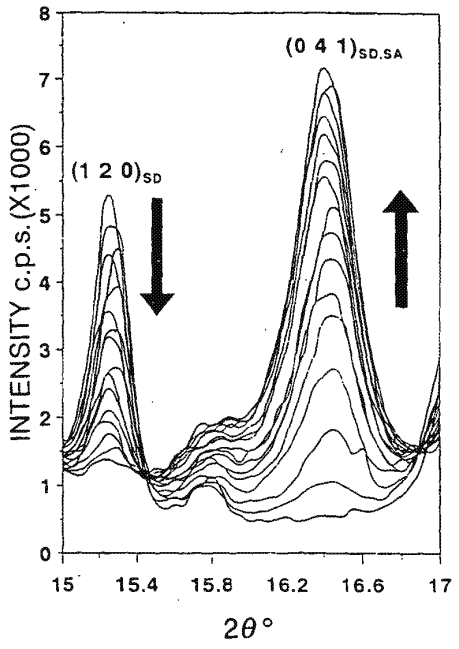


Fig. 3 Variation in peak intensities for reflections (1 2 0) of SD and (0 4 1) of the cocrystal SD·SA as co-grinding of SD and SA proceeded

Table 1 Melting points and N–H stretching frequencies for cocrystals SD·A (A = aromatic carboxylic acid)

A	Mp (°C)	N–H stretch/cm^{-1}
—	197	3436, 3337, 3236
BA	215	3464, 3375, 3259
AA	206	3490, 3463, 3371
SA	196	3475, 3381, 3256
AC	138	3487, 3398
PHA	180	3493, 3379
PCL	207	3469, 3376, 3256

was used to plot the extent of reaction (α) *versus* time curves shown in Fig. 4(*a*). Analysis of the latter curve yielded a fit of the data to the equation $-\ln(1-\alpha) = kt$ with k = 0.11 min^{-1}. The plot of $-\ln(1-\alpha)$ *versus* t is shown in Fig. 4(*b*). This first-order behaviour indicates that cocrystallization involves a

UM00013093
NOVARTIS EXHIBIT 1517
Novartis v. Regents, IPR2023-01347
Page 1839 of 4460

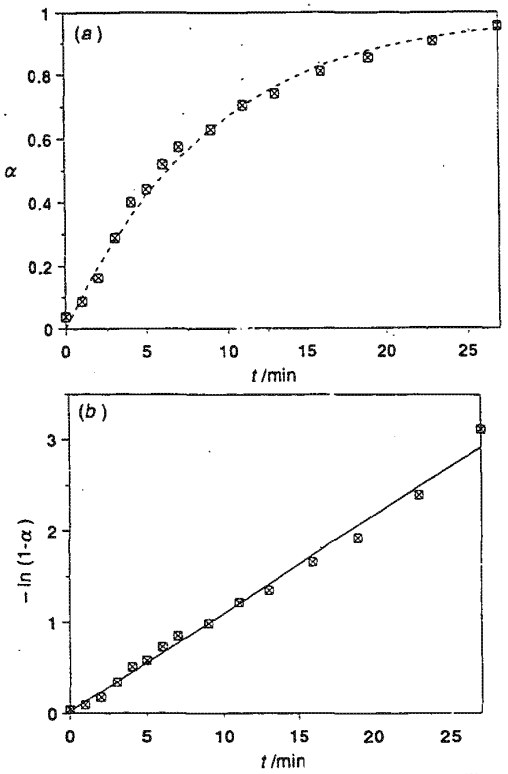


Fig. 4 (*a*) Extent of reaction (α) *versus* time for the cocrystallization of SD and SA in the solid state, experimental points are indicated by squares while dashed curve represents theoretical first-order behaviour; (*b*) plot of $-\ln(1-\alpha)$ *versus* time for the formation of cocrystal SD·SA

random nucleation mechanism.[14] Analogous results were obtained for the formation of the cocrystal SD·AA, with a rate constant $k = 0.08\ \text{min}^{-1}$.

Competition experiments

Competition experiments involved co-grinding equimolar ternary mixtures of SD and selected pairs of acids. The results of a typical experiment, in which SD was co-ground with SA and AA, are shown in Fig. 5. The XRD pattern of the product of co-grinding is dominated by peaks for the cocrystal SD·AA. It also contains peaks of low intensity representing the unreacted SA and traces of the phase SA·AA. (The existence of the latter cocrystal was proven by a separate experiment in which the acids SA and AA were co-ground. The XRD pattern of the product contained peaks not present in the patterns of either of the pure components.) The reaction occurring in the competition experiment can thus be represented by eqn. (1) with the product SD·AA predominating.

$$\text{SD} + \text{AA} + \text{SA} \longrightarrow \text{SD·AA} + \text{SA} + \text{SA·AA} \quad (1)$$

Analogous experiments using SD and the pairs AC and AA, BA and AA, were carried out and the major products of cocrystallization were similarly identified by XRD. The reactions occurring were confirmed as (2) and (3). In (2),

$$\text{SD} + \text{AC} + \text{AA} \longrightarrow \text{SD·AA} + \text{AC} \quad (2)$$

$$\text{SD} + \text{BA} + \text{AA} \longrightarrow \text{SD·AA} \quad (3)$$

exclusive formation of the cocrystal SD·AA was indicated. In

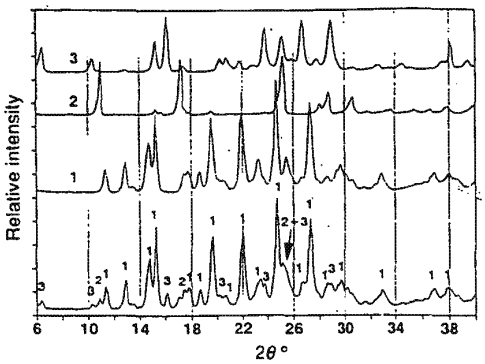


Fig. 5 XRD traces for interpretation of the competition reaction (1): (1) calculated from the crystal structure of SD·AA; (2) the acid SA; (3) the cocrystal SA·AA; (4) product of co-grinding SD, SA, and AA [reaction (1)]

peaks for unreacted BA were not observed. The presence of only one extraneous peak among those for SD·AA suggested that BA was converted into an essentially amorphous phase (possibly BA·AA).

A solid state substitution reaction

Noting the tendency for preferential formation of SD·AA in competition experiments, we carried out an experiment to test whether reaction of AA with a complex SD·A′ (A′ = an acid other than AA) might lead to formation of SD·AA, as this would represent an unusual instance of substitution in the solid state.

The cocrystal SD·SA and the pure acid AA in 1 : 1 molar ratio were co-ground for 3 min. The XRD pattern of the resulting material is shown in Fig. 6 where it is compared with the XRD pattern for the product obtained from the competition reaction (1). The identical nature of these patterns proves that the major product of co-grinding SD·SA and AA is SD·AA and that pure SA and the cocrystal SA·AA are also present in the final mixture. The substitution reaction we observed may therefore be represented by eqn. (4).

$$\text{SD·SA} + \text{AA} \longrightarrow \text{SD·AA} + \text{SA} + \text{SA·AA} \quad (4)$$

The displacement of SA from the cocrystal SD·SA and its replacement by AA in the solid state is remarkable and we are not aware of a previous account of such a process.

Similar co-grinding experiments with a mixture of SD·SA and BA did not, however, result in substitution of SA by BA and the success of reaction (4) appears to depend on the unusual stability of the cocrystal SD·AA.

Our experiments have demonstrated the ready formation of 1 : 1 cocrystals between SD and aromatic carboxylic acids in the solid state, as well as proving that the cocrystals thus formed have identical structures to their counterparts crystallizing from solutions containing the two components. The kinetic study shows that XRD is a useful method for following the course of solid state cocrystallization and that further experiments may give us more insight into the mechanism of solid state reactions of this type.

In attempting to explain the outcome of the competition reactions (1)–(3), we have considered the relative strengths of binding between the components of the cocrystals as reflected in their N···O intermolecular hydrogen bonded distances. In the case of reaction (2), where the cocrystals SD·SA and SD·AA are potential products, the relevant N···O distances for the hydrogen bonds N–H···O, O–H···N are respectively 2.784(4), 2.639(3) Å in SD·SA[8] and 2.838(2), 2.663(2) Å in SD·AA.[9] If stronger hydrogen bonds in the product were the

UM00013094
NOVARTIS EXHIBIT 1517
Novartis v. Regents, IPR2023-01347
Page 1840 of 4460

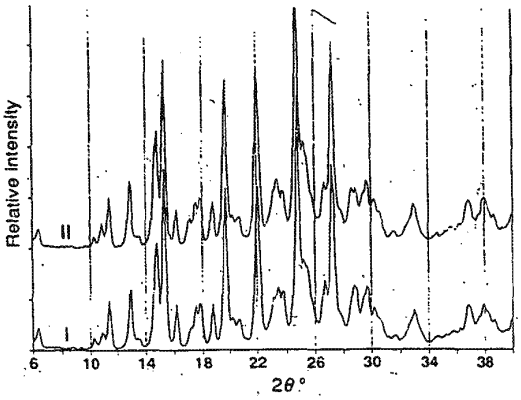


Fig. 6 XRD traces obtained by co-grinding (I) SD·SA and AA [reaction (4)], (II) SD, AA and SA [reaction (1)]

and stronger hydrogen bonds in SD·SA should favour its formation over SD·AA, whereas the reverse was observed. We have in fact indicated previously[10] that the intermolecular N · · · O hydrogen bond distances in this series of cocrystals vary significantly and, in the case of SD·PCL which crystallizes with two complex units in the asymmetric unit,[11] we have found significantly different N · · · O distances for chemically identical bonds in the two complex units. These observations clearly indicate that considerations of additional factors, *e.g.*, crystal packing and lattice energies, are also important in explaining the results of competition experiments. With regard to the preferred formation of SD·AA, the following qualitative explanation is offered. Cocrystal formation between SD and an acid A involves competition between homomeric aggregation (SD · · · SD, A · · · A) and heteromeric aggregation (SD · · · A). When two acids A and A′ are present, as in the competition reactions (1)–(3) above, weaker intermolecular attractive forces in crystals of, *e.g.*, A, compared with those in A′, should favour the formation of the cocrystal SD·A over SD·A′. In crystals of SA, AC and BA, the molecules aggregate in a manner typical of carboxylic acids, namely by formation of stable hydrogen bonded dimers with a graph set $R_2^2(8)$.[12] However, in crystals of AA, the situation differs.[15] The crystallographic asymmetric unit comprises two molecules, one neutral and the other a zwitterion. Consequently, stable hydrogen bonded dimers do not occur in the crystal and instead, the hydrogen bonding arrangement propagates unidirectionally in a helical pattern parallel to the polar axis of the crystal. We have confirmed that the sample of AA used in our experiments is the same polymorph as that described above and we conclude that the tendency for the cocrystal SD·AA to form preferentially in competition experiments (1)–(3) is probably due to the relative ease of de-aggregation of AA, owing to the absence of stable dimers, as compared with the other acids.

competition reactions in solution and computer modelling of the cocrystallization process, are needed for a deeper insight into the mechanisms involved.

We have found a plausible explanation for some of the results obtained here, but several questions require further investigation, *e.g.* the mechanism of the substitution reaction, which involves subtle processes between homomeric and heteromeric hydrogen bonded aggregates, quite distinct from those occurring between dissolved molecules. This complexity was underscored in a recent account of self-organization of nucleotide bases in the solid state by Etter *et al.*,[4] where the failure to explain certain observations relating to selectivity was attributed to our current lack of understanding of the intricate processes involved in cooperative hydrogen bonding arrangements and solid state phase transformations.

Acknowledgements

We thank the FRD (Pretoria) and the University of Cape Town for financial support.

References

1 J. Bernstein, M. C. Etter and L. Leiserowitz, in *Structure Correlation*, eds. H.-B. Bürgi and J. D. Dunitz, VCH Publishers, 1994, New York, vol. 2, p.431.
2 V. A. Russell, M. C. Etter and M. D. Ward, *Chem. Mater.*, 1994, **6**, 1210.
3 J. H. Loehlin, M. C. Etter, C. Gendreau and E. Cervasio, *Chem. Mater.*, 1994, **6**, 1218.
4 M. C. Etter, S. M. Reutzel and C. G. Choo, *J. Am. Chem. Soc.*, 1993, **115**, 4411.
5 M. C. Etter, *J. Phys. Chem.*, 1990, **95**, 4601.
6 M. C. Etter, Z. Urbańczyk-Lipkowska, M. Zia-Ebrahimi and T. W. Panunto, *J. Am. Chem. Soc.*, 1990, **112**, 8415.
7 M. C. Etter and D. A. Adsmond, *J. Chem. Soc., Chem. Commun.*, 1990, 589.
8 U. Patel, M. Haridas and T. P. Singh, *Acta Crystallogr., Sect. C*, 1988, **44**, 1264.
9 M. R. Caira, *J. Crystallogr. Spectrosc. Res.*, 1991, **21**, 641.
10 M. R. Caira, *J. Crystallogr. Spectrosc. Res.*, 1992, **22**, 193.
11 M. R. Caira, *J. Chem. Crystallogr.*, in preparation.
12 M. C. Etter, *Acc. Chem. Res.*, 1990, **23**, 120.
13 K. Yvon, W. Jeitschko and E. J. Parthé, *J. Appl. Crystallogr.*, 1977, **10**, 73.
14 M. E. Brown, *Introduction to Thermal Analysis–Techniques and Applications*, Chapman and Hall, London and New York, 1988.
15 C. J. Brown and M. Ehrenberg, *Acta Crystallogr., Sect. C*, 1985, **41**, 441.

Paper 5/04357C
Received 5*th July* 1995
Accepted 24*th August* 1995

UM00013095
NOVARTIS EXHIBIT 1517
Novartis v. Regents, IPR2023-01347
Page 1841 of 4460

This Page is Inserted by IFW Indexing and Scanning Operations and is not part of the Official Record

BEST AVAILABLE IMAGES

Defective images within this document are accurate representations of the original documents submitted by the applicant.

Defects in the images include but are not limited to the items checked:

- ☐ BLACK BORDERS
- ☐ IMAGE CUT OFF AT TOP, BOTTOM OR SIDES
- ☐ FADED TEXT OR DRAWING
- ☐ BLURRED OR ILLEGIBLE TEXT OR DRAWING
- ☐ SKEWED/SLANTED IMAGES
- ☐ COLOR OR BLACK AND WHITE PHOTOGRAPHS
- ☐ GRAY SCALE DOCUMENTS
- ☐ LINES OR MARKS ON ORIGINAL DOCUMENT
- ☐ REFERENCE(S) OR EXHIBIT(S) SUBMITTED ARE POOR QUALITY
- ☐ OTHER: _____

IMAGES ARE BEST AVAILABLE COPY.
As rescanning these documents will not correct the image problems checked, please do not report these problems to the IFW Image Problem Mailbox.

Journal of Chemical Crystallography, Vol. 28, No. 1, 1998

Structure of a 1:1 complex between the anthelmintic drug mebendazole and propionic acid

Mino R. Caira,[1]* Theo G. Dekker,[2] and Wilna Liebenberg[2]

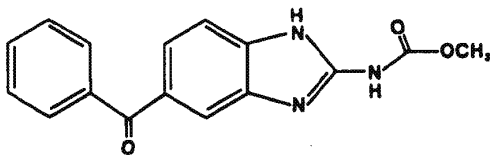
Received August 5, 1997

Recrystallization of the anthelmintic drug mebendazole from propionic acid yields a 1:1 molecular complex which crystallizes in the triclinic system space group $P\bar{1}$, a = 5.928(2), b = 11.066(2), c = 14.337(6)Å, α = 94.89(3), β = 101.56(3), γ = 96.18(2)°, and Z = 2 complex units in the unit cell. An x-ray diffraction study revealed an $R_2^2(8)$ hydrogen bonding system in the complex, involving the unprotonated imidazole N and amide N−H function of the drug and the acid carboxylic group. Complex molecules form centrosymmetric dimers by intermolecular N−H···O hydrogen bonding involving the protonated imidazole N atom and the benzoyl O atom of the drug molecule.

KEY WORDS: Mebendazole−propionic acid complex; molecular complex; crystal structure.

Introduction

Mebendazole, [(5-benzoyl-1H-benzimidazol-2-yl)-carbamic acid methyl ester, Fig. 1], is a broad spectrum anthelmintic drug producing high cure rates in infestations by Ascaris, threadworms, hookworms, and whipworms.[1] The drug is practically insoluble in water and a study of its polymorphism has led to the identification and characterisation of three polymorphic forms (A, B, C) displaying significantly different solubilities and therapeutic differences.[2,3] X-ray powder data are available for these polymorphs[2] but no single crystal structures have been reported.[4] The only documented crystal structure of a mebendazole species is that of its hydrobromide salt.[5]



Mebendazole

Fig. 1. Chemical structure of mebendazole.

In this paper, we report the preparation of a 1:1 molecular complex between mebendazole and propionic acid and its X-ray crystal structure. Since the drug molecule presents a variety of functional groups potentially capable of interacting with the carboxylic group of propionic acid, molecular complexation analogous to that which we have reported for sulfa drugs and carboxylic acids[6] was considered a distinct possibility. Alternatively, association between drug molecules could provide a clathrating environment for the propionic acid molecules. Enclathration of propionic acid molecules in zeolitic organic networks has recently been reported.[7]

Experimental

A solution of 50 mg of mebendazole (Cipla) in 8 cm^3 of propionic acid was stirred for 25 min at 56°C

[1] Department of Chemistry, University of Cape Town, Rondebosch 7701, South Africa.
[2] Research Institute for Industrial Pharmacy, Potchefstroom University for C.H.E., Potchefstroom 2531, South Africa.
* To whom correspondence should be addressed.

1074-1542/98/0100-0011$15.00/0 © 1998 Plenum Publishing Corporation

UM00013097
NOVARTIS EXHIBIT 1517
Novartis v. Regents, IPR2023-01347
Page 1843 of 4460

and left to crystallize at 20°C. Fine yellow needles which appeared initially were left to grow for 6 months to attain a size suitable for X-ray analysis.

Thermogravimetric analysis was performed with a Shimadzu TGA-50 instrument using a sample of mass 2.86 mg. The sample was placed in a platinum cell, heated at 10°C min^{-1} and purged with nitrogen gas flowing at 20 cm^3 min^{-1}.

Diffraction symmetry and preliminary cell data were determined from X-ray precession photographs and intensity data were collected diffractometrically. All data were corrected for Lorentz-polarization effects but not for absorption which was negligibly small for the specimen chosen. Intensity statistics confirmed centrosymmetry and the structure was solved in space group $P\bar{1}$ by direct methods.[8] All H atoms were located in difference electron density maps. Refinement with program SHELX76[9] proceeded routinely. All non-H-atoms were treated anisotropically. H atoms attached to carbons were included in idealized positions in a riding model with C−H 1.00Å. H atoms on N and O were allowed to refine subject to a distance constraint of 1.00Å from their parent atoms. Common variable isotropic thermal parameters were assigned to chemically distinct H atoms.

Table 1. Crystal data, details of data-collection and refinement

Compound	$C_{16}H_{13}N_3O_3 \cdot C_2H_5COOH$
Formula weight	369.38
Temperature	294(1)K
Crystal system	Triclinic
Space group	$P\bar{1}$
Unit cell dimensions (24 refls., θ 16–17°)	a = 5.928(2) Å, α = 94.89(3)° b = 11.066(2) Å, β = 101.56(3)° c = 14.337(6) Å, γ = 96.18(2)°
Volume	910.5(5) Å^3
Z	2
Density (calculated)	1.347 mg m^{-3}
Absorption coefficient	0.927 cm^{-1}
Diffractometer/scan	Enraf-Nonius CAD4/ω-2θ
Radiation/wavelength	MoKα (graphite monochrom.)/ 0.71069 Å
F(000)	388
Crystal size	0.19 × 0.19 × 0.38 mm
Data collection θ-range	1 to 25
Index ranges	$-7 \le h \le 7$, $-13 \le k \le 13$, $0 \le l \le 17$
Reflections collected	3325
Independent/ observed refls.	2884 (R_{int} = 0.057)/2165 [$I > 2\sigma(I)$]
Refinement method	Full-matrix least-squares on F
Data/restraints/ parameters	2884/2/261
Average Δ/σ	$<10^{-3}$
Goodness-of-fit on F	1.623
SHELX76 weights	$[\sigma^2(F_o) + 2.57 \times 10^{-3} F_o^2]^{-1}$
Final R indices	R = 0.068, wR = 0.073
Largest diff. peak, hole	0.15, −0.22.1 eÅ^{-3}

Table 2. Fractional atomic coordinates (×10^4) and equivalent isotropic thermal parameters (Å^2 × 10^3) with esd, s in parentheses

Atom	x/a	y/b	z/c	U_{eq}[a]
N(1)	3774(5)	1304(3)	2170(2)	46(1)
C(2)	5098(6)	1637(3)	3024(2)	41(1)
N(3)	4225(5)	1194(2)	3743(2)	43(1)
C(4)	523(6)	−177(3)	3705(2)	42(1)
C(5)	−1403(6)	−790(3)	3073(2)	41(1)
C(6)	−1709(6)	−716(3)	2086(2)	45(1)
C(7)	−96(6)	−22(3)	1714(2)	47(1)
C(8)	1852(6)	581(3)	2341(2)	41(1)
C(9)	2126(6)	504(3)	3319(2)	40(1)
C(10)	−3170(6)	−1513(3)	3482(3)	42(1)
O(11)	−3583(4)	−1142(2)	4250(2)	55(1)
C(12)	−4353(6)	−2723(3)	2982(2)	40(1)
C(13)	−6485(6)	−3174(3)	3146(3)	50(1)
C(14)	−7483(7)	−4347(4)	2766(3)	61(2)
C(15)	−6341(8)	−5071(4)	2239(4)	71(2)
C(16)	−4222(8)	−4625(4)	2070(3)	67(2)
C(17)	−3243(7)	−3447(3)	2431(3)	52(1)
N(18)	7189(5)	2362(3)	3151(2)	47(1)
C(19)	8626(6)	2736(3)	4014(3)	47(1)
O(20)	8270(5)	2499(3)	4777(2)	65(1)
O(21)	10512(4)	3402(2)	3884(2)	59(1)
C(22)	12226(7)	3872(4)	4734(3)	69(2)
C(23)	10003(10)	3167(6)	−238(4)	101(3)
C(24)	7634(9)	2511(5)	−334(3)	85(2)
C(25)	6959(7)	2338(4)	603(3)	55(1)
O(26)	8077(5)	2816(3)	1368(2)	66(1)
O(27)	5013(6)	1617(3)	512(2)	79(1)

[a] $U_{eq} = (1/3)\Sigma_i\Sigma_j U_{ij} a_i^* a_j^* a_i \cdot a_j$.

Table 1 lists data collection and refinement details. Fractional atomic coordinates and equivalent isotropic thermal parameters are listed in Table 2.

Results and discussion

Thermogravimetry indicated a one-step mass loss of 19.85% in the temperature range 100–150°C, confirming a 1:1 mebendazole-propionic acid complex (theoretical mass loss 20.05%).

The X-ray analysis revealed that the drug molecule is intimately associated with the propionic acid molecule by complementary hydrogen bonding to form

UM00013098
NOVARTIS EXHIBIT 1517
Novartis v. Regents, IPR2023-01347
Page 1844 of 4460

a 1:1 complex unit. The structure and atomic numbering of this unit are shown in Fig. 2,[10] which includes a centrosymmetrically related complex unit. Bond lengths and bond angles are listed in Table 3.

This is the first x-ray structure of a species containing the neutral mebendazole molecule. Bond lengths and bond angles for the drug molecule are in good agreement with chemically equivalent ones observed in the mebendazole HBr salt.[5] However, in the latter case, both N atoms of the imidazole ring are protonated and the distances N(1)–C(2) and C(2)–N(3) are the same (1.35(1), 1.33(1)Å) whereas in the title compound these C–N distances are significantly different (Table 3) and consistent with N(3) as the protonation site.

A least-squares (LS) plane calculation including all non-H-atoms of the benzimidazole moiety shows it to be planar to within 0.01Å. Table 4 lists selected torsion angles in the mebendazole molecule. For comparison, corresponding data for the hydrobromide salt[5] are included. For the unprotonated and protonated forms of mebendazole occurring in these respective compounds, significant differences are noted for torsion angles describing the orientation of substituents attached to C(2) and C(5). In particular, the torsion angle N(1)–C(2)–N(18)–C(19) is anti-periplanar in the complex but is periplanar in the HBr salt. In addi-

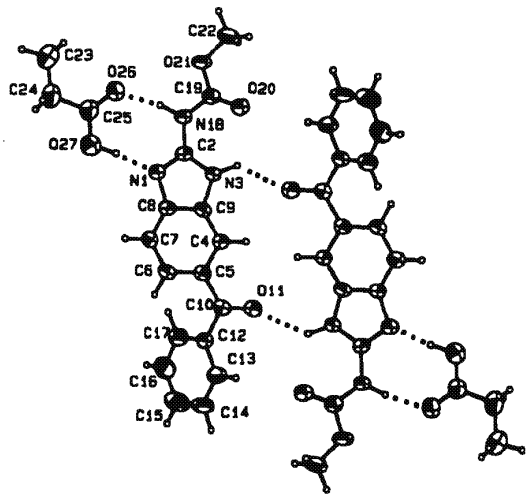


Fig. 2. Structure of the title complex showing the asymmetric unit (labeled atoms) and the centrosymetrically related complex unit. Thermal ellipsoids are drawn at the 50% probability level for non-H-atoms while H-atoms are drawn as spheres with arbitrary radii. Dotted lines represent hydrogen bonds.

Table 3. Bond lengths (Å) and bond angles (°)

N(1)–C(2)	1.314(4)
N(1)–C(8)	1.395(5)
C(2)–N(3)	1.348(5)
C(2)–N(18)	1.372(4)
N(3)–C(9)	1.383(4)
C(4)–C(5)	1.378(4)
C(4)–C(9)	1.379(5)
C(5)–C(6)	1.401(4)
C(5)–C(10)	1.492(5)
C(6)–C(7)	1.380(5)
C(7)–C(8)	1.380(4)
C(8)–C(9)	1.391(4)
C(10)–O(11)	1.222(5)
C(10)–C(12)	1.494(4)
C(12)–C(13)	1.380(5)
C(12)–C(17)	1.383(6)
C(13)–C(14)	1.384(5)
C(14)–C(15)	1.375(7)
C(15)–C(16)	1.374(7)
C(16)–C(17)	1.381(5)
N(18)–C(19)	1.358(5)
C(19)–O(20)	1.198(5)
C(19)–O(21)	1.326(4)
O(21)–C(22)	1.439(4)
C(23)–C(24)	1.484(8)
C(24)–C(25)	1.498(7)
C(25)–O(26)	1.208(5)
C(25)–O(27)	1.307(5)
C(2)–N(1)–C(8)	104.5(3)
N(1)–C(2)–N(18)	121.9(3)
N(1)–C(2)–N(3)	114.0(3)
N(3)–C(2)–N(18)	124.1(3)
C(2)–N(3)–C(9)	106.2(3)
C(5)–C(4)–C(9)	117.0(3)
C(4)–C(5)–C(10)	117.5(3)
C(4)–C(5)–C(6)	121.2(3)
C(6)–C(5)–C(10)	121.4(3)
C(5)–C(6)–C(7)	121.1(3)
C(6)–C(7)–C(8)	118.1(3)
N(1)–C(8)–C(7)	130.6(3)
C(7)–C(8)–C(9)	120.1(3)
N(1)–C(8)–C(9)	109.3(3)
C(4)–C(9)–C(8)	122.6(3)
N(3)–C(9)–C(8)	106.0(3)
N(3)–C(9)–C(4)	131.5(3)
C(5)–C(10)–C(12)	120.3(3)
C(5)–C(10)–O(11)	120.1(3)
O(11)–C(10)–C(12)	119.6(4)
C(10)–C(12)–C(17)	120.8(4)
C(10)–C(12)–C(13)	119.5(3)
C(13)–C(12)–C(17)	119.5(3)
C(12)–C(13)–C(14)	119.9(4)
C(13)–C(14)–C(15)	120.2(4)
C(14)–C(15)–C(16)	120.1(4)
C(15)–C(16)–C(17)	119.8(5)
C(12)–C(17)–C(16)	120.4(4)
C(2)–N(18)–C(19)	124.5(3)
N(18)–C(19)–O(21)	109.1(4)
N(18)–C(19)–O(20)	125.9(4)
O(20)–C(19)–O(21)	125.0(4)
C(19)–O(21)–C(22)	116.3(3)
C(23)–C(24)–C(25)	114.0(4)
C(24)–C(25)–O(27)	113.2(4)
C(24)–C(25)–O(26)	124.0(4)
O(26)–C(25)–O(27)	122.8(4)

UM00013099
NOVARTIS EXHIBIT 1517
Novartis v. Regents, IPR2023-01347
Page 1845 of 4460

Table 4. Comparison of selected torsion angles (°) in the title complex and in the HBr salt of mebendazole

	Title complex	HBr salt[a]
N(1)–C(2)–N(18)–C(19)	179.9(4)	−5(3)
C(4)–C(5)–C(10)–O(11)	35.7(5)	−171(1)
C(4)–C(5)–C(10)–C(12)	−141.1(4)	−4(2)
C(5)–C(10)–C(12)–C(17)	29.4(5)	63(2)
O(11)–C(10)–C(12)–C(13)	26.3(6)	48(2)
C(2)–N(18)–C(19)–O(20)	−0.7(7)	7(3)
C(2)–N(18)–C(19)–O(21)	178.8(3)	178(2)
N(18)–C(19)–O(21)–C(22)	−180.0(3)	179(2)
O(20)–C(19)–O(21)–C(22)	−0.5(6)	−12(3)

[a] Calculated from coordinate data in Ref. 5.

tion, torsion angle C(4)–C(5)–C(10)–O(11), which measures the extent of rotation of O(11) out of the benzimidazole plane, is synclinal in the complex and anti-periplanar in the HBr salt.

Figure 2 shows that unprotonated atom N(1) acts as an acceptor of a hydrogen bond from the −OH function of the propionic acid molecule and N(18) is a donor in a hydrogen bond to the carbonyl O atom of the acid, these bonds resulting in the formation of a stable ring with a graph-set description[11] $R_2^2(8)$. The latter indicates an eight-membered ring motif in which there are two hydrogen bond donors and two hydrogen bond acceptors. The six nonhydrogen atoms included in the $R_2^2(8)$ system are coplanar to within 0.08Å. The propionic acid molecule adopts an extended conformation with torsion angle C(23)–C(24)–C(25)–O(27) −171.1(4)° and is thus practically coplanar with the bulk of the mebendazole molecule.

Table 5 lists hydrogen bond data. The N···O, H···O, and N···H distances for these bonds indicate strong intermolecular association and compare favorably with corresponding distances which we reported for stable 1:1 complexes between the sulfa drug sulfadimidine and various aromatic carboxylic acids, in all of which analogous $R_2^2(8)$ hydrogen bonding motifs occur.[6]

Table 5. Hydrogen bond data for the title complex

D–H···A	D···A (Å)	H···A (Å)	D–H···A (°)
N(18)–H(18)···O(26)	2.786(4)	1.80(3)	170(4)
O(27)–H(27)···N(1)	2.664(5)	1.70(5)	161(6)
N(3)–H(3)···O(11)^{i}	2.982(4)	2.20(1)	133(1)

(i) = $-x, -y, 1-z$

Figure 2 also shows the association of complex molecules into centrosymmetric dimers. The dimers are maintained by two identical intermolecular N–H···O hydrogen bonds which involve the protonated imidazole atom N(3) and the benzoyl oxygen atom O(11) (Table 5). The motif thus generated is described in graph set notation[11] as $R_2^2(14)$.

The bulk of each dimer unit forms a plane, the phenyl ring substituents attached to C(10) making a dihedral angle of approximately 60° with the former plane. The space group requires the molecular planes to be parallel and they are all found to lie on the (−1 3 0) crystal planes, whose intensity is consequently higher than that of any other reflection. Since complex formation and dimerisation utilize virtually all donor and acceptor functions, only weaker van der Waals forces and C–H···O hydrogen bonds maintain the crystal structure.

Recrystallization of an organic substance from propionic acid can result either in crystallization of the pure substance as a polymorph or inclusion of the acid in the product. In the latter case, possible modes of incorporation of the acid include molecular complexation, as found here and elsewhere,[12] or clathration of the acid either as monomers[7] or as hydrogen bonded dimers in a framework provided by the host substance.[13] Our results indicate that the heterogeneous interactions observed between drug and acid molecules in the title complex are more favorable than homogeneous interactions which could instead lead to clathrate formation.

Acknowledgments

We thank the Foundation for Research Development (Pretoria), the University of Cape Town, and the University of Potchefstroom and Adcock Ingram Limited for financial assistance.

Supplementary Material. Crystallographic data (excluding structure factors) for the structures reported in this paper have been deposited with the Cambridge Crystallographic Data Centre as supplementary publication no. CCDC-1003/5265. Copies of available material can be obtained, free of charge, on application to the CCDC, 12 Union Road, Cambridge CB2 1EZ, UK, (fax: +44-(0)1223-336033 or e-mail: deposit@ccdc.cam.ac.uk.)

UM00013100
NOVARTIS EXHIBIT 1517
Novartis v. Regents, IPR2023-01347
Page 1846 of 4460

References

1. Al-Badr, A.A.; Tariq, M. In *Analytical Profiles of Drug Substances*, Florey, K., Ed.; Academic Press, New York, 1987, Vol. 16, p 291.
2. Himmelreich, M.; Rawson, B.J.; Watson, T.R. *Austral. J. Pharm. Sci.* **1977**, *6*, 123.
3. Rodrigues-Caabeiro, F.; Criado-Fornelio, A.; Jiminez-Gonzalez, A.; Guzman, L.; Igual, A.; Perez, A.; Pujol, M. *Chemotherapy* **1987**, *33*, 266.
4. Cambridge Structural Database and Cambridge Structural Database System, (Version 5.11), Cambridge Crystallographic Data Centre, University Chemical Laboratory, Cambridge, England, April 1996.
5. Blaton, N.M.; Peeters, O.M.; De Ranter, C.J. *Cryst. Struct. Comm.* **1980**, *9*, 181.
6. Caira, M.R.; Nassimbeni, L.R.; Wildervanck, A.F. *J. Chem. Soc. Perkin Trans.* **1995**, *2*, 2213.
7. Wang, X.; Simard, M.; Wuest, J.D. *J. Am. Chem. Soc.* **1994**, 12119.
8. Sheldrick, G.M. *Acta Crystallogr.* **1990**, *A46*, 467.
9. Sheldrick, G.M. *SHELX76. A System of computer programs for X-ray structure determination*; England, University of Cambridge, 1976.
10. Zolnai, L. *Zortep*: Programme for plotting molecular structures with thermal ellipsoids, University of Heidelberg: Germany, unpublished.
11. Etter, M.C. *Acc. Chem. Res.* **1990**, *23*, 120.
12. Simard, M.; Su, D.; Wuest, J.D. *J. Am. Chem. Soc.* **1991**, *113*, 4696.
13. Csöregh, I.; Czugler, M.; Weber, E.; Ahrendt, J. *J. Incl. Phenom.* **1990**, *8*, 309.

UM00013101
NOVARTIS EXHIBIT 1517
Novartis v. Regents, IPR2023-01347
Page 1847 of 4460

Hydrogen bonding interaction of diphenylbarbituric acid and 9-ethyladenine. Crystal structure of a 1:1 complex

Arthur Camerman, Donald Mastropaolo, Andrew Hempel, and Norman Camerman

Abstract: There are several different types of adenosine receptors found in the brain and molecules capable of interacting with the adenine ring system may have an effect on brain activity. Phenobarbital and diphenylhydantoin, two commonly used antiepileptic drugs have been shown to form hydrogen bonded complexes with adenine derivatives. Although 5,5-diphenylbarbituric acid has anticonvulsant properties equivalent to phenobarbital, neither its structure nor possible interactions with adenine have been investigated. 5,5-Diphenylbarbituric acid and 9-ethyladenine were, therefore, cocrystallized and the three-dimensional 1:1 hydrogen bonded complex was determined by X-ray diffraction. The crystals are monoclinic, *C2/c*, a = 28.457(9), b = 10.633(3), c = 13.995(4) Å, β = 100.20(2)°, Z = 8, R = 0.067 for 1680 reflections with $I > 3\sigma(I)$. The molecules propagate along the b crystallographic axis in an alternating fashion in which adjacent adenine and barbiturate molecules interact through a pair of hydrogen bonds. Two-fold symmetry related barbiturate carbonyl groups in neighboring planes of hydrogen bonded ribbons are involved in dipole–dipole attractive interactions. This hydrogen bonding pattern is compared to patterns found in other barbiturate–adenine complexes.

Key words: hydrogen bonding, crystal structure, barbiturates, adenine, anticonvulsants.

Résumé : On connaît plusieurs types différents de récepteurs de l'adénosine et de molécules capables d'interagir avec le système cyclique de l'adénine qui peuvent avoir un effet sur l'activité cérébrale. On a démontré que deux médicaments fréquemment utilisés contre l'épilepsie, le phénobarbital et la diphénylhydantoïne, forment des complexes avec les dérivés de l'adénine par le biais de liaisons hydrogènes. Même si l'acide 5,5-diphénylbarbiturique possède des propriétés anticonvulsantes équivalentes à celles du phénobarbital, aucune étude n'a été faite sur sa structure ou sur ses interactions possibles avec l'adénine. On a donc cocristallisé de l'acide 5,5-diphénylbarbiturique et de la 9-éthyladénine et, faisant appel à la diffraction des rayons X, on a déterminé la nature tridimensionnelle du complexe 1:1 lié par liaisons hydrogènes. Les cristaux sont monocliniques, groupe d'espace *C2/c*, avec a = 28,457(9), b = 10633(3) et c = 13,995(4) Å, β = 100,20(2)°, Z = 8, R = 0,067 pour 1680 réflexions avec $I > 3\sigma(I)$. Les molécules se propagent le long de l'axe cristallographique d'une façon alternée dans laquelle les molécules adjacentes d'adénine et de barbiturate interagissent par le biais d'une paire de liaisons hydrogènes. La symétrie binaire apparentée aux groupes carbonyles du barbiturate de plans voisins des rubans de liaisons hydrogènes est impliquée dans les interactions d'attraction dipôle–dipôle. Ce patron de liaison hydrogène se compare à ceux retrouvés dans d'autres complexes barbiturate–adénine.

Mots clés : liaison hydrogène, structure cristalline, barbiturates, adénine, anticonvulsant.

[Traduit par la Rédaction]

Introduction

5,5-Diphenylbarbituric acid (DPB) is chemically very similar to diphenylhydantoin (DPH) and phenobarbital (PB), two of the drugs most widely used for the control of epileptic seizures. All three compounds possess two hydrophobic (phenyl, ethyl) groups attached to the tetrahedral carbon of a heterocyclic ring which contains at least two hydrogen bond acceptor atoms (see Fig. 1). Placement of these atoms with respect to each other in three-dimensional space is considered an important stereochemical factor in determining anticonvulsant activity (1). Despite its similarities with DPH and PB, early pharmacological studies of DPB (2–4) reported only weak anticonvulsant activity and dismissed DPB as a potentially new agent for the treatment of epilepsy. However, more than 25 years later another study (5) compared the anticonvulsant activity of DPB, DPH, and PB in the mouse by gavage administration of the drugs in conjunction with two standard laboratory tests most commonly used for the measurement of anticonvulsant efficacy, pentylenetetrazol (PTZ), and maximal electroshock (MES) induced seizures. The results showed that DPB when administered

Received April 3, 2000. Published on the NRC Research Press website on July 28, 2000.

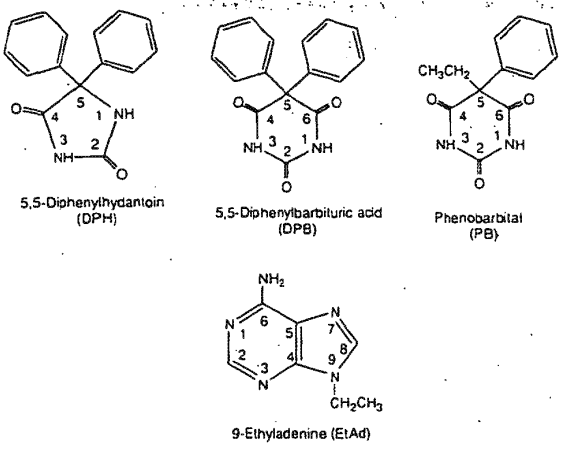
A. Camerman[1] **and D. Mastropaolo.** ARDONO Research, 8515-C 35th Ave. N.E., Seattle, WA 98115, U.S.A.
A. Hempel and N. Camerman. Biochemistry Department, University of Toronto, Toronto, ON M5S 1A8, Canada.

[1]Author to whom correspondence may be addressed. Telephone (206) 529-9421. e-mail: ardonoresearch@hotmail.com

© 2000 NRC Canada

UM00013102
NOVARTIS EXHIBIT 1517
Novartis v. Regents, IPR2023-01347
Page 1848 of 4460

Fig. 1. Chemical drawings and numbering scheme of the heterocyclic rings of 5-5-diphenylhydantoin, 5,5-diphenylbarbituric acid, phenobarbital, and 9-ethyladenine.



by gavage has anticonvulsant properties comparable to PB. Experiments with intraperitoneally administered DPB also concluded that poor solubility of DPB in the gastrointestinal lumen was a major factor in limiting potency. These results suggest that solubility problems were most likely responsible for the weak anticonvulsant activity reported for DBP in the early trials.

At present the mechanisms of action of the antiepileptic drugs PB and DPH are not completely understood. Although the inhibition of membrane sodium channels has been shown to be a basic action of DPH (6) there is no single action of DPH that can account for all its effects on both neuronal and nonneuronal tissue. Other mechanisms of action could include regulation and inhibition of voltage-dependent neurotransmitter release at synapses and regulation of calmodulin and cyclic nucleotide second messenger systems (7). PB shows similar but less potent effects on Na^+ channels and also interacts with GABA-mediated receptors (8). Early on, the similarity of barbiturates to uracil was recognized and prompted several investigations into whether and how barbiturates and similar drugs might associate with adenine in an attempt to explain their pharmacological effects. Such studies have observed selective hydrogen bond interactions between barbiturates and adenine derivatives (9–14) and between substituted hydantoins and 9-ethyladenine (EtAd) (15, 16) in the solid state and in solution. As yet it is still unclear whether these specific hydrogen bond interactions can be correlated with any pharmacologic activity. However, these interactions have gained added significance with the more recent discovery of adenosine receptors in brain membranes (17) and the evidence of the anticonvulsant action of endogenous adenosine (18, 19). Thus it has been suggested that modification or modulation of this purinergic system might also provide a basis for a possible antiepileptic drug mechanism. For example, barbiturates and benzodiazepines have been shown (20, 21) to inhibit adenosine uptake in rodent brain synaptosomes which results in elevated synaptic adenosine levels. Similarly, DPH has been shown to inhibit adenosine uptake in rat cerebral cortical neurons (22). These increased levels of adenosine could be correlated with some of the depressant effects these compounds have on neuronal tissue. The complementarity that DPH and PB have shown to the purine ring system through hydrogen-bond formation might well be an indicator of their ability to effect changes in the purinergic system that has been postulated to be linked to antiepileptic drug action.

In light of the role adenosine may play in regulation of seizure activity, the more recent results showing DPB to be a better anticonvulsant than previously thought and the fact that DPH and PB form hydrogen-bonded complexes with adenine derivatives, we decided to investigate DPB's three-dimensional structure and its hydrogen bonding capabilities with adenine molecules. We successfully cocrystallized DPB and EtAd with the aim of elucidating the structure of the intermolecular complex which can then be compared to the structures of adenine complexes with DPH, with PB, and with other barbiturates. In addition, DPB's three-dimensional stereochemistry obtained from the crystal structure determination can be used for comparisons with known structures of the other anticonvulsants. Such information may prove helpful in understanding some modes of action of this important class of drugs.

Experimental

Equimolar amounts of DPB and EtAd were dissolved in a 50:50 acetone–water mixture. Slow solvent evaporation yielded colorless, thin, plate-like crystals. Weissenberg photographic methods revealed the monoclinic space group *C2/c* which was confirmed by structural analysis.

The crystal data including data collection and refinement parameters are summarized in Table 1. The data were corrected for Lorentz and polarization factors; no absorption correction was applied.

MULTAN 80 (23) was used to solve the structure. An E-map calculated with the phases from the solution with the best combined figure of merit revealed all 33 non-hydrogen atoms of the asymmetric unit. Hydrogen atoms were located from subsequent difference Fourier electron density maps and their positional parameters were refined along with nonhydrogen positional and anisotropic temperature factors. Hydrogen atoms were given fixed isotropic temperature factors equal to $B = 3.6$ Å^2. The refinement converged to a final residual of $R = 0.067$. The program used in the refinement was from the XRAY76 System (24). Table 2 lists the atom fractional coordinates.[2]

[2] Anisotropic temperature factors, hydrogen atom coordinates, interatomic distances, and angles and equations of selected least-square planes have been deposited as supplementary material and may by purchased from: The Depository of Unpublished Data, Document Delivery, CISTI, National Research Council Canada, Ottawa, Ontario, Canada, K1A 0S2. Crystallographic data for the structure(s) reported in this paper have been deposited with the Cambridge Crystallographic Data Centre (CDCC). Copies of the data can be obtained, free of charge on application to : The Director, Cambridge Crystallographic Data Centre, 12 Union Road, Cambridge, CB2 1EZ, U.K. (Fax: 44 1223 336033 or e-mail: deposit@ccdc.cam.ac.uk).

© 2000 NRC Canada

UM00013103
NOVARTIS EXHIBIT 1517
Novartis v. Regents, IPR2023-01347
Page 1849 of 4460

Table 1. Crystal data, data collection parameters, solution and refinement.

Crystal data	
Chemical formula	$(C_{16}H_{12}N_2O_3)\bullet(C_7H_9N_5)$
Molecular weight	443.47
Crystal system	Monoclinic
Space group	*C2/c*
a (Å)	28.457(9)
b (Å)	10.633(3)
c (Å)	13.995(4)
β (°)	100.20(2)
V (Å^3)	4168(1)
Z	8
Dx(g cm^{-3})	1.368
No. of reflections for cell measurements	15
Range of cell parameters	$45 < \theta < 65$
Absorption μ (cm^{-1})	7.85
Temperature (K)	295
Crystal shape	plate
Crystal size (mm)	0.46 × 0.18 × 0.11
Crystal color	clear
Data collection	
Diffractometer	Picker FACS I
Radiation	Cu Kα
Wavelength (Å)	1.5418
Scan type	ω/2θ
θmax	65
Range of *h*, *k*, *l*	0→30
	0→12
	−16→16
No. of measured reflections	3510
No. of independent reflections	3510
No. of observed reflections	1680, $I > 3\sigma(I)$
No. of standard reflections	3 every 200 reflections
Intensity variation (%)	< 5
Data Reduction	
Corrections	Lorentz and polarization corrections
Solution and Refinement	
Solution	Direct methods (23)
Refinement	full-matrix refinement (24)
Atomic scattering	XRAY76
No. parameters used	361
Treatment of hydrogens	positions refined with fixed isotropic factors
R	0.067
wR	0.074
S	1.85
Weighting	$1/\sigma^2(Fo)$
Δ/σ_{max}	0.316
$\Delta\rho_{max}$ (e Å^{-3})	0.223
$\Delta\rho_{min}$ (e Å^{-3})	−0.317

Results and discussion

The crystal asymmetric unit contains one molecule of DPB and one molecule of EtAd. The adenine and barbiturate molecules are highly planar. The standard deviation of the nine atoms of the purine group from the least-squares plane defined by these atoms is 0.02 Å with the amino nitrogen situated only 0.01 Å from this plane. The standard deviation of the barbiturate atoms N(1), C(2), N(3), C(4), and C(6) from their least-squares plane is 0.05 Å with atoms O(4), C(5), and O(6) exhibiting the maximum deviations of −0.11, 0.06, and 0.09 Å, respectively. The phenyl groups are planar to within 0.01 Å. Bond distances and angles for DPB and EtAd are all within the normal range and are typical of barbiturate and adenine derivatives.

The pyrimidine ring of DPB is decidedly more planar than those of other barbiturates in which one of the C(5) substituents is a phenyl ring (11, 25 and refs. therein). Those

UM00013104
NOVARTIS EXHIBIT 1517
Novartis v. Regents, IPR2023-01347
Page 1850 of 4460

Table 2. Atomic coordinates ($\times 10^4$) and equivalent isotropic displacement parameters ($Å^2 \times 10^3$).

Atom	X	Y	Z	U_{eq}[a]
AN(1)	4808(2)	7104(5)	1232(4)	35(1)
AC(2)	5246(2)	6848(7)	1059(6)	43(1)
AN(3)	5594(2)	7637(5)	950(4)	38(1)
AC(4)	5454(2)	8832(6)	1066(5)	30(1)
AC(5)	5015(2)	9241(6)	1227(5)	30(1)
AC(6)	4682(2)	8318(6)	1319(5)	36(1)
AN(7)	5009(2)	10545(5)	1292(4)	33(1)
AC(8)	5441(3)	10866(6)	1175(6)	40(1)
AN(9)	5729(2)	9893(5)	1035(4)	34(1)
AN(6)	4237(2)	8562(6)	1475(5)	44(1)
AC(10)	6232(3)	9891(8)	921(7)	46(1)
AC(11)	6552(3)	9375(9)	1792(7)	51(1)
BN(1)	4390(2)	2614(5)	1505(4)	37(1)
BC(2)	4622(2)	3749(6)	1452(5)	30(1)
BO(2)	5033(2)	3792(4)	1327(4)	47(1)
BN(3)	4360(2)	4808(5)	1547(4)	35(1)
BC(4)	3914(2)	4856(6)	1755(4)	29(1)
BO(4)	3732(1)	5863(4)	1907(3)	39(1)
BC(5)	3627(2)	3631(6)	1704(4)	29(1)
BC(6)	3924(2)	2445(6)	1568(4)	28(1)
BO(6)	3752(2)	1391(4)	1530(3)	40(1)
BC(7)	3237(2)	3800(6)	804(5)	32(1)
BC(8)	3320(3)	3441(7)	−106(6)	40(1)
BC(9)	2987(3)	3696(8)	−928(6)	54(1)
BC(10)	2569(3)	4302(7)	−852(7)	54(1)
BC(11)	2483(3)	4662(8)	38(7)	52(1)
BC(12)	2813(2)	4432(7)	863(6)	41(1)
BC(13)	3453(2)	3416(6)	2672(5)	32(1)
BC(14)	3025(2)	2820(7)	2723(6)	38(1)
BC(15)	2899(3)	2578(7)	3615(6)	48(1)
BC(16)	3192(3)	2898(8)	4461(7)	57(1)
BC(17)	3628(3)	3452(7)	4426(6)	50(1)
BC(18)	3755(2)	3726(7)	3535(6)	42(1)

Note. Prefixes A and B refer to EtAd and DPB, respectively.
[a] $U_{eq} = (1/3)\Sigma_i\Sigma_j U_{ij} a_i^* a_j^* a_i a_j$.

structures contain pyrimidine rings described as enveloped-shaped with C(5) 0.30–0.43 Å out of the plane in the direction of the phenyl group and atoms O(4) and O(6) displaced by more than 0.10 Å from the plane in the direction away from the phenyl group. It is not known whether the more planar conformation of the barbiturate ring observed in the crystal structure of DPB is a chemical effect related to the presence of two phenyl rings attached to C(5) or is a consequence of the crystal packing forces. It should be pointed out that others (26) have found no correlation between the chemical nature of the C(5) substituent and the extent of barbiturate ring puckering. Furthermore, the variation in barbiturate ring puckering reported in crystal structures all containing 5,5-diethylbarbituric acid (12, 27–30) indicates that the puckering in the solid state is dominated by crystal packing forces. Other than these small differences in the barbiturate ring planarity, DPB and PB are very similar in overall structural geometry and stereochemistry. In the reported three-dimensional structures of DPH (16,31) the hydantoin rings are planar to within experimental error.

DPB and EtAd form a 1:1 complex organized into infinite ribbons of alternating adenine and barbiturate residues in which adjacent adenine and barbiturate molecules interact through pairs of hydrogen bonds. The dihedral angle between the adenine and barbiturate planes is only 1.2°. DPB donates its N(1) hydrogen to N(7) of EtAd and the DPB carbonyl oxygen O(6) accepts a hydrogen from the EtAd amino group forming a Hoogsteen type pair of hydrogen bonds. The second pair of hydrogen bonds is of the Watson–Crick type and involves the N(3) hydrogen and O(4) carbonyl of DPB with N(1) and the other amino hydrogen of EtAd. The hydrogen bonding scheme is illustrated in Fig. 2 and Table 3 gives the hydrogen bonding geometry. The basic structural pattern is very similar to those of the crystalline complexes EtAd–5-isopropyl-5-bromoallylbarbiturate (I) (11) and EtAd–5,5-diethylbarbituric acid (II) (12). Figure 3 (Top) is a schematic drawing which summarizes the hydrogen bonding features of I, II, and the current structure. A unique feature of these structures is the positioning of two symmetry related barbiturate carbonyl groups, C(2)-O(2), which lie in neighboring planes of the hydrogen bonded ribbons with their bond vectors pointing in opposite directions as is shown in Fig. 2. The C(2)— O(2)′ intermolecular contact of 3.090(9) Å found in the present study is shorter than the same contact found in I (3.165(20) Å) and longer than that found in II (2.983(4) Å). Such an arrangement of carbonyl groups has also been observed in crystal structures of hydrated barbiturate derivatives (25). These noncovalent contacts which are less than or approximately equal to the normal van der Waals distance of 3.1 Å appear to be due to an attractive dipole–dipole interaction. The differences in the contact distances observed in these structures are most likely due to crystal packing requirements of the different sized barbiturate C(5) substituents which fill the spaces between the planar hydrogen-bonded layers. One other significant difference between the current structure and structures I and II is the dihedral angle between the hydrogen-bonded barbiturate and adenine ring planes. In I and II this angle is 10.5 and 10.2° respectively compared with just 1.2° found for the DPB–EtAd structure.

In all three structures the carbonyl oxygens adjacent to the C(5) atom of the barbiturates form extremely weak hydrogen bonds and the N(3) of EtAd and O(2) of the barbiturates are not involved in any hydrogen bonds. As previously suggested (11), the long contacts involving the adenine N(6) hydrogens and barbiturate O(4) and O(6) carbonyls might be explained by geometrical constraints placed on the molecular arrangement due to translational symmetry which propagates the 1:1 complex and forms the infinite hydrogen-bonded ribbon. Since there is one independent molecule of EtAd and one of DPB, any change in the contact on one side of N(6) will effect a change in the opposite direction on the other side. The observed distances are thus a result of a compromise between crystal packing symmetry and hydrogen bond forces. As we will see below, when there is a greater degree of freedom with two crystallographically independent molecules involved in forming the adenine–barbiturate hydrogen bonded pair, the N(6)—carbonyl oxygen hydrogen bond distances are less than 3.2 Å and in the more normal range. In structures I and II there was some speculation about hydrogen bond formation between adenine C2

UM00013105
NOVARTIS EXHIBIT 1517
Novartis v. Regents, IPR2023-01347
Page 1851 of 4460

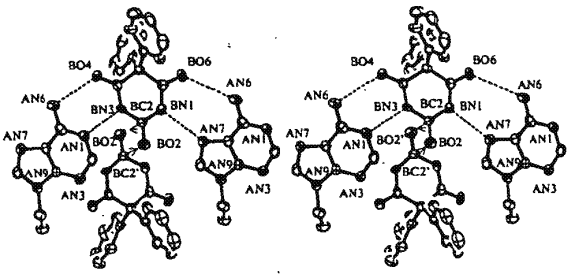
Table 3. Hydrogen bond distances (Å) and angles (°)

	H···O (or N)[a]	N···O (or N)[a]	< N-H···O (or N) >[a]
BN(1)-H···AN(7)	2.03(7)	2.867(8)	170(6)
	1.89(3)	2.827(3)	171(3)
BN(3)-H···AN(1)	2.00(6)	2.825(8)	175(6)
	1.91(4)	2.832(3)	176(3)
AN(6)-H(1)···BO(6)	2.45(7)	3.316(6)	169(5)
	2.47(4)	3.387(4)	176(3)
AN(6)-H(2)···BO(4)	2.51(7)	3.312(7)	158(6)
	2.35(4)	3.218(4)	172(3)

Note. The prefixes A and B refer to EtAd and DPB, respectively.

[a]The second row of numbers per hydrogen bond are equivalent parameters reported in the 9-ethyladenine-5,5-diethylbarbituric acid 1:1 complex referred to as Structure II in the text.

Fig. 2. Stereoscopic drawing showing hydrogen bonding and bond–dipole interactions in the 1:1 EtAd–DPB crystal. Hydrogen bonds are represented by dashed lines and the C(2)—O(2) dipole interaction is indicated by arrows. Hydrogen atoms have been omitted for clarity.



and C8 hydrogens with the barbiturate O2. In the DPB–EtAd complex we find these C—O distances to be 3.34 Å with the C-H-O(2) angles less than 140° suggesting only normal van der Waals contacts. In I the adenine C8 and C2 distances to the barbiturate O2 are 3.28 and 3.31 Å, respectively which also indicate relatively weak interactions. In II the adenine C8 and barbiturate O2 distance is 3.18 Å indicating a stronger hydrogen bond-like interaction but the C-H-O(2) angle is only 129°. The adenine C2—barbiturate O2 distance of 3.37 Å found in II is more typical of a normal van der Waals contact.

In the structures of the complexes 8-bromo-9-ethyladenine–phenobarbital (III) (10) and 8-bromo-9-ethyladenine–5-allyl-5-isobutylbarbituric acid (IV) (13) a different hydrogen bonding scheme is found with no evidence of carbonyl dipole interactions (see Fig. 3 (Bottom)). In III and IV the barbiturate molecules form separate Watson–Crick-type hydrogen-bonded pairs with each of two crystallographically independent adenine derivatives utilizing the barbiturate hydrogen bond donors N(1) and N(3) and acceptors O(2) and O(4). In structure IV there is a second barbiturate molecule which hydrogen bonds to two independent adenine derivatives as depicted in Fig. 3. Also in IV there is no hydrogen-bonded dimer formed between the second of the two independent adenine molecules.

It should be pointed out that structure III is the only 2:1 adenine to barbiturate complex observed which might account for its different hydrogen bonding pattern. However the major factor in determining the two different hydrogen bonding schemes shown in Fig. 3 is the presence of the 8-bromo-substituent on the adenine molecules in the III and IV structures. This bulky substituent prevents the formation of the Hoogsteen-type pair that is observed in structures I, II, and the DPB–EtAd structure due to a sterically forbidden contact it would make with the barbiturate O(2) carbonyl oxygen. Since adenine moieties of nucleic acids and coenzymes are not usually substituted at the 8-position (especially with a bromine atom), it seems reasonable to suggest that if barbiturates complex with adenine bases or interact with similar receptors in vivo, the likely hydrogen bonding scheme is that found between DPB and EtAd

The comparisons made between the present structure and the others cited above thus indicate that the presence of the C(2)-O(2) dipole interaction is dependent on the adenine derivative and its hydrogen bonding requirements while the strength of the interaction appears to be balanced against the packing requirements of the different sized C(5) barbiturate substituents.

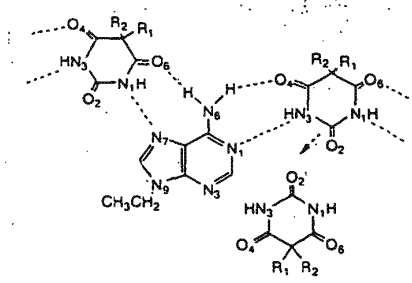
Unlike DPH (16), barbiturate molecules do not form self-associated hydrogen-bonded dimers when a complementary alternative molecule is available in the structure even if in some cases the other molecule happens to be water (25). Given an unrestricted choice of hydrogen bond pair formation with adenine molecules, barbiturates seem to prefer a mixed Watson–Crick, Hoogsteen-type pairing leaving the C(2)-O(2) available for dipole–dipole type interactions. Our crystal structure results along with the others discussed above suggest that in addition to hydrogen bonding these nonbonded carbonyl associations may also be important in determining molecular packing. Whether such dipole interactions might be involved in barbiturate–receptor binding or pharmacological signal transmission is not known.

It is of interest to note that primidone, the phenobarbital congener with the C(2)=O(2) replaced by CH2, is also a useful antiepileptic agent. Its spectrum of anticonvulsant effects resembles that of phenobarbital except that it is much less potent in antagonizing PTZ induced seizures. As barbiturate C(2)=O(2) carbonyls do not hydrogen bond to EtAd, it is likely that primidone could interact with adenine by forming the same pairs of hydrogen bonds as observed in the DPB–EtAd complex. Thus if some barbiturate anticonvulsant or other pharmacologic actions are mediated through this type of interaction they are likely to be those actions common to both phenobarbital and primidone.

© 2000 NRC Canada

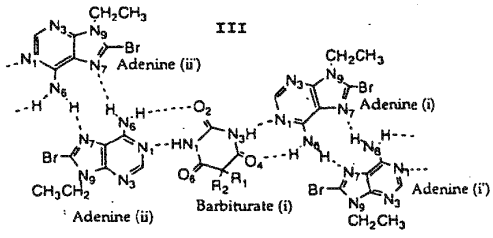
UM00013106
NOVARTIS EXHIBIT 1517
Novartis v. Regents, IPR2023-01347
Page 1852 of 4460

Fig. 3. Schematic drawing illustrating the different hydrogen bonding arrangements observed in crystal structures of adenine–barbiturate complexes.



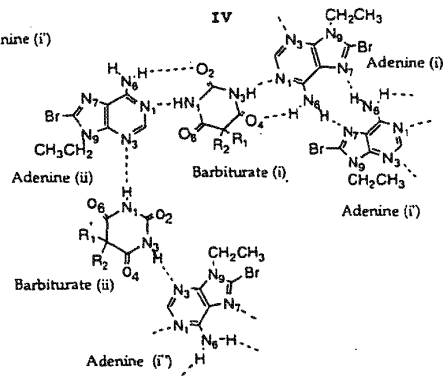
Distances (Å)

	I	II	This Work
AN6-BO6	3.12	3.39	3.32
AN7-BN1	2.81	2.83	2.87
AN6-BO4	3.34	3.22	3.31
AN1-BN3	2.79	2.83	2.83
BC2-BO2'	3.17	2.98	3.09



Distances (Å)

	III	IV
A(i)N6-B(i)O4	3.19	2.96
A(i)N1-B(i)N3	2.78	2.79
A(ii)N6-B(i)O2	2.97	3.07
A(ii)N1-B(i)N1	2.80	2.94
A(ii)N3-B(ii)N1	----	2.97
A(i'')N3-B(ii)N3	----	3.03
A(i)N6-A(i')N7	3.09	2.97
A(ii)N6-A(ii')N7	3.02	----



References

1. A. Camerman and N. Camerman. *In* Molecular and quantum pharmacology. *Edited by* E. Bergman and B. Pullman. D. Reidel, Dordrecht, Holland. 1975. pp. 213–228.
2. P.K. Knoefel and G. Lehman. J. Pharmacol. Exp. Ther. **76**, 194 (1942).
3. H.H. Merrit and T.J. Putnam. Epilepsia, **3**, 51 (1945).
4. G.C.H. Alles, G. A. Ellis, and M.A. Redmann. J. Pharmacol. Exp. Ther. **89**, 346 (1947).
5. A. Raines, J.M. Niner, and D.G. Pace. J. Pharmacol. Exp. Ther. **186**, 315 (1973).
6. J. Francis and W.M. Burnham. Mol. Pharmacol. **42**, 1097 (1992).
7. R. Levy, F.E. Dreifuss, R.H. Mattson, B.S. Meldrum, and J.K. Penry. (*Editors*). Antiepileptic drugs. Raven Press, New York. 1989. p. 155.
8. R.L Macdonald. Epilepsia, **34**(Suppl. 5), S1 (1993).
9. Y. Kyogoku, R.C. Lord, and A. Rich. Nature (London), **218**, 69 (1968).
10. S.H. Kim and A. Rich. Proc. Natl. Acad. Sci. U.S.A. **60**, 402 (1968).
11. D. Voet and A. Rich. J. Am. Chem. Soc. **94**, 5888 (1972).
12. D. Voet. J. Am. Chem. Soc. **94**, 8213 (1972).
13. R.H. Epstein, A.V. Zeiger, C. Crocker, and D. Voet. Acta Crystallogr. Sect. B: Struct. Crystallogr. Crys. Chem. **B32**, 2180 (1976).
14. E. Gentric, J.F. Meney, J. Lauransan, L.G. Bardou, and P. Saumagne. Chem. Biol. Interact. **54**, 117 (1985).
15. G.L. Jones and J.W. Kemp. Mol. Pharmacol. **10**, 48 (1974).
16. D. Mastropaolo, A. Camerman, and N. Camerman. Mol. Pharmacol. **23**, 273 (1983).
17. R.F. Bruns, J.W. Daly, and S.H. Snyder. Proc. Natl. Acad. Sci. U.S.A. **77**, 5547 (1980).
18. M. Dragunow. Prog. Neurobiol. (Oxford), **31**, 85 (1988).
19. G. Zhang, P.H. Franklin, and T.F. Murray. J. Pharmacol. Exp. Ther. **264**, 1415 (1993).
20. R.A. Gonzalez and S.W. Leslie. Biochem. Pharmacol. **34**, 1619 (1985).
21. J.W. Phillis, P.H. Wu, and A.S. Bender. Gen. Pharmacol. **12**, 67 (1981).
22. J.W. Phillis. Epilepsia, **25**, 765 (1984).
23. P. Main, S.J. Fiske, S.E. Hull, L. Lessinger, G. Germain, J.P. DeClercq, and M.M. Woolfson. MULTAN 80. A system of

© 2000 NRC Canada

UM00013107
NOVARTIS EXHIBIT 1517
Novartis v. Regents, IPR2023-01347
Page 1853 of 4460

computer programs for the automatic solution of crystal structures from x-ray diffraction data. Univs. of York, England and Louvain, Belgium. (1980).
24. J.M. Stewart. The Xray System. University of Maryland, College Park, Maryland. (1976).
25. P.P. Williams. Acta Crystallogr. Sect. B: Struct. Crystallogr. Crys. Chem. B29, 1572 (1973).
26. B.M. Gatehouse and B.M. Craven. Acta Crystallogr. Sect. B: Struct. Crystallogr. Crys. Chem. B27, 337 (1971).
27. B.M. Craven, E.A. Vizzini, and M.M. Rodrigues. Acta Crystallogr. Sect. B: Struct. Crystallogr. Crys. Chem. B25, 1978 (1969).
28. B.M. Craven and E.A. Vizzini. Acta Crystallogr. Sect. B: Struct. Crystallogr. Crys. Chem. B27, 1917 (1971).
29. B.M. Craven and G.L. Gartland. J. Pharm. Sci. 59, 1666 (1970).
30. S. Kiryu. J. Pharm. Sci. 60, 699 (1971).
31. A. Camerman and N. Camerman. Acta Crystallogr. Sect. B: Struct. Crystallogr. Crys. Chem. B27, 2205 (1971).

© 2000 NRC Canada

This Page is Inserted by IFW Indexing and Scanning Operations and is not part of the Official Record

BEST AVAILABLE IMAGES

Defective images within this document are accurate representations of the original documents submitted by the applicant.

Defects in the images include but are not limited to the items checked:

- ☐ BLACK BORDERS
- ☐ IMAGE CUT OFF AT TOP, BOTTOM OR SIDES
- ☐ FADED TEXT OR DRAWING
- ☐ BLURRED OR ILLEGIBLE TEXT OR DRAWING
- ☐ SKEWED/SLANTED IMAGES
- ☐ COLOR OR BLACK AND WHITE PHOTOGRAPHS
- ☐ GRAY SCALE DOCUMENTS
- ☐ LINES OR MARKS ON ORIGINAL DOCUMENT
- ☐ REFERENCE(S) OR EXHIBIT(S) SUBMITTED ARE POOR QUALITY
- ☐ OTHER: _____

IMAGES ARE BEST AVAILABLE COPY.
As rescanning these documents will not correct the image problems checked, please do not report these problems to the IFW Image Problem Mailbox.

gave (±)-2b (7.31 g, 38% from the acid): bp 129–136 °C (17 mm). Anal. ($C_8H_9NCl_2$) C, H, N.

(*S*)-α-(3,5-Dichlorophenyl)ethylamine [(*S*)-2b]. Racemic **2b** (6.95 g, 36.6 mmol) and (+)-10-camphorsulfonic acid (8.49 g, 36.6 mmol) were dissolved in hot methanol (50 mL). The methanol was removed at reduced pressure. Recrystallization (4×) of the residue from 30–50% ethanol in water gave the pure salt (1.26 g, 16%): $[\alpha]^{25}_D$ +6.8° (*c* 1.38, NaOH–CH_3OH[34]). Decomposition of the salt gave (*S*)-**2b**: $[\alpha]^{26}_D$ −24° (*c* 1.45, CH_3OH); >95% ee.[35]

(*S*)-α-Benzylethylamine [(*R*)-3a] had $[\alpha]^{22}_D$ +33.1° (neat, d^{20}_4 0.949, 0.5 dm) [lit.[15] $[\alpha]^{15}_D$ +35.6° (neat)].

(*S*)-α-Benzylethylamine hydrochloride [(*S*)-3a·HCl] had $[\alpha]^{25}_D$ +21.6° (*c* 9.0, H_2O) [lit.[15] $[\alpha]^{15}_D$ +24.8° (*c* 9.00, H_2O)].

(*S*)-α-(*p*-Chlorobenzyl)ethylamine hydrochloride [(*S*)-3b·HCl] had $[\alpha]^{25}_D$ +22° (*c* 2.10, H_2O) [lit.[16] $[\alpha]^{25}_D$ +22° (*c* 2.10, H_2O)]; >95% ee.[35]

(*R*)-α-(*p*-(Trifluoromethyl)benzyl)ethylamine [(*R*)-3c]. Racemic **3c**·HCl,[20] mp 202–204 °C (lit.[19] mp 195–197 °C) (4.83 g, 20.2 mmol), in 95% ethanol (25 mL) was mixed with 20% NaOH (4.1 g, 20 mmol). To the mixture was then added L-*N*-acetylleucine[38] (3.55 g, 20.5 mmol) in 95% ethanol (25 mL), and the mixture was heated to boiling and filtered. The solvent was evaporated, and the residue was recrystallized from methanol. A second recrystallization from methanol gave the salt (1.12 g, 29%): $[\alpha]^{26}_D$ −15° (*c* 1.47, CH_3OH). Decomposition of the salt gave (*R*)-**3c**: $[\alpha]^{26}_D$ −19° (*c* 1.76, CH_3OH); >95% ee.[35] The hydrochloride salt [(*R*)-3c·HCl] formed by the addition of concentrated HCl to an ether solution of the amine had mp 170–172 °C and $[\alpha]^{26}_D$ −7° (*c* 1.23, CH_3OH).

(*R*)-*N*,*N*-Dimethyl-α-benzylethylamine [(*R*)-4a]. A mixture of formic acid (2.4 g of 97%, 51 mmol) and formaldehyde (2.0 mL of 36%) was added with cooling to (*R*)-α-benzylethylamine [(*R*)-9a], $[\alpha]^{22}_D$ −35.0° (neat, d^{20}_4 0.949) (1.35 g, 10.0 mmol). The mixture was boiled for 15 h, acidified with 6 N hydrochloric acid (2.0 mL), and concentrated at reduced pressure. The concentrate was made basic with 10% sodium hydroxide (10 mL) and then extracted with ether (2 × 10 mL). The ether solution was dried (KOH) and evaporated. Distillation of the residue gave (*R*)-**4a** (0.828 g, 51%): bp 116–120 °C (32 mm) [lit.[41] bp 115–118 °C (20 mm) for (±)-**4a**]; $[\alpha]^{26}_D$ +7.8° (*c* 1.96, CH_3OH) [lit.[17] $[\alpha]_D$ +7.8° (*c* 2.6, CH_3OH)].

(*S*)-*N*,*N*-Dimethyl-α-(p-chlorobenzyl)ethylamine hydrochloride [(*S*)-4b·HCl] had $[\alpha]^{25}_D$ +11° (*c* 2.09, H_2O) [lit.[16] $[\alpha]^{25}_D$ +11° (*c* 2.09, H_2O)].

(*S*)-*O*-Methylmandelic acid was prepared as described previously[22,42] and had mp 63–66 °C $[\alpha]^{26}_D$ +161° (*c* 1.20, H_2O) [lit.[22] mp 65–67 °C and $[\alpha]^{23}_D$ −161.9° (*c* 1.66, H_2O) for the *R* isomer].

Registry No. (*S*)-**1a**, 2627-86-3; (*S*)-**1a**·HCl, 17279-30-0; (±)-**1b**, 42070-98-4; (*S*)-**1b**, 27298-98-2; (*S*)-**1b**·HCl, 84499-72-9; (±)-**1c**, 35588-60-4; (*R*)-**1c**, 27298-99-3; (*S*)-**1c**, 4187-56-8; (*S*)-**1c**·HCl, 56782-68-4; (*S*)-**1d**, 27298-97-1; (*S*)-**1d**·HCl, 84499-77-4; (*S*)-**1e**, 36244-70-9; (±)-**1f**, 84580-06-3; (*S*)-**1f**, 84499-73-0; (*S*)-**1f**·L-*N*-acetylleucine, 84499-82-1; (*S*)-**1f**·HCl, 84499-78-5; (±)-**2a**, 84580-07-4; (*S*)-**2a**, 84499-76-3; (*S*)-**2a**·L-*O*,*O*′-dibenzoyltartrate, 84520-44-5; (*R*)-**2a**·HCl, 84499-74-1; (*S*)-**2a** (*N*-5-bromosalicylidene derivative), 84499-81-0; (±)-**2b**, 84499-83-2; (*S*)-**2b**, 84499-75-2; (*S*)-**2b**·(+)-10-camphorsulfonic acid, 84580-08-5; (*S*)-**2b**·HCl, 84499-79-6; (*S*)-**3a**, 51-64-9; (*S*)-**3a**·HCl, 1462-73-3; (*S*)-**3b**, 405-46-9; (*S*)-**3b**·HCl, 16064-30-5; (*R*)-**3c**, 84580-99-4; (*R*)-**3c**·HCl, 84580-09-6; (*R*)-**3c**·L-*N*-acetylleucine, 84620-15-5; (*S*)-**3c**, 84580-04-1; (*S*)-**3c**·HCl, 84580-05-2; (*R*)-**4a**, 52691-87-9; (*S*)-**4a**·HCl, 36913-04-9; (*S*)-**4a**, 17279-39-9; (*S*)-**4b**, 84499-80-9; (*S*)-**4b**·HCl, 16064-30-5; (*R*)-**9a**, 156-34-3; *p*-methylacetophenone, 122-00-9; *p*-chloroacetophenone, 99-91-2; *p*-(trifluoromethyl)-acetophenone, 709-63-7; 3,5-dimethylacetophenone, 5379-16-8; methyllithium, 917-54-4; 3,5-dichlorobenzoic acid, 51-36-5; 3,5-dichloroacetophenone, 14401-72-0; 2-(3,5-dichlorophenyl)-2-propanol, 68575-35-9.

(41) Simon, I. B. *Zh. Obshch. Khim.* **1949**, *28*, 2586–2587; *J. Gen. Chem. USSR* (*Engl. Transl.*) **1949**, *28*, 2619–2620.
(42) Reeve, W.; Christoffel, I. *J. Am. Chem. Soc.* **1950**, *72*, 1480–1483.

Molecular Structure of Acetylacetone. A Crystallographic Determination

Arthur Camerman,*[1a] Donald Mastropaolo,[1a] and Norman Camerman[1b]

Contribution from the Department of Medicine (Neurology) and Pharmacology, University of Washington, Seattle, Washington 98195, and the Department of Biochemistry, University of Toronto, Toronto, Canada M5S 1A8. *Received September 21, 1982*

Abstract: A drug complex crystallized from acetylacetone (2,4-pentanedione) was found by X-ray crystal structure determination to contain one molecule of acetylacetone per asymmetric unit in the crystal lattice. The acetylacetone does not interact with the other molecules in the crystal but displays a keto–enol configuration stabilized by an intramolecular hydrogen bond. In contrast to electron diffraction studies of acetylacetone and crystal structure studies of other β-diketones, bond distances, including the hydrogen bond, are not symmetric but are indicative of localized single and double bonds throughout the molecule. Past estimates of acetylacetone diketo/keto–enol ratios in the liquid and gas phases may be in error if they assume complete bond length symmetry for the enol form.

The β-diketones have been among the most widely studied chelating compounds because of their strong hydrogen-bonding property and their ability to form coordination complexes with almost every metal in the periodic table. Although scores of such metal chelates have been investigated crystallographically,[2] only limited structural data have been collected on β-diketones themselves. The questions of whether the diketo or enol form predominates for these molecules and whether or not the enol intramolecular hydrogen bond is symmetrical have been examined in the crystal structure determinations of bis(*m*-bromobenzoyl)-methane,[3] bis(*m*-chlorobenzoyl)methane,[4] dibenzoylmethane,[5] and tetraacetylethane.[6] All of these compounds were found to be in the enol configuration in the crystalline state and all except dibenzoylmethane are characterized by equidimensional C–O distances and a symmetric intramolecular hydrogen bond. The latter

Table I. Acetylacetone Intermolecular Contacts Less Than 3.2 A

O(2)- - -H(C), A[a]	2.56	O(2)- - -H(C), D	2.76
O(2)- - -C, A	3.15	O(2)- - -H(C), D	3.11
O(2)- - -H(N), A	2.80	O(4)- - -H(N), A	2.95
O(4)- - -H(C), D[a]	2.91	O(4)- - -N, A	3.18

[a] A, 9-ethyladenine; D, diphenylhydantoin.

(1) (a) University of Washington. (b) University of Toronto.
(2) For a review, see: Mehrotra, R. C.; Bohra, R.; Gaur, D. P. "Metal β-Diketonates and Allied Derivatives"; Academic Press: London, 1978.
(3) Williams, D. E.; Dumke, W. L.; Rundle, R. E. *Acta Crystallogr.* **1962**, *15*, 627–635.
(4) Engebretson, G. R.; Rundle, R. E. *J. Am. Chem. Soc.* **1964**, *86*, 574–581.
(5) Williams, D. E. *Acta Crystallogr.* **1966**, *21*, 340–349.
(6) Schaefer, J. P.; Wheatley, P. J. *J. Chem. Soc. A.* **1966**, 528–532.

0002-7863/83/1505-1584$01.50/0 © 1983 American Chemical Society

UM00013110
NOVARTIS EXHIBIT 1517
Novartis v. Regents, IPR2023-01347
Page 1856 of 4460

Table II. Acetylacetone Fractional Coordinates

atom	x	y	z	atom	x	y	z
C(1)	0.33316	0.23193	0.21553	H(4)	0.29120	0.12245	0.40162
C(2)	0.29359	0.17827	0.28212	H(3)	0.12853	0.18204	0.24414
O(2)	0.36466	0.14964	0.32240	H(1a)	0.33169	0.19336	0.15168
C(3)	0.17876	0.15790	0.29863	H(1b)[a]	0.2767	0.2758	0.2096
C(4)	0.13991	0.10369	0.35445	H(1c)[a]	0.4285	0.2971	0.2580
O(4)	0.20748	0.06785	0.40078	H(5a)	0.03709	0.05951	0.43582
C(5)	0.01389	0.07521	0.37188	H(5b)[a]	−0.0078	0.1488	0.3918
				H(5c)[a]	−0.0612	−0.0020	0.3066

[a] Calculated positions.

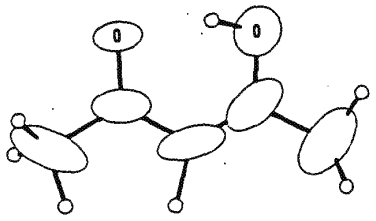


Figure 1. Perspective drawing of acetylacetone. Thermal ellipsoids are drawn at the 40% probability level.

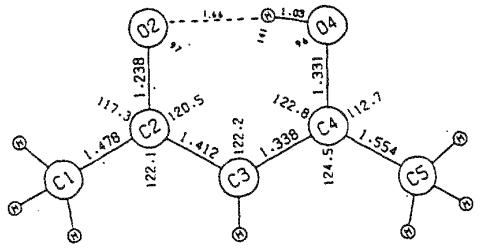


Figure 2. Bond distances and angles for acetylacetone. Errors in the heavy atom distances and angles are 0.01 Å and 0.9°, respectively. The H atom distances range between 0.89 and 1.15 Å, with errors of 0.09 Å; angles range between 96 and 132°, with errors of 5°. The O(2)–O(4) distance is 2.535 Å.

compound deviates slightly from this symmetry, but differences between related C–O, O–H, and C–C bond lengths are only barely outside experimental error.

The prototype β-diketone, acetylacetone (2,4-pentanedione), is a liquid at room temperature (mp −23 °C) and has not been until now subjected to crystallographic examination. An NMR study[7] concluded that liquid acetylacetone at 25 °C is approximately 80% enol and 20% ketone, while two electron diffraction experiments have suggested that in the gas phase the ratios are 97% enol at 27 °C[8] and 67% enol at 105 °C.[9] Although they differ on bond-length estimates, both electron diffraction studies conclude that the enol form of acetylacetone, like the substituted β-diketones, possesses aromatic character and a symmetric intramolecular hydrogen bond.

As part of a research project on antiepileptic drugs we have recently crystallized a complex of diphenylhydantoin and 9-ethyladenine, using acetylacetone as solvent.[10] Elucidation of the three-dimensional structure of the crystals revealed that one molecule of acetylacetone per asymmetric unit is present in the crystal lattice. The acetylacetone does not interact in any way with the other molecules in the crystal; thus we are able to observe its molecular structure in a rather isolated environment. This environment is illustrated quantitatively in Table I, which lists all contacts less than 3.2 Å between acetylacetone atoms and those of diphenylhydantoin and ethyladenine. No contacts shorter than van der Waal's distances are observed. We now report that acetylacetone in the solid state is in the enol configuration with bond lengths that indicate nonequivalence of related atoms (no aromatic character) and a definitively asymmetric intramolecular hydrogen bond.

The complex of diphenylhydantoin and 9-ethyladenine with acetylacetone included in the lattice crystallized in space group $P\bar{1}$ with cell constants $a = 12.256$ (2) Å, $b = 13.691$ (2) Å, $c = 14.835$ (2) Å, $\alpha = 112.04$ (1)°; $\beta = 98.72$ (1)°, $\gamma = 110.99$ (1)°, $Z = 2$. The structure was solved by direct methods and refined by least-squares methods to a final discrepancy index $R = (\sum||F_o| - |F_c||)/\sum F_o = 0.054$. Positions of most of the acetylacetone hydrogen atoms including H(4) were located in difference electron-density maps. The exceptions were two hydrogens of each of the methyl groups whose positions were calculated. Hydrogen atom coordinates were refined in the final least-squares cycle, but their thermal parameters were kept equal to those of the heavy atoms to which they are bonded. Final acetylacetone fractional coordinates are listed in Table II.

Table III. Selected Bond Distances (Å) in Acetylacetone and Related Compounds

bond	BrBM[a]	ClBM[b]	BM[c]	TAE[d]	AcAc[e]	AcAc[f]	AcAc[g]
C–O	1.306	1.299	1.292	1.295	1.315	1.287	1.238
		1.318	1.317	1.310			1.331
C–C	1.393	1.397	1.385	1.395	1.416	1.405	1.338
		1.402	1.413	1.411			1.412
O–H	1.23		1.18		1.19	1.26	1.03
			1.34				1.66
O–O	2.464	2.475	2.468	2.424	2.38	2.52	2.535

[a] Bis(*m*-bromobenzoyl)methane.[3] Space-group symmetry requires equivalence of the two C–O bonds and of the two C–C bonds in this molecule. [b] Bis(*m*-chlorobenzoyl)methane.[4] [c] Dibenzoylmethane.[5] [d] Tetraacetylethane.[6] [e] Acetylacetone, electron diffraction.[8] [f] Acetylacetone, electron diffraction.[9] [g] Acetylacetone, X-ray crystallography (this work).

A perspective drawing of the molecule is shown in Figure 1. The seven non-hydrogen atoms define a plane from which the maximum deviation is 0.038 Å and the average deviation is 0.018 Å. The hydrogen atom attached to O(4) lies 0.36 Å out of the plane. Bond distances and angles are listed in Figure 2. These values present a clear indication that acetylacetone, in the solid-state isolated environment at least, does not exhibit aromatic ring characteristics with a symmetric intramolecular hydrogen bond, but rather adopts a discrete keto–enol configuration with an O–H···O hydrogen bond that is asymmetric and nonlinear. Differences between the C–C distances (0.074 Å), C–O distances (0.093 Å), and O–H distances (0.63 Å) are far greater than the standard deviations of the bond lengths and clearly distinguish between single and double bonds joining the respective atoms.

Comparisons of bond lengths found for acetylacetone in the solid state, those postulated for the molecule from the electron diffraction radial distribution curves, and those found in substituted β-diketones in other crystallographic investigations are shown in Table III. These comparisons suggest that the apparent acetylacetone keto–enol ratios in the liquid and gas phase may be in error if they include an assumption of symmetry of bond lengths for the enol form. They also suggest that either a trend toward aromatic character in the intramolecular hydrogen-bond ring system of the β-diketones increases with increasing substitution

(7) Reeves, L. W. *Can. J. Chem.* **1957**, *35*, 1351–1365.
(8) Lowry, A. H.; George, C.; D'Antonio, P.; Karle, J. *J. Am. Chem. Soc.* **1971**, *93*, 6399–6403.
(9) Andreassen, A. L.; Bauer, S. H. *J. Mol. Struct.* **1972**, *12*, 381–403.
(10) Mastropaolo, D.; Camerman, A.; Camerman, N. *Abstr. Am. Crystallogr. Assn.* **1977**, *5* (1), 36.

UM00013111
NOVARTIS EXHIBIT 1517
Novartis v. Regents, IPR2023-01347
Page 1857 of 4460

or alternatively the symmetry observed in some β-diketone structures is the result of statistical disorder.

Acknowledgment. The research was supported in part by National Institutes of Health, Grants NS09839 and CA15879.

Registry No. Acetylacetone, 123-54-6.

Supplementary Material Available: Table of anisotropic thermal parameters (1 page). Ordering information is given on any current masthead page.

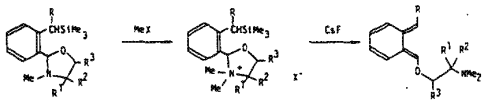
A New Approach to Asymmetric Synthesis of Polycycles on the Basis of *o*-Quinodimethane Generation

Yoshihiko Ito,* Yusuke Amino, Masashi Nakatsuka, and Takeo Saegusa*

Contribution from the Department of Synthetic Chemistry, Faculty of Engineering, Kyoto University, Yoshida, Kyoto 606, Japan. *Received June 2, 1982*

Abstract: The fluoride anion induced 1,4 elimination of 2-[*o*-[1-(trimethylsilyl)alkyl]phenyl]-3,3-dimethyloxazolidinium salts generates (*E*,*E*)-α-alkyl-α′-[2-(dimethylamino)alkyl]-*o*-quinodimethane intermediates, which are trapped stereoselectively with dienophiles to give polycycles. Intramolecular cyclization of 2-[*o*-[1-(trimethylsilyl)hept-6-enyl]phenyl]-3,3-dimethyl-4-(*R*)-methyl-5(*R*)-phenyloxazolidinium triflate at 0 °C produces a 3:1 diastereoisomeric mixture of 6-[2(*R*)-(dimethylamino)-1(*R*)-phenylpropoxyl]-*trans*-octahydrophenanthrene, which is converted by hydrogenolysis on Pd/C to *trans*-octahydrophenanthrene with $[\alpha]_D$ +46.6° (50% ee). Similarly, intramolecular cyclization of 2-[*o*-[1-(trimethylsilyl)hept-6-enyl]phenyl]-3,3-dimethyl-4(*S*)-methoxymethyl-5(*S*)-phenyloxazolidinium triflate produces, after hydrogenolysis on Pd/C, *trans*-octahydrophenanthrene with $[\alpha]_D$ −51.1° (55% ee). The enantioselection in the cycloaddition with *o*-quinodimethane intermediate may be accounted for on the basis of π-stacking interaction in the Diels–Alder transition state.

A variety of methodologies[1] have so far been developed to generate in situ *o*-quinodimethane and applied to synthesize polycycles including steroidal structures by their cycloaddition reactions. However, a generation of *o*-quinodimethanes with electron-donating heteroatom substituents[2] at the α position, which may be expected to exert higher regioselectivity and higher reactivity in Diels–Alder cycloaddition, has been scarcely known. In the preceding papers[3], we reported a mild and efficient generation of *o*-quinodimethanes by the fluoride anion induced 1,4-elimination of *o*-[1-(trimethylsilyl)alkyl]benzyltrimethylammonium halides. The methodology for the generation of *o*-quinodimethanes has been successfully extended to 2-[*o*-[1-(trimethylsilyl)alkyl]phenyl]-3,3-dimethyloxazolidinium salts (**2**),



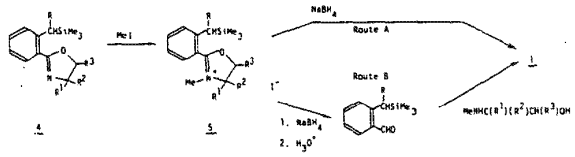
1 **2** **3**

a, R = H; $R^1 = R^2$ = Me; R^3 = H
b, R = $R^1 = R^2$ = H; R^3 = Me
c, R = -$(CH_2)_4CH{=}CH_2$; $R^1 = R^2$ = H; R^3 = Me
d, R = -$(CH_2)_4CH{=}CH_2$; $R^1 = R^2$ = H; R^3 = (*R*)-Ph
e, R = -$(CH_2)_4CH{=}CH_2$; R^1 = (*S*)-Me; R^2 = H; R^3 = (*R*)-Ph
f, R = -$(CH_2)_4CH{=}CH_2$; R^1 = (*R*)-Me; R^2 = H; R^3 = (*R*)-Ph
g, R = -$(CH_2)_4CH{=}CH_2$; R^1 = (*S*)-CH_2OMe; R^2 = H; R^3 = (*S*)-Ph
h, R = -$(CH_2)_4CH{=}CH_2$; R^1 = (*R*)-Ph; $R^2 = R^3$ = H
i, R = -$(CH_2)_4CH{=}CH_2$; R^1 = (*S*)-CH_2Ph; $R^2 = R^3$ = H
j, R = H; R^1 = (*S*)-Me; R^2 = H; R^3 = (*R*)-Ph

leading to the formation of (*E*,*E*)-α-alkyl-α′-[2-(dimethylamino)alkoxy]-*o*-quinodimethane intermediates (**3**).

In this paper, we describe a synthesis of polycycles by the inter- and intramolecular cycloadditions of **3**. Of special interest is that some 2-[*o*-[1-(trimethylsilyl)alkyl]phenyl]-3,3-dimethyloxazolidinium salts (**2**) with a phenyl substituent at the C-5 on the oxazolidinium ring were cyclized enantioselectively via the corresponding *o*-quinodimethanes to afford polycycles. This reaction, which is the first use of *o*-quinodimethane in asymmetric synthesis, may present a new approach to asymmetric synthesis of polycycles. The 2-(dimethylamino)alkoxy substituent of **3**, which conferred high reactivity in reactions with dienophiles and brought about the asymmetric induction, was easily removed after the reactions.

Scheme I



4 **5** **6**

a, R = H; $R^1 = R^2$ = Me; R^3 = H
b, R = $R^1 = R^2$ = H; R^3 = Me
c, R = -$(CH_2)_4CH{=}CH_2$; $R^1 = R^2$ = Me; R^3 = H
d, R = -$(CH_2)_4CH{=}CH_2$; $R^1 = R^2$ = H; R^3 = Me

Results and Discussions

Preparation of the requisite oxazolidines **1**[4] for the generation of *o*-quinodimethanes **3** could be carried out via quaternization and reduction of the corresponding 2-[*o*-[(trimethylsilyl)-methyl]phenyl]oxazolines (**4**) and 2-[*o*-[1-(trimethylsilyl)alkyl]phenyl]oxazolines (**4**, R = alkyl), which were accessible from alkylations at the silicon-stabilized carbanion of **4** R = H[4a] (route A in Scheme I). Thus, 2-[*o*-[(trimethylsilyl)methyl]phenyl]-3,4,4-trimethyloxazolidine (**1a**) and 2-[*o*-[1-(trimethylsilyl)-hept-6-enyl]phenyl]-3,5-dimethyloxazolidine (**1c**) were prepared

(1) Oppolzer, W., *Synthesis*, **1978**, 793.
(2) Sammes, P. G. *Tetrahedron* **1976**, *32*, 405.
(3) (a) Ito, Y.; Nakatsuka, M.; Saegusa, T. *J. Am. Chem. Soc.* **1980**, *102*, 863. (b) Ito, Y.; Nakatsuka, M.; Saegusa, T. *J. Am. Chem. Soc.* **1981**, *103*, 476.
(4) (a) Gschwend, H. W.; Hamdan, A. *J. Org. Chem.* **1975**, *40*, 2008. (b) Nordin, I. C. *J. Heterocycl. Chem.* **1966**, *3*, 531. (c) Meyers, A. I.; Nabeya, A.; Adickes, H. W.; Politzer, I. R.; Malone, G. R.; Kovelesky, A. C.; Nolen, R. L.; Portnoy, R. C. *J. Org. Chem.* **1973**, *38*, 36.

0002-7863/83/1505-1586$01.50/0 © 1983 American Chemical Society

UM00013112
NOVARTIS EXHIBIT 1517
Novartis v. Regents, IPR2023-01347
Page 1858 of 4460

This Page is Inserted by IFW Indexing and Scanning Operations and is not part of the Official Record

BEST AVAILABLE IMAGES

Defective images within this document are accurate representations of the original documents submitted by the applicant.

Defects in the images include but are not limited to the items checked:

- ☐ BLACK BORDERS
- ☐ IMAGE CUT OFF AT TOP, BOTTOM OR SIDES
- ☐ FADED TEXT OR DRAWING
- ☐ BLURRED OR ILLEGIBLE TEXT OR DRAWING
- ☐ SKEWED/SLANTED IMAGES
- ☐ COLOR OR BLACK AND WHITE PHOTOGRAPHS
- ☐ GRAY SCALE DOCUMENTS
- ☐ LINES OR MARKS ON ORIGINAL DOCUMENT
- ☐ REFERENCE(S) OR EXHIBIT(S) SUBMITTED ARE POOR QUALITY
- ☐ OTHER: _____

IMAGES ARE BEST AVAILABLE COPY.
As rescanning these documents will not correct the image problems checked, please do not report these problems to the IFW Image Problem Mailbox.

CRYSTAL GROWTH & DESIGN
2002
VOL. 2, NO. 4
255–257

Noncovalent Derivatization: Green Chemistry Applications of Crystal Engineering

Amy S. Cannon and John C. Warner*

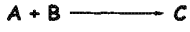
Department of Chemistry, UMB Center for Green Chemistry, University of Massachusetts Boston, 100 Morrissey Boulevard, Boston, Massachusetts 02125-3393

Received April 17, 2002; Revised Manuscript Received May 14, 2002

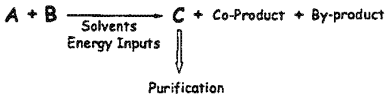
ABSTRACT: The field of crystal engineering is rapidly expanding. As our understanding of the mechanism of construction and relationship between structure and function of molecular crystals increases, it is important to recognize that this field offers significant toxicological and environmental benefits. The processes of molecular recognition and self-assembly are inherently benign in terms of its impact on human health and the environment. These benefits must be articulated and exploited.

As the field of crystal engineering continues to grow, it is worthwhile to consider some philosophical implications of its impact to the chemical sciences. We live in a society based on materials. We depend on chemical products for virtually every aspect of our lives. We have come to expect a continuous stream of new pharmaceuticals to cure life-threatening diseases or for the incremental improvement in the quality of our lives. We expect an ever-expanding food supply based on an agricultural industry that is designing new fertilizers and pesticides. We rely on new materials for the construction of buildings, clothing, and microelectronic gadgetry. Society has come to expect innovation from industry in the form of material goods. The economic fabric of our society is based for the most part on the design, manufacture, marketing, and sale of these materials, but the creation of these new "things" does not come without cost. Industry must use whatever state-of-the-art scientific tools available to meet the consumer's ever increasing appetite for new products. Under the pressure imposed by the expectations of "increased shareholder value" and patent timelines, there is less opportunity for industry to perform basic research. It must largely rely on the current literature for most of the new chemical processes and transformations it will use. Many of the chemical reactions available to the chemical industries use or generate substances that have a detrimental effect on human health and the environment. Ironically, at the same time that society has increased its expectations of materials production, it is also becoming more demanding in terms of toxicological and environmental issues. The negative reputation of the chemical industry on the general public has been propagated in large by the reoccurring reports in the media of chemical accidents, spills, leaks, and explosions. Much, if not all, of this criticism is well deserved. Green chemistry is the philosophy that the best method of pollution prevention, from an ethical and economic perspective, is to focus on toxicological and environmental implications at the earliest stage of product design. It is simply better to carry our processes that have minimal use of hazardous material. Industry certainly recognizes this fact. Unfortunately, most of the tools currently available are not environmentally benign.

Scheme 1



Scheme 2



Consider a simple schematic of a chemical reaction. In general, an ideal chemical transformation can be represented as a simple combination of reactants to form a single product (Scheme 1).

In practice, chemical reactions are rarely, if ever, this simple. There are many other implications (Scheme 2). Often there is the stoichiometric generation of coproducts and a number of byproducts that are formed during the reaction. These reaction products can have serious consequences from a toxicological or environmental analysis. The solvents that are used can constitute the majority of the total mass of the reaction materials. The energy used for the heating, cooling, or mixing of the reaction can account for the greatest cost, both environmentally and economically. It is also important to recognize that product isolation and purification, with the use of chromatography, distillation, or other solvent- or energy-intensive processes can have serious impact.

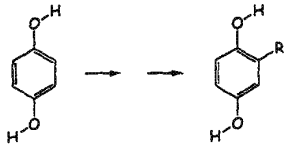
Why are chemical reactions carried out in the first place? What is the objective of chemical synthesis? It is safe to say that chemical synthesis is always carried out for the purpose of manipulating the chemical and physical properties of a material. Very often an individual molecule is identified that has several desirable physical and chemical properties for a specific application, but this molecule is not perfect. As an example,

* To whom correspondence should be addressed.

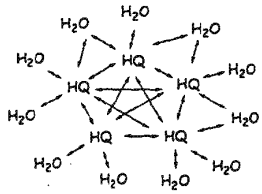
10.1021/cg0255218 CCC: $22.00 © 2002 American Chemical Society
Published on Web 06/01/2002

UM00013114
NOVARTIS EXHIBIT 1517
Novartis v. Regents, IPR2023-01347
Page 1860 of 4460

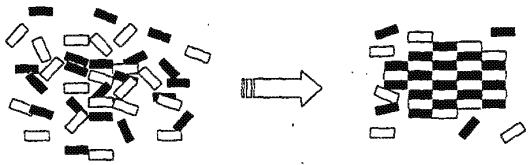
Scheme 3



Scheme 4



Scheme 5



imagine that the molecule hydroquinone (HQ) has many desirable properties for some application, except that it is too water soluble. The typical research and development approach would be to synthetically modify the molecule to increase its hydrophobicity. For example, a research effort could be undertaken to synthesize a number of alkyl derivatives (Scheme 3). Of course, these synthetic reactions will most likely produce coproducts and byproducts, make use of solvents and energy inputs, and require separation and purification.

What is being accomplished, at the molecular level, by adding an alkyl group to HQ? To render HQ less water soluble, the intermolecular interactions between the HQ molecules must be strengthened while simultaneously reducing the strength of the intermolecular interactions between the HQ molecules and water (H_2O) molecules (Scheme 4). The addition of the alkyl group will accomplish this by increasing the nonpolar, lipophilic surface area of the molecule, strengthening the van der Waals interactions between the HQ derivatives.

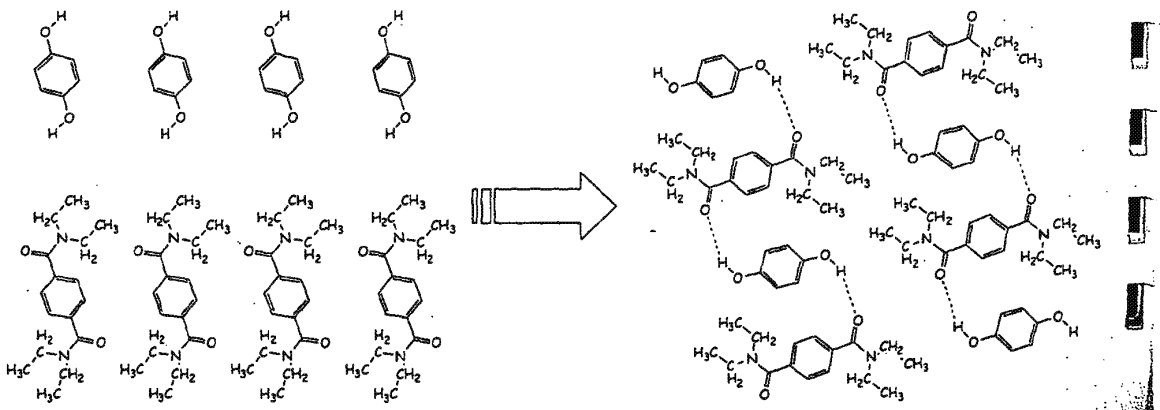
The process of molecular recognition and self-assembly occurs spontaneously in nature. Crystal engineering studies the mechanisms by which functional groups on molecules interact so as to align and orient molecular aggregates in ordered matrixes (Scheme 5).[1]

By taking advantage of this "natural tendency" of molecules to self-assemble in ordered matrixes, physical properties can be manipulated. In the same way that an HQ molecule can be made less water soluble by conventional covalent derivatization, its solubility can be equally reduced by incorporating it into a binary cocrystalline matrix.[2] For example, HQ can be cocrystallized with a terephthalamide molecule (Scheme 6). This 1:1 complex of HQ and, in this case, bis-[*N*,*N*-diethyl]terephthalamide can be considered a noncovalent derivative of HQ.[3]

The physical properties of the HQ are now modified by the terephthalamide (TPA) molecule by interfering with the intermolecular interactions between the HQ molecules and between the intermolecular interactions between the HQ molecules and the H_2O molecules (Scheme 7).

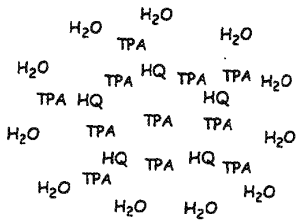
Using molecular recognition and self-assembly in the design of materials is an example of green chemistry.[4] Because the coproducts, byproducts, solvents, energy inputs, and purification procedures are often unnecessary when constructing noncovalent derivatives, the process is more environmentally sound. In terms of economic and environmental cost, it is far better to manipulate intermolecular interactions than breaking and forming covalent bonds. Noncovalent derivatization is not amenable to all material syntheses, but there certainly is application for this technique in many instances. If we can learn what molecules "want" to do in the first place, and then design processes to be consistent with these "natural tendencies", the result will be more environmentally benign mechanisms in terms of materials and energy consumption. As the field of crystal engineering continues to advance, hopefully

Scheme 6



NOVARTIS EXHIBIT 1517
Novartis v. Regents, IPR2023-01347
Page 1861 of 4460

Scheme 7



practitioners will attempt to embrace these toxicological and environmental benefits that this field affords.

Acknowledgment. We wish to thank the EPA (R825327), the Massachusetts Toxics Use Reduction Institute, and Pfizer, Inc., for financial support.

References

(1) (a) Desiraju, G. R. *Curr. Sci.* **2001**, *81*(8), 1038–1042. (b) Rogers, R. D. *NATO ASI Series, Series C: Math. Phys. Sci.* **1999**, *539*, 155–189. (c) Aakeroy, C. B.; Seddon, K. R. *Chem. Soc. Rev.* **1993**, *22*(6), 397–407.

(2) Warner, J. C. Pollution Prevention via Molecular Recognition and Self-Assembly: Non-Covalent Derivatization. In *Green Chemistry: Frontiers in Benign Chemical Synthesis and Processes*; Anastas, P., Williamson, T., Eds.; Oxford University Press: London, 1998; pp 336–346.

(3) (a) Guarrera, D.; Taylor, L. D.; Warner, J. C. *Chem. Mater.* **1994**, *6*, 1293. (b) Foxman, B. M.; Guarrera, D. J.; Taylor, L. D.; Warner, J. C. *Cryst. Eng.* **1998**, *1*, 109.

(4) Anastas, P. T.; Warner, J. C. *Green Chemistry: Theory and Practice*; Oxford University Press: London, 1998.

CG0255218

UM00013116

NOVARTIS EXHIBIT 1517
Novartis v. Regents, IPR2023-01347
Page 1862 of 4460

This Page is Inserted by IFW Indexing and Scanning Operations and is not part of the Official Record

BEST AVAILABLE IMAGES

Defective images within this document are accurate representations of the original documents submitted by the applicant.

Defects in the images include but are not limited to the items checked:

- ☐ BLACK BORDERS
- ☐ IMAGE CUT OFF AT TOP, BOTTOM OR SIDES
- ☐ FADED TEXT OR DRAWING
- ☐ BLURRED OR ILLEGIBLE TEXT OR DRAWING
- ☐ SKEWED/SLANTED IMAGES
- ☐ COLOR OR BLACK AND WHITE PHOTOGRAPHS
- ☐ GRAY SCALE DOCUMENTS
- ☐ LINES OR MARKS ON ORIGINAL DOCUMENT
- ☐ REFERENCE(S) OR EXHIBIT(S) SUBMITTED ARE POOR QUALITY
- ☐ OTHER: _____

IMAGES ARE BEST AVAILABLE COPY.
As rescanning these documents will not correct the image problems checked, please do not report these problems to the IFW Image Problem Mailbox.

Wood, A. W., Chang, R. L., Katz, M., Conney, A. H., Jerina, D. M., Sikka, H. C., Levin, W. & Kumar, S. (1989). *Cancer Res.* 49, 6981–6985.

Acta Cryst. (1999). C55, 399–401

2-Aminopyrimidine and *p*-phenylenediacetic acid (1:1) co-crystal

KANDASAMY CHINNAKALI,[a]† HOONG-KUN FUN,[a] SHYAMAPRASAD GOSWAMI,[b] AJIT KUMAR MAHAPATRA[b] AND GUR DAYAL NIGAM[c]

[a]*X-ray Crystallography Unit, School of Physics, Universiti Sains Malaysia, 11800 USM, Penang, Malaysia,* [b]*Department of Chemistry, Bengal Engineering College (Deemed University), Howrah 711 103, India, and* [c]*Department of Physics and Meteorology, Indian Institute of Technology, Kharagpur 721 302, West Bengal, India. E-mail: hkfun@usm.my*

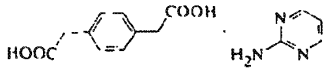
(*Received 16 September 1998; accepted 19 October 1998*)

Abstract

In the title co-crystal, each 2-aminopyrimidine molecule, $C_4H_5N_3$, participates in two eight-membered hydrogen-bonded rings with carboxylic acid groups from two different phenylenediacetic acid molecules, $C_{10}H_{10}O_4$. This results in infinite hydrogen-bonded chains. In the supramolecular structure, the chains are held together by weak C—H···O contacts.

Comment

Hydrogen bonds are used extensively as a tool to design the structure of molecular crystals, because of their strength, as well as their directional nature, compared to other intermolecular non-covalent interactions (Lehn, 1995). Most of the supramolecular crystals originate from strong N—H···*X* and O—H···*X* (*X* = O, N) hydrogen bonds. Weak C—H···O bonds are known to play a significant role in determining the molecular packing of organic solids (Taylor & Kennard, 1982). 2-Aminopyrimidine forms heterodimeric structures with different mono- and dicarboxylic acids (Etter & Adsmond, 1990; Etter *et al.*, 1990), rather than their individual self assembly (Scheinbeim *et al.*, 1976). We have also recently shown (Goswami *et al.*, 1999) that terephthalic acid forms chain-like heteroassemblies with 2-aminopyrimidine, similar to those formed by 2-aminopyrimidine and succinic acid (Etter *et al.*, 1990). In this paper, we report the supramolecular structure of the 2-aminopyrimidine–*p*-phenylenediacetic acid co-crystal, (I), *via* C—H···O hydrogen bonding.



(I)

The asymmetric unit consists of one half-molecule each of 2-aminopyrimidine and *p*-phenylenediacetic acid; the 2-aminopyrimidine lies on a crystallographic twofold axis passing through atoms N2, C6 and C8, and the *p*-phenylenediacetic acid is on an inversion centre.

Bond lengths and angles in the 2-aminopyrimidine agree with other reported values (Byriel *et al.*, 1992; Lynch *et al.*, 1994). The carboxylic acid group (O1, O2, C4 and C5) makes dihedral angles of 77.6 (1) and 2.5 (1)° with the planes of the phenyl ring and the 2-aminopyrimidine moiety, respectively. The planar 2-aminopyrimidine is linked to the *p*-phenylenediacetic acid by N2—H1N2···O1 and O2—H1O2···N1 intermolecular hydrogen bonds; along with C5 and C6, they form an eight-membered ring, which is coplanar with the pyrimidine moiety. Since both molecules lie across crystallographic symmetry elements, the hydrogen-bond system is extended to form an infinite chain-like structure in the solid state. Neighbouring chains along the *a* axis are linked by weak C4—H4*B*···O1^{i} contacts to form a supramolecular assembly (Fig. 2), in which the pyrimidine and phenyl rings are stacked with perpendicular separations of 3.605 (4) and 3.614 (4) Å, respectively [symmetry code: (i) $x-1, y, z$].

† On leave from: Department of Physics, Anna University, Chennai 600 025, India.

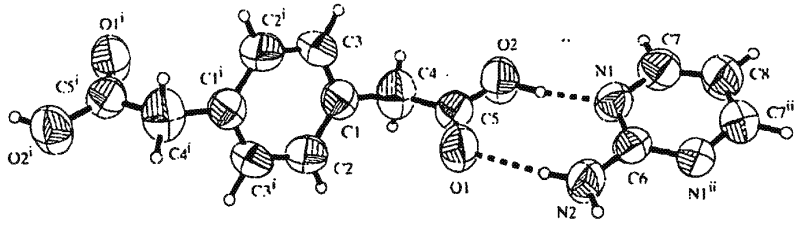


Fig. 1. The structure of the title co-crystal, showing 50% probability displacement ellipsoids and the atom-numbering scheme [symmetry codes: (i) $-x, 1-y, 1-z$; (ii) $1-x, y, \frac{1}{2}-z$].

© 1999 International Union of Crystallography
Printed in Great Britain – all rights reserved

UM00013118
NOVARTIS EXHIBIT 1517
Novartis v. Regents, IPR2023-01347
Page 1864 of 4460

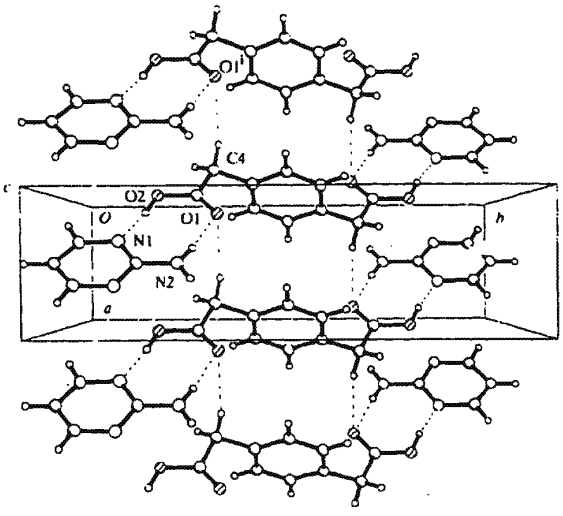


Fig. 2. A view of the supramolecular structure of (I) [symmetry code: (i) $x-1, y, z$].

Experimental

Single crystals of (I) were grown by slow evaporation of a dry acetone solution of 2-aminopyrimidine and *p*-phenylenediacetic acid (1:1 molar ratio).

Crystal data

$C_4H_5N_3{\cdot}C_{10}H_{10}O_4$	Mo $K\alpha$ radiation
M_r = 289.29	λ = 0.71073 Å
Orthorhombic	Cell parameters from 3724 reflections
Pbcn	θ = 2.77–33.18°
a = 4.5686 (1) Å	μ = 0.099 mm^{-1}
b = 15.7687 (2) Å	T = 293 (2) K
c = 20.1621 (4) Å	Block
V = 1452.50 (5) Å^3	0.58 × 0.44 × 0.38 mm
Z = 4	Colourless
D_x = 1.323 Mg m^{-3}	
D_m not measured	

Data collection

Siemens SMART CCD area-detector diffractometer	1286 reflections with $I > 2\sigma(I)$
ω scans	R_{int} = 0.033
Absorption correction: none	θ_{max} = 32°
11 260 measured reflections	$h = 0 \rightarrow 6$
2515 independent reflections	$k = 0 \rightarrow 23$
	$l = 0 \rightarrow 30$

Refinement

Refinement on F^2	$(\Delta/\sigma)_{max} < 0.001$
$R[F^2 > 2\sigma(F^2)]$ = 0.059	$\Delta\rho_{max}$ = 0.119 e Å^{-3}
$wR(F^2)$ = 0.161	$\Delta\rho_{min}$ = −0.096 e Å^{-3}
S = 1.084	Extinction correction: *SHELXTL* (Sheldrick, 1997)
2515 reflections	Extinction coefficient: 0.026 (3)
128 parameters	
All H-atom parameters refined	

$w = 1/[\sigma^2(F_o^2) + (0.045P)^2 + 0.2796P]$ where $P = (F_o^2 + 2F_c^2)/3$

Scattering factors from *International Tables for Crystallography* (Vol. C)

Table 1. *Fractional atomic coordinates and equivalent isotropic displacement parameters (Å^2)*

$U_{eq} = (1/3)\sum_i\sum_j U^{ij}a^i a^j \mathbf{a}_i\cdot\mathbf{a}_j$.

	x	y	z	U_{eq}
O1	0.1400 (3)	0.35048 (8)	0.64565 (7)	0.0956 (5)
O2	0.0011 (4)	0.22373 (9)	0.61149 (8)	0.0961 (5)
N1	0.3388 (4)	0.15077 (9)	0.70366 (7)	0.0756 (5)
N2	1/2	0.27532 (15)	3/4	0.0903 (8)
C1	−0.0970 (4)	0.42296 (11)	0.52668 (9)	0.0692 (5)
C2	−0.1812 (5)	0.49945 (14)	0.55305 (11)	0.0881 (6)
C3	0.0850 (5)	0.42488 (13)	0.47323 (10)	0.0867 (6)
C4	−0.1966 (6)	0.33973 (16)	0.55521 (14)	0.0929 (7)
C5	−0.0014 (4)	0.30613 (12)	0.60887 (9)	0.0718 (5)
C6	1/2	0.19082 (16)	3/4	0.0680 (6)
C7	0.3460 (5)	0.06616 (13)	0.70459 (10)	0.0864 (6)
C8	1/2	0.0207 (2)	3/4	0.0928 (9)

Table 2. *Selected bond lengths (Å)*

O1—C5	1.207 (2)	N1—C6	1.3469 (18)
O2—C5	1.300 (2)	N2—C6	1.333 (3)
N1—C7	1.335 (2)		

Table 3. *Hydrogen-bonding geometry (Å, °)*

D—H···A	D—H	H···A	D···A	D—H···A
O2—H1O2···N1	1.02 (3)	1.66 (3)	2.675 (2)	171 (2)
N2—H1N2···O1	0.90 (2)	2.02 (2)	2.922 (2)	174 (2)
C4—H4B···O1^i	1.00 (3)	2.56 (3)	3.541 (3)	168 (2)

Symmetry code: (i) $x-1, y, z$.

The data collection covered a hemisphere of reciprocal space by a combination of three sets of exposures; each set had a different φ angle (0, 88 and 180°) for the crystal and each exposure of 10 s covered 0.3° in ω. The crystal-to-detector distance was 4 cm ($2\theta_{max}$ = 66.36°) and the detector swing angle was −35°. Crystal decay was monitored by repeating 30 initial frames at the end of data collection and analysing the duplicate reflections, and was found to be negligible. Only reflections having 2θ less than 64° were used for structure solution and refinement, as only a few reflections were found to be observed at higher angles. The structure was solved by direct methods and refined by full-matrix least-squares techniques. All H atoms were located from a difference Fourier map and refined isotropically.

Data collection: *SMART* (Siemens, 1996). Cell refinement: *SAINT* (Siemens, 1996). Data reduction: *SAINT*. Program(s) used to solve structure: *SHELXTL* (Sheldrick, 1997). Program(s) used to refine structure: *SHELXTL*. Molecular graphics: *SHELXTL*. Software used to prepare material for publication: *SHELXTL* and *PLATON* (Spek, 1990).

SG and AKM are grateful to the CSIR, New Delhi, India, for financial support. The authors would also like to thank the Malaysian Government for research grant R&D No. 190-9609-2801. KC thanks the Universiti Sains Malaysia for a Visiting Post-Doctoral Fellowship.

Supplementary data for this paper are available from the IUCr electronic archives (Reference: HA1242). Services for accessing these data are described at the back of the journal.

UM00013119
NOVARTIS EXHIBIT 1517
Novartis v. Regents, IPR2023-01347
Page 1865 of 4460

References

Byriel, K. A., Kennard, C. H. L., Lynch, D. E., Smith, G. & Thompson, J. G. (1992). *Aust. J. Chem.* **45**, 969–981.

Etter, M. C. & Adsmond, D. A. (1990). *J. Chem. Soc. Chem. Commun.* pp. 589–591.

Etter, M. C., Adsmond, D. A. & Britton, D. (1990). *Acta Cryst.* C**46**, 933–934.

Goswami, S., Mahapatra, A. K., Ghosh, K., Nigam, G. D., Chinnakali, K. & Fun, H.-K. (1999). *Acta Cryst.* C**55**, 87–89.

Lehn, J. M. (1995). *Supramolecular Chemistry*, edited by U. Anton, pp. 1–171. New York: VCH.

Lynch, D. E., Smith, G., Freney, D., Byriel, K. A. & Kennard, C. H. L. (1994). *Aust. J. Chem.* **47**, 1097–1115.

Scheinbeim, J. & Schempp, E. (1976). *Acta Cryst.* B**32**, 607–609.

Sheldrick, G. M. (1997). *SHELXTL. Structure Determination Programs*. Version 5.10. Bruker Analytical X-ray Systems, Madison, Wisconsin, USA.

Siemens (1996). *SMART* and *SAINT. Area Detector Control and Integration Software*. Siemens Analytical X-ray Instruments Inc., Madison, Wisconsin, USA.

Spek, A. L. (1990). *Acta Cryst.* A**46**, C-34.

Taylor, R. & Kennard, O. (1982). *J. Am. Chem. Soc.* **104**, 5063–5070.

Acta Cryst. (1999). C**55**, 401–403

2-[3-(Pyrrolidin-1-yl)cyclohex-2-en-1-ylidene]propanedinitrile

S. Selladurai,[a] R. Chandrasekaran,[a] L. Govindasamy,[b] P. Murugan[c] and V. T. Ramakrishnan[c]

[a]*Department of Physics, Madras Institute of Technology, Anna University, Chromepet, Chennai-44, India,* [b]*Department of Crystallography and Biophysics, University of Madras, Guindy Campus, Chennai-25, India, and* [c]*Department of Organic Chemistry, University of Madras, Guindy Campus, Chennai-25, India. E-mail: mit@md2.vsnl.net.in*

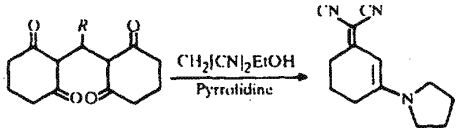
(*Received 30 March 1998; accepted 14 July 1998*)

Abstract

In the title compound, $C_{13}H_{15}N_3$, the cyclohexene ring adopts a conformation intermediate between sofa and half-chair, and the substituted pyrrolidine ring assumes a conformation intermediate between envelope and half-chair. The dihedral angle between the pyrrolidine and cyclohexene rings is 7.2 (1)°. The propanedinitrile group occupies the equatorial position with respect to the cyclohexene ring.

Comment

Applications of malononitrile in organic chemistry comprise the synthesis of unique heterocyclic systems, pharmaceuticals, pesticides, fungicides and solvato-chromic dyes (Fatiadi, 1978). The pyrrolidine part of the title compound has useful medicinal properties. Pyrrolidine derivatives inhibit the production of prostaglandin E2 and intracellular phospholipase A2, and are useful for prevention and treatment of rheumatoid arthritis, asthma, allergies, rhinitis and related diseases (Mitsuaki *et al.*, 1997). Some of the aminopyrrolidine products are used as pharmaceutical and agrochemical intermediates (Fumiaki & Shozo, 1997). The pyrrolidine–cyclohexyl compounds act as highly-lipophilic chemically-novel potent selective kappa opioid agonists (Sabin *et al.*, 1997) and were found to be preferential dopamine autoreceptor antagonists (Haekan *et al.*, 1997). Some of the arylpyrrolidine derivatives are used as insecticides, acaricides and herbicides (Santel *et al.*, 1997). In view of the above medicinal significance, the title compound was investigated to define the conformation of the cyclohexene ring with respect to the pyrrolidine ring of the molecule.



(1) R = H
(2) R = CH_3

(3)

An *ORTEP* drawing (Zsolnai, 1997) of the molecule with atomic numbering scheme is shown in Fig. 1. Cremer & Pople (1975) puckering parameters show that the cyclohexene ring is in a half-chair conformation, distorted towards a half-boat [Q = 0.461 (2) Å, θ = 56.0 (2)° and φ = −111.8 (3)°] (Duax & Norton, 1975; Caracelli *et al.*, 1997). The conformation of the pyrrolidine ring assumes an intermediate between an envelope and a half-chair conformation as seen by the ring puckering parameters [Q = 0.129 (4) Å and φ = 52.1 (1)°] (Zukerman-Schpector *et al.*, 1984). C11 and C12 in the pyrrolidine ring have high anisotropic dis-

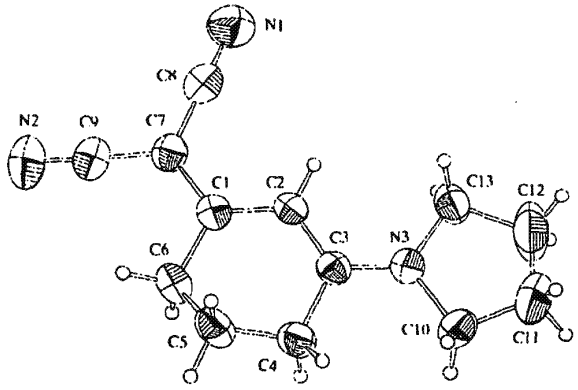


Fig. 1. Molecular structure of the title compound with 50% probability displacement ellipsoids. H atoms have been assigned as circles of an arbitrary radius.

© 1999 International Union of Crystallography
Printed in Great Britain – all rights reserved

UM00013120
NOVARTIS EXHIBIT 1517
Novartis v. Regents, IPR2023-01347
Page 1866 of 4460

Acta Crystallographica Section C
Crystal Structure Communications
ISSN 0108-2701

Cocrystallization of melaminium levulinate monohydrate

Chan Soo Choi,[a,b] Ramaiyer Venkatraman,[b] Eun Hee Kim,[c] Hae Sook Hwang[a] and Sung Kwon Kang[c]*

[a]Division of Hi-Tech. Materials Science, Daejeon University, Daejeon 300-716, South Korea, [b]Department of Chemistry, Jackson State University, Mississippi 39217, USA, and [c]Department of Chemistry, Chungnam National University, Daejeon 305-764, South Korea
Correspondence e-mail: skkang@cnu.ac.kr

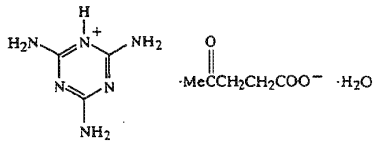
Received 5 January 2004
Accepted 5 March 2004
Online 31 March 2004

Crystals of 2,4,6-triamino-1,3,5-triazin-1-ium levulinate (4-oxopentanoate) monohydrate, $C_3H_7N_6^+\cdot C_5H_7O_3^-\cdot H_2O$, are formed *via* self-assembled hydrogen bonding by cocrystallization of melamine and levulinic acid. Two N—H···N hydrogen bonds and four N—H···O hydrogen bonds connect two melaminium entities such that each of two pairs of N—H···O bonds bridges two H atoms belonging to the amine groups of two different melaminium cations *via* the carbonyl O atom of one levulinate molecule.

Comment

One of the primary objectives of crystal engineering is the construction of self-assembled hydrogen-bonded molecular materials (Desiraju, 1996; Philip & Stoddart, 1996). Currently, many research groups are involved in synthesizing one-, two- and three-dimensional clustered self-assembled hydrogen-bonding superlattice structures (Zerkowski *et al.*, 1990; Whitesides *et al.*, 1991; Ghadiri *et al.*, 1993; Mathias, Simanek & Whitesides, 1994; Mathias, Simanek, Zerkowski *et al.*, 1994; Kimizuka *et al.*, 1995; Lange *et al.*, 1997), while others are synthesizing metal-ion-incorporated systems (Goddgame *et al.*, 1999; Zhang *et al.*, 1999). Various studies have been carried out using melamine and its derivatives as versatile components, because the presence of amino groups in these compounds means that they can easily form several types of self-organized superlattices with suitable hydrogen-bonding donor and acceptor molecules (Janczak & Perpétuo, 2001*a*,*b*,*c*,*d*; Perpétuo & Janczak, 2002). The combination of levulinic acid with melamine leads to the formation of a 1:1 adduct, namely 2,4,6-triamino-1,3,5-triazin-1-ium levulinate monohydrate, $C_3H_7N_6^+\cdot C_5H_7O_3^-\cdot H_2O$, (I), the crystal structure of which is reported here.

The asymmetric unit of (I) consists of two oppositely charged ions, *viz.* a protonated melaminium ion and a levulinate ion, and one water molecule (Fig. 1). Two melaminium entities are connected to one another *via* two N6—H···N3 hydrogen bonds, two N5—H···O3 hydrogen bonds and two N6—H···O3 hydrogen bonds; specifically, the four N—H···O interactions bridge four amine H atoms belonging to two different melaminium entities *via* the carbonyl O atoms of two levulinate ions. In addition, two N4—H···O1*W* and two O1*W*—H···O1 hydrogen bonds link the two cations and two anions. The bridging water molecules and the bridging carbonyl O atoms between the melaminium and levulinate entities form large pores (0*L* and 0*R* in Fig. 1). Finally, two water molecules, O1W^{ii} and O1W^{iii}, are involved in bridging melaminium and levulinate entities in the next row along the *b* axis [symmetry codes: (ii) $-x, -\frac{1}{2}+y, \frac{1}{2}-z$; (iii) $x, \frac{1}{2}-y, \frac{1}{2}+z$]. There are hydrogen bonds between water molecules and the O1 atoms of the levulinate anions (Table 2).



(I)

The six-membered aromatic ring of the melaminium ion exhibits slight distortions from the ideal hexagonal form (Janczak & Perpétuo, 2001*c*) and from the structure of neutral melamine (Hughes, 1941). The C2—N2—C1 angle (Table 1) at the protonated N atom of the melaminium entity is 4° larger than the C1—N1—C3 angle at a non-protonated N atom. Also, the N1—C3—N3 angle, involving the non-protonated ring N atoms, is about 5° larger than the N3—C2—N2 angle, involving protonated and non-protonated N atoms. The contraction of the C1—N1—C3 and C2—N3—C3 angles from 120 to ~115° appears to be correlated with expansion of the

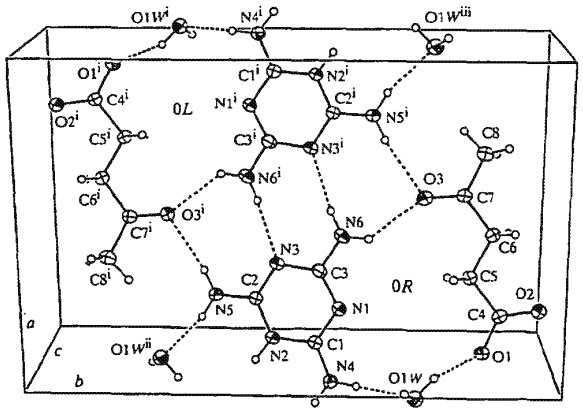


Figure 1
The molecular structure and unit-cell contents of (I), showing the atom-numbering scheme and 30% probability displacement ellipsoids. Pores formed by hydrogen bonds between melaminium cations and levulinate anions are designated 0*L* and 0*R*. [Symmetry codes: (i) $1-x, -y, 1-z$; (ii) $-x, -\frac{1}{2}+y, \frac{1}{2}-z$; (iii) $x, \frac{1}{2}-y, \frac{1}{2}+z$.]

 DOI: 10.1107/S0108270104005207 © 2004 International Union of Crystallography

UM00013121
NOVARTIS EXHIBIT 1517
Novartis v. Regents, IPR2023-01347
Page 1867 of 4460

N1—C3—N3 angle to ~127°, while the N1—C1—N2 and N3—C2—N2 angles are both close to ideal, as is the C2—N2—C1 angle. On the other hand, the C2—N2—C1 and C1—N1—C3 angles are 3° larger than the equivalent angle (116°) in neutral melamine (Hughes, 1941). The N1—C3—N3 and N3—C2—N2 angles are similar to those in neutral melamine.

Experimental

An aqueous solution (50 ml) of levulinic acid (0.22 g, 2 mmol) was added to melamine (0.26 g, 2 mmol) dissolved in hot water (100 ml). The resulting solution was cooled slowly to ambient temperature and filtered. Colorless crystals of (I) appeared after the solution had been left to stand for several days in the presence of air at room temperature.

Crystal data

$C_3H_7N_6^+ \cdot C_5H_7O_3^- \cdot H_2O$
$M_r = 260.27$
Monoclinic, $P2_1/c$
$a = 10.538\ (2)$ Å
$b = 16.214\ (3)$ Å
$c = 7.1988\ (14)$ Å
$\beta = 95.85\ (3)°$
$V = 1223.6\ (4)$ Å^3
$Z = 4$
$D_x = 1.413$ Mg m^{-3}
Mo $K\alpha$ radiation
Cell parameters from 23 reflections
$\theta = 11.3–13.9°$
$\mu = 0.11$ mm^{-1}
$T = 293\ (2)$ K
Block, colorless
0.46 × 0.43 × 0.36 mm

Data collection

Enraf–Nonius CAD-4 diffractometer
Non-profiled $\omega/2\theta$ scans
5931 measured reflections
2806 independent reflections
1899 reflections with $I > 2\sigma(I)$
$R_{int} = 0.030$
$\theta_{max} = 27.5°$
$h = -13 \rightarrow 13$
$k = -21 \rightarrow 21$
$l = 0 \rightarrow 9$
3 standard reflections
every 400 reflections
intensity decay: 1%

Refinement

Refinement on F^2
$R[F^2 > 2\sigma(F^2)] = 0.048$
$wR(F^2) = 0.137$
$S = 1.02$
2806 reflections
175 parameters
H atoms treated by a mixture of independent and constrained refinement
$w = 1/[\sigma^2(F_o^2) + (0.0639P)^2 + 0.3261P]$ where $P = (F_o^2 + 2F_c^2)/3$
$(\Delta/\sigma)_{max} < 0.001$
$\Delta\rho_{max} = 0.28$ e Å^{-3}
$\Delta\rho_{min} = -0.19$ e Å^{-3}

Table 1
Selected geometric parameters (Å, °).

O1—C4	1.277 (2)	N2—C1	1.372 (2)
O2—C4	1.224 (2)	N3—C2	1.325 (2)
O3—C7	1.208 (2)	N3—C3	1.355 (2)
N1—C1	1.328 (2)	N4—C1	1.312 (2)
N1—C3	1.337 (2)	C4—C5	1.515 (2)
N2—C2	1.351 (2)		
C1—N1—C3	115.18 (16)	N1—C3—N3	127.00 (16)
C2—N2—C1	119.03 (15)	O2—C4—O1	123.83 (17)
C2—N3—C3	115.05 (15)	O2—C4—C5	119.90 (16)
N1—C1—N2	121.66 (16)	O1—C4—C5	116.27 (16)
N3—C2—N2	122.03 (17)		

Table 2
Hydrogen-bonding geometry (Å, °).

D—H···A	D—H	H···A	D···A	D—H···A
N2—H2···O1^{iv}	0.89 (2)	1.80 (2)	2.689 (2)	179 (2)
O1W—H1W···O1	0.86 (3)	1.90 (3)	2.697 (2)	154 (3)
O1W—H2W···O1^{v}	0.85 (3)	1.99 (3)	2.825 (2)	168 (3)

Symmetry codes: (iv) $-x, y-\frac{1}{2}, \frac{1}{2}-z$; (v) $x, \frac{1}{2}-y, z-\frac{1}{2}$.

H atoms on atoms N2 and O1W were located in a difference map and their parameters were refined isotropically. All other H atoms were positioned geometrically and constrained to ride on their parent atoms, with U_{iso}(H) values of $1.2U_{eq}$(C,N) (CH_2 and NH_2 H atoms) or $1.5U_{eq}$(C) (CH_3 H atoms).

Data collection: *CAD-4 EXPRESS* (Enraf–Nonius, 1994); cell refinement: *CAD-4 EXPRESS*; data reduction: *XCAD4* (Harms & Wocadlo, 1995); program(s) used to solve structure: *SHELXS97* (Sheldrick, 1997); program(s) used to refine structure: *SHELXL97* (Sheldrick, 1997); molecular graphics: *ORTEP-3 for Windows* (Farrugia, 1997); software used to prepare material for publication: *WinGX* (Farrugia, 1999).

This work was supported by a grant (No. R01-2001-000-00055-0) from the Korea Science and Engineering Foundation and by a grant from Chungnam National University.

Supplementary data for this paper are available from the IUCr electronic archives (Reference: SQ1149). Services for accessing these data are described at the back of the journal.

References

Desiraju, G. R. (1996). *The Crystal as a Supermolecular Entity*. New York: Wiley.
Enraf–Nonius (1994). *CAD-4 EXPRESS*. Enraf–Nonius, Delft, The Netherlands.
Farrugia, L. J. (1997). *J. Appl. Cryst.* **30**, 565.
Farrugia, L. J. (1999). *J. Appl. Cryst.* **32**, 837–838.
Ghadiri, M. R., Granja, J. R., Milligan, R. A., McRee, D. E. & Khazanovich, N. (1993). *Nature (London)*, **366**, 324–327.
Goddgame, D. M. L., Hussain, I., White, A. J. P. & Williams, D. J. (1999). *J. Chem. Soc. Dalton Trans.* pp. 2899–2900.
Harms, K. & Wocadlo, S. (1995). *XCAD4*. University of Marburg, Germany.
Hughes, E. W. (1941). *J. Am. Chem. Soc.* **63**, 1737–1752.
Janczak, J. & Perpétuo, G. J. (2001*a*). *Acta Cryst.* C**57**, 123–125.
Janczak, J. & Perpétuo, G. J. (2001*b*). *Acta Cryst.* C**57**, 873–875.
Janczak, J. & Perpétuo, G. J. (2001*c*). *Acta Cryst.* C**57**, 1120–1122.
Janczak, J. & Perpétuo, G. J. (2001*d*). *Acta Cryst.* C**57**, 1431–1433.
Kimizuka, N., Kawasaki, T., Hirata, K. & Kunitake, T. (1995). *J. Am. Chem. Soc.* **117**, 6360–6361.
Lange, R. F. M., Beijer, F. H., Sijbesma, R. P., Hooft, R. W. W., Kooijman, H., Spek, A. L., Kroon, J. & Meijer, E. W. (1997). *Angew. Chem. Int. Ed. Engl.* **36**, 969–971.
Mathias, J. P., Simanek, E. E. & Whitesides, G. M. (1994). *J. Am. Chem. Soc.* **116**, 4326–4340.
Mathias, J. P., Simanek, E. E., Zerkowski, J. A., Seto, Ch. T. & Whitesides, G. M. (1994). *J. Am. Chem. Soc.* **116**, 4316–4325.
Perpétuo, G. J. & Janczak, J. (2002). *Acta Cryst.* C**58**, o112–o114.
Philip, D. & Stoddart, J. F. (1996). *Angew. Chem. Int. Ed. Engl.* **35**, 1154–1196.
Sheldrick, G. M. (1997). *SHELXL97* and *SHELXS97*. University of Göttingen, Germany.
Whitesides, G. M., Mathias, J. P. & Seto, C. T. (1991). *Science*, **254**, 1312–1319.
Zerkowski, J. A., Seto, C. T., Wierda, D. A. & Whitesides, G. M. (1990). *J. Am. Chem. Soc.* **112**, 9025–9026.
Zhang, Y., Jianmin, L., Nishiura, M. & Imamoto, T. (1999). *Chem. Lett.* pp. 543–544.

UM00013122
NOVARTIS EXHIBIT 1517
Novartis v. Regents, IPR2023-01347
Page 1868 of 4460

ACKNOWLEDGMENTS AND ADDRESSES

Received March 10, 1972, from the *Medical Research Department, ICI America Inc., Wilmington, DE 19899*

Accepted for publication May 5, 1972.

Presented in part at the 55th Annual Meeting of the Federation of American Societies for Experimental Biology, April 12–17, 1971.

▲ To whom inquiries should be directed.

Complexation of Acetaminophen with Methyl Xanthines

Y. P. CHOW and A. J. REPTA▲

Abstract □ The interaction, in aqueous solution, of acetaminophen with caffeine, theophylline, and theobromine was investigated. Caffeine and theophylline form isolatable crystalline 1:1 complexes with acetaminophen, while theobromine apparently does not complex with acetaminophen. The caffeine–acetaminophen complex was found to exist in three forms, differing only in the degree of solvation. The solubility and dissolution rates of some of the caffeine–acetaminophen and theophylline–acetaminophen complexes were determined.

Keyphrases □ Acetaminophen—complexation with methyl xanthines, particularly caffeine and theophylline □ Caffeine–acetaminophen complexes—isolation, solubility, dissolution rates, stability constants □ Theophylline–acetaminophen complexes—isolation, solubility, dissolution rates, stability constants □ Complex formation—acetaminophen with methyl xanthines □ Analgesic availability—effect of complexation

Many studies have shown that caffeine and related xanthines are capable of interacting in aqueous media with a variety of drugs through complexation (1).

In a recent search of the literature relative to the possible influence of complexation on the availability of analgesics, it became obvious that the effect of the interaction of acetaminophen with the methyl xanthines had not been reported.

Although acetaminophen and caffeine are present in many commercial analgesic products (2), the role or purpose of caffeine as a therapeutically active ingredient may be doubtful. However, such combinations may exhibit physical–chemical interactions of pharmaceutical interest and importance from a formulation standpoint.

EXPERIMENTAL

Equipment[1]—Constant-temperature water baths were used which maintained the temperature at 25 ± 0.1°. Tablets for the dissolution studies were prepared using a Carver press and a flat-face punch and die with a diameter of 1.27 cm. (0.5 in.). The dissolution apparatus consisted of a 500-ml., two-necked round-bottom flask immersed in a constant-temperature bath. The dissolution medium (350 ml. of water) was stirred through the central neck of the flask using a stirring motor[2] and an L-shaped glass stirrer located 2.5 cm. above the bottom of the flask. The stirring rod was fashioned from a 7-mm. glass rod, as shown in Fig. 1.

Table I—Amounts of Substrate and Ligand Used in the Various Solubility Studies

Substrate	Ligand
Acetaminophen, 2 g.	Caffeine, 0–3.1 g.
Acetaminophen, 1.5 g.	Theophylline, 0–2.4 g.
Theobromine, 0.03 g.	Acetaminophen, 0–0.32 g.

Materials—Caffeine, theophylline, theobromine, and acetaminophen were recrystallized from distilled water, dried to constant weight, and shown to be anhydrous by differential scanning calorimetry and/or NMR. Melting points were found to be in good agreement with literature values (3). All water used was distilled from acid permanganate solution in an all-glass apparatus. The NMR spectra were obtained in deuterated dimethyl sulfoxide (97.5% isotopic purity). All other reagents were of analytical or reagent grade.

Methods—*Solubility Study*—A certain quantity of substrate, in excess of its aqueous solubility, was placed in 30-ml. glass, screw-capped vials together with increasing but accurately weighed amounts of ligand (Table I) and 20 ml. of distilled water. The vials were sealed and fixed on a rotating shaft in a constant-temperature bath and equilibrated for 48 hr. at 25 ± 0.1°. Aliquot portions of the

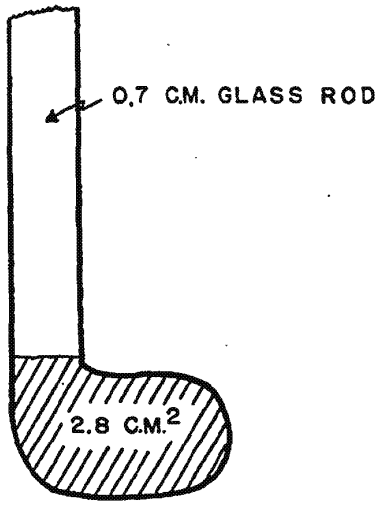


Figure 1—*Shape and dimensions of glass stirrer used in dissolution rate studies.*

[1] Spectrophotometric measurements were made using a Cary model 14 or 15 spectrophotometer. Differential scanning calorimetry was performed using a Perkin-Elmer model DSC-1B differential scanning calorimeter. The Varian model T-60 was used for obtaining NMR spectra.

[2] Inframo model RZR64.

UM00013123
NOVARTIS EXHIBIT 1517
Novartis v. Regents, IPR2023-01347
Page 1869 of 4460

Table II—Molar Absorptivities of the Various Components at 25° and the Conditions under which They Were Determined

Components	Absorptivities, l cm.$^{-1}$ M^{-1}: 257.5 nm. in pH 12 Aqueous Solution	276.5 nm. in Chloroform	248.5 nm. in Methanol	271 nm. in Methanol	272 nm. in Methanol	273 nm. in Methanol
Acetaminophen	10,380	—	13,300	3700	3230	2970
Caffeine	—	9600	2,640	—	—	9240
Theophylline	—	—	3,140	9680	—	—
Theobromine	—	—	2,680	—	9260	—

supernatant liquid were removed using a pipet (whose tip had been wrapped with glass wool) and analyzed by the procedures described later. In the acetaminophen–caffeine system, glass wool (or a tiny crystal of the complex) was added to induce crystal formation prior to sampling.

Isolation of Complexes—The complexes were isolated during the solubility studies. The acetaminophen–caffeine complex did not precipitate spontaneously during solubility studies, and it was necessary to induce crystallization by introducing a small piece of glass wool into the solutions and allowing them to remain at 25° for about 1 hr. The resulting precipitate was then separated by filtration. The damp residue melted over a range of 40–45°. When the precipitate was allowed to air dry for several hours and then placed in a vacuum oven at 40° and a pressure of 2 mm. of mercury for 24–48 hr., the resulting anhydrous material melted at about 145°. The preparation of the monohydrate acetaminophen–caffeine complex (melting point ~85°) is described below.

In the case of the acetaminophen–theophylline complexes, precipitation occurred spontaneously during the solubility studies. The precipitate was removed by filtration, and the damp precipitate melted at about 55°. Complete drying in a vacuum oven resulted in the anhydrous complex which melted at ~192–195°.

Dissolution Rate Study—All dissolution studies were performed according to the following method.

Approximately 300 mg. of the material to be tested was compressed at 2270 kg. (5000 lb.) into a tablet. The weight and surface area of the tablet were then determined. The tablet was then placed in the 350 ml. of water contained in the dissolution apparatus and the time was noted. One- or two-milliliter samples were withdrawn at the appropriate times through the side arm of the flask. A pipet whose tip was wrapped in glass wool was used to remove the sample. The samples were analyzed as described below.

Analytical Procedure—The analysis of all compounds was done by spectrophotometric measurements after appropriate treatment of the various samples. The absorptivities of the various compounds under the conditions at which they were measured are given in Table II.

1. Acetaminophen–caffeine—In the acetaminophen–caffeine system, caffeine was separated from acetaminophen by adjusting the pH of the aqueous solution of the compounds to 12 with 0.1 *N* NaOH solution [pKa of acetaminophen was determined as 10.15, pKa of caffeine is 14 (3)] and extracting with chloroform. Aliquots of the aqueous portion, containing the sodium salt of acetaminophen, were diluted with an equal volume of pH 12 buffer, and the absorbance was measured at 257.5 nm. The aliquot of chloroform extract, containing caffeine, was diluted with an equal volume of chloroform and the absorbance was measured at 276.5 nm. (Table II).

2. Acetaminophen–theophylline—Multicomponent analysis by spectrophotometry (4) was used in this system. The absorptivities (Table II) were obtained from Beer's law plots which were made by dissolving known weights of sample in methanol. The concentrations of acetaminophen and theophylline were determined by taking 1 ml. of aqueous sample, diluted 1:5000 or 1:10,000 with methanol, and measuring the absorbances at 248.5 and 271 nm.

3. Acetaminophen–theobromine—Multicomponent analysis (4) by spectrophotometry was also used in this system. The concentrations of acetaminophen and theobromine were determined at 248.5 and 272 nm. after appropriate dilution of the samples.

Structure of Complexes—To determine the degree of hydration of the acetaminophen–caffeine complex which was precipitated, and to demonstrate that the acetaminophen–caffeine complexes differed only in the degree of hydration, the following experiment was carried out.

A sample of the appropriate complex was place in an open vial, and the vial was then placed in a vessel containing a saturated aqueous barium chloride solution and excess barium chloride. This system was then sealed and placed in a water bath at 25°. The activity of water on the saturated barium chloride solution was reported (5) to be 0.90. The experimental design did not permit direct contact beteen the barium chloride solution and the sample, but it did allow water to be transferred *via* the vapor phase. The melting behavior, as reflected by differential scanning calorimetric recording, was checked at various times under the conditions employed. When no further change was observed for the "freshly filtered sample" (after about 3–4 weeks), a portion of the sample was weighed and then dried completely and reweighed. The loss in weight was attributed to water loss. The complex was shown in this way to contain about 6.4 molecules of water. The NMR spectrum also showed 6 moles of water/mole of the 1:1 acetaminophen–caffeine complex.

RESULTS AND DISCUSSION

The complexation of acetaminophen with each of the compounds (caffeine, theophylline, and theobromine) was studied at 25° in

Table III—Initial Dissolution Rate of Acetaminophen, Caffeine, and Theophylline from Tablets at 25° in Water[a]

Tablet Composition	Initial Dissolution Rate[b] of Components, *M* cm.$^{-1}$ min.$^{-1}$ × 10^5: Acetaminophen	Caffeine	Theophylline
Pure acetaminophen	0.90	—	—
Pure caffeine	—	1.10	—
Pure theophylline	—	—	0.50
Hexahydrate complex of acetaminophen–caffeine	0.67	0.67	—
Monohydrate complex of acetaminophen–caffeine	2.75	2.75	—
Anhydrous complex of acetaminophen–caffeine	2.50	2.50	—
Anhydrous complex of acetaminophen–theophylline	0.66	—	0.76
Physical mixture of[c] acetaminophen–caffeine	3.80	3.80	—
Physical mixture of[d] acetaminophen–theophylline	0.72	—	1.07

[a] Stirring rate was 120 r.p.m. [b] Based on initial surface area of tablet. [c] Coprecipitate (see text for further discussion). [d] Mixture of powdered acetaminophen and theophylline.

UM00013124
NOVARTIS EXHIBIT 1517
Novartis v. Regents, IPR2023-01347
Page 1870 of 4460

Table IV—Summary of Data for the Complexation of Acetaminophen with Caffeine, Theophylline, and Theobromine at 25° in Water

System	Evidence of Complexation	Stoichiometry of Complex —(Acetaminophen–Xanthine)— Chemical	Calculated	Initial Slope (Fig. 1)	$K_{1:1}$ (l. mole)	Solubility[a] of Complex (mole l.)
Acetaminophen–caffeine	Yes	1	1.10	0.838	59.4	~0.1
Acetaminophen–theophylline	Yes	1	1.03	0.614	16.1	~0.05
Acetaminophen–theobromine	No	—	—	—	—	—

[a] Estimated from increase in total acetaminophen concentration in Fig. 2.

water using the solubility method (1). The equilibrium phase solubility diagrams obtained for the acetaminophen–caffeine and acetaminophen–theophylline systems are shown in Fig. 2. In both of these systems, the solubility of the substrate (acetaminophen) was found to be increased by the addition of the ligand. Furthermore, both systems deposited crystalline complexes at higher concentration of ligand. These complexes were isolated, dried, and analyzed. Both were found to contain 1 mole of ligand/mole of substrate. The acetaminophen–theobromine system, however, did not give any evidence of complexation. Even when theobromine was employed as the substrate in the presence of a 12-fold excess of acetaminophen, there was no detectable changes in solubility and no crystalline complex was formed. These results may have been due in part to a lack of sensitivity of the analytical method employed; but it is safe to say that if any complexation did occur, it was negligible relative to that observed for the acetaminophen–caffeine and acetaminophen–theophylline systems.

Calculation of the stoichiometry of the acetaminophen–caffeine and acetaminophen–theophylline complexes based on the data in the plateau region (1) of the respective diagrams in Fig. 2 were in good agreement with those obtained by isolation and analysis of the crystalline complexes as indicated in Table II. The slightly greater value of the stoichiometric ratio of acetaminophen to caffeine in the complex as found from calculation based on the solubility diagram suggests that complexes consisting of two or more molecules of acetaminophen per molecule of caffeine exist in solution but are not precipitated. On the basis of the formation of the 1:1 complex, the stability constants for both systems were calculated (1). These are listed in Table IV along with the approximate solubility of each complex as calculated from the increased solubility of acetaminophen for each system. The stability constants are in general agreement in both rank and magnitude with those found for similar systems (1).

An interesting observation made in the studies involving acetaminophen and caffeine was that the precipitation of the complex was not spontaneous. When sealed vials containing acetaminophen and caffeine in four- to fivefold excess of their equilibrium solubility were equilibrated at 25°, a clear solution resulted which did not produce a precipitate over periods of up to 2 weeks. Only when glass wool or a crystal of complex was introduced did crystallization occur.

In the process of isolating and determining the stoichiometry of the crystalline complexes, it was noted that the melting point of the solids changed with time. This was especially noticeable with the acetaminophen–caffeine complex. When the freshly filtered solid was air dried for 1–2 hr. and then heated in a sealed capillary, the solid (AC-I) melted at about 42–50°. When allowed to air dry for about 24–48 hr., the resultant material (AC-II) melted at about 75–80°. If the solid was exhaustively dried in a vacuum oven at 40° and about 2 mm. of mercury, the resulting anhydrous solid (AC-III) melted at about 145°. Analysis of all three solids demonstrated that each contained acetaminophen and caffeine in an equimolar ratio and that the difference in melting points was due to water of hydration.

In the case of AC-II, spectrophotometric analysis, weight loss on drying, and NMR showed the complex to be a monohydrate. AC-III was found to be anhydrous. The water content of AC-I was not easily determined, however, due to the rapidity of water loss. To determine the composition of AC-I and to establish whether or not the hydration and dehydration were reversible, the following experiment was carried out. Samples of AC-III, AC-II, and the freshly filtered complex (presumably wet AC-I) were equilibrated at 25° with an aqueous solution in which the water activity was 0.9 (3). The resulting changes in the samples were followed by differential scanning calorimetry as a function of time.

The appearance, shape, and location of endotherms at various times of equilibration are shown schematically in Fig. 3. As indicated, all samples exhibited only a single endotherm before

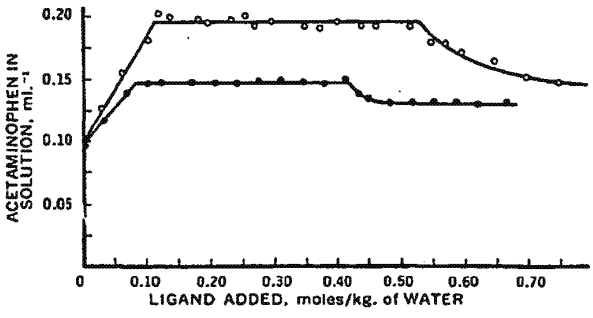


Figure 2—*Solubility of acetaminophen as a function of caffeine* (○) *or theophylline* (●) *added.*

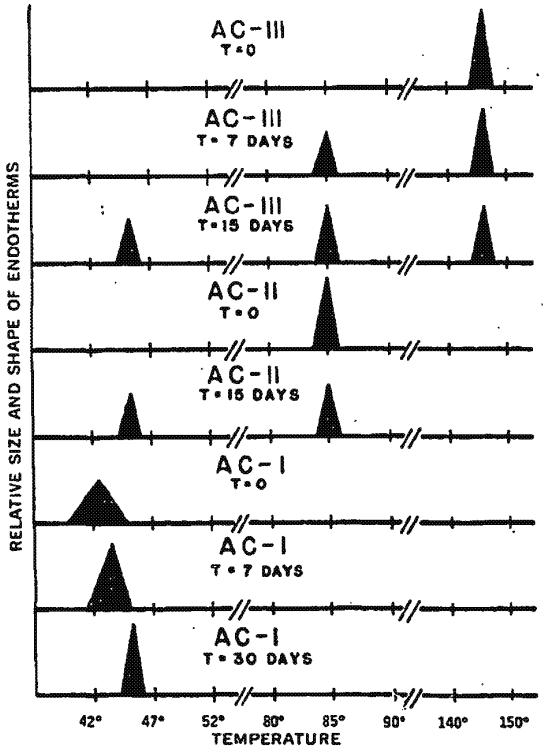


Figure 3—*Schematic diagram of the changes in differential scanning calorimetric recording of samples of AC-III, AC-II, and wet AC-I as a function of the time of equilibration at 25°. (See text for further discussion.)*

UM00013125
NOVARTIS EXHIBIT 1517
Novartis v. Regents, IPR2023-01347
Page 1871 of 4460

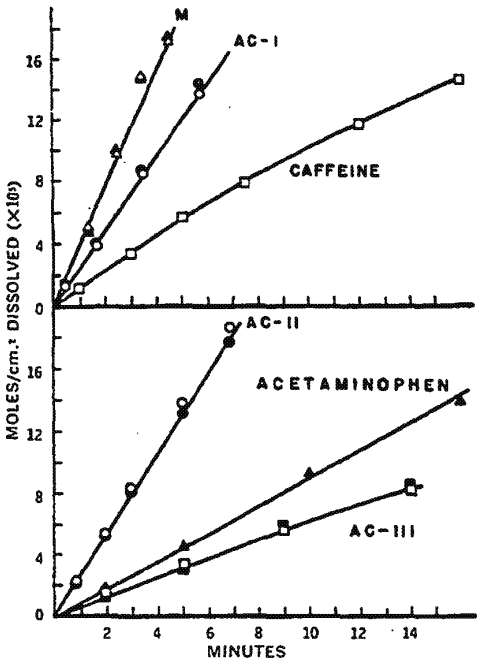


Figure 4—*Dissolution in water at 25° of acetaminophen (closed symbols) and caffeine (open symbols) from tablets of AC-III, AC-II, AC-I, caffeine, acetaminophen, and an equimolar mixture of acetaminophen and caffeine (M).*

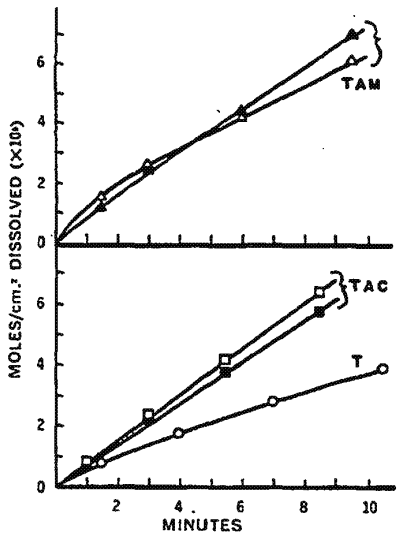


Figure 5—*Dissolution in water at 25° of acetaminophen (closed symbols) and theophylline (open symbols) from tablets of anhydrous theophylline (T), an anhydrous theophylline–acetaminophen complex (TAC), and an equimolar physical mixture of acetaminophen and theophylline (TAM).*

equilibration. With AC-III and AC-II the endotherms were quite sharp, in contrast with those seen for AC-I. As the time of equilibration increased, both AC-II and AC-III developed additional endotherms corresponding to more hydrated species. AC-I, on the other hand, appeared to lose water as evidenced by: (*a*) the decrease in the broadness of the single endotherm, and (*b*) the increase in the temperature corresponding to the maximum of the endotherm. After 4 weeks of equilibration of AC-I, there were no additional changes in the differential scanning calorimetric readings. The material which melted at about 50° was analyzed for water content by integration of NMR spectra and by loss of weight on drying. Both methods showed AC-I to contain six molecules of water associated with each mole of complex.

Thus, the equilibration studies confirmed the fact that the complexes differ only in degree of hydration and, furthermore, that all of the species are in equilibrium. In addition, the presence of only three distinct endotherms suggested that the anhydrous, monohydrate, and hexahydrate species are the only species involved in the equilibrium.

Similar changes in the melting point of the acetaminophen–theophylline complex with drying were observed. The initially isolated crystalline material melted at about 55°. After air drying for 24–48 hr., it exhibited a melting point of about 130°. Complete drying in a vacuum oven resulted in a solid which melted at 192–195°. This high melting solid was found to be anhydrous. However, no attempt was made to determine the composition with respect to water of the other, lower melting, acetaminophen–theophylline complexes.

Since acetaminophen does complex with both caffeine and theophylline, the effects of the complexation on the dissolution rate of each compound were investigated. These dissolution studies were carried out at 25° in water as described in the *Experimental* section. The initial dissolution rates obtained for acetaminophen, caffeine, and theophylline from various systems are summarized in Table III. The dissolution curves for each system were followed for periods of times during which at least 30% of the material in the tablet had dissolved.

Figure 4 shows the dissolution curves obtained for tablets of AC-I, AC-II, AC-III, and an equimolar mixture of acetaminophen and caffeine prepared by evaporation of a methanolic solution of acetaminophen and anhydrous caffeine. In all cases where acetaminophen and caffeine were present in equimolar amounts, the rate of dissolution of both species occurred at about the same rate to within ±5%. For this reason the solid curves in Fig. 4 were drawn to approximate the dissolution behavior of both species from a given tablet.

Inspection of the dissolution curves in Fig. 4 and the initial dissolution rates in Table III shows that the rate of release of acetaminophen and caffeine was greatest from the equimolar mixture prepared by precipitation from methanol solution. Although it was anticipated that the anhydrous complex would dissolve more rapidly than either acetaminophen or caffeine alone, it was rather surprising that the equimolar mixture of acetaminophen and caffeine dissolved at a rate about 70% greater than that for the anhydrous complex. The reason for these results is not clear. It was felt that the equimolar mixture prepared by precipitation may have been a more energetic solid than would be obtained with a simple physical mixture. To determine if similar results could be obtained from a true physical mixture, equimolar quantities of acetaminophen and caffeine were powdered and intimately mixed. The resulting mixture was compressed into tablets and an attempt was made to determine the dissolution rates. These attempts were not successful since the tablets almost immediately began to disintegrate when placed in the dissolution medium. Because of the changes in surface area associated with disintegration, the dissolution rates obtained could not be compared with those obtained for the other system where the tablet remained intact.

An additional unexpected result was the greater dissolution rate of AC-II relative to AC-III. Related work on hydrated and anhydrous systems showed the solubility and dissolution rate of the anhydrous solid to be greater than the hydrated form at 25° (6, 7).

It seems reasonable in the present case that the dissolution rates obtained reflect the relative solubilites of AC-II and AC-III in water at 25°. Thus, by using the initial dissolution rate together with the heats of solution of AC-II and AC-III, which were calorimetrically determined[3] to be about 10.1 and 6.5 kcal./mole, respectively, a transition temperature of about 20° was calculated. Thus, at temperatures of less than about 20°, the dissolution rate of AC-III would be expected to be greater than the dissolution rate of AC-II.

[3] These values were determined (at 25°) in these laboratories by S. Lindenbaum. A solution batch calorimeter was used.

UM00013126
NOVARTIS EXHIBIT 1517
Novartis v. Regents, IPR2023-01347
Page 1872 of 4460

Although the results shown in Fig. 2 and Table IV clearly show that the presence of caffeine and acetaminophen in equimolar amounts has a significant effect on the dissolution rate of acetaminophen (and caffeine), they still left some question as to whether or not the presence of smaller ratios of caffeine to acetaminophen, such as are found in many commercial analgesic preparations (2), would have any significant physical effects on the release of acetaminophen from such tablets. Therefore, tablets containing one part anhydrous caffeine (30 mg.) and 10 parts acetaminophen (300 mg.) were prepared. The dissolution behavior of such tablets was then compared to pure acetaminophen tablets (300 mg.). The tablets containing the mixture began to disintegrate within 2 min. and dissolved completely within 50 min. The pure acetaminophen tablets, on the other hand, dissolved without disintegration and required more than 100 min. for complete dissolution.

Whether or not these results can be extrapolated to commercial tablets that contain various additives such as binders and diluents is doubtful. However the results do suggest that caffeine has a substantial effect on the release of acetaminophen from tablets. Therefore, in any formulation attempts or changes, the possible effects of the presence of caffeine in such a system should be considered.

The dissolution rates of theophylline and acetaminophen from various systems are shown in Fig. 5. It is obvious that in these systems the dissolution rates of acetaminophen and theophylline from the same tablet are not as similar as in the acetaminophen–caffeine systems. Furthermore, there is no significant difference between the anhydrous complex and the equimolar physical mixture which, in this case, was prepared by blending of powders. The initial rate of dissolution for theophylline from the physical mixture and the pure theophylline tablet should be noted. The theophylline dissolves approximately 100% faster from the physical mixture than from pure theophylline tablets. This increase in dissolution rate, together with the neutral to slightly acid pH of the resulting solution, suggests that the anhydrous complex may have some utility in the formulation of more rapidly dissolving oral dosage forms of theophylline which could replace, in some cases, the highly alkaline theophylline salts presently employed.

REFERENCES

(1) "Advances in Analytical Chemistry and Instrumentation," vol. 4, C. N. Reilley, Ed., Interscience, New York, N. Y., 1965, pp. 117–212.

(2) "Handbook of Non-Prescription Drugs," 1971 ed., G. B. Griffenhagen and L. L. Hawkins, Eds., American Pharmaceutical Association, Washington, D. C., 1971, pp. 44, 45.

(3) "The Merck Index," 8th ed., Merck and Co., Inc., Rahway, N. J., 1968.

(4) K. A. Connors, "A Textbook of Pharmaceutical Analyses," Wiley, New York, N. Y., 1967, pp. 166–168.

(5) R. A. Robinson and R. H. Stokes, "Electrolyte Solutions," 2nd ed., Butterworths, London, England, 1959, p. 510.

(6) J. W. Poole and C. K. Bahal, *J. Pharm. Sci.*, 57, 1945(1968).

(7) E. Shefter and T. Higuchi, *ibid.*, 52, 781(1963).

ACKNOWLEDGMENTS AND ADDRESSES

Received March 6, 1972, from the *School of Pharmacy, University of Kansas, Lawrence, KS 66044*

Accepted for publication May 16, 1972.

Presented to the Basic Pharmaceutics Section, APhA Academy of Pharmaceutical Sciences, Houston meeting, April 1972.

Abstracted in part from a dissertation submitted by Y. P. Chow to the University of Kansas in partial fulfillment of the M.S. degree requirements.

Supported in part by the Warner-Lambert Pharmaceutical Co., Morris Plains, N. J.

▲ To whom inquiries should be directed.

DRUG STANDARDS

Desorption of Belladonna Alkaloids from Antacids for Analysis

V. DAS GUPTA▲ and K. L. EULER

Abstract □ The desorption of belladonna alkaloids from antacids for analysis was investigated. The antacids studied were dried aluminum hydroxide gel, calcium carbonate, magnesium carbonate, magnesium oxide, and magnesium trisilicate. It appears that the alkaloids are strongly adsorbed only on the surface of magnesium trisilicate. The complete desorption of alkaloids requires boiling the complex with concentrated hydrochloric acid and then using a dye method for the analysis.

Keyphrases □ Belladonna alkaloids—desorption from antacids for analysis □ Desorption, belladonna alkaloids—from antacids, analysis □ Antacids—adsorption of belladonna alkaloids, desorption for analysis □ Magnesium trisilicate—adsorption of belladonna alkaloids, desorption for analysis

The pharmaceutical industry is marketing some liquid antacid preparations in combination with belladonna alkaloids. One typical product of this nature was brought to the authors' notice for the development of an assay procedure for *l*-hyoscyamine. During the investigations, *l*-hyoscyamine was found to be strongly adsorbed onto the surface of one or more of the ingredients. An effective method was required to desorb the alkaloids for analysis. The purpose of this paper is to report the details of these investigations.

UM00013127
NOVARTIS EXHIBIT 1517
Novartis v. Regents, IPR2023-01347
Page 1873 of 4460

This Page is Inserted by IFW Indexing and Scanning Operations and is not part of the Official Record

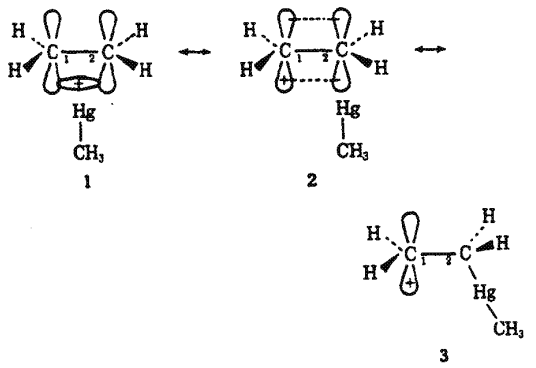
BEST AVAILABLE IMAGES

Defective images within this document are accurate representations of the original documents submitted by the applicant.

Defects in the images include but are not limited to the items checked:

- ☐ BLACK BORDERS
- ☐ IMAGE CUT OFF AT TOP, BOTTOM OR SIDES
- ☐ FADED TEXT OR DRAWING
- ☐ BLURRED OR ILLEGIBLE TEXT OR DRAWING
- ☐ SKEWED/SLANTED IMAGES
- ☐ COLOR OR BLACK AND WHITE PHOTOGRAPHS
- ☐ GRAY SCALE DOCUMENTS
- ☐ LINES OR MARKS ON ORIGINAL DOCUMENT
- ☐ REFERENCE(S) OR EXHIBIT(S) SUBMITTED ARE POOR QUALITY
- ☐ OTHER: _____

IMAGES ARE BEST AVAILABLE COPY.
As rescanning these documents will not correct the image problems checked, please do not report these problems to the IFW Image Problem Mailbox.



1 2 3

The relatively low barrier for interconversion of 1 to 2 is also consistent with experimental[11] and theoretical[12] studies on the importance of carbon–metal $\sigma-\pi$ conjugation in the stabilization of mercurinium ions.[13] The extent of perturbation of the double bond by $HgCH_3^+$ may be estimated by a comparison of the Mulliken overlap population for ethylene, $\rho_\pi = 0.503$, with that of the π system of the mercurinium ions 1–3. The Mulliken overlap population for the C_1–C_2 π bond in 1 has been reduced to 0.368. In the unsymmetrical ion 2 this value is slightly increased to 0.381. The overlap population between the carbon 2p π orbital on C_1 and electron density on mercury is only 0.110 in 2. Thus, 78% of the stabilization of the positive charge on C_1 in 2 is due to delocalization of the polarizable carbon–mercury σ bond and only 22% to neighboring group participation by mercury. With the classical ion 3 ρ_π is 0.346 and the overlap population between the neighboring group $HgCH_3$ and the π orbital on carbon, ρ_{C_1-Hg}, is reduced to 0.052. Thus, in 3 both $\sigma-\pi$ conjugative stabilization and neighboring group participation are reduced. The increase in energy of 3 is also reflected in an increase in positive charge on C_1 which is 0.114, 0.123, and 0.177 for ions 1, 2, and 3, respectively.

Acknowledgment. Acknowledgment is made to the donors of the Petroleum Research Fund, administered by the American Chemical Society, and to the National Institutes of Health (ES 00761-01) for support of this work.

(11) T. G. Traylor, W. Hanstein, J. J. Berwin, N. A. Clinton, and R. S. Brown, *J. Amer. Chem. Soc.*, 93, 5715 (1971).
(12) R. D. Bach and P. A. Scherr, *ibid.*, 94, 220 (1972).
(13) T. G. Traylor, *Accounts Chem. Res.*, 2, 152 (1969).

Robert D. Bach,* Johannes Gauglhofer, Larry Kevan
Department of Chemistry, Wayne State University
Detroit, Michigan 48202
Received April 4, 1972

Activity Coefficient Effects in Spectral and Solubility Studies of Molecular Complex Equilibria

Sir:

Information about molecular complexes of iodine has played a key role in the development of theories of electron donor–acceptor interaction.[1] Yet, in spite of the importance of these adducts, there remains considerable disagreement regarding the magnitudes of spectral and thermodynamic constants of iodine complexes in nonpolar media.[1-6] When different physical methods are employed to study the same series of complexes, discrepancies are particularly large. For example, formation constant (K_c) values determined by the solubility method are as much as twice as great as those inferred from spectral techniques.[4,5]

It has been stated that the solubility method and similar thermodynamic techniques yield K_c values which account for the total effect of donor–acceptor interactions (specific plus nonspecific),[5b] whereas K_c values determined spectrally reflect only the effects of donor–acceptor contacts occurring in excess of random collisions.[7] This communication treats explicitly the effect of variation in activity coefficients on values of thermodynamic constants inferred from the solubility method and compares the corrected solubility results with constants determined spectrally.

Consider the reaction $D + I_2 \rightleftharpoons DI_2$ which occurs between dissolved donor (D) and iodine in dilute solution in a solvent (*e.g.*, heptane). The thermodynamic equilibrium constant for the reaction (in reciprocal molarity units) is

$$K_c = a_{DI_2}/(a_D a_{I_2}) = (c_{DI_2}/c_D c_{I_2})\,(\gamma_{DI_2}/\gamma_D\gamma_{I_2})$$

where a_i, c_i, and γ_i represent the activity, molar concentration, and activity coefficient of a solute species i (DI_2, D, or I_2). The activity coefficients are based on ideal dilute solution (unit molarity) standard states; the γ_i values individually approach unity as the total solute concentration approaches zero. In conventional spectral studies it is common to assume that $\gamma_{DI_2} \simeq \gamma_D\gamma_{I_2}$, even in treating data for quite concentrated solutions. This assumption has been criticized and defended by various workers.[8-10] At first glance, it would appear that constants derived from solubility results should be less influenced by activity coefficient effects, since meaningful measurements of solubility increases can be made in the very dilute solution range.[5] However, the total concentration of dissolved iodine, at constant activity in the presence of an added donor, can be expressed as

$$[I_2] = c_{I_2} + c_{DI_2} = (a_{I_2}/\gamma_{I_2}) + c_{DI_2} \qquad (1)$$

where a_{I_2} is fixed and known.[11] As more donor is

(1) For general references, see (a) R. S. Mulliken and W. B. Person, "Molecular Complexes. A Lecture and Reprint Volume," Wiley-Interscience, New York, N. Y., 1969; (b) R. Foster, "Organic Charge-Transfer Complexes," Academic Press, London and New York, 1969; (c) G. Briegleb, "Elektronen-Donator-Acceptor-Komplexe," Springer-Verlag, Berlin, 1961.
(2) L. E. Orgel and R. S. Mulliken, *J. Amer. Chem. Soc.*, 79, 4839 (1957).
(3) P. J. Trotter and M. W. Hanna, *ibid.*, 88, 3724 (1966).
(4) G. Kortüm and W. M. Vogel, *Z. Elektrochem.*, 59, 16 (1955); J. A. A. Ketelaar, C. Van de Stolpe, A. Goudsmit, and W. Dzcubas, *Recl. Trav. Chim. Pays-Bas*, 71, 1104 (1952).
(5) (a) J. D. Childs, S. D. Christian, and J. Grundnes, *J. Amer. Chem. Soc.*, 94, 5657 (1972); (b) J. D. Childs, Ph.D. Dissertation, The University of Oklahoma, 1971.
(6) R. L. Scott and D. V. Fenby, *Annu. Rev. Phys. Chem.*, 20, 111 (1969).
(7) R. L. Scott, *J. Phys. Chem.*, 75, 3843 (1971).
(8) S. K. Alley and R. L. Scott, *ibid.*, 67, 1182 (1963).
(9) Reference 1a, pp 91, 98–100.
(10) M. W. Hanna and D. G. Rose, *J. Amer. Chem. Soc.*, 94, 2601 (1972).
(11) In the polyiodide solubility method, mixtures of tetramethylammonium polyiodides are utilized to maintain a constant activity of iodine in a solution phase or gaseous phase containing added donor.[6,12] Studies of aromatic donor–iodine complexes in heptane are conveniently performed by using tetramethylammonium triiodide and pentaiodide solid mixtures, which in contact with liquid heptane at 25° give an equilibrium concentration of molecular iodine equal to 1.97×10^{-4} *M*. In these experiments, $c_D \gg c_{I_2}$ or c_{DI_2}, which implies that activity coefficient effects in the solution phase are determined by the relative concentrations of heptane and donor.

UM00013129
NOVARTIS EXHIBIT 1517
Novartis v. Regents, IPR2023-01347
Page 1875 of 4460

added, c_{DI_2}, will increase, but owing to nonspecific effects, γ_{I_2}, may vary also. It can be shown that in very dilute solutions both c_{DI_2} and γ_{I_2} (or its reciprocal) vary linearly with donor concentration;[13,14] therefore, the total solubility increase reflects both specific and nonspecific effects. It should be obvious from eq 1 that knowledge of γ_{I_2} would permit the unambiguous determination of c_{I_2} and, by difference, c_{DI_2}; knowledge of c_{DI_2} permits determination of the concentration of uncomplexed donor (c_D). Therefore, if γ_{I_2} were known as a function of c_D, it would be possible to obtain values of $c_{DI_2}/(c_D c_{I_2})$ in the very dilute concentration region and to extrapolate these values to infinite dilution to obtain the thermodynamic equilibrium constant K_c.

The equations of solubility parameter theory (for a mixed solvent)[15] may be used to estimate γ_{I_2} as a function of c_D for several aromatic donor–iodine systems for which K_c has been determined by both the polyiodide solubility method and the Benesi–Hildebrand (BH) spectral technique.[16] Table I shows values of K_c

Table I. Equilibrium Constants for Several Donor–Iodine Complexes in Heptane at 25°[a]

Donor	$K_c^{(a)}$,[b] l. mol^{-1}	$K_c^{(corr)}$,[c] l. mol^{-1}	$K_c^{(BH)}$,[d] l. mol^{-1}
Benzene	0.37	0.15	0.20
Toluene	0.50	0.28	0.32
o-Xylene	0.64	0.37	0.42
p-Xylene	0.64	0.40	0.41
m-Xylene	0.70	0.46	0.54
Mesitylene	0.98	0.71	0.74

[a] From ref 5b. [b] $K_c^{(a)}$ values are obtained directly from the polyiodide solubility results, assuming $\gamma_{I_2} = 1$. [c] $K_c^{(corr)}$ values have been corrected for γ_{I_2}, estimated from solubility parameter theory. [d] $K_c^{(BH)}$ values have been inferred using the Benesi–Hildebrand analysis, assuming $\gamma_{DA} = \gamma_D\gamma_A$.

obtained directly from the uncorrected solubility method, values corrected for changes in γ_{I_2}, and values obtained using the BH analysis of spectral data for more concentrated solutions. The agreement between the corrected solubility results and the BH results is remarkably good, indicating that $\gamma_{DI_2} \simeq \gamma_D\gamma_{I_2}$ in these systems. This is not to suggest that activity coefficient effects will in general cancel so neatly, but, at least in the case of the important aromatic hydrocarbon complexes, the spectral and solubility results can be brought into near agreement by estimating γ_{I_2} from simple nonelectrolyte solution theory.

Finally, it should be noted that properties of the electronic spectral bands of donor–iodine complexes inferred from the uncorrected solubility results (ignoring activity coefficient effects) are in better agreement with trends predicted from the Mulliken theory[1,17] than are results inferred from the BH or corrected solubility methods.[5,18] In the case of relatively weak complexes it may be argued that the total effect of donor–iodine interactions (random plus specific) should be considered in relating spectral intensities and frequency shifts to donor strength. Since the uncorrected solubility results comprise both types of effects, they should therefore be simpler to interpret theoretically. This point of view is not very different from that expressed by Orgel and Mulliken,[2] who introduced the concept of "contact charge transfer" to explain the anomalous variation of spectral band intensities with donor strength for weak complexes which had been investigated with the BH technique.

Acknowledgment. This work was supported in part by National Science Foundation Grants No. GP-8029 and GP-23278.

(12) J. D. Childs, S. D. Christian, J. Grundnes, and S. R. Roach, *Acta Chem. Scand.*, 25, 1679 (1971); S. D. Christian and J. Grundnes, *J. Amer. Chem. Soc.*, 93, 6363 (1971).
(13) W. B. Person, *ibid.*, 87, 167 (1965).
(14) J. H. Hildebrand and R. L. Scott, "The Solubility of Nonelectrolytes," 3rd ed, Reinhold, New York, N. Y., 1950, p 34.
(15) J. H. Hildebrand, J. M. Prausnitz, and R. L. Scott, "Regular and Related Solutions," Van Nostrand-Reinhold, Princeton, N. J., 1970.
(16) H. A. Benesi and J. H. Hildebrand, *J. Amer. Chem. Soc.*, 71, 2703 (1949).
(17) R. S. Mulliken, *ibid.*, 74, 811 (1952).
(18) A puzzling result of the BH spectral studies is that in a series o, weak complexes such as those between the aromatic donors and iodinef the molar absorptivities of the charge-transfer band do not increase uniformly as the donor strength increases;[1,3] in fact, there is an abrupt drop in absorptivity in the series benzene·I_2–toluene·I_2–xylene·I_2, and the absorptivity rises again as more highly alkylated donors are employed. The polyiodide solubility results yield absorptivity values which are all in the range 6900 ± 1200 l. mol^{-1} cm^{-1} for the complexes listed in Table I.[5b] Moreover, the uncorrected solubility results lead to simple correlations between complex stability and the intensities and frequency shifts of the blue-shifted iodine bands of the aromatic donor complexes.[5b]

Sherril D. Christian,* Jerry D. Childs, Edwin H. Lane
Department of Chemistry, The University of Oklahoma
Norman, Oklahoma 73069
Received May 16, 1972

Substituent Effects in Gas-Phase Ionic Nitration and Acetylation of Aromatics

Sir:

We report the observation using ion cyclotron resonance (icr) spectroscopy of marked substituent effects on the gas-phase reaction rates of $(NO_2)^+$ and $(CH_3CO)^+$ transfer to a variety of substituted benzenes and heteroaromatic compounds. Although substituent effects in gas-phase ionic reactions have never been examined under conditions comparable to those employed in this work a number of studies have dealt with ion–molecule reactions involving aromatic compounds.[1-10] Of particular interest are the results of Cacace,[4,5] *et al.*, on tritiation by strong Brønsted acids, in which a substantial positional selectivity is observed, but little rate selectivity.

(1) S. A. Benezra, M. K. Hoffman, and M. M. Bursey, *J. Amer. Chem. Soc.*, 92, 7501 (1970); M. K. Hoffman and M. M. Bursey, *Tetrahedron Lett.*, 2539 (1971).
(2) M. M. Bursey, T. A. Elwood, M. K. Hoffman, T. A. Lehman, and J. M. Tesarek, *Anal. Chem.*, 42, 1370 (1970); S. A. Benezra and M. M. Bursey, *J. Amer. Chem. Soc.*, 94, 1024 (1972).
(3) V. Aquilanti, A. Giardini-Guidoni, and G. G. Volpi, *Trans. Faraday Soc.*, 64, 3282 (1968).
(4) F. Cacace and S. Caronna, *J. Amer. Chem. Soc.*, 89, 6848 (1967).
(5) F. Cacace, R. Cipollini, and G. Occhiucci, *J. Chem. Soc., Perkin Trans. 2*, 84 (1972).
(6) M. S. B. Munson and F. H. Field, *J. Amer. Chem. Soc.*, 89, 1047 (1967).
(7) S. Wexler and R. P. Clow, *ibid.*, 90, 3940 (1968); S. Wexler and L. G. Pobo, *ibid.*, 91, 7233 (1969), and references therein.
(8) L. I. Bone and J. H. Futrell, *J. Chem. Phys.*, 47, 4366 (1967).
(9) S. Takamuku, K. Iseda, and H. Sakurai, *J. Amer. Chem. Soc.*, 93, 2420 (1971).
(10) E. W. McDaniel, "Collision Phenomena in Ionized Gases," Wiley, New York, N. Y., 1964, Chapter 3.

UM00013130
NOVARTIS EXHIBIT 1517
Novartis v. Regents, IPR2023-01347
Page 1876 of 4460

Journal of Biomolecular Structure & Dynamics, ISSN 0739-1102
Volume 8, Issue Number 2 (1990), ©Adenine Press (1990).

Molecular Structure of the Complex Formed Between the Anticancer Drug Cisplatin and d(pGpG): $C222_1$ Crystal Form

Miquel Coll[1], Suzanne E. Sherman[2], Dan Gibson[2], Stephen J. Lippard[2] and Andrew H. -J. Wang[3]*
Department of Biology[1] and Department of Chemistry[2]
Massachusetts Institute of Technology
Cambridge, MA 02139

[3]Department of Physiology and Biophysics
University of Illinois at Urbana-Champaign
Urbana, IL 61801

Abstract

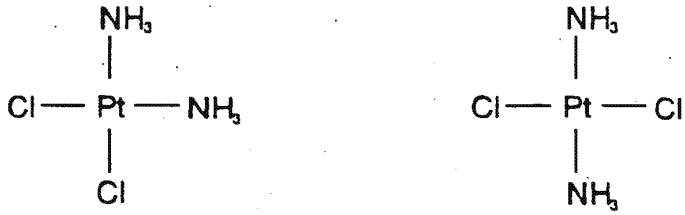
The three dimensional molecular structure of the adduct formed between the anticancer drug cisplatin and a DNA dinucleotide d(pGpG) has been determined by x-ray diffraction analysis at 1.37 Å resolution and refined to a final R-factor of 0.11. This structure, solved by using data from a previously reported crystal form in the space group $C222_1$, resembles that found in the space group $P2_12_12$ (Sherman, et al., *Science, 230*, 412-417, 1985; ibid, *J. Amer. Chem. Soc. 110*, 7368-7381, 1988). In both structures, four crystallographically independent *cis*-$[Pt(NH_3)_2\{d(pGpG)\}]$ molecules aggregate into a tetrameric cluster that is stabilized by a large number of intermolecular hydrogen bonds and base-base stacking interactions. In each molecule, the platinum atom is coordinated to the N7 atoms of two guanine bases arranged in a head-to-head orientation, resulting in a large dihedral angle between the guanines. Intermolecular guanine-guanine base pairings between different intrastrand crosslinked molecules are used extensively in the crystal lattice.

Introduction

cis-Diamminedichloroplatinum(II) (*cis*-$[Pt(NH_3)_2Cl_2]$, *cis*-DDP or cisplatin; Figure 1) is an important anticancer drug widely used in the treatment of several human tumors (1,2). The trans isomer of this square-planar inorganic platinum coordination compound (*trans*-DDP) is inactive, although it can pass through the cell membrane like the cis isomer. Substantial evidence has accumulated indicating that the principal target of both isomers is nuclear DNA (1,2). When dissolved in aqueous solution, cisplatin loses both chloride ions to afford activated, hydrolyzed species that react with the guanines of DNA and form two Pt-N covalent bonds to the N7 atoms of two adjacent nucleotides. This interaction produces a stable adduct and induces significant conformational distortion in DNA, bending the DNA

*Author to whom correspondence should be addressed.

UM00013131
NOVARTIS EXHIBIT 1517
Novartis v. Regents, IPR2023-01347
Page 1877 of 4460



cis-Diamminedichloroplatinum(II) *trans*-Diamminedichloroplatinum(II)

Figure 1: Structural formulas of *cis*-diamminedichloroplatinum(II) (Cisplatin) and *trans*-diamminedichloroplatinum(II).

double helix, and unstacking the adjacent guanines (3,4). The biological activity of cisplatin is presumably due in large part to the formation of this major bidentate intrastrand crosslink, which the inactive *trans*-DDP cannot form. This binding mode is quite different from those formed by other types of anticancer drugs, most of which bind DNA by noncovalent interactions such as intercalation (5) or groove binding (6).

There has been substantial interest in the three dimensional structure of the cisplatin-(bis-guanine) adduct since it may provide us with some clues regarding the conformational distortions in the DNA double helix caused by the binding of cisplatin that have biological implications about its use in cancer chemotherapy. We have approached this problem by, inter alia, synthesizing a series of cisplatin-oligonucleotide adducts for crystallization and studying them by x-ray diffraction. One such adduct, *cis*-$[Pt(NH_3)_2\{d(pGpG)\}]$, was crystallized from similar conditions producing two different but closely related crystal forms in the space groups $P2_12_12$ and $C222_1$. The three dimensional structure of the $P2_12_12$ crystal form was determined to high resolution and reported previously (7,8). That structure revealed the dinucleotide adduct to form a tetrameric aggregate using extensive intermolecular hydrogen bonds and stacking interactions. We were interested in knowing the possible influence of lattice forces on the structure of the platinum adduct and, therefore, solved the structure of the other crystal form ($C222_1$) in order to make detailed comparisons between them. The global features of both structures are very similar, although some differences occur both in the molecular structures and in the ways in which the molecules are packed in their respective crystal lattice. The crystal structure of another cisplatin adduct with a DNA trinucleotide d(CpGpG) has also been determined recently (9).

Experimental

The cisplatin DNA complex was prepared by allowing the ammonium form of the dinucleotide d(pGpG) to react with an equimolar amount of 2 mM aqueous solution of *cis*-$[Pt(NH_3)_2(NO_3)_2]$ at 37°C for 80 minutes. The product was purified by anion exchange and reversed phase HPLC. Two crystal forms were obtained by the vapor diffusion technique from solutions containing 9 mM *cis*-$[Pt(NH_3)_2\{d(pGpG\}]$, 33 mM glycine · HCl buffer (pH 3.8), 33 mM NaCl and 9.2% 2-methyl-2,4-pentanediol

UM00013132
NOVARTIS EXHIBIT 1517
Novartis v. Regents, IPR2023-01347
Page 1878 of 4460

(2-MPD), equilibrated against 70% 2-MPD. Long prismatic crystals of the orthorhombic form I (space group $C222_1$) were obtained first, with the unit cell dimensions $a=30.55, b=33.90, c=41.25$ Å. At higher 2-MPD concentration and the addition of 17 mM $MgCl_2$, a second crystal form (form II) appeared which belonged to the space group $P2_12_12$ with the unit cell dimensions $a=31.326$, $b=35.679$ and $c=19.504$ Å. Form II crystal structure was solved and refined as described previously (7,8). By examining the unit cell dimensions of both crystal forms, it is obvious that they are closely related. The *a*- and *b*-axes of the two forms are nearly the same and the *c*-axis dimension of Form I is nearly twice that of Form II. The volume of the asymmetric unit in both crystal forms is about the same, however, ~5,400 Å^3.

X-ray diffraction data were collected for the $C222_1$ crystal by using a CAD4 Enraf-Nonius diffractometer with MoK_α radiation to a resolution of 1.37 Å at room temperature. 4677 reflections were measured and 2233 reflections with $I > 2\sigma(I)$ were used in the refinement. Earlier attempts to solve the structure by direct methods with programs such as MULTAN77 (10) were unsuccessful. Finally, using the direct methods program SHELXS86 (11), four platinum atoms were located in the asymmetric unit. Neither the tangent recycling in the direct method package nor the difference Fourier maps could produce the rest of the structure, however. At this point, we surmised that the two crystal forms might have similar molecular structures owing to the similarity in their unit cell dimensions. Therefore, we used the structure of the tetrameric aggregate of the $P2_12_12$ crystal form and the positions of the four Pt atoms to determine the complete structure of the $C222_1$ form with a molecular replacement technique as described below.

Since the volume of the asymmetric units in both crystal forms is very similar (~5400 Å^3), it seemed likely that the cluster of four platinum-dinucleotide complexes found in the $P2_12_12$ form would also exist in the $C222_1$ form. There are four different ways to position four molecules such that the four platinum atoms in the cluster can be superimposed onto the new locations of the four platinums found with SHELXS86. Accordingly four different models were constructed by carrying out least squares fittings of the platinums between the two sets. A rigid body refinement was carried out with the program SHELX76 (12) allowing the four dinucleotides to move independently but pivoting around the corresponding platinum atom. Only one of the four models could be successfully refined and it was used for further studies.

The correct model was further refined with the Hendrickson-Konnert constraint refinement program (13) because of the limited resolution (1.37 Å) of the diffraction data. A (2Fo-Fc) Fourier map was calculated at 2 Å resolution and it revealed that indeed the DNA molecules fitted the electron density quite reasonably. During refinement the DNA geometry was held close to the ideal values with strong constraints. After several cycles and the addition of 20 water and 3 glycine molecules, the R-factor dropped to 0.18. In view of the large contributions of the platinum atoms to the structure factors, we decided to refine their positions with individual atomic refinement while maintaining the complete nucleotide moiety (all eight guanine nucleotides) as a rigid body. Alternate cycles of Hendrickson-Konnert refinement of the entire complex and anisotropic refinement with SHELX76 for the platinum atoms were carried out to obtain a final R-factor of 0.11. The final atomic

NOVARTIS EXHIBIT 1517
Novartis v. Regents, IPR2023-01347
Page 1879 of 4460

Table I
Atomic Fractional coordinates of *cis*-[$Pt(NH_3)_2$[d(pGpG)]]

	X	Y	Z	X	Y	Z
PT	0.2794	0.5350	0.1778			
N1	0.2747	0.5275	0.2247			
N2	0.2151	0.5397	0.1683			
O3P	0.4003	0.5572	0.2618			
P	0.3792	0.5982	0.2594	0.4170	0.6881	0.1337
O1P	0.3293	0.5953	0.2546	0.3864	0.6999	0.1601
O2P	0.3858	0.6239	0.2898	0.4371	0.7254	0.1188
O5'	0.4015	0.6174	0.2288	0.3991	0.6616	0.1056
C5'	0.4472	0.6292	0.2303	0.4159	0.6579	0.0745
O4'	0.4685	0.5730	0.2004	0.3740	0.6005	0.0633
C4'	0.4662	0.6164	0.1980	0.3854	0.6377	0.0503
O3'	0.4543	0.6630	0.1518	0.3365	0.6630	0.0075
C3'	0.4424	0.6258	0.1674	0.3430	0.6597	0.0414
C2'	0.4512	0.5892	0.1457	0.3087	0.6353	0.0578
C1'	0.4585	0.5571	0.1695	0.3277	0.5948	0.0571
N9	0.4180	0.5339	0.1763	0.3120	0.5683	0.0832
C8	0.3767	0.5476	0.1706	0.3024	0.5758	0.1150
N7	0.3451	0.5264	0.1804	0.2855	0.5470	0.1312
C6	0.3552	0.4549	0.2046	0.2758	0.4751	0.1105
O6	0.3184	0.4408	0.2089	0.2642	0.4565	0.1329
C5	0.3693	0.4908	0.1922	0.2880	0.5155	0.1077
C4	0.4141	0.4984	0.1904	0.3015	0.5291	0.0782
N3	0.4461	0.4733	0.1983	0.3032	0.5099	0.0491
C2	0.4319	0.4390	0.2094	0.2905	0.4724	0.0528
N2	0.4591	0.4106	0.2198	0.2921	0.4475	0.0273
N1	0.3881	0.4285	0.2117	0.2765	0.4563	0.0809
			molecule 2			
PT	0.7193	0.3796	0.1911			
N1	0.7173	0.3840	0.2404			
N2	0.7838	0.3742	0.1982			
O3P	0.5774	0.3263	0.2942			
P	0.6176	0.3184	0.2693	0.5915	0.2264	0.1461
O2P	0.6443	0.2838	0.2807	0.6246	0.2212	0.1730
O1P	0.6412	0.3571	0.2763	0.5690	0.1855	0.1437
O5'	0.5987	0.3127	0.2356	0.6092	0.2430	0.1144
C5'	0.5576	0.2909	0.2317	0.5927	0.2715	0.0928
O4'	0.5278	0.3442	0.1990	0.6427	0.3213	0.0735
C4'	0.5371	0.3038	0.2001	0.6257	0.2825	0.0672
O3'	0.5560	0.2562	0.1599	0.6757	0.2494	0.0299
C3'	0.5658	0.2950	0.1706	0.6660	0.2565	0.0633
C2'	0.5512	0.3271	0.1466	0.7029	0.2794	0.0797
C1'	0.5413	0.3605	0.1674	0.6914	0.3214	0.0742
N9	0.5812	0.3816	0.1775	0.7038	0.3506	0.0993
C8	0.6220	0.3648	0.1794	0.7079	0.3468	0.1313
N7	0.6520	0.3854	0.1932	0.7195	0.3807	0.1447
C6	0.6412	0.4564	0.2162	0.7217	0.4506	0.1252
O6	0.6777	0.4667	0.2268	0.7258	0.4684	0.1511
C5	0.6271	0.4212	0.2020	0.7155	0.4087	0.1230
C4	0.5845	0.4165	0.1941	0.7080	0.3911	0.0935
N3	0.5507	0.4420	0.1986	0.7051	0.4089	0.0646
C2	0.5645	0.4749	0.2135	0.7094	0.4488	0.0681
N2	0.5384	0.5051	0.2205	0.7076	0.4685	0.0398
N1	0.6071	0.4830	0.2222	0.7177	0.4677	0.0958

UM00013134

NOVARTIS EXHIBIT 1517
Novartis v. Regents, IPR2023-01347
Page 1880 of 4460

Table I
continued

molecule 3						
PT	0.2169	0.3757	0.1771			
N1	0.2823	0.3760	0.1723			
N2	0.2171	0.4309	0.1980			
O3P	0.3118	0.3210	0.0635			
P	0.2663	0.3448	0.0583	0.0853	0.3067	0.0548
O1P	0.2688	0.3602	0.0252	0.1203	0.3346	0.0443
O2P	0.2663	0.3793	0.0808	0.0497	0.3043	0.0303
O5'	0.2275	0.3145	0.0661	0.0680	0.3135	0.0902
C5'	0.2138	0.2861	0.0407	0.0355	0.2859	0.1033
O4'	0.2180	0.2445	0.0865	0.0368	0.3106	0.1577
C4'	0.1913	0.2538	0.0601	0.0103	0.3066	0.1293
O3'	0.1108	0.2647	0.0579	-0.0457	0.3582	0.1396
C3'	0.1489	0.2652	0.0773	-0.0063	0.3483	0.1221
C2'	0.1458	0.2363	0.1062	0.0336	0.3720	0.1338
C1'	0.1950	0.2332	0.1140	0.0392	0.3512	0.1665
N9	0.2033	0.2610	0.1403	0.0795	0.3607	0.1830
C8	0.2085	0.3020	0.1370	0.1208	0.3617	0.1700
N7	0.2131	0.3183	0.1643	0.1516	0.3754	0.1889
C6	0.2154	0.2896	0.2215	0.1415	0.4052	0.2457
O6	0.2218	0.3178	0.2394	0.1807	0.4138	0.2554
C5	0.2114	0.2901	0.1878	0.1297	0.3863	0.2169
C4	0.2060	0.2537	0.1723	0.0836	0.3804	0.2128
N3	0.2035	0.2175	0.1862	0.0517	0.3875	0.2345
C2	0.2078	0.2188	0.2182	0.0659	0.4049	0.2602
N2	0.2059	0.1885	0.2393	0.0409	0.4143	0.2861
N1	0.2139	0.2527	0.2359	0.1104	0.4136	0.2678

molecule 4						
PT	0.7784	0.5387	0.1963			
N1	0.7160	0.5403	0.1762			
N2	0.7706	0.4795	0.2040			
O3P	0.6846	0.6069	0.0950			
P	0.7148	0.5737	0.0814	0.8973	0.6022	0.0653
O1P	0.7143	0.5444	0.1093	0.9225	0.6182	0.0366
O2P	0.7148	0.5591	0.0486	0.8682	0.5707	0.0531
O5'	0.7649	0.5967	0.0864	0.9216	0.5941	0.0969
C5'	0.7675	0.6326	0.0676	0.9601	0.6204	0.1049
O4'	0.7734	0.6736	0.1165	0.9511	0.5964	0.1585
C4'	0.7931	0.6617	0.0880	0.9822	0.5986	0.1318
O3'	0.8665	0.6419	0.0731	1.0412	0.5528	0.1406
C3'	0.8386	0.6453	0.0996	0.9975	0.5564	0.1268
C2'	0.8488	0.6766	0.1258	0.9645	0.5317	0.1450
C1'	0.8038	0.6828	0.1409	0.9560	0.5589	0.1737
N9	0.7965	0.6538	0.1671	0.9163	0.5486	0.1919
C8	0.7820	0.6159	0.1639	0.8736	0.5488	0.1794
N7	0.7795	0.5985	0.1928	0.8438	0.5350	0.2002
C6	0.7965	0.6252	0.2489	0.8597	0.5049	0.2561
O6	0.7910	0.5976	0.2686	0.8199	0.4976	0.2658
C5	0.7910	0.6259	0.2153	0.8697	0.5222	0.2260
C4	0.8041	0.6602	0.1996	0.9146	0.5282	0.2200
N3	0.8171	0.6947	0.2133	0.9474	0.5204	0.2407
C2	0.8196	0.6923	0.2454	0.9351	0.5040	0.2676
N2	0.8333	0.7246	0.2607	0.9656	0.4939	0.2893
N1	0.8102	0.6606	0.2629	0.8916	0.4958	0.2765

UM00013125
NOVARTIS EXHIBIT 1517
Novartis v. Regents, IPR2023-01347
Page 1881 of 4460

Table I
continued

Glycine molecules						
N1	0.8677	0.4671	0.1000	0.9240	0.8696	0.1617
C1	0.8549	0.4327	0.1194	0.9361	0.8601	0.1275
C2	0.8802	0.4370	0.1504	0.9221	0.8973	0.1080
O1	0.9216	0.4299	0.1485	0.8998	0.8920	0.0823
O2	0.8622	0.4415	0.1766	0.9416	0.9284	0.1156
N1	0.6561	0.9575	0.0923			
C1	0.6091	0.9613	0.1000			
C2	0.6030	0.9748	0.1347			
O1	0.5634	0.9762	0.1456			
O2	0.6337	0.9695	0.1546			
Water molecules						
W01	0.5583	0.2911	-0.0054	0.8005	0.2860	0.1457
W02	0.6366	0.6418	0.0038	0.8209	0.8018	0.1664
W03	0.7919	0.5463	0.0035	0.6855	0.6432	0.1558
W04	0.9391	0.0856	0.0254	0.6934	0.2729	0.2070
W05	0.9473	0.2658	0.0082	0.5108	0.9784	0.0490
W06	1.0000	0.2804	0.2500	0.9450	0.9402	0.0456
W07	0.9196	0.7324	0.0327	0.9952	0.3927	0.0223
W08	0.5230	0.5384	0.0507	0.5710	0.1379	0.2190
W09	0.8887	0.9771	0.0049	0.5377	0.3743	0.0367
W10	0.7915	0.3688	0.0839	0.5975	0.5862	0.0552
W11	0.6461	0.9119	0.0341	0.5820	0.0203	0.0483
W12	0.5716	0.1583	0.0815	0.9535	0.7575	0.1786
W13	0.5864	0.4988	0.0980	0.7804	0.2113	0.2065
W14	0.6802	0.8857	0.1100	0.8954	0.3066	0.1120
W15	0.5308	0.7013	0.1116	0.5411	0.4309	0.1217
W16	0.5645	0.6314	0.0932	0.5863	0.5297	0.1596
W17	0.6579	0.0196	0.1177	0.5523	0.7398	0.2041
W18	0.8195	0.5340	0.1055	0.8148	0.1469	0.1612
W19	0.9580	0.7399	0.1237	0.5005	0.1725	0.2272
W20	0.6137	0.1149	0.1301	0.5894	0.7754	0.2588
W21	0.8972	0.2425	0.2045			

UM00013136
NOVARTIS EXHIBIT 1517
Novartis v. Regents, IPR2023-01347
Page 1882 of 4460

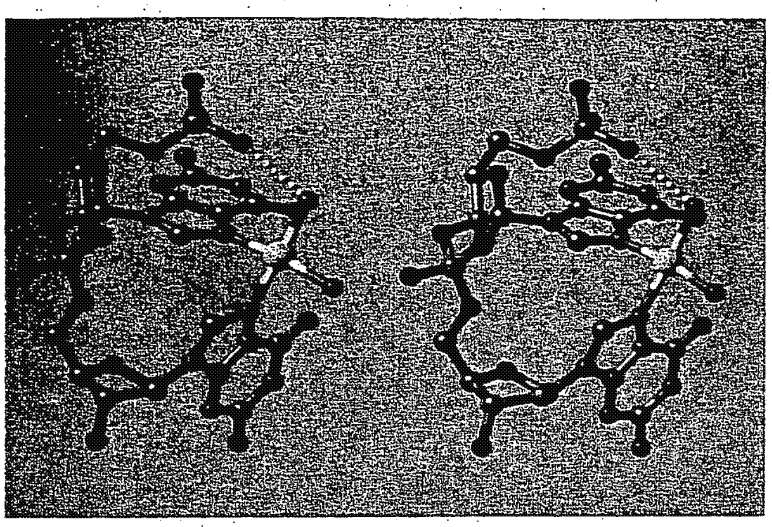


Figure 2: Stereoscopic skeletal drawing of the cisplatin-d(pGpG) complex. This is molecule 1 from the tetrameric aggregate seen in the asymmetric unit in the crystal. The large dihedral angle between the two guanines in the dinucleotide is evident. This diagram is generated by the program MARS (Molecular Architecture Rendering System) developed at UIUC and it is run on a Silicon Graphics IRIS computer.

coordinates are listed in Table I.

Results and Discussion

The structure of the cisplatin-d(pGpG) complex, *cis*-$[Pt(NH_3)_2\{d(pGpG)\}]$, of the $P2_12_12$ form has been described in detail recently (7,8). The present structure is similar in many respects; consequently only relevant structural features are discussed in this paper.

Molecular Structure

As in the $P2_12_12$ form, four Pt-d(pGpG) complexes form a tetrameric aggregate. Figure 2 shows one such complex in which the platinum atom is coordinated to the N7 atoms of both guanines of the dinucleotide, resulting in the formation of a 17-membered ring. All four complexes have a similar conformation with the two guanines almost perpendicular to one another in a "head-to-head" arrangement.

The skeletal stereo diagram (Figure 3) compares tetrameric clusters of the two crystal forms by carrying out a least squares fit between them. It can be seen that the overall conformation is similar with the root-mean-square difference between the two structures being 0.567 Å. The four platinum atoms (represented as circles) form an array with the shape of a flattened tetrahedron in the center of the cluster. The aggregate is stabilized by an extensive network of intermolecular hydrogen bonds and a number of guanine-guanine base stacking interactions between the dinucleotide complexes.

UM00013137
NOVARTIS EXHIBIT 1517
Novartis v. Regents, IPR2023-01347
Page 1883 of 4460

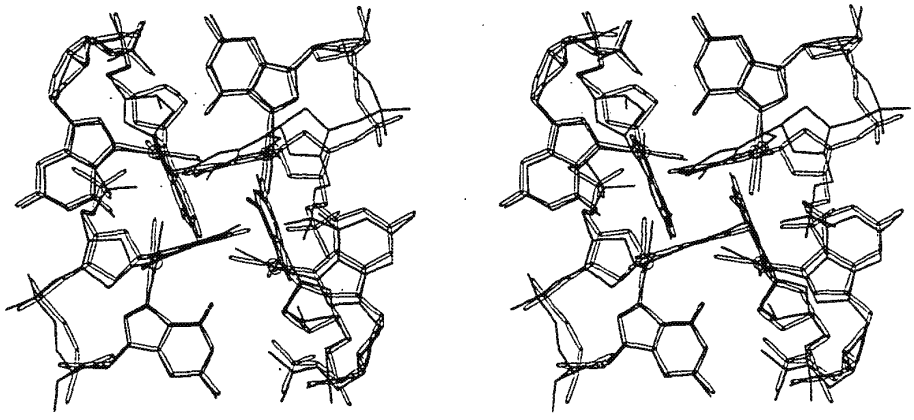


Figure 3: A comparsion of the cisplatin-d(pGpG) tetrameric aggregates from the two crystal forms. Solid bonds correspond to the $C222_1$ crystal form, while open bonds represent the $P2_12_12$ form.

Figure 4 compares the four independent complexes in the aggregate by viewing them from the direction perpendicular to the plane of the Pt-N_4 coordination square. The sugar phosphate backbones in all four platinum-dinucleotide complexes are very similar. This similarity is clearly evident when we compare the torsion angles for all four molecules listed in Table II. All β-γ-δ torsion angles are in the *trans-gauche*$^+$*-gauche*$^+$ conformation for the 5′ deoxyguanosine residues and *trans-gauche*$^+$*-trans* conformation for the 3′ residues. These angles result in an extension of the backbone between the two guanine nucleotides crosslinked by cisplatin.Even though the guanines can adopt slightly different conformations with respect to the plane of the square-planar platinum coordination plane, all sugar-phosphate backbones are driven to a more rigid conformation by coordination of adjacent N7 atoms to the drug molecule. All glycosyl angles are in the *anti* conformation range. The sugar pucker, defined by the pseudorotation angle, is C3′-endo for all four 5′-deoxyguanosines, but it is C2′-endo for all 3′-deoxyguanosines. Similar results were observed in the $P2_12_12$ form (7,8), although the 3′-sugar in molecule 2 in the latter structure contained a disordered deoxyribose. It should be pointed out that the latter structure was refined at substantially higher resolution (0.94 Å) with individual atomic parameters revealing finer details of the structure.

In this view (Figure 4) the large dihedral angle between the guanine bases generated by bidentate coordination to platinum is clearly evident. Despite similar overall conformations, however, some subtle differences are seen. Each complex is comprised of one cisplatin and two deoxyguanosines, 5′-G and 3′-G. The dihedral angles between the pair of guanines are 84°, 75°, 80° and 68° for molecules 1, 2, 3 and 4 respectively. In addition, a comparison of dihedral angles between the guanine and platinum coordination planes also reveals differences among the molecules. A consistent pattern, apparent in Figure 4 is that pairs of molecules 1 and 2, and 3 and 4, have comparable 3′-G/cisplatin and 5′-G/cisplatin dihedral angles. This result reflects the pseudo two-fold symmetry of the tetrameric cluster in which molecules 1

UM00013138

NOVARTIS EXHIBIT 1517
Novartis v. Regents, IPR2023-01347
Page 1884 of 4460

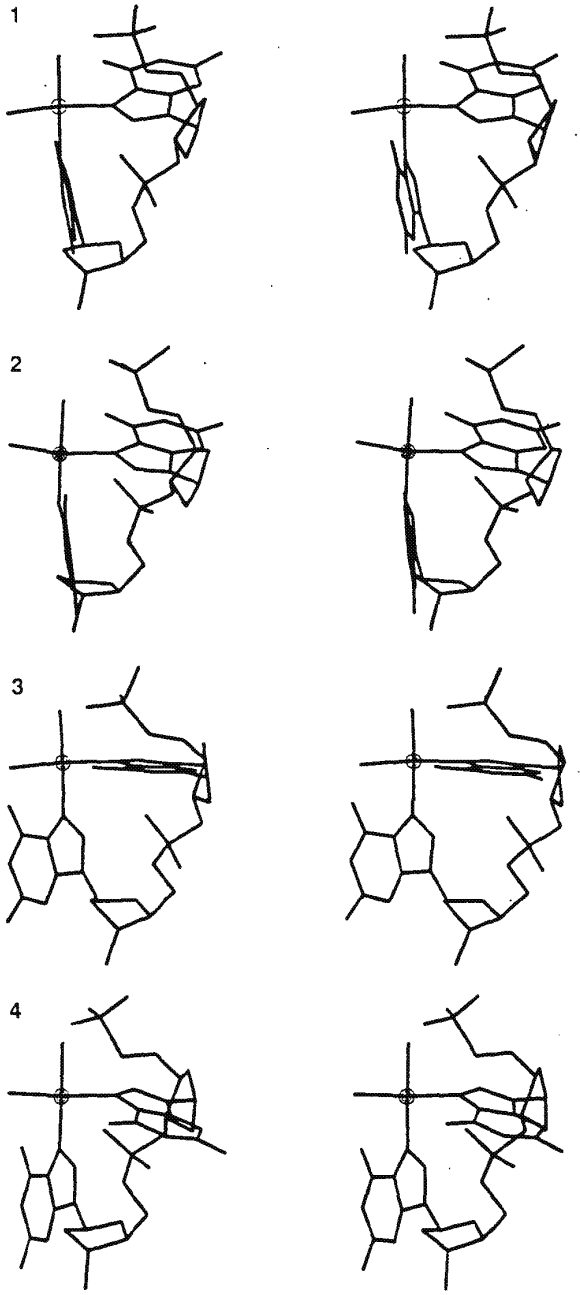


Figure 4: Comparsion of individual cisplatin-d(pGpG) complexes in the tetrameric aggregate. It can be seen that molecules 1 and 2 are similar with their 3'-G's almost perpendicular to the PtN_4 planes, while molecule 3 has its 5'-G almost perpendicular to the PtN_4 plane.

UM00013139
NOVARTIS EXHIBIT 1517
Novartis v. Regents, IPR2023-01347
Page 1885 of 4460

Table II
Backbone Torsion Angles (deg) of Cisplatin-d(pGpG) Complexes

	α	β	γ	δ	ε	ζ	χ
G1		138	47	91	−145	−62	− 78
G2	−86	−166	66	129			−107
G3		157	61	88	−143	−66	− 75
G4	−19	171	13	137			− 86
G5		159	66	82	−120	−67	−146
G6	−65	−156	46	151			−128
G7		143	54	69	−133	−51	−151
G8	−77	−166	57	136			−146

Torsion angles along the backbone of the oligonucleotide are defined as $P\overset{\alpha}{-}O5'\overset{\beta}{-}C5'\overset{\gamma}{-}C4'\overset{\delta}{-}C3'\overset{\varepsilon}{-}O3'\overset{\zeta}{-}P$ and χ is the glycosyl angle. The nucleotides are numbered from G1 to G8 in the tetrameric aggregate.

and 2 have similar conformations, while molecules 3 and 4 are similar to one another but different from 1 and 2. It is clear from Figure 4 that one of the two guanines is not perpendicular, whereas the other guanine remains almost perpendicular, to the Pt-N4 plane in three of the four complexes. The only exception is found in molecule 4, in which both the 5′-G/cisplatin and 3′-G/cisplatin dihedral angles deviate significantly from 90°.

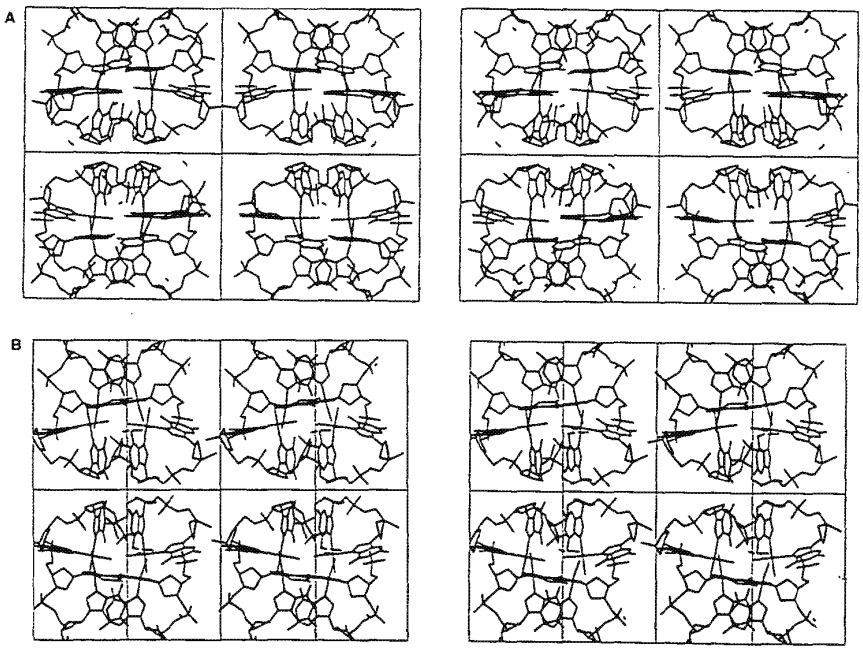


Figure 5: Crystal packing diagrams of the two crystal forms. Four clusters are shown which are located between $b=0.0$ to 0.5. a-axis is vertical and c-axis is horizontal. (A). $C222_1$ form with $a=0.0$ to 1.0 and $c=0.0$ to 1.0 (B) $P2_12_12$ form with $a=0.0$ to 1.0 and $c=-0.5$ to 1.5.

UM00013140
NOVARTIS EXHIBIT 1517
Novartis v. Regents, IPR2023-01347
Page 1886 of 4460

Crystal Packings

Figure 5 compares the molecular packing of the two crystal forms viewed along the *b*-axis (i.e. perpendicular to the *ac* plane). As mentioned earlier, the two crystal forms are closely related: the unit cell dimensions *a* and *b* are very similar, while $c(C222_1) \sim 2c(P2_12_12)$. The solution of the present new crystal structure confirms the similarity of the two lattices, which are depicted in Figure 5a for the $C222_1$ form and Figure 5b for the $P2_12_12$ form. In both Figures, four clusters are shown. The global features of the crystal packing are remarkably similar. Upon closer examination, however, it can be seen that the relationship between neighboring molecules is different in the two crystal forms. Specifically, in Figure 5a ($C222_1$ form) the two clusters on the left are related to the two clusters on the right by a crystallographic two fold axis along the *a*-axis at $c=0.5$. In contrast, in Figure 5b ($P2_12_12$ form) they are related to each other by the unit cell translation in the *c*-axis direction. Consequently, the principal interactions between neighboring clusters due to guanine-guanine associations are different in the two crystal forms, as described below.

Guanine-Guanine Interactions

The tetrameric clusters are held together in the crystal lattices by extensive guanine-guanine base pairing along the directions of the *a* and *c* unit cell axes. In the *a*-axis direction, there are two different sets of G-G base pairing interactions. Figure 6a shows the first of the two sets of G-G base pairing which has a two-fold axis lying parallel to and between the planes of the bases. This occurs across the line at $a=0.5$ along the *b*-axis direction (see Figure 5A). The G-G base pair is formed with two symmetrical hydrogen bonds (2.98 and 3.02 Å) between the N2 and N3 atoms of one guanine (G1) to the corresponding N3 and N2 atoms of the other guanine (G3). Interestingly, there is a large propeller twist angle (42°) between the paired guanines.

Figure 6b shows the second set of such similar interactions along *a*, with the two-fold axis now perpendicular to the planes of the guanines. Figure 6c shows a single G-G base pair in the *c*-axis direction. Finally, a different kind of guanine/guanine interaction contributes to cluster interactions in the *b*-axis direction, a partial guanine guanine stacking as shown in Figure 6d.

Although the tetrameric clusters in the $P2_12_12$ crystal form use different guanine-guanine pairs to hold the lattice together (8), similar types of G-G interactions occur (N2 of one G to N3 of another G and vice versa) except in one case. Figure 7a shows the G1-G1* and the G3-G3* base pairings with a two-fold axis perpendicular to the base planes observed in the $P2_12_12$ structure. If we compare this drawing with that of Figure 6b, we can see that the bases in the upper pair (G1-G1*) have slipped with respect to one another such that N3 is no longer involved in base pairing with the N2 of the paired guanine. Instead, the N2 amino group makes a hydrogen bond (3.04 Å) to O4′ of the deoxyribose and simultaneously to the O5′ (3.12 Å) of the molecule (G3*) below.

It is worth noting that similar G-G base pairing interactions are found between two

UM00013141
NOVARTIS EXHIBIT 1517
Novartis v. Regents, IPR2023-01347
Page 1887 of 4460

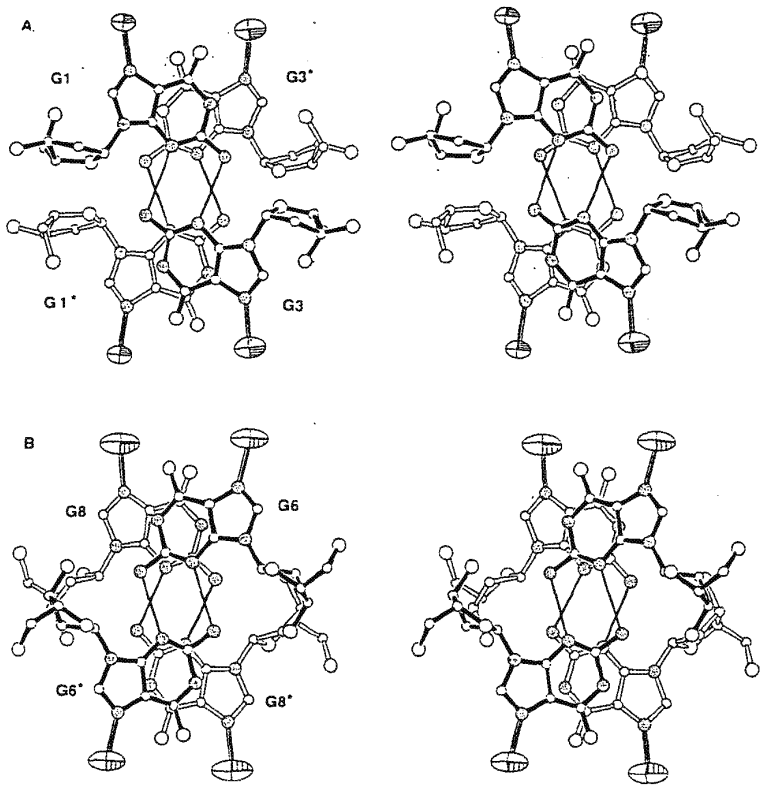


Figure 6: Guanine-guanine interactions in the $C222_1$ crystal lattice. (A). G1-G3*. The * represents the symmetry-related molecule at (-x, y, 0.5-z). There is a large propeller twist angle between the G-G pairs (49°). A two-fold rotational axis along *b* is between the two G-G pairs in the horizontal direction. (B). G6-G6* over G8-G8*. The * represents the symmetry-related molecule at (1-x, y, 0.5-z). The propeller twist angles in both pairs are 51°. The two-fold axis along *b* is at the center and perpendicular to the paper. (C). G2-G2*. The * represents the symmetry-related molecule at (x, -y, 1-z). The two-fold axis along *a* is at the center and perpendicular to the paper. The propeller twist angle is 38°. (D). G5-G7 base-base stacking. The * represents the symmetry-related molecule at (0.5-x, 0.5+y, 0.5-z). The two-fold screw axis along *b* is between the two bases vertically.

B-DNA dodecamer [e.g., d(CGCGAATTCGCG)] double helices in several isomorphous crystal lattices (14,15), as shown in Figure 7b. Two GC base pairs from one end of the helix lie close to two other GC base pairs from the opposite end of a symmetry-related helix, in an interlocking manner in their minor grooves. These G-G interactions are important in fixing two dodecamer molecules along the helical axis in the unit cell *c*-axis direction. From these studies we identify a common pattern of guanine-guanine interactions used extensively in building up different crystal lattices of many guanine-containing DNA molecules. This feature was also found in the structures of many purine derivatives (16) and in two d(CpG) dinucleoside monophosphates (17,18). It is interesting to inquire whether such G-G interactions

UM00013142

NOVARTIS EXHIBIT 1517
Novartis v. Regents, IPR2023-01347
Page 1888 of 4460

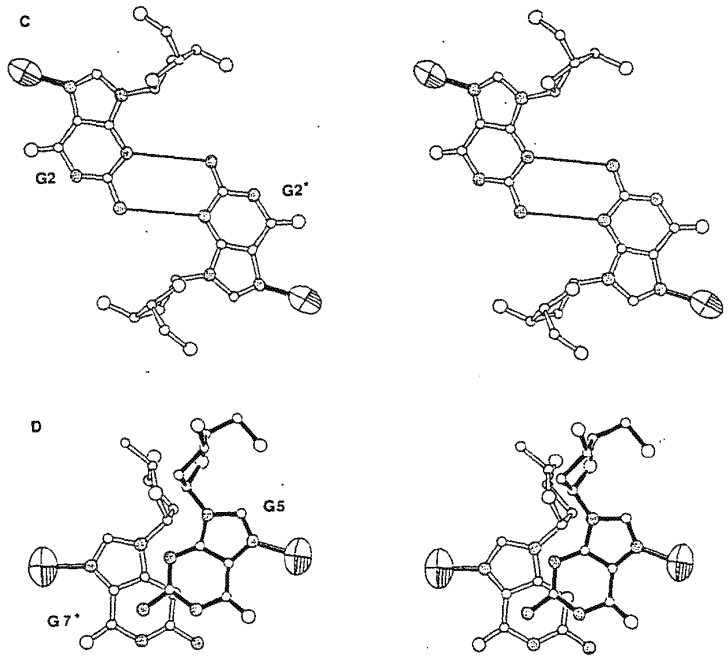


Figure 6 *continued*

might have any biological implications. Guanine is well-known for its associative properties. For example, poly(G) strands can associate with each other forming a four-stranded structure with parallel sugar-phosphate backbones by pairing four guanine bases in a head-to-tail manner (19,20). In this structure, hydrogen bonds are formed between N1 and N2 of one guanine to O6 and N7 of another guanine. This self-associated tetra-guanine structure has recently been proposed to be important in cell meiosis (21). The G-G association observed in the structure described here is different from that in the poly(G) structure. In the present case, all G-G base pairing involving N2 and N3 atoms is between parallel DNA strands. Such pairing is not possible in a regular antiparallel DNA. Recently, several studies have suggested that certain unique structures, including hairpin dimers, might occur at the end of the eukaryotic chromosomal telomer DNA molecules and that such structures might involves some kinds of G-G base pairs (22-24). Those studies pointed out the fact that nature will use many novel base pairing schemes for various biological functions. Whether the G-G pairing observed in the present structure is used in nature, for example in RNA molecules, remains to be determined.

UM00013143
NOVARTIS EXHIBIT 1517
Novartis v. Regents, IPR2023-01347
Page 1889 of 4460

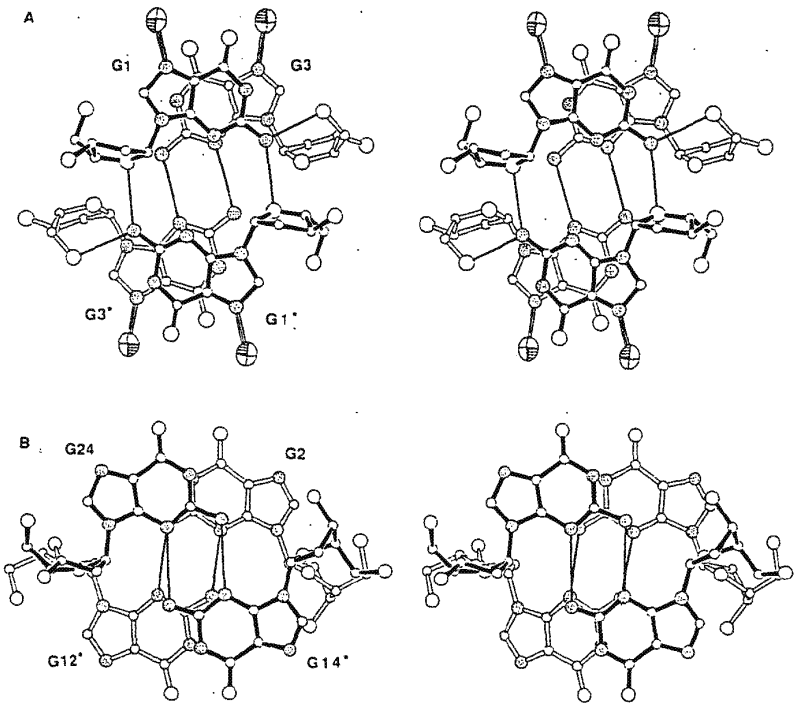


Figure 7: Similar guanine-guanine base pairing interactions in other crystal lattices. (A). G1-G1* over G3-G3* base pairs in the $P2_12_12$ form (7,8). In this structure, the N2 amino group of G1 is now hydrogen bonded to O4' from the deoxyribose, instead of the N3 of the N3 of guanine, of its paired guanine. The * represents the symmetry-related (by the two-fold axis along *c*) molecule at (1-x, 1-y, z). (B). Guanine-guanine base pairings in DNA dodecamer d(CGCAAATTTGCG) (26). The two GC base pairs (G2 and G24) from one end of the helix interlock with two other GC base pairs (G12 and G14) from the other end of the helix of a symmetry-related molecule.

Conclusions

The most conspicuous feature of the present structure is the large dihedral angle between guanines and its concomitant destacking of bases caused by the binding of the drug cisplatin. This geometry is seen in every molecule of the tetrameric aggregates of both $C222_1$ and $P2_12_12$ crystal forms. Solution studies have revealed that the cisplatin adduct of DNA has a distorted conformation similar to what have been seen in the crystal structures. This distortion presumably induces a bend (estimated to be ~32-35°) in the DNA double helix as evident from polyacrylamide gel electrophoresis work revealing that cisplatin complexation retards the mobility of DNA (3,25). Unstacking of two consecutive bases upon cisplatin induced d(GpG) intrastrand crosslinking creates a "kink" in the helix that is probably responsible for the DNA bending. Similar, although less drastic, unstacking of bases at the junction of an oligo-dA tract and a "normal" B-DNA tract due to the high propeller twisted base pairs in the $(dA)_n$·$(dT)_n$ tract has been proposed as a mechanism of DNA bending (26).

UM00013144
NOVARTIS EXHIBIT 1517
Novartis v. Regents, IPR2023-01347
Page 1890 of 4460

Several models of DNA double helices incorporating a single cisplatin binding site have been made based on molecular mechanical calculations (27,28). The stereochemistry depicted by these models could form the basis for the recognition of cisplatin adducts on DNA by the recently discovered damage recognition protein (29,30). Failure to repair such adducts in the tumor cell could lead to the observed anticancer activity of the drug (31).

Acknowledgements

This work is supported by grants from NSF, NIH to AHJW and NIH (CA34992) to SJL. MC was a Fulbright fellow. DG acknowledges the Chaim Weizmann Postdoctoral Fellowship, and SES was an NIH predoctoral trainee. We thank Dr. H. Robinson for his help in generating the color figures.

References

1. Hacker, M.P., Douple, E.B., Hrakoff, I.H., Eds., *Platinum Coordination Complexes in Cancer Chemotherapy*, Martinus Nijhof, Boston, 1984.
2. Sherman, S.E. and Lippard, S.J., *Chem. Rev. 87*, 1153-1181 (1987).
3. Bellon, S.L. and Lippard, S.J., *Biophy. Chem. 35*, 179-188 1990).
4. den Hartog, J.H.J., Altona, C., van Boom, J.H., van der Marel, G.A., Haasnoot, C.A.G. and Reedijk, J., *J.Biomol. Struct. Dyn. 2*, 1137-1155 (1985).
5. Wang, A.H.-J., in *Nucleic Acids and Molecular Biology Vol. 1*, (eds. Eckstein, F. & Lilley, D.M.) pp. 32-54 (Springer, Berlin, 1987).
6. Wang, A.H.-J. and Teng, M.-k., in *Crystallographic and Modeling Methods in Molecular Design*, (Eds. C. Bugg and S. Ealick) Springer-Verlag pp 123-150 (1990).
7. Sherman, S.E., Gibson, D., Wang, A.H.-J. and Lippard, S.J., *Science, 230*, 412-417 (1985).
8. Sherman, S.E., Gibson, D., Wang, A.H.-J. and Lippard, S.J., *J. Amer. Chem. Soc. 230*, 412-417 (1988).
9. Admiraal, G., van der Veer, J.L., de Graaff, R.A., den Hartog, J.H.J. and Reedijk, J., *J. Amer. Chem. Soc. 109*, 592-594 (1987).
10. Main, P., Lessinger, L., Woolfson, M.M., Germain, G., Declercq, J.-P. MULTAN77. Univeristy of York, York, England, and University of Louvain, Louvain, Belgium.
11. Sheldrick, G.M., in *Crystallographic Computing 3*, (Eds. G.M. Sheldrick, C. Kruger and R. Goddard), Clarendon Press, Oxford. 1985.
12. Sheldrick, G.M., in *Computing in Crystallography.*, (Eds. Schenk, H., Olthof-Hazenkemp, R., van Konigsveld, H., Bassi, G.C.) Delft University Press, Delft, The Netherlands, 1978.
13. Hendrickson, W.A. and Konnert, J., in *Biomolecular Structure, Conformation, Function and Evolution*, (ed. Srinvasan, R.) 43-57 (Pergamon, Oxford,1979).
14. Drew, H.R. and Dickerson, R.E., *J. Mol. Biol. 152*, 723-736 (1981).
15. Wang, A.H.-J. and Teng, M.-k., *J. Crystal Growth 90*, 295-310 (1988).
16. Sobell, H.M., *J. Mol. Biol. 18*, 1-7 (1966).
17. Cruse, W.B.T., Egert, E. Kennard, O., Sala, G.B., Salisbury, S.A. and Viswamitra, M.A., *Biochemistry 22*, 1833-1839 (1983).
18. Coll, M., Solans, X., Font-Altaba, M. and Subirana, J.A., *J. Biomol. Struct. Dyn. 4*, 797-811 (1987).
19. Arnott, S., Chandrasekaran, R. and Marttila, C.M., *Biochem. J. 141*, 537-543 (1974).
20. Zimmerman, S.B., Cohen, G.H. and Davies, D.R., *J. Mol. Biol. 92*, 181-192 (1975).
21. Sen, D. and Gilbert, W., *Nature (London), 334*, 364-366 (1988).
22. Henderson, E., Hardin, C.C., Walk, S.K., Tinoco, I. and Blackburn, E.H., *Cell 51*, 899-908 (1987).
23. Sundquist, W.I. and Klug, A., *Nature (London) 342*, 825-829 (1989).
24. Williamson, J.R., Raghuraman, M.K. and Cech, T.R., *Cell 59*, 871-880 (1989).
25. Rice, J.A., Crothers, D.M., Pinto, A.L. and Lippard, S.J., *Proc. Natl. Acad. Sci. USA 85*, 4158-4161 (1988).
26. Coll, M., Frederick, C.A., Wang, A.H.-J. and Rich, A., *Proc. Natl. Acad. Sci. USA 84*, 8385-8389 (1987).

UM00013145
NOVARTIS EXHIBIT 1517
Novartis v. Regents, IPR2023-01347
Page 1891 of 4460

27. Kozelka, J., Petsko, G.A., Lippard, S.J. and Quigley, G.J., *J. Amer. Chem. Soc. 107*, 4079-4081 (1985).
28. Kozelka, J., Archer, S., Petsko, G.A., Lippard, S. J. and Quigley, G. J., *Biopolymers 107*, 4079-4081 (1985).
29. Toney, J.H., Donahue, B.A., Kellett, P.J., Bruhn, S.L., Essigmann, J.M. and Lippard, S.J., *Proc. Natl. Acad. Sci. USA 86*, 8328-8332 (1989).
30. Donahue, B.A., Augot, M., Bellon, S.F., Treiber, D.K., Toney, J.H., Lippard, S.J. and Essigmann, J.M., *Biochemistry 29*, 5872-5880 (1990).
31. Ciccarelli, R.B., Solomon, M.J., Varshavesky, A., Lippard, S., *J. Biochemistry, 24*, 7533-7540 (1985).

Date Received: June 15, 1990

Communicated by the Editor R.H. Sarma

UM00013146

NOVARTIS EXHIBIT 1517
Novartis v. Regents, IPR2023-01347
Page 1892 of 4460

This Page is Inserted by IFW Indexing and Scanning Operations and is not part of the Official Record

BEST AVAILABLE IMAGES

Defective images within this document are accurate representations of the original documents submitted by the applicant.

Defects in the images include but are not limited to the items checked:

- ☐ BLACK BORDERS
- ☐ IMAGE CUT OFF AT TOP, BOTTOM OR SIDES
- ☐ FADED TEXT OR DRAWING
- ☐ BLURRED OR ILLEGIBLE TEXT OR DRAWING
- ☐ SKEWED/SLANTED IMAGES
- ☐ COLOR OR BLACK AND WHITE PHOTOGRAPHS
- ☐ GRAY SCALE DOCUMENTS
- ☐ LINES OR MARKS ON ORIGINAL DOCUMENT
- ☐ REFERENCE(S) OR EXHIBIT(S) SUBMITTED ARE POOR QUALITY
- ☐ OTHER: _____

IMAGES ARE BEST AVAILABLE COPY.
As rescanning these documents will not correct the image problems checked, please do not report these problems to the IFW Image Problem Mailbox.

tively, were prepared, giving correspondingly amplified ellipsometric thickness and absorbance. Respective emission decays were identical to those of the unquenched and quenched bilayer structures discussed above.

In summary, we have reported the synthesis, film-forming properties, and photophysical data on **1** and **2**. The films are stable to hot solvents and may be built up repetitively with reproducible thickness per layer and fluorescence behavior. Thus, we introduce a photocharge-generating element to a material class where nonlinear optical, rectifying, and insulating components could also be present at arbitrary positions. Work is in progress to observe and measure lifetimes of the photoinduced charge separated species directly, and to explore the electrical and optical properties of multiple-component superlattices prepared by Zr phosphonate deposition.

Acknowledgment. We are grateful to C. Chidsey, M. L. Schilling, and L. Brus for valuable discussions during the course of this work.

Supplementary Material Available: Synthetic schemes for **1** and **2** (2 pages). Ordering information is given on any current masthead page.

Supramolecular Chemistry of $[Mn(CO)_3(\mu_3\text{-}OH)]_4$: Assembly of a Cubic Hydrogen-Bonded Diamondoid Network with 1,2-Diaminoethane

Steven B. Copp, S. Subramanian, and Michael J. Zaworotko*

Department of Chemistry, Saint Mary's University Halifax, Nova Scotia, B3H 3C3 Canada

Received July 2, 1992

Predictable self-organization of molecules into one-, two-, or three-dimensional hydrogen-bonded architectures is an area of supramolecular chemistry that is of great current interest.[1] Such research is particularly relevant in the context of solid-state chemistry since rational design, i.e., crystal engineering, of solids has important ramifications for the development of new materials with unusual physical properties.[2] An aspect of this chemistry that is particularly pleasing from an aesthetic perspective and has a number of potential applications, particularly in the area of host–guest chemistry, concerns the construction of three-dimensional hydrogen-bonded diamondoid open networks. The concept was delineated by Ermer in 1988, who demonstrated that if tetrafunctionalized organics with approximate tetrahedral symmetry have the capability to associate via hydrogen bonds, then diamondoid networks may result.[3] Unfortunately, the relative sizes of the cavities formed by adamantane-1,3,5,7-tetracarboxylic acid and 3,3-bis(carboxymethyl)glutaric acid ("methanetetraacetic acid") facilitate interpenetration of five[3a] and three[3b] networks, respectively, thereby precluding formation of internal chambers. However, Ermer subsequently demonstrated that enclathration

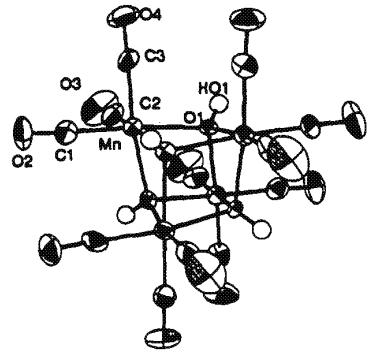
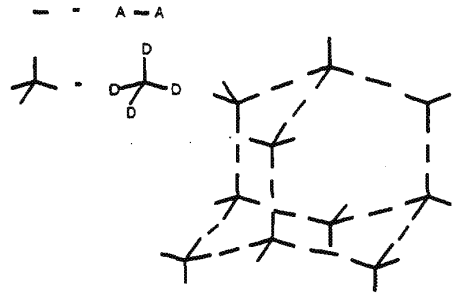
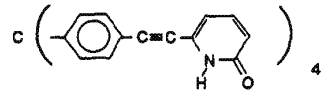


Figure 1. Perspective view of a molecule of **2** as it exists in **3**. Intramolecular distances and angles are within expected ranges.[6,7]

Chart I



can be attained with double-diamond 2,6-dimethylidene-adamantane-1,3,5,7-dicarboxylic acid networks,[4] and in a significant development, Wuest recently demonstrated that tecton **1** can self-assemble to form a diamondoid network that does not



1

interpenetrate and is capable of enclathration.[5] In this communication we develop the theme further by outlining an alternate approach to assembly of diamondoid networks: assembly of a rigid tetrafunctional hydrogen-bond donor with complementary difunctional hydrogen-bond-acceptor molecules (Chart I).

A molecule which possesses S_4 symmetry and the requisite four H-bond donors[6] is the cubane-like cluster $[Mn(CO)_3(\mu_3\text{-}OH)]_4$, **2**, which can be synthesized quantitatively in one step from $Mn_2(CO)_{10}$.[7] Reaction of **2** with excess 1,2-diaminoethane, en, in toluene immediately affords a yellow-orange precipitate, which may be recrystallized from $CHCl_3/CH_3CN$ to afford cocrystals of composition **2**·2en, **3**.[8] X-ray crystallographic analysis[9] reveals

(1) For recent reports, see: (a) Krishnamohan, C. V.; Panneerselvam, K.; Pilati, T.; Desiraju, G. R. *J. Chem. Soc., Chem. Commun.* **1992**, 832. (b) Garcia-Tellado, F.; Geib, S. J.; Goswami, S.; Hamilton, A. D. *J. Am. Chem. Soc.* **1991**, *113*, 9265. (c) Geib, S. J.; Hirst, S. C.; Vicent, C.; Hamilton, A. D. *J. Chem. Soc., Chem. Commun.* **1991**, 1283. (d) Zhao, X.; Chang, Y.-L.; Fowler, F. W.; Lauher, J. W. *J. Am. Chem. Soc.* **1990**, *112*, 6627. (e) Lehn, J.-M.; Mascal, M.; DeCian, A.; Fischer, J. *J. Chem. Soc., Chem. Commun.* **1990**, 479. (f) Etter, M. C. *Acc. Chem. Res.* **1990**, *23*, 120.

(2) (a) Lehn, J.-M. *Angew. Chem., Int. Ed. Engl.* **1990**, *29*, 1304. (b) Allcock, H. R. *Science* **1992**, *255*, 1106. (c) Aakeroy, C. B.; Hitchcock, P. B.; Seddon, K. R. *J. Chem. Soc., Chem. Commun.* **1992**, 553. (d) Desiraju, G. R. *Crystal Engineering. The Design of Organic Solids*; Elsevier: Amsterdam, 1989. (e) Frankenbach, G. M.; Etter, M. C. *Chem. Mater.* **1992**, *4*, 272.

(3) (a) Ermer, O. *J. Am. Chem. Soc.* **1988**, *110*, 3747. (b) Ermer, O.; Eling, A. *Angew. Chem., Int. Ed. Engl.* **1988**, *27*, 829.

(4) Ermer, O.; Lindenberg, L. *Helv. Chim. Acta* **1991**, *74*, 825.

(5) Simard, M.; Su, D.; Wuest, J. D. *J. Am. Chem. Soc.* **1991**, *113*, 4696.

(6) **2** is able to form isolable 1:4 adducts with H-bond acceptors as diverse in nature as water and triphenylphosphine oxide: Clerk, M. D.; Copp, S. B.; Subramanian, S.; Zaworotko, M. J. *Supramol. Chem.* **1992**, *1*, 7.

(7) Clerk, M. D.; Zaworotko, M. J. *J. Chem. Soc., Chem. Commun.* **1991**, 1607.

(8) In a typical reaction, a recrystallized yield of **3** of 80% is afforded. IR (KBr, cm^{-1}): ν_{CO} 2011 s, 1916 s; $\nu_{NH,OH}$ 3375 bs. Anal. Found: (calcd) C, 26.12 (25.84); H, 2.68 (2.69); N, 7.26 (7.53).

0002-7863/92/1514-8719$03.00/0 © 1992 American Chemical Society

UM00013148
NOVARTIS EXHIBIT 1517
Novartis v. Regents, IPR2023-01347
Page 1894 of 4460

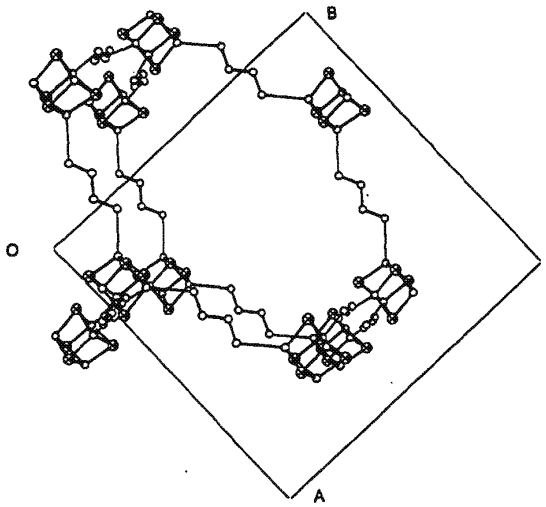


Figure 2. Perspective view of the tertiary structure of 3 viewed down the c-axis. For the sake of clarity, an adamantane-like unit of only one of the three networks is illustrated and all hydrogen atoms and carbonyl ligands are omitted.

that 3 exists in the solid state as an undistorted triple diamondoid network of 2 linked by en bridges. O···N and O–H···N distances of 2.774 (8) and 1.94 (6) Å, respectively, O–H···N angles of 165 (5)°, and IR spectroscopy[8] confirm the presence of hydrogen bonds. The O–H···en···H–O linkages therefore serve the same geometric function as C–C bonds in diamond but can be much more readily disassembled and reassembled. The rigid tetrahedral geometry of 2, which is illustrated in Figure 1, is reinforced crystallographically since 2 lies around a $\bar{4}$ position. The adamantane-like architecture of one of the independent diamondoid networks of 3 is illustrated in Figure 2.

The relative size and shape of 2, the length of en, and the interpenetration of the networks do not facilitate enclathration of guest molecules; however, the concept of assembly of complementary molecules to generate diamondoid networks is confirmed. A significant feature of this concept (as opposed to self-assembly of identical molecules) is that judicious choice of the bridging H-bond-acceptor moiety should permit rational design of cavity size without extensive synthetic procedures (i.e., breakage or formation of covalent bonds). As noted previously,[3,4] there are numerous potential applications of diamondoid networks. In addition to those already discussed, we point out that molecules such as 2 may be photoreactive[10] and that 2 is not the only cubane cluster with such geometric features.[11] The generality of the approach to construction of diamondoid and other hydrogen-bonded networks outlined herein is currently under further investigation in our laboratory.[12]

Acknowledgment. We thank the NSERC, Canada (operating grant, M.J.Z.), and Saint Mary's University (Senate research grants, purchase of the X-ray diffractometer) for support of this work.

Supplementary Material Available: Crystallographic report, atomic parameters, U values, and interatomic distances and angles for 3 (3 pages); listing of observed and calculated structure factors for 3 (4 pages). Ordering information is given on any current masthead page.

(9) Crystals of 3 belong to the noncentrosymmetric cubic space group $I\bar{4}3d$ (T_d^6, No. 220) with a = 20.733 (3) Å, V = 8912.2 (13) Å^3, D_{calcd} = 1.66 g cm^{-3}, and Z = 12. Molecules of 2 lie around a $\bar{4}$ position whereas the bridging en molecules lie around 2-fold axes. Full matrix least-squares refinement of all non-hydrogen atoms with anisotropic thermal parameters, the μ_3-OH hydrogen atom with an isotropic thermal parameter, and with all other hydrogen atoms fixed in calculated positions, afforded R = 0.027 and R_w = 0.026. The tertiary structure consists of three independent diamondoid networks based upon molecules of 2 that lie 11.59 Å from each other around corresponding sets of four $\bar{4}$ positions (Set 1: $^7/_8$, 0, $^1/_4$; $^5/_8$, 0, $^3/_4$; $^3/_8$, $^1/_2$, $^3/_4$, $^1/_8$, $^1/_2$, $^1/_4$. Set 2: $^1/_4$, $^7/_8$, 0; $^3/_4$, $^5/_8$, 0; $^5/_4$; $^3/_8$, $^1/_2$; $^1/_4$; $^1/_8$; $^1/_2$. Set 3: 0, $^1/_4$, $^7/_8$; 0, $^3/_4$, $^5/_8$; $^1/_2$, $^1/_4$, $^3/_8$; $^1/_2$, $^1/_4$, $^5/_8$). The network illustrated in Figure 2 is based upon set 2.

(10) Mn_4O_4 cubes are considered a model for one of the "S-states" of PS-II, a water oxidation enzyme: Proserpio, D. M.; Hoffmann, R.; Dismukes, G. C. *J. Am. Chem. Soc.* **1992**, *114*, 4364 and references therein.

(11) There are numerous examples of rigid M_4X_4 cubanes spanning a wide range of metals (including main group) and X moieties. 2 has close analogues in $[Mo(CO)_2(NO)(\mu_3\text{-}OH)]_4$, which also forms a 1:4 adduct with triphenylphosphine oxide (Albano, V.; Bellon, P.; Ciani, G.; Manassero, M. *J. Chem. Soc., Chem. Commun.* **1969**, 1242) and $[Re(CO)_3(\mu_3\text{-}OH)]_4$ (Herberhold, M.; Suss, G.; Ellermann, J.; Gabelein, H. *Chem. Ber.* **1978**, *111*, 2931). X could also be an H-bond acceptor, thereby facilitating assembly of diamondoid networks with rigid tetrafunctional H-bond acceptors and simple difunctional H-bond-donor molecules.

(12) A plethora of potential bridging molecules exists. A double diamondoid network is obtained when 2 is cocrystallized with the bulkier but longer hydrogen-bond acceptor 1,2-bis(diphenylphosphinyl)ethane). The two interweaved diamondoid networks are tetragonally distorted, and the phenyl rings are disordered, resulting in an R value of 0.11. Space group $P4_2/n$, a = 14.290 (5) Å, c = 18.028 (8) Å, V = 3681.4 Å^3, Z = 2. Full details will be published at a later date.

Trisilaallyl Anion Structures. Is Conjugation Effective?

Anatoli A. Korkin and Paul von Ragué Schleyer*

Institut für Organische Chemie der Friedrich-Alexander Universität Erlangen-Nürnberg Henkestrasse 42, D-8520 Erlangen, Germany

Received July 13, 1992

To what extent can analogies between carbon and silicon species be applied to the trisilaallyl anion $SiH_2SiHSiH_2^-$, 1? Is the potential resonance energy in 1 sufficient to overcome the inherent nonplanar preferences of the related silicon species? While the methyl anion inversion barrier is only 2.3 kcal/mol at MP2/6-31+G*,[1] the SiH_3^- barrier is an order of magnitude higher (25.9 kcal/mol).[2] Unsaturated carbon species are planar, while the silicon analogs are not. The bent structures of disilaethylene[3] and hexasilabenzene[4] are examples.[4c]

The structure and stabilization energy of the allyl anion (2) have been determined both experimentally and theoretically,[5] but

(1) See: Salzner, U.; Schleyer, P. v. R. *Chem. Phys. Lett.* **1992**, in press and references cited for other values.

(2) Reliable earlier estimations of the SiH_3^- inversion barrier are in the 25.4–26.5 kcal/mol range: (a) Keil, F.; Ahlrichs, R. *Chem. Phys.* **1975**, *8*, 384. (b) Eades, R. A.; Dixon, D. A. *J. Chem. Phys.* **1980**, *72*, 3309. (c) Reed, A. E.; Schleyer, P. v. R. *Chem. Phys. Lett.* **1987**, *133*, 553. (d) Shen, M.; Xie, Ya.; Schaefer, H. F., III. *J. Chem. Phys.* **1990**, *93*, 8098–8104. (e) Hopkinson, A. C.; Rodriquez, C. F. *Can. J. Chem.* **1990**, *68*, 1309–1316.

(3) (a) Apeloig, Y.; Kerni, M.; Chandrasekhar, J.; Schleyer, P. v. R. *J. Am. Chem. Soc.* **1986**, *108*, 270. (b) Olbrich, G. *Chem. Phys. Lett.* **1986**, *130*, 115. (c) Teramae, H. *J. Am. Chem. Soc.* **1987**, *109*, 4140. (d) Hrovat, D. A.; Sun, H.; Borden, W. T. *THEOCHEM* **1988**, *163*, 51. (e) Boatz, J. A.; Gordon, M. S. *J. Phys. Chem.* **1990**, *94*, 7331. (f) Trinquier, G. *J. Am. Chem. Soc.* **1990**, *112*, 2130.

(4) (a) Nagase, S.; Kudo, T.; Aoki, M. *J. Chem. Soc., Chem. Commun.* **1985**, 1121. (b) Clabo, D. A.; Schaefer, H. F., III. *J. Chem. Phys.* **1986**, *84*, 1664. (c) Nagase, S.; Teramae, H.; Kudo, T. *J. Chem. Phys.* **1987**, *86*, 4513. (d) Sax, A. F.; Kalcher, J.; Janoschek, R. *J. Comput. Chem.* **1988**, *9*, 564. (e) Apeloig, Y. In *The Chemistry of Organic Silicon Compounds Part 1*; Patai, S., Rappoport, Z., Eds.; Wiley Interscience: New York, 1989; pp 57–225.

(5) (a) Schleyer, P. v. R. *J. Am. Chem. Soc.* **1985**, *107*, 4793. (b) Charton, M.; Greenberg, A.; Stevenson, T. A. *J. Org. Chem.* **1985**, *50*, 2643–2646. (c) Schleyer, P. v. R.; Spitznagel, G. W.; Chandrasekhar, J. *Tetrahedron Lett.* **1986**, *27*, 4411–4414. (d) Lindh, R.; Roos, B. O.; Jonsäll, G.; Ahlberg, P. *J. Am. Chem. Soc.* **1986**, *108*, 2853–2862. (e) Gonzalez-Luque, R.; Nebot-Gil, I.; Merchan, M.; Thomas, F. *Theor. Chim. Acta* **1986**, *69*, 101. (f) Froelicher, S. W.; Freiser, B. S.; Squires, R. R. *J. Am. Chem. Soc.* **1986**, *108*, 2853–2862. (g) Dorigo, A. E.; Li, Y.; Houk, K. N. *J. Am. Chem. Soc.* **1989**, *111*, 6942–6948. (h) Wiberg, K. B.; Breneman, C. M.; LePage, T. J. *J. Am Chem. Soc.* **1990**, *112*, 61–72. (i) Oakes, J. M.; Ellison, G. B. *J. Am. Chem. Soc.* **1984**, *106*, 7734.

0002-7863/92/1514-8720$03.00/0 © 1992 American Chemical Society

UM00013149
NOVARTIS EXHIBIT 1517
Novartis v. Regents, IPR2023-01347
Page 1895 of 4460

(S)-Spiro[(1,3-diazacyclopent-1-ene)-5,2′-(7′-methyl-1′,2′,3′,4′-tetrahydronaphthalene)]: Resolution, Stereospecific Synthesis, and Preliminary Pharmacological Characterization as a Partial α-Adrenergic Agonist

Alex A. Cordi,* Jean-Michel Lacoste, Fabrice Le Borgne,† Yolande Herve,† Lucile Vaysse-Ludot,† Jean-Jacques Descombes, Christine Courchay, Michel Laubie, and Tony J. Verbeuren

Institut de Recherches Servier, 11, rue des Moulineaux, 92150 Suresnes, France, and ORIL, 13, rue Auguste Desgenétais-B.P.17-76210 Bolbec, France

Received April 29, 1997®

Recently, we reported on the design, synthesis, and structure–activity relationships of a series of spiroimidazolines endowed with α-adrenergic agonist activities. Among the compounds described, (*R*,*S*)-spiro(1,3-diazacyclopent-1-ene)-[5,2′](7′-methyl-1′,2′,3′,4′-tetrahydronaphthalene) fumarate (**5*RS***) was chosen for further development as a venotonic agent. The resolution of this compound, as well as the pharmacological characterization of the enantiomers, stereospecific synthesis of eutomer (**5*S***, S 18149), and determination of absolute configuration by single-crystal X-ray diffraction analysis, are described.

Introduction

Recently, we reported on the design, synthesis, and structure–activity relationships of a series of spiroimidazolines endowed with α adrenergic agonist activities.[1] Among the compounds described, (*R*,*S*)-spiro(1,3-diazacyclopent-1-ene)-5,2′]-(7′-methyl-1′,2′,3′,4′-tetrahydronaphthalene) fumarate (**5*RS***) was chosen for further development as a venotonic agent. Indeed, this compound is the prototype of a venospecific constrictor as it is able to constrict the saphenous vein of the dog without noticeable effects on the mean arterial pressure.

As this compound contains an asymmetric center at carbon 5-2′, it was important to assess the influence of chirality on the pharmacological properties of compound **5*RS***. In fact, regulatory agencies are increasingly concerned[2] by the administration of racemic compounds as drugs if no benefit can be related to the presence of each of the enantiomers. In addition, it is preferential to investigate whether the observed pharmacological properties reside in one enantiomer, an eventuality which could accelerate development.[3]

We now report on the resolution of this racemic compound, describe the preliminary pharmacological characterization of the most active enantiomer, and document the determination of its absolute configuration as well as its stereospecific synthesis.

Chemistry

The resolution of the two enantiomers of **5*RS*** was initially achieved by recrystallization of the dibenzoyl-L-tartaric salt in ethanol. Resolution was monitored by chiral HPLC. After three crystallizations the enantiomeric purity exceeded the limit of detection of the analytical method (ee >96%), the salt was decomposed in strong basic media, and the free base was transformed into the fumarate in 2-propanol to afford **5*R***. The opposing enantiomer was obtained by evaporation of the initial filtrates, followed by decomposition of the salt by the addition of a strong base and dichloromethane extraction. The crude free base was combined with an equimolecular amount of the D enantiomer of dibenzoyltartaric acid and crystallized twice in ethanol to afford the opposite enantiomer **5*S*** in ee >96%.

Our approach toward the stereospecific synthesis of **5*S*** was inspired by the work of Weinges et al.[4] who synthesized (*R*)-α-methylphenylalanine by a stereospecific Strecker synthesis using (1*R*)-phenylethylamine as chiral inducer. Stereospecific Strecker synthesis[5] have been successfully exemplified in recent years starting mainly from aromatic aldehydes;[6–13] however comparatively little success has been achieved starting from ketone substrates.[14,15] In our case (Scheme 1) we used the 7-methyl-2-tetralone as template, a ketone with little difference between its two arms: a benzyl residue and a phenylethyl residue. The reaction proceeded cleanly and in high yield to give a diastereoisomerically pure solid endowed with the desired 2*S* configuration. As the Strecker reaction is a reversible process, the complete diastereoselectivity observed during this procedure is probably linked to the crystallization of one pure diastereoisomer exhibiting much lower solubility than the other and therefore displacing the whole equilibrium in favor of the production of this sole enantiomeric adduct. In this respect, it is worth mentioning that improvements of yield were obtained by increasing the water content of the solvent mixture, leading to better recovery of the poorly soluble product. Attempts to characterize the presence of the other diastereoisomer in the mother liquors failed. As expected, the mirror-image reaction starting from (1*S*)-phenylethylamine led, in the same conditions, to **5*R*** in comparable yields (data not shown).

Biology

The two enantiomers **5*S*** and **5*R*** as well as the racemic **5*RS*** described above were tested for their biological activity in the pithed rat (*in vivo*) and on contractibility of isolated canine saphenous veins and femoral arteries (*in vitro*). The pithed rat assay allows quantitative determination of the impact of the tested

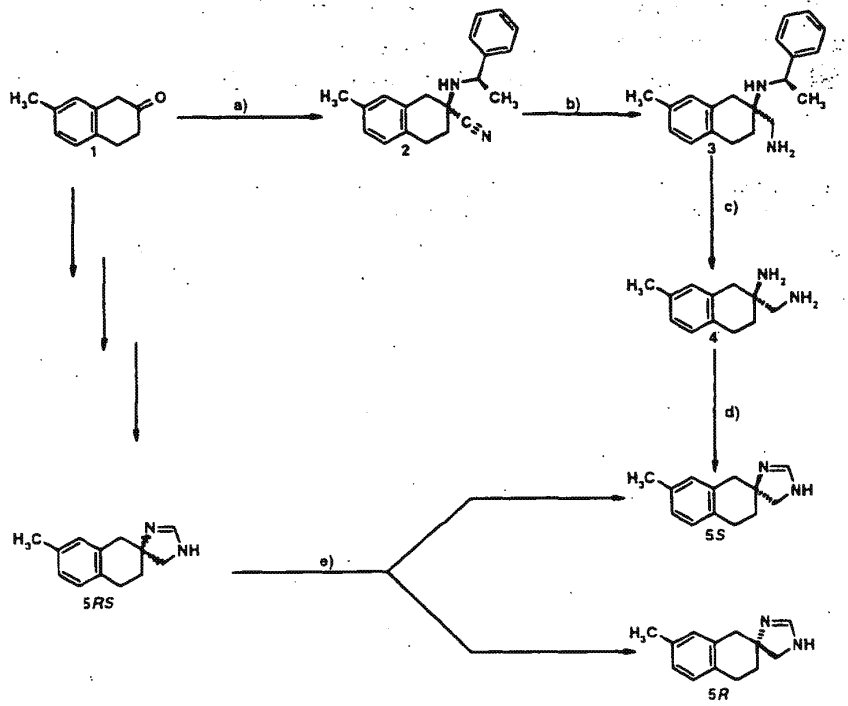
† ORIL.

® Abstract published in *Advance ACS Abstracts*, August 1, 1997.

S0022-2623(97)00282-3 CCC: $14.00 © 1997 American Chemical Society

UM00013150
NOVARTIS EXHIBIT 1517
Novartis v. Regents, IPR2023-01347
Page 1896 of 4460

Scheme 1[a]



[a] Reagents and conditions: (a) (*R*)-α-methylbenzylamine, NaCN, AcOH, EtOH, MeOH, H_2O, 94% yield; (b) $LiAlH_4$, THF, 93% yield; (c) H_2, 5% Pd/C, MeOH, 78% yield; (d) HC(=NH)NH_2·AcOH, EtOH, 87% yield; (e) dibenzoyl-D-tartaric acid or dibenzoyl-L-tartaric acid, EtOH, 11 and 6% yield, respectively.

Table 1. *In Vitro* and *in Vivo* α-Adrenergic Activity of Compounds **5**

Cpd #	Structure	Pithed rat: Control C_{20}[a]	Pithed rat: Control Max[b]	Pithed rat: $C_{20antag}$[c]/$C_{20control}$ Praz	Pithed rat: $C_{20antag}$[c]/$C_{20control}$ Yohim	Isolated blood vessel: Femoral Artery EC_{50}[d] (μM)	Isolated blood vessel: Femoral Artery E_{max}[e]	Isolated blood vessel: Saphenous Vein EC_{50}[d] (μM)	Isolated blood vessel: Saphenous Vein E_{max}[e]
6	St 587	8.6±1.6	129±4	16	1.8	10.9±7.9	19.7±2.1	2.02±0.77	54.4±10.2
5RS		6.7±0.6	112±2	6.1	7.9	>3	7.7±2.2	0.36±0.01	68.5±8.6
5R		44.8±4.6	109±5	20	12	>3	8.4±2.8	2.8±0.39	39.4±10.2
5S		5.8±1.5	106±4	6.5	4.2	>3	15.8±3	0.22±0.05	78.3±9.1

[a] Concentration which increases the arterial pressure by 20 mmHg in the pithed rat, expressed in μg/kg iv (mean ± SEM, $n = 5$). [b] Maximal pressure response (mean ± SEM) caused by the agonist, expressed in mmHg (the maximum obtained with phenylephrine is 150 mmHg). [c] Ratio of C_{20} obtained in the absence or presence of 0.1 mg of prazosin or 1 mg of yohimbine. [d] EC_{50} value for the agonist in the isolated blood vessel shown in μM (mean ± SEM, $n = 6-12$). [e] E_{max} = maximal contractile response obtained with the agonist expressed as percentage (mean ± SEM) of the maximal contraction to KCl (100 mM) in the blood vessel indicated.

compounds on the vascular tone defined by the dose (in μg/kg iv) which increases the arterial blood pressure by 20 mmHg (C_{20} in Table 1). Additionally, the maximal pressor response caused by the agonist (Max), expressed in mmHg, is an indication of the efficacy of the tested compounds. In the same assay, the use of selective α_1- and α_2-adrenoceptor antagonists (prazosin and yohimbine) in the presence of the tested compounds allows the definition of a C_{20} ratio (Praz and Yohim, respectively), which are indicative of the contribution of α_1- and α_2-adrenergic mechanisms to the pressor response. The *in vitro* evaluation allows the comparison in terms of affinity (EC_{50}) and efficacy (E_{max}) on two types of vascular beds which might be responsible for either the expected therapeutic efficacy (saphenous vein) or the potential side effect (femoral artery).

UM00013151
NOVARTIS EXHIBIT 1517
Novartis v. Regents, IPR2023-01347
Page 1897 of 4460

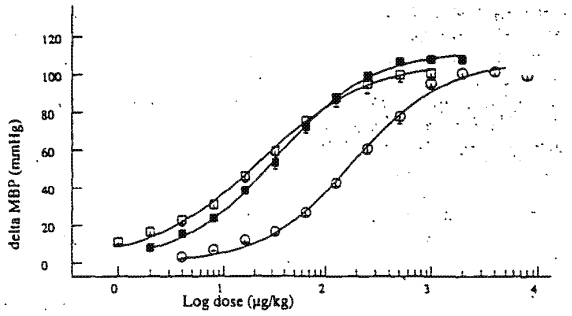


Figure 1. Effect of compounds **5** in the pithed rat. Dose–response effect of **5*RS*** (n = 5) (■), **5*R*** (n = 5) (○), and **5*S*** (n = 8) (□) on mean arterial blood pressure (MBP) in the pithed rat. Data are shown as means ± SEM.

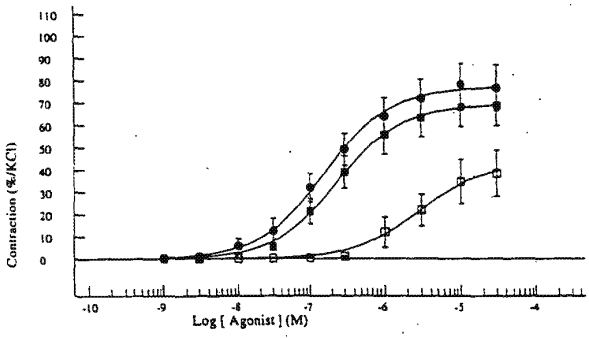


Figure 2. Effect of compounds **5** on the dog saphenous vein without Endothelium. Contractile activity of increasing concentrations of **5*RS*** (■), **5*R*** (□), and **5*S*** (●) on the dog saphenous vein without endothelium. Data are the means ± SEM of 6–12 experiments.

Results and Discussion

The results of the biological evaluations of compounds **5** are presented in Figures 1 and 2, as well as in Table 1. In the pithed rat (Figure 1), the three compounds were administered in cumulative doses iv to three groups of rats. These doses caused dose-related pressor responses. The effect of **5*S*** was comparable to that of **5*RS***. **5*R*** was significantly less potent than **5*RS*** and **5*S*** but caused comparable increases in arterial blood pressure at the highest doses used. The maximal pressor response was reached with **5*R*** at 4 mg/kg but with **5*RS*** and **5*S*** at 1 mg/kg. The experiments were repeated using the same cumulative doses after blockade of α_1-adrenoceptors with prazosin (100 μg/kg iv 10 min before) and after blockade of α_2-adrenoceptors with yohimbine (1 mg/kg iv 10 min before). Both the α_1- and α_2-adrenoceptor antagonists led to significant and comparable displacement of the dose–response curve to the right (data not shown). Prasozin also decreased the maximal pressor response induced by compounds **5**. The maximal responses were reached with **5*RS*** and **5*S*** at 1 mg/kg in the control group and at 4 mg/kg in both prazosin- and yohimbine-treated animals. These experiments offer *in vivo* evidence that **5*S*** is the eutomer of the racemic mixture **5*RS*** and acts as a partial agonist at both α_1- and α_2-adrenoceptors.

In dog femoral arteries, compounds **5** evoked weak concentration-dependent contractions (data not shown); the maximal responses and the affinities of the three compounds were not significantly different and averaged

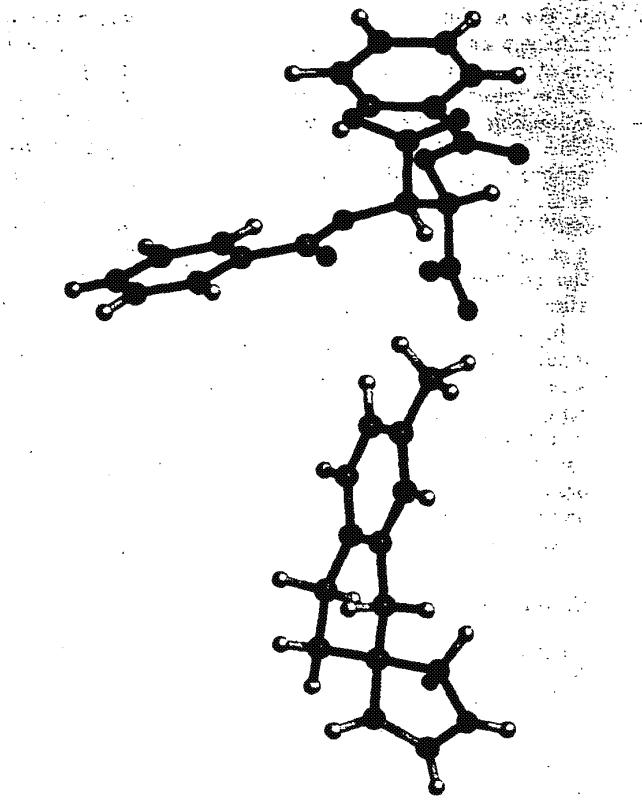


Figure 3. Single-crystal X-ray structure of **5*S*** as a dibenzoyl-D-tartaric acid salt.

less than 16% of the responses obtained with KCl (100 mM). In dog saphenous veins, compounds **5** evoked concentration-dependent contractions (Figure 2); the maximal response and the affinities of the three compounds were in the following order of potency: **5*S*** > **5*RS*** ≫ **5*R***, indicating that in this tissue also, **5*S*** is the active enantiomer of **5*RS***. A comparison of the maximal effects of **5*S*** in the dog saphenous vein (78.3 ± 9.1%) and femoral artery (15.8 ± 3%) shows that the response was significantly ($p \leq 0.001$) greater in the vein than in the artery.

In our previous report,[1] we discussed the use of an empirical ratio between the C_{20} value in the pithed rat and the EC_{50} value obtained in the vein as a discriminator in the search of venous specific compounds. When the same calculations were made from the number displayed in Table 1, the following order of venous specificity is obtained **5*S*** (26) > **5*RS*** (19) > **5*R*** (16), confirming that all the favorable properties of the racemic (potency and selectivity) are present in only one enantiomer: **5*S***. As all the curves were parallel, one can speculate that the residual activity of **5*R*** in these assays is linked to the likely presence of small amounts of **5*S*** (<2% according to the accuracy of the analytical method) in "pure" *R* enantiomer samples.

The absolute configuration of **5*S*** was obtained through single-crystal X-ray diffraction analysis performed on the dibenzoyl-D-tartaric acid salt, by Dr. C. Pascard at ICSN (Gif sur Yvette). The absolute configuration of the tartaric acid being known, the configuration of carbon 2 is *S* (Figure 3). One atom of hydrogen appeared on each nitrogen atom, the two C–N bonds

UM00013152
NOVARTIS EXHIBIT 1517
Novartis v. Regents, IPR2023-01347
Page 1898 of 4460

in the imidazoline are equal (1.29 Å), and the N1 nitrogen atom is in equatorial position as anticipated in the design process.[1] Additionally, two hydrogen bonds joined each of the nitrogens to two oxygen atoms belonging to different molecules N1−H−O (2.73 Å) and N3−H−O (2.76 Å). It is worth mentioning that the absolute configuration disclosed in the eutomer is the same as that seen for SDZ-NVI 085[16] and SK&F 1-89748,[17] two other α-adrenoceptor agonists exhibiting a comparable chiral center which is in fact absent in the endogenous hormones adrenaline and noradrenaline.

In conclusion, our quest for a potent and selective α-adrenoceptor agonist endowed with a particular venous selectivity has terminated with the selection of **5S**. The compound is currently under development as S 18149 to test the initial hypothesis that such compounds might be useful in the treatment of venous disease and the prevention of ulcers. Further characterization of the pharmacological properties of **5S** has already appeared in abstract forms.[18,19]

Experimental Section

Biology. Methods (pithed rat and isolated blood vessels) described in ref 1 were used without changes.

Chemistry. Reagents were commercially available and of synthetic grade. ^{1}H NMR spectra relative to TMS were recorded on Bruker 200 or 400 MHz spectrometers. Infrared spectra were obtained as Nujol emulsion, on a Bruker Fourier transform spectrometer. All new substances were homogeneous in TLC and exhibited spectroscopic data consistent with the assigned structures. Elemental analyses (C, H, N) were performed on a Carlo Erba 1108 instrument and agree with the calculated values within the ±0.4% range. Melting points were obtained on a Reichert hot stage microscope and are uncorrected. Silica gel 60, Merck 230−400 mesh, was used for both flash and medium-pressure chromatography. TLC were performed on precoated 5 × 10 cm, Merck silica gel 60 F254 plates (layer thickness 0.25 mm). Gas chromatography was performed on a 5890 Hewlett-Packard instrument with a CP Sil 5 CB column (50 m × 0.32 mm), on column injection (150 °C), FID detection (280 °C), $t°$ raising from 100 to 250 °C at the rate of 15 °C/min and then holding this $t°$ for 20 mn. Chiral HPLC were performed on a Hewlett-Packard series 1050 instrument equipped with a UV variable detector set at 220 nm and a DAICEL Chiralpack AS column eluted with a mixture of *n*-heptane/2-propanol/diethylamine (920/80/0.5).

(*R*)-Spiro[(1,3-diazacyclopent-1-ene)-5,2′-(7′-methyl-1′,2′,3′,4′-tetrahydronaphthalene)], Fumarate (5*R*). Resolution by Formation of Diastereoisomeric Salts. A solution of dibenzoyl-L-tartaric acid (9.41 g, 25 mmol) in ethanol (200 mL) was added to a stirred solution of (*R,S*)-spiro-[(1,3-diazacyclopent-1-ene)-5,:2′-(7′-methyl-1′,2′,3′,4′-tetrahydronaphthalene)][1] (**5*RS***, 5 g, 25 mmol) in ethanol (170 mL). The solution was filtered and concentrated under reduced pressure to provide an amorphous residue which was dissolved in boiling ethanol (550 mL). After cooling at 20 °C for 2 h and then at 5 °C overnight, crystals formed which were filtered, washed with a small amount of cold ethanol, and dried under reduced pressure (4.7 g, ee: 76%). This crystallization procedure was repeated three times under the same conditions (minimum amount of ethanol to ensure the complete dissolution ≃ 100 mL/g) until enantiomeric purity was superior to 98%, as indicated by chiral HPLC. The pure diastereoisomeric salt (1.3 g, ee: ≥96%) was taken up in water (10 mL) and treated with concentrated aqueous NaOH (5 mL); the free base was extracted with CH_2Cl_2 (3 × 15 mL). The combined organic phases were dried over $MgSO_4$, filtered, and evaporated to yield a white solid (0.44 g, 2.2 mmole). The solid was dissolved in boiling 2-propanol (20 mL) in the presence of fumaric acid (0.255 g, 2.2 mmol) and the resulting solution filtered hot. A minimum of diethyl ether was added until a haze appeared; the system was cooled to 5 °C and left overnight. The desired compound was obtained after filtration and drying, as colorless crystals (0.46 g, 6%): mp 163−164 °C; ^{1}H NMR (DMSO-d_6) δ 8.5−11.5 (m exchanged with D_2O), 8.25 (s, 1H), 7 (d, 1H), 6.95 (dd, 1H), 6.9 (d, 1H), 6.45 (s, 2H), 3.55 (AB system, 2H), 2.95 (AB system, 2H), 2.7−2.9 (m, 2H), 2.25 (s, 3H), 1.8−2.1 (m, 2H); $[\alpha]^{20}_D$ = +52° (*c* = 1, ethanol 95%). Anal. ($C_{13}H_{16}N_2 \cdot C_4H_4O_4$) C, H, N.

(*S*)-Spiro[(1,3-diazacyclopent-1-ene)-5,2′-(7′-methyl-1′,2′,3′,4′-tetrahydronaphthalene)], Fumarate (5*S*). The compound was prepared as described for the *R* enantiomer. (*R,S*)-Spiro[(1,3-diazacyclopent-1-ene)-5,2′-(7′-methyl-1′,2′,3′,4′-tetrahydronaphthalene)] (**5*RS***, 3 g, 15 mmol, ee: 50%) was employed as starting material, resulting from the neutralization with aqueous NaOH, of the mother liquors from the resolution of the *R* enantiomer and using dibenzoyl-D-tartaric acid (5.65 g, 15 mmol) as chiral agent. After three crystallizations in ethanol (100 mL/g), the pure diastereoisomeric salt was neutralized and the free base converted to the fumaric acid salt. The title compound was isolated as colorless crystals (0.51 g, 11%), mp 163−165 °C. Spectroscopic characteristics were identical to those of the *R* enantiomer: $[\alpha]^{20}_D$ −53° (*c* = 1, ethanol 95%). Anal. ($C_{13}H_{16}N_2 \cdot C_4H_4O_4$) C, H, N.

7-Methyl-3,4-dihydro-(1*H*)-naphthalen-2-one (1). Step a: *m*-Tolylacetyl Chloride. Thionyl chloride (984 g, 7.3 mol) was added to a solution of *m*-tolylacetic acid (**1**, 1,000 g, 6.66 mol) in toluene (3 L), while the temperature was maintained at 50 °C. At the end of the addition, the reaction mixture was heated at 80−85 °C until the gas evolution ceased. The solution was then cooled at 40 °C and the solvent carefully removed under reduced pressure. The acid chloride was used without further purification in the following step.

Step b: 7-Methyl-3,4-dihydro-(1*H*)-naphthalen-2-one (1). *m*-Tolylacetyl chloride (1.000 g, 5.9 mol) in CH_2Cl_2 (3.5 L) was added dropwise to a stirred solution of $AlCl_3$ (925 g, 6.95 mol) in CH_2Cl_2 (7.5 L) at 0 °C. At the end of the addition, the reaction mixture was maintained at 0 °C for 15 min and then lowered to −40 °C. Ethylene (468 g, 16.7 mol) was bubbled slowly (430 g/h) into the mixture while the temperature was kept below −30 °C. Reaction progress was followed by gas chromatography. When starting material concentration was below 5%, the reaction mixture was poured over a mixture of water and ice (50/50, 18 kg) while the temperature was kept in the 15−20 °C range. The mixture was diluted with CH_2Cl_2 (4.5 L). The phases were separated, the aqueous solution was extracted with more CH_2Cl_2, and the pooled organic phases were washed with aqueous $NaHCO_3$ until neutrality. The organic phase was dried over $MgSO_4$ and evaporated under reduced pressure. The solid residue was washed with diisopropyl ether to remove the isomeric 1,2,3,4-tetrahydro-5-methyl-2(1*H*)-naphthalenone and dried under reduced pressure (445 g, 47%), mp 61 °C with decomposition.

7-Methyl-2(*S*)-[[1(*R*)-phenylethyl]amino]-1,2,3,4-tetrahydronaphthalene-2-carbonitrile (2). 1(*R*)-Phenylethylamine (757 g, 6.24 mol) was added dropwise, followed by acetic acid (375 g, 6.24 mol) to a solution of 7-methyl-3,4-dihydro-(1*H*)-naphthalen-2-one (**1**) (1000 g, 6.24 mol) in a mixture of ethanol, methanol, and water (6 L, 4/1/1), at such a rate that the temperature did not exceed 35 °C. A solution of sodium cyanide (337 g, 6.86 mol) in water (1.5 L) was then added dropwise and the reaction mixture heated to 40 °C for 1 h during which the suspension became difficult to stirr. Water (4.5 L) was added, and the mixture was stirred for 2.5 h at 40 °C, followed by 24 h at room temperature. Water (3 L) was added again, and the suspension was cooled at −15 °C for 1 h, filtered, rinsed with ice cold ethanol, and dried under reduced pressure to afford a white solid (1700 g, 94.5%): mp 112 °C; ^{1}H NMR ($CDCl_3$) δ 7.1−7.4 (m, 5H), 7 (d, 1H), 6.9 (dd, 1H), 6.4 (d, 1H), 4.25 (q, 1H), 3 (m, 2H), 2.6 (AB system, 2H), 2.2 (s, 3H), 2−2.3 (m, 2H), 1.65 (m exchanged with D_2O), 1.45 (d, 3H).

[2(*S*)-(Aminomethyl)-7-methyl-1,2,3,4-tetrahydronaphthalen-2-yl][1(*R*)-phenylethyl]amine, Dihydrochloride (3). A solution of 7-methyl-2(*S*)-[1(*R*)-phenylethyl]amino]-1,2,3,4-tetrahydronaphthalene-2-carbonitrile (**2**, 1000 g, 3.44

UM00013153
NOVARTIS EXHIBIT 1517
Novartis v. Regents, IPR2023-01347
Page 1899 of 4460

mol) in THF (7 L) was added dropwise to a suspension of $LiAlH_4$ (304 g, 8 mol) in THF (13 L) at such a rate that gas evolution remained controlable and the temperature did not exceed 20 °C. The suspension was stirred at 20 °C for 3 h until the starting material had disappeared on TLC (methanol/acetone, 80/20). The reaction mixture was hydrolyzed by careful and succesive additions of water (0.3 L), 2 N NaOH (0.35 L), and water (0.575 L) while the temperature was maintained below 20 °C. The solid was filtered and washed with THF (2 × 1 L), and the pooled organic solutions were evaporated under reduced pressure. The residue was taken up in ethyl acetate (6.5 L), and the hydrochloride salt was formed by addition of 3.5 N HCl in ethyl acetate (2 L) at 0 °C. The solid was filtered, washed with ethyl acetate, and dried under reduced pressure to afford a white solid (1180 g, 93%): mp 190 °C; ^{1}H NMR (DMSO-d_6) δ 10.15 (br s exchanged with D_2O, 2H), 8.74 (br s exchanged with D_2O, 3H), 7.80 (br s, 2H), 7.46 (br s, 3H), 6.96 (AB system, 2H), 6.50 (s, 1H), 3.61−3.32 (m, 2H), 3.13−2.61 (m, 4H), 2.39−1.92 (m, 3H), 2.17 (s, 3H), 1.77 (d, 3H).

2(*S*)-(Aminomethyl)-7-methyl-1,2,3,4-tetrahydronaphthalen-2-ylamine, Dihydrochloride (4). A solution of [2(*S*)-aminomethyl-7-methyl-1,2,3,4-tetrahydronaphthalen-2-yl][1(*R*)-phenylethyl]amine, dihydrochloride (**3**) (1000 g, 2.74 mol) in methanol (12 L) was hydrogenated at 20 °C under 1 bar of hydrogen and in the presence of Pd (5% Pd/C, 50% humidity, 100 g). Each time the flow of hydrogen decreased (twice), the suspension was filtered and a new batch of catalyst (5% Pd/C, 50% humidity, 100 g) was added to the reactor. At the end of the theoretical absorption (68 L), the catalyst was filtered off and the solution was concentrated under reduced pressure. The residue was stirred with hot acetone (5 L), cooled at 0 °C, and filtered to afford, after drying under reduced pressure, a white solid (559 g, 78%): mp 250 °C; ^{1}H NMR (DMSO-d_6) δ 8.87 (br s exchanged with D_2O, 6H), 6.97 (dd, 2H), 6.9 (s, 1H), 3.21 (AB system, 2H), 3.03 (br s, 2H), 2.66 (AB system, 2H), 2.21 (s, 3H), 2.06 (t, 2H).

(*S*)-Spiro[(1,3-diazacyclopent-1-ene)-5,2′-(7′-methyl-1′,2′,3′,4′-tetrahydronaphthalene)], Fumarate (5S). NaOH pellets (353 g, 8.83 mol) were added to a suspension of 2(*S*)-(aminomethyl)-7-methyl-1,2,3,4-tetrahydronaphthalen-2-ylamine, dihydrochloride (**4**, 1000 g, 3.8 mol), and formamidine acetate (491 g, 4.75 mol) in ethanol (15.7 L). The reaction mixture was stirred for 1 h at 20 °C, concentrated under reduced pressure, and then taken up in 1.5 N HCl (14 L) and extracted with ethyl acetate (2 × 2 L). The aqueous phase was brought to pH 12.5 by the slow addition of 10 N NaOH while the temperature was kept at 20 °C. The solid was filtered, washed with water, and dried under reduced pressure to afford a white powder (661 g, 87%), mp 182−183 °C. The fumarate salt was prepared quantitatively in ethanol or 2-propanol at the concentration of 1/15: mp 162−165 °C. Spectroscopic characteristics were identical to those of the compound obtained by the other route.

Acknowledgment. The authors thank Michele Hipeaux, Pascal Vrillaud, Yvette Menant, Elisabeth Adnet, and Veronique Barou for their expert technical assistance, and Angela D. Morris is thanked for help in preparation of the manuscript.

Supporting Information Available: X-ray analysis data (5 pages). Ordering information is given on any current masthead page.

References

(1) Cordi, A. A.; Lacoste, J.-M.; Descombes, J.-J.; Courchay, C.; Vanhoutte, P. M.; Laubie, M.; Verbeuren, T. J. Design, Synthesis and Structure-Activity Relationships of a New Series of Alpha Adrenergic Agonists: the Spiro[(1,3-diazacyclopent-1-ene)-5:2′-(1′,2′,3′,4′-tetrahydronaphthalene)]. *J. Med. Chem.* **1995**, *38*, 4056−4069.
(2) Seiler, J. P. Chiral Drugs-The View of the Swiss Intercantonal Office for the Control of Medecines. *Drug Inf. J.* **1993**, *27*, 485−489.
(3) Smith, R. L.; Caldwell, J. Racemates: Towards a New Year Resolution? *Trends Pharmacol. Sci.* **1988**, *9*, 75−79.
(4) Weinges, K.; Gries, K.; Stemmle, B.; Schrank, W. Über die Asymmetrische Strecker-Synthese mit (S)-(−)-1-Phenylethylamine als Chiralem Hilfsreagens. *Chem. Ber.* **1977**, *110*, 2098−2105.
(5) Harada, K. Asymmetric Synthesis of α-Amino-acids by the Strecker Synthesis. *Nature* **1963**, *200*, 1201. Harada, K.; Fox, S. W. Stereospecific Synthesis of an Optically Active α-Amino Acid. *Naturwiss.* **1964**, *51*, 106−107.
(6) Mai, K.; Patil, G. Asymmetric Synthesis of α-Aminonitriles. *Synth. Commun.* **1984**, *14*, 1299−1304.
(7) Weinges, K.; Brachmann, H.; Stahnecker, P.; Rodewald, H.; Nixdorf, M.; Irngartinger, H. Synthese der Enantiomerenreinen 2-(2-Thienyl)- und 2-(3-Thienyl)-glycine - Molekülstruktur der als Zwischenprodukte Auftretenden Schiffschen Basen. *Liebigs Ann. Chem.* **1985**, 566−578.
(8) Kunz, H.; Sager, W. Diastereoselective Strecker Synthesis of α-Aminonitriles on Carbohydrate Templates. *Angew. Chem., Int. Ed. Engl.* **1987**, *26*, 557−559.
(9) Kunz, H.; Pfrengle, W.; Rück, K.; Sager, W. Stereoselective Synthesis of L-Amino Acids via Strecker and Ugi Reactions on Carbohydrate Templates. *Synthesis* **1991**, *26*, 1039−1042.
(10) Bousquet, C.; Tadros, Z.; Tonnel, J.; Mion, L.; Taillades, J. Auxiliaires Cétoniques Chiraux dans la Synthèse Asymétrique des α-Aminoacides selon Strecker. *Bull. Soc. Chim. Fr.* **1993**, *130*, 513−520.
(11) Davis, F. A.; Portonova, P. S.; Reddy, R. E.; Chiu, Y. Asymmetric Strecker Synthesis Using Enantiopure Sulfinimines and Diethylaluminium Cyanide: The Alcohol Effect. *J. Org. Chem.* **1996**, *61*, 440−441.
(12) Iyer, M. S.; Gigstad, K. M.; Namdev, N. D.; Lipton, M. Asymmetric Catalysis of the Strecker Amino Acid Synthesis by a Cyclic Dipeptide. *J. Am. Chem. Soc.* **1996**, *118*, 4910−4911.
(13) For a recent review on this subject, see: Kunz H. Stereoselective Synthesis: Formation of C-C bond by Addition to Imino Group via Strecker and Ugi Reactions. In *Houben-Weyl Methoden der Organischen Chemie Band E21b*; Müller, E., Ed.; Georg Thieme Verlag: Stuttgart, New York, 1995; pp 1933−1945.
(14) Weinges, K.; Graab, G., Nagel, D.; Stemmle, B. Die Externe Asymmetrische Strecker-Synthese von α-Methyl-aminosäuren. *Chem. Ber.* **1971**, *104*, 3594−3606.
(15) Subralanian, P. K.; Woodard, R. W. An Asymmetric Strecker Synthesis of (R)-(+)-2-Methyl-3-Phenylalanine: An Efficient Preparation. *Synth. Commun.* **1986**, *16*, 337−342.
(16) Nozulak, J.; Vigouret, J. M.; Jaton, A. L; Hofmann, A.; Dravid, A. R.; Weber, H. P.; Kalkman,H. O.; Walkinshaw, M. D. Centrally Acting α_1-Adrenoceptor Agonist Based on Hexahydronapht[2,3-b]-1,4-oxazines and Octahydrobenzo[g]quinolines. *J. Med. Chem.* **1992**, *35*, 480−489.
(17) De Marinis, R. M.; Hieble, J. P. l-1,2,3,4-Tetrahydro-8-methoxy-5-(methylthio)-2-naphthalenamine: A Potent and Selective Agonist at α_1-Adrenoceptors. *J. Med Chem.* **1983**, *26*, 1215−1218.
(18) Verbeuren, T. J.; Vayssettes-Courchay, C.; Descombes, J.-J.; Simonet, S.; Lacoste, J.-M.; Cordi, A. A.; Laubie, M. S 18149 is a Partial Agonist at α-Adrenoceptors: Studies in Pithed Rats and isolated Canine and Human Blood Vessels. *Br. J. Pharmacol.* **1996**, *117*, 277P.
(19) Vayssettes-Courchay, C.; Lacoste, J.-M.; Cordi, A. A.; Laubie, M.; Verbeuren, T. J. In vivo Cardiovascular Effects of the α-Adrenoceptor Agonist S 18149 in the Anaesthetized Dog. *Br. J. Pharmacol.* **1996**, *117*, 255P.

JM970282M

UM00013154
NOVARTIS EXHIBIT 1517
Novartis v. Regents, IPR2023-01347
Page 1900 of 4460

This Page is Inserted by IFW Indexing and Scanning Operations and is not part of the Official Record

BEST AVAILABLE IMAGES

Defective images within this document are accurate representations of the original documents submitted by the applicant.

Defects in the images include but are not limited to the items checked:

- ☐ BLACK BORDERS
- ☐ IMAGE CUT OFF AT TOP, BOTTOM OR SIDES
- ☐ FADED TEXT OR DRAWING
- ☐ BLURRED OR ILLEGIBLE TEXT OR DRAWING
- ☐ SKEWED/SLANTED IMAGES
- ☐ COLOR OR BLACK AND WHITE PHOTOGRAPHS
- ☐ GRAY SCALE DOCUMENTS
- ☐ LINES OR MARKS ON ORIGINAL DOCUMENT
- ☐ REFERENCE(S) OR EXHIBIT(S) SUBMITTED ARE POOR QUALITY
- ☐ OTHER: _____

IMAGES ARE BEST AVAILABLE COPY.
As rescanning these documents will not correct the image problems checked, please do not report these problems to the IFW Image Problem Mailbox.

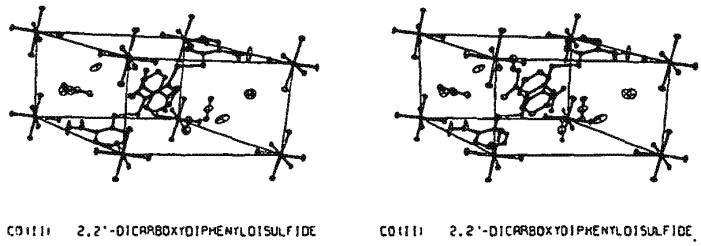


Fig. 3. A stereo view of the packing within the unit cell using ellipsoids of 15% probability. Three-atom 'molecules' are methanol oxygen atoms with two disordered half-carbon atoms. Two-atom molecules are methanol, and a water molecule is represented by only its oxygen atom. The view is nearly along c, with b horizontal and a vertical in the plane of the page.

etry of the disulfide linkage. The C(11)–S(5)–S(6)–C(18) dihedral angle is 86·7° and the S(5)–S(6) bond is 2·047 (3) Å. These values can be compared to those of 90·5° and 2·060 (3) Å found in an analogous compound, 2,2'-diaminodiphenyl disulfide (Lee & Bryant, 1970), (to illustrate the similarity, the present anion may be named hydrogen-2,2'-dicarboxylate diphenyl disulfide), as well as to many other organic disulfides (Hordvik, 1966; Lee, 1972). A stereo view of the packing is shown in Fig. 3.

This work was supported by the National Institutes of Health (grant no. GM-18813-01). We are also indebted to the National Science Foundation for their assistance (grant no. GP-13213) in the purchase of the diffractometer, and to the University of Hawaii Computing Center.

References

BOSCHI, T., CROCIANI, B., TONIOLO, L. & BELLUCO, U. (1970). *Inorg. Chem.* **9**, 532–537.

CHALLENGER, F. (1959). *Aspects of the Organic Chemistry of Sulphur*. London: Butterworths.

DOYLE, P. A. & TURNER, P. S. (1968). *Acta Cryst.* A**24**, 390–397.

HEMMERICH, P. (1966). *The Biochemistry of Copper*, edited by PEISACH, AISEN & BLUMBERG, pp. 15–34. New York: Academic Press.

HORDVIK, A. (1966). *Acta Chem. Scand.* **20**, 1885–1891.

HUBBARD, C. R., QUICKSALL, C. O. & JACOBSON, R. A. (1971). *ALFF*, Ames Laboratory Fast Fourier, Iowa State Univ., U.S.A.

KAWANISHI, S., YOKOYAMA, A. & TANAKA, H. (1972). *Chem. Pharm. Bull.* **20**, 262–268.

JOHNSON, C. K. (1965). *ORTEP*. Report ORNL-3794, Oak Ridge National Laboratory, Oak Ridge, Tennessee.

LEE, J. D. (1972). *Naturwissenschaften*, **59**, 36–37.

LEE, J. D. & BRYANT, M. W. R. (1970). *Acta Cryst.* B**26**, 1729–1735.

OTTERSEN, T., WARNER, L. G. & SEFF, K. (1973). *Chem. Commun.* 876–877.

ZALKIN, A., RUBEN, H. & TEMPLETON, D. H. (1962). *Acta Cryst.* **15**, 1219–1223.

Acta Cryst. (1974). B**30**, 1191

The 2:1 Crystal Complex of 5,5-Diethylbarbituric Acid (Barbital) and Caffeine

BY B. M. CRAVEN AND G. L. GARTLAND*

Department of Crystallography, University of Pittsburgh, Pittsburgh, Pennsylvania 15260, *U.S.A.*

(*Received* 5 *September* 1973; *accepted* 19 *October* 1973)

Triclinic, $P\bar{1}$; $a=14{\cdot}627$ (4), $b=14{\cdot}160$ (4), $c=6{\cdot}902$ (2) Å, $\alpha=92{\cdot}25$ (4), $\beta=92{\cdot}80$ (4), $\gamma=100{\cdot}75$ (4)°; $Z=2$ for $2C_8H_{12}N_2O_3.C_8H_{10}N_4O_2$; $D_{meas}=1{\cdot}344$ g cm^{-3}, $D_x=1{\cdot}334$ g cm^{-3}; m.p. 142°C; μ(Cu $K\alpha$)= 8·67 cm^{-1}. The crystal structure was determined by direct methods from 4665 intensity data which were measured with a computer-controlled four-circle diffractometer and nickel-filtered Cu $K\alpha$ radiation. Refinement by a block-diagonal least-squares procedure gave a final R index of 0·053. Bond lengths and angles are similar to those observed in related crystal structures.

Introduction

The crystals were prepared as described by Higuchi & Lach (1954). Integrated intensity data were collected from a crystal elongated along c and exhibiting the forms {100}, {010}, and {001}. The crystal was mounted with the c^* reciprocal axis along the diffractometer φ axis. 4665 independent reflections in the range $\sin\theta/\lambda \leq 0{\cdot}59$ Å^{-1} were scanned in the θ–2θ mode at a rate of 2° min^{-1}. A variable 2θ scan width was used, based on a minimum of 1·5°. Stationary

* Present address: The University of Alabama Medical Center, Birmingham, Alabama 35233, U.S.A.

UM00013156
NOVARTIS EXHIBIT 1517
Novartis v. Regents, IPR2023-01347
Page 1902 of 4460

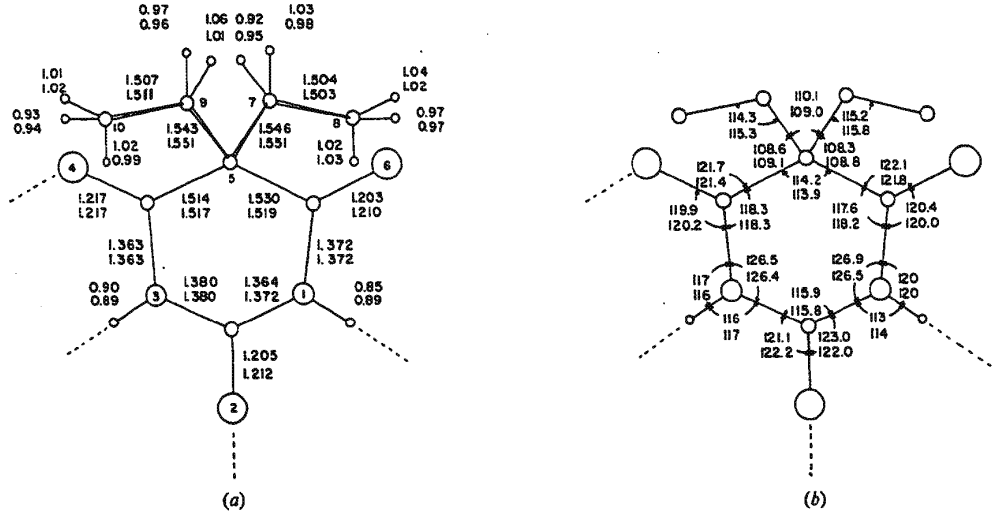


Fig. 1. Bond lengths (*a*) and angles (*b*) for the barbital molecules. Circles of decreasing radius represent oxygen, nitrogen, carbon and hydrogen atoms. For each parameter, the values given are for molecule *A* (above) and molecule *B* (below). Estimated standard deviations in distances are: 0·006 Å for ring and carbonyl bonds, 0·007 Å for C(5)–C(α) bonds of the ethyl groups, 0·008 Å for the C(α)–C(β) bonds, 0·05 Å for N–H bonds, and 0·06 Å for C–H bonds. The estimated error in a bond angle determination is 0·4°. Dashed lines indicate atoms involved in hydrogen bonding.

Table 1. *Atomic parameters*

Positional parameters are given as fractions of the lattice translations. Anisotropic temperature factors correspond to the expression: $\exp[-(h^2\beta_{11}+k^2\beta_{22}+l^2\beta_{33}+2hk\beta_{12}+2hl\beta_{13}+2kl\beta_{23})]$, and isotropic temperature factors to the expression: $\exp(-B\sin^2\theta/\lambda^2)$. The entry U_k is the r.m.s. atomic vibrational amplitude (Å) in the direction of the kth principal axis of the thermal ellipsoid. These were calculated from the experimental β_{ij} values. For barbital parameters, the values given are for molecule *A* (above) and molecule *B* (below). E.s.d.'s shown in parentheses refer to the least significant figures in parameter values.

(*a*) Carbon, nitrogen and oxygen atoms

(All parameters $\times 10^4$, except $\beta_{33}\times 10^3$ and $U_k\times 10^2$)

	x	y	z	β_{11}	β_{22}	β_{33}	β_{12}	β_{13}	β_{23}	U_1	U_2	U_3
(i) Barbital												
N(1)	2054 (3)	2105 (2)	7951 (6)	43 (2)	30 (2)	27 (1)	6 (2)	21 (4)	33 (3)	16	21	26
	2618 (2)	5810 (2)	7305 (5)	23 (2)	37 (2)	24 (1)	5 (1)	−2 (3)	25 (3)	15	18	25
C(2)	1185 (3)	1928 (3)	8635 (7)	42 (2)	38 (2)	22 (1)	11 (2)	14 (4)	22 (4)	18	21	24
	2958 (3)	5039 (3)	7918 (6)	31 (2)	35 (2)	20 (1)	6 (2)	6 (3)	15 (4)	18	18	22
O(2)	723 (3)	2544 (2)	8903 (6)	60 (2)	46 (2)	40 (1)	24 (2)	45 (4)	47 (4)	18	24	32
	2477 (2)	4238 (2)	7837 (5)	43 (2)	34 (2)	33 (1)	0 (1)	−3 (3)	21 (3)	17	22	28
N(3)	861 (2)	993 (2)	9043 (6)	36 (2)	33 (2)	25 (1)	6 (1)	30 (3)	19 (3)	17	18	25
	3883 (2)	5231 (2)	8602 (5)	28 (2)	33 (2)	24 (1)	9 (1)	3 (3)	29 (3)	16	18	24
C(4)	1330 (3)	246 (3)	8868 (6)	37 (2)	32 (2)	20 (1)	4 (2)	9 (4)	9 (4)	18	20	22
	4466 (3)	6111 (3)	8810 (6)	26 (2)	38 (2)	21 (1)	8 (2)	12 (3)	21 (4)	16	19	23
O(4)	994 (2)	−527 (2)	9423 (5)	50 (2)	34 (2)	28 (1)	4 (1)	33 (3)	22 (3)	17	22	27
	5241 (2)	6208 (2)	9619 (5)	30 (1)	51 (2)	28 (1)	8 (1)	−10 (3)	33 (3)	17	21	27
C(5)	2251 (3)	399 (3)	7919 (7)	37 (2)	33 (2)	24 (1)	7 (2)	23 (4)	20 (4)	18	19	24
	4139 (3)	6944 (3)	7929 (7)	26 (2)	32 (2)	25 (1)	4 (2)	1 (4)	21 (4)	17	17	25
C(6)	2594 (3)	1437 (3)	7451 (7)	38 (2)	40 (2)	27 (1)	5 (2)	19 (4)	28 (4)	18	21	26
	3119 (3)	6720 (3)	7180 (7)	27 (2)	38 (2)	27 (1)	6 (2)	5 (4)	30 (4)	17	18	26
O(6)	3317 (3)	1674 (3)	6708 (7)	51 (2)	58 (2)	49 (1)	8 (2)	77 (4)	58 (4)	18	24	36
	2748 (2)	7320 (2)	6489 (6)	37 (2)	51 (2)	51 (1)	10 (1)	−19 (4)	76 (4)	17	21	37
C(7)	2131 (4)	−275 (3)	5994 (7)	55 (3)	45 (3)	26 (1)	11 (2)	42 (5)	12 (4)	20	21	27
	4748 (3)	7194 (3)	6200 (7)	32 (2)	44 (2)	25 (1)	2 (2)	4 (4)	36 (4)	17	20	26
C(8)	1328 (4)	−188 (4)	4617 (8)	80 (4)	67 (4)	23 (1)	5 (3)	8 (6)	14 (5)	23	25	30
	4764 (3)	6371 (4)	4669 (7)	45 (3)	65 (3)	23 (1)	8 (2)	5 (4)	13 (5)	22	23	25
C(9)	3000 (4)	139 (4)	9317 (9)	43 (3)	57 (3)	37 (2)	10 (2)	0 (5)	52 (6)	20	22	31
	4298 (3)	7832 (3)	9482 (8)	38 (2)	38 (2)	30 (1)	6 (2)	11 (4)	14 (4)	19	20	27
C(10)	3195 (4)	779 (5)	11216 (9)	54 (3)	111 (5)	31 (2)	−7 (3)	−17 (6)	47 (7)	22	26	36
	3636 (4)	7765 (4)	11101 (9)	67 (3)	57 (3)	32 (2)	19 (3)	35 (6)	22 (5)	22	25	29

UM00013157
NOVARTIS EXHIBIT 1517
Novartis v. Regents, IPR2023-01347
Page 1903 of 4460

Table 1 (*cont.*)

(ii) Caffeine

N(1)	1972 (2)	3786 (3)	2937 (5)	28 (2)	53 (2)	22 (1)	15 (2)	4 (3)	10 (4)	16	23	23
C(1)	2890 (3)	3500 (4)	3000 (9)	32 (2)	82 (4)	36 (2)	28 (2)	13 (5)	22 (6)	15	29	29
C(2)	1216 (3)	3071 (3)	3253 (7)	40 (2)	49 (3)	21 (1)	16 (2)	5 (4)	12 (4)	18	22	23
O(2)	1312 (3)	2260 (3)	3534 (6)	57 (2)	56 (2)	39 (1)	27 (2)	14 (4)	42 (4)	19	26	31
N(3)	352 (2)	3327 (2)	3247 (5)	31 (2)	35 (2)	21 (1)	7 (1)	7 (3)	9 (3)	18	19	22
C(3)	−461 (3)	2590 (3)	3512 (8)	40 (2)	37 (2)	31 (1)	4 (2)	19 (4)	18 (4)	18	21	27
C(4)	267 (3)	4238 (3)	2849 (6)	27 (2)	37 (2)	15 (1)	7 (2)	3 (3)	2 (3)	17	18	20
C(5)	1022 (3)	4911 (3)	2499 (6)	29 (2)	40 (2)	17 (1)	8 (2)	5 (3)	2 (3)	17	19	21
C(6)	1946 (3)	4731 (3)	2510 (6)	28 (2)	52 (3)	17 (1)	5 (2)	5 (3)	−5 (4)	17	19	24
O(6)	2653 (2)	5298 (3)	2213 (5)	30 (2)	64 (2)	33 (1)	1 (1)	15 (3)	8 (4)	17	26	28
N(7)	675 (2)	5731 (2)	2186 (5)	29 (2)	36 (2)	18 (1)	4 (1)	6 (3)	9 (3)	17	19	21
C(7)	1215 (3)	6654 (3)	1730 (7)	41 (2)	40 (2)	26 (1)	0 (2)	18 (4)	13 (4)	18	22	25
C(8)	−247 (3)	5504 (3)	2341 (6)	31 (2)	40 (2)	18 (1)	8 (2)	2 (3)	6 (4)	18	20	21
N(9)	−534 (2)	4596 (2)	2763 (5)	26 (2)	36 (2)	18 (1)	7 (1)	4 (3)	4 (3)	16	19	21

Table 1 (*cont.*)

(*b*) Hydrogen atoms

Positional parameters $\times 10^3$

(i) Barbital

	x	*y*	*z*	*B* (Å²)
H(1)	223 (4)	269 (4)	771 (8)	6 (1)
	200 (3)	569 (4)	705 (7)	5 (1)
H(3)	30 (3)	88 (4)	954 (7)	5 (1)
	410 (3)	475 (3)	911 (7)	4 (1)
H(71)	205 (3)	−89 (4)	639 (7)	4 (1)
	535 (3)	748 (3)	681 (7)	4 (1)
H(72)	276 (4)	−12 (4)	535 (7)	5 (1)
	451 (3)	771 (4)	563 (7)	4 (1)
H(81)	69 (4)	−40 (4)	521 (8)	6 (1)
	502 (4)	582 (4)	524 (7)	5 (1)
H(82)	140 (4)	48 (4)	432 (9)	7 (1)
	415 (4)	605 (4)	411 (7)	5 (1)
H(83)	131 (5)	−64 (5)	336 (9)	8 (2)
	514 (4)	656 (4)	350 (8)	6 (1)
H(91)	282 (4)	−53 (4)	961 (8)	6 (1)
	493 (4)	790 (4)	998 (7)	5 (1)
H(92)	363 (4)	20 (4)	858 (9)	6 (1)
	423 (4)	841 (4)	876 (7)	5 (1)
H(101)	264 (5)	74 (5)	1184 (9)	9 (2)
	361 (4)	719 (4)	1167 (9)	7 (1)
H(102)	345 (5)	145 (5)	1086 (9)	8 (2)
	300 (4)	780 (4)	1060 (9)	6 (1)
H(103)	367 (5)	55 (5)	1208 (9)	8 (2)
	383 (4)	833 (4)	1214 (9)	7 (1)

(ii) Caffeine

	x	*y*	*z*	*B* (Å²)
H(11)	338 (5)	409 (5)	340 (10)	9 (2)
H(12)	297 (5)	327 (5)	173 (10)	9 (2)
H(13)	297 (5)	311 (5)	414 (11)	9 (2)
H(31)	−101 (4)	287 (4)	374 (7)	5 (1)
H(32)	−56 (4)	207 (5)	247 (9)	8 (2)
H(33)	−34 (4)	227 (4)	471 (9)	7 (1)
H(71)	80 (4)	709 (4)	159 (8)	6 (1)
H(72)	152 (4)	654 (4)	52 (9)	7 (1)
H(73)	167 (4)	692 (4)	281 (8)	5 (1)
H(8)	−65 (3)	596 (3)	217 (7)	4 (1)

background counts of 20 s were recorded at each of the 2θ scan limits. There were 882 reflections for which the integrated intensity I was less than $1{\cdot}2\ \sigma(I)$. They were assigned intensities of $\sigma(I)/2$, where $\sigma(I)$ is the standard deviation of I as estimated from counting statistics. No corrections were made for X-ray absorption or extinction.

The structure was solved by direct methods with the symbolic addition procedure followed by automated tangent refinement (Karle & Karle, 1966). All 40 non-hydrogen atoms were found in the first E map, and all 34 hydrogen atoms were subsequently found in a difference Fourier synthesis.

The positional and anisotropic thermal parameters for heavier atoms and positional and isotropic thermal parameters for hydrogen atoms were refined by a block-diagonal least-squares procedure. The atomic form factors used were those of Cromer & Waber (1965) for carbon, nitrogen and oxygen, and Stewart, Davidson & Simpson (1965) for hydrogen. The function minimized was $\sum w_H \Delta_H^2$, where $\Delta_H = |F_H^{obs}| - |F_H^{calc}|$ and $w_H^{-1} = 1{\cdot}2 + |0{\cdot}05F_H|^2$. Convergence occurred with R (all reflections) $= \sum|\Delta_H|/\sum|F_H^{obs}| = 0{\cdot}053$. The atomic parameters and their e.s.d.'s are in Table 1.*

Discussion

The present discussion is restricted to the molecular structures of the components, because the intermolecular aspects of the crystal structure, including the hydrogen bonding, ring stacking and carbonyl–carbonyl interactions, have been described elsewhere (Craven & Gartland, 1970).

(*a*) *Barbital*

Bond lengths and angles for the two crystallographically independent molecules of barbital are shown in Fig. 1(*a*) and (*b*). These have not been corrected for thermal motion effects. There are no significant differences between the values determined for the two different molecules. In addition, the values are in good agreement with those found in polymorphs of barbital itself (Craven, Vizzini & Rodrigues, 1969).

Both molecules *A* and *B* exhibit small differences (0·01 Å) in the lengths of pairs of C–N and C=O bonds,

* Final observed and calculated structure amplitudes have been deposited with the British Library Lending Division as Supplementary Publication No. SUP 30255 (28 pp., 1 microfiche). Copies may be obtained through the Executive Secretary, International Union of Crystallography, 13 White Friars, Chester CH1 1NZ, England.

UM00013158
NOVARTIS EXHIBIT 1517
Novartis v. Regents, IPR2023-01347
Page 1904 of 4460

e.g. C(6)N(1) and C(4)N(3) which should be equivalent in an isolated molecule. These differences are not significant in terms of their e.s.d.'s. However, Craven, Cusatis, Gartland & Vizzini (1973) have pointed out that these differences occur with the same sense in a number of barbiturate crystal structures, and that they seem to arise whenever atom O(4) is hydrogen bonded, but O(6) is not. The slight puckering of the oxopyrimidine ring in molecules *A* and *B* is similar to that observed in other barbiturate crystal structures [see Fig. 3 in Craven *et al.* (1973)].

In both molecules *A* and *B*, the hydrocarbon chains consisting of the ethyl groups and C(5) are distorted from idealized all-*trans* conformations by small twists about C(5)–C(α) bonds. In molecule *B* the distortions are slightly larger. Torsion angles about the C(5)–C(α) bonds are 182·4 and 182·5° for molecule *A* and 183·6 and 186·5° for molecule *B*. When viewed along the C(5)···C(2) direction, the hydrocarbon backbone for each molecule assumes a slight 'S' shape such that the terminal atom C(8) lies closer to O(4) than to O(6) and *vice versa* for the terminal atom C(10).

(*b*) *Caffeine*

Bond lengths and angles for caffeine in the 2:1 barbital–caffeine complex are shown in Fig. 2(*a*) and (*b*). Differences between the caffeine molecular dimensions determined in this complex and those found in a 1:1 complex with 5-chlorosalicylic acid (Shefter, 1968) are also shown in Fig. 2. There is overall agreement between the two sets of parameters. The only possibly significant differences are in the bond length C(6)–O(6) ($\Delta = 2{\cdot}6\sigma$), and the bond angle C(5)–N(7)–C(7) ($\Delta = 3{\cdot}2\sigma$). The smaller C(5)–N(7)–C(7) angle in the complex with barbital may be attributed to a repulsion between the caffeine methyl group C(7) and the barbital oxygen atom O(2) of molecule *A* (Craven & Gartland, 1970).

Although the atoms of the purine ring system are almost coplanar, there are small but significant displacements of the methyl carbon atoms (0·06, 0·02 and 0·01 Å) and the carbonyl O(2) atom (0·06 Å) from this plane (Fig. 3). A similar pattern of atomic displacements is reported for the caffeine molecule in the complex with 5-chlorosalicylic acid (Shefter, 1968). However, in this case, there is also a slight folding of the molecule about the C(4)–C(5) bond. The orientation of the methyl hydrogen atoms is similar in both crystal complexes for the methyl substituents at the nitrogen atoms N(1) and N(7). In the complex with 5-chlorosalicylic acid, the methyl group at N(3) is twisted about 40° around the N(3)–C bond relative to the configuration shown in Fig. 3. Presumably these differences are the result of crystal packing effects.

This work was supported by Grant No. NS-02763 of the U. S. Public Health Service, National Institutes of Health. We thank Dr R. Shiono for use of programs for the IBM 1130 and 7090 computers.

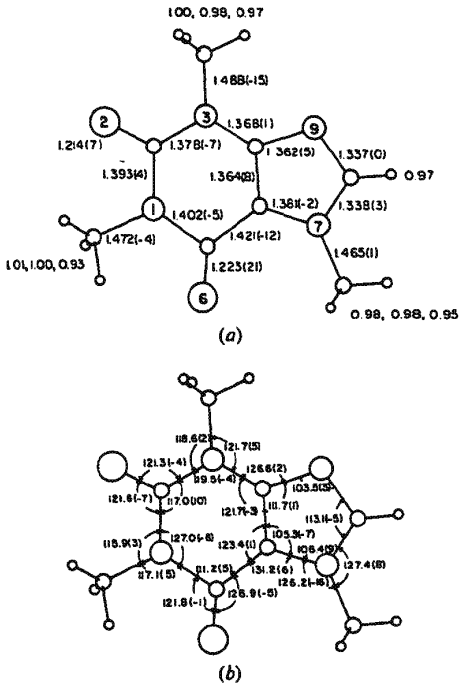


Fig. 2. Bond lengths (*a*) and angles (*b*) for caffeine. The values shown are for the 2:1 complex of barbital with caffeine. The quantities in parentheses are differences between the presently reported values and those found in a 1:1 complex of caffeine with 5-chlorosalicyclic acid (Shefter, 1968). Thus a negative number indicates that the larger parameter was found in the latter complex. Estimated standard errors in distances are 0·06 Å for bonds involving hydrogen; otherwise, 0·006 Å. The estimated error in an angle is 0·4°.

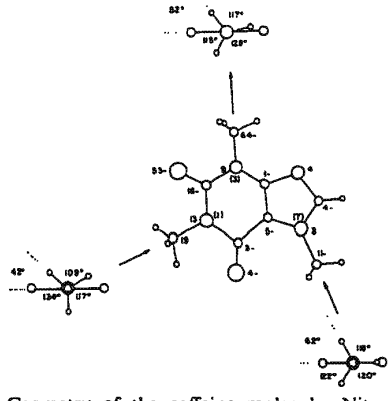


Fig. 3. Geometry of the caffeine molecule. Nitrogen atoms which have methyl substituents are numbered in parentheses. For each non-hydrogen atom, the distance (Å × 10^3) above or below the best least-squares plane through the purine atoms is indicated. The orientations of methyl hydrogen atoms are shown in projections down appropriate N–C bonds.

UM00013159
NOVARTIS EXHIBIT 1517
Novartis v. Regents, IPR2023-01347
Page 1905 of 4460

References

CRAVEN, B. M., CUSATIS, C., GARTLAND, G. L. & VIZZINI, E. A. (1973). *J. Mol. Struct.* **16**, 331–342.

CRAVEN, B. M. & GARTLAND, G. L. (1970). *J. Pharm. Sci.* **59**, 1666–1670.

CRAVEN, B. M., VIZZINI, E. A. & RODRIGUES, M. M. (1969). *Acta Cryst.* B**25**, 1978–1993.

CROMER, D. T. & WABER, J. T. (1965). *Acta Cryst.* **18**, 104–109.

HIGUCHI, T. & LACH, J. L. (1954). *J. Amer. Pharm. Assoc. Sci. Ed.* **43**, 349–354.

KARLE, J. & KARLE, I. L. (1966). *Acta Cryst.* **21**, 849–859.

SHEFTER, E. (1968). *J. Pharm. Sci.* **57**, 1163–1168.

STEWART, R. F., DAVIDSON, E. R. & SIMPSON, W. T. (1965). *J. Chem. Phys.* **42**, 3175–3187.

Acta Cryst. (1974). B**30**, 1195

The Geometry of Polyhedral Distortions. Predictive Relationships for the Phosphate Group

BY WERNER H. BAUR

Department of Geological Sciences, University of Illinois at Chicago, Chicago, Illinois 60680, *U.S.A.*

(*Received* 4 *June* 1973; *accepted* 26 *September* 1973)

The shapes of 211 phosphate tetrahedra have been studied. Their dimensions are known precisely from published X-ray and neutron-diffraction investigations. Results: (1) The site symmetry of the P atoms is found in 85% of the cases to be 1. Other observed symmetries are *m*, 2, 3, $\bar{4}$, *mm*, $\bar{4}2m$, 222 and 23. (2) The deviations from regular symmetry, $\bar{4}3m$, are pronounced. The distortions can be measured by defining for every phosphate group three distortion indices: $DI(TO)=(\sum|TO_i-TO_m|)/4TO_m$, $DI(OTO)=(\sum|OTO_i-OTO_m|)/6OTO_m$ and $DI(OO)=(\sum|OO_i-OO_m|)/6OO_m$, where TO is the distance P–O, OTO the angle O–P–O, OO the distance O–O, the subscripts *m* refer to the mean and *i* to individual values. The average distortion indices for all groups are: DI(TO) = 0·021, DI(OTO) = 0·028, DI(OO) = 0·012. This means that distortions are more pronounced in the P–O distances than in O–O and thus the phosphate group can be viewed, to a first approximation, as a rigid regular arrangement of O atoms, with the P atoms displaced from their centroid. (3) *Mean* P–O distances of the phosphate groups vary from 1·506 to 1·572 Å. (4) *Individual* P–O distances are correlated with the bond strengths received by the individual oxygen atoms. (5) The individual O–P–O angles are strongly correlated with the average of the P–O distances on the sides of the angle, and with the opposite O–O distance. The various correlations are strong enough to formulate six equations which are useful for predictive purposes: the mean P–O distances can be calculated from the coordination numbers and the distortion indices; the individual P–O distances follow from the bond strength distribution; the bond angles are based on the normalized bond lengths; the mean O–O distances are a function of the mean P–O distances and the distortion indices; the lengths of shared tetrahedral edges depend on the number of shared edges per tetrahedron. Some of the correlations are affected by the presence of shared edges in the phosphate groups and differ for various subpopulations of the sample (ortho-, di-, ring-, poly-, acid or organic phosphates). The calculated shapes can be used as input to computer simulation of crystal structures.

Introduction

The arrangement of four oxygen atoms around a central pentavalent phosphorus atom is called the tetrahedral phosphate group because the oxygen ligands are distributed over the four corners of a tetrahedron. A regular tetrahedron possesses point group symmetry $\bar{4}3m$ or 23. However, to my knowledge no phosphate tetrahedron observed so far in a crystalline solid is located at a site with $\bar{4}3m$ symmetry. The site symmetries of the phosphate group in Ag_3PO_4 (Helmholz, 1936) and of one of the PO_4^{3-} groups in $Na_6F(OH_2)_{18}(NaH_2O)(PO_4)_2$ (Tillmanns & Baur, in preparation) are 23. However, these data are not used here because in the first case the structure is not determined precisely, while in the second case the phosphate group is disordered and therefore its actual dimensions are not precisely known. The site symmetry of 85% of the phosphate groups studied in this paper is 1 (Table 1). Most phosphate tetrahedra deviate significantly in their dimensions from the values expected for a regular tetrahedral arrangement. The geometry of these deviations and the extent and the limits of the distortions are the topics of this study. 'Tetrahedron' is used to

Table 1. *Site symmetries of a sample of* 211 *phosphate groups observed in crystalline solids* (*see Appendix*)

Symmetry	Number of groups	% of total
1	179	84·8
m	16	7·6
2	7	3·3
3	4	1·9
$\bar{4}$	2	0·9
mm	1	0·5
222	1	0·5
$\bar{4}2m$	1	0·5

UM00013160
NOVARTIS EXHIBIT 1517
Novartis v. Regents, IPR2023-01347
Page 1906 of 4460

bonded chains with H(5) atoms in such positions are not observed.

A twist of the O(5)–H(5) bond in the opposite sense, *i.e.* away from the line of centres O(5)---O(5′), would weaken the hydrogen bond O(5)–H(5)---O(5′), but would strengthen the attractive interaction O(5)–H(5)---O(*W*) with the water oxygen atom at the bottom right of Fig. 2, by decreasing the H(5)---O(*W*) distance from 2·5 Å and increasing the angle at H(5) from 117°. The water molecule would then become involved in four, rather than three, hydrogen bonds, and these would be tetrahedrally disposed.

It appears that, within the observed range of twist of the O(5)–H(5) bond about the C(5)–O(5) bond, no one position is particularly favourable for intermolecular hydrogen bonding.

The greater part of this work was carried out while B.M.C. was a Senior Rothmans Research Fellow at Sydney University. Research facilities were kindly made available by Dr H.C. Freeman of the School of Chemistry, and by a grant from the Australian Institute for Nuclear Science and Engineering. The work was completed with support by a research grant NB-02763 from the U.S. Public Health Service, National Institutes of Health. Computer programs for IBM 7040 used in this work were written by Mrs Suzanne Hogg and Dr G.W. Cox (A.A.E.C. Research Establishment). Programs used for the IBM 7090 were written by Dr R. Shiono (University of Pittsburgh) and Dr C.K. Johnson (Oak Ridge National Laboratory, Tennessee). We thank the A.A.E.C. Reactor Operations Section for assistance with data collection.

References

ALEXANDER, L. E. & PITMAN, D. T. (1956). *Acta Cryst.* **9**, 501.
BOLTON, W. (1965). *Acta Cryst.* **19**, 1051.
BUSING, W. R. & LEVY, H. A. (1964). *Acta Cryst.* **17**, 142.
International Tables for X-ray Crystallography (1962). Vol. III. Birmingham: Kynoch Press.
PAULING, L. (1960). *The Nature of the Chemical Bond.* Ithaca: Cornell Univ. Press.

Acta Cryst. (1969). B25, 1978

The Crystal Structures of Two Polymorphs of 5,5′-Diethylbarbituric Acid (Barbital)

BY B. M. CRAVEN, E. A. VIZZINI AND M. M. RODRIGUES*

Crystallography Laboratory, University of Pittsburgh, Pittsburgh, Pennsylvania 15213, *U.S.A.*

(*Received* 21 *May* 1968 *and in revised form* 13 *November* 1968)

Crystal morphological, X-ray and infrared spectral data are presented for the identification of three (I, II and IV) of the four reported polymorphs of 5,5′-diethylbarbituric acid (barbital). Three-dimensional X-ray crystal structure determinations of barbital I and II are reported. The crystal data are: I (trigonal, m.p. 190°C) $a=26{\cdot}921$, $c=6{\cdot}828$ Å (hexagonal lattice), space group $R\bar{3}$, with 18 molecules per cell; II (monoclinic, m.p. 183°C) $a=7{\cdot}120$, $b=14{\cdot}162$, $c=9{\cdot}810$ Å, $\beta=89°14'$, space group $C2/c$ with 4 molecules per cell. For barbital I X-ray intensity data were collected from two different crystals and two independent structure determinations (I*a*, I*b*) were carried out. These agreed within experimental error. The X-ray intensity data (1526, 1617 and 840 reflections in I*a*, I*b* and II) were collected with a four-circle automatic diffractometer. Refinement of atomic positional and anisotropic thermal parameters was by full-matrix least-squares, resulting in final R values of 0·057, 0.041 and 0·062 for I*a*, I*b*, II, excluding the unobservably weak reflections. All hydrogen atoms were found. The molecule is in the 2·4,6-trioxo tautomeric form in both I and II. The molecular point symmetry is approximately 2 *mm*, but with distortions in the barbiturate ring and hydrocarbon chain which are most marked in I. Molecules are linked by NH···OC hydrogen bonds to form ribbons in which the barbiturate rings are almost coplanar, although the mode of hydrogen bonding is different in I and II. Van der Waals interactions are of greater importance in the stable form I. Variations of 0·014 Å in C–N ring bond lengths are near the limit of experimental error, but appear to be systematic and may be related to hydrogen bonding effects. The atomic thermal vibrational behaviour is strikingly similar in I and II.

Introduction

Since 1903 when Fischer and von Mering discovered the hypnotic action of 5,5′-diethylbarbituric acid (also known as barbital, veronal, or diemal, Fig. 1†), the relationship between chemical structure and drug action

* Present address: Escola de Engenharia de São Carlos, Universidade de São Paulo, São Carlos, S.P., Brazil.

† The atomic nomenclature in the present work was chosen to conform as closely as possible to the chemical nomenclature. A twofold rotation axis of crystallographic symmetry passes through atoms O(2), C(2) and C(5) in the case of barbital II.

UM00013161
NOVARTIS EXHIBIT 1517
Novartis v. Regents, IPR2023-01347
Page 1907 of 4460

of barbiturates has been widely studied. Doran (1959) has reviewed the structures, physical and chemical properties, and pharmacological activity of several hundred different barbiturates.

In order to possess effective hypnotic activity, a barbiturate must be disubstituted at the C(5) ring position either by ethyl or by larger nonpolar groups, *e.g.* allyl, isoamyl, phenyl or cyclohexyl groups. Thus barbital is chemically the simplest hypnotic barbiturate. Hypnotic activity generally increases up to a total of about six to ten carbon atoms in the C(5) substituents. A second requirement for hypnotic action is that the barbiturate ring should have at least a minimum capability for hydrogen bonding, *i.e.* no more than one of the two ring imide groups may be methylated, and no more than two of the three carbonyl oxygen atoms may be replaced by sulfur.

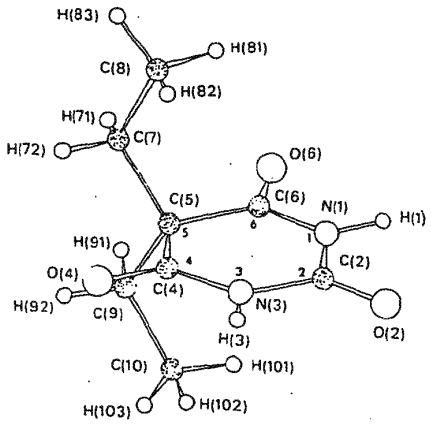


Fig. 1. Molecular formula of barbital.

In about 1900, Meyer & Overton correlated increased activity of anaesthetic agents with their increased lipid solubility. According to this theory, an anaesthetic (or barbiturate) with lipid solubility may pass from an aqueous biological medium and become associated with the lipids or lipoproteins of biological membranes, thus disrupting the normal metabolic process of the cell. Recently, progress has been made by Chance & Hollunger (1963) in determining the role of barbiturates in inhibiting the complex enzymatic processes of oxidative phosphorylation. It is perhaps significant that the enzymes concerned are believed to be either embedded in, or held in close proximity to, a mitochondrial membrane. The importance of a newly discovered specific hydrogen bonding of barbiturates to adenine derivatives has been stressed (Kyogoku, Lord & Rich, 1968; Kim & Rich, 1968). Although the detailed mechanism of barbiturate drug action at the molecular level is not understood, this must involve intermolecular interactions between barbiturate molecules and the drug acceptor site.

As a result of the chemical nature of the drug active barbiturates, these molecules are expected to exhibit

Table 1. *Crystal data for the polymorphs of barbital*

The lattice parameters are the result of the present work. These are in agreement with those previously reported for forms I (Ghose, Jeffrey, Craven & Warwicker, 1960) and II (Bertinotti, Bonamico, Braibanti, Coppola & Giacomello, 1959).

	I	II	III	IV
m.p.	190°C	183°C	181°C	176°C
Crystal system	Trigonal	Monoclinic	Monoclinic	Monoclinic*
Habit	Rhombohedral needles	Prisms	Needles	Twinned rectangular plates or flat pyramids
Space group†	$R\bar{3}$	$C2/c$	?	$P2_1$
a	26·921 ± 0·006 Å	7·120 ± 0·005 Å		12·585 ± 0·008 Å
b		14·162 ± 0·010 Å		22·083 ± 0·010 Å
c	6·828 ± 0·009 Å	9·810 ± 0·007 Å		6·788 ± 0·009 Å
β		89° 14 ± 2′		90° 55 ± 2′
Z	18	4		8
D_m	1·287 ± 0·007 g.cm^{-3}	1·238 ± 0·007 g.cm^{-3}		1·296 ± 0·007 g.cm^{-3}
D_x	1·284 g.cm^{-3}	1·242 g.cm^{-3}		1·303 g.cm^{-3}
Cleavage plane	(10$\bar{1}$0)	($\bar{1}$01)		(010)

* Previously reported as triclinic (Huang, 1951; Köfler, 1948) and incorrectly as orthorhombic (Ghose, Jeffrey, Craven & Warwicker, 1960).

† By crystal structure determination.

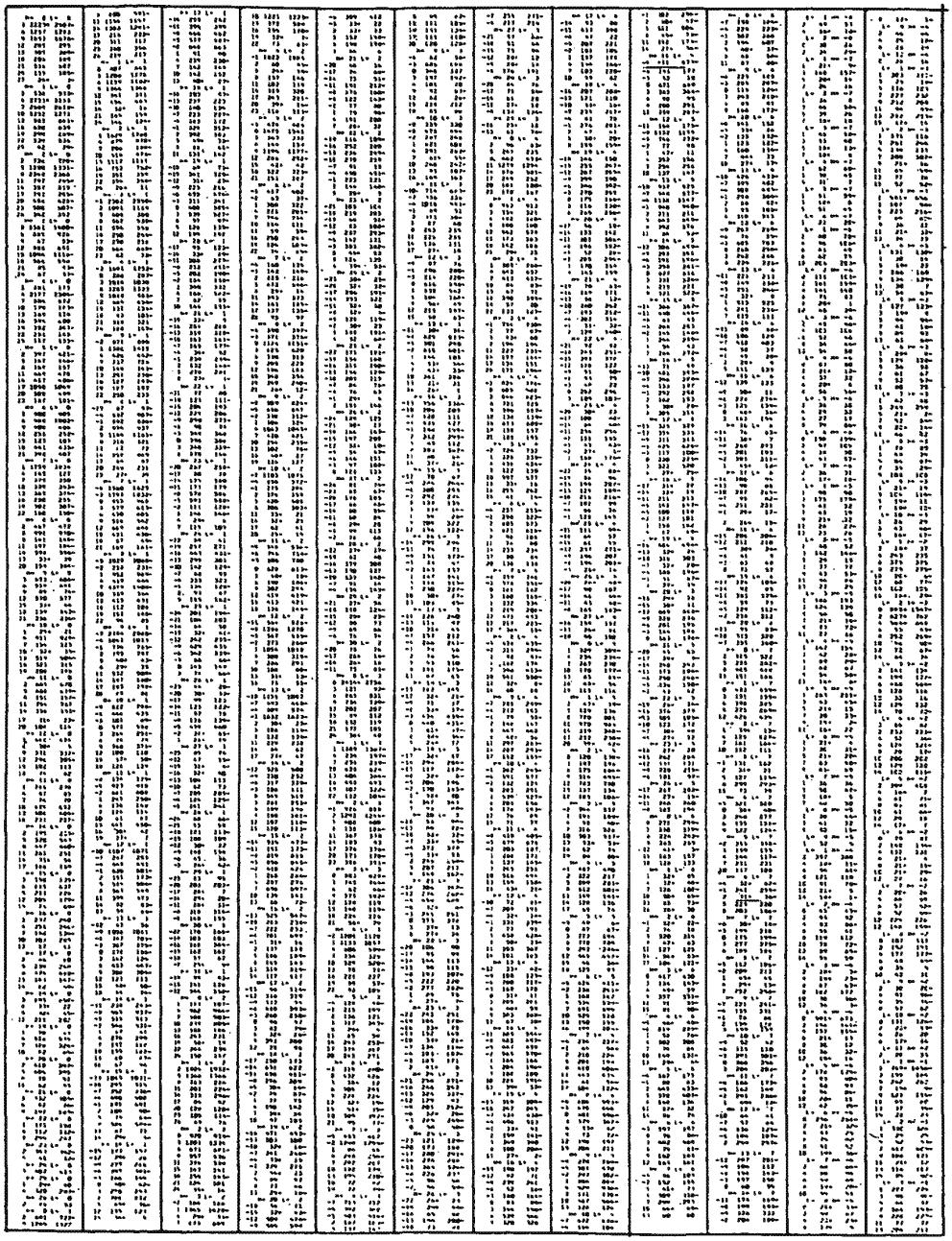
Table 2. *Intensity data for barbital* I *and* II

	Barbital I		Barbital II
	1st data set	2nd data set	
Crystal dimensions (mm) (c given first)	0·3, 0·1, 0·1	0·46, 0·24, 0·16	0·3, 0·2, 0·2
Crystal axis parallel to diffractometer φ-axis	c	c	b
Number of independent reflections	1526	1617	840
Number of unobserved reflections	495	220	149
R value, including unobserved reflections	8·4%	4·7%	10·2%
R value, excluding unobserved reflections	5·7%	4·1%	5·2%
Standard deviation in observation of unit weight	0·6139	0·5141	0·7221

UM00013162
NOVARTIS EXHIBIT 1517
Novartis v. Regents, IPR2023-01347
Page 1908 of 4460

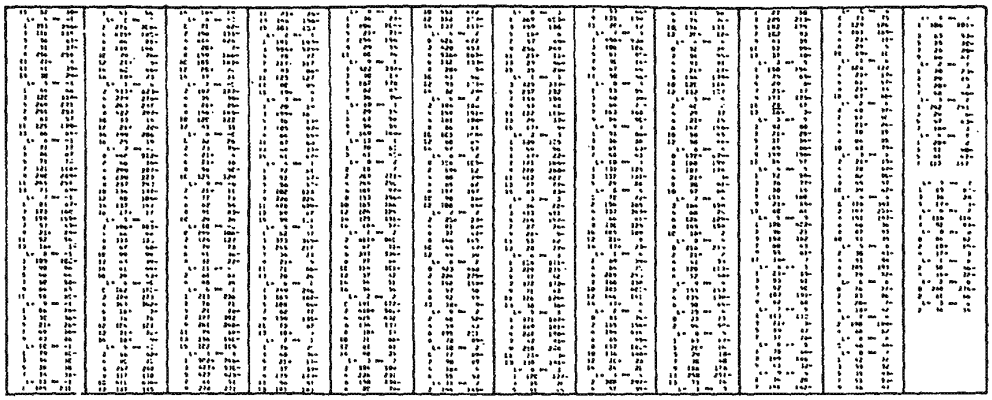
Table 3. *Observed and calculated structure factors*

Successive columns list k, $10|F_{obs}|$ and $10F_{calc}$. Reflections marked with an asterisk are either unobservably weak or very strong and considered to be affected by extinction. The latter were given zero weight in the least-squares refinement. The Table begins with the second data set for form I and continues with the data for form II at the top of the 11th column.



UM00013163
NOVARTIS EXHIBIT 1517
Novartis v. Regents, IPR2023-01347
Page 1909 of 4460

Table 3 (*cont.*)



considerable versatility in their intermolecular associations. Hydrogen bonding, van der Waals interactions between flat pyrimidine rings or between nonpolar hydrocarbon groups, dipole–dipole interactions between polar carbonyl groups and possibly charge-transfer interactions may be involved. Indeed, such versatility may eventually prove to be highly significant in determining the role of barbiturate molecules in their drug action.

We are now reporting the first results of a program of crystal structure determinations of the drug-active barbiturates, in which our principal objective is the study of recurring features in the various modes of barbiturate molecular association. We hope to establish features which, although based on homomolecular assemblies, may, because of the presence of both polar and nonpolar moieties in the barbiturate molecule, be relevant to the likely structural relationships at heteromolecular barbiturate drug-acceptor sites.

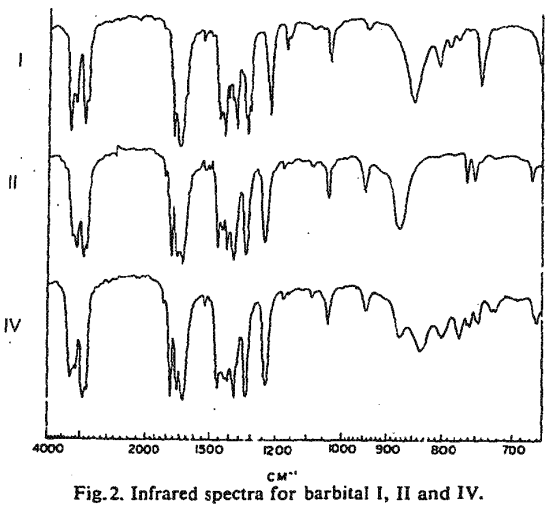


Fig. 2. Infrared spectra for barbital I, II and IV.

It is of interest that drug-active barbiturates are commonly polymorphous in their crystal structures and in the solid state readily form solutions and binary compounds with each other (Brandstätter-Kuhnert & Vlachopoulos, 1967; Cleverley & Williams, 1959). The molecular basis for polymorphism may depend on conformational variations when the C(5) substituents are flexible, but the results so far obtained for barbital and amobarbital (Craven & Vizzini, 1969) indicate that the major factor is in the interplay among the various types of molecular interaction, *e.g.* in barbital, van der Waals interactions appear to be more effective in polymorph I than in II. The crystal structure of polymorph II is dominated by hydrogen bonding.

Characterization of the polymorphs of barbital

Four polymorphs (I, II, III, IV) of barbital have been characterized by Köfler (1948) and Huang (1951) on the basis of crystal morphology, melting points and X-ray powder data. Cleverley & Williams (1959) have reported the infrared spectra of forms I, II and IV. More recently, Brandstätter-Kuhnert & Aepkers (1962) reported the existence of six (not four) polymorphs of barbital on the basis of thermal analyses of binary barbiturate systems. However, forms V and VI have not been isolated as single crystals. The melting points for these forms were obtained by extrapolation of the melting point curves for barbiturate solid solutions as a function of concentration.

Köfler and Huang also describe techniques for obtaining the various polymorphs both by sublimation and from solution. From studies on two-component systems, such as barbital–methylacetanilide, Köfler (1948) observed only one reversible phase transformation for barbital (III⇌IV at 135°C). Above 135°C, form I is most stable, followed by II, III, IV, in the order of decreasing melting points, while below 135° C, the order is I, II, IV, III.

UM00013164

NOVARTIS EXHIBIT 1517
Novartis v. Regents, IPR2023-01347
Page 1910 of 4460

Table 4. *Atomic parameters with e.s.d.'s*

Positional parameters are given as fractions of the lattice translations. Thermal parameters are given according to the expression:

$$T = \exp\left[-(\beta_{11}h^2+\beta_{22}k^2+\beta_{33}l^2+2\beta_{12}hk+2\beta_{13}hl+2\beta_{23}kl)\right].$$

The e.s.d.'s given in brackets refer to the least significant figures in the parameter values.

	x	y	z	β_{11}	β_{22}	β_{33}	β_{12}	β_{13}	β_{23}
Barbital I (parameters obtained from second data set)									
N(1)	0·10452 (7)	0·48245 (7)	0·7215 (2)	0·00161 (3)	0·00207 (3)	0·0093 (3)	0·00120 (3)	−0·00008 (7)	−0·00006 (7)
H(1)	0·1032 (11)	0·4817 (12)	0·861 (4)						
C(2)	0·06321 (7)	0·48923 (7)	0·6293 (2)	0·00145 (3)	0·00147 (3)	0·0105 (4)	0·00083 (3)	0·00001 (8)	−0·00005 (8)
O(2)	0·02548 (6)	0·49129 (6)	0·7190 (2)	0·00162 (2)	0·00245 (3)	0·0133 (3)	0·00134 (3)	0·00056 (7)	0·00000 (7)
N(3)	0·06649 (6)	0·49317 (6)	0·4280 (2)	0·00144 (3)	0·00167 (3)	0·0099 (3)	0·00101 (3)	−0·00020 (7)	−0·00019 (7)
H(3)	0·0410 (12)	0·4991 (11)	0·368 (4)						
C(4)	0·10727 (8)	0·49143 (7)	0·3135 (2)	0·00159 (3)	0·00141 (3)	0·0103 (4)	0·00087 (3)	0·00010 (8)	−0·00002 (8)
O(4)	0·10697 (6)	0·49804 (6)	0·1382 (2)	0·00240 (3)	0·00254 (3)	0·0094 (3)	0·00162 (3)	0·00045 (7)	0·00041 (7)
C(5)	0·15065 (8)	0·47882 (8)	0·4109 (3)	0·00157 (4)	0·00189 (4)	0·0128 (4)	0·00114 (3)	0·00047 (9)	−0·00009 (9)
C(6)	0·14719 (7)	0·47635 (8)	0·6324 (3)	0·00161 (4)	0·00188 (4)	0·0128 (4)	0·00111 (3)	−0·00028 (9)	−0·00020 (9)
O(6)	0·18018 (7)	0·46900 (8)	0·7316 (2)	0·00231 (5)	0·00370 (5)	0·0172 (4)	0·00222 (4)	−0·00111 (9)	−0·00011 (10)
C(7)	0·21165 (10)	0·52430 (11)	0·3486 (4)	0·00171 (4)	0·00269 (6)	0·0227 (6)	0·00119 (4)	0·00135 (12)	0·00070 (13)
H(71)	0·2128 (13)	0·5273 (14)	0·210 (5)						
H(72)	0·2385 (13)	0·5089 (14)	0·385 (4)						
C(8)	0·23168 (12)	0·58369 (12)	0·4289 (5)	0·00208 (6)	0·00213 (5)	0·0407 (9)	0·00074 (5)	−0·00073 (17)	0·00131 (17)
H(81)	0·2032 (15)	0·5962 (15)	0·389 (6)						
H(82)	0·2354 (15)	0·5842 (15)	0·580 (6)						
H(83)	0·2743 (15)	0·6095 (14)	0·382 (6)						
C(9)	0·13795 (11)	0·41917 (10)	0·3346 (3)	0·00265 (5)	0·00218 (5)	0·0182 (5)	0·00173 (4)	−0·00026 (12)	−0·00094 (12)
H(91)	0·1715 (14)	0·4163 (13)	0·389 (4)						
H(92)	0·1417 (13)	0·4237 (13)	0·186 (4)						
C(10)	0·08089 (14)	0·36998 (11)	0·3947 (5)	0·00135 (7)	0·00175 (5)	0·0404 (9)	0·00133 (5)	−0·00031 (20)	−0·00072 (17)
H(101)	0·0734 (17)	0·3672 (15)	0·540 (6)						
H(102)	0·0466 (18)	0·3757 (15)	0·367 (6)						
H(103)	0·0763 (16)	0·3347 (15)	0·353 (6)						
Barbital II									
C(2)	0	0·3228 (3)	0·25	0·0134 (6)	0·00323 (18)	0·0067 (4)	0	−0·0023 (4)	0
O(2)	0	0·4073 (2)	0·25	0·0238 (7)	0·00235 (14)	0·0120 (4)	0	−0·0066 (4)	0
N(3)	−0·0971 (3)	0·2506 (1)	0·1551 (2)	0·0165 (5)	0·00284 (12)	0·0066 (2)	0·0005 (2)	−0·0053 (3)	0·00024 (12)
H(3)	−0·160 (5)	0·300 (2)	0·096 (3)						
C(4)	−0·1040 (3)	0·1744 (2)	0·1456 (2)	0·0130 (4)	0·00311 (13)	0·0059 (3)	0·0000 (2)	−0·0029 (3)	−0·00026 (14)
O(4)	−0·1925 (3)	0·1371 (1)	0·0543 (2)	0·0262 (5)	0·00341 (11)	0·0087 (2)	0·0003 (2)	−0·0100 (3)	−0·00072 (11)
C(5)	0	0·1160 (2)	0·25	0·0157 (7)	0·00221 (15)	0·0054 (3)	0	−0·0028 (4)	0
C(7)	0·1441 (4)	0·0536 (2)	0·1736 (3)	0·0216 (6)	0·00418 (16)	0·0082 (3)	0·0030 (3)	−0·0031 (4)	−0·00086 (17)
H(71)	0·210 (5)	0·012 (3)	0·242 (4)						
H(72)	0·063 (5)	0·003 (3)	0·119 (4)						
C(8)	0·2882 (6)	0·1066 (3)	0·0878 (4)	0·0247 (9)	0·00878 (29)	0·0152 (5)	0·0038 (4)	0·0063 (6)	−0·00052 (30)
H(81)	0·352 (7)	0·152 (4)	0·144 (5)						
H(82)	0·208 (6)	0·144 (3)	0·011 (5)						
H(83)	0·383 (6)	0·064 (3)	0·045 (5)						

UM00013165

NOVARTIS EXHIBIT 1517
Novartis v. Regents, IPR2023-01347
Page 1911 of 4460

Previous single-crystal X-ray studies have been concerned only with forms I, II and IV. The crystal structure of II has been determined in projection (Bertinotti, Bonamico, Braibanti, Coppola & Giacomello, 1959).

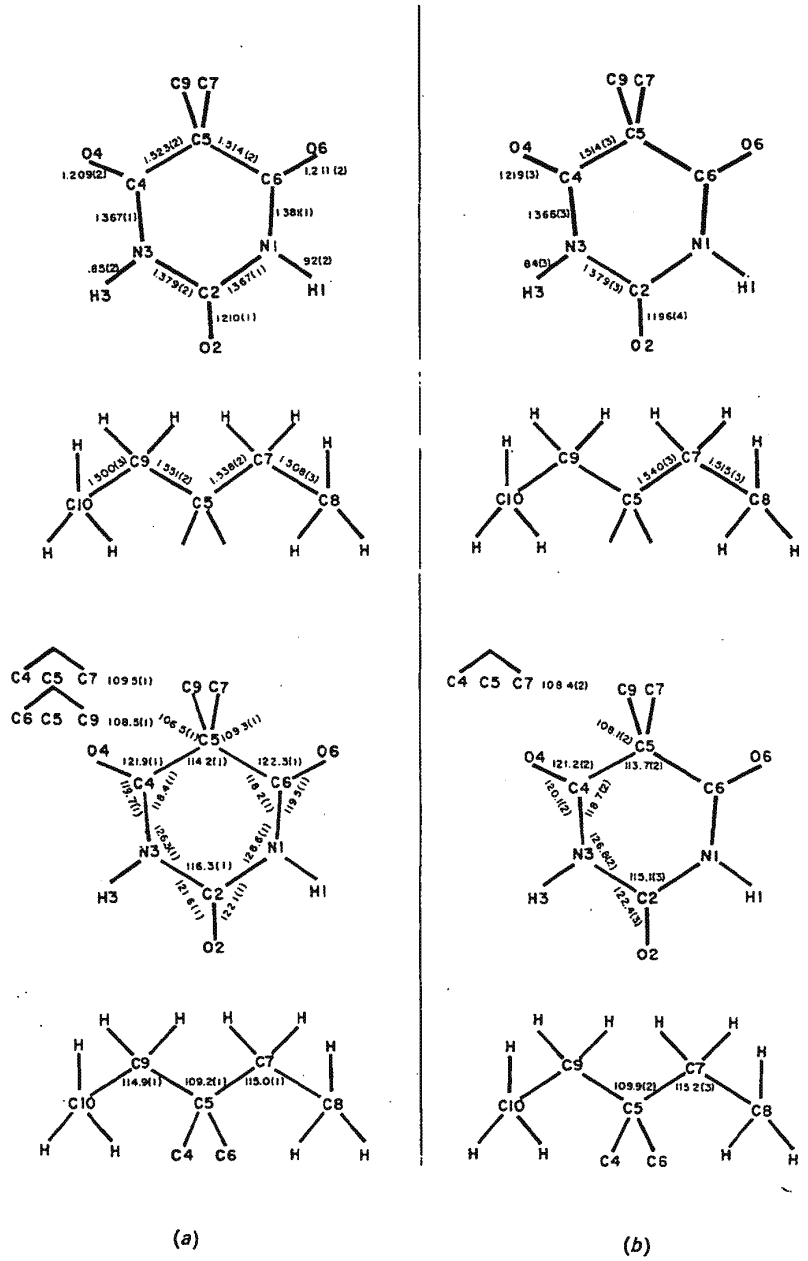


Fig. 3. Bond angles and bond lengths for barbital I and II. Bond lengths are in Å units, and are not corrected for the effect of anisotropic thermal motion. The e.s.d.'s in bond lengths and angles are given in brackets, and correspond to the least significant digits of the parameters involved. (*a*) The average values for the two independent structure determinations for barbital I. (*b*) Barbital II.

UM00013166
NOVARTIS EXHIBIT 1517
Novartis v. Regents, IPR2023-01347
Page 1912 of 4460

approximate cell data and space groups have been reported for forms I and IV (Ghose, Jeffrey, Craven & Warwicker, 1960).

The present crystal data (Table 1) and infrared spectra (Fig. 2) for forms I and II agree with those previously reported. However, there are inconsistencies concerning form IV, which we assume to be the same 'rectangular' plates described by Köfler (1948) and subsequent workers. In Fig. 2, the infrared spectrum of IV is now shown to be different from that of II, whereas Cleverley & Williams (1959) found these spectra to be identical. Also, single-crystal X-ray data for form IV now show this to be monoclinic rather than triclinic, as previously reported by Huang (1951) and Köfler (1948) on crystal morphological evidence. It should be noted that form IV can be obtained either as 'rectangular' plates which are in fact monoclinic, but twinned on the well-developed (010) face, or occasionally as flattened-pyramidal crystals with morphological symmetry 2, (pseudo *m*2*m*). Only with the latter single crystals were the X-ray crystal data unambiguously determined for this polymorph. Hence, the orthorhombic crystal data for form IV previously reported by Ghose, Jeffrey, Craven & Warwicker (1960) are incorrect, since these were obtained by the use of the pseudo-orthorhombic twinned crystals. Attempts to obtain form III, either from solution or by sublimation, were unsuccessful.

Experimental

Single crystals of polymorphs I, II and IV were obtained from the same ethanol solution by slow evaporation at room temperature. The infrared spectra (Fig. 2) were recorded with a Perkin-Elmer Model 137 spectrometer. Crystals were individually sorted according to their morphology, and for each polymorph a sample was prepared as a Nujol mull confined between rocksalt plates. Crystal densities were measured at room temperature by the flotation method. Lattice parameters (Table 1) and X-ray intensity data (Table 2) were measured with a Picker four-circle automatic diffractometer and Cu $K\alpha$ radiation. Intensity measurements

Table 5(*a*). *Interatomic distances and angles in barbital* I *determined from the second data set*

Atoms not in the crystal chemical unit (*i.e.* not listed in Table 4) are specified by a subscript. The four-digit subscript denotes how the atomic parameters can be derived from the corresponding atom in the crystal chemical unit. The first three digits code a lattice translation, *e.g.* 564 means a translation of $(5-5)a+(6-5)b+(4-5)c$ or $(b-c)$. The fourth digit refers to one of the following symmetry operations:

1: x, y, z	5: $\frac{1}{2}+(y-x), \frac{1}{2}-x, \frac{1}{2}+z$
2: $\bar{y}, (x-y), z$	6: $\frac{1}{2}+y, \frac{1}{2}+(y-x), \frac{1}{2}-z$
3: $\frac{1}{2}-y, \frac{1}{2}+(x-y), \frac{1}{2}+z$	7: $\frac{1}{2}+(x-y), \frac{1}{2}+y, \frac{1}{2}-z$
4: $\frac{1}{2}+(y-x), \frac{1}{2}+(x-y), \frac{1}{2}+z$	

Interatomic distances and angles are expressed as follows:

1·379 (3) Å means a distance of 1·379 Å with an e.s.d. of 0·003 Å.
120·1 (2)° means an angle of 120·1° with an e.s.d. of 0·2°.

(i) Bond distances

Column (1) lists uncorrected distances,
(2) lists distances with corrections based on the rigid body mode of molecular thermal motion.

	(1)	(2)
C(2)—O(2)	1·211 (2) Å	1·212 Å
C(2)—N(1)	1·368 (2)	1·372
N(1)—H(1)	0·95 (3)	
N(1)—C(6)	1·381 (2)	1·384
N(3)—H(3)	0·88 (3)	
C(2)—N(3)	1·378 (3)	1·384
C(6)—O(6)	1·210 (2)	1·212
C(6)—C(5)	1·514 (3)	1·521
C(5)—C(4)	1·523 (3)	1·528
C(4)—N(3)	1·370	1·371
C(4)—O(4)	1·211 (3)	1·213
C(5)—C(7)	1·538 (3)	1·545
C(5)—C(9)	1·555 (3)	1·562
C(7)—H(71)	0·96 (3)	
C(7)—H(72)	1·02 (3)	
C(9)—H(91)	1·01 (3)	
C(9)—H(92)	1·02 (3)	
C(7)—C(8)	1·512 (4)	1·517
C(9)—C(10)	1·499 (4)	1·504
C(8)—H(81)	1·01 (4)	
C(8)—H(82)	1·03 (4)	
C(8)—H(83)	1·04 (4)	
C(10)–H(101)	0·99 (4)	
C(10)–H(102)	1·01 (4)	
C(10)–H(103)	0·95 (4)	

UM00013167

NOVARTIS EXHIBIT 1517
Novartis v. Regents, IPR2023-01347
Page 1913 of 4460

Table 5(*a*) (*cont.*)

(ii) Bond angles

C(2)—N(3)—C(4)	126·3 (2)°
N(3)—C(2)—N(1)	116·4 (2)
N(3)—C(2)—O(2)	121·6 (2)
C(2)—N(3)—H(3)	116 (2)
H(3)—N(3)—C(4)	117 (2)
N(1)—C(2)—O(2)	122·0 (2)
C(2)—N(1)—H(1)	116 (2)
C(2)—N(1)—C(6)	126·4 (2)
C(6)—N(1)—H(1)	118 (2)
N(1)—C(6)—O(6)	119·7 (2)
N(1)—C(6)—C(5)	118·2 (2)
C(5)—C(6)—O(6)	122·2 (2)
C(6)—C(5)—C(4)	114·1 (2)
C(6)—C(5)—C(9)	108·2 (2)
C(6)—C(5)—C(7)	109·2 (2)
C(5)—C(4)—N(3)	118·4 (2)
C(5)—C(4)—O(4)	121·8 (2)
C(4)—C(5)—C(7)	109·5 (2)
N(3)—C(4)—O(4)	119·8 (2)
C(4)—C(5)—C(9)	106·6 (2)
C(9)—C(5)—C(7)	109·0 (2)
C(5)—C(7)—C(8)	114·6 (2)
C(5)—C(9)—C(10)	114·8 (2)
H(71)—C(7)—H(72)	107 (3)
H(81)—C(8)—H(82)	110 (3)
H(82)—C(8)—H(83)	103 (3)
H(83)—C(8)—H(81)	117 (3)
H(91)—C(9)—H(92)	110 (2)
H(101)–C(10)–H(102)	92 (3)
H(102)–C(10)–H(103)	114 (3)
H(103)–C(10)–H(101)	107 (3)

(iii) Hydrogen-bond distances and angles

N(3)···O(2)$_{4552}$	2·888 (4) Å	N(1)···O(4)$_{5561}$–C(4)$_{5561}$	163·4 (1)°
H(3)···O(2)$_{4552}$	2·02 (4)	H(1)···O(4)$_{5561}$–C(4)$_{5561}$	160 (1)
		N(1)—H(1)···O(4)$_{5561}$	173 (1)
N(1)···O(4)$_{5561}$	2·871 (4)	N(3)···O(2)$_{4552}$–C(2)$_{4552}$	129·2 (2)
H(1)···O(4)$_{5561}$	1·94 (3)	H(3)···O(2)$_{4552}$–C(2)$_{4552}$	132·1 (7)
		N(3)—H(3)···O(2)$_{4552}$	170 (2)

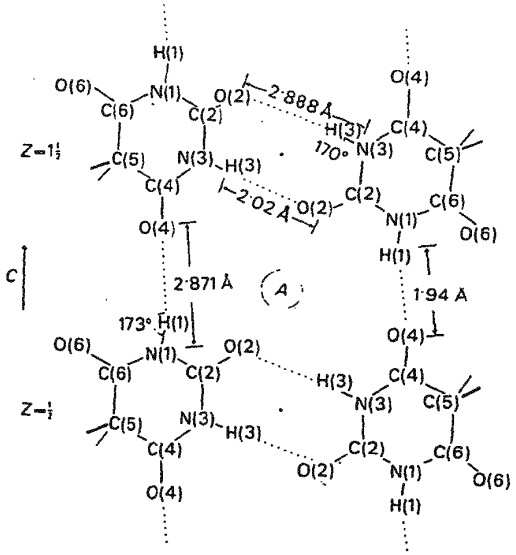


Fig.4. The hydrogen bonding in barbital I.

were made by scanning reflections in the θ:2θ mode at a rate of 2° min^{-1} with scans of 2° and a background count of 20 seconds at each of the scan limits. Data were collected for which 2θ was less than 130° (sin θ/λ <0·59 Å^{-1}). An integrated intensity, I, was assumed to be unobservably weak if I was less than 1·5$\sigma(I)$, where $\sigma(I)$ is the estimated standard deviation in I as determined from counting statistics. These reflections were assigned an intensity of 0·5$\sigma(I)$. X-ray absorption corrections were neglected.

For form I, two sets of intensity data were obtained, each from a different crystal, and independent structure determinations were carried out (Table 2).

Determination of the crystal structures

(*a*) *Barbital* I

The observed Laue symmetry, $(\bar{3})$, and the systematic spectral absences for form I indicated that the space group was either $R3$ or $R\bar{3}$. The space group was initially assumed to be $R\bar{3}$, which was subsequently confirmed by detailed structure determination.

In the three-dimensional Patterson function for the space group $R\bar{3}$ the Harker vectors at $w=0$ arising from

UM00013168

NOVARTIS EXHIBIT 1517
Novartis v. Regents, IPR2023-01347
Page 1914 of 4460

Table 5(*a*) (*cont.*)

(iv) Other close intermolecular approaches

The atom listed at the left of each pair belongs to the crystal chemical unit (*i.e.* has the parameters listed in Table 4). Intermolecular distances marked *v* lie within 0·2 Å of the sum of the appropriate van der Waals radii (Pauling, 1960).

C(2)·····O(6)$_{5556}$	3·115 (4)*v* Å
C(10)····C(10)$_{4555}$	3·981 (4)*v*
····H(102)$_{4555}$	3·09 (4)*v*
····O(4)$_{4555}$	3·635 (4)
····C(4)$_{4555}$	3·937 (4)*v*
····O(2)$_{4554}$	3·539 (4)*v*
H(101)···H(102)$_{4555}$	2·41 (6)*v*
···C(10)$_{4555}$	2·81 (4)*v*
H(102)···H(102)$_{5543}$	3·07 (5)
···H(103)$_{5543}$	3·04 (6)
H(103)···O(4)$_{4555}$	2·81 (4)
C(8)·····C(8)$_{5556}$	4·120 (7)*v*
·····C(8)$_{4556}$	4·369 (7)
·····C(7)$_{4556}$	3·879 (5)*v*
·····H(71)$_{4557}$	3·17 (3)*v*
C(7)·····C(7)$_{5557}$	4·364 (3)
·····H(81)$_{5557}$	3·16 (4)*v*
H(71)····H(81)$_{5557}$	2·37 (4)*v*
H(72)····O(4)$_{5557}$	2·83 (3)
H(81)····C(7)$_{4556}$	3·16 (4)*v*
····H(71)$_{4556}$	2·37 (5)
····H(72)$_{4556}$	3·15 (5)
O(4)·····H(72)$_{4556}$	2·83 (3)
·····H(91)$_{4556}$	2·88 (3)
·····C(2)$_{5541}$	3·639 (5)

Table 5(*b*). *Interatomic distances and angles in barbital* II

Atomic subscripts are as above, except that the fourth digit specifies one of the following symmetry operations:

1 x, y, z	5 $\frac{1}{2}+x, \frac{1}{2}+y, z$
2 $-x, y, \frac{1}{2}-z$	6 $\frac{1}{2}-x, \frac{1}{2}+y, -z$
3 $-x, -y, -z$	7 $\frac{1}{2}+x, \frac{1}{2}-y, \frac{1}{2}+z$
4 $x, -y, \frac{1}{2}+z$	8 $\frac{1}{2}-x, \frac{1}{2}+y, \frac{1}{2}-z$

Thus the atom C(4)$_{5552}$ has fractional coordinates (0·10398, 0·17440, 0·35437) and is related to C(4) by the crystallographic (and molecular) twofold rotation axis at ($x=0$, $z=\frac{1}{4}$).

(i) Bond distances

Column (1) lists uncorrected distances,
(2) lists distances with corrections based on the rigid body mode of molecular thermal motion.

	(1)	(2)
C(2)–O(2)	1·196 (4) Å	1·197 Å
C(2)–N(3)	1·379 (3)	1·384
N(3)–H(3)	0·84 (3)	
N(3)–C(4)	1·366 (3)	1·370
C(4)–O(4)	1·219 (3)	1·222
C(4)–C(5)	1·514 (3)	1·520
C(5)–C(7)	1·540 (3)	1·548
C(7)–H(71)	1·01 (4)	
C(7)–H(72)	1·07 (4)	
C(7)–C(8)	1·515 (5)	1·521
C(8)–H(81)	0·96 (5)	
C(8)–H(82)	1·09 (5)	
C(8)–H(83)	0·99 (5)	

(ii) Bond angles

N(3)–C(2)–N(3)$_{5552}$	115·1 (3)°	C(5)—C(7)–H(71)	109 (2)°
C(2)–N(3)–C(4)	126·8 (3)	C(5)—C(7)–H(72)	106 (2)
N(3)–C(4)–C(5)	118·7 (2)	C(8)—C(7)–H(71)	110 (2)
C(4)–C(5)–C(4)$_{5552}$	113·7 (2)	C(8)—C(7)–H(72)	115 (2)
N(3)–C(2)–O(2)	122·4 (3)	H(71)–C(7)–H(72)	102 (3)
C(2)–N(3)–H(3)	118 (2)	C(7)—C(8)–H(81)	110 (3)
C(4)–N(3)–H(3)	115 (2)	C(7)—C(8)–H(82)	105 (3)
N(3)–C(4)–O(4)	120·1 (2)	C(7)—C(8)–H(83)	112 (3)
C(5)–C(4)–O(4)	121·2 (2)	H(81)–C(8)–H(82)	109 (4)
C(4)–C(5)–C(7)	108·4 (2)	H(81)–C(8)–H(83)	109 (4)
C(4)–C(5)–C(7)$_{5552}$	108·1 (2)	H(82)–C(8)–H(83)	112 (4)
C(7)–C(5)–C(7)$_{5552}$	109·9 (2)		
C(5)–C(7)–C(8)	115·2 (3)		

UM00013169
NOVARTIS EXHIBIT 1517
Novartis v. Regents, IPR2023-01347
Page 1915 of 4460

Table 5(*b*) (*cont.*)

(iii) Hydrogen bond distances and angles

N(3)···C(4)$_{4556}$	2·867 (3) Å	N(3)—H(3)·····O(4)$_{4555}$	117 (3)°
H(3)···O(4)$_{4556}$	2·03 (3)	H(3)···O(4)$_{4556}$—C(4)$_{4556}$	128 (1)
		N(3)···O(4)$_{4556}$—C(4)$_{4556}$	127·2 (2)
		C(4)—N(3)·····O(4)$_{4556}$	112·8 (2)

(iv) Other close intermolecular approaches

The atom listed at the left of each pair belongs to the crystal chemical unit (*i.e.* has parameters listed in Table 4). Since atoms C(2) and O(2) lie on a twofold rotation axis, the close approaches to these atoms occur in symmetry-related pairs, only one of which is listed.

Intermolecular distances marked *v* lie within 0·2 Å of the sum of the appropriate van der Waals radii (Pauling, 1960).

C(2)····C(8)$_{5556}$	3·745 (4)*v* Å	H(72)···H(72)$_{5553}$	2·50 (5)*v* Å
····H(83)$_{5556}$	3·40 (5)	···O(4)$_{5553}$	2·76 (4)*v*
····H(71)$_{4555}$	3·39 (4)	···H(82)$_{5553}$	3·12 (6)
O(2)····C(7)$_{4555}$	3·365 (4)*v*	C(8)····C(2)$_{5556}$	3·745 (5)*v*
····H(71)$_{4555}$	2·55 (4)*v*	····O(2)$_{5556}$	3·615 (5)
····C(8)$_{4555}$	3·580 (5)*v*	····N(3)$_{5556}$	3·654 (5)
····H(83)$_{4555}$	3·11 (5)	····O(2)$_{5455}$	3·580 (5)
····C(8)$_{5556}$	3·615 (5)	····C(8)$_{6552}$	4·404 (6)
····H(83)$_{5556}$	3·02 (5)	····C(8)$_{5556}$	4·445 (7)
O(4)····C(7)$_{5553}$	3·514 (4)*v*	H(81)···H(81)$_{6552}$	2·97 (7)
····H(72)$_{5553}$	2·76 (4)*v*		
		H(82)···C(2)$_{5556}$	3·30 (5)
C(7)····O(2)$_{5455}$	3·365 (4)*v*	···O(2)$_{5556}$	3·35 (5)
····O(4)$_{5553}$	3·514 (4)*v*		
····C(7)$_{5553}$	4·265 (5)	H(83)···C(2)$_{5556}$	3·40 (5)
		···O(2)$_{5455}$	3·11 (5)
H(71)···O(2)$_{5455}$	2·55 (4)*v*	···O(2)$_{5556}$	3·02 (5)
···C(2)$_{5455}$	3·39 (4)	···H(83)$_{6553}$	2·61 (7)

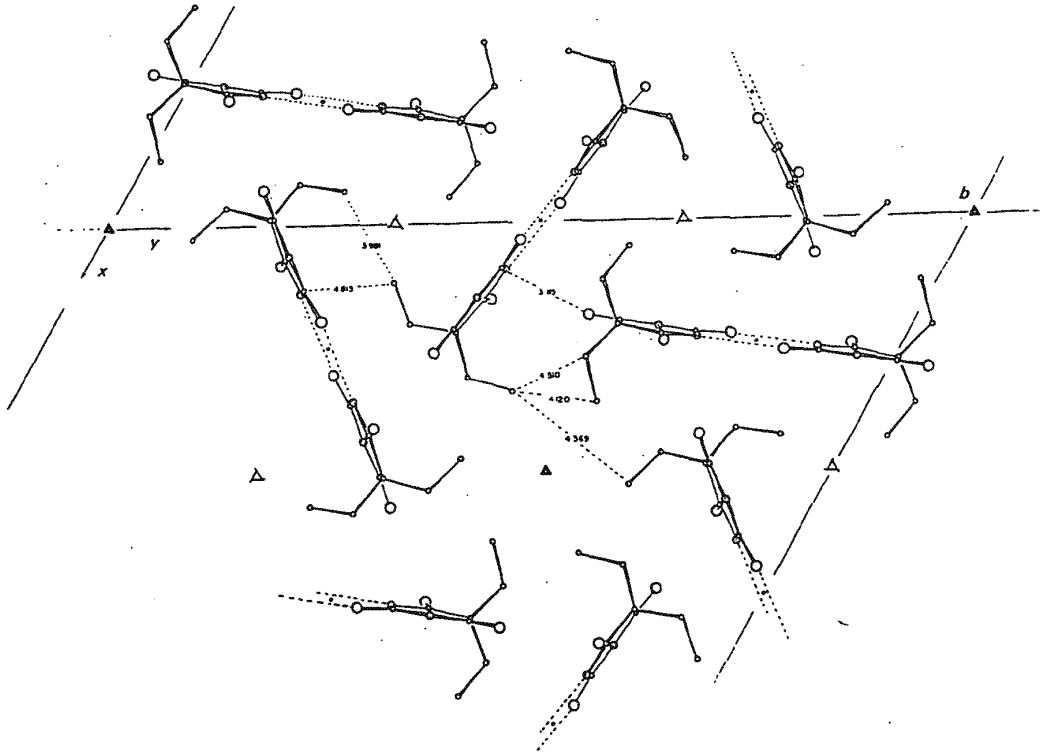


Fig. 5. The crystal structure of barbital I viewed down the *c* axis.

UM00013170
NOVARTIS EXHIBIT 1517
Novartis v. Regents, IPR2023-01347
Page 1916 of 4460

Table 6. *Least squares planes and dihedral angles*

	Barbital I	Barbital II
Plane 1:	Least-squares plane through the six pyrimidine ring atoms, all atoms being equally weighted.	The best least-squares plane through the six pyrimidine ring atoms, all atoms being equally weighted.
Plane 2:	The plane passing through the atoms N(1), C(2), N(3) and C(4).	The plane parallel to the crystallographic plane (10$\bar{1}$) and passing through the crystallographic twofold rotation axis which contains atoms O(2), C(2), C(5); *i.e.* the idealized plane of an extended ribbon of hydrogen bonded oxypyrimidine rings.
Plane 3:	The plane passing through the atoms N(1), C(4), C(5) and C(6).	The plane passing through atoms C(2), C(5) and the α-carbon atom, C(7), of the ethyl group substituents.

(i) Equations of planes

The equations of these planes are in the form $AX+BY+CZ=D$, referred to the crystallographic axes with X, Y, Z in Å units.

Plane	*A*	*B*	*C*	*D*	*A*	*B*	*C*	*D*
1	0·13059	0·79136	0·06670	10·95041	−0·80050	0	0·58854	1·43722
2	0·08971	0·81540	0·07226	11·20009	−0·80292	0	0·58526	1·42921
3	0·16654	0·76879	0·06496	10·78306	0·59226	0	0·81360	1·98683

(ii) Distances $d(i)$ of atoms from the ith plane

(The e.s.d.'s given in brackets refer to the least significant digit of the distances quoted.)

	Atoms forming the plane			Atoms not forming the plane			
	d(1)	*d*(2)	*d*(3)		*d*(1)	*d*(2)	*d*(3)
Barbital I							
N(1)	0·024 (2) Å	−0·001 (2) Å	−0·009 (3) Å	O(2)	−0·067 (2) Å	0·001 (2) Å	
C(2)	−0·019 (2)	0·002 (2)		O(4)	0·099 (3)	0·059 (3)	
N(3)	−0·015 (2)	−0·002 (2)		O(6)	−0·015 (3)	−0·133 (3)	
C(4)	0·039 (2)	0·001 (2)	0·008 (2)	C(5)		−0·123 (2)	
C(5)	−0·033 (2)		−0·015 (2)	C(6)		−0·076 (2)	
C(6)	0·003 (2)		0·016 (2)	Center at $(0,\frac{1}{2},\frac{1}{2})$		0·022	
				C(2)			−0·095 (2) Å
				N(3)			−0·088 (2)
Barbital II							
C(2)	0			H(3)	0·03 (3)	0·03 (3)	
N(3)	0·008 (2)			N(3)		0·013 (2)	
C(4)	−0·007 (2)			C(4)		−0·002 (2)	
C(5)	0			O(4)	−0·028 (2)	−0·018 (2)	
				H(71)			0·83 (4)
				H(72)			−0·78 (4)
				C(8)			−0·074 (4)
				H(81)			0·64 (5)
				H(82)			−1·03 (5)
				H(83)			−0·01 (5)

(iii) Dihedral angles

Barbital I

(2)∧(3) 4·5° fold along the C(4)–N(1) line.

Barbital II (These angles are positive for an anticlockwise twist when viewing the molecule along the axis from atom C(5) to C(2).

(1)∧(2) 0·23° (1)∧(3) 90·5 (2)° (2)∧(3) 90·3 (2)°

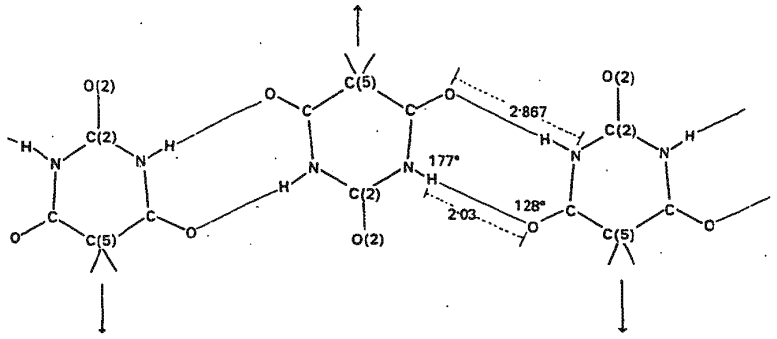


Fig. 6. The hydrogen bonding in barbital II.

UM00013171
NOVARTIS EXHIBIT 1517
Novartis v. Regents, IPR2023-01347
Page 1917 of 4460

Table 7. *Comparison of rigid body vibrational tensors* (**T**,**ω**) *for barbital* I *and* II

The tensors **T** and **ω** are referred to right handed orthogonal molecular axes directed with
(1) along the vector from atoms C(5) to C(2),
(2) the normal to the pyrimidine ring on the side of atom C(9),
(3) in the plane of the pyrimidine ring, approximately parallel to the vector from atoms C(5) to O(6).
The origin is at the molecular center of mass.

	T (Å²)			σ(**T**) (Å²)			r	ω (deg.²)			σ(ω) (deg.²)	
Barbital I	0·0346	0·0039	−0·0016	0·0006	0·0006	−0·0005	29·4	−1·2	−2·9	0·9	0·6	−0·6
		0·0363	0·0004		0·0041	−0·0034		3·9	0·7		3·5	−3·0
			0·0277			0·0034			18·1			2·8
Barbital II	0·0307	0	0	0·0016	0	0	35·7	0	0	1·9	0	0
		0·0281	−0·0014		0·0004	−0·0005		2·9	−1·1		0·5	−0·3
			0·0191			0·0034			23·4			2·5

Direction cosines of the principal values of **T** and **ω** with respect to the molecular axes.

	T (Å²)	$T^{1/2}$ (Å)	Direction cosines Molecular axes (1)	(2)	(3)	**ω** (deg.²)	$\omega^{1/2}$ (deg.)	Direction cosines Molecular axes (1)	(2)	(3)
Barbital I	0·0396	0·199	0·6327	0·7714	−0·0629	30·2	5·5	0·9708	−0·0499	−0·2339
	0·0320	0·179	−0·7136	0·6125	0·3393	17·4	4·2	0·2358	0·0283	0·9708
	0·0272	0·165	0·3004	−0·1698	0·9380	3·8	2·0	−0·0418	−0·9978	0·0392
Barbital II	0·0307	0·175	1	0	0	35·7	6·0	1	0	0
	0·0284	0·169	0	0·9894	−0·1449	23·5	4·8	0	−0·0528	0·9986
	0·0189	0·138	0	0·1449	0·9894	2·9	1·7	0	−0·9986	0·0528

the $\bar{3}$-axial symmetry constitute the c projection of the crystal structure transformed by a rotation of 30° and magnified by a factor of $\sqrt{3}$ (Buerger, 1959). The correct interpretation of the Harker section $w=0$ for barbital I was not immediately obvious, because of the presence of what subsequently proved to be non-Harker peaks. However, after the determination of the orientation of the barbiturate ring from the characteristic pattern of the intra-ring atom vectors near the three-dimensional Patterson origin, the c projected structure was recognized in the Harker section $w=0$. The atomic z parameters were obtained from a consideration of the molecular packing and the hydrogen bonding.

(*b*) *Barbital* II

Approximate atomic positional parameters were derived by inspection of the three-dimensional sharpened Patterson function. These agreed satisfactorily with the parameters determined by the two-dimensional structure analysis of Bertinotti *et al.* (1959).

The refinement of parameters

The refinement procedure was very similar for both crystal structures. Several cycles of structure factors and three-dimensional Fourier syntheses of the electron density were calculated in order to confirm the initial trial structures. X-ray atomic scattering factors were taken from *International Tables for* X-*ray Crystallography* (1962).The atomic positional and isotropic thermal parameters were refined by full-matrix least-squares procedures to give R values of 0·15 and 0·11 for forms I and II, respectively. A three-dimensional difference Fourier synthesis revealed all hydrogen atom positions in both crystal structures. Subsequent least-squares refinement involved the positional parameters of all atoms and anisotropic thermal parameters only for non-hydrogen atoms. The hydrogen atoms were assumed to have the same thermal parameters as the atoms to which they were covalently bonded.

The least-squares calculations were based on structure amplitudes, F, with the e.s.d. in a structure amplitude assumed to be given by the expression

$$\sigma(F)=\sigma+0{\cdot}05|F|\,,$$

where σ is the e.s.d. derived from counting statistics. In the final two cycles of least-squares refinement, the largest structure amplitudes were assigned zero weight when it became apparent that, with increasing magnitude of structure amplitude, the observed structure amplitudes were systematically less than the calculated values, indicating extinction effects. The results of the refinement for both crystal structures are given in Tables 3, 4 and 5. The observed and calculated structure factors for barbital I (Table 3) are those of the second of the two data sets. The corresponding atomic parameters with e.s.d.'s are listed in Table 4. Final R values are given in Table 2.

UM00013172
NOVARTIS EXHIBIT 1517
Novartis v. Regents, IPR2023-01347
Page 1918 of 4460

The molecular structure of barbital

In the crystal structures of both polymorphs I and II, molecules of barbital are in the trioxopyrimidine tautomeric form (Fig. 1). There are no significant differences between the values obtained for the two independent structure determinations of barbital I (Vizzini, 1968). In Fig. 3, the weighted average values of bond lengths and angles for barbital I are shown together with the values obtained for barbital II. In Table 5, distances and angles are given only for the more precise second structure determination of barbital I and for barbital II. In Tables 5(*a*)(i) and 5(*b*)(i) the bond lengths are shown with corrected values obtained by assuming rigid body thermal motion according to Cruickshank (1956, 1961).

In both barbital I and II, the C–N bond lengths alternate between values close to 1·384 and 1·370 Å around the pyrimidine rings. These differences (0·014 Å) have an e.s.d. of 0·004 Å and so are probably real. In barbital I, there are no significant differences in the C–O bond lengths, but in barbital II, the bond lengths of the hydrogen bonded carbonyl groups are longer than the other C–O bond lengths (1·222 *vs.* 1·97 Å, with e.s.d. of 0·005 Å in the difference). The evidence for a correlation between C–N and C–O bond length variations and the mode of hydrogen bonding in barbital and other 5,5-dialkylbarbiturates is discussed by Craven, Cusatis, Gartland & Vizzini (1969).

The C–C bonds in barbital are of three types, *i.e.* the ring bonds at C(5), each between a tetrahedrally and a trigonally bonded carbon atom, the bonds between atom C(5) and the α-carbon atoms of the ethyl groups and the bonds between α- and β-carbon atoms of the ethyl groups. Averaging over both barbital I and II, these have bond lengths of 1·52, 1·55 and 1·51 Å respectively, after correction for rigid body motion. The C(α)–C(β) bond length average becomes 1·53 Å assuming the riding motion correction (Busing & Levy, 1964). In either case, there are significant variations in this bond length sequence. A comparison of the barbital ring C–C bond lengths with the C–C bond length in acetaldehyde (1·501 Å from microwave spectra; Kilb, Lin & Wilson, 1957) and the ethyl C–C bond lengths with those in normal hydrocarbons (1·532 Å from electron diffraction; Bartell & Kohl, 1963) shows a lengthening of the bonds in barbital involving atom C(5). This is attributed to the non-bonded repulsive effects between the substituents at the C(5) position.

The internal angles at barbiturate ring atoms in barbital are very similar to those observed in the crystal structure of barbituric acid (Bolton, 1963). In particular the steric requirements of ring formation lead to an opening of the angle at the tetrahedrally bonded atom C(5) from the tetrahedral angle (109·4°) to 114°, for both barbital I and II and for barbituric acid. In the ethyl groups of barbital, a comparison with the average C–C–C angles in normal hydrocarbons (112·6°; Bartell & Kohl, 1963) shows that the steric repulsion between the terminal methyl groups and the ring atoms has given rise to a small increase in the angle at the α-carbon atoms (115°) with a corresponding decrease of the C(α)–C(5)–C(α) angle (109·0° and 109·9° in barbital I and II, respectively.).

The differences in molecular conformation in barbital I and II are small but real. The pyrimidine ring in barbital I is slightly folded along the line C(4)–N(1). Atoms N(1), C(2), N(3) and C(4) are coplanar, while atoms C(4), C(5), C(6) and N(1) are almost coplanar. The dihedral angle between the best least-squares planes of the halves of the pyrimidine ring is 4·5° (Table 6). However, in barbital II the pyrimidine ring is planar within experimental error (Table 6). The

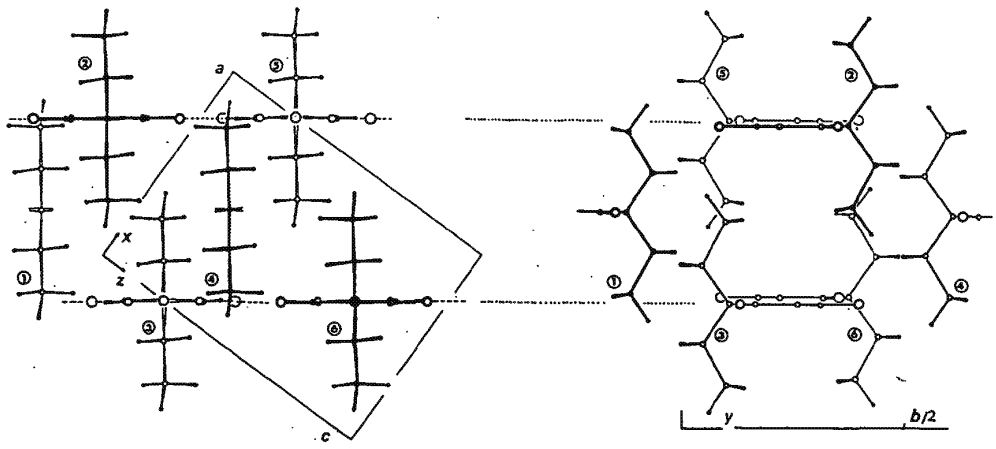


Fig. 7. The crystal structure of barbital II. The projection on the left is down the crystallographic *b* axis. The projection at the right is down [101]. In the latter projection, molecules which actually superimpose are shown slightly displaced. Molecules are numbered in the same way in both projections.

UM00013173
NOVARTIS EXHIBIT 1517
Novartis v. Regents, IPR2023-01347
Page 1919 of 4460

hydrocarbon chains are distorted from the idealized all *trans* conformation by twists about the C(5)–C(α) bonds of 5·2°, 4·3° in barbital I and 3·7° in barbital II. In barbital I, the spine of the hydrocarbon chain as viewed down the line C(5)→C(2) is slightly bowed, bringing the terminal atoms C(10) and C(8) both closer to O(6) than to O(4). The twofold rotation axis relating the ethyl groups in barbital II gives the hydrocarbon spine a slight 'S' shape. For Newman projections including the hydrogen atoms, see Vizzini (1968). It should be noted that the deviations from an idealized geometry with molecular point symmetry *2mm* are greater in barbital I than in barbital II, as might be expected from the crystal environments discussed below.

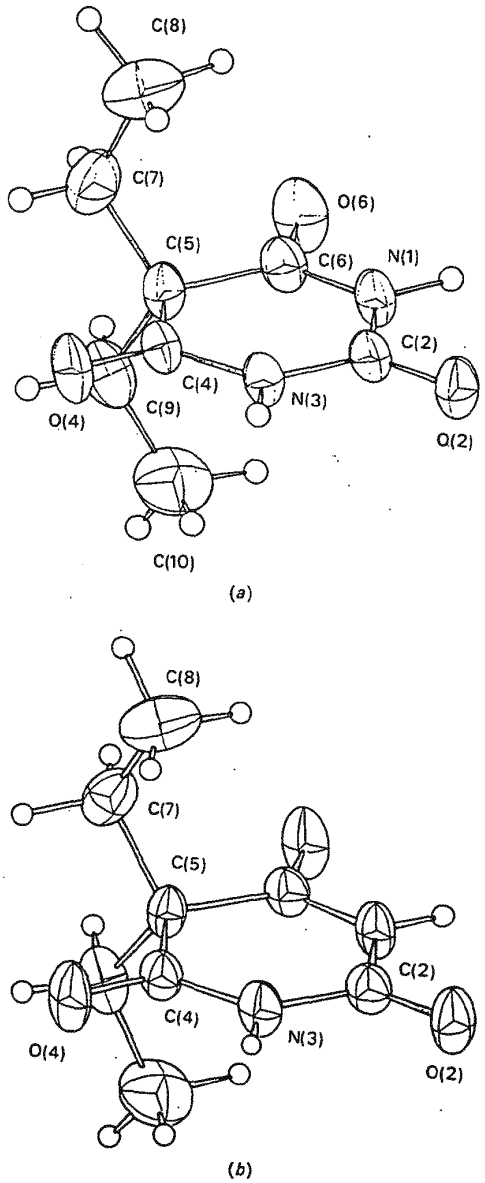


Fig. 8. The ellipsoidal representation of anisotropic thermal parameters (*a*) barbital I, (*b*) barbital II.

The crystal structures

(*a*) *Barbital* I

The hydrogen bonds in barbital I link barbiturate rings to form approximately planar ribbons running parallel to c, as shown in Fig. 4.

In Fig. 5, the packing of hydrogen bonded barbiturate ribbons is viewed down the trigonal *c* axis. In this mode of packing there are a number of van der Waals interactions between ethyl groups, as shown by the C···C (Fig. 5) and H···H distances listed in Table 5(*a*). The C(7)–C(8) ethyl groups are arranged about the threefold inversion axes, and the C(9)–C(10) ethyl groups are arranged about the threefold screw axes, but there are no van der Waals interactions between the two crystallographically distinct ethyl groups.

The carbonyl group C(6)–O(6), which is not hydrogen bonded, is directed towards the C(2) atom of a carbonyl group in an adjacent molecule, so that the angle C(6)–O(6)···C(2′) is 137°. The O(6)···C(2′) distance (3·12 Å) corresponds to a normal van der Waals interaction. Bolton (1964) has drawn attention to a number of crystal structures, including barbiturates, in which there appear to be dipole–dipole intermolecular interactions between carbonyl groups. These are characterized by C···O distances as much as 0·3 Å less than the van der Waals distance and C–O···C angles near 160°. Although the carbonyl–carbonyl interaction in barbital I is weak, as indicated by the larger C···O distance, it is believed that it does have some structure determining influence. It should be noted that the molecules which interact with a given hydrogen bonded ribbon in this way (Fig. 5) are arranged so that their C(9)–C(10) ethyl groups approach the ribbon on either side of the open area labelled '*A*' in Fig. 4.

An inspection of a model of the crystal structure of barbital I shows that the observed molecular distortions from idealized geometry result in closer intermolecular packing than would otherwise be the case. For example, the 4·5° 'folding' of the pyrimidine ring about the C(4)–N(1) axis, which is almost parallel to the *c* axis of projection in Fig. 6, leads to closer approaches by about 0·3 Å among both of the two sets of terminal methyl groups. The observed distances are C(8)···C(8′) at 4·1 Å and C(10)···C(10′) at 4·0 Å.

(*b*) *Barbital* II

In this crystal structure, the molecules are hydrogen bonded N(3) H(3)···O(4′) in ribbons in which the barbiturate rings are very nearly parallel to the crystal-

UM00013174
NOVARTIS EXHIBIT 1517
Novartis v. Regents, IPR2023-01347
Page 1920 of 4460

lographic plane ($10\bar{1}$). One such ribbon is shown in Fig.6.

The carbonyl oxygen atom O(2) is not hydrogen bonded, nor is it involved in a carbonyl–carbonyl interaction similar to that of the non-hydrogen bonded carbonyl group in barbital I. However, the hydrogen bonded ribbons pack so that atom O(2), lying on a twofold rotation axis, is in van der Waals contact with an ethyl group from each of two symmetry related molecules. The van der Waals distances are listed in Table 5(*b*).

It is of particular interest that there are so few close intermolecular approaches between the ethyl group atoms in this crystal structure. The only intermolecular distance involving these atoms which lies within 0·2 Å of the sum of the appropriate van der Waals radii (1·2 Å for hydrogen, 2·0 Å for methyl or methylene carbon atoms; Pauling, 1960) is the distance H(72)···H(72′) of 2·50 Å, for which the corresponding C(7)···C(7′) distance is 4·27 Å. Thus the mode of molecular packing in this crystal structure is dominated by the hydrogen bonding requirements of the barbiturate rings, the attractive interactions between the nonpolar ethyl groups being of little importance.

Adjacent parallel ribbons of hydrogen-bonded barbiturate rings are separated by 5·72 Å. These ribbons form the 'walls' of tunnels parallel to the [101] direction and running through the structure, with spanning ethyl groups forming the 'floor' and 'roof' (Fig. 7). The closest intermolecular approach between floor and roof is the H(82)···H(82′) distance of 3·08 Å, with corresponding C(8)···C(8′) distance of 4·445 Å.

Relationship between barbital I and II

In both barbital I and II, there are NH···OC hydrogen bonds involving the two imine groups and two of the three carbonyl groups. These hydrogen bonds link the barbiturate rings to form almost planar ribbons. However, in barbital II, these are simple ribbons in which each molecule is hydrogen bonded to only two adjacent molecules, while in barbital I, a more complex double ribbon is formed in which each molecule is hydrogen bonded to three others.

In forming a crystal structure, the hydrogen bonded ribbons in barbital I pack more efficiently than those of barbital II. This can be seen in the appreciable difference in crystal densities (1·29 *vs.* 1·24 g.cm^{-3} in barbital I and II respectively), as well as from a consideration of the detailed intermolecular structural features. It is concluded that barbital I is the more stable structure because of the more effective van der Waals interactions, particularly those between ethyl groups.

In spite of environmental differences, the molecular thermal vibrational behaviour in both crystal structures is similar. This can be seen from the ellipsoidal representation of atomic thermal parameters in Fig.8(*a*) and (*b*) and a comparison of the molecular rigid body translational and librational tensor components (Table 7). The rigid body model is invoked not because this is claimed to be the true description of the molecular vibrational behaviour, but rather as a convenient description of the similarity of this behaviour in the two crystal structures.* The close correspondence in rigid body parameters for the two molecules, however, does provide evidence that this model is a useful approximation.

The two translational tensors (T) correspond to almost isotropic motions of similar amplitudes. The principal values of the librational tensors (ω) are in directions which are close to the chosen molecular axes. Furthermore, the librational amplitudes about corresponding molecular axes are almost the same. The librational motion is markedly anisotropic, such that the amplitude of libration about the molecular axis which is normal to the pyrimidine ring (and hydrogen bonded ribbon of molecules) is smaller than the libration about the other two axes. The larger amplitudes of libration correspond to flexing motions within a hydrogen bonded ribbon of molecules.

It is concluded that the molecular vibrational behaviour in the two crystal structures is largely determined by the hydrogen bonding of molecules to form ribbons. The amplitude of flexing motions in these ribbons seems to be insensitive to the precise structure of the ribbons, and to the manner in which these are packed together to form the crystal structure.

This work was supported by a grant NB-02763 from the U.S. Public Health Service, National Institutes of Health. Part of the work was carried out while one of us (MMR) held a Fulbright Scholarship.

Computer programs for IBM 7090 used in this work were written by Drs Busing, Martin & Levy (full-matrix least squares) and Johnson (thermal ellipsoid plot) of Oak Ridge National Laboratory, and by Drs Zalkin (Fourier) and Gantzel, Coulter and Trueblood (rigid body analysis) of the University of California. These programs were modified by Dr Shiono of University of Pittsburgh. Drs Shiono, Chu and Schwarzenbach are responsible for the IBM 1620 programs used in data collection and processing.

References

Bartell, L. S. & Kohl, D. A. (1963). *J. Chem. Phys.* **39**, 3097.

Bertinotti, F., Bonamico, M., Braibanti, A., Coppola, R. & Giacomello, G. (1959). *Ann. Chim. (Rome)*, **49**, 825.

Bolton, W. (1963). *Acta Cryst.* **16**, 166.

Bolton, W. (1964). *Nature, Lond.* **201**, 987.

* Schomaker & Trueblood's (1968) recent treatment of rigid body motion is more appropriate for a barbital molecule with point symmetry 2*mm*, since it does not require the present assumption of librational axes intersecting at the molecular center of mass. For *comparison* of the two crystal structures, Cruickshank's procedure (1956, 1961) is adequate.

UM00013175
NOVARTIS EXHIBIT 1517
Novartis v. Regents, IPR2023-01347
Page 1921 of 4460

BRANDSTÄTTER-KUHNERT, M. & AEPKERS, M. (1962). *Mikrochim. Acta*, p. 1055.
BRANDSTÄTTER-KUHNERT, M. & VLACHOPOULOS, A. (1967). *Mikrochim. Acta*, p. 201.
BUERGER, M. (1959). *Vector Space*, 2nd Edition. New York: John Wiley.
BUSING, W. R. & LEVY, H. A. (1964). *Acta Cryst.* **17**, 142.
CHANCE, B. & HOLLUNGER, G. (1963). *J. Biol. Chem.* **238**, 418.
CLEVERLEY, B. & WILLIAMS, P. P. (1959). *Tetrahedron*, **7**, 277.
CRAVEN, B. M., CUSATIS, C., GARTLAND, G. L. & VIZZINI, E. A. (1969). To be published.
CRAVEN, B. M. & VIZZINI, E. A. (1969). *Acta Cryst.* **25**, 1993.
CRUICKSHANK, D. W. J. (1956). *Acta Cryst.* **9**, 754.
CRUICKSHANK, D. W. J. (1961). *Acta Cryst.* **14**, 896.
DORAN, W. J. (1959). *Medicinal Chemistry*. Vol. IV. New York: John Wiley.
GHOSE, S., JEFFREY, G. A., CRAVEN, B. M. & WARWICKER, J. O. (1960). *Acta Cryst.* **13**, 1034.
HUANG, T.-Y. (1951). *Acta Pharm. Intern.* **11**, 106.
International Tables for X-ray Crystallography (1962). Vol. III. Birmingham: Kynoch Press.
KILB, R. W., LIN, C. C. & WILSON, E. B. (1957). *J. Chem. Phys.* **26**, 1695.
KIM, S. H. & RICH, A. (1968). *Proc. Nat. Acad. Sci. Wash.* **60**, 402.
KÖFLER, A. (1948) *Mikrochemie*, **33**, 4.
KYOGOKU, Y., LORD, R. C. & RICH, A. (1968). *Nature, Lond.* **218**, 69.
PAULING, L. (1960). *The Nature of the Chemical Bond*. 3rd ed. Ithaca: Cornell Univ. Press.
SCHOMAKER, V. & TRUEBLOOD, K. N. (1968). *Acta Cryst.* B**24**, 63.
VIZZINI, E. A. (1968). Ph. D. Thesis, Univ. of Pittsburgh.

Acta Cryst. (1969). B**25**, 1993

The Crystal Structures of Two Polymorphs of 5-Ethyl-5-isoamylbarbituric Acid (Amobarbital)

BY B. M. CRAVEN AND E. A. VIZZINI

Crystallography Laboratory, University of Pittsburgh, Pittsburgh, Pennsylvania 15213, *U.S.A.*

(*Received* 21 *May* 1968 *and in revised form* 13 *November* 1968)

Two crystalline forms of 5-ethyl-5-isoamylbarbituric acid (amobarbital) are known. Three-dimensional X-ray crystal structure determinations of these are reported. The crystal data are: I (monoclinic, m.p. 154–156°C) $a=21{\cdot}480$, $b=11{\cdot}590$, $c=10{\cdot}370$ Å, $\beta=97°4'$, space group $C2/c$ with 8 molecules per cell; II (monoclinic, m.p. 160–162°C) $a=10{\cdot}281$, $b=22{\cdot}601$, $c=11{\cdot}679$ Å, $\beta=109°6'$, space group $P2_1/c$ with 8 molecules per cell. The X-ray intensity data (1861 and 4139 reflections in I and II) were collected with a four-circle automatic diffractometer and Cu $K\alpha$ radiation. Refinement of atomic positional and anisotropic thermal parameters was by a least-squares procedure, resulting in final R values of 9·6 and 7·2 per cent for all reflections or 6·9 and 7·1 per cent excluding unobserved and extinction affected reflections. The positions of the three isoamyl terminal atoms are not well-defined in either I or II because of unusually large amplitudes of thermal vibration and possibly some degree of conformational disorder. Hydrogen atoms were found except for those associated with the isoamyl terminal groups. The molecules are in the 2,4,6-trioxo tautomeric form. Variations of 0·012 Å in C–N ring bond lengths are observed which appear to be systematic and may be correlated with the effects of hydrogen bonding. The main difference between I and II is in the mode of assembly of the same structural unit, the so-called double ribbon. A single ribbon is formed from (NH···OC) hydrogen bonded barbiturate rings with all isoamyl groups projecting on one side and all ethyl groups on the other. In the double ribbon, the two component ribbons are interlocked with their ethyl group surfaces in close contact.

Introduction

A study of polymorphism in drug-active barbiturates has been undertaken in this laboratory.* In this paper, the crystal structure determinations of the two polymorphs of 5-ethyl-5-isoamyl barbituric acid, or amobarbital (Fig. 1) are reported.

Experimental

Single crystals of amobarbital I and II were obtained from the same aqueous ethanol solution by slow evaporation at room temperature. The melting points, crystal morphology, and infrared spectra of these two forms as presently observed are in agreement with those previously reported (Williams, 1959; Cleverley & Williams, 1959; Brandstätter-Kuhnert & Aepkers, 1962). The crystal data are listed in Table 1.

The intensity data were collected in the same way as for barbital (Craven, Vizzini & Rodrigues, 1969). For both forms I and II, the crystals were oriented with the symmetry axis b along the φ axis of the diffractometer. X-ray absorption corrections were applied only to the data for amobarbital I.

* See the previous paper (Craven, Vizzini & Rodrigues, 1969).

UM00013176
NOVARTIS EXHIBIT 1517
Novartis v. Regents, IPR2023-01347
Page 1922 of 4460

This Page is Inserted by IFW Indexing and Scanning Operations and is not part of the Official Record

BEST AVAILABLE IMAGES

Defective images within this document are accurate representations of the original documents submitted by the applicant.

Defects in the images include but are not limited to the items checked:

- ☐ BLACK BORDERS
- ☐ IMAGE CUT OFF AT TOP, BOTTOM OR SIDES
- ☐ FADED TEXT OR DRAWING
- ☐ BLURRED OR ILLEGIBLE TEXT OR DRAWING
- ☐ SKEWED/SLANTED IMAGES
- ☐ COLOR OR BLACK AND WHITE PHOTOGRAPHS
- ☐ GRAY SCALE DOCUMENTS
- ☐ LINES OR MARKS ON ORIGINAL DOCUMENT
- ☐ REFERENCE(S) OR EXHIBIT(S) SUBMITTED ARE POOR QUALITY
- ☐ OTHER: _____

IMAGES ARE BEST AVAILABLE COPY.
As rescanning these documents will not correct the image problems checked, please do not report these problems to the IFW Image Problem Mailbox.

Acta Cryst. (1994). D50, 414–423

Screening and Optimization Strategies for Macromolecular Crystal Growth

By Bob Cudney and Sam Patel

University of California Riverside, Department of Biochemistry, Riverside, CA 92521, USA, and Hampton Research, Riverside, CA, USA

Karl Weisgraber and Yvonne Newhouse

The Gladstone Institute, San Francisco, CA, USA

and Alexander McPherson

University of California Riverside, Department of Biochemistry, Riverside, CA 92521, USA

(*Received* 13 *August* 1993; *accepted* 9 *March* 1994)

Abstract

Today the determination of successful crystallization conditions for a particular macromolecule remains a highly empirical process. Sparse-matrix and grid-screening procedures are rapid and economical means to determine preliminary crystallization conditions. During optimization the variable set (pH, precipitant type and precipitant concentration) utilized in these procedures is screened in an attempt to determine appropriate conditions for the nucleation and growth of single crystals suitable for X-ray diffraction analysis. Unfortunately, in many cases this strategy will not produce single crystals suitable for X-ray diffraction analysis. We have explored, in an empirical sense, other tools for use during optimization. First, a new screening protocol is evaluated which employs less classical precipitating agents. Second, a set of 24 electrostatic crosslinking agents are evaluated for their ability to promote crystallization. Third, a panel of more than 30 detergents are evaluated for their ability to prevent sample aggregation and influence crystal growth.

1. Introduction

In spite of recent innovations and an expanded base of experience, the growth of single crystals of macromolecules generally remains an empirical and frequently tedious process. The variable set over which successful crystallization conditions must be sought is vast while the quantity of macromolecule available may be extremely limited (McPherson, 1990). Nonetheless, the number of macromolecules crystallized during the past decade has increased at a near exponential rate (Gilliland & Bickham, 1990). A major contribution to this increased success has been the development of novel screening protocols and optimization strategies which have provided investigators with an expanded portfolio of effective crystallization tools (Carter & Carter, 1979; Jancarik & Kim, 1991; McPherson, 1992; Samudzi & Fivash, 1992; Stura, Nemerow & Wilson, 1992; Weber, 1990). In addition, the increasing number of investigators engaged in the crystallization of macromolecules has further enhanced the database of successful crystallization conditions and approaches.

The process of crystallizing macromolecules can be divided into three discrete stages. These are (1) screening for useful crystallization conditions or leads; (2) optimization of one or more initial condition to produce single crystals suitable for X-ray diffraction analysis; and (3) reproducible production of single crystals for X-ray data collections. The first stage, locating successful crystallization conditions, is essentially the search of an extensive matrix of parameters to identify an initial combination of variables which produce crystals. In less successful cases they may yield only solubility information which must in turn be used to design subsequent crystallization trials. An effective screening technique often termed 'grid screening' evaluates the variance of pH and precipitant concentration for different kinds of precipitants to promote crystal growth (Weber, 1990; McPherson, 1990). Typically, such a crystallization trial utilizes a four by six grid to screen pH (example 4, 5, 6, 7, 8, 9) *versus* a concentration range of a single precipitant which may be a salt, polymer or organic solvent. Based upon microscopic examination, generally, of vapor-diffusion crystallization trials, a more refined screen can then be set up and searched in the neighborhood of the initial, promising condition. The advantage of the 'grid-screening' technique is the ease and rapidity in creating and interpreting the crystallization trials as a consequence of the limited range of variables. The

©1994 International Union of Crystallography
Printed in Great Britain – all rights reserved

ISSN 0907-4449 ©1994

UM00013178
NOVARTIS EXHIBIT 1517
Novartis v. Regents, IPR2023-01347
Page 1924 of 4460

principal disadvantage of this approach is that an exhaustive search of potential crystallization conditions by varying pH *versus* precipitant type and concentration would consume a large amount of macromolecule. An effective compromise to such an exhaustive search is to evaluate ranges of pH, precipitant type and precipitate concentration which have yielded high rates of success in other crystallization investigations. Based primarily upon personal experience and the contents of the NIST/CARB Biological Macromolecule Crystallization Database (BMCD), grid-screening strategies using polyethylene glycol (M_r 400 to 20 000; 6000 being the most frequently used PEG), ammonium sulfate and 2-methyl-2,4-pentanediol (MPD) have proven very successful in providing initial crystallization conditions for a wide variety of proteins (Samudzi & Fivash, 1992; McPherson, 1990; Weber, 1990).

More recently, approaches for expanding the ranges of salts, polymers, organic solvents and pH included in a screen and at the same time conserving macromolecule sample, have appeared (Carter & Carter, 1979; Jancarik & Kim, 1991; McPherson, 1992; Samudzi & Fivash, 1992; Stura *et al.*, 1992; Weber, 1990). These have seen great success in identifying initial crystallization conditions for a wide variety of macromolecules including proteins, viruses, peptides and nucleic acids. These strategies, termed 'incomplete-factorial' and 'sparse-matrix' screens are designed to evaluate a large number of pH and precipitant combinations with a limited amount of macromolecule sample. Here we describe a general approach for developing a novel 'sparse-matrix' screen, specifically that presented in Fig. 1.

2. Development of the screen

A focus of our research is to produce crystals of as many different macromolecules, under as many different conditions, as possible, and then to apply a variety of phyical techniques to delineate the essential characteristics of the growth process. Therefore, in developing this novel 'sparse-matrix' screen our objective was to expand the current set of successful, initial screening conditions by utilizing hanging- or sitting-drop vapor-diffusion crystallization in a single 24-well plate. Another intention was to employ a novel set of precipitants, or combination of precipitants, in order to escape the limitation of the salts and polymeric precipitants one typically uses. In so doing we hoped to uncover new additional leads for further optimization. With a more diverse set of leads in hand, the opportunities for successful optimization or the discovery of different crystal forms might be enhanced.

The determination of a suitable pH range was based upon a review of the NIST/CARB BMCD (Gilliland & Bickham, 1990). We selected a pH range between 4 and 9 reflecting the observation that more than 90% of all macromolecules reported crystallized were within this pH range. The decision to use Good's (Good *et al.*, 1966) series of buffers was based upon our objective of minimizing the occurence of inorganic crystals as phosphate, carbonate and borate salts when combined with ions possibly used during screening and optimization procedures. A comprehensive panel of precipitants (salts, polymers and organic solvents) were selected from the NIST/CARB BMCD and from the literature (McPherson, 1990, 1992; Weber, 1990). For each precipitant a suitable concentration range was selected based again upon a review of the NIST/CARB BMCD and the literature. Weight was given to entries in the NIST/CARB BMCD which had been successful in the crystallization of multiple macromolecules. Combinations of precipitants and pH were then generated based upon a further analysis of the NIST/CARB BMCD but clearly biased by our own personal experience and inclinations.

The initial list of precipitant and pH combinations was comprised of more than 250 unique solutions. Those which closely approximated one another by having very similar precipitant types and concentration, as well as similar pH's were consolidated. Those solutions which resembled or appeared in published screening procedures (McPherson, 1990, 1992; Jancarik & Kim, 1991; Stura *et al.*, 1992) were eliminated. This process pared the list of screening solutions to slightly more than 50. During formulation several solutions were removed from the

1. 30%(*v*/*v*) MPD, 0.5 *M* ammonium sulfate, 0.1 *M* Hepes pH 7.5
2. 5%(*v*/*v*) MPD, 10%(*w*/*v*) PEG 6000, 0.1 *M* Hepes pH 7.5
3. 20%(*v*/*v*) Jeffamine M-600, 0.1 *M* Hepes pH 7.5
4. 2.0 *M* Sodium chloride, 0.1 *M* Na acetate pH 4.5
5. 30%(*v*/*v*) MPD, 0.2 *M* sodium chloride, 0.1 *M* Na acetate pH 4.5
6. 1.6 *M* Magnesium sulfate, 0.1 *M* MES pH 6.5
7. 2.0 *M* Sodium chloride, 0.2 *M* K/Na tartrate, 0.1 *M* MES pH 6.5
8. 2.0 *M* Sodium chloride, 0.2 *M* Na/K phosphate, 0.1 *M* MES pH 6.5
9. 2.0 *M* Ammonium sulfate, 0.2 *M* K/Na tartrate, 0.1 *M* Na citrate pH 5.6
10. 1.0 *M* Lithium sulfate, 0.5 *M* ammonium sulfate, 0.1 *M* Na citrate pH 5.6
11. 30%(*v*/*v*) MPD, 0.2 *M* Na/K phosphate, 0.1 *M* Na citrate pH 5.6
12. 1.6 *M* Ammonium sulfate, 0.1 *M* sodium chloride, 0.1 *M* Hepes pH 7.5
13. 2 *M* Ammonium formate, 0.1 *M* Hepes pH 7.0
14. 12%(*w*/*v*) PEG 20000, 0.1 *M* MES pH 6.0
15. 1.6 *M* Ammonium sulfate, 10% dioxane, 0.1 *M* MES pH 6.0
16. 15%(*v*/*v*) Jeffamine M-600, 0.1 *M* MES pH 6.0
17. 8% Polyethyleneimine, 0.5 *M* sodium chloride, 0.1 *M* Na citrate pH 5.0
18. 40% Ethanol, 0.1 *M* Na citrate pH 5.0
19. 10% Jeffamine M-600, 0.8 *M* ammonium sulfate, 0.1 *M* Na citrate pH 5.0
20. 20% Jeffamine T-403, 0.8 *M* ammonium sulfate, 0.1 *M* Na citrate pH 5.0
21. 20% Ethanol, 0.1 *M* Tris pH 8.0
22. 40%(*v*/*v*) Hexanediol, 0.2 *M* magnesium chloride, 0.1 *M* Tris pH 8.0
23. 25%(*v*/*v*) *tert*-Butanol, 0.1 *M* Tris pH 8.0
24. 2.0 *M* Sodium chloride, 0.2 *M* lithium sulfate, 0.1 *M* Tris pH 8.0

Fig. 1. Novel matrix screening solutions.

UM00013179

NOVARTIS EXHIBIT 1517
Novartis v. Regents, IPR2023-01347
Page 1925 of 4460

screen when it was noted that there was a failure to form stable homogeneous solutions for more than 30 d. The final screen contained 32 unique solutions. Based upon the success of crystallization trials with a library of more than 20 unique macromolecules, the final composition of the screen was reduced to 24. Thus, the screen was conveniently formatted for use in a 24-well plate that consumed approximately 1 mg of macromolecule. This screen was then evaluated against the same library of 20 unique macromolecules which includes two peptides and a virus (Fig. 2). Of the 20 macromolecules screened with the protocol, 14 produced crystals. In most cases crystals were produced under several conditions included in the screen.

We have used this screen to grow crystals which have been crystallized previously, and those which have not. For those macromolecules where previous crystallization conditions have been known, this screen identified new conditions to consider for optimization. In several cases better crystals were obtained than had previously been grown using other screening approaches. In some instances different crystal forms were obtained from some of the proteins investigated as well as differences in the frequency of nuclei, overall morphology and and crystal quality. This screen was not intended to replace the use of the sparse-matrix screen which we commonly use (Jancarik & Kim, 1991), but rather it extends the number of screening solutions which can be applied to macromolecules where the sparse-matrix screen fails. In addition, this screen provides an even greater number of leads from which the best candidates for optimization can be selected.

3. Optimization strategies

Successes in initial screening protocols may range from microcrystals to small single crystals, and include a wide variety of both favorable and unfavorable habits, as well as occasional single crystals suitable for X-ray analysis. In most instances, the next step in producing single crystals is optimization of the preliminary set of crystallization conditions. Although the variables for optimization are extensive (McPherson, 1990) a systematic optimization plan can be formulated. In most cases one can further optimize conditions by incrementing precipitant and/or macromolecule concentration, making slight pH adjustments, or evaluating different temperatures between 277 and 300 K. If these procedures fail then one must look to other variables which influence crystal growth and to the unique characteristics of the macromolecule.

1. Satellite tobacco mosaic virus	1, 2, 5, 7, 8, 10, 11, 12, 14, 16, 17, 18, 23, 24
2. Lysozyme	4, 7, 11, 16, 17, 18
3. Thaumatin	7, 9
4. Ribonuclease A	9
5. DPDPE	3, 17, 19, 20
6. Xanthine oxidase	16
7. Yeast Phe tRNA	24
8. Edestin	2, 24
9. Catalase	2
10. Leupeptin	9, 19
11. Leutenizing hormone beta	14
12. Lactate dehydrogenase	2, 14
13. Papain	20
14. Hemoglobin	4

Other macromolecules screened but not crystallized include peanut peroxidase, ribonuclease B, α-amylase, aldolase, leutenizing hormone alpha, and glyceraldehyde-3-phosphate dehydrogenase. All initial macromolecule concentrations were 20 mg ml^{-1}.

Fig. 2. Macromolecules crystallized using the novel matrix screen.

3.1. *Electrostatic crosslinkers as additives*

We have evaluated, though by no means exhaustively, two classes of additives which may have value for optimization of crystallization conditions. Here we would like to share our somewhat limited experience with these additives since our results in some cases indicate that these compounds may be useful for increasing the probability of obtaining high-quality crystals.

Ionic and electrostatic interactions between macromolecules certainly play a role in the crystallization of macromolecules. The exterior surfaces of macromolecules expose an array of unique functional groups and these form favorable interactions with other macromolecules as they condense under conditions of supersaturation. We were interested in seeing if manipulation of intermolecular interactions by addition of small charged polymers would alter and perhaps enhance the crystallization of macromolecules. To test our hypothesis we selected a group of low-molecular-weight (< 500), short-chained, branched and unbranched polymers with carboxyl and amino functional groups which would be expected to engage in electrostatic interactions with macromolecules through non-covalent bonds. Our initial collection of 24 reagents, which we term electrostatic crosslinking agents (linkers), is illustrated in Fig. 3. This collection of molecules samples varying lengths of dicarboxylic and diamine alkyl compounds with both similar and dissimilar charges at either end of the chain, as well as along the chain in some instances. Stock solutions ranging from 0.01 to 1 *M* for each compound were made in water, titrated to neutrality, and sterile filtered using a 0.2 μm filter. We evaluated the influence of these compounds on macromolecular crystallization using the panel of 20 macromolecules which included a variety of proteins, two peptides and a virus. Sitting-drop vapor-diffusion crystallization trials were performed at room temperature with Cryschem plates

UM00013180

NOVARTIS EXHIBIT 1517
Novartis v. Regents, IPR2023-01347
Page 1926 of 4460

(Charles Supper Company, Natick, MA) or Costar (No. 3424) plates with Micro-Bridges (Crystal Microsystems, England). In the experiments, drops of a macromolecule solution were comprised of 10 μl of macromolecule, 5 μl of an electrostatic crosslinking agent and 5 μl of an appropriate precipitant. Drops were equilibrated against 700 μl of an appropriate reservoir precipitant. Plates were sealed with clear tape (Manco No. 07307). All experiments were conducted at room temperature (296 K). Each trial was performed in duplicate. Controls for each macromolecule with the appropriate precipitant substituting water in place of the linker were run in parallel and a second control using the linkers in the presence of the macromolecule but without precipitant in either drop or reservoir were also run for each macromolecule. No crystals were observed to grow in the presence of a linker without a precipitant in the drop and reservoir. The following are the observations we recorded for a selection of the macromolecules evaluated.

(*a*) Lactate dehydrogenase (LDH) was crystallized in 12%(*w*/*v*) polyethylene glycol 20 000, 0.1 *M* 2-morpholinoethanesulfonic acid (MES) pH 6.0. In the absence of linker we typically observe a shower of small polyhedral crystals. Crystals grown in the presence of linkers 4, 6 and 17 were slightly larger, fewer in number and had improved surface features. Crystals grown in linker 13 showed a marked improvement. In the control, more than 150 crystals are typically observed, approximately 0.1 mm in length and less than 0.1 mm in width and height. The crystals grown in the presence of linker 13 were fewer in number, typically ten crystals per drop, two to three times as long, and with increased breadth. No crystals were grown in other linker solutions.

(*b*) Crystals of satellite tobacco mosaic virus (STMV) were grown in the presence of 10–16% saturated ammonium sulfate over a range of pH levels. Crystals grown in linker 20 (Fig. 4*a*, control is 4*b*) demonstrated the best morphology while also being fewer in number and larger than the control. Smaller crystals were grown in the presence of linker 16 and fewer, larger crystals with morphology as good or better than the control crystals were grown in linkers 4, 6, 7, 11, 12, 14, 15 and 19. No crystals were grown in linkers 3, 5, 19, 22 and 23.

(*c*) Hemoglobin crystals were grown in 30% polyethylene glycol 8000, 0.2 *M* ammonium sulfate, 0.1 *M* sodium cacodylate pH 6.5. The control crystals were very thin blades dispersed in a microcrystalline precipitate. The crystals were virtually transparent. In linkers 2, 12 and 22, single well defined crystals with a deep red color were grown (Fig. 4*c*, control is 4*d*). Fewer nucleation sites were observed using these linkers. The remaining linkers yielded crystals similar to the control. Crystals were grown in the presence of all linkers.

(*d*) Lysozyme was crystallized in 6.5%(*w*/*v*) sodium chloride, 0.1 *M* sodium actetate pH 4.2. In the presence of linkers 1, 3–12, 14, 15, 17, 18 and 19 we observed increased nucleation, as well as crystals being interpenetrated and twinned more than in the control. No crystals appeared in linker 2. In linker 13 thin plates grew (a different morphology to the control). In linker 16 a rhombic habit along with a tetragonal blade form were noted. In linker 20 there was less nucleation than for the control and in linker 23 we observed half the number of nucleation sites with crystals approximately twice the size of those in the control sample.

(*e*) Thaumatin crystals were grown from of 1 *M* potassium, sodium tartrate, 0.1 *M* *N*-(2-acetamido)-iminodiacetic acid (ADA) pH 6.5. Crystals similar to the control were observed in linkers 1, 4, 9, 11, 17, 21, 23 and 12. No crystals were observed in linkers 5 and 19. Fewer nucleation sites were observed in linkers 2, 3, 6, 7, 8, 10, 13, 14, 15, 16, 18, 20 and 22. Linker 12 contained two crystal forms, the typical tetragonal bipyramid and a previously unobserved long thin tetragonal blade (Fig. 4*e*, control is 4*f*).

(*f*) Catalase crystals were grown in the presence of 5% MPD, 10% polyethylene glycol 6000 and 0.1 *M* HEPES pH 7.5. Typically, we observed six to eight long thin, but wide, blades in a single drop, with some secondary growth of needles. Crystals of different appearance, but with no improvement in quality, were observed in linkers 1, 3, 7, 10, 11, 13, 14, 16 and 19. No crystals were grown in the presence of linkers 2, 5 and 20. Crystals similar to the control were

1. Dextran sulfate (1.5 mg ml^{-1})
2. 6-Aminocaproic acid (1.0 *M*)
3. 1,5-Hexanediamine (1.0 *M*)
4. 1,10-Decanedicarboxylic acid (100% saturated)
5. 1,8-Diaminooctane (1.0 *M*)
6. 1,12-Dodecanedioic acid (100% saturated)
7. Spermine tetrahydrochloride (0.01 *M*)
8. Cadaverine (0.5 *M*)
9. *trans*-2-Dodecenedioic acid (100% saturated)
10. Spermine (0.2 *M*)
11. Azelaic acid (100% saturated)
12. Poly-L-aspartic acid (0.01 *M*)
13. Poly-DL-lysine hydrobromide (0.01 *M*)
14. Spermidine (1.0 *M*)
15. Poly-L-glutamic acid (0.01 *M*)
16. Poly-L-lysine (0.01 *M*)
17. Hexadecanoic acid (0.4 *M*)
18. Hexaglycine (0.01 *M*)
19. 1,7-Diaminoheptane (1.0 *M*)
20. Glycylglycine (1.0 *M*)
21. Triglycine (0.3 *M*)
22. Tetraglycine (0.02 *M*)
23. 1,10-Diaminodecane (100% saturated)
24. Glycylglycine (0.3 *M*), triglycine (0.1 *M*), tetraglycine (0.007 *M*) mixture

All stock solutions are unbuffered, titrated to pH 7.0 using HCl or NaOH. Concentrations listed are stock values prior to dilution in droplet.

Fig. 3. Electrostatic crosslinking agents.

UM00013181

NOVARTIS EXHIBIT 1517
Novartis v. Regents, IPR2023-01347
Page 1927 of 4460

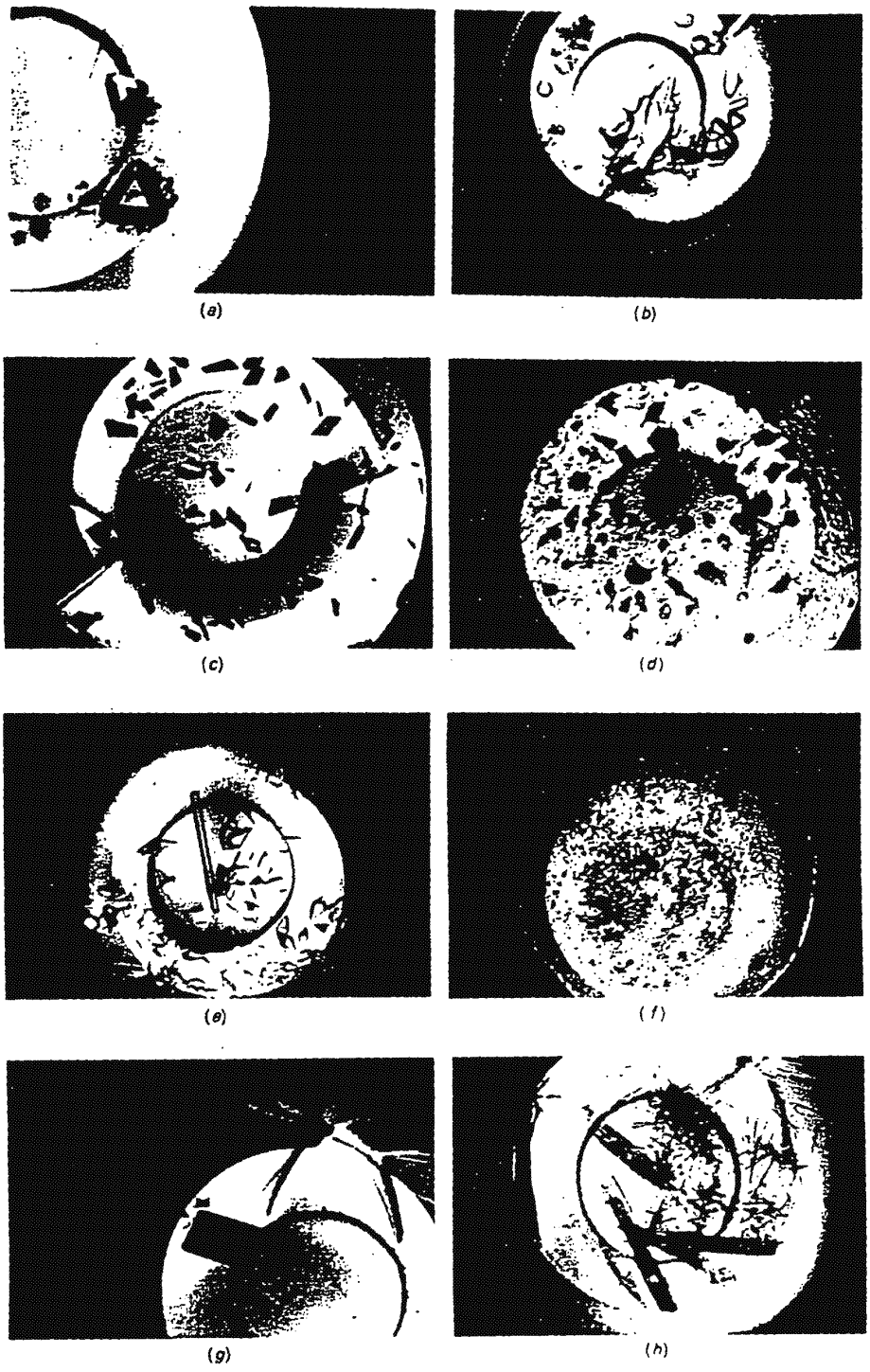


Fig. 4. Crystals in the presence of electrostatic crosslinking agents.

UM0001318

NOVARTIS EXHIBIT 1517
Novartis v. Regents, IPR2023-01347
Page 1928 of 4460

grown in linkers 6, 9, 11, 15, 17, 21 and 22. Fewer and slightly larger, thicker crystals were grown in the presence of linkers 4, 8, 12, 18 and 23 (Fig. 4*g*, control is 4*h*). A different crystal form, small and short, and numerous tetragonal bipyramids appeared in the presence of linkers 3, 14 and 19.

(*g*) Valine tRNA crystals were grown in the presence of 30% PEG 4000, 0.1 *M* sodium acetate pH 4.6, 0.2 *M* ammonium acetate. These were a shower of needles. In the presence of linkers 4, 9, 17 and 23 the needles were fewer and slightly larger but of a size still not suitable for diffraction analysis.

(*h*) Crystals of 3-phosphoglycerate kinase were grown in the presence of 30% PEG 4000, 0.1 *M* Tris–HCl pH 8.5, 0.2 *M* sodium acetate. These crystals are in general small, of poor quality and have a needle morphology. In the presence of linkers 17 and 22, however, fewer needles of greater size were observed. Nonetheless, these crystals were not of sufficient quality for diffraction analysis.

(*i*) Leupeptin, a small peptide, was crystallized in the presence of ammonium sulfate as long thin blades. Fewer thicker blades were observed in the presence of linker 16.

(*j*) Edestin was crystallized in the presence of 0.5 *M* ammonium phosphate, 0.05 *M* Na HEPES pH 5.0. These crystals have a hexagonal morphology with irregular surface features. The best crystals, suitable for diffraction analysis, were grown in the presence of linker 6.

Although this survey of macromolecules is limited we consistently noted several features that we feel deserve attention. In all cases where macromolecules were grown in the presence of linkers, we observed at least one linker that demonstrated a perceptible improvement in the crystallization. This improvement was either an increase in size, a reduction in the number of nucleation sites, or an improvement in crystal quality. In the cases of LDH, STMV, hemoglobin, lysozyme, thaumatin, catalase and edestin this effect was obvious, suggesting that we might profitably pursue the use of such linkers as a variable for optimization of crystal growth.

The change of crystal form with thaumatin, lysozyme and catalase in the presence of certain linkers implies, as well, that the use of similar linkers might provide a useful approach for the modification of crystal habit.

The inclusion of electrostatic crosslinking agents may serve as a useful extension of the broadly empirical approach to obtaining useful crystals. We currently use the methodology described in Fig. 3 during optimization after we have limited the conditions with regards to precipitant type, concentration and pH. Such a screen typically requires less than 1 mg of macromolecule. Hopefully, the identification of other even more effective linkers may be useful for producing different crystal forms and increase the number of available paths for optimization of crystal growth. In terms of mechanism, it appears to us that short flexible charged polymers could act as multivalent tethers where one end of the linker would interact with a charged surface group of one macromolecule while a second charged group on the same tether could interact with another. Such favorable interactions might influence both pre- and post-nucleation events, altering the kinetics of association leading to crystal growth, and lending enhanced stability to crystals once they have matured.

3.2. *Detergents as additives*

Detergents are a crystallization additive tool that has been widely and successfully used to produce and improve the quality of crystals of macromolecules, particularly where aggregation is a serious problem (McPherson *et al.*, 1986*a*,*b*; Reiss-Husson, 1992). β-Octylglucoside, especially, has been found to be a useful additive for the crystallization of a number of proteins and nucleic acids (Dock *et al.*, 1984; McPherson *et al.*, 1986*a*,*b*). The inclusion of β-octylglucoside can have a positive, and in the case of membrane proteins, a striking effect on the parameters of crystal growth.

For the optimization of crystal growth of a variety of macromolecules we have frequently utilized β-octylglucoside in the mother liquor where observations have suggested that specific and/or non-specific heterogeneity due to aggregation may be a problem. This occurs with particular frequency in the case of hydrophobic or lipophilic proteins. Unfortunately, the use of β-octylglucoside is not an ultimate solution of this problem and the question remains whether other detergents might be of greater effectiveness.

With the development of membrane protein biochemistry there has been an attendant increased availability of non-ionic detergents. These are often used for the isolation and purification of membrane proteins. There has also been an increased diversity of detergents applied to the crystallization of membrane proteins. It seems to follow that one should evaluate detergents as one would classes of salts, polymers or organic solvents for the crystallization of macromolecules.

To test this idea we evaluated a panel of 32 detergents (Fig. 5) against the library of 20 macromolecules for their influence on crystal growth. Detergents were formulated at 10%(*w*/*v*) (lyophilized detergents) or (*v*/*v*) (solution detergent) stocks and stored at 277 K for short periods (30 d) and at 203 K in the long term (6 months to 1 year). The experiment trials were set up and evaluated within one week. This was done to minimize the effect of

UM00013183

NOVARTIS EXHIBIT 1517
Novartis v. Regents, IPR2023-01347
Page 1929 of 4460

decomposition, as some detergents are unstable and degrade within 30–60 d. It is our experience that detergent stocks stored at 277 K are generally stable for about 30 d but after that should be discarded. We typically formulate small volumes of working stocks, flood the tube with nitrogen and store frozen aliquots at 203 K. Using this procedure the solutions appear stable for extended periods of up to at least one year. Final detergent concentrations in the drops of mother liquor were 0.14%(*w*/*v*) unless specified otherwise. Solutions were always dispensed in the following order: protein first, followed by detergent and finally precipitant from the reservoir. It should also be noted that detergents were not added to the reservoir.

(*a*) Lysozyme was crystallized from 6.5% sodium chloride, 0.1 *M* sodium acetate pH 4.2. The best crystals of lysozyme were obtained using the detergents 5, 8, 9, 12, 13, 14 and 15. A long square rod, different from the typical polyhedral crystal form, appeared in detergent 9. Crystals grown in the presence of other detergents had generally poorer morphologies, often demonstrated excessive nucleation and showed interpenetration among crystals.

(*b*) Thaumatin was crystallized in 1.0 *M* potassium, sodium tartrate, 0.1 *M* ADA pH 6.5. The best crystals were obtained in detergents 9, 14, 19, 21, 22, 23, 24, 26, 27, 28, 29, 30, 31 and 32. Of these, detergent 30 (Fig. 6*a*) yielded perfectly formed tetragonal bipyramids on a more consistent basis than any other detergent as well as for controls. Excessive nucleation, and twinned, interpenetrating crystals were observed in the remaining detergents (Fig. 6*b*).

(*c*) LDH was crystallized in 12%(*w*/*v*) polyethyleneglycol 20 000, 0.1 *M* MES pH 6.0. Good crystals were grown in detergents 6, 7, 8, 12, 13, 14, 17, 18, 19, 20, 21, 24, 31 and 32. Reduced nucleation and crystals having improved surface features developed in detergent 23 (Fig. 6*c*). Crystals grown in the remaining detergents showed no improvement and, in general, were of poorer quality, again showing excessive nucleation as well as the formation of amorphous precipitate (Fig. 6*d*).

(*d*) Catalase crystals were grown in 5% MPD, 10% PEG 6000, 0.1 *M* Na HEPES pH 7.5. No improvements were observed in any of the crystals as a consequence of the inclusion of detergents. Most of the crystals demonstrated a deterioration in quality (3, 5, 6, 9, 11, 12, 22, 23, 24, 25, 26, 27, 28, 29, 30, 31 and 32) while the remaining crystals were similar to the control – long thin blades.

(*e*) Papain was crystallized in the presence of 1.6 *M* ammonium sulfate, 10% dioxane, 0.1 *M* MES pH 6.0. Under these conditions we typically observe clusters of small thin plates and some larger, individual, thin plates with rhombic faces. These same crystal forms were observed in the presence of detergents 14, 16, 21, 26 and 30. Some deterioration was observed in detergents 1–12, 13, 15, 17, 18, 19, 20, 22, 24, 28 and 29. In the presence of detergents 23, 25 and 28, however, many single thin blades of unique habit were observed. This is the first observation of this crystal form, at least in this precipitant system.

(*f*) 3-Phosphoglycerate kinase, ficin, edestin, hemoglobin and protease crystals showed no improvement when grown in the presence of the detergents. It was observed that for all but a few of the detergents tested with these proteins, the crystals were identical to those in control samples. In only a few cases was there any degradation in the quality of the crystals.

(*g*) We have been working with vitamin D binding protein (VDBP) which is purified from pooled human plasma and comes to us in lyophilized form. This protein has been crystallized previously (Koszelak, McPherson, Bouillon & Van Baelen, 1985) but subsequent preparations have proved futile for crystal growth. Current samples of the protein form heavy brown precipitates or oils in virtually every precipitant we have investigated. The addition of 0.01–1% β-octylglucoside seemed to have no effect on the formation of either precipitate or oil. Because the material is limited, we did not have the means to test all 32 detergents against all available precipitants. To obviate the problem we used the

1. Triton X-45
2. Triton X-111
3. Triton X-60
4. Triton X-101
5. Triton X-200
6. Sigma Triton X-114
7. Sigma Triton X-100
8. Sigma Nonident P-40
9. Triton X-405
10. Triton X-102
11. BASF Pluronic L-62
12. BASF Pluronic L-64
13. BASF Tetronic 901
14. Lonza Barlox 105
15. Continental Conco XA-L
16. β-Octylthioglucoside
17. Isotridecylpoly(ethylene glycol ether)$_n$
18. Triton X-100 (Boehringer)
19. Triton X-114 (Boehringer)
20. Thesit
21. *n*-Octylglucoside
22. *N*-Dodecyl-1-*N*,*N*-dimethyl-3-ammonio-1-propanesulfonate
23. Mega-8
24. *n*-Dodecylmaltoside
25. CHAPS
26. CHAPSO
27. Octylmethylammonioacetate
28. Dimethyloctylphosphine oxide
29. Dimethyloctylammoniopropylsulfate
30. Methyloctylsulfide
31. *N*,*N*-Dimethyloctylamine oxide
32. Dodecyl-D-maltoside

Fig. 5. Detergent screening solutions.

UM00013184

NOVARTIS EXHIBIT 1517
Novartis v. Regents, IPR2023-01347
Page 1930 of 4460

DynaPro-801 dynamic light scattering instrument (Protein Solutions, Charlottesville, West Virginia, USA) to evaluate whether the sample was mono- or poly-dispersed. 200 μl samples of 2 mg ml^{-1} VDBP were prepared and filtered with a 0.1 μm filter. Prior to the analysis in the presence of detergent the sample appeared to be fairly mono-dispersed, but actually had an approximate molecular weight of 800 000. The monomer of VDBP has a molecular weight of 40 000. Thus it was clear that the protein was present as a large aggregate in solution. We then repeated our light-scattering measurements using 200 μl of VDBP in the presence of 0.2%(*v/v*) detergent, evaluating each of the detergents listed in Fig. 6. Large aggregates were observed in the presence of β-octylglucoside as well as all other surfactants, except for detergents 20 and 30. In the presence of the latter two detergents the analysis clearly showed the protein to correspond approximately to the size of a monomer. Using these two detergents we have begun screening a variety of precipitants to identify crystallization conditions. We have yet to reproduce crystals of VDBP, but we have observed a significant decrease in the number of samples which yield precipitate or oils, and of those samples which do precipitate, this typically occurs after 3–7 d rather than immediately as was previously observed. We plan to continue our crystallization trials using these two detergents and VDBP. We have recently initiated a similar set of experiments where we have applied these detergents to six different intact monoclonal antibodies and Fab fragments, and have again noted a significant reduction in the number of samples yielding precipitants or oils. We are optimistic that future experiments will support the value of detergents in the crystallization of antibodies.

An impressive result using the detergent screen was obtained in collaboration with Dr Karl Weisgraber at the Gladstone Institute (San Francisco, CA). This laboratory has been working on the crystallization of apolipoprotein CI for some time

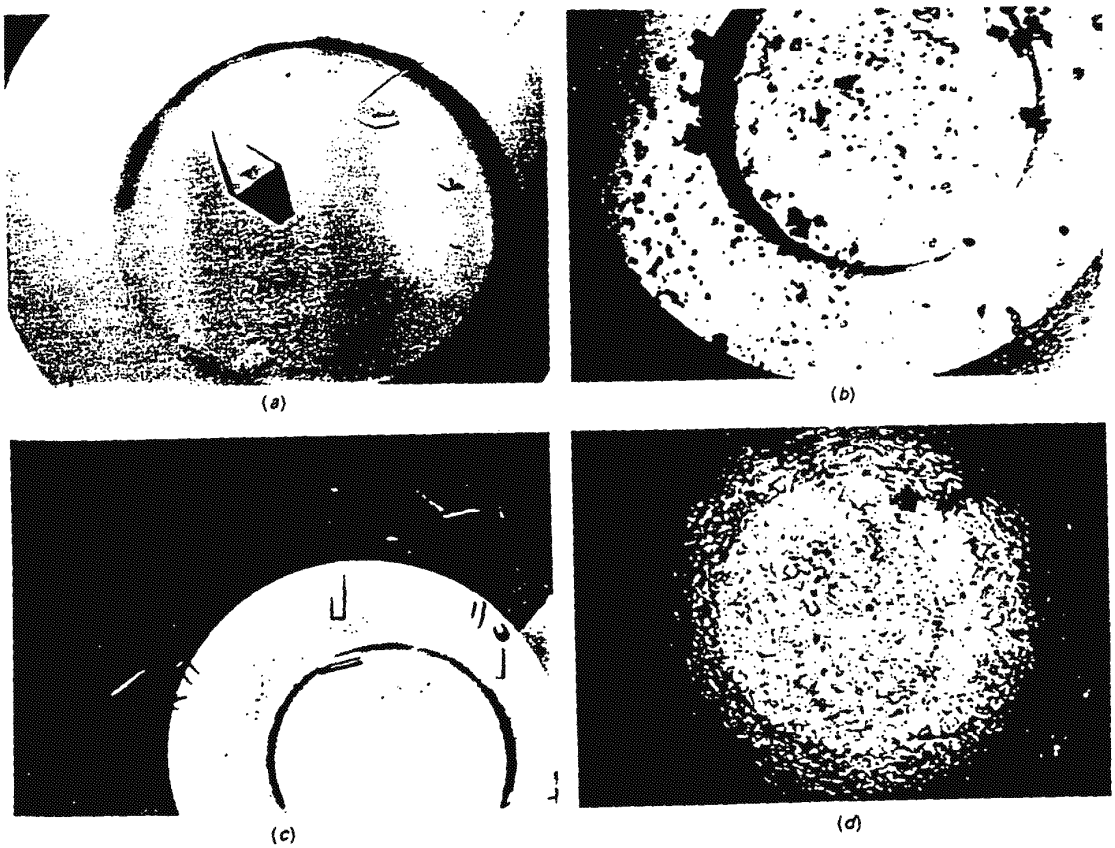


Fig. 6. Crystals in the presence of detergents.

UM00013185

NOVARTIS EXHIBIT 1517
Novartis v. Regents, IPR2023-01347
Page 1931 of 4460

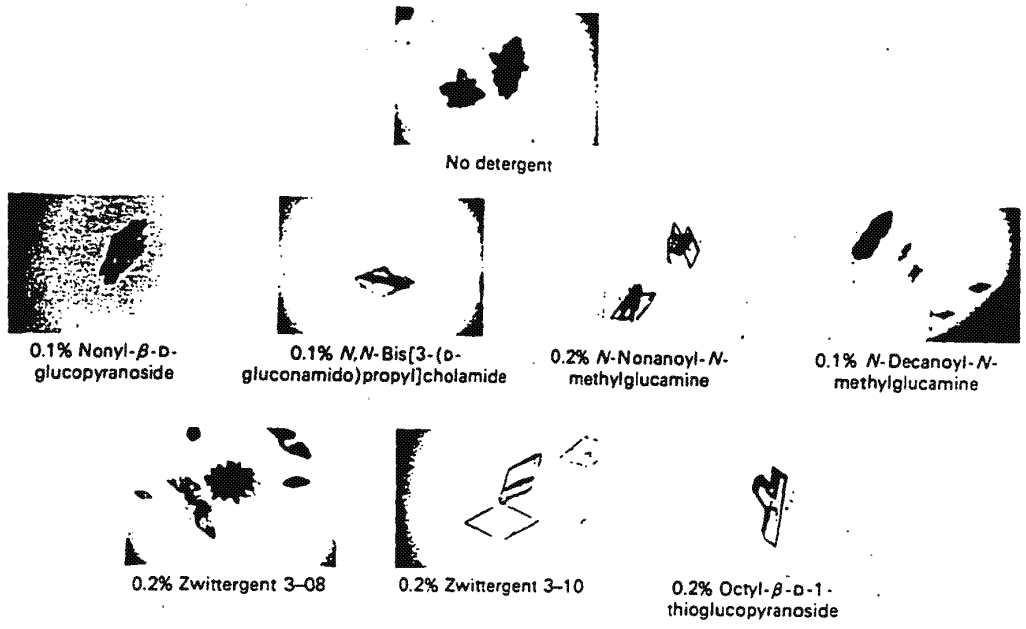


Fig. 7. Crystals of apolipoprotein C1 with and without the addition of various detergents.

with good results except that the crystals were always clustered, thin plates or blades and unsuitable for X-ray diffraction analysis. Using an optimized precipitant formulation an evaluation of 18 detergents similar to those studied here as well as additional compounds was studied for their influence on crystal growth. A summary of the results is illustrated in Fig. 7 where the importance of using the appropriate detergent is clearly demonstrated. The best crystals were grown in the presence of 0.2% octyl-β-D-1-thioglucopyranoside. Single crystals, although thin, were grown in the presence of 0.2% Zwittergent 3–10 while small disordered clusters were grown in 0.2% Zwittergent 3–08. It is interesting to note the reduction in chain length of the detergent could result in such a drastic change in crystal quality.

Although the evaluation of protein crystallization in the presence of detergents in our laboratory was strictly limited, and the selection of detergents incomplete, we feel our observations support other evidence (Reiss-Husson, 1992) suggesting the value of a detergent screen for increased improvements, particularly where aggregation is suspected to be a complication. The screen we describe is simple and rapid to perform and it requires only about 1 mg of macromolecule for 32–48 detergents. An important point, we feel, is that use of a single detergent is inadequate and that a variety should be investigated. Evaluating the role of a single detergent in preventing aggregation would be analogous to accepting the role of ammonium sulfate as indicative of the expected results for all salts. Thus, detergent screens are now an integral part of our optimization strategy.

This research was supported with grant funding from NASA. We wish to thank Dr Karl Weisgraber and Yvonne Newhouse for their valuable contribution in work with detergents. We would like to thank the Texaco Chemical Company for the samples of Jeffamine. We also thank the Procter and Gamble Company, Rohm and Haas, Continental Chemical Company, Lonza, and BASF for the detergent samples. Finally, we would like to thank Alan Nenius of Glaxo Research Institute, for programming and statistical support and Annie Hassell, also from Glaxo Research Institute, for assisting us in evaluating our ideas with her own unique proteins.

References

Carter, C. W. Jr & Carter, C. W. (1979). *J. Biol. Chem.* 254, 12219–12223.

Dock, A. C., Lorber, B., Moras, D., Pixa, G., Thierry, J. C. & Giegé, R. (1984). *Biochimie*, 66, 179.

Gilliland, G. L. & Bickham, D. M. (1990). *Methods: a Companion to Methods in Enzymology*, Vol. 1, pp. 31–37. New York: Academic Press.

Good, N. E., Winget, G. D., Winter, W., Connolly, T. N., Izana, K. M. & Singh, R. M. M. (1966). *Biochemistry*, 5, 467.

Jancarik, J. & Kim, S. H. (1991). *J. Appl. Cryst.* 24, 409–411.

UM00013186

NOVARTIS EXHIBIT 1517
Novartis v. Regents, IPR2023-01347
Page 1932 of 4460

KOSZELAK, S., MCPHERSON, A., BOUTILLON, R. & VAN BAELEN, H. (1985). *J. Steroid Biochem.* **23**, 1077–1078.
MCPHERSON, A. (1990). *Eur. J. Biochem.* **189**, 1–23.
MCPHERSON, A. (1992). *J. Cryst. Growth*, **122**, 161–167.
MCPHERSON, A., KOSZELAK, S., AXELROD, H., DAY, J., ROBINSON, L., MCGRATH, M., WILLIAMS, R. & CASCIO, C. (1986*a*). *J. Cryst. Growth*, **76**, 547–553.
MCPHERSON, A., KOSZELAK, S., AXELROD, H., DAY, J., ROBINSON, L., MCGRATH, M., WILLIAMS, R. & CASCIO, C. (1986*b*). *J. Biol. Chem.* **261**(4), 1969–1975.
REISS-HUSSON, F. (1992). *Crystallization of Proteins and Nucleic Acids, a Practical Approach*, pp. 175–193. Oxford Univ. Press.
SAMUDZI, C. T. & FIVASH, M. J. (1992). *J. Cryst. Growth*, **123**, 47–58.
STURA, E. A., NEMEROW, R. & WILSON, I. A. (1992). *J. Cryst. Growth*, **122**, 273–285.
WEBER, P. (1990). *Methods: a Companion to Methods in Enzymology*, Vol. 1, pp. 31–37. New York: Academic Press.
WEBER, P. (1991). *Adv. Protein Chem.* **41**, 1–36.

UM00013187
NOVARTIS EXHIBIT 1517
Novartis v. Regents, IPR2023-01347
Page 1933 of 4460

This Page is Inserted by IFW Indexing and Scanning Operations and is not part of the Official Record

BEST AVAILABLE IMAGES

Defective images within this document are accurate representations of the original documents submitted by the applicant.

Defects in the images include but are not limited to the items checked:

- ☐ BLACK BORDERS
- ☐ IMAGE CUT OFF AT TOP, BOTTOM OR SIDES
- ☐ FADED TEXT OR DRAWING
- ☐ BLURRED OR ILLEGIBLE TEXT OR DRAWING
- ☐ SKEWED/SLANTED IMAGES
- ☐ COLOR OR BLACK AND WHITE PHOTOGRAPHS
- ☐ GRAY SCALE DOCUMENTS
- ☐ LINES OR MARKS ON ORIGINAL DOCUMENT
- ☐ REFERENCE(S) OR EXHIBIT(S) SUBMITTED ARE POOR QUALITY
- ☐ OTHER: _____

IMAGES ARE BEST AVAILABLE COPY.
As rescanning these documents will not correct the image problems checked, please do not report these problems to the IFW Image Problem Mailbox.

© 2003 The Chemical Society of Japan

Molecular Complex Formation between Riboflavin and Salicylate in an Aqueous Medium

Silpi Datta, Chaitali Mukhopadhyay, and Swapan Kumar Bose*

Department of Chemistry, University of Calcutta, 92, A.P.C. Road, Kolkata-700 009, India

Received March 6, 2003; E-mail: chaitalicu@yahoo.com

Evidence for an intermolecular interaction of riboflavin and sodium salicylate in an aqueous medium was obtained from the presence of isosbestic points in the absorption spectra and an isoemissive point in the emission spectra. The equilibrium constant was estimated from absorption and emission studies, and also from the solubility of riboflavin in an aqueous solution of sodium salicylate, and was found to be in the range of 10–14 mol dm^{-3}. Lifetime measurements indicate a predominantly static mechanism of quenching. The Stern–Volmer constant for the quenching of riboflavin by sodium salicylate was significantly reduced upon the addition of urea. An MD simulation study on the system revealed a stacked conformation, which is probably due to a hydrophobic interaction of the two components.

The term flavin refers to a generic set of compounds containing the heterocyclic isoalloxazine chromophore. They are very versatile compounds and are involved in a host of biological processes.[1] In aerobic metabolic processes, they catalyze two-electron dehydrogenations of different substrates, and participate in one-electron transfers to various metal centers.[1] They are cofactors of the flavoenzymes, which are ubiquitous and can catalyze a wide variety of chemical reactions essential for sustaining the living conditions of each organism.[2] The mechanism of cofactor (i.e. flavins) binding by the flavoenzymes involve a stacking interaction between a conserved aromatic residue (e.g., tyrosine, tryptophan or histidine) at the cofactor binding site and the isoalloxazine ring of the flavin. This has been observed in the cases of the flavoenzyme, ferredoxin-NADHreductase, where the isoalloxazine ring of flavin is stabilized by a stacking interaction with the Tyr 303 residue.[3] In the crystal structure of D-amino acid oxidase-*o*-amino benzoate complex, a similar interaction between the flavin and the aromatic ring of the Tyrosine 224 residue is observed at the binding site.[1] Flavodoxin reductase, on the other hand, contains Trp 248 at the cofactor binding site.[4] In flavoenzymes that do not have a bound cofactor, e.g., NAD(P)H: Flavin oxidoreductase from *E. coli*, do not have such an aromatic residue at the cofactor binding site.[4] Thus, the stacking interaction appears to be important in stabilizing the cofactor in the bound form.

Stacking interaction is important in the functioning of the flavoenzymes, where the substrates containing an aromatic ring system gain additional stability in the binding site upon stacking onto the flavin cofactor. One of the earliest known flavoenzyme is 'Old Yellow Enzyme', obtained from yeast. Although the exact physiological function of this enzyme is not known, many studies have been conducted with this enzyme because of its ability to form beautiful charge transfer complexes with aromatic and heteroaromatic compounds containing an ionizable hydroxy group. The crystal structure of the enzyme with bound phenol clearly shows that a parallel stacking of flavin and phenol is required for the observed charge-transfer interaction.[2] A stacking interaction between Trp 27 and the isoalloxazine ring of flavin forms the structural basis of the binding of riboflavin to the *Schizosaccharomyces pombe* 6,7-dimethyl-8-ribityllumazine synthase.[5]

Thus, the interaction of the flavin moiety with aromatic ring systems appears to be a vital factor in stabilizing it as a cofactor as well as in the functioning of many flavoenzymes. In order to understand the nature of this interaction we chose a model system comprising of riboflavin and a salicylate anion, and characterized the interaction in an aqueous medium. Riboflavin, vitamin B_2, is a water-soluble, yellow, fluorescent compound, which functions as a coenzyme in numerous redox reactions in metabolic pathways and in energy production. Salicylic acid, on the other hand, is one of the most widely used drugs with analgesic and antipyretic activity. Studies have suggested that salicylic acid may serve as one-electron-donating substrates for catalases/peroxidases.[6] Studies on the interaction of flavin derivatives with salicylic acid and its derivatives in a non-aqueous medium, such as chloroform and benzene, were reported earlier. In these studies, a hydrogen-bonding interaction between salicylic acid and riboflavin has been suggested.[7] Riboflavin and salicylic acid form a 1:1 cyclic hydrogen-bonded dimer through the N-3 proton and the C-2 carbonyl oxygen of the isoalloxazine ring of RF and the carboxylic hydroxy proton and carbonyl oxygen of SA in an aprotic solvent.[7] The optimum hydrogen-bonding requires that RF and SA be placed side-by-side, so that the arrangement of the donor and acceptor groups is linear. Since these studies have been made in aprotic solvents, stacking interactions between flavins and salicylic acid have not been emphasized. We have studied the binding of riboflavin to salicylic acid in an aqueous medium. It is quite conceivable that in an aqueous medium a stacking interaction will be crucial rather than hydrogen-bonding.

Published on the web September 15, 2003; DOI 10.1246/bcsj.76.1729

UM00013189
NOVARTIS EXHIBIT 1517
Novartis v. Regents, IPR2023-01347
Page 1935 of 4460

Experimental

Materials and Methods. Riboflavin (RF) was purchased from Sigma Chemicals Co. AR-grade salicylic acid (SA) was obtained from S.D. fine-chem Ltd. (India). GR-quality sodium salicylate (NAS), urea, potassium nitrate (KNO_3) and potassium iodide (KI) were obtained from E. Merck (India). AR-grade sodium dihydrogenorthophosphate and disodium hydrogenorthophosphate were obtained from Qualigens Fine Chemicals (India). Water distilled twice in an all glass apparatus was used for preparing all solutions.

The UV–visible absorption spectra were recorded using a Hitachi U-3501 spectrophotometer with 1 cm quartz cuvettes. The concentration of RF used for absorption experiments with NAS was 5×10^{-5} mol dm^{-3}. The range of the NAS used was (0.0125–0.4) mol dm^{-3}. A phosphate buffer (0.10 mol dm^{-3}) was used for maintaining pH values of 6, 7, and 8. The pH of the solutions was measured by an Elico LI127 pH meter.

The fluorescence spectra were recorded on a Perkin-Elmer LS50B emission spectrofluorimeter. The concentration of the RF used for all steady state fluorescence experiments was of the order of 10^{-5} mol dm^{-3}. For the quenching of RF by KI in the presence of salicylic acid, the KI concentration was varied from (1–7) mmol dm^{-3} and that of salicylic acid was (1.7–13.6) mmol dm^{-3}. For the quenching of RF by NAS, the concentration range for NAS was (1–8) mmol dm^{-3} in the presence of 0.10 (M) phosphate buffers of pH 6, 7, and 8. The effect of the ionic strength on the fluorescence spectra were studied by repeating the fluorescence quenching experiments of RF by NAS in a medium of 0.20 mol dm^{-3} KNO_3 at pH 6.0. The fluorescence quenching experiments were studied using excitation wavelengths of 350 nm and 440 nm with both excitation and emission slit widths of 5.0 nm. The peaks of RF and NAS were monitored at 522 nm and 412 nm, respectively. The absorption and emission experiments of the RF–NAS pair were repeated in the presence of varying amounts of urea at a concentration of (1–5) mol dm^{-3} at pH 6.0. The temperatures for the absorption and emission experiments were maintained within 22–26 °C.

Solubility experiments were performed by saturating solutions of NAS ranging between (0–8) mmol dm^{-3} with RF in the presence of 0.2 mol dm^{-3} KNO_3 at pH 6.0 using a magnetic stirrer, and filtering. Two mL of the filtrate was diluted to 10 mL and the absorbance was noted at 450 nm using 1 cm cuvettes. Fluorescence lifetimes were determined from total emission intensity decay measurements using a time-domain assembled fluorimeter with components from Edinburgh Analytical Instruments and EG&GORTEC, and operated in the time-correlated single-photon counting mode. Excitation was provided by a pulsed high-pressure 152 kPa N_2 lamp operating at 1.3 ns. The RF was excited at 380 nm and the emission decay profile was monitored at 522 nm. The time-resolved measurements were performed with 10^{-4} (M) RF collecting 5000 photon counts in the peak channel. Three different concentrations of NAS (3, 6 and 9 mmol dm^{-3}) were used. All of the solutions were prepared in a medium of 0.03 (M) phosphate buffer of pH 7.5.

For Molecular Modeling, Insight II software package (Accelrys, Inc., USA, Version 98.0) running on a Silicon Graphics O2 workstation was used. A DISCOVER module[8] and a CVFF force field were used for molecular mechanics and dynamics calculations. This force field has been used earlier for studying small molecules.[9] Three-dimensional models of RF and salicylate ion were generated using standard molecular templates. The initial models were energy minimized to remove any strain. Several initial conformations of the complex of RF and salicylate were generated by keeping the molecules side-by-side within a hydrogen-bonding distance of the 2 carbonyl and N-3 hydrogen of RF and phenolic OH and carboxylate group of the salicylate anion. After energy minimization of the complex, it was solvated with an 8 Å water layer. The total number of water molecules needed was 315. The solvated complex was energy minimized. A molecular dynamics simulation of the solvated complex was performed for 100 ps after an initial 10 ps equilibration period.

Results and Discussions

Evidence for Complex Formation and Determination of the Equilibrium Constant by an Absorption Method. The absorption spectra of mixtures of RF and salicylic acid showed a decrease in the intensity of both the 445 and 372 nm absorption bands of RF. Since the solubility of salicylic acid in water is very low, NAS was used in place of salicylic acid for a quantitative analysis of the intensities of the RF bands. The absorption spectra of mixtures of RF and NAS (Fig. 1) showed a decrease in the intensity of the two RF bands upon increasing the concentration of NAS for a fixed RF concentration and pH. Three isosbestic points were discerned in the absorption spectra of the mixtures. This is indicative of a complex formation between RF and NAS. The decreased absorbance values recorded at 445 and 490 nm were used to calculate the equilibrium constants, K. These two wavelengths were selected because they are well removed from the isosbestic points.

The equilibrium constant of the complex was obtained using the following form of the Benesi–Hildebrand equation:[10,11]

$$\frac{1}{\Delta A} = \frac{1}{K\Delta\varepsilon} \cdot \frac{1}{C_b^0} + \frac{1}{\Delta\varepsilon}, \quad (1)$$

where ΔA is the difference between the absorbance of the RF solution and that of a mixture containing the same amount of RF and an excess amount of NAS at a fixed pH and an appropriate wavelength. $\Delta\varepsilon$ is the difference between the molar absorptivity of the complex and that of the RF. C_b^0 is the stoichiometric concentration of NAS in the mixture of RF and NAS. A plot of $(\Delta A)^{-1}$ versus $(C_b^0)^{-1}$ is shown in Fig. 2 at two different wavelengths of 445 and 490 nm at pH 6.0.

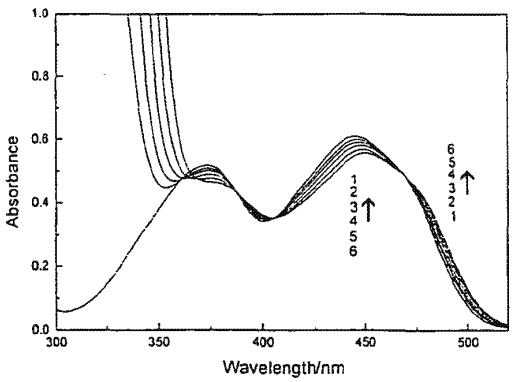


Fig. 1. Effect of NAS on the absorption spectra of RF at pH 6.0. Numbers (1–6) indicate the variation of [NAS] in the order 0, 0.0125, 0.05, 0.10, 0.20, 0.4 mol dm^{-3}.

UM00013190
NOVARTIS EXHIBIT 1517
Novartis v. Regents, IPR2023-01347
Page 1936 of 4460

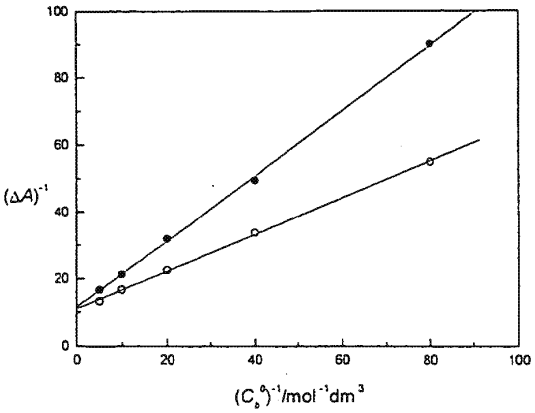


Fig. 2. Plot of $(\Delta A)^{-1}$ versus $(C_b{}^0)^{-1}$ for the RF–NAS system, pH 6.0 at (i) 445 nm (●) ($r = 0.99969$), (ii) 490 nm (○) ($r = 0.99962$).

The equilibrium constant values were calculated by taking the ratio of the intercept and the slope of the graph, and were found to lie between 10–14 mol^{-1} dm^3 at pH 6, 7 and 8. The K values are pH independent as well as wavelength independent. The close agreement of the K values, determined from two different wavelengths, indicates the presence of a single association complex in aqueous solution. In this context it is worth mentioning that the individual spectrum of RF and NAS are pH independent.

Determination of Complex Formation by Fluorescence Spectroscopy. The Stern–Volmer quenching constants of RF fluorescence by KI were determined at different salicylic acid concentrations. A plot of K_{sv} versus the concentration of salicylic acid is shown in Fig. 3. It was found that K_{sv} decreases with increasing the salicylic acid concentrations, and ultimately reaches a plateau for concentrations higher than 6.0 mmol dm^{-3}. The variation of K_{sv} as a function of the salicylic acid concentration is supporting evidence for complex formation between RF and salicylic acid. The emission spectra for the quenching of RF by NAS at an excitation wavelength of 350 nm shows an isoemissive point at 498 nm (Fig. 4). The intensity of the emission maxima of RF at 522 nm for both excitation wavelengths of 350 nm and 440 nm were found to decrease with increasing concentrations of NAS. From the quenching data at two different wavelengths, the K_{sv} values in the range of (50–60) mol^{-1} dm^3 were obtained. The equilibrium constant, (K) was calculated using

$$\frac{F_0}{\Delta F} = \frac{F_0}{(F_0' - F_0)} + \frac{F_0}{K(F_0' - F_0)} \cdot \frac{1}{C_b{}^0}, \qquad (2)$$

where F_0, F_0', and F are the fluorescence intensities of the RF solution, a solution of totally complexed RF with NAS and the experimental solution, respectively. ΔF is the difference in the fluorescence intensities of the RF solution and that of a mixture containing the same amount of RF and varying excess amounts of NAS for a particular excitation wavelength and pH. The above equation was used to find the association constant of lumichrome and β-cyclodextrin.[12] The ratio of the intercept and slope obtained from a plot of $(F_0/\Delta F)$ versus $(C_b{}^0)^{-1}$ (Fig. 5) gives the value of the equilibrium constant, K. The K values obtained at two different wavelengths of 350 nm and 440 nm are almost identical, and range between (45–55) mol^{-1} dm^3. This indicates that a similar quenching mechanism is involved in both cases. The K values are almost equal to the K_{sv} values at these two wavelengths. However, the K values obtained here are significantly higher than those obtained from absorption experiments.

The disparity in the K values obtained from fluorescence quenching and absorption experiments may have been due to the effect of the ionic strengths of the solutions used. The ionic strength of the NAS solution used in the absorption method is much higher than that used in the fluorescence quenching experiments. The fluorescence quenching experiments were repeated in a medium of 0.20 mol dm^{-3} KNO_3 at pH 6.0. This particular concentration of KNO_3 is the average of the concentration range of NAS used in the absorption experiments. In this medium of increased ionic strength, the equilibrium constant, (K) was reduced to 14 mol dm^{-3} [Figure not shown]. This is in fair agreement with those obtained from absorption

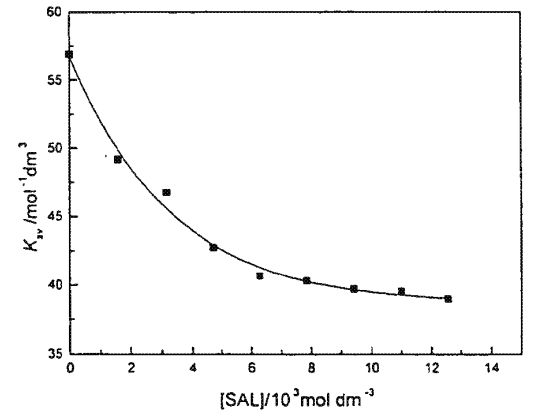


Fig. 3. Effect of salicylic acid on K_{sv} for the quenching of RF fluorescence by KI in aqueous solution.

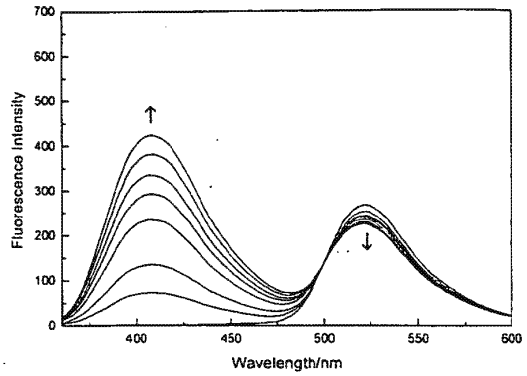


Fig. 4. Emission spectra of RF and NAS at $\lambda_{ex} = 350$ nm, pH 6.0. Upward ↑ indicate the variation of [NAS] in the order (1, 2, 3, 4, 5, 6, 7, 8) × 10^{-3} mol dm^{-3} and downward ↓ indicate the decreasing fluorescence intensity of RF on addition of NAS.

UM00013191
NOVARTIS EXHIBIT 1517
Novartis v. Regents, IPR2023-01347
Page 1937 of 4460

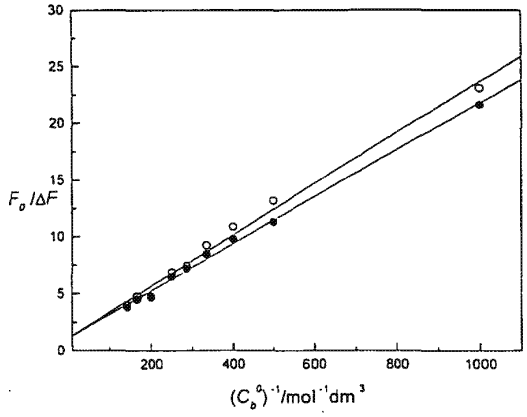


Fig. 5. Plot of $(F_0/\Delta F)$ versus $(C_b^0)^{-1}$ for the RF–NAS system, pH 6.0 at (i) 350 nm (●) ($r = 0.9981$), (ii) 440 nm (○) ($r = 0.99537$).

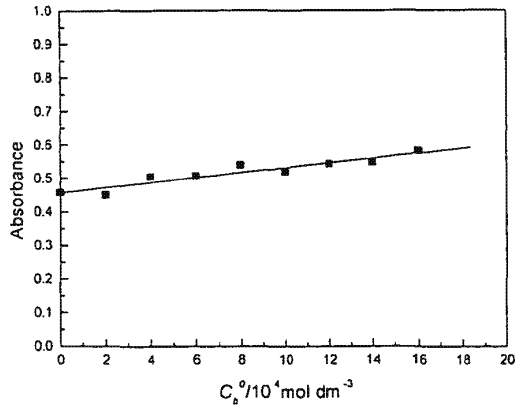


Fig. 7. Plot for the solubility of RF in aqueous solution of NAS at pH 6.0 in presence of 0.20 mol dm^{-3} KNO_3 ($r = 0.93972$).

studies. The reduction of K with an increase in the ionic strength indicates that the association complex is a charged species.

Determination of Mechanism of Quenching by Lifetime Measurements. To substantiate the mechanism of quenching, fluorescence lifetime measurements were carried out. All of the decay curves were found to fit a single exponential decay function, which is shown in Fig. 6. The fluorescence lifetimes (τ) of RF were 4.00 ns, 4.20 ns, 4.40 ns for NAS concentrations of 3, 6, and 9 mmol dm^{-3}, respectively, and that for RF in absence of NAS was 4.63 ns, very close to the previously reported value of 4.64 ns.[13] The change in the τ values obtained upon the addition of NAS is marginal, and can be considered to be insignificant. This indicates that the above quenching mechanism is predominantly static, the dynamic quenching involved being negligible.

Determination of the Equilibrium Constant by the Solubility Method. The solubility of RF in water was found to increase considerably in the presence of NAS. For determining the equilibrium constants by solubility methods, a series of solutions of NAS were taken in the presence of phosphate buffer of pH 6.0 and 0.20 mol dm^{-3} KNO_3. The solubilities of RF in these solutions were determined according to a procedure described in the Materials and Methods section. The absorbances for the above-mentioned solutions at 450 nm were processed using the following equation:[12]

$$A_{mix} = A_{RF} + KA_{RF}C_b^0, \quad (3)$$

where A_{mix} and A_{RF} are the absorbances of the complexed RF and RF in an aqueous solution respectively. C_b^0 is the stoichiometric concentration of NAS. The plot of A_{mix} versus C_b^0 (Fig. 7) is linear. From the ratio of the slope and intercept of the curve, an equilibrium constant of 12 mol dm^{-3} was obtained which, is in close agreement with the K values obtained from absorption methods. The presence of any hydrotropic effect is ruled out because the concentration range of the NAS used was much lower than that required for a hydrotropic effect.[14]

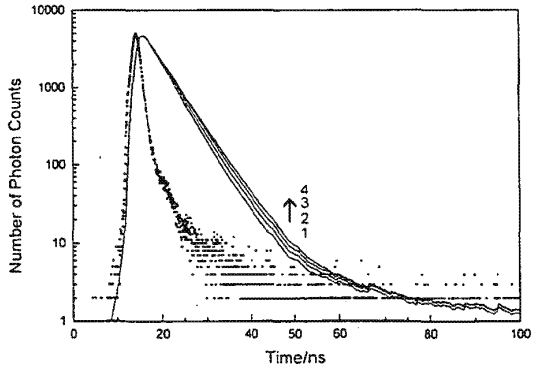


Fig. 6. Single exponential fits to the fluorescence intensity decay profiles of RF in (1) aqueous solution and in presence of (2) 3 mmol dm^{-3}, (3) 6 mmol dm^{-3}, and (4) 9 mmol dm^{-3} NAS.

Effect of Urea on the Absorption and Fluorescence Spectra. Urea is a well-known chemical denaturant for proteins, and at concentrations above 6–8 M, destroys the tertiary structure of proteins. Although the exact mechanism by which urea destroys the protein tertiary structure is not known, several proposals have been made which include a breakdown of the water structure by urea,[15] preferential solvation of hydrophobic residues,[15] as well as adsorption onto the surface residues, leading to the swelling of protein, and finally denaturation.[15] To test whether urea can break the complex formed between RF and NAS in an aqueous medium, the effects of urea on the absorption and fluorescence spectra of RF and NAS were studied. The absorption spectra of a mixture of RF (10^{-5} mol dm^{-3}) and NAS (0.20 mol dm^{-3}) in the presence of varying concentrations of urea at pH 6.0 are shown in Fig. 8. The two absorption bands of RF at 445 and 372 nm were found to increase in intensity with respect to the spectra for the mixture of RF and NAS in absence of urea, the more significant change being observed in the case of the 372 nm band. Fluorescence-quenching experiments of RF by NAS were repeated in the presence of varying urea concentrations at pH 6.0. A plot of

UM00013192
NOVARTIS EXHIBIT 1517
Novartis v. Regents, IPR2023-01347
Page 1938 of 4460

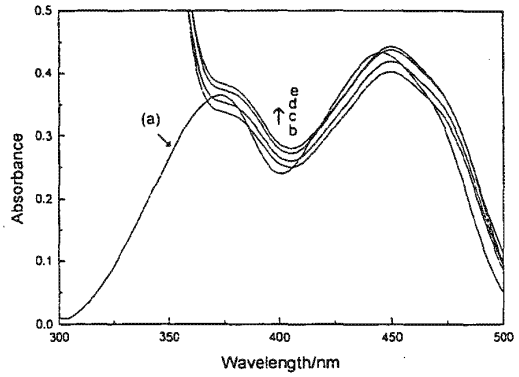


Fig. 8. Effect of urea on the absorption spectra of a mixture of RF (5×10^{-2} mmol dm^{-3}) and NAS (0.20 mol dm^{-3}), labels b, c, d, e indicating the varying urea concentrations 0 mol dm^{-3}, 1 mol dm^{-3}, 2 mol dm^{-3}, 4 mol dm^{-3} and 'a' indicating spectra of pure RF.

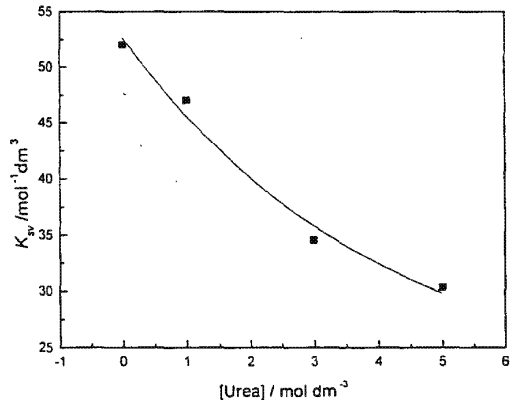


Fig. 9. Effect of urea on K_{sv} for the quenching of RF fluorescence by NAS at pH 6.0.

K_{sv} as a function of the urea concentration is shown in Fig. 9. The K_{sv} value decreases with increasing urea concentrations, ultimately reaching a constant value of about 30 mol^{-1} dm^3 at higher concentrations of urea. However, absorption and emission spectra of RF and NAS separately remains unaffected in the presence of urea.

In a non-aqueous medium, a hydrogen-bonding mechanism was proposed earlier[7] for the formation of an association complex between flavins and small organic molecules. In an aqueous medium, however, other mechanisms, e.g., stacking interactions, charge transfer, etc., may be important for complex formation. The changed absorption spectra as well as the reduction of the K_{sv} values with increasing urea concentrations indicate that the RF–NAS interaction is weakened in the presence of urea. Although the K_{sv} value is reduced, it does not become insignificantly small. This indicates that interactions, which are unaffected by urea, might also be operative. We suggest a charge-transfer mechanism between the salicylate anion as a donor and the RF as an acceptor was observed for the RF–NaN_3 pair[16] where the association constant was calculated to be as low as 4 mol dm^{-3}. The association constants in the order of 300–400 mmol dm^{-3}, as reported in the literature for flavin–substrate systems in a non-aqueous medium, involved hydrogen-bonding interactions. It was reported that the sites of RF involved in that interaction were the C-2 carbonyl oxygen and the N-3 proton. In this work, a low association constant signifies a weaker interaction.

Molecular Modeling. One of the two starting conformations chosen for the RF–NAS complex had the N-3 hydrogen atom placed within the hydrogen-bonding distance of the carboxylic group of the salicylate anion, while the other had the C-2 carbonyl oxygen placed near to the phenolic OH group. During MD simulations, however, the salicylate anion moved away from the side-by-side position within the equilibration period, itself, and became stacked onto the isoalloxazine ring of RF with an average distance of (4–5) Å between the aromatic ring of SA and the heteroaromatic rings of RF, and remained in that position throughout the entire simulation time. This indicates that in the presence of water the stacked complex is more favourable than the side-by-side complex. It is conceivable that the van der Waals interaction will be more favourable in the stacked form than in the side-by-side form. Also, in presence of water, RF and NAS can form hydrogen bonds with water molecules instead of forming the inter-molecular hydrogen bonds needed to stabilize the side-by-side complex. Thus, water might play a crucial role in stabilizing the stacked form of the complex. The diagram (Fig. 10) shows the stacked conformation of the complex. From the trajectory-averaged conformation of the complex, it was observed that the stacking interaction of the hydrophobic rings of RF and NAS as well as the electrostatic interaction between the phenolic OH and the carboxylate groups of salicylate anion and the C-2 carbonyl oxygen and the N-3 hydrogen of RF are crucial for stabilizing the complex.

Experimental evidence confirms the formation of a complex between riboflavin and sodium salicylate. The association-constant value for the formation of a complex obtained from different experimental methods gave a consistent value, and its magnitude was in the range of 10–14 mol dm^{-3}. In an aqueous solution, the low association constant is indicative of the formation of a weak complex; whereas the association

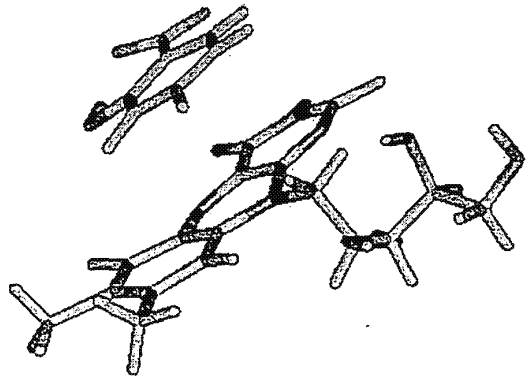


Fig. 10. Trajectory averaged structure of the interaction of RF and NAS.

UM00013193
NOVARTIS EXHIBIT 1517
Novartis v. Regents, IPR2023-01347
Page 1939 of 4460

constant obtained for the same system under aprotic conditions is very high, indicating a stronger interaction in a non-polar environment. The presence of urea, a known structure breaker, weakens the binding of the RF–NAS complex. Molecular modeling studies also indicate the presence of a stacked complex.

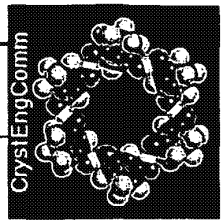
The authors gratefully acknowledge Prof. S. Basak, Chemical Sciences Division, Saha Institute of Nuclear Physics, Kolkata for providing the facilities for fluorescence lifetime measurements. S.D. acknowledges University of Calcutta for financial assistance.

References

1 R. Miura, *Chem. Rec.*, **1**, 183 (2001).
2 V. Massey, *Biochem. Soc. Trans.*, **28**, 283 (2000).
3 J. A. Hermoso, T. Mayoral, M. Faro, C. Gomez-Moreno, J. Sanz-Aparicio, and M. Medina, *J. Mol. Biol.*, **319**, 1133 (2002).
4 T. M. Louie, H. Yang, P. Karnchanaphanurach, and X. S. Xie, *J. Biol. Chem.*, **277**, 39450 (2002).
5 S. Gerhardt, I. Haase, S. Steinbacher, J. T. Kaiser, M. Cushman, A. Bacher, R. Huber, and M. Fischer, *J. Mol. Biol.*, **318**, 1317 (2002).
6 J. Durner and D. F. Klessig, *J. Biol. Chem.*, **271**, 28492 (1996).
7 B. S. Yu, S. J. Lee, S. J. Lee, and H. H. Chung, *J. Pharm. Sci.*, **72**, 592 (1983).
8 Discover Manual, Version 98.0.
9 C. Mukhopadhyay, *Biopolymers*, **45**, 177 (1998).
10 H. A. Benesi and J. H. Hildebrand, *J. Am. Chem. Soc.*, **71**, 270 (1949).
11 P. Douglas, G. Waechter, and A. Mills, *Photochem. Photobiol.*, **52**, 473 (1990).
12 B. Sarkar, U. Das, S. Bhattacharya, and S. K. Bose, *Bull. Chem. Soc. Jpn.*, **68**, 1807 (1995).
13 K. Bystra-Mieloszyk, A. Balter, and R. Drabent, *Photochem. Photobiol.*, **41**, 141 (1985).
14 R. E. Coffman and D. O. Kildsig, *J. Pharm. Sci.*, **85**, 951 (1996).
15 A. Wallqvist, D. G. Covell, and D. Thirumalai, *J. Am. Chem. Soc.*, **120**, 427 (1998).
16 B. Sarkar, U. Das, S. Bhattacharya, and S. K. Bose, *J. Chem. Res., Synop.*, **72**, 123 (1995).

UM00013194
NOVARTIS EXHIBIT 1517
Novartis v. Regents, IPR2023-01347
Page 1940 of 4460

Crystal engineering – nucleation, the key step†



Highlight

R. J. Davey,* K. Allen,‡ N. Blagden,§ W. I. Cross,¶ H. F. Lieberman,‖ M. J. Quayle, S. Righini,†† L. Seton‡‡ and G. J. T. Tiddy**

Crystals, Colloids and Interfaces Group, Department of Chemical Engineering, UMIST, Manchester, UK M60 1DQ. E-mail: roger.davey@umist.ac.uk

Received 10th April 2002, Accepted 17th April 2002
Published on the Web 16th July 2002

In the world of crystal engineering in which the focus of effort is on the assembly of molecular species by crystallisation, surprisingly little attention has been paid to the actual nucleation and crystallisation processes involved. This Highlight explores the structural aspects of the nucleation process in a range of small molecule systems. It uses a combination of thermodynamic, structural and modelling approaches in order to progress our understanding of the link between liquid phase molecular assemblies, which constitute crystal growth units, and their solid state counterparts, the supramolecular synthons.

Introduction

In the world of crystal engineering, where materials are assembled from predetermined building blocks, the use of solution phases as media for the homogenisation of starting compositions and crystallisation for the subsequent assembly processes are common.[1] The crystallisation episode itself can involve a range of procedures by which the solution phases are brought to a supersaturated (non-equilibrium) state so that crystallisation can proceed.[2,3] Since the final materials are often salts it is common to find salting out reactions (addition of a common ion), evaporation of common organic solvents and drowning out (the addition of a miscible non-solvent) used for this purpose. To those whose major concern is the structural determination of the final product the nature of this crystallisation step may be a mystery, an irritation, or rely on serendipity, and yet few would deny that the manner in which it occurs can often determine the final outcome of the process in terms of, for example, the size and morphology of the crystals and indeed the intimate details of the molecular packing as evidenced by the occurrence of polymorphism and solvate formation.[1,4]

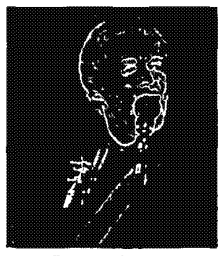
This contribution sets out to explore some aspects of the nucleation process and in particular to begin to unravel the relationship between solid-state molecular packing, as evidenced *via* crystal structure data, and the intermolecular interactions which exist in solution. In this way it is hoped to begin to make a structural link between the solvent-mediated kinetic processes of molecular assembly, that underlie nucleation, and the structure of the resultant crystals.

Historical

The process of nucleation has been the subject of almost continuous study over at least the past 150 years.[5] Notably, Ostwald[6] in the 19th century made a number of important experimental observations concerning the effect of sample volume, seeding and metastable states. One of his most important contributions in this field was the statement of his rule of stages in 1897[6,7] in which he recognised that frequently the most kinetically accessible crystal structure was not the most stable one but rather the least stable of the known forms. In this observation we have the first indication that for a given material its crystal structure is not a fixed parameter but that it can be determined by kinetic processes as reflected in the crystallisation pathway used and the composition of the starting liquid phase. Paracetamol, for example, crystallised from acetone solution will always yield crystals of the stable monoclinic form I whereas crystallisation from the melt will

†Based on the presentation given at CrystEngComm Discussion, 29th June–1st July 2002, Bristol, UK.
‡Current address: Pharmacia, Skokie, IL, USA.
§Current address: School of Pharmacy, University of Bradford, Bradford, UK.
¶Current address: GlaxoSmithKlein, Medicines Research Centre, Stevenage, UK.
‖Current address: Aventis Pharmaceuticals Inc., Bridgewater, NJ, USA.
**Current address: BNFL Technology Centre, Seascale, Cumbria, UK.
††Current address: Rhodia, Centre de Recherches de Lyon, Saint-Fons Cedex, France.
‡‡Current address: School of Pharmacy and Chemistry, John Moores University, Liverpool, UK.

Roger Davey graduated from Bristol University in 1969 with BSc Hons in Chemistry. He studied for his PhD at University College London and held post-doctoral positions at Imperial College London and the ETH Zurich, Switzerland until 1977 when he joined the chemical company ICI (later to become Zeneca). In 1993 he joined the Department of Chemical Engineering at UMIST where he has established a successful research group and helped to create a new centre for the study of Molecular Materials. Throughout his career he has studied problems associated with crystal nucleation and growth and is particularly well known for his work on molecular crystals, polymorphism and applications of crystal chemistry to industrial problems. In 2001 he was awarded a prestigious EPSRC Senior Research Fellowship allowing him to devote his time to research and in particular to studies of crystal nucleation. Outside of his professional life Roger sings and plays in a local rock band – he is seen here performing at the Department's Christmas party!



Roger Davey

DOI: 10.1039/b203521a

This journal is © The Royal Society of Chemistry 2002

UM00013195
NOVARTIS EXHIBIT 1517
Novartis v. Regents, IPR2023-01347
Page 1941 of 4460

always produce the orthorhombic metastable layer structure, form II.[8] Also known at the time of Ostwald were the twin phenomena of metastability and undercooling – the thermal hysteresis – of saturated liquids and melts, and it was inferred from this that a barrier existed to nucleation. It was not until the kinetic formalism developed by Volmer[9] that the basis of this barrier was understood and the parameters determining the nucleation process were unravelled. The importance of the link between molecular behaviour in the fluid phase and the ultimate crystal packing was implicit in this analysis – nucleation, just like a chemical reaction, is an activated process in which the transition state is associated with an assembly of molecules held together by intermolecular interactions – hydrogen bonds, π–π and van der Waals interactions, coulombic forces and co-ordinate bonds. For nucleation, unlike a chemical reaction, the viability of this assembly depends on its size. The reason for this now seems obvious to us: in creating the nucleus of a crystal a new interface is created for which a penalty must be paid in terms of free energy. The amount of free energy available to create this interface depends on the supersaturation, and to ensure overall viability of the nucleus this penalty has to be recoverable from the free energy gain of creating the bulk material. Thus in a supersaturated solution there will be a steady state distribution of assemblies, and depending on the supersaturation imposed there will be a critical size, above which the assemblies can grow and below which they are unstable. The higher the supersaturation the smaller the size, the easier nucleation becomes and the more crystals will be formed.

In terms of the classic formalism[10] this process is represented in the overall reaction

$$z\mathrm{A} \rightleftharpoons \mathrm{A_c}$$

in which a number, z, of A molecules self-assemble to create a single critical nucleus $\mathrm{A_c}$. The equilibrium constant associated with this process is then

$$K_z = [\mathrm{A_c}]/[\mathrm{A}]^z$$

and the associated free energy change is given by:

$$\ln K_z = -\Delta G_c/RT$$

From this it becomes apparent that the larger K_z, and hence the higher the proportion of critically sized nuclei, the more favourable the nucleation process will be – in other words, self-assembly favours nucleation. Overall, this formal analysis gives rise to the well known exponential relationship between nucleation rate and supersaturation which explains the existence of a metastable zone and indicates the difficulty of controlling crystallisation processes which are dominated by primary nucleation.[10]

These kinetic relationships were derived to explain macroscopic phenomena at a time when the most intimate probe of crystallising systems was the optical microscope, which gave a resolution of *ca.* 1.0 μm at best. Modern techniques and methodologies, including atomic probe microscopies, X-ray and neutron diffraction and scattering and molecular modelling, have led us routinely to expect resolution and visualisation down to 0.1 nm, an advance which has only just begun to be reflected in experimental and theoretical studies[11,12] of the nucleation process. For example, structural studies of multilayers spread on water indicate[13] that even bi- and tri-layers of molecules can adopt the ultimate packing of bulk crystal structures; recent neutron scattering data show that even in systems such as methanol and ethanol, which one might think of as well solvated, there is significant molecular clustering[14] and molecular dynamics calculations increasingly support the notion of solute assembly as a prerequisite to nucleation.[12] In reassessing the core assumptions of general nucleation theory within the context of a structural framework, three key questions (at least!) arise:

(1) Do critically sized clusters have to be 'crystalline' or could they be 'amorphous'?

(2) Do clusters exist with packings corresponding to all the potential polymorphs in a system?

(3) Are the cluster structures biased in any way by the nature of the solvent–solute interactions?

The answers to these questions are not known and will almost certainly not have universal answers but here we set out to review some of our recent work which begins to shed light on the structural elements of the assembly processes and how they are controlled. One point of clarification is needed: crystal engineering has spawned the notion of the *supramolecular synthon*. This idea has come from the vast amount of crystal structure data available and the identification of certain common building blocks from trends in crystal packing motifs. The world of crystallisation is more familiar with the idea of a *growth unit*, the essential building block that transfers structural information from the solution to the crystal surface. The understanding of the link between the growth unit and the structural synthon is then the basic structural problem for nucleation theory.

The growth unit and solution chemistry: the case of saccharin

In its crystal structure saccharin is dimerised in a ring, $R_2^2(8)$, using its amide functionality[15] as seen in Fig. 1. These dimers are packed in the familiar herring-bone motif of the space group $P2_1/c$. It was noticed[16] that when saccharin crystallises from acetone solution large numbers of the nucleated crystals are twinned (on $\{10\bar{2}\}$[17]), whereas upon crystallisation from ethanolic solution the majority of crystals are single. Fig. 2 shows the experimentally determined frequency of twinning in acetone and ethanolic solutions at different supersaturations. Unexpectedly it is clear that the most twins are found at low supersaturations in acetone. This result is important because it appears counterintuitive since conventionally twinning is seen, in crystal growth terms, as the result of packing errors. Because 'more mistakes' are anticipated at high supersaturation so might be more twins. There are important additional features of this process. It is clearly solvent dependent and no multiple twins were ever seen, only pairs in which each member was of approximately equal size. The addition to crystallising solutions (0.27 mM) of indigo, a molecule designed to span the twin interface yielded molecules in which the twin boundary was dyed blue,[18] as seen in Fig. 3, and increased the frequency of twinning in ethanol[18] by almost an order of magnitude.

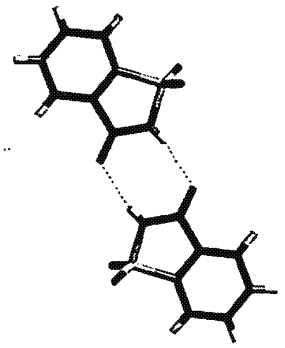


Fig. 1 Hydrogen bonded $R_2^2(8)$ saccharin dimer extracted from its crystal structure.

UM00013196
NOVARTIS EXHIBIT 1517
Novartis v. Regents, IPR2023-01347
Page 1942 of 4460

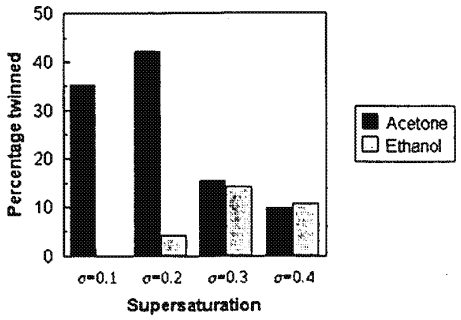


Fig. 2 Experimentally determined frequency of twinning at 40 °C measured in acetone and ethanol in the supersaturation range 0 to 0.4.

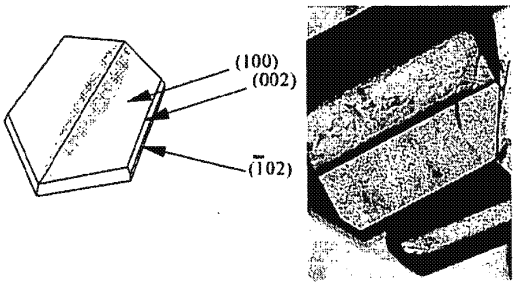


Fig. 3 Optical micrograph and schematic diagram of a twinned crystal grown in the presence of 0.27 mM indigo and a supersaturation of 0.4. The crystal is *ca.* 70 μm in length.

Solubility data indicate that in acetone solutions saccharin exists predominantly as solvated monomers whereas in, near ideal, ethanolic solutions both solvated monomers and dimers exist.[16] This is visualised in Fig. 4, which displays the result of calculations performed using the program GRID[19] to calculate the interaction energies between probe hydroxy (ethanol)

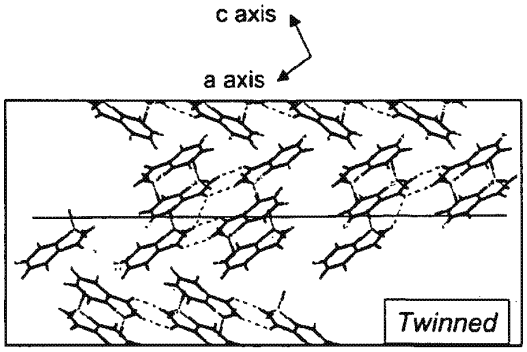


Fig. 5 The {10$\bar{2}$} twin interface in saccharin showing the new three-centre C=O···H–N hydrogen bond (0.2123 nm) which joins dimers across the plane.

and carbonyl (acetone) groups and a monomer and dimer of saccharin taken from its crystal structure. Together these data indicate firstly that twinning occurs only at the point of nucleation – all twins are symmetric, no multiple twins were ever seen – and secondly that twinning is favoured by the existence of monomeric saccharin in (acetone) solution. In creating a molecular picture which reconciles all these observations it becomes clear that this example offers a fine probe of the molecular assembly process occurring at nucleation.

Modelling of the {10$\bar{2}$} twin plane[17] allowed the precise nature of the twin interface to be determined and indicated that it was stabilised by the formation of the three-centre hydrogen bond shown in Fig. 5. In considering the surface structure of the {10$\bar{2}$} plane it is evident that two possibilities exist, as shown in Fig. 6. If the fundamental growth unit is monomeric, as it would be in acetone, then the nucleating molecular cluster may be expected to have a {10$\bar{2}$} interface, as seen in Fig. 6A, terminated by the polar amide and sulfoxide functionalities. Other monomers can then join this interface to form the three-centre hydrogen bond and hence the twin. If the crystal nucleates from a solution containing dimers then its surface will

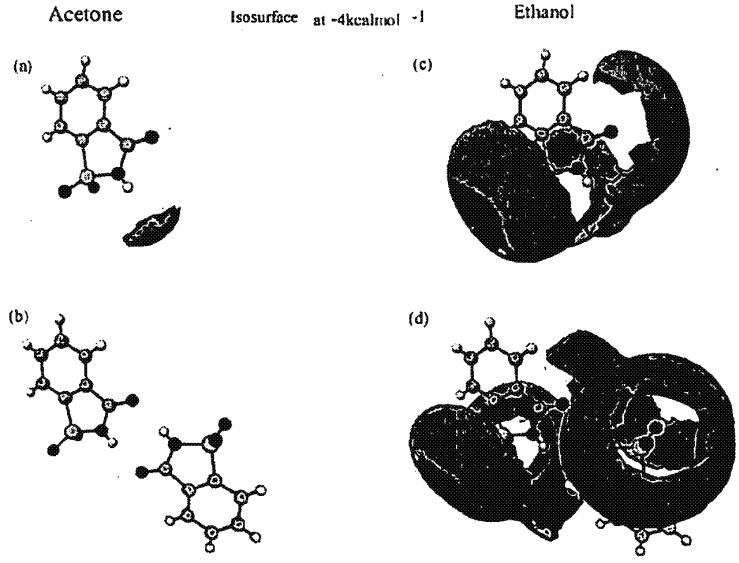


Fig. 4 The interaction of carbonyl (a and b) and hydroxy (c and d) probes with a saccharin dimer and monomer. Isosurfaces have been drawn corresponding to an interaction energy of −4 kcal mol^{-1}.

UM00013197
NOVARTIS EXHIBIT 1517
Novartis v. Regents, IPR2023-01347
Page 1943 of 4460

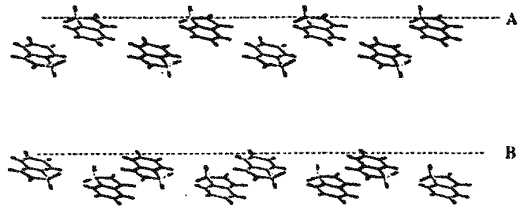


Fig. 6 Possible surface structures of the $\{10\bar{2}\}$ facet: cut A exposes the non-polar phenyl hydrogens and is inconsistent with twin formation whereas cut B exposes the polar sulfoxide and amide functionalities and allows twinning to proceed.

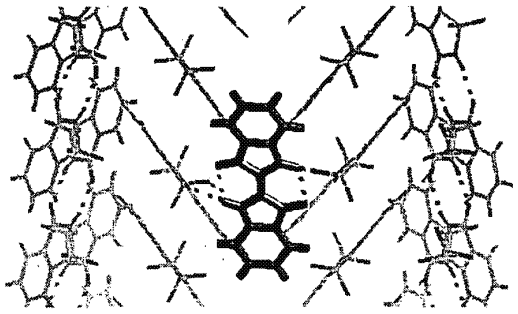


Fig. 7 Indigo molecule hydrogen bonded across the twin interface of saccharin.

be terminated as in Fig. 6B by the non-polar phenyl rings, and the creation of a twin is inhibited by the steric hindrance imposed on the formation of the three-centre bond.[16] This picture is consistent with the solution chemistry indicating that in acetone solution nucleation takes place from monomeric species while in ethanol it involves the assembly of dimers. Thus, we uncover in this simple system both the solvent dependence of the initial assembly process resulting from changes in solution chemistry and evidence that the fundamental building block is not necessarily a monomer but may involve pre-assembled dimers.

The presence of indigo at the twin interface and its catalytic activity implicates it in the nucleation process. Through hydrogen bonding to the sulfoxide oxygens as shown in Fig. 7 it is able to modify the assembly of growth units to create nuclei which possess the twin plane even though in ethanolic solution growth takes place *via* dimers.

Polymorphism as probe to self-assembly: the cases of sulfathiazole and 2,6-dihydroxybenzoic acid

Saccharin exhibits only one known crystal structure; however, it may be anticipated that materials which exhibit more than one crystal structure (polymorphs) may hold further keys to the nature and extent of the self-assembly process particularly when the kinetic processes surrounding polymorph appearance are solvent dependent. Sulfathiazole is an excellent example of a polymorphic material exhibiting five crystal structures.[20,21] In each structure the molecule exists in its *imine* form and hence the crystals are composed of equal numbers of enantiomerically- (referred to as L and R) related molecules. All five structures are richly hydrogen bonded and for structures I, II, III, and IV it is possible to define a fundamental dimer building block from which each crystal form is constructed. Form V is derived from $R_3^3(10)$ rings linked in chains along the *b*-axis – no

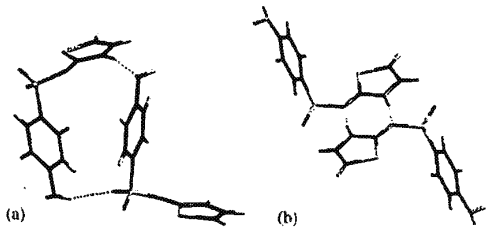


Fig. 8 Dimers of sulfathiazole: (a) the β dimer $R_2^2(18)$ of forms II, III and IV, and (b) the α dimer $R_2^2(8)$ taken from form I.

dimers are apparent in this structure. Forms II, III and IV all use an identical β dimer $R_2^2(18)$ constructed from LL or RR enantiomer pairs utilising sulfato oxygen to aniline hydrogen and aniline nitrogen to thiazole hydrogen contacts as shown in Fig. 8(a). The form I, α, $[R_2^2(8)]$ dimer is unique, being constructed only from LR pairs in which the molecules have slightly different conformations and which utilises [Fig. 8(b)] two imine nitrogen to thiazole hydrogen contacts. The actual assembly of the dimers uses essentially the same interactions: forms II, III and IV utilise the amine and thiazole hydrogens as donors and both the sulfoxide oxygen and amine nitrogen as acceptors to build the common C(8) dimer chain whereas form I uses only the amine hydrogens and sulfoxide oxygens to build C(8) chains. Some light is shed on the nature of the growth unit from the subsequent kinetic stability of these structures which indicates[20] that form I is the least stable, converting stepwise to II, III and IV given the correct solvent conditions. In this case we find that whereas water permits the full transformation series from I through IV in a 24 hour time period, in n-propanol form I alone persists in suspensions for at least one year. This result is again, as in the case of saccharin, consistent with the existence of dimers as growth units for the nucleation process. In water, both α and β dimers have the potential to build nuclei, whilst in n-propanol solvent binding blocks the amine hydrogen bonding sites sufficiently to offer a significant steric barrier to the assembly of the β dimer and hence selectively preventing the formation of forms II, III and IV.[20]

A further example is to be found in the nucleation of 2,6-dihydroxybenzoic acid. This is a much simpler case for study than sulfathiazole, as the acid exists in only two known polymorphic forms whose hydrogen bonded motifs are relatively easy to describe: form 1 is a metastable monoclinic form based on centrosymmetric carboxyl dimers[22] while the stable form 2 is noncentric based on a catemer motif which utilises a carbonyl–hydroxy interaction.[23] Fig. 9 shows the elements of these two structures. In this case it was found that in quiescent solutions the metastable dimer structure nucleated preferentially from toluene, whereas in chloroform direct nucleation to the stable form was possible. A combination of solubility data, UV/vis spectroscopy and calculation of solvation enthalpies all pointed to the preferential assembly of dimers in toluene solutions and catemers in chloroform, yielding again a clear link between the assembly process in solution and the nucleation event.[24] Fig. 10, for example, shows the solvation of both acid and phenolic dimers by toluene ($Ar–CH_3$ probe) and chloroform (RH–Cl probe) calculated using GRID.[19] Here the enhanced solvation of the phenolic dimer (catemer) in chloroform is clearly evident. This conclusion was substantiated in two ways. Firstly, an additive, benzaldehyde, was chosen which, as seen in Fig. 11, is able to enter the form 1 structure without causing disruption to the dimer units but which on joining a form 2 chain cluster will cause chain termination and inhibit its nucleation. When present in toluene solution this additive was found, as expected,

UM00013198
NOVARTIS EXHIBIT 1517
Novartis v. Regents, IPR2023-01347
Page 1944 of 4460

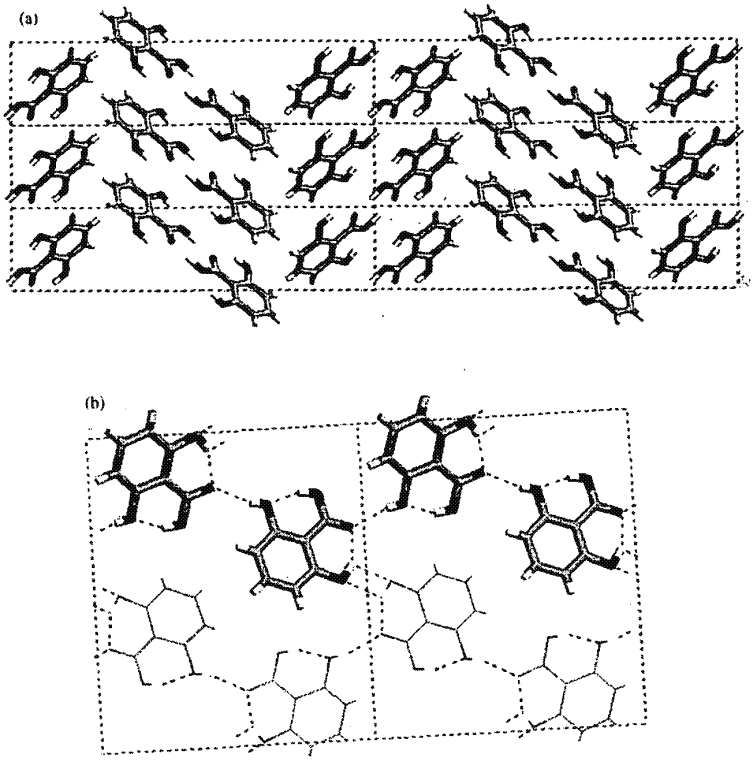


Fig. 9 Two polymorphic forms of 2,6-dihydroxybenzoic acid: (a) the metastable form 1 dimer structure, and (b) the stable form 2 catemeric structure.

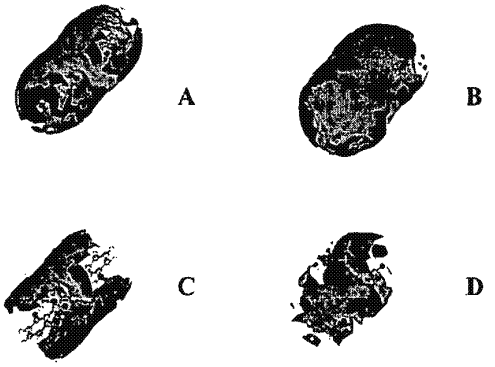


Fig. 10 Solvation of acid and phenolic dimers by toluene ($Ar–CH_3$) and chloroform (CH–Cl): isosurfaces drawn corresponding to an interaction energy of -4 kcal mol^{-1}. **A** and **B** are, respectively, the dimer and catemer solvated by chlorform; **C** and **D** are, respectively, the dimer and catemer solvated by toluene.

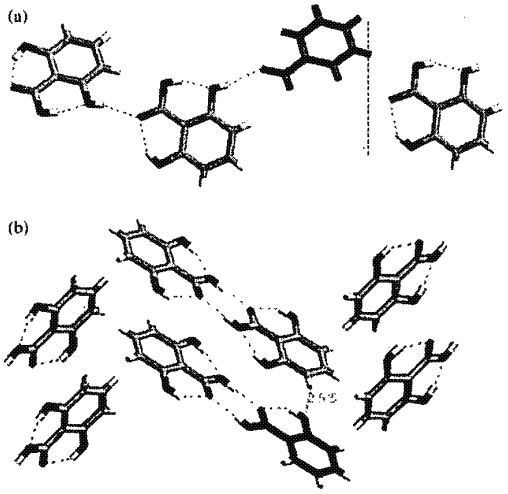


Fig. 11 Benzaldehyde inserted into the form 1 and 2 structures showing the termination of a chain (a) and the incorporation into a dimer (b).

to allow the usual nucleation of the metastable form 1 but to delay the appearance of form 2 by almost two orders of magnitude from 2 to 150 h.[25] Secondly, it was found that when form 1 crystals were grown from chloroform[24] the {310} faces appeared in the external morphology of the crystals. Examination of the surface structure of this face, Fig. 12, shows how it appears to be a mimic of the form 2 chain motif – hence a solvent which stabilises the form 2 chains also stabilises the {310} faces of form 1.

Overall, these examples give an indication of how polymorphism can be used to probe the liquid phase assembly processes and again lead to the conclusion that molecular assembly does direct the nucleation event and that it can be controlled by solvent–solute interactions.

UM00013199
NOVARTIS EXHIBIT 1517
Novartis v. Regents, IPR2023-01347
Page 1945 of 4460

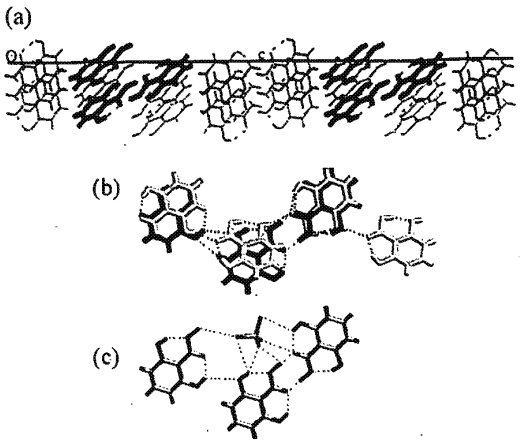


Fig. 12 Visualisation of the binding of chloroform to the {310} face of form 1: (a) the {310} surface; (b) the binding site mimics the form 2 chain; (c) chloroform docked into the binding site.

Solvent-directed self-assembly – learning from structure predictions

In the examples given so far, interpretation has been based on knowledge of known crystal structures taken together with experimental solution chemistry, computational results and details of crystallisation events. These data have been used to deduce certain modes of self-assembly and to explore the possible intermolecular events surrounding the nucleation process. A further test of this thesis has been made by performing structural predictions on previously uncharacterised systems and attempting to use the ideas as a basis for directing the nucleation to yield certain types of packing. All reports of structural prediction[26] indicate that very large numbers of potential structures exist within a rather narrow range of lattice energies and densities. Given our previous examples, however, it would seem likely that in a supersaturated solution there are in fact limited classes of clusters present whose packings may be determined by the solution chemistry of the solute–solvent systems chosen. If this is indeed the case then it should be feasible, *via* solvent selection, to induce interactions to favour crystal structures with certain packings. This was first demonstrated for the simple molecule 2-amino-4-nitrophenol[27] for which no previous crystal structures had been determined. Predictions were run using the Cerius^2 Polymorph Predictor module[28] together with the most common space groups, $P\bar{1}$, $C2/c$, $P2_1$, $P2_12_12_1$, and $P2_1/c$. Fig. 13(a) shows the commonly occurring intermolecular interactions within 250 predicted structures.[27] In attempting to crystallise structures composed of dimers V and VI, toluene was chosen as a solvent since it was thought that this would maximise the chances of intermolecular hydrogen bonding in the solution. Consequently, as expected, the structure (a toluenate) shown in Fig. 13(b) was prepared which indeed shows both dimers V and VI connected by chains of type II' and III. In a second such experiment, nitromethane was used as a solvent in an attempt to solvate the amine hydrogens and direct the crystal packing towards nitro–hydroxy interactions. This met with some success in that the resulting crystal structure [Fig. 13(c)] contained type II' chains and no type VI dimers but it still contained type V dimers. Finally, methanol was chosen to solvate the hydroxy groups and direct the nucleation towards the type IV and V contacts. This again met with some success: at high supersaturations the non-solvated form identical to that from nitromethane appeared, whereas at low supersaturations a methanol solvate crystallised. In this form (not shown) the methanol is hydrogen bonded to hydroxy groups of the solute and chains of type IV appear, as planned. These chains are linked by type VI dimers. It is clear that the results of this approach to directed crystallisation support our conclusions from studies of twinning and polymorphism – molecular pre-assembly does accompany nucleation and this can be directed in a logical way *via* the solvent. The limitations of this approach are also evident: some assemblies, notably dimers, are too stable to be discouraged in this way.

Evidence for long range pre-assemblies – nucleation of *para*-azoxyanisole and glycine from mesophases

A separate class of systems in which the impact of preordering on nucleation might be anticipated and used as a means of exploring links between self-assembly and nucleation are those that form thermotropic nematic and smectic liquid crystalline phases. In these single component systems the long range liquid crystalline order prior to crystal formation is easily probed by conventional SAXS and may then be compared to the WAXD that appears on crystallisation. One of the simplest systems of this type is *para*-azoxyanisole which is reported to form a nematic liquid crystal phase and three crystal phases, of which only the crystal structure of the stable form III is known.[29,30] *In situ* SAXS experiments, performed on station 16.1 at the Daresbury SRS, indictate[31] [Fig. 14(a)] that the nematic phase at 125 °C shows significant evidence of both orientational and positional order having clear d and $d/2$ diffraction peaks at 2.7 and 1.3 nm. Cooling of this phase to room temperature leads to the direct crystallisation of the stable form III. Subcooling of the liquid crystal to 90 °C, however, yields a new higher order reflection at 0.7 nm, and cooling of this material leads to the formation of a metastable crystal structure which transforms to the stable phase on cooling [Fig. 14(b)]. Although the structure of this phase is unknown it is evident that in the known stable structure the molecules are packed in a 0.7 nm layer as dimers shown in Fig. 14(c), and it maybe that such layers also form the basis of this new form. Systems of this type offer a new and exciting avenue for this research.

In solutions the use of scattering and diffraction to probe pre-assembly during nucleation is more limited due to poor contrast and low phase volumes. Nevertheless, some evidence can be gleaned from alternative experiments. For example, from aqueous solutions, at the isoelectric pH of 6.1, glycine crystallises in its centrosymmetric α form. At high supersaturations the noncentric β polymorph appears, and at high and low pHs the most stable, noncentric γ polymorph may be crystallised.[32] The consistent appearance of α from solutions has been explained by the existence of centrosymmetric zwitterionic dimers in aqueous solution which naturally pack to yield the α structure.[31] However, we have recently found[32] that when crystallised from within lamellar and microemulsion phases prepared from the anionic surfactant AOT [sodium bis(2-ethyl)sulfosuccinate] the nucleation of the γ form is induced even at pH 6.1 where it has never previously been seen. Fig. 15 shows such crystals suspended from an AOT-containing oil–water interface with their fast growing c-axes pointing down into the aqueous solution. Earlier studies of the induced nucleation of α glycine using hydrophobic amino acids[11,33] have indicated that single molecules of glycine are bound to a monolayer that has the structure of the {020} plane of α glycine. In the case of AOT, however, the anionic SO_3^- groups cannot mimic the fast growing {001} plane of the γ polymorph since neither the functionality nor the surface area per molecule[34] (40–60 Å^2) offer a structural match. Futhermore, it is known categorically[35] that glycine is not solubilised by AOT. This means that glycine molecules have no specific interaction at an aqueous–AOT interface and that the only way in which the induction of γ nucleation by AOT can be

UM00013200
NOVARTIS EXHIBIT 1517
Novartis v. Regents, IPR2023-01347
Page 1946 of 4460

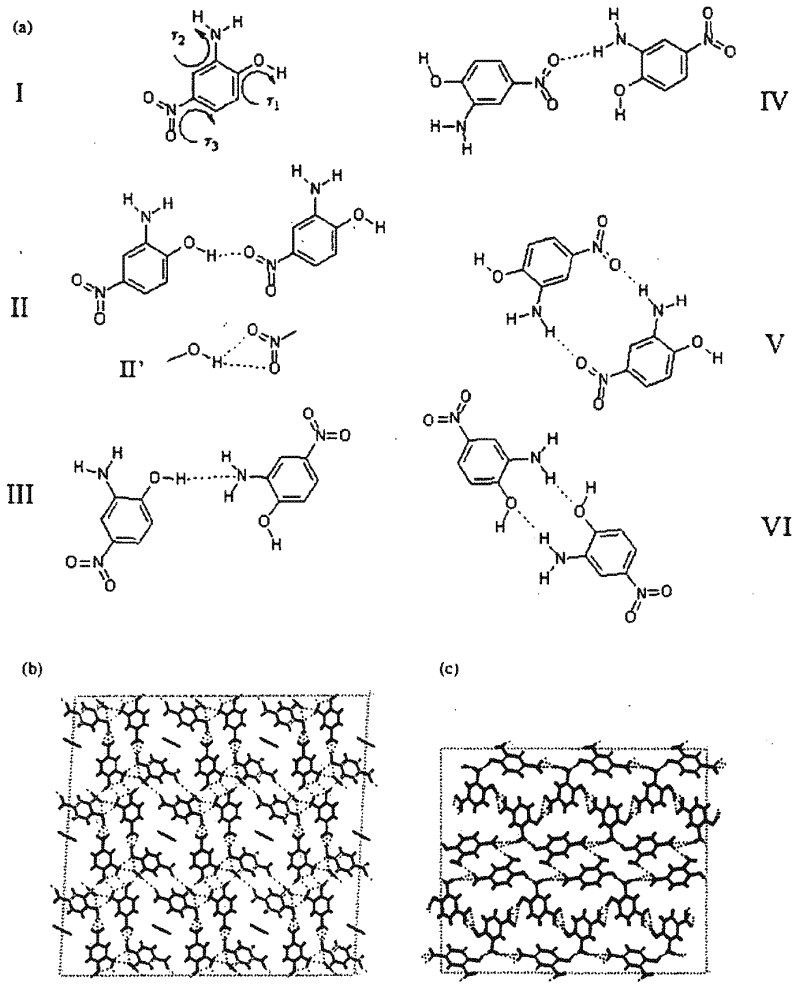


Fig. 13 Synthesising predicted structures of 2-amino-4-nitrophenol: (a) commonly found motifs, (b) form I prepared from toluene, (c) form II prepared from nitromethane.

understood is *via* a cluster capture model. In this model it has to be assumed that a supersaturated solution contains clusters corresponding in structure to each of the available polymorphs and that these are recognised and bound to the interface on the basis of their polarity. The structural specificity of the nucleation process must then be the result of the overall polarity of the clusters involved. For example, given a supersaturated glycine solution containing α, β and γ clusters of identical packing to their known crystal structures a comparison of the polarity along the fastest growth direction of the three sets of clusters then indicates γ to be the most polar with molecules aligned along the *c*-axis. The β type is the next most polarized with molecules partially aligned along the *b*-axis, and the centric α structure offers no inherent polarization. In terms of the interactions of such clusters with a charged AOT monolayer it then seems totally reasonable to suppose that the most polarized clusters, in this case those of the γ structure, would bind most strongly. Interestingly, this concept of cluster capture is supported by previous kinetic data[36] on the nucleation of ice under alcohol monolayers. In this case the ability of a $C_{30}H_{61}OH$ monolayer, spread onto water droplets, to catalyse ice nucleation was found to result not from a decrease in the critical size through a lowering of the interfacial tension but to an increase in the pre-exponential factor. This result may now be seen to be compatible with the capture, stabilisation and enhanced viability of clusters by the monolayer in a manner similar to that proposed above for glycine.

Engineering crystals through control of nucleation – concluding remarks

Returning to questions posed at the beginning of this paper it is clear that actually no direct data exist that relate to the crystallinity of the molecular clusters – we do not know whether they are 'crystalline' or 'amorphous'. Data on the templated nucleation of glycine and on nucleation in other polymorphic systems such as dihydroxybenzoic acid and sulfathiazole suggest that molecular assembly in the liquid phase can indeed mirror the packings of the potential polymorphs in a system. The nature of the solvent–solute interactions, however, can play a significant role in determining the viability of these clusters and hence direct the structural outcome of the crystallisation. The understanding of the link

UM00013201
NOVARTIS EXHIBIT 1517
Novartis v. Regents, IPR2023-01347
Page 1947 of 4460

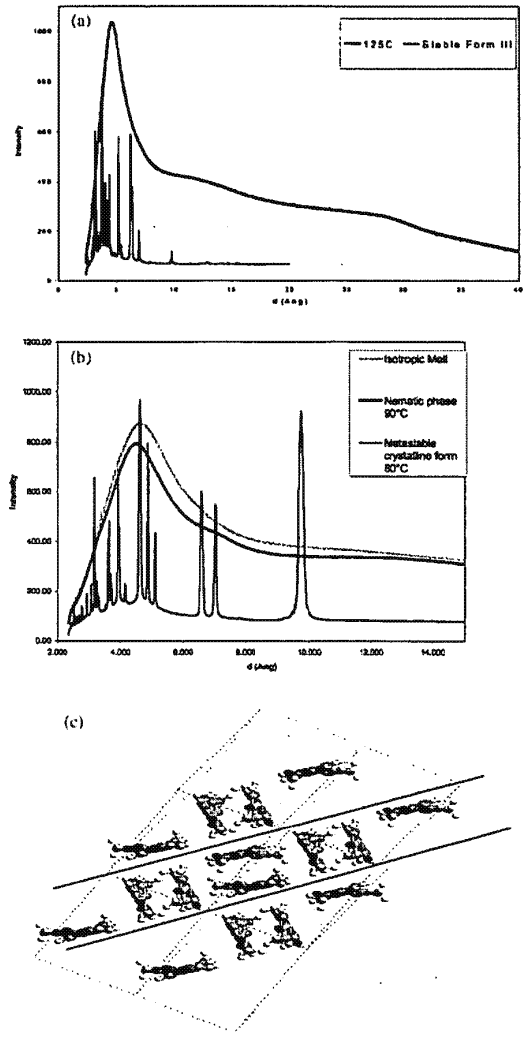


Fig. 14 Crystallisation of *para*-azoxyanisole: (a) the nematic and stable phases crystallised by cooling, (b) the metastable form crystallised from the undercooled nematic, (c) the 0.7 nm layer of form III.

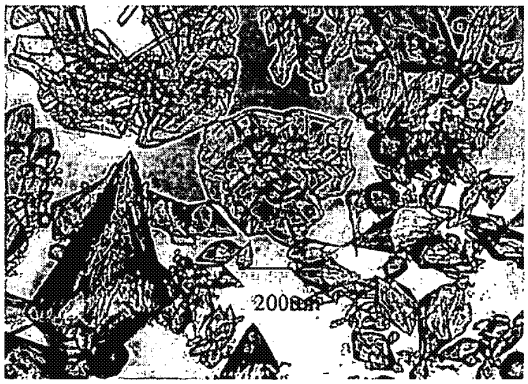


Fig. 15 Crystallisation of γ glycine from an AOT-containing oil–water interface. The tips of the conical crystals are anchored in the interfacial region.

between the *growth unit* and the *structural synthon* remains the basic problem for nucleation theory – the cases discussed shed some light on this issue with dimers evidently being common building blocks and having the necessary flexibility to act as a kind of structural messenger between solution and crystal.

This is the beginning of the development of a structural perspective of the nucleation process and much exciting work remains to be done.

References

1 D. Braga, *J. Chem. Soc., Dalton Trans.*, 2000, 3705.
2 C. Horn, L. Berben, H. Chow, M. Scudder and I. Dance, *CrystEngComm*, 2002, 4(2), 7.
3 J. Breu, H. Domel and A. J. Stoll, *Eur. J. Inorg. Chem.*, 2000, 2401.
4 D. Braga, G. Cojazzi, D. Paolucci and F. Grepioni, *CrystEngComm*, 2001, 3(38), 159.
5 *Nucleation*, A. C. Zettlemoyer, ed., Marcel Dekker, New York, 1969, ch. 1 and 5.
6 W. Ostwald, *Z. Phys. Chem.*, 1897, **22**, 289.
7 J. Bernstein, R. J. Davey and J.-O. Henck, *Angew. Chem., Int. Ed.*, 1999, **38**, 3440.
8 G. Nichols and C. S. Frampton, *J. Pharm. Sci.*, 1998, **87**, 648.
9 M. Volmer, *Kinetic der Phasenbildung*, Steinkopf, Leipzig, 1939.
10 R. J. Davey and J. Garside, *From Molecules to Crystallisers*, Oxford Science Publications, Oxford University Press, Oxford, 2000.
11 I. Weissbuch, R. Popovitz-Biro, L. Leiserowitz and M. Lahav, in *The Lock and Key Principle*, J. P. Behr, ed., Wiley, New York, 1994, p. 173.
12 A. Gavezotti and G. Fillippini, *Chem. Commun.*, 1998, 287.
13 S. P. Weinbach, K. Kjaer, J. Als-Nielsen, M. Lahav and L. Leiserowitz, *J. Phys. Chem.*, 1993, **97**, 5200.
14 D. T. Bowron, A. K. Soper and J. L. Finney, *J. Chem. Phys.*, 2001, **114**, 6203.
15 Y. Okaya, *Acta Crystallogr., Sect. B*, 1969, **25**, 2257.
16 L. Williams-Seton, R. J. Davey and H. F. Lieberman, *J. Am. Chem. Soc.*, 1999, **121**, 4563.
17 H. F. Lieberman, L. Williams, R. J. Davey and R. G. Pritchard, *J. Am. Chem. Soc.*, 1998, **120**, 686.
18 R. J. Davey, L. Williams-Seton, H. F. Lieberman and N. Blagden, *Nature*, 1999, **402**, 797.
19 P. J. Goodford, *J. Med. Chem.*, 1985, **28**, 849.
20 N. Blagden, R. J. Davey, H. F. Lieberman, L. Williams, R. Payne, R. Roberts, R. Rowe and R. Docherty, *J. Chem. Soc., Faraday Trans.*, 1998, **94**, 1035.
21 D. S. Hughes, M. B. Hursthouse, T. Threlfall and S. Taverner, *Acta Crystallogr., Sect. C*, 1999, **55**, 1831.
22 L. R. MacGillivray and M. J. Zaworotko, *J. Chem. Crystallogr.*, 1994, **24**, 703.
23 M. Gdaniec, M. Gilski and G. Denisov, *Acta Crystallogr., Sect. C*, 1994, **50**, 1622.
24 R. J. Davey, N. Blagden, S. Righini, H. Alison, M. J. Quayle and S. Fuller, *Cryst. Growth Des.*, 2001, **1**, 59.
25 R. J. Davey, N. Blagden, S. Righini, H. Alison and E. Ferrari, *J. Phys. Chem. B*, 2002, **106**, 1954.
26 T. Beyer, T. Lewis and S. L. Price, *CrystEngComm*, 2001, **3**(44), 178.
27 N. Blagden, W. I. Cross, R. J. Davey, M. Broderick, R. G. Pritchard, R. J. Roberts and R. C. Rowe, *Phys. Chem. Chem. Phys.*, 2001, **3**, 3819.
28 Available within Cerius^2, version 3, Accelrys, Cambridge, UK, 2000.
29 J. D. Bernal and D. Crowfoot, *Trans. Faraday Soc.*, 1933, **29**, 1032.
30 C. Chebli and F. Brisse, *Acta Crystallogr., Sect. C*, 1995, **51**, 1164.
31 R. J. Davey, W. Liu, M. J. Quayle and G. J. T. Tiddy, *Cryst. Growth Des.*, accepted.
32 K. Allen, R. J. Davey, E. Ferrari, C. Towler, G. J. T. Tiddy, M. Jones and R. Pritchard, submitted to *Langmuir*, March 2002.
33 E. M. Landau, M. Levanon, L. Leiserowitz, M. Lahav and J. Sagiv, *Nature*, 1985, **318**, 353.
34 K. Fontell, *J. Colloid Interface Sci.*, 1973, **44**, 318.
35 J. Yano, H. Furedi-Milhofer, E. Wachtel and N. Garti, *Langmuir*, 2000, **16**, 9996.
36 R. J. Davey, S. J. Maginn, R. B. Steventon, J. M. Ellery, A. V. Murrell, J. Booth, A. D. Goodwin and J. E. Rout, *Langmuir*, 1994, **10**, 1673.

UM00013202
NOVARTIS EXHIBIT 1517
Novartis v. Regents, IPR2023-01347
Page 1948 of 4460

Crystallisation in polymer films: control of morphology and kinetics of an organic dye in a polysilicone matrix

Roger J. Davey,*[a] Simon N. Black,[b] Alan D. Goodwin,[b] Duncan Mackerron,[b] Steven J. Maginn[b] and Emma J. Miller[b]

[a]*Colloids, Crystals, and Interfaces Group, Department of Chemical Engineering, UMIST, PO Box 88, Manchester, UK M60 1QD*

[b]*Research and Technology Department, ICI Chemicals and Polymers, The Heath, Runcorn, Cheshire, UK WA7 4QD*

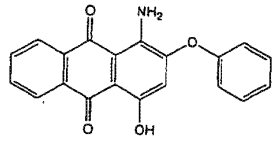
The successful selection, design and synthesis of additives for the control of nucleation and crystallisation of a red anthraquinone based dye is described. This procedure is based on the crystal structure and morphology of solution grown crystals and in this study the possibility of using the same approach to control crystallisation within an amorphous polymeric matrix is explored. The work has been motivated by the desire to prepare stable dye sheets for thermal transfer printing applications, yet the parallel with natural biomineralisation processes is clear.

Recent years have seen significant advances in the understanding of structural mechanisms available for the control of crystallisation processes.[1–3] Thus, the factors leading to the design of auxiliary molecules for the control of nucleation and growth of both organic and inorganic materials are now well understood.[4,5] One area of particular interest, largely in the context of materials design, has been biomineralisation. Here, biological systems are seen as models for the expression of highly organised structures comprising simple inorganic crystals located in macromolecular matrices (*e.g.* calcium phosphate in collagen). A number of studies have already been reported which attempt to mimic these processes using synthetic polymers as matrices in which simple inorganic species are nucleated and grown.[6,7] In this study we present for the first time an example of an organic molecule crystallising within a polymer film and show how the existing strategies for the control of crystallisation from solutions and melts can be successfully transferred to crystallisation from an amorphous polymeric matrix. The work was motivated by the commercial need to develop dye sheets for use in thermal transfer colour printing,[8–10] in which the dye was stabilised against crystallisation during storage.

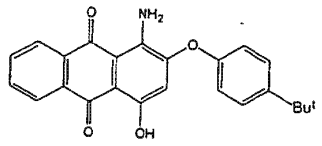
Experimental

The dye chosen for this work was the red, anthraquinone-based 1-amino-4-hydroxy-2-phenoxyanthraquinone **1**, supplied by ICI. Crystallisation was carried out both from solutions in butanone and from films comprising crosslinked polydimethylsiloxane, also supplied by ICI. These films were prepared by coating a solution of dye, polymer, crosslinker and catalyst (dibutyltin) in CH_2Cl_2 onto a 6 μm melinex support [biaxially oriented poly(ethylene terephthalate)] using a K-bar (R K Print-Coat Instruments Ltd.) to give coatings 24–54 μm in thickness. After spreading, the solvent was evaporated using a hot air drier and the film cured at 100 °C for 30 s to complete the crosslinking. This left a final film of *ca.* 1 μm thickness. By carrying out the final cure for variable times and on a microscope hot stage, the nucleation and growth of dye crystals at 100 °C in these initially amorphous films was monitored. Dye concentrations in the original solutions were chosen to be 0.28, 0.56 and 0.85 wt.% and each measurement reported is the mean of seven experiments.

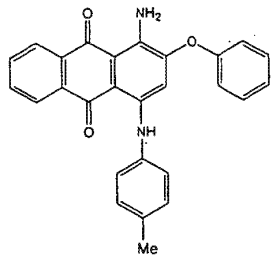
Crystals of the dye were grown from solution by slow evaporation of 1% butanone solutions at 30 °C. Owing to the



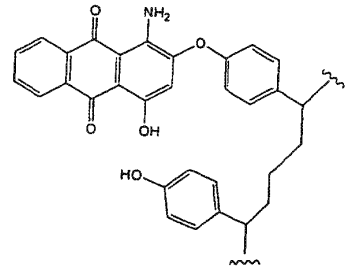
1



2



3



4

UM00013203
NOVARTIS EXHIBIT 1517
Novartis v. Regents, IPR2023-01347
Page 1949 of 4460

colour intensity of such solutions it was not possible to monitor the progress of these experiments. When only a little solvent remained the solutions were filtered and the crystals examined by SEM. Crystals grown from pure solutions were examined by optical microscopy and optical goniometry in order to define their morphology. The theoretical morphology was calculated using the program HABIT[3] and the potentials of Momany *et al.*[11]

Small molecule additives [1-amino-2-(4-*tert*-butylphenoxy)-4-hydroxyanthraquinone 2 and 1-amino-2-phenoxy-4-toluidinoanthraquinone 3] were supplied by ICI. These materials were characterised by NMR spectroscopy, thin layer chromatography (TLC) and microanalysis and found to have purities in excess of 98%. The polymeric additives were the products of grafting 1-amino-2-bromo-4-hydroxyanthraquinone onto copolymers of styrene and vinylphenol (4). Poly(vinylphenol)s of varying vinylphenol contents were synthesised by reacting vinylphenol (prepared by the method of Hatakeyama *et al.*[12]) (0.044, 0.11, and 0.15 mole fraction) with styrene at 60 °C for 50 h using azoisobutyronitrile (AIBN) as an initiator. The copolymers were recovered by dissolving the reaction mixture in butanone and precipitating the polymer with MeOH. 1-Amino-2-bromo-4-hydroxyanthraquinone was then grafted onto these polymers by reaction in *N*-methylpyrrolidone at 135 °C for 20 h. The resultant grafted polymers were recovered by precipitation with MeOH. Characterisation was performed by gel permeation chromatography (GPC), to measure the molecular weight relative to a polystyrene standard, and proton NMR, FTIR and UV–VIS spectroscopy to assess the extent of grafting.

For subsequent solution growth experiments additives were added at levels of 1 wt.% on dye, while in the polymer films levels up to 15 wt.% on dye were used.

Crystal structure and additive design

The crystal structure of the dye used here has been reported previously.[10] It belongs to the monoclinic space group $P2_1/c$ with four molecules in the unit cell and $a=1.4972$, $b=0.5141$ and $c=1.9853$ nm and $\beta=94.15°$. The anthraquinone and phenoxy rings adopt a dihedral angle of 97° and the molecules are held in the structure by van der Waals and π–π interactions. There are no intermolecular hydrogen bonds. Fig. 1(*a*) viewed down the *a*-axis shows the herringbone motif and indicates that the π–π interactions lie along [010]. Fig. 1(*b*) is a view down the *b*-axis. Fig. 2(*a*) is a scanning electron micrograph of solution grown crystals which adopt a needle morphology in which the needle axis corresponds to [010] with large {101} and smaller {101} and {002} side faces, as determined by optical goniometry. The predicted morphology is shown in Fig. 2(*b*) and is in reasonable agreement with experiment with elongation along [010] as expected from the π–π interactions, with {002}, {200} and {101} as the most important side faces.

The overall objective of this study was to prevent crystallisation of dye molecules within the polymeric films by including in the formulations additives which would inhibit nucleation and growth of crystals. It was on the basis of the above structural and morphological data that such additives were selected and designed as molecules likely to inhibit crystallisation of specific faces of the dye crystals. For example, in the {101} faces molecules present either their phenoxy or their anthraquinone rings to the growth environment [Fig. 1(*b*)]. Hence substitution at the *para* position on the phenoxy ring by a bulky group should yield a molecule that is recognised by the crystal surface but which, once in position, will sterically

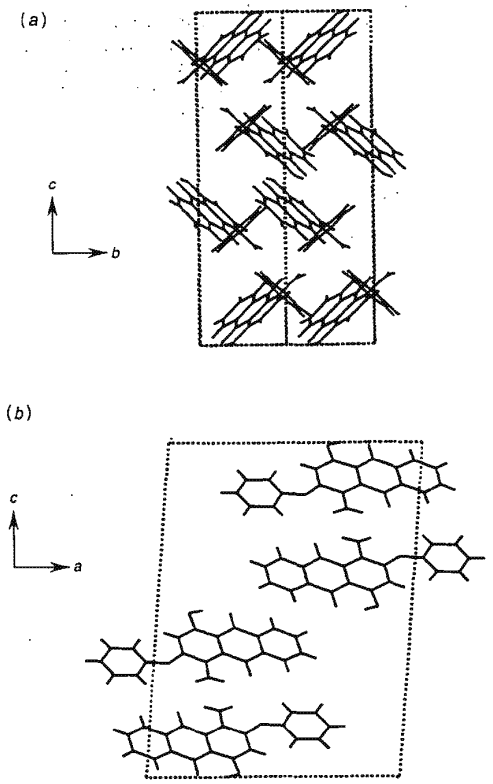


Fig. 1 The crystal structure of 1 (*a*) viewed down [100], and (*b*) viewed down [010]

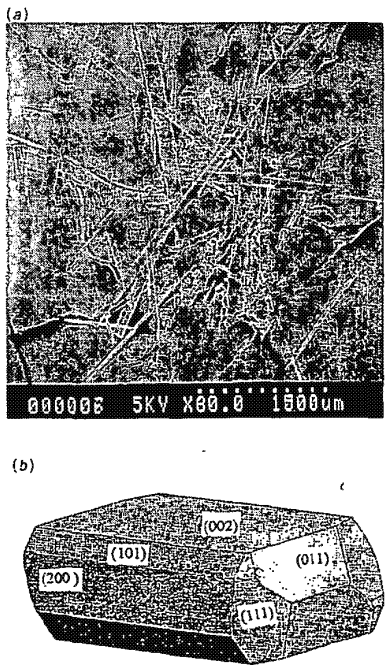


Fig. 2 The morphology of 1-amino-4-hydroxy-2-phenoxyanthraquinone crystals: (*a*) solution grown and (*b*) predicted from the crystal structure

UM00013204
NOVARTIS EXHIBIT 1517
Novartis v. Regents, IPR2023-01347
Page 1950 of 4460

prevent addition of further molecules to the growing crystal. For {020} there are four different molecular orientations [Fig. 1(*a*)], however in two of these the hydroxy group is directed away from the surface such that its replacement by a bulkier substituent might be expected to inhibit growth in this direction. Bearing these conclusions in mind two potential additives were selected, one in which the phenoxy ring was substituted at the *para* position by a *tert*-butyl group (2) and was designed to inhibit growth on the (101) face, and a second in which the hydroxy group was replaced by a toluidino group (3) designed to inhibit (020). Their likely positions in the two surfaces are shown in Fig. 3(*a*) and (*b*). In addition, the polymeric additives (4) described above were synthesised with the aim of providing the possibility of multidentate binding to the surfaces to compare with the small unidentate molecules. This is shown schematically in Fig. 3(*c*) for the {101} faces.

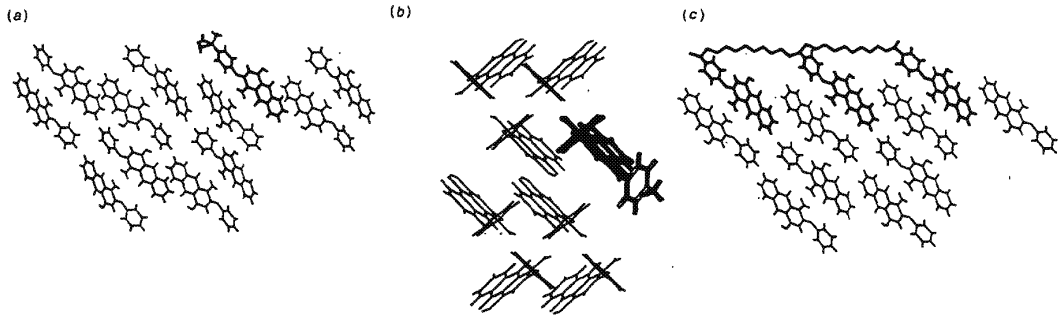


Fig. 3 Possible binding sites of additives: (*a*) 2 on (101), (*b*) 3 on (020), and (*c*) 4 on (101)

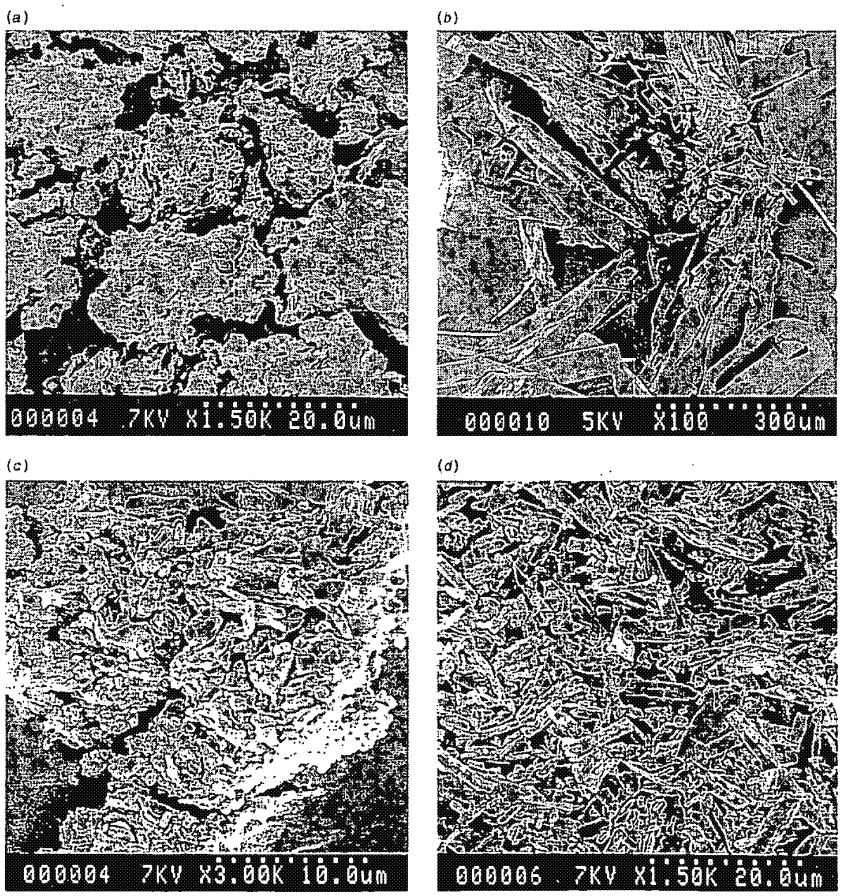


Fig. 4 Crystals grown from solution in the presence of (*a*) 2, (*b*) 3, (*c*) a mixture of 2 and 3 and (*d*) polymer 4c

UM00013205
NOVARTIS EXHIBIT 1517
Novartis v. Regents, IPR2023-01347
Page 1951 of 4460

Results

Characterisation of polymers

Three copolymers were prepared, having mole fractions (as determined by FTIR) of 0.048, 0.11, and 0.16 vinylphenol. This suggests a reactivity ratio of vinylphenol with styrene of unity, in agreement with related studies.[13] After grafting, 2.25, 4.7 and 12.8% (w/w) of 1-amino-2-bromo-4-hydroxyanthraquinone had been incorporated, and the copolymers had weight mean molar masses (M_w) of 168100, 103300 and 85700, respectively. They are referred to subsequently as polymers **4a**, **b** and **c**.

Solution grown crystals

Fig. 4(*a*)–(*d*) shows crystals grown in the presence of the *tert*-butyl derivative **2**, the 4-methylaniline derivative **3**, a mixture of **2** and **3**, and polymer **4c**, respectively. When compared with crystals grown from pure solutions [Fig. 2(*a*)] it is quite clear that all the additives tested had a significant effect on the crystallisation process. The *tert*-butyl derivative appeared to prevent the formation of well defined crystals, yielding a powder of irregular plate-like crystals. The toluidino derivative significantly reduced growth along the *b*-axis as expected, while polymer **4c** appeared to give enhanced nucleation (smaller crystals) but little morphological change. Overall these results indicated that the additives chosen were of sufficient potency to test in polymer films.

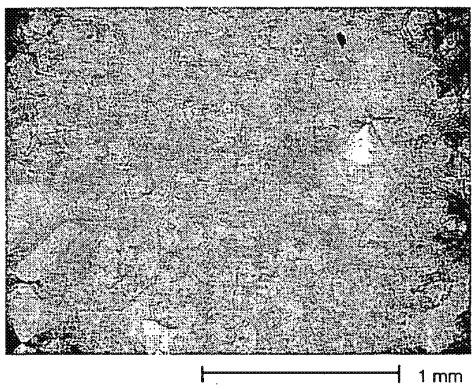


Fig. 5 Spherulitic crystallisation of **1** in a polymer film

Crystallisation in polymer films

In polymer films dye nucleation was followed by radial growth, giving polycrystalline spherulitic or rosette type morphologies which eventually spread through the entire film. This is seen in Fig. 5. Similar behaviour has been reported previously for anthraquinone crystallising from polystyrene films.[14] Powder X-ray diffraction of crystallised films had major reflections corresponding to *d*-spacings of 1.23, 1.15, 0.62 and 0.49 nm as expected for *b*-axis needles of this dye having predominant {101} and {002} faces.[13] This implies radial growth of the spherulites along the fast growing [010] direction. Increasing the dye concentration from 0.28 to 0.85 wt.% led, as expected, to an increase in the nuclei density from 0.7 to 3.5 rosettes per mm^2 due to the associated rise in supersaturation.

In agreement with the solution growth experiments reported above, all the additives influenced the crystallisation of the dye in the polymer film. The morphological changes are shown in Fig. 6. Fig. 6(*a*) and (*b*) show the effect of increasing levels of **2** while Fig. 6(*c*) and (*d*) show the effects of **3** and polymer **4c**, respectively. Clearly, all these additives inhibit the formation of the space-filling rosettes and appear to inhibit the crystallisation process such that large areas of the film remain uncrystallised.

In order to quantify the magnitude of crystallisation inhibition, simple kinetic studies were undertaken in which the rosette numbers and radii were measured. The resulting crystallisation times and nucleation densities are shown in Fig. 7(*a*) and (*b*), where it is clear that stabilisation of the dye films is enhanced by increasing concentrations of additive. Compound **3** is most active in this respect, presumably because it was designed to inhibit the fastest growth direction, [010]. The polymers appear to be particularly successful at inhibiting nucleation, an observation that appears to be in complete contrast to their solution behaviour, where they appear to enhance the nucleation rate. This may well be related to reduced mobility and conformational flexibility in the polymer film. Finally, the behaviour of the three grafted copolymers was compared and the kinetic data are shown in Fig. 7(*c*). For comparison, polystyrene was also tested and found to be ineffective in modifying the crystallisation and also to be immiscible with the silicone binder system used here. Given that these copolymers contain significant polystyrene blocks it would be expected that their solubility in the polymer film would be a key factor in their efficacy. For example, polymer **4a** is 95.5% polystyrene, which implies a low solubility in the film and hence explains its poor efficacy in Fig. 7(*c*). Polymers **4b** and **4c** showed improved performance, although at high (10%) levels they also phase separate in the film. It is perhaps surprising that the efficacy does not increase monotonically with level of grafting, yet it is encouraging that all the polymers

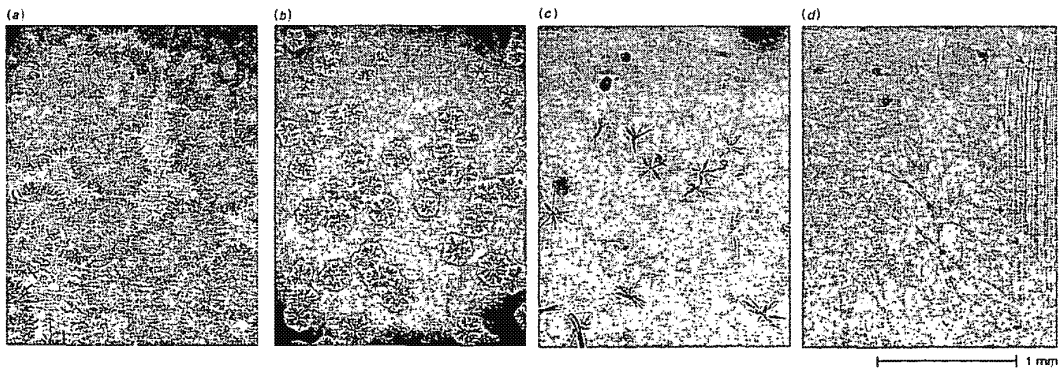


Fig. 6 The influence of additives on the morphology of crystallised polymer films: (*a*) 5% of **2**, (*b*) 14% of **2**, (*c*) 2% of **3** and (*d*) 5% of **4c**

UM00013206
NOVARTIS EXHIBIT 1517
Novartis v. Regents, IPR2023-01347
Page 1952 of 4460

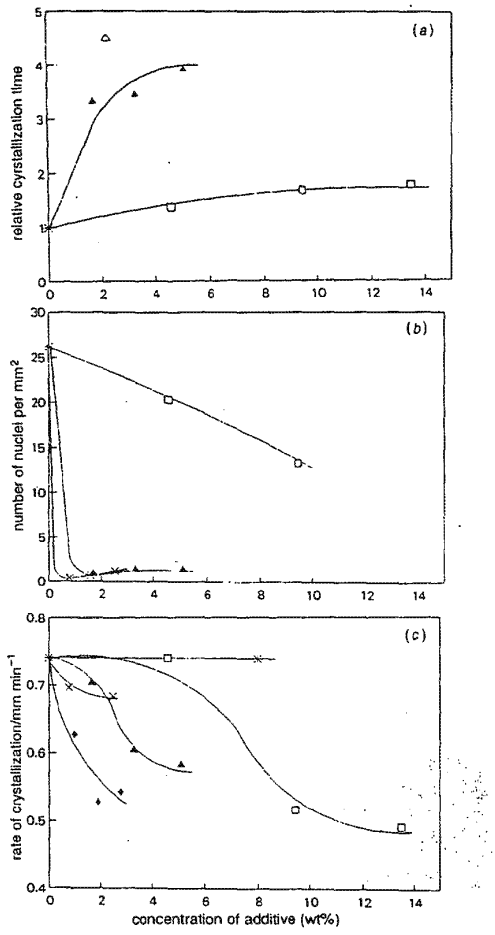


Fig. 7 The influence of additives on the kinetics of crystallisation of **1** in polymer films: (*a*) the effect of (□) **2**, (△) **3**, and (▲) polymer **4c** on times taken for films to fully crystallise, (*b*) the effect of (□) **2** and polymers (×) **4a** and (▲) **4c** on the nucleation in films, and (*c*) the effect of (*) polystyrene, (□) **2** and polymers (×) **4a**, (◆) **4b** and (▲) **4c** on crystallisation rates

show enhanced activity over the single small molecule *tert*-butyl derivative. This supports the idea that efficacy may be enhanced through multidentate binding.

Conclusions

This study has applied the structurally based strategy for selection and design of tailor-made growth auxiliaries to the case of an anthraquinone dye crystallising from an amorphous polymer film. Crystallisation inhibitors, selected on the basis of the known crystal structure of the dye, were tested for efficacy in solution growth experiments and shown to be powerful crystallisation modifiers. It is interesting to note that unlike previous studies of tailor-made inhibitors the molecular recognition features involved utilise only van der Waals and π–π interactions rather than more specific hydrogen bonding. It was found that this behaviour could be transferred directly to crystallisation in a polymer matrix, with the result that crystallisation could be significantly inhibited and the dye films stabilised even at temperatures as high as 100 °C. This correspondence between solution and polymeric media has not been addressed before, although it is clearly of significance both technologically and from the biomineralisation viewpoint.

The authors acknowledge the assistance of Drs. B. D. Chen and H. Lieberman in the preparation of this manuscript.

References

1 I. Weissbuch, R. Popoviz-Biro, L. Leiserowitz and M. Lahav, in *The Lock and Key Principle*, ed. J. P. Behr, John Wiley and Sons, Chichester, 1994, ch. 6.
2 R. J. Davey, in *Separation Technology The Next Ten Years*, ed. J. Garside, I. Chem E., Rugby, 1994, ch. 4.
3 G. Clydesdale, K. J. Roberts and R. Docherty, in *Colloid and Surface Engineering: Controlled Particle, Droplet, and Bubble Formation*, ed. D. Wedlock, Butterworth-Heineman, London, 1993, pp. 95–135.
4 A. L. Rohl, D. H. Gay, R. J. Davey and C. R. A. Catlow, *J. Am. Chem. Soc.*, 1996, **118**, 642.
5 S. Mann, *Nature (London)*, 1993, **365**, 499.
6 J. Lin, E. Cates and P. A. Bianconi, *J. Am. Chem. Soc.*, 1994, **116**, 4738.
7 B. J. Brisdon, B. R. Heywood, A. G. W. Hodson, S. Mann and K. W. Wong, *Adv. Mater.*, 1993, **5**, 49.
8 P. Gregory, *Chem. Br.*, 1989, January, 47.
9 R. J. Davey and D. H. Mackerron, *Eur. Pat. Appl.*, EP 294 109, 1988.
10 S. N. Black, R. J. Davey, C. A. O'Mahoney and D. J. Williams, *Acta Crystallogr., Sect. C*, 1992, **48**, 321.
11 F. A. Momany, L. M. Carruthers, R. F. McGuire and H. A. Scheraga, *J. Phys. Chem.*, 1974, **78**, 1595.
12 T. Hatakeyama, K. Nakamura and H. Hatakeyama, *Polymer*, 1978, **19**, 593.
13 A. D. Jenkins, K. Petrak, G. A. F. Roberts and D. R. M. Walton, *Eur. Polym. J.*, 1975, **11**, 653.
14 Y. Murata and T. Kiyotsukuri, *Kobunshi Ronbunshu*, 1984, **41**, 111.

Paper 6/05614H; *Received* 12*th August*, 1996

UM00013207
NOVARTIS EXHIBIT 1517
Novartis v. Regents, IPR2023-01347
Page 1953 of 4460

This Page is Inserted by IFW Indexing and Scanning Operations and is not part of the Official Record

BEST AVAILABLE IMAGES

Defective images within this document are accurate representations of the original documents submitted by the applicant.

Defects in the images include but are not limited to the items checked:

- ☐ BLACK BORDERS
- ☐ IMAGE CUT OFF AT TOP, BOTTOM OR SIDES
- ☐ FADED TEXT OR DRAWING
- ☐ BLURRED OR ILLEGIBLE TEXT OR DRAWING
- ☐ SKEWED/SLANTED IMAGES
- ☐ COLOR OR BLACK AND WHITE PHOTOGRAPHS
- ☐ GRAY SCALE DOCUMENTS
- ☐ LINES OR MARKS ON ORIGINAL DOCUMENT
- ☐ REFERENCE(S) OR EXHIBIT(S) SUBMITTED ARE POOR QUALITY
- ☐ OTHER: _____

IMAGES ARE BEST AVAILABLE COPY.
As rescanning these documents will not correct the image problems checked, please do not report these problems to the IFW Image Problem Mailbox.

phase was separated and evaporated at 37 °C under a light current of nitrogen. To the dry extract was added 200 μL of a solution of heptafluorobutyric anhydride (HFBA) in ethyl acetate (1:10; v/v). The mixture was heated for 20 min at 60 °C and then evaporated to eliminate any excess of HFBA. The residue was washed twice with 300 μL of ethyl acetate, and then 200 μL of n-hexane was added. Two microliters of this organic solution was injected by means of an automatic injector (HP 7672 A) into a gas chromatograph (HP 5880) fitted with a capillary quartz column (25 m and 0.22 mm i.d.). The phase film used was OV1 (0.11 μM). Vector and make-up gases was argon–methane (95:5, v/v) delivered at 0.5 and 40 mL/min, respectively. The split ratio was 1:10. The temperatures of the column, injector, and detector were 215, 300, and 300 °C, respectively. The detection was achieved by electron capture (^{63}Ni source).

Under these conditions, the retention times for 8, 11, 16, and metoprolol were 12.3, 15.6, 18.9, and 6.5 min, respectively. The calibration curves of these compounds were linear for reaction mixtures containing from 0 to 200 ng/mL of substrate and their minimal detectable quantities by this method were 10 ng/mL.

The initial rates of disappearance within the 10-min reaction time were determined for 8, 11, 16, and metoprolol. These values were corrected for the spontaneous degradation of these compounds. The apparent constant of Michaelis–Menten (K_M) and the maximal rate of disappearance of the substrate (V_{max}) were calculated according to the procedure described by Mazel.[39] It should be mentioned that the chosen incubation time (10 min) permitted to obtain, for all the compound tested, a linear relationship between the logarithm of the rate concentration and the reciprocal of the rate of the reaction, allowing a correct determination of V_{max} and K_M.

(39) Mazel, P. *Fundam. Drug Metab. Drug Dispos.* 1971, *19*, 527.

Conformationally Defined Adrenergic Agents. 5. Resolution, Absolute Configuration, and Pharmacological Characterization of the Enantiomers of 2-(5,6-Dihydroxy-1,2,3,4-tetrahydro-1-naphthyl)imidazoline: A Potent Agonist at α-Adrenoceptors†

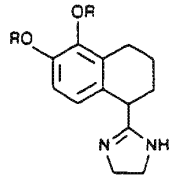
John F. DeBernardis,* Daniel J. Kerkman, David L. Arendsen, Steve A. Buckner, John J. Kyncl, and Arthur A. Hancock

Division of Cardiovascular Research, Abbott Laboratories, Abbott Park, Illinois 60064. *Received September 23, 1986*

(±)-2-(5,6-Dimethoxy-1,2,3,4-tetrahydro-1-naphthyl)imidazoline has been resolved into its (+) and (−) enantiomers, and the absolute configuration was established by single-crystal X-ray diffraction studies. The more active isomer has been assigned the *R* absolute configuration. Cleavage of the respective (+)- and (−)-dimethyl ethers with boron tribromide provided the corresponding (+)- and (−)-2-(5,6-dihydroxy-1,2,3,4-tetrahydro-1-naphthyl)imidazoline hydrobromides and these were pharmacologically characterized. In various preparations, the *R* enantiomer has been shown to be an extremely potent α agonist with preferential activity at the α_2-adrenergic receptor.

Imidazoline derivatives are well recognized as an important class of drugs that interact with α-adrenergic receptors.[1-5] Studies have even appeared in the literature on optically active derivatives of various imidazolines.[6-11] Generally speaking, these optical isomers were derivatives of the parent achiral molecule in which an asymmetric center was generated through modifications on the imidazoline ring[6,7] or incorporation of a benzylic hydroxyl atom.[8] The biological activity of the antipodes of tetrahydrazoline has also been reported.[9-11]

Recently,[12] we reported that the compound (±)-2-(5,6-dihydroxy-1,2,3,4-tetrahydro-1-naphthyl)imidazoline (1a) is an agonist at both the α_1- and α_2-adrenoceptors with modest selectivity for the latter. A remarkable feature associated with 1a was the extraordinary potency it displayed in vitro for both the α_1- as well as the α_2-adrenergic receptors, being 13 and 184 times, respectively, more potent than norepinephrine (NE).[12] Our interest in the relationship between stereochemical drug–receptor interactions and the resulting biological effects led us to resolve 1a into its respective enantiomers. Furthermore, we



1a, R = H
b, R = CH_3

† A preliminary account of this work has been presented to the Division of Medicinal Chemistry, 192nd National Meeting of the American Chemical Society, Anaheim, CA, 1986; DeBernardis, J. F.; Kerkman, D. J., paper MEDI-70.

(1) Boudier, H. S.; deBoer, J.; Smeets, G.; Lien, E. J.; van Rossum, J. *Life Sci.* 1975, *17*, 377.
(2) Boudier, H. S.; Smeets, G.; Brouwer, G.; van Rossum, J. *Life Sci.* 1973, *15*, 887.
(3) Kobinger, W.; Pichler, L. *Naunyn-Schmiedeberg's Arch. Pharmacol.* 1975, *291*, 175.
(4) Mujic, M.; van Rossum, J. M. *Arch. Int. Pharmacodyn.* 1965, *155*, 432.
(5) Ruffolo, R. R., Jr.; Rosing, E. L.; Waddell, J. E. *J. Pharmacol. Exp. Ther.* 1979, *209*, 429.
(6) Miller, D. D.; Hsu, F.-L.; Ruffolo, R. R., Jr.; Patil, P. N. *J. Med. Chem.* 1976, *19*, 1382.
(7) Hsu, F.-L.; Hamada, A.; Booher, M. E.; Fuder, H.; Patil, P. N.; Miller, D. D. *J. Med. Chem.* 1980, *23*, 1232.
(8) Miller, D. D.; Hamada, A.; Craig, E. C.; Christoph, G. G.; Gallucci, J. C.; Rice, P. J.; Banning, J. W.; Patil, P. N. *J. Med. Chem.* 1983, *26*, 957.
(9) Yellin, T. O.; Katchen, M. S.; Lavenhar, S. R.; Nelson, E. G. *Acta Physiol. Scand., Spec. Suppl.* 1978, 219.
(10) Ruffolo, R. R., Jr.; Rice, P. J.; Patil, P. N.; Hamada, A.; Miller, D. D. *Eur. J. Pharmacol.* 1983, *86*, 471.
(11) Fuder, J.; Nelson, W. L.; Miller, D. D.; Patil, P. N. *J. Pharmacol. Exp. Ther.* 1981, *217*, 1.
(12) DeBernardis, J. F.; Kyncl, J. J.; Basha, F. Z.; Arendsen, D. L.; Martin, Y. C.; Winn, M.; Kerkman, D. J. *J. Med. Chem.* 1986, *29*, 463.

UM00013209
NOVARTIS EXHIBIT 1517
Novartis v. Regents, IPR2023-01347
Page 1955 of 4460

wanted to crystallize one of the enantiomers and subject it to a single-crystal X-ray analysis in order to establish the absolute configuration so as to obtain additional information regarding the interaction of **1a** with the α_1- and the α_2-adrenergic receptors. This paper describes a facile resolution and the pharmacological characterization of both the (+)- and (−)-2-(5,6-dihydroxy-1,2,3,4-tetrahydro-1-naphthyl)imidazolines as well as the X-ray diffraction studies and determination of absolute configuration for one of the corresponding resolved dimethoxy derivatives.

Resolution

(±)-2-(5,6-Dimethoxy-1,2,3,4-tetrahydro-1-naphthyl)-imidazoline (**1b**) was prepared as previously described.[12] Resolution of the racemic mixture was accomplished through fractional crystallization of the salt formed by the addition of 1.1 molar equiv of (+)-dibenzoyl-D-tartaric acid monohydrate to a solution of **1b** in methanol. One recrystallization from methanol afforded one of the diastereomeric salts. Decomposition of the salt with cold NH_4OH afforded the free base, $[\alpha]^{25}_D$ −13.6°. Initial attempts to free the diastereomeric salt of **1b** at room temperature with NH_4OH resulted in considerable racemization. We have since found that if the salt is neutralized with NH_4OH at 0 °C, extracted into CH_2CL_2, and evaporated without external heating, the resulting free base maintains its optical purity.

We decided to follow the change in rotation (if any) with time for the free base of **1b** in ethanol at 34 °C. We found that the free base itself without added NH_4OH underwent racemization under these conditions. When the ln of the observed rotation was plotted vs. the elapsed time, a least-squares fit of the data gave a rate constant of $k = 1.02 \times 10^{-2}$ min^{-1} corresponding to a half-life of $t_{1/2} = 98$ min with a correlation coefficient of $r = 0.9974$. The relationship was linear for at least 3 half-lives. When the HCl salt of **1b**, formed from the free base with ethereal HCl, was dissolved in distilled water (pH 5), there was no change in the observed rotation at 34 °C over a 5-h period.

The above experiments showed that **1b** was susceptible to racemization as the free base but not as the salt. Since there was concern about possible racemization of the respective enantiomers during biological testing, we chose to follow the change in observed rotation with time of both **1a** and **1b** under the most basic pH conditions used in any of the biological assays. This required observation of the rotation in pH 7.7 Tris-HCl buffer at 25 °C. Compound **1b** showed no racemization over a 16-h observation period, and **1a** also gave no evidence of racemization under these conditions during a 4-h time period. As a result, we are confident that the biological activity observed with the respective enantiomers is not confounded by racemization during the biological experiments.

The (+) enantiomer was recovered from the filtrates of the initial resolution. Formation of the diastereomeric salt was accomplished as described for the (−) enantiomer with, however, (−)-dibenzoyl-L-tartaric acid monohydrate. One recrystallization from methanol afforded, after decomposition of the salt as before, the free base, $[\alpha]^{25}_D$ +13.8°.

The optical purity of the enantiomers was established after formation of the respective hydrochloride salts and utilization of NMR spectroscopy in the presence of the aqueous chiral shift reagent CoATP.[13] Inspection of the NMR spectra revealed a general upfield shift of the resonances of **1b** with the addition of the paramagnetic CoATP complex. Of particular interest was the behavior

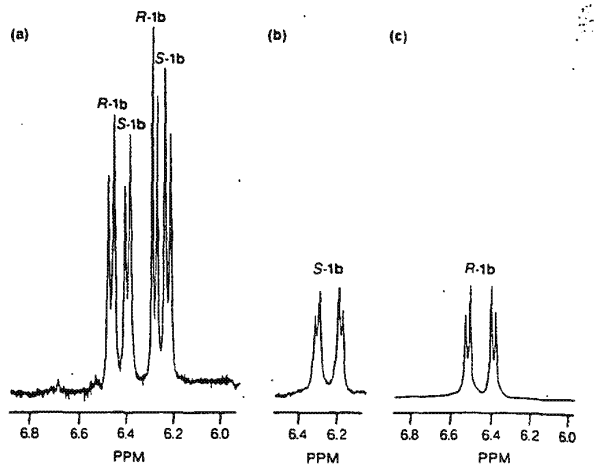


Figure 1. NMR determination of optical purity: (a) racemic **1b** in D_2O + 400 μL of CoATP, (b) (−)-*S* enantiomer in D_2O + 400 μL of CoATP, (c) (+)-*R* enantiomer in D_2O + 300 μL of CoATP.

of the two aromatic doublets. In the presence of the chiral shift reagent the aromatic resonances were separated into a pair of doublets, as shown in Figure 1a. This effect presumably arises due to formation of pseudocontact diastereomers between the chiral CoATP complex and each of the two enantiomers of **1b**. As seen in Figure 1a the two pairs of resonances are nearly completely resolved, allowing separate integration of the signals from each enantiomer. Consequently, the relative amount of each enantiomer of **1b** present in the resolved samples could be determined. Sample integration of the racemic mixture yielded a ratio of 1.1 to 1, within experimental error of the value expected. Figure 1b,c shows the results obtained for the (−) and (+) isomers, respectively, in the presence of the chiral shift reagent. As is readily seen, the enantiomers are resolved to a conservatively estimated enantiomeric excess (ee) of >98%.

The respective (+) and (−) isomers were cleaved to the corresponding catechols with boron tribromide at reduced temperatures. It was found that when the reaction was run at −22 °C, under an inert atmosphere for 3 h, a clean conversion to the desired catechols resulted; $[\alpha]^{25}_D$ +12.5° and $[\alpha]^{25}_D$ −11.8°. At an elevated temperature (0 °C for 3 h) some apparent racemization resulted as evidenced by NMR studies on the catechol enantiomers.

Optical purity of the (+) and (−) enantiomers of **1a** was again determined with the aqueous chiral shift reagent CoATP. As shown in Figure 2a–c, the aromatic resonances are nearly completely separated as was the case for the dimethoxy derivatives. Once again, the ee was conservatively estimated to be >98%.

Crystallography

An X-ray structure determination of the (+)-dibenzoyl-D-tartaric acid salt (from unnatural (−)-D-tartaric acid) of **1b** was performed in order to determine the absolute configuration of the imidazoline derivative relative to the known[14] configuration of the tartaric acid salt. A ball and stick representation of the molecular structure showing all non-hydrogen atoms is shown in Figure 3. Analysis of the structure revealed that the asymmetric carbon at position 1 has the *S* configuration. Therefore, the enantiomer obtained from the diastereomeric salt formed with (−)-dibenzoyl-L-tartaric acid was assigned the *R* configuration.

(13) Granot, J.; Reuben, J. *J. Am. Chem. Soc.* **1978**, *100*, 5209.

(14) *Merck Index* **1983**, *10*, 8943.

UM00013210
NOVARTIS EXHIBIT 1517
Novartis v. Regents, IPR2023-01347
Page 1956 of 4460

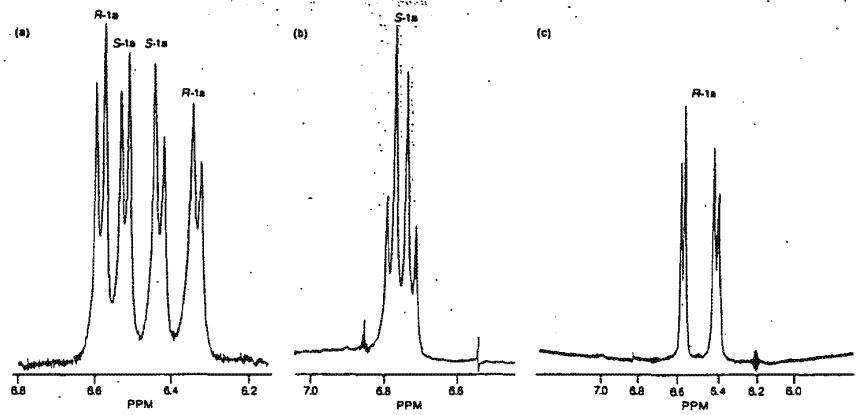


Figure 2. NMR detemination of optical purity: (a) racemic **1a** in D_2O + 200 μL of CoATP, (b) (−)-*S* enantiomer in D_2O + 300 μL of CoATP, (c) (+)-*R* enantiomer in D_2O + 150 μL of CoATP.

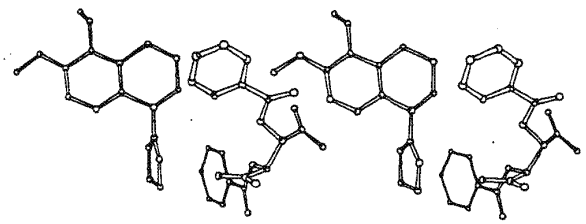


Figure 3. Ball and stick representation[27] of the X-ray structure of all the non-hydrogen atoms of (*S*)-**1b** as the (+)-dibenzoyl-D-tartaric acid salt.

Pharmacological Evaluation

In order to evaluate the α_1- and α_2-adrenergic properties associated with the respective (*R*)- and (*S*)-**1a** enantiomers (tested as the hydrobromide salts), we utilized in vitro tissue preparations that contained a homogeneous population of a single-receptor subtype, the isolated rabbit aorta (α_1),[15] as well as the phenoxybenzamine-pretreated dog saphenous vein (postjunctional α_2) (PBZ-DSV).[16,17] The potency of each test compound was expressed as a molar ED_{50}, and an index number was obtained by calculating the ratio of the ED_{50} of NE to that of the test compound (CPD). The larger the index number the more potent the compound relative to NE.

Our previous studies[12] had demonstrated that the treatment of the isolated DSV with PBZ (10^{-7} M) selectively inactivated the postsynaptic α_1 receptors and, thereby, provided a functional tissue model containing a homogeneous population of postsynaptic α_2 receptors. The contractile response of this tissue proved to be suitable for the quantitative evaluation of the postsynaptic α_2 component of both selective α_2 agents, as well as nonselective (α_1/α_2) adrenergic compounds. However, since it was observed that the PBZ (10^{-7} M) utilized in this DSV preparation did not significantly affect the function of the presynaptic α_2 receptors in this tissue, we developed[18] an experimental model capable of simultaneously assessing the effects of compounds interacting at the presynaptic and the postsynaptic α_2-adrenergic receptors. This model provided a means whereby we could investigate the effects of racemic **1a**, as well as the respective enantiomers. This allowed us to investigate any pre/post α_2-receptor selectivity and also investigate the stereochemical requirements of these imidazolines at pre- and postjunctional α_2 receptors.

Table I. Radioligand-Binding Affinities for (*R*)- and (*S*)-**1a**

	α_1		α_2	
compd	K_i,[a] nM	*n*	K_i,[a] nM	*n*
(*R*)-**1a**	523 (402–681)	6	0.55 (0.3–0.9)	4
(*S*)-**1a**	817 (526–1269)	6	28 (25–32)	6
(±)-**1a**	400 (340–470)	8	6.5 (5.6–7.7)	6
NE	390 (370–410)	6	37 (35–39)	6
UK 14,304	740 (150–3700)	3	30 (25–38)	3
clonidine	520 (300–900)	5	30 (23–40)	3

[a] Geometric mean with 90% confidence limits in parentheses.

The affinity of the *R* and *S* enantiomers for the α_1- and α_2-adrenergic receptors was obtained from radioligand-binding assays with rat liver and [^{3}H]prazosin (α_1)[19] or rat cortex and [^{3}H]rauwolscine (α_2).[20] The values (Table I) are expressed as an equilibrium affinity constant (K_i), with lower K_i values reflecting better affinities for the respective adrenergic receptor.

Comparisons of the K_i values for the respective *R* and *S* enantiomers indicate both isomers have selectivity for the α_2 receptor. However, the *R* enantiomer shows much greater affinity for the α_2 receptor than does its enantiomeric counterpart. In fact, the *R* isomer shows extremely good affinity for the α_2-adrenergic receptor having a K_i of 550 pM, which is remarkable for agonist binding at adrenergic sites. Included in Table I is NE along with some known α_2 agonists for comparative purposes. As seen, none of the standard α_2-adrenergic agents approach the affinity seen with (*R*)-**1a**.

The more potent catechol enantiomer in all the various in vitro screens was shown to be the (+) enantiomer, which has the *R* absolute configuration. As shown in Table II, both the *R* and *S* enantiomers are full α_1-adrenergic agonists in the rabbit aorta with the *R* isomer being approximately 30-fold more potent than both the *S* enantiomer, as well as NE.

Interestingly, the affinity of (*R*)-**1a** and (*S*)-**1a** for the α_1 receptor is quite similar (cf. Table I) whereas the α_1

(15) Docherty, J. R.; Constantine, J. W.; Starke, K. *Naunyn-Schmiedeberg's Arch. Pharmacol.* **1981**, *317*, 5.
(16) Kyncl, J. J.; Buckner, S. A.; Bush, E. N.; DeBernardis, J. F.; Lin, C. T.; Warner, R. B. *Fed. Proc., Fed. Am. Soc. Exp. Biol.* **1985**, *44*, 1466.
(17) Constantine, J. W.; Lebel, W.; Archer, R. *Eur. J. Pharmacol.* **1982**, *85*, 325.
(18) Buckner, S. A.; Morse, P.; DeBernardis, J. F.; Kyncl, J. J. *Fed. Proc., Fed. Am. Soc. Exp. Biol.* **1986**, *45*, 2379.
(19) Hoffman, B. B.; et al. *Life Sci.* **1981**, *28*, 265.
(20) Perry, B. D.; U'Prichard, D. C. *Eur. J. Pharmacol.* **1981**, *76*, 461.

UM00013211
NOVARTIS EXHIBIT 1517
Novartis v. Regents, IPR2023-01347
Page 1957 of 4460

Table II. Indexes and ED_{50} Values for (*R*)- and (*S*)-1a in the Rabbit Aorta (α_1)

compd[a]	index[b] (ED_{50} NE/ED_{50} CPD)	*n*	E_{max}[b,c]	ED_{50} NE ($\times 10^7$)[d]	ED_{50} CPD ($\times 10^7$)[d]
(*R*)-1a	29 ± 4	5	128 ± 3	0.72 (0.42–1.23)	0.02 (0.01–0.03)
(*S*)-1a	1.0 ± 0.08	5	94 ± 8	0.68 (0.47–0.98)	0.67 (0.47–0.94)
(±)-1a	13 ± 2	31	114 ± 1	0.93 (0.68–1.25)	0.10 (0.08–0.13)

[a] All compounds were tested as their hydrobromide salts. CPD = test compound; NE = (−)-norepinephrine. [b] Mean of *n* experiments ± SEM. [c] Expressed as a percent of the maximum response of the tissue to NE. [d] Geometric mean with 90% confidence limits in parentheses.

Table III. Indexes and ED_{50} Values for (*R*)- and (*S*)-1a in the PBZ-DSV (α_2)

compd[a]	index[b] (ED_{50} NE/ED_{50} CPD)	*n*	E_{max}[b,c]	ED_{50} NE ($\times 10^7$)[d]	ED_{50} CPD ($\times 10^7$)[d]
(*R*)-1a	248 ± 58	5	102 ± 3	5.26 (3.16–8.76)	0.02 (0.01–0.04)
(*S*)-1a	15.4 ± 2.3	5	74 ± 4	6.02 (4.46–8.12)	0.41 (0.26–0.66)
(±)-1a	184 ± 25	8	102 ± 2	7.02 (5.85–8.42)	0.04 (0.03–0.06)

[a–d] See notes for Table II.

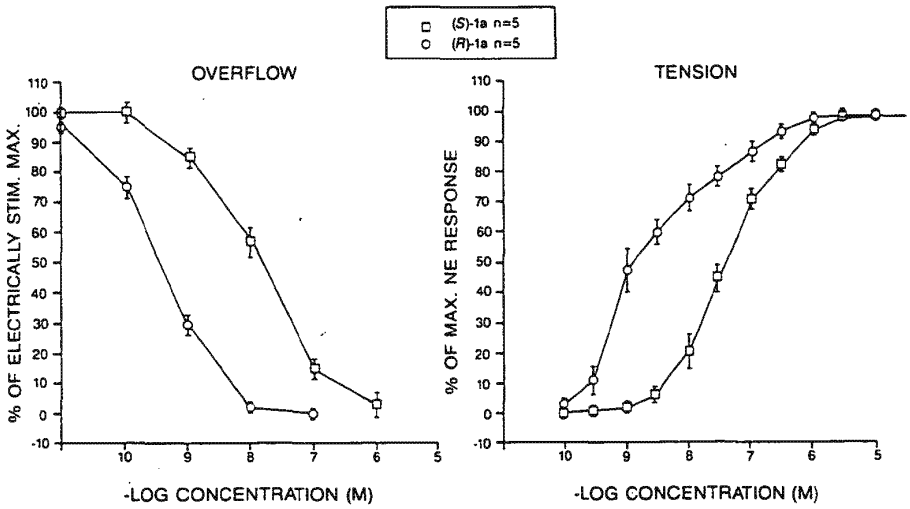


Figure 4. (a) Presynaptic α_2 activity in the PBZ-DSV. The electrical field stimulation (2 Hz, 9 V, 0.3 ms, 3 min) defines the maximum response. (b) Postsynaptic α_2 activity in the PBZ-DSV. Exogenous NE was used to define the maximum response.

potency of the two compounds differs considerably (cf. Table II). The reason for this is not apparent; however, as pointed out previously by Timmermans,[21] binding selectivity may not necessarily parallel agonist activiy since the former is a measure of receptor affinity, whereas the latter results from both affinity and intrinsic activity (efficacy).

When the enantiomers were evaluated for postjunctional α_2-adrenergic activity in the PBZ-DSV, once again the *R* enantiomer was more potent than the *S* enantiomer as seen in Table III. Both of these enantiomers were, however, very potent relative to NE. The *R* enantiomer was an extraordinarily potent α_2-adrenergic full agonist, approximately 250-fold more potent than NE. The *R* enantiomer is the most potent α_1- and α_2-adrenergic full agonist of which we are aware.

Comparisons of the α-subtype selectivity (ratio of the indexes; α_2/α_1) indicate that the *S* enantiomer is, perhaps, slightly more selective for the α_2-adrenergic receptor than is the corresponding *R* enantiomer, although the former is much less potent than the latter at α_2 sites.

In view of the potency associated with both of the catechol enantiomers at the postjunctional α_2 receptors of the DSV (cf. Table III, especially (*R*)-1a), we decided to investigate the biological activity of these imidazolines at the presynaptic α_2 receptors in this tissue. Additionally, we felt that information pertaining to the stereochemical requirements of imidazolines at both the pre- and postsynaptic α_2 receptors could thus be determined. The results of these studies from the DSV are shown in Figure 4a,b. Figure 4a illustrates the results obtained at the presynaptic α_2 receptor of the DSV for both enantiomers. As seen, (*R*)-1a was the more potent enantiomer at the presynaptic α_2 site causing the electrically stimulated release of [^{3}H]NE overflow to cease at approximately 10^{-8} M (IC_{50} = (0.39 ± 0.08) × 10^{-9} M) whereas (*S*)-1a required a concentration of 10^{-6} M to achieve the same effect (IC_{50} = (14.5 ± 4.4) × 10^{-9} M). For comparative purposes, the concentration–response curves for both enantiomers at the postsynaptic α_2 site in the DSV are shown in Figure 4b. As mentioned previously, (*R*)-1a is a more potent enantiomer (ED_{50} = (3 ± 1) × 10^{-9} M) than (*S*)-1a (ED_{50} = (44 ± 9) × 10^{-9} M). Both enantiomers are slightly selective for the presynaptic α_2 receptor relative to the postjunctional α_2 site on the basis of a comparison of the ED_{50} and IC_{50} values.

We feel the slight presynaptic selectivity of these enantiomers is not sufficient evidence on which to base a claim that the pre- and postsynaptic α_2-adrenoceptors of the DSV are different receptor proteins. However, it is apparent that the stereochemical requirements of the pre- and postsynaptic α_2 receptor in the DSV are identical since in both cases the *R* enantiomer was substantially more potent than the *S* antipode. This study represents the first

(21) Timmermans, P. B. M. W. M.; Matthews, W. D.; DeMarinis, R. M.; Hieble, J. P.; Mathy, M.-J.; Doods, H. N.; Thoolen, M. J. M. C.; DeJonge, A.; Wilffert, B.; VanZwieten, P. A. *Eur. J. Pharmacol.* 1984, *101*, 45.

UM00013212
NOVARTIS EXHIBIT 1517
Novartis v. Regents, IPR2023-01347
Page 1958 of 4460

reported case in which the α_2-receptor pharmacology of optically active imidazoline derivatives has been characterized at both presynaptic and postsynaptic α_2 sites in the same tissue. We have subsequently investigated α_2-presynaptic activity in the rabbit pulmonary artery[22] and reproduced the same results as reported above for the α_2 presynaptic receptor in the DSV (data not shown). It remains to be determined if the stereochemical requirements of these optically active imidazolines will be identical at other presynaptic α_2 receptors, from different tissues and/or animal species.

In summary, the resolution of the potent α-adrenergic agent 2-(5,6-dihydroxy-1,2,3,4-tetrahydro-1-naphthyl)-imidazoline has been accomplished and the absolute configuration of the enantiomers established. The more potent enantiomer was shown to have the *R* absolute configuration and in various in vitro screens was found to be extraordinarily potent at both α_1- and α_2-adrenergic receptors. In fact, (*R*)-**1a** is the most potent α_2 full agonist reported to date. In addition, (*R*)-**1a** possesses extremely good affinity for the α_2 receptor, far greater than any previously reported α_2 agonist. We have shown with these optically active imidazolines that, for the α_2 receptors in the DSV, the stereochemical requirements of imidazoline-containing compounds appears to be identical for activation of both the presynaptic as well as the postsynaptic α_2-adrenoceptors. Compound (*R*)-**1a** should prove to be of considerable value in pharmacologically characterizing α-adrenoceptors in other tissues and/or species. This is particularly true since only a limited number of optically active imidazolines have been reported, and (*R*)-**1a** has both good affinity and efficacy at α-adrenoceptors.

Experimental Section

Chemistry. Proton magnetic resonance (^{1}H NMR) spectra were recorded on a Nicolet NT-360 MHz instrument. Melting points were determined on a Thomas-Hoover Unimelt and are uncorrected. Elemental analyses were done in-house, and determined values are within 0.4% of theoretical values. The organic chemicals including *l*-NE were purchased from Aldrich Chemical Co., Milwaukee, Wi, and the PBZ was obtained from Smith Kline and French Laboratories, Philadelphia, PA.

Resolution of (±)-2-(5,6-Dimethoxy-1,2,3,4-tetrahydro-1-naphthyl)imidazoline (1b). Compound **1b** was resolved by fractional crystallization of the diastereomeric salts of both the (+)-dibenzoyl-D-tartaric and (−)-dibenzoyl-L-tartaric acids. Crystallization of the (+)-dibenzoyl-D-tartaric acid salt gave (*S*)-**1b** as the less soluble principal component of the diastereomeric mixture, while crystallization of the (−)-dibenzoyl-L-tartaric acid salt gave (*R*)-**1b**.

(±)-**1b** (13.4 g, 52 mmol) in 400 mL of MeOH was combined with 22.6 g (60 mmol) of (−)-dibenzoyl-L-tartaric acid monohydrate in 400 mL of MeOH. The flask was swirled and after several minutes precipitation of the salt occurred. The white solid was filtered and recrystallized from 1200 mL of hot MeOH, with slow cooling to room temperature. The resulting crystals were filtered and dried. The free base was obtained by the addition of cold aqueous NH_4OH to a CH_2Cl_2 solution of the salt. The organic layer was separated, dried ($MgSO_4$), filtered, and evaporated, affording a white solid (*R*)-**1b**, $[\alpha]^{25}_D$ +13.8° (free base, EtOH, c 0.0173). The sample was converted to the hydrochloride salt, mp 250–251 °C; $[\alpha]^{25}_D$ −11.0° (HCl salt, H_2O, *c* 0.010). Anal. ($C_{15}H_{21}ClN_2O_2$) C, H, N.

(±)-**1b** (10.35 g, 40 mmol) in 200 mL of MeOH was combined with 17.09 g (45 mmol) of (+)-dibenzoyl-D-tartaric acid monohydrate in 250 mL of MeOH. Precipitation of the salt occurred within minutes. This was filtered and recrystallized from 900 mL of hot MeOH and slowly cooled to room temperature. The crystals were filtered and the free base regenerated by cold NH_4OH as before, affording a white solid (*S*)-**1b**, $[\alpha]^{25}_D$ −13.6° (free base, EtOH, *c* 0.0119). The HCl salt was immediately formed, mp 250–251 °C; $[\alpha]^{25}_D$ +10.6° (HCl salt, H_2O, *c* 0.0126). Anal. ($C_{15}H_{21}ClN_2O_2$) C, H, N.

(*R*)- and (*S*)-2-(5,6-Dihydroxy-1,2,3,4-tetrahydro-1-naphthyl)imidazoline Hydrobromide (1a). The appropriate enantiomeric free base (1.6 g, 6 mmol) was dissolved in 25 mL of CH_2Cl_2 and then cooled to −22 °C, under N_2. Boron tribromide (1.95 mL, 20 mmol) in 5 mL of CH_2Cl_2 was added dropwise. Upon complete addition (ca. 5 min) the reaction mixture was stirred at −22 °C for 3 h. The reaction was quenched by dropwise addition of 20 mL of MeOH, and the solution was evaporated to dryness. The residue was taken up in 30 mL of EtOH and then evaporated to dryness once again. The resulting residue was triturated with CH_2Cl_2, filtered, and washed with Et_2O, affording the desired HBr salt. (*S*)-**1a**·HBr: yield, 1.36 g (72%); mp 270–271 °C; $[\alpha]^{25}_D$ −11.8° (HBr salt, EtOH, *c* 0.012), $[\alpha]^{25}_{436}$ −33.0° (HBr salt, MeOH, *c* 0.012); ^{1}H NMR (Me_2SO-d_6) δ 1.3–2.0 (4 H, m), 2.3–2.6 (2 H, m), 3.70 (4 H, s), 6.25 (1 H, d, *J* = 8 Hz), 6.60 (1 H, d, *J* = 8 Hz). Anal. ($C_{13}H_{17}BrN_2O_2$) C, H, N. (*R*)-**1a**·HBr: yield, 0.5 g (64%); mp 270–271 °C; $[\alpha]^{25}_D$ +12.5° (HBr salt, EtOH, *c* 0.024), $[\alpha]^{25}_{436}$ +33.3° (HBr salt, MeOH, *c* 0.013); ^{1}H NMR spectra (Me_2SO-d_6) identical with that of (*S*)-**1a**·HBr. Anal. ($C_{13}H_{17}BrN_2O_2$) C, H, N.

Estimation of the Enantiomeric Purity of (*R*)- and (*S*)-1a·HBr by ^{1}H NMR. ^{1}H NMR spectra of **1a** and **1b** were obtained in D_2O with *p*-dioxane as an internal reference. Initial concentrations of **1a** and **1b** were typically about 15 mM. After a preliminary spectrum was obtained, the sample was titrated with a 120 mM solution of CoATP in D_2O. Optimal spectral resolution was obtained at concentrations of approximately 5–7 mM in **1a** or **1b** and 40–60 mM in CoATP. Continued addition of CoATP resulted in extensive line broadening due to the rapid relaxation caused by the presence of the paramagnetic complex.

Rate Determinations for the Racemization of 1a and 1b. Reagent grade solvents or distilled water was used without further purification. The concentration of compounds for rate determinations was (3–4) × 10^{-2} M, and the concentration of Tris·HCl buffer was 50 mM. The pH of the solution of the compound in the Tris·HCl buffer was adjusted to 7.7 with 1 N KOH (a volume of only ca. 0.2% of the total solution volume was required). A water jacketed sample cell, 1 dm in length, with a volume of ca. 1 mL was used in a Perkin-Elmer 241 polarimeter equipped with a Haake FE2 thermostatically controlled circulating water bath for measurement of optical rotation. The first-order rate constant (for **1b** free base in ethanol) was taken from the slope of the line obtained by a least-squares fit of the ln (observed rotation) vs. time.

Crystallization and X-ray Analysis of (*S*)-1b. A crystal for single-crystal X-ray analysis was found in the salt of **1b** and (+)-dibenzoyl-D-tartaric acid. The compound crystallizes in the space group $P2_12_12_1$ from systematic absences, with the following crystal data: $C_8H_{14}O_8 \cdot C_{15}H_{20}O_2N_2$, *M* = 619, orthorhombic, *a* = 7.478 (2) Å, *b* = 18.336 (6) Å, *c* = 22.447 (10) Å, *V* = 3078 (2) Å^3, *Z* = 4, ρ(calcd) = 1.32 g/cm^3, *F*(000) = 1280, (Cu Kα) = 7.27.

Crystallographic data were collected with Cu Kα X-rays and a graphite monochromatic on a Syntex P3 four-circle diffractometer with the θ–2θ scan technique out to a 2θ of 116.0°. A variable-scan rate was used with a maximum of 29.30°/min and a minimum of 7.32°/min. The scan range was from 1.2° less than $K\alpha_1$ to 1.2° more than $K\alpha_2$; backgrounds, equivalent to the scan time, were counted at each end of the scan range. Three standard reflections were measured every 50 reflections; the data were corrected linearly for the 5% decay of the standards observed during data collection.

Of the 2436 reflections collected, 25 were rejected as systematically absent, leaving 2411 unique reflections of which 2011 met the condition $F_o > 5_\sigma(F_o)$ [OMIT 5]. The 25 non-hydrogen atoms of the acid were located by the MULTAN 80 program, and then by recycling these through MULTAN, the 19 non-hydrogen atoms of the base were also located. These 45 atoms were refined in SHELX 76 isotropically to *R* = 0.1403 and anisotropically with OMIT 5 to *R* = 0.0823. All hydrogens except the two OH hydrogens and the one NH hydrogen were fixed for the final two anisotropic refinements of the non-hydrogen atoms, giving a final *R* = 0.0631. The highest peak on the EMAP was 0.22 e/Å^3.

(22) Su, C.; Bevan, J. A. *J. Pharm. Exp. Ther.* **1970**, *172*, 62.

UM00013213
NOVARTIS EXHIBIT 1517
Novartis v. Regents, IPR2023-01347
Page 1959 of 4460

Pharmacology. α_1 Activities Using Isolated Rabbit Aorta. Female rabbits, weighing 2–5 kg, were sacrificed by cervical dislocation. The thoracic cavity was immediately opened and the descending aorta was removed and placed in a petri dish containing Krebs buffer saturated with 95% O_2 and 5% CO_2. The Krebs buffer solution was prepared as follows (mM concentrations): NaCl 119, $NaHCO_3$ 25, KCl 4.7, $MgSO_4$ 1.5, KH_2PO_4 1.2, $CaCl_2$ 2.5, glucose 11, Na_2EDTA 0.03, and ascorbic acid 0.3. The buffer was prepared daily from fresh dry reagents and was adjusted to a pH of 7.4.

A helical strip of aorta was mounted in a 10-mL tissue bath containing Krebs buffer and was attached to a force transducer (Grass or Statham) so that an initial tension of 2 g was applied. The tissue was allowed to equilibrate for 1 h during which time the tissue was washed four times and the tension reset to 2 g until it had stabilized. A mixture of 95% O_2 and 5% CO_2 was continuously bubbled through the tissue bath and reservoir. Stirring in the bath was provided by vigorous bubbling of the gas mixture. The temperature of the tissue bath was maintained at 37 ± 0.5 °C by means of a constant-temperature bath that circulated approximately 8 L/min of warmed water through the water jacket of the tissue bath. Standard weights were hung on the force transducers to calibrate them. Contractions, measured by the force transducers, were recorded on a Grass Model 7 polygraph, and periodic samples of the data were acquired by an on-line computer system that included a PDP 11/45 and DEC 10 computer.

A cumulative dose–response curve of contraction was produced with the standard agonist NE from 10^{-8} to 10^{-3} M doses. Drugs were adminstered by means of an adjustable microliter pipet in volumes usually from 10 to 100 μL. The response to each dose of standard or test compound was allowed to plateau before the administration of the next dose. Following a dose–response series, the tissue was washed with aliquots of buffer every 10–15 min for 60–90 min until the tension returned to base line or reached a plateau near the base-line level. The tension of the tissues was readjusted until it stabilized at 2 g before the next dose–response series.

Postsynaptic α_2 Activities Using PBZ-Pretreated DSV. Rings (3–4 mm wide) of lateral saphenous veins excised from beagle dogs of either sex were suspended in 10-mL tissue baths containing bicarbonate buffer of the following mM composition: NaCl 119, KCl 4.7, $CaCl_2$ 2.5, $MgSO_4$ 1.5, KH_2PO_4 1.2, $NaHCO_3$ 20, dextrose 11, ascorbic acid 0.3, Na_2EDTA 0.03, cocaine 0.03, hydrocortisone hemisuccinate 0.04, and propranolol 0.004. The solution was gassed with 95% O_2 and 5% CO_2 at 37 °C, pH 7.40. Isometric contractions of the tissues, preloaded with a tension of 2 g, were measured with Grass FTO3 strain gauges and recorded on a Grass Model 7 polygraph. Following an equilibration period of 15–20 min and maximal contraction by NE (10^{-4} M), the tissues were washed for 60 min at which time they were exposed to PBZ (10^{-7} M) for 30 min. At the end of the PBZ treatment, a thorough washout followed for 60 min. Tissues were then adjusted to 2-g tension, and a control cumulative dose–response curve was obtained for the standard agonist NE. After washout of norepinephrine (45–60 min), tissues were again equilibrated, and a cumulative dose–response curve of the tested agonist was obtained.

Simultaneous Evaluation of the Pre- and Postsynaptic α_2-Receptor Interactions. Helical strips of the DSV were preincubated for 1 h at 37 °C in 1 mL of vehicle containing [^{3}H]NE (0.375×10^{-6} M; 10 Ci/mmol) and then rinsed. The strips were exposed to PBZ (10^{-7} M) for 30 min and then mounted vertically between two platinum wire electrodes and attached to a force gauge transducer with a 2-g preload. The preparation was then superfused at a constant rate of 2 mL/min with the buffer composition as described above, saturated with 95% O_2 and 5% CO_2, at pH 7.40. An electrical field stimulation (2 Hz, 9 V, 0.3 ms, 3 min) was applied to the tissue in 48-min intervals to evoke release of endogenous NE. This was reflected by an increase of tritium overflow in the fractional 3-min collections of superfusate (presynaptic α_2 response) and mediation of the isometric contraction of the tissue (postsynaptic α_2 response). The test compounds were dissolved in the vehicle buffer in increasing molar concentrations and superfused over the tissue.

Radioligand-Binding Assays. Tissue Preparation. Twenty male Sprague–Dawley rats weighing 250–350 g were anesthetized with pentobarbital sodium (50 mg/kg, ip), and the brains and livers were quickly removed and placed in assay buffer (Tris·HCl, 50 mM, pH 7.7 at 25 °C) at 4 °C. Cerebral cortices were separated from the remainder of the brains, and tissues were pooled prior to homogenization. The organs were weighed, and pooled tissues were separately homogenized in 20 volumes of preparation buffer (Tris·HCl, 50 mM pH 7.7 at 25 °C containing 5 mM EDTA), with a Tekmar SDT homogenizer at full speed for two 10-s bursts. The homogenates were centrifuged at 50000g (4 °C) for 10 min, and the supernatant was discarded. The pellets were resuspended by homogenization as above in 20 volumes of preparation buffer and recentrifuged for 10 min, and the supernatant was again discarded. The final pellet was resuspended in 6.25 volumes of assay buffer, flash frozen in liquid nitrogen, and stored at −70 °C until the day of the experiment. Tissues were thawed at room temperature and thereafter maintained at 4 °C.

Assay Methods. All assays were performed in a light-subdued laboratory with a total incubation volume of 1.0 mL. Radioligand (450 μL) [either [^{3}H]prazosin (sp act. ~80 Ci/mmol, Amersham, Arlington Heights, IL) for α_1 assays[19] or [^{3}H]rauwolscine[20] (sp act. 80–90 Ci/mmol, New England Nuclear, Boston, MA) for α_2 assays] in assay buffer was incorporated with 50 μL of 0.3 mM ascorbic acid, containing phentolamine, 10^{-5} M (nonspecific binding), varying concentrations of test compounds, or no addition (total binding). Incubation commenced upon the addition of 500 μL of membrane homogenate in assay buffer, resulting in a final protein concentration of 50–150 μg/mL, determined by the method of Bradford.[23] Equilibrium binding was evaluated after a 50-min incubation at 25 °C for α_1-assays or a 2-h incubation period at 0 °C for α_2 assays. Receptor-bound radioligand was separated from free ligand by filtration under −180 mmHg vacuum through Whatman GF/B filters, which were dried in a hot-air oven at 60 °C. Three milliliters of Ready-Solv NA (Beckman) was added and the solubilized ligand was counted to a 4.5% 2σ error level in a Beckman LS3800 liquid scintillation counter at approximately 63% counting efficiency. The "added" radioligand tubes were not filtered, but 0.1 mL was dried on a filter, combined with 3 mL of Ready-Solv, and counted. Quenching was determined by the H# method.

In saturation binding experiments, eight to ten concentrations of radioligand between 10^{-11} and 10^{-8} M were utilized. Total (buffer control) and nonspecific (10^{-5} M phentolamine) binding were determined in triplicate at each concentration of radioligand. The radioligand affinity (K_D) and apparent receptor density (B_{max}) were evaluated by using the method of Scatchard.[24] Total and nonspecific binding data were also analyzed via the SCAFIT program of Munson and Rodbard,[25] to determine if the data could be best described by either a one- or two-site model.

In competition binding assays, total and nonspecific binding were each determined with five replicates. Specific binding was the arithmetic difference between total binding and nonspecific binding. Affinities of each of the tested compounds were evaluated by measuring the percent inhibition of specific binding, using at least four concentrations between 10^{-10} and 10^{-3} M, with duplicate determinations at each concentration. The concentration at which 50% inhibition of specific binding was observed, and the pseudo-Hill coefficients were calculated from the linear relationship between logit percent specific bound (log [% /|1 − %|]) vs. log concentration. The dissociation constant (K_i) was derived according to the equation of Cheng and Prusoff:[26]

$$K_i = IC_{50}/(1 + [L]/K_D)$$

The ligand concentration (L) used in this calculation was the arithmetic difference between the total ligand added to each incubation tube as determined from the counts in the "added" tubes and the radioligand bound at the IC_{50} concentration. The

(23) Bradford, M. M. *Anal. Biochem.* 1976, *72*, 248.
(24) Scatchard, G. *Ann. N.Y. Acad. Sci.* 1949, *51*, 660.
(25) Munson, P. J.; Rodbard, D. *Anal. Biochem.* 1980, *107*, 220.
(26) Cheng, Y. C.; Prusoff, W. H. *Biochem. Pharmacol.* 1973, *22*, 3099.
(27) Generated with in-house molecular graphics software. This view is for convergent or "cross-eyed" viewing. The use of a "stereoviewer" will present the reader with an image of the opposite absolute configuration.

UM00013214
NOVARTIS EXHIBIT 1517
Novartis v. Regents, IPR2023-01347
Page 1960 of 4460

ligand affinity for the receptors (K_D) was held constant for each radioligand.

Acknowledgment. We thank Dr. Richard Stephens for NMR spectroscopy, Dr. Steve Byrn for the X-ray data, and Karen Oheim, John Cain, Dusanka Stanisic, Robert Warner, Pat Morse, and Josef Cerny for technical assistance as well as Cyndy Davis and Joan Doerrer for typing this manuscript.

Supplementary Material Available: Tables of fractional atomic coordinates, thermal parameters, and bond lengths and bond angles for (*S*)-1b (3 pages). Ordering information is given on any current masthead page.

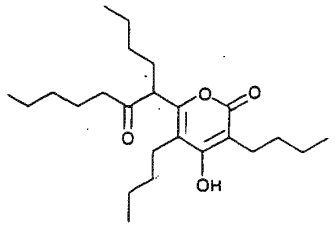
Inhibition of Human Sputum Elastase by Substituted 2-Pyrones[1]

Luisa Cook,[†] Bela Ternai,*[†] and Peter Ghosh[‡]

Department of Chemistry, La Trobe University, Bundoora 3083, Australia, and Raymond Purves Research Laboratories, University of Sydney, Royal North Shore Hospital, St. Leonards 2065, Australia. *Received September 10, 1986*

Nineteen 4-hydroxy- and 4-methoxy-2-pyrones related to elasnin (I) have been assayed for in vitro inhibition of human sputum elastase (HSE), porcine pancreatic elastase, α-chymotrypsin, and trypsin. Inhibition is reported as K_i and K_i'; percentage inhibition was dependent on [S] in a number of cases, making it unsuitable as a measure of relative inhibition. The 3-(1-oxoalkyl)-4-hydroxy-6-alkyl-2-pyrones were found to be most effective, the octyl homologue 11 being the most potent inhibitor (K_i = 4.6 μM, 30 times better than the lead compound). A further reduction in inhibition was observed when the hitherto hydrophobic 6-substituent was substituted by a branched functionality of hydrophilic nature. Conversely, methylation of the 4-hydroxy group of the 6-alkyl-2-pyrones increased inhibitory activity. The mechanism of inhibition varied from pure noncompetitive to mixed type to uncompetitive and was found to be dependent on the pattern of substitution. We believe that the 4-hydroxy-2-pyrone binds to the S_4 subsite, with the 6-substituent extending across the S_4–S_1 subsites and the 3-substituent occupying the S_5 subsite. The length of the inhibitor binding region was calculated to be approximately 24 Å. None of the hydrophobic compounds were found to have any appreciable inhibition (<10%) with porcine pancreatic elastase, bovine α-chymotrypsin, and bovine trypsin when tested at the limit of their solubility. The hydrophilic compounds were nonspecific, inhibiting all four enzymes. Dialysis was used to show that the interaction is fully reversible.

Human sputum elastase (HSE) has been implicated in many inflammatory disease states such as pulmonary emphysema, acute arthritis, and destruction of connective tissue.[2-5] The report by Omura et al.[6] that elasnin (I), an alkylated 2-pyrone of microbial origin, was a good inhibitor of HSE prompted us to use elasnin as a lead compound in the search for specific and potent inhibitors of HSE.



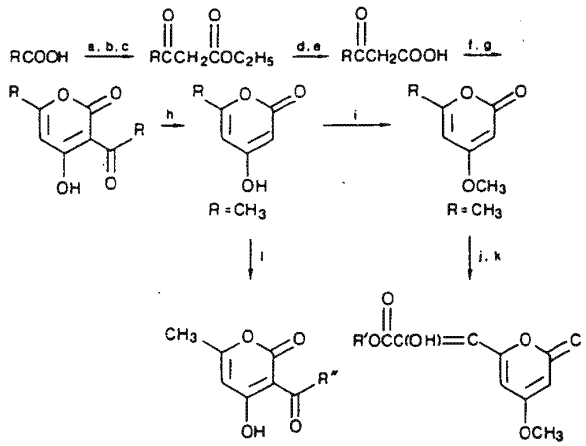
I

We report here the in vitro enzyme inhibitory properties of 19 elasnin analogues, their mechanism of action, the requirements of the inhibitor binding region, and its relationship to the substrate binding region.

Chemistry

The substituted 2-pyrones were prepared according to Scheme I. The 3-oxo carboxylate[7] was formed by reacting an acid imidazolide (formed in situ) with the neutral magnesium salt of ethyl hydrogen malonate.[8] Hydrolysis of the ester in 1 M NaOH afforded the 3-oxo carboxylic acid, which was cyclized by using 1.1 equiv of carbonyldiimidazole in THF[9] to afford the 3-(1-oxoalkyl)-4-hydroxy-6-alkyl-2-pyrones (pentyl to undecyl). Deacylation was easily carried out[10] by heating these 2-pyrones at 130 °C in 90% H_2SO_4. The 4-hydroxy group was methylated[11] by using dimethyl sulfate and anhydrous K_2CO_3

Scheme I[a]



[a] (a) Carbonyldiimidazole, THF, room temperature; (b) Mg(OOCCH$_2$COOC$_2$H$_5$); (c) H$^+$; (d) 1 M NaOH; (e) H$^+$; (f) carbonyldiimidazole, THF, room temperature; (g) H$^+$; (h) 90% H_2SO_4, 130 °C; (i) $(CH_3)_2SO_4$, K_2CO_3, petroleum ether (60–80 °C); (j) (R′OOC)$_2$, Na; (k) H$^+$; (l) R″COCl, CF_3COOH.

[†] La Trobe University.
[‡] University of Sydney.

(1) This is part 2 of a series. For part 1, see: Lentini, A.; Ternai, B.; Ghosh, P. *Biochem. Int.* 1985, *10*, 221.
(2) Janoff, A. *Annu. Rev. Med.* 1972, *23*, 177.
(3) Mittman, C., Ed. *Pulmonary Emphysema and Proteolysis*; Academic: New York, 1972.
(4) Lieberman, J. *Chest* 1976, *70*, 62.
(5) Janoff, A.; Feinstein, G.; Malemud, C.; Elias, J. M. *J. Clin. Invest.* 1976, *57*, 615.
(6) Omura, S.; Ohno, H.; Saheki, T.; Yoshida, M.; Nakagawa, A. *Biochem. Biophys. Res. Commun.* 1978, *83*, 704.

0022-2623/87/1830-1017$01.50/0 © 1987 American Chemical Society

UM00013215
NOVARTIS EXHIBIT 1517
Novartis v. Regents, IPR2023-01347
Page 1961 of 4460

This Page is Inserted by IFW Indexing and Scanning Operations and is not part of the Official Record

BEST AVAILABLE IMAGES

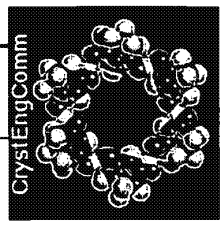
Defective images within this document are accurate representations of the original documents submitted by the applicant.

Defects in the images include but are not limited to the items checked:

- ☐ BLACK BORDERS
- ☐ IMAGE CUT OFF AT TOP, BOTTOM OR SIDES
- ☐ FADED TEXT OR DRAWING
- ☐ BLURRED OR ILLEGIBLE TEXT OR DRAWING
- ☐ SKEWED/SLANTED IMAGES
- ☐ COLOR OR BLACK AND WHITE PHOTOGRAPHS
- ☐ GRAY SCALE DOCUMENTS
- ☐ LINES OR MARKS ON ORIGINAL DOCUMENT
- ☐ REFERENCE(S) OR EXHIBIT(S) SUBMITTED ARE POOR QUALITY
- ☐ OTHER: _____

IMAGES ARE BEST AVAILABLE COPY.
As rescanning these documents will not correct the image problems checked, please do not report these problems to the IFW Image Problem Mailbox.

Crystal and co-crystal



Letter

Gautam R. Desiraju

School of Chemistry, University of Hyderabad, Hyderabad 500 046, India.
E-mail: desiraju@uohyd.ernet.in

Received 27th October 2003, Accepted 4th November 2003
First published as an Advance Article on the web 13th November 2003

Problems with nomenclature are necessary evils in the development of a new subject. As the subject of crystal engineering progresses, it is possible and indeed advantageous to assess terminology, keep what is good, and discard what is not required. Names are coined easily in the early days of a subject. This arises partly from enthusiasm and partly because it is difficult to describe new concepts with old names. Or so we seem to feel. As crystal engineering has evolved into a more mature discipline, one also realizes that some of the terms that we used during the last 15 years or so in describing crystals and their design and properties might not have been really necessary and that standard terminology in the existing chemical and crystallographic literature might well have sufficed. More particularly, I refer to the term *co-crystal* (also written as *cocrystal*).

I do not know exactly when this term came into the literature. Perhaps it was in the paper of Etter and Panunto on the complexing ability of 1,3-bis(*m*-nitrophenyl)urea.[1] Whatever the case, the term gained easy acceptance. The operational word here is 'easy'. Anyone could understand that a co-crystal was what one got in a co-crystallization experiment, and gradually the term came to be used for just about any two- and higher-component crystal. At this point, it would do one good to remember that we had (and still have) a perfectly good word to describe multi-component crystals, which have specific non-covalent interactions between the distinct molecules, and this is *molecular complex*.[2] For someone whose serious early chemical education included the study of Foster's book[3] on donor–acceptor complexes and Herbstein's illuminating work in this area[4] (for those too young to know or care, my Ph.D. topic was in the area of quinone–hydroquinone donor acceptor complexes), the term *molecular complex* was perfectly acceptable and I have used it invariably in my papers. Recently, however, the term *co-crystal* slipped into a paper (that too in the title) where I was not the corresponding author[5] and this has prompted the present letter.

I was always uncomfortable with the term *co-crystal* but not in ways I could express satisfactorily. For a start, the word *crystal* is too important, too meaningful and too evocative.[6] For those in the subject of crystal engineering, it is a sacrosanct word—something like *bond* to a chemist. Given the centrality of the concept of a crystal, what is a *co*-crystal? I never had any problems with *co-crystallization* or *co-crystallize* and indeed I use these terms regularly. It was the simple, easy word *co-crystal* that caused me problems. Now, a crystal is described both by a lattice, which gives us the symmetry information, and also by the atoms/ions/molecules that are contained in it, the chemical information. So how can something like 1 : 1 1,3-bis(*m*-nitrophenyl)urea–triphenylphosphine oxide masquerade as a co-crystal, when it has nothing in common with the crystal of either 1,3-bis(*m*-nitrophenyl)urea or that of triphenylphosphine oxide? What is co- to what? In the end, would brass become a co-crystal of copper and zinc? Or are my questions too naïve?

It was Herbstein again who, through his recent paper on composite crystals of 5-oxatricyclo[5.1.0.0^{1,3}]octan-4-one,[7] resolved my nebulous doubts and brought my objections to the present use of the term *co-crystal* into sharper focus. He defines a *composite crystal* as something that is formed by 'ordered agglutination of crystals of the same or different type'. He is speaking literally about two different crystals stuck together at the molecular level. This to my mind is a real co-crystal—two crystals that are joined together. In his paper written 40 years ago on hexabromobenzene, he provides us with another beautiful example of a composite crystal.[8] Because this crystal is pseudo-hexagonal with $c/a \sim 1/\sqrt{3}$, planes like (101) and (1 0 −1) or (301) and (001) coincide, but not exactly, and what one gets is a mosaic of crystals joined along these nearly common planes. In a recent authoritative work, Chapuis and his group discuss urotropin azelate.[9] These authors actually call this an 'unwilling co-crystal' in their paper title because each of the components, urotropin and azelaic acid, retain many of their original crystal traits in the conjunction of these substances. Now this is what I would call a good co-crystal because, once more, vestigial influences of former beings persist. However, so prevalent has the present connotation of the term *co-crystal* become that something that is a really good example of a co-crystal is referred to in almost exactly the opposite terms! The Chapuis group have another paper on the σ-structure of β-tantalum, and here the composite portions of a true co-crystal have different space groups.[10] This is not all. Alivisatos and co-workers have recently shown how a nanocrystal tetrapod of CdTe grows.[11] When it nucleates, it starts off as a cubic phase and when it branches out it switches to a hexagonal phase. Two crystals living together—I'd call this a co-crystal for sure. I will round off this selection of examples with Boese's fascinating studies of what he calls oligo-diffractometry.[12] Here we have crystals of polymorphs that are necessarily examined together in the diffraction experiment and their patterns deconvoluted later—a different type of co-crystal maybe but still a co-crystal. In none of these cases, however, has my image of a crystal been dimmed and yet we have two or more crystals somehow connected with each other intimately.

So what do we do with the 1 : 1 1,3-bis(*m*-nitrophenyl)urea–triphenylphosphine oxide co-crystal? For a start, I'd revert to calling it the 1 : 1 1,3-bis(*m*-nitrophenyl)urea–triphenylphosphine oxide molecular complex. This is a good term and a clear one at that. It tells us what is happening, and it is general enough. It may be distinguished from the terms *solid solution* or *inclusion compound* and the reader who is further interested in all these terminologies is well advised to read Kitaigorodskii's book.[2]

To conclude, when new terms enter the literature in a big way, and there is some controversy regarding their use, I would suggest that there are two possible courses of action. If the term is merely ambiguous, it may be easiest to just retain it because it has become too common. A good example of this situation is the use of the term *pseudopolymorph*.[13] But if something is scientifically suspect it must go, howsoever popular it might be. What is easy is sometimes not what is best.

 DOI: 10.1039/b313552g

This journal is © The Royal Society of Chemistry 2003

UM00013217
NOVARTIS EXHIBIT 1517
Novartis v. Regents, IPR2023-01347
Page 1963 of 4460

References

1 M. C. Etter and T. W. Panunto, *J. Am. Chem. Soc.*, 1988, **110**, 5896.
2 A. I. Kitaigorodskii, *Mixed Crystals*, Springer, Berlin, 1984, p. 275.
3 R. Foster, *Organic Charge-Transfer Complexes*, Academic Press, New York. 1969.
4 F. H. Herbstein, in *Perspectives in Structural Chemistry*, ed. J. D. Dunitz and J. A. Ibers, vol. IV, pp. 166–394, 1971.
5 J. Zyss, I. Ledoux-Rak, H. -C. Weiss, D. Bläser, R. Boese, P. K. Thallapally, V. R. Thalladi and G. R. Desiraju, *Chem. Mater.*, 2003, **15**, 3063.
6 G. R. Desiraju, *Nature (London)*, 2003, **423**, 485.
7 F. H. Herbstein, *Acta Crystallogr., Sect. B*, 2003, **59**, 303.
8 E. G. Boonstra and F. H. Herbstein, *Acta Crystallogr.*, 1963, **16**, 252.
9 M. Bonin, T. R. Welberry, M. Hostettler, M. Gardon, H. Birkedal, G. Chapuis, P. Mockli, C. A. Ogle and K. J. Schenk, *Acta Crystallogr., Sect. B*, 2003, **59**, 72.
10 A. Arakcheeva, G. Chapuis, H. Birkedal, P. Pattison and V. Grinevitch, *Acta Crystallogr., Sect. B*, 2003, **59**, 324.
11 L. Manna, D. J. Milliron, A. Meisel, E. C. Scher and A. P. Alivisatos, *Nat. Mater.*, 2003, **2**, 382.
12 R. Boese, M. T. Kirchner, W. E. Billups and L. R. Norman, *Angew. Chem. Int. Ed.*, 2003, **42**, 1961.
13 R. K. R. Jetti, R. Boese, P. K. Thallapally and G. R. Desiraju, *Cryst. Growth Des. ASAP.*

UM00013218
NOVARTIS EXHIBIT 1517
Novartis v. Regents, IPR2023-01347
Page 1964 of 4460

Crystal engineering: Outlook and prospects

Gautam R. Desiraju

School of Chemistry, University of Hyderabad, Hyderabad 500 046, India

Crystal engineering continues to attract the interest of organic and physical chemists, crystallographers and materials scientists. This article discusses some current challenges in this area and outlines some prospects. Owing to the rapid recent advances, the scope of the present article is necessarily subjective.

CRYSTAL engineering or the design of organic solids with specific physical and chemical properties continues to elicit intense interest[1]. This new subject encompasses a wide variety of research activity ranging from the understanding of crystal packing in organic molecular solids to the design of open network structures based on metal–ligand coordinate bonds, the so-called coordination polymers. On the other hand, one is able to analyse and understand with increasing certainty the vast amounts of accurate data currently available from crystallographic databases, while on the other, an appreciation of a phenomenon like polymorphism can lead to immediate benefits in applied areas such as pharmaceutical development[2]. The work of Schmidt on topochemistry is considered by many to represent the formal beginnings of crystal engineering (Box 1). The seventies could be considered as something of a hiatus, but interest widened in the eighties to more general studies of intermolecular interactions. With a better appreciation of these interactions, the identification of a crystal as a supermolecule in the nineties appears natural. In the early 2000s, crystal engineering is moving from structure engineering to property engineering.

The brief chronological scheme outlines the progress of crystal engineering during the last 50 years, and more so since the late 1980s from when onwards the attention of the chemical community has become more fully focused on it.

Crystal structure from molecular structure

Around sixty years ago, Pauling and Delbrück stated that in any kind of molecular recognition, and this includes the recognition between identical molecules, it is the dissimilar rather than the similar functionalities that come into closest contact[3]. Because the supramolecular behaviour of a particular functional group depends on the nature and location of other groups in the molecule, crystal structures of organic molecules need not necessarily be derived in a straightforward way from the functional groups present. Crystal engineering is, in this respect, distinct from traditional organic chemistry. Simple relationships between molecular and crystal structure are ideal but in practice, only obtained when *interference* between orthogonal sets of interactions is minimal. In such cases, the interactions are said to be insulated from one another but when and why such *insulation* occurs is still not evident. Accordingly, the crystal structures of many 'simple' organic compounds are hard to understand and harder to predict.

Since functional groups do not adequately reflect molecules → crystal transforms, how then does one attempt to understand recognition and crystallization events in chemical terms? In this regard, there have been attempts to identify multimolecular units that more accurately reflect the relationships between molecular and supramolecular structure. The descriptor *supramolecular synthon* signifies a larger structural unit, within the most robust and useful of which is encoded the optimal information inherent in the mutual recognition of molecules to yield crystals. Inherent in this term 'synthon' are ideas of size economy and maximum information content. Very large structural units will naturally contain more information, but these are accompanied by unnecessary detail, while very small units may lack sufficient and critical information regarding supramolecular structure. For example, the crystal structures of all the three isomeric aminophenols, **1**–**3**, contain the O–H···N and N–H···O synthon **4**. Knowing that the *ortho* and *meta* isomers, **1** and **2**, have a very different crystal structure from the *para* compound, **3**, one may then conclude that synthon **4** is too small to discriminate between alternative structural possibilities. A better, that is more representative, supramolecular synthon is **5**; this is found in the crystal structures of **1** and **2** but absent in the structure of **3**. In effect, the most useful supramolecular synthons combine form with compactness[4].

Weak intermolecular interactions and crystal packing

Conventional hydrogen bonding is the pivotal interaction in many crystal structures but a number of weaker and softer interactions have been shown to play a role

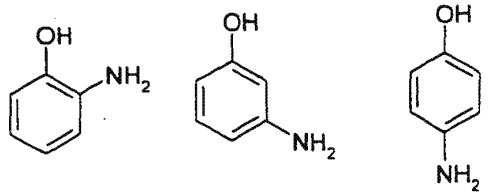
e-mail: desiraju@uohyd.ernet.in

UM00013219
NOVARTIS EXHIBIT 1517
Novartis v. Regents, IPR2023-01347
Page 1965 of 4460

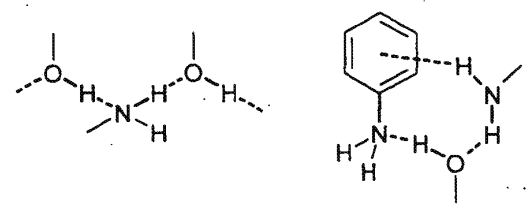
Box 1. Chronology of crystal engineering.

1951	J. M. Robertson's paper (*Proc. R. Soc. London*, 1951, **A207**, 101) on crystal structures of polynuclear aromatic hydrocarbons.
1964	G. M. J. Schmidt's series of papers (*J. Chem. Soc.*, 1964, 2000; 2014; 2041; 2051; 2060; 2068) on the solid state photochemistry of cinnamic acids and other alkenes – the topochemical principle.
1971	Introduction of the term *crystal engineering* by Schmidt (*Pure Appl. Chem.*, 1971, **27**, 647).
1970s till mid-1980s	Development of organic solid state chemistry in the Weizmann Institute (reaction cavity and hydrogen bonding: M. D. Cohen, M. Lahav, L. Leiserowitz), University of Illinois (phase transformations, gas–solid reactions and crystal polarity: D. Y. Curtin, I. C. Paul), University of Freiburg (diacetylene polymerisation: G. Wegner, V. Enkelmann) and University of Cambridge (topotaxy: J. M. Thomas, W. Jones).
1988	First systematic analysis of an interpenetrated structure of a molecular solid. O. Ermer's paper on adamantane-1,3,5,7-tetracarboxylic acid, *J. Am. Chem. Soc.*, 1988, **110**, 3747.
1989	Robertson revisited. Paper by G. R. Desiraju and A. Gavezzotti entitled 'From molecules to crystal structure: Polynuclear aromatic hydrocarbons', *Chem. Commun.*, 1989, 621.
1989	G. R. Desiraju's monograph *Crystal Engineering. The Design of Organic Solids*, Elsevier, Amsterdam, 1989. This work showed that the subject of crystal engineering goes far beyond organic solid state chemistry, and is still the only single author book on the subject.
1990	R. Robson's paper on interpenetrated structures of transition metal coordination compounds, *J. Am. Chem. Soc.*, 1990, **112**, 1546.
1991	Identification of an organic crystal as a 'supramolecule par excellence' (J. D. Dunitz, *Pure Appl. Chem.*, 1991, **63**, 177) and a few years later by J.-M. Lehn, *Supramolecular Chemistry: Concepts and Perspectives*, VCH, Weinheim, 1995.
mid-1990s	The subject enters mainstream organic chemistry. Crystal engineering is identified as a form of supramolecular synthesis. Three definitive reviews appear in this and related contexts: (a) G. M. Whitesides *et al.*, Noncovalent synthesis: Using physical organic chemistry to make aggregates, *Acc. Chem. Res.*, 1995, **28**, 37; (b) G. R. Desiraju, Supramolecular synthons in crystal engineering – a new organic synthesis, *Angew. Chem. Int. Ed. Engl.*, 1995, **34**, 2311; (c) J. F. Stoddart *et al.*, Synthetic supramolecular chemistry, *Acc. Chem. Res.*, 1997, **30**, 393.
1996	The first edited book on the subject appears. *The Crystal as a Supramolecular Entity* (ed. G. R. Desiraju), *Perspectives in Supramolecular Chemistry*, Wiley, Chichester, 1996, vol. 2.
1996	Crystal engineering is the theme of keynote lectures for the first time in a Congress of the International Union of Crystallography. Lectures are given by A. Gavezzotti and G. R. Desiraju at the Seattle Congress.
1996	First conference devoted exclusively to crystal engineering is held at Digby, Nova Scotia and is organized by M. J. Zaworotko and K. R. Seddon. The study of coordination polymers begins to develop as a distinct branch of crystal engineering, especially in North America (O. M. Yaghi, R. D. Rogers). Inorganic chemists get involved (A. Müller, J. Atwood, D. Braga).
1998	Crystal engineering makes its debut in the Erice series of conferences with a school organised by F.H. Allen and J.A.K. Howard. This is followed a year later by a very similar meeting organized there by D. Braga and A. G. Orpen.
1998	Launching of the first journal on the subject: *Crystal Engineering* (Elsevier).
1999	Crystal engineering becomes a microsymposium topic for the first time in an I.U.Cr. Congress. G. R. Desiraju, M. J. Zaworotko and R. D. Rogers co-chair at the Glasgow Congress.
1999	The Royal Society of Chemistry launches its own journal *Cryst. Eng. Comm.* It is the second all-electronic journal of the RSC. The subject now has clear contours and may be distinguished from materials chemistry for which the society has a separate journal.
2000	The first dramatic application of crystal engineering – a crystalline sensor that can detect gaseous SO_2 at ppm level is described in a paper by van Koten *et al.* (*Nature*, 2000, **406**, 970). The subject is moving from structure engineering to property engineering.
2001	The subject has come of age. The American Chemical Society unveils its journal *Crystal Growth and Design*, to cover all aspects of crystal engineering.
2001	Crystal engineering and supramolecular chemistry in biological and material sciences is featured in a *Nature* review by G. R. Desiraju, *Nature*, 2001, **412**, 397.
2002	The first *CrystEngComm* discussion meeting on innovations in crystal engineering will be held at Bristol University, July, 2002 and will be sponsored by the RSC.

UM00013220
NOVARTIS EXHIBIT 1517
Novartis v. Regents, IPR2023-01347
Page 1966 of 4460



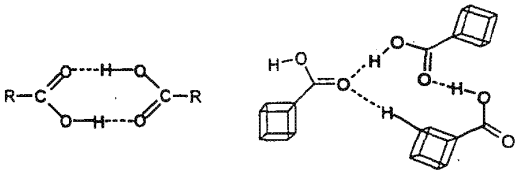
1 2 3



4 5

also in structure stabilization. This role can vary from unimportant to supportive to one that is actually intrusive. In this last case, the weak interactions may actually distort and modify the topology and arrangement of the conventional and stronger interactions[5]. Weak hydrogen bonding and polarization-induced heteroatom interactions are examples of these secondary interactions whose exact nature has still not been fully elucidated. As mentioned above, interaction insulation is always desirable and one would like to study the weaker interactions from this viewpoint.

The study of weak interactions will continue to be important in the design of supramolecular structures, because these interactions are able to alter predicted structures in dramatic ways[6]. Take for instance the crystal packing of carboxylic acids. The common mode of association of carboxyl groups is via the centrosymmetric dimer synthon 6. However, in the family of cubanecarboxylic acids, the dimer synthon gives way to an



6 7

exotic pattern–carboxyl groups of alternating syn and anti-conformation form an infinite O–H...O hydrogen bonded catemer, 7, that is stabilized by a C–H...O hydrogen bond from an activated cubyl C–H group. The assumption is that in the absence of the cubyl group, the unusual catemer structure would not be obtained but rather that the more common dimer would be found.

Supramolecular synthetic strategies

The study of a family of compounds provides insight into packing characteristics that may be exploited in the design of new and related structures. The identification of a crystal as a retrosynthetic target follows from the depiction of a crystal structure as a network with the molecules as the nodes and the supramolecular synthons as the node connectors. In this context, the organic diamondoid network solids are of relevance. Our interest in the study of such solids originated from observations of molecular-supramolecular equivalence in the tetraphenylmethane family of structures. For example, tetraphenylmethane, and CBr_4 form a 1:1 molecular complex, that is nearly isostructural with tetrakis-(4-bromophenyl)methane[7]. Following on these lines, we have recently described a diamondoid structure built up with $I\cdots NO_2$ interactions for diiododinitrotetraphenylmethane[8].

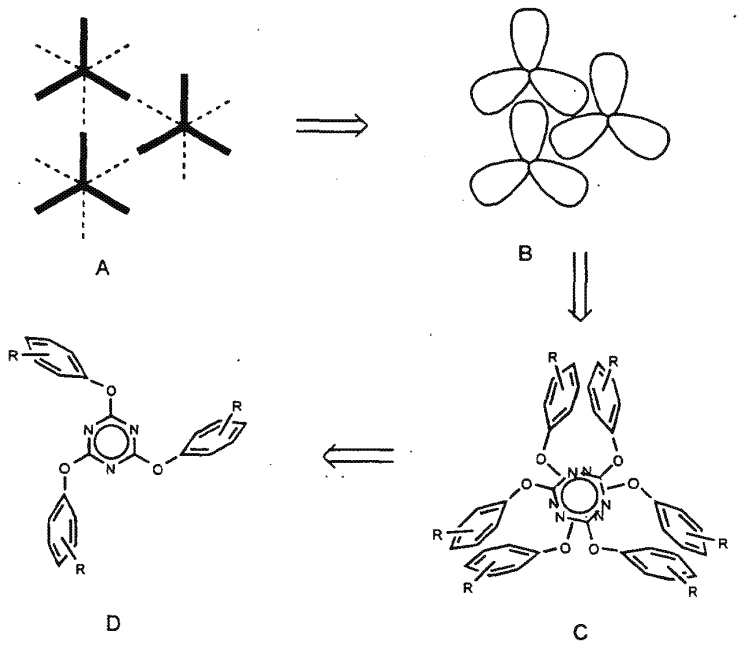
Crystal structures from X-ray powder diffraction data

With the tremendous increase in the range of chemical systems being studied in crystal engineering, an all-too common occurrence is the failure to obtain diffraction quality single crystals. Clearly one would not like to abandon a research project for such a reason. The growth and development of methods of structure determination from X-ray diffraction patterns of polycrystalline samples is therefore becoming of increasing importance[9]. Among the difficulties encountered commonly in the use of such methods are the overlap of non-equivalent reflections in powder patterns, the indexing of patterns of low crystal symmetry and the dependence of the pattern on inhomogeneities in microcrystal size and orientation. Structures of purely organic compounds are difficult to solve because of the absence of strong scatterers, but direct space methods offer a new approach[10]. Synchrotron X-ray and high resolution neutron diffraction sources are very useful but are not commonly available and conventional X-rays are therefore used also.

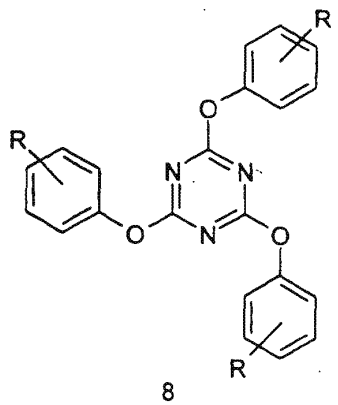
Functionalized solids

Crystal engineering targeted at solids exhibiting large optical non-linearities has attracted much interest[11]. The traditional design of NLO active materials has concentrated exclusively on dipolar molecules and in effect ignored the wealth of possibilities that could arise from two- and three-dimensional self-assembly. Diversified

UM00013221
NOVARTIS EXHIBIT 1517
Novartis v. Regents, IPR2023-01347
Page 1967 of 4460



Scheme 1.



8

investigations of more isotropic molecules, such as 2,4,6-triamino-1,3,5-trinitrobenzene, with attached octupolar and multipolar and non-linearities have been proposed but these investigations have been confined to the molecular rather than extended to the supramolecular or crystalline level.

A typical symmetry pattern that leads to crystalline octupolar non-linearity is the trigonal network **A** constituted with trigonal molecules (Scheme 1). Retrosynthetic analysis applied to **A** leads one to think in terms of synthons such as **B**. Crystalline triaryloxy substituted 1,3,5-triazines from stacked molecular diads called *Piedfort Units* (PUs) and such PUs, which in themselves are supramolecular species, **C** may be derived retrosynthetically from **B**. The ultimate molecular starting point of this supramolecular synthesis is a series of substituted 2,4,6-triphenoxy-1,3,5-triazines, **D**. To summarize, the retrosynthetic analysis **A** ⇒ **B** ⇒ **C** ⇒ **D** has to ensure that the three-fold hierarchy is preserved at each stage of supramolecular construction from **D** to **A**. This is by no means trivial because it implies a carry over of molecular symmetry into the supramolecular structure. However, in a family of triazines, **8**, quasi-trigonal or trigonal networks are the rule rather than the exception[12], and measurable SHG powder signals of around 0.10 × urea are obtained.

Polymorphism

Originally an enigma, then a curiosity, polymorphism[13] today may be central to our understanding of crystallization mechanisms. Crystallization is inherently a very efficient process and nature seems to have developed ways and means to eliminate alternative pathways[2]. Given the complementary nature of molecular recognition and the importance of enthalpic, entropic and kinetic factors, it would appear reasonable that the events during crystallization should be quite specific to the

UM00013222
NOVARTIS EXHIBIT 1517
Novartis v. Regents, IPR2023-01347
Page 1968 of 4460

molecule in question and that the possibility of obtaining two or more forms (especially in the same crystallization batch) is unlikely. Polymorphism is a complex phenomenon. Its occurrence is more frequent in compounds that are conformationally flexible and also contain groups that are able to form strong hydrogen bonds, like –OH, $-NH_2$, $-CO_2H$, and $-CONH_2$. The fact that these groups are commonly found in drug molecules makes this phenomenon of outstanding significance in pharmaceutical development.

Conclusions

The design of organic solids with potential applications as useful materials is an evolving subject. However, this new subject of crystal engineering contains features additional to those that are characteristic of molecule-based organic chemistry. Ability to plan and design crystal structures will depend very largely on thinking supramolecularly and on viewing a crystal structure as a blend of a very large number of interactions of various types and strengths. Within this complexity one must try to identify interactions or supramolecular synthons that will carry through across an entire family of structures with the aim of identifying a set of related molecules that yield a set of related crystal structures. The need to minimise interaction interference is therefore paramount. The resulting modularity in the crystal design process will render feasible three-dimensional structure control. The study of polymorphism is not a distinct endeavour from the control of crystal packing in that the need to understand the nature of weak interactions is acutely felt in both cases. The challenging nature of many of these tasks should ensure lively activity in the future.

1. Desiraju, G. R., *Chem. Commun.*, 1997, 1475–1482.
2. Desiraju, G. R., *Science*, 1997, **278**, 404–405.
3. Pauling, L. and Delbrück, M., *Science*, 1940, **92**, 77–79.
4. Allen, F. H., Hoy, V. J., Howard, J. A. K., Thalladi, V. R., Desiraju, G. R., Wilson, C. C. and McIntyre, G. J., *J. Am. Chem. Soc.*, 1997, **119**, 3477–3480.
5. Desiraju, G. R. and Steiner, T., *The Weak Hydrogen Bond in Structural Chemistry and Biology*, Oxford, 1999.
6. Kuduva, S. S., Craig, D. C., Nangia, A. and Desiraju, G. R., *J. Am. Chem. Soc.*, 1999, **121**, 1936–1944.
7. Reddy, D. S., Craig, D. C. and Desiraju, G. R., *J. Am. Chem. Soc.*, 1996, **118**, 4090–4093.
8. Thaimattam, R., Sharma, C. V. K. M., Clearfield, A. and Desiraju, G. R. *Cryst. Growth Des.*, 2001, **1**, 103–106.
9. Poojary, D. M. and Clearfield, A., *Acc. Chem. Res.*, 1997, **30**, 414–422.
10. Tedesco, E., Harris, K. D. M., Johnston, R. L., Turner, G. W., Raja, K. M. P. and Balaram, P., *Chem. Commun.*, 2001, 1460–1461.
11. Zyss, J. (ed.), *Molecular Nonlinear Optics: Materials, Physics and Devices*, Academic, Boston, 1994.
12. Thalladi, V. R., Brasselet, S., Weiss, H.-C., Bläser, D., Katz, A. K., Carrell, H. L., Boese, R., Zyss, J., Nangia, A. and Desiraju, G. R., *J. Am. Chem. Soc.*, 1998, **120**, 2563–2577.
13. Threlfall, T. L., *Analyst*, 1995, **120**, 2435–2460.

Other key references are provided in the chronology.

ACKNOWLEDGEMENT. I thank the Department of Science and Technology, Government of India for its support of my research programmes.

UM00013223
NOVARTIS EXHIBIT 1517
Novartis v. Regents, IPR2023-01347
Page 1969 of 4460

Acta Cryst. (1972). B28, 1864

The Structure of the Crystalline Complex Estradiol.Urea (1:1)

BY WILLIAM L. DUAX

Medical Foundation of Buffalo, 73 High Street, Buffalo, New York 14203, *U.S.A.*

(*Received* 12 *April* 1971 *and in revised form* 17 *November* 1971)

The crystal data for the complex estradiol.urea (1:1), $C_{18}H_{24}O_2.CON_2H_4$, are $a=24{\cdot}631$ (1), $b=7{\cdot}951$ (1), $c=9{\cdot}302$ (1) Å, orthorhombic $P2_12_12_1$, $Z=4$, $D_x=1{\cdot}20$, $D_m=1{\cdot}20$ g.cm^{-3}. Three-dimensional data were collected on a single-crystal counter diffractometer. The structure was solved from a set of phases derived from two-dimensional structure invariants, with phasing extended by application of the tangent formula. Refinement by a block-diagonal least-squares procedure resulted in a final R of 6·3% for 1886 observed reflections. All hydrogen atoms were located in difference electron density syntheses, and their coordinates were refined by least-squares methods. The basic packing pattern observed in numerous steroid crystals, infinite chains of steroids hydrogen-bonded head to tail, is retained in the complex. The urea molecules bind the steroids together with an extensive hydrogen-bonding network in which each urea is hydrogen-bonded to four different steroid chains. Comparison of the thermal motion of the urea molecule in the complex with that of urea crystallized in a tetragonal space group, suggests that the nonrigid body motion observed in the complex is a result of differences in hydrogen-bonding to the two nitrogen atoms and the absence of crystallographically imposed symmetry.

Introduction

As part of an investigation of steroid complex formation and crystallization, the stable crystalline complexes cortisol.urea (1:1) and estradiol.urea (1:1) have been prepared. The crystal-structure study of the estrogen complex was undertaken in order to determine the configuration of the complex, the extent of hydrogen bonding in the crystal structure, and the alteration, if any, of the steroid packing pattern as a result of complex formation. A schematic representation of the steroid molecule, showing the numbering of atoms and ring designations, is given in Fig. 1. Hydrogen atoms are omitted from the diagram, but are given the same numbering as the carbon atoms to which they are attached. Where appropriate, the hydrogen atoms are also designated β or α, depending on their orientation relative to the top (β) or under (α) side of the molecule.

Experimental

Large columnar crystals of estradiol.urea (1:1) were grown from a benzene solution containing a 1:10 molar ratio of steroid to urea. A cuboid crystal, 0·2 mm on an edge, was used for data collection. All X-ray measurements were made on a General Electric single-crystal counter diffractometer. The crystal was mounted with the c axis parallel to the φ axis of the instrument. The systematic extinctions ($h00$, $h=2n+1$; $0k0$, $k=2n+1$; $00l=2n+1$) indicate the orthorhombic space group $P2_12_12_1$. The unit-cell dimensions were obtained from a least-squares calculation, based on 2θ measurements of 35 hkl α_1 and α_2 reflections having $2\theta>85°$. The density was measured by flotation in an aqueous potassium iodide solution. The crystal data are presented in Table 1.

Table 1. *Crystal data for estradiol.urea* (1:1)

$C_{18}H_{24}O_2.CON_2H_4$	F.W.332·4
Orthorhombic	Space group $P2_12_12_1$
$a=24{\cdot}631$ (1) Å	$Z=4$
$b=7{\cdot}951$ (1)	$F(000)=720$
$c=9{\cdot}302$ (1)	$D_m=1{\cdot}20$ g.cm^{-3}
λ(Cu $K\alpha_1$) = 1·54051 Å	$D_x=1{\cdot}20$
λ(Cu $K\alpha_2$) = 1·54438	

The intensities of 2088 independent reflections, with 2θ less than 145°, were measured by the stationary-crystal stationary-counter technique. The background was a uniform function of 2θ above 45°, and a background correction curve was constructed from balanced nickel–cobalt measurements of 15% of the data in this range. Reflections were considered unobserved

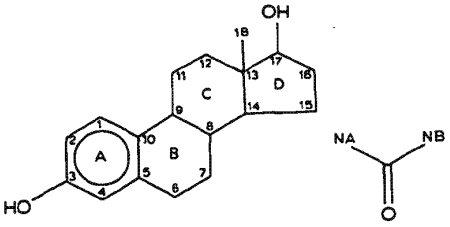
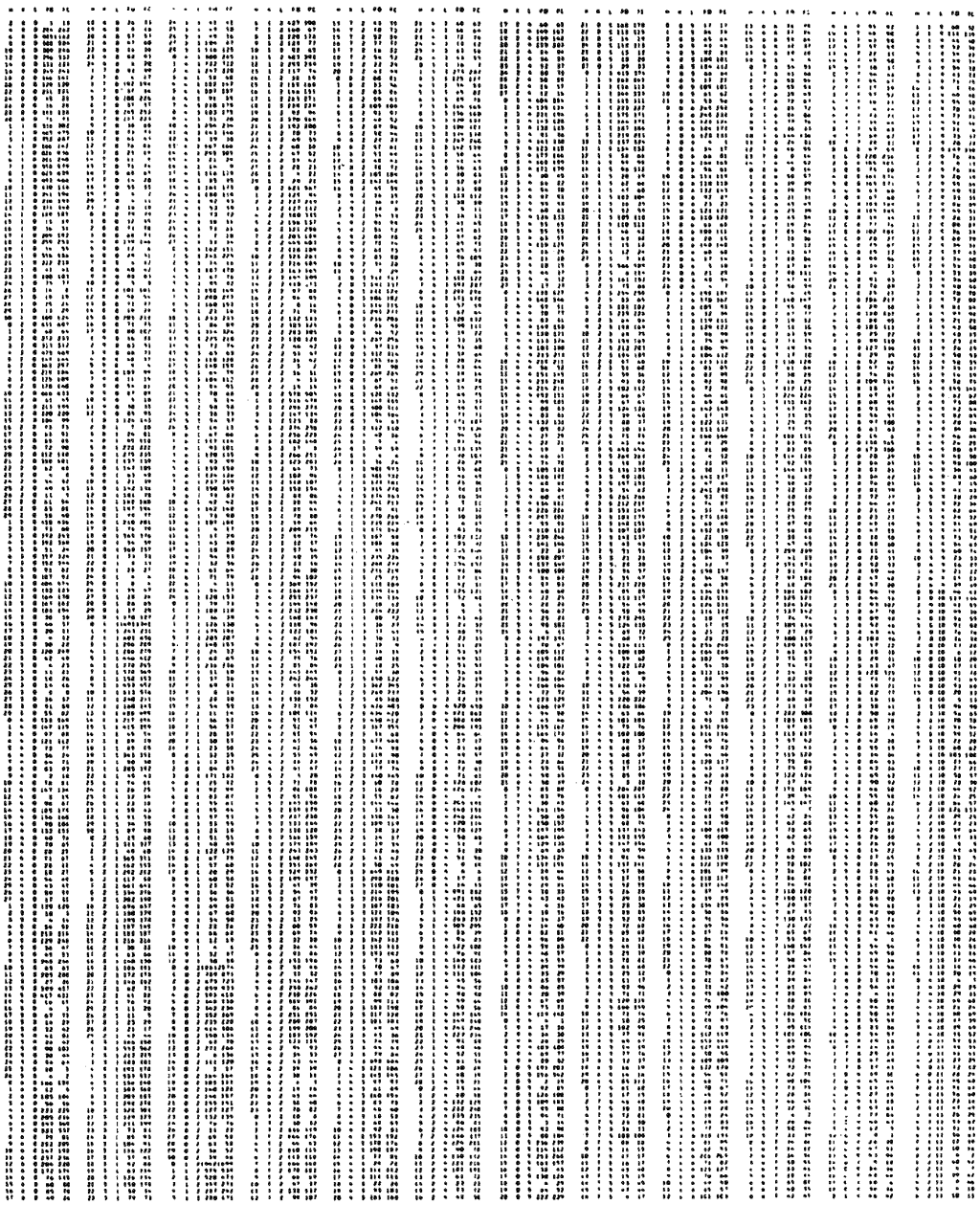


Fig. 1. Schematic representation of the steroid molecule showing the numbering of atoms and ring designation.

UM00013224
NOVARTIS EXHIBIT 1517
Novartis v. Regents, IPR2023-01347
Page 1970 of 4460

if the net count was less than twice the standard deviation of the background. Cobalt-filtered background measurements were made for all data with 2θ less than 45°. Calibrated nickel filters were used in the measurement of the most intense reflections. No significant changes were observed in the intensities of five standard reflections measured daily during the period of data collection. The intensity of the 006 reflection ($\chi = 90°$, $2\theta = 59{\cdot}6°$) varied up to a maximum of $\pm 2{\cdot}0\%$ from its mean value within the φ range in which data were

Table 2. *Comparison of the observed structure factor amplitudes with those calculated* ($\times 10$) *from the refined atomic parameters for the structure of estradiol.urea* (1:1)



UM00013225
NOVARTIS EXHIBIT 1517
Novartis v. Regents, IPR2023-01347
Page 1971 of 4460

collected. Intensities were corrected for Lorentz and polarization factors but not for absorption ($\mu R = 0{\cdot}07$).

Structure determination

The structure was determined by a phasing procedure, based on the two-dimensional structure invariants $\cos(\varphi_1+\varphi_2+\varphi_3)$ whose values were calculated by a recently developed formula. The phasing process is described fully in the preceding paper (Duax, Weeks & Hauptman, 1971). A structure-factor calculation, based on positional parameters for the 24 nonhydrogen atoms taken from the E map, resulted in an R index ($R=\sum||F_o|-|F_c||/\sum F_o$) of 0·46. After five cycles of refinement of the positional parameters and anisotropic thermal parameters of the nonhydrogen atoms, R was lowered to 0·11. A three-dimensional Fourier difference synthesis, calculated without the contributions of the hydrogen atoms to the structure factors, produced well-defined electron densities corresponding to the 28 hydrogen atoms. Introduction of these atoms into the structure-factor calculations lowered R to 0·08. Three more refinement cycles were performed, which included refinement of the positional and isotropic thermal parameters of the hydrogen atoms. The scattering factors used throughout the refinement were taken from *International Tables for X-ray Crystallography* (1962). The refined thermal parameters for the hydrogen atoms ranged from 0·5 for hydrogen atoms of the bridgehead carbon atoms to 5·0 for the hydrogen atoms of carbon atoms having the largest anisotropic motion. This variation of thermal motion was considered to be largely spurious, and the hydrogen thermal parameters were held constant at 2·5 in the last three cycles of refinement. The calculated intensities of the two most intense reflections were 25% higher than the observed intensities. This was assumed to be due to extinction and these reflections were not included in the final refinement. In the last refinement cycles, a weighting scheme in which $1/w=[(|F_o|-15)/15^2+1]^{1/2}$ was used in order that $\langle w\triangle^2\rangle$ remain invariant with $|F_o|$. Refinement was terminated when all parameter shifts were less than one-half their standard deviations and the minimization function, $\sum_w(|F_o|-|F_c|)^2/(m-n)$, was 0·80. The final R values were 0·07 for all reflections and 0·063 for the 1886 observed reflections. Table 2 lists the final observed and calculated structure factor amplitudes. Final atomic positional and thermal parameters are given in Tables 3 and 4.

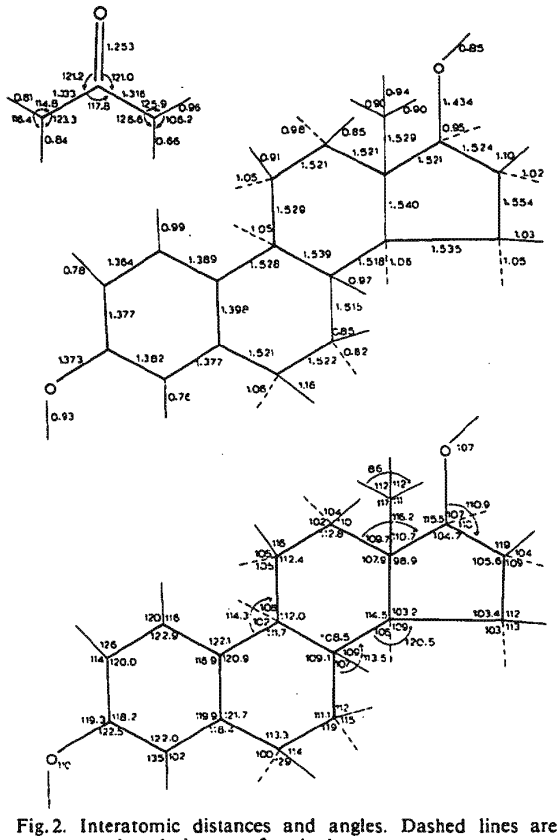


Fig. 2. Interatomic distances and angles. Dashed lines are used to designate α-face hydrogen atoms.

Table 3. *Positional and thermal parameters of the nonhydrogen atoms, at the end of the least-squares refinement*

Temperature factors are of the form: $\exp -[2\pi^2(U_{11}h^2a^{*2}+2U_{12}hka^*b^*+\ldots)]$.

	x/a	y/b	z/c	U11	U22	U33	U12	U13	U23
C(1)	0.0836 (1)	0.4431 (4)	0.4110 (4)	0.0329(19)	0.0217(18)	0.0384(22)	-0.0055(16)	-0.0032(18)	-0.0056(18)
C(2)	0.1350 (1)	0.3749 (4)	0.4080 (4)	0.0361(20)	0.0188(16)	0.0465(24)	-0.0006(17)	-0.0016(19)	-0.0059(19)
C(3)	0.1784 (1)	0.4857 (5)	0.4219 (4)	0.0293(18)	0.0291(20)	0.0345(21)	0.0031(16)	0.0009(17)	-0.0021(19)
C(4)	0.1690 (1)	0.6537 (5)	0.4496 (5)	0.0279(19)	0.0369(20)	0.0637(30)	-0.0064(17)	-0.0002(20)	-0.0076(22)
C(5)	0.1172 (1)	0.7173 (4)	0.4595 (5)	0.0310(19)	0.0312(18)	0.0544(28)	-0.0045(16)	0.0031(20)	-0.0047(20)
C(6)	0.1101 (1)	0.9019 (5)	0.4979 (8)	0.0290(20)	0.0225(20)	0.1319(54)	-0.0021(18)	0.0060(29)	-0.0204(32)
C(7)	0.0535 (1)	0.9889 (4)	0.4657 (8)	0.0306(20)	0.0176(18)	0.0850(38)	-0.0032(16)	0.0036(23)	-0.0051(23)
C(8)	0.0102 (1)	0.8479 (4)	0.5172 (4)	0.0249(17)	0.0147(17)	0.0416(22)	-0.0018(15)	-0.0025(17)	0.0006(18)
C(9)	0.0169 (1)	0.6824 (4)	0.4321 (4)	0.0243(17)	0.0217(18)	0.0384(20)	-0.0028(15)	-0.0012(17)	0.0000(18)
C(10)	0.0726 (1)	0.6118 (4)	0.4166 (4)	0.0261(17)	0.0231(18)	0.0311(19)	-0.0016(15)	-0.0021(16)	0.0017(17)
C(11)	-0.0292 (1)	0.5564 (4)	0.4747 (5)	0.0304(19)	0.0200(18)	0.0681(32)	-0.0061(17)	0.0008(21)	0.0005(22)
C(12)	-0.0859 (1)	0.6309 (5)	0.4446 (5)	0.0288(19)	0.0255(19)	0.0645(30)	-0.0073(17)	-0.0024(20)	-0.0077(22)
C(13)	-0.0919 (1)	0.7930 (4)	0.5409 (4)	0.0241(17)	0.0296(19)	0.0333(21)	-0.0051(16)	-0.0021(16)	0.0011(18)
C(14)	-0.0471 (1)	0.9149 (4)	0.5013 (5)	0.0247(17)	0.0194(17)	0.0499(24)	-0.0035(15)	0.0025(18)	0.0012(20)
C(15)	-0.0636 (1)	1.0822 (6)	0.5702 (7)	0.0313(22)	0.0362(23)	0.1115(47)	-0.0029(20)	0.0078(29)	-0.0170(32)
C(16)	-0.1267 (1)	1.0757 (6)	0.5690 (7)	0.0325(22)	0.0322(23)	0.1151(48)	0.0018(20)	0.0073(29)	-0.0110(32)
C(17)	-0.1413 (1)	0.9005 (5)	0.5167 (5)	0.0231(17)	0.0277(20)	0.0496(25)	-0.0015(16)	0.0008(18)	-0.0002(22)
C(18)	-0.0895 (1)	0.7544 (4)	0.5107 (5)	0.0407(24)	0.0230(19)	0.0531(25)	-0.0025(20)	0.0022(21)	0.0127(20)
C(19)	0.2643 (1)	-0.0046 (6)	0.1365 (4)	0.0283(19)	0.0261(16)	0.0691(22)	0.0052(12)	0.0030(15)	-0.0066(17)
O(3)	0.2304 (1)	0.4213 (3)	0.4108 (3)	0.0294(13)	0.0344(16)	0.0535(18)	-0.0040(12)	0.0032(13)	-0.0078(16)
O(17)	-0.1916 (1)	0.9445 (3)	0.5757 (3)	0.0421(17)	0.0336(14)	0.0384(17)	0.0068(13)	0.0074(20)	0.0014(21)
O(19)	0.2248 (1)	0.0474 (3)	0.0208 (3)	0.0325(17)	0.0306(20)	0.0401(21)	0.0142(12)	-0.0124(21)	0.0008(19)
N(1)	0.2607 (1)	-0.1636 (4)	0.1507 (4)	0.1293(43)	0.0445(24)	0.0374(22)	0.0179(29)	-0.0057(27)	-0.0075(21)
N(2)	0.2505 (2)	0.0906 (5)	0.2475 (4)	0.0543(28)	0.0398(17)	0.0387(17)	0.0147(15)	-0.0051(15)	0.0019(15)

UM00013226
NOVARTIS EXHIBIT 1517
Novartis v. Regents, IPR2023-01347
Page 1972 of 4460

Table 4. *Positional parameters for the hydrogen atoms in estradiol.urea* (1:1)

Values are × 10^3.

	X	*Y*	*Z*
H(1)	52 (2)	372 (8)	382 (6)
H(2)	143 (2)	288 (7)	387 (6)
H(4)	185 (2)	726 (7)	478 (6)
H(6*A*)	131 (2)	957 (8)	410 (7)
H(6*B*)	121 (2)	902 (9)	620 (7)
H(7*A*)	42 (1)	970 (6)	382 (5)
H(7*B*)	51 (1)	1062 (6)	509 (5)
H(8)	17 (1)	826 (6)	618 (5)
H(9)	9 (1)	710 (6)	322 (5)
H(11*A*)	− 26 (2)	458 (8)	398 (7)
H(11*B*)	− 20 (1)	508 (5)	560 (5)
H(12*A*)	− 90 (2)	642 (9)	361 (8)
H(12*B*)	−110 (2)	561 (8)	488 (6)
H(14)	− 54 (1)	921 (6)	387 (4)
H(15*A*)	− 47 (1)	1173 (6)	499 (5)
H(15*B*)	− 48 (2)	1092 (9)	673 (7)
H(16*A*)	−141 (1)	1165 (6)	501 (6)
H(16*B*)	−141 (2)	1114 (9)	676 (7)
H(17)	−146 (1)	906 (6)	413 (4)
H(18*A*)	− 86 (2)	849 (7)	762 (6)
H(18*B*)	− 56 (2)	726 (8)	746 (7)
H(18*C*)	−117 (2)	684 (8)	745 (6)
H(N1*A*)	245 (2)	−230 (7)	98 (6)
H(N1*B*)	273 (1)	−202 (6)	227 (5)
H(N2*A*)	239 (1)	212 (6)	252 (5)
H(N2*B*)	256 (1)	74 (6)	314 (5)
H(170)	−199 (1)	750 (6)	536 (5)
H(30)	255 (2)	507 (6)	394 (5)

Steroid geometry

The intramolecular bond distances and valency angles (Fig. 2) are in good agreement with values observed in determinations of similar steroid structures. The estimated standard deviations in bond lengths are 0·006 and 0·06 Å for bonds involving nonhydrogen and hydrogen atoms, respectively. E.s.d.'s in valency angle are 0·4, 2·5, and 4·0° for angles of the types C–C–C, C–C–H, and H–C–H respectively. The average C(sp^3)–C(sp^3) bond length in this determination is 1·528 Å as compared with expected values of 1·533 Å (Bonham & Bartell, 1959) or 1·526 Å (Lide, 1962). Only the C(15)–C(16) bond length is more than two standard deviations away from either of these expectep values. A lengthening of bond distances in the *D* ring is common in steroids. The average of the C–C bond lengths in the aromatic *A* ring is 1·381 Å, which is slightly shorter than the values of 1·390 and 1·394 Å observed for the two estriol molecules (Cooper, Norton & Hauptman, 1969). The bond lengths and valency angles in the urea molecule are within 0·015 Å and 0·2° of the values observed in crystalline urea by Caron & Donohue (1964).

The bonds and angles involving hydrogen atoms are within three standard deviations of standard values. Because of strains imposed at ring junctions, some deviations from theoretical values would be expected, particularly in valency angles. The average C–H bond distance is 0·96 Å and the average C–C–H bond angle is 108·7°. The most questionable hydrogen position is that of H(N2*b*) of the urea molecule, which results in the short N–H distance of 0·66 Å. The Newman projections (Fig. 3) illustrate the orientation of the hydrogen atom of the angular methyl group over the *C*/*D* junction, and the relative orientation of hydrogen atoms on adjacent carbon atoms in the bonds C(6)–C(7), C(11)–C(12), and C(15)–C(16). The hydrogen atoms of the methyl groups are oriented in the expected *gauche* positions relative to the bonds to C(13). Staggered conformations are also observed for the hydrogen atoms on the carbon atoms of the C(6)–C(7) and the C(11)–C(12) bonds. These bonds occur in the half-chair conformation *B* ring and the normal-chair conformation *C* ring respectively. The hydrogen atoms on the carbon atoms of the C(15)–C(16) bond in the β-envelope *D* ring are almost fully eclipsed. Such hydrogen atoms are not always eclipsed. One example of a structure with a twisted β-envelope conformation *D* ring, in which the hydrogen atoms of C(15) and C(16) are staggered, is 2,4-dibromoestradiol [Fig. 3(*e*)] (Cody, DeJarnette, Duax & Norton, 1971).

Steroid conformation

In Fig. 4 the conformation of the molecule is illustrated in two *ORTEP* drawings (Johnson, 1965). The torsional angles, a sensitive quantitative index of ring conformation, are presented in Table 5.

The *D* ring conformation is a distorted β-envelope and can be described by the parameters $\Delta = 48{\cdot}99$ and $\varphi_m = 22{\cdot}31$ (Altona, Geise & Romers, 1968). The *C* ring is in the normal-chair conformation. The average of the absolute values of the torsional angle in the *C*

Table 5. *Torsional angles in the rings**

Ring *A*		Ring *B*		Ring *C*		Ring *D*	
Bond	$\varphi(A-B)$†	Bond	$\varphi(A-B)$	Bond	$\varphi(A-B)$	Bond	$\varphi(A-B)$
C(1)–C(2)	−2·2	C(5)–C(6)	−17·0	C(8)—C(9)	−53·6	C(13)–C(14)	48·1
C(2)–C(3)	3·0	C(6)–C(7)	45·4	C(9)—C(11)	53·3	C(14)–C(15)	−33·6
C(3)–C(4)	−0·9	C(7)–C(8)	−64·2	C(11)–C(12)	−54·2	C(15)–C(16)	5·9
C(4)–C(5)	−2·1	C(8)–C(9)	52·5	C(12)–C(13)	54·1	C(16)–C(17)	24·3
C(5)–C(10)	2·9	C(9)–C(10)	−25·1	C(13)–C(14)	−57·7	C(13)–C(17)	−44·3
C(1)–C(10)	−0·8	C(5)–C(10)	7·2	C(8)—C(14)	57·6		

* The sign convention for torsional angles is that of Klyne & Prelog (1960).

† $\varphi(A-B)$ is the torsional angle about the *A*–*B* bond, in which the other two atoms required to define the angle are those attached to either end of the bond and are in the ring in question.

UM00013227
NOVARTIS EXHIBIT 1517
Novartis v. Regents, IPR2023-01347
Page 1973 of 4460

ring is 55·1°, indicating typical flattening of the ring due to junction strain. The *B* ring is in the half-chair conformation, which is the most common form observed in the 1,3,5(10)-estratriene series (*e.g.* Cooper, Norton & Hauptman, 1969; Norton, Kartha & Lu, 1964; Busetta & Hospital, 1969). The algebraic sum of the torsional angles C(9)–C(10)–C(5)–C(6) and C(10)–C(5)–C(6)–C(7) for this structure is 10°, indicating a half-chair conformation. When the sum of these torsional angles in a 1,3,5(10)-estratriene molecule is 0°, the conformation is 'sofa', as in one of the three molecules of 2,4-dibromoestradiol (Cody *et al.*, 1971). The deviations of individual atoms of the phenolic *A* ring from the least-squares plane of atoms C(1), C(2), C(3), C(4), C(5), and C(10) are given in Table 6.

Table 6. *The deviations, D, of individual atoms from the least-squares plane through* (*a*) *atoms* C(1), C(2), C(3), C(4), C(5), *and* C(10) *in the phenolic A ring of estradiol, and* (*b*) *through atoms* C(19), O(19), N(19*A*), *and* N(19*B*) *of the urea molecule*

(*a*)

	D
C(1)	−0·004 Å
C(2)	0·017
C(3)	−0·014
C(4)	−0·004
C(5)	0·018
C(10)	−0·013
O(3)	−0·048
C(6)	0·100
C(9)	−0·130
H(1)	−0·14
H(2)	−0·02
H(4)	0·15
H(O3)	−0·33
C(7)	−0·265
C(8)	0·405

(*b*)

	D
C(19)	−0·007 Å
O(19)	0·003
N(*A*)	0·002
N(*B*)	0·002
H(N*A*1)	−0·32
H(N*A*2)	−0·03
H(N*B*1)	−0·01
H(N*B*2)	−0·10

The deviations of individual atoms from the least-squares plane of the nonhydrogen atoms of the urea molecule are given in Table 6(*b*). Only one of the hydrogen atoms deviates appreciably from the plane of the molecule.

Thermal vibration analysis

Analysis of the thermal motion of estriol (Cooper, Norton & Hauptman, 1969) and 12α-bromo-11β-hydroxyprogesterone (Cooper & Norton, 1968) showed these steroids to behave as rigid bodies, with some

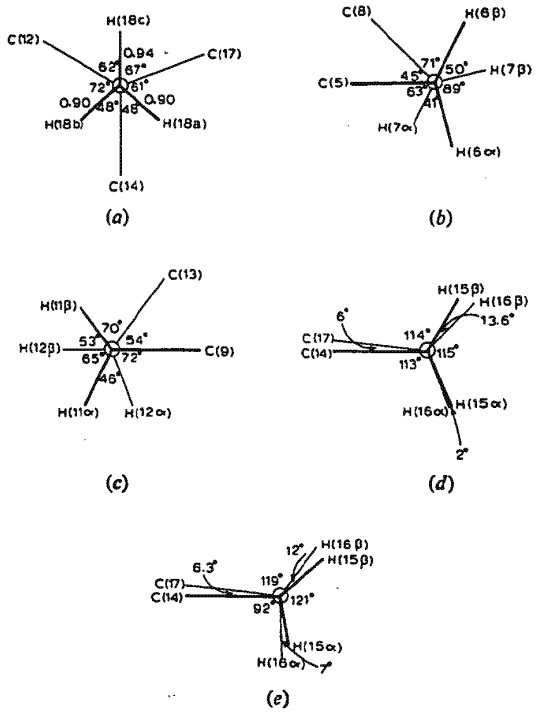


Fig. 3. Newman projections, illustrating the conformations of hydrogen atoms about selected bonds in estradiol [(*a*), (*b*), (*c*), (*d*)] and 6α-fluorocortisol [(*e*)].

Table 7. *Comparison of the rigid-body vibrational parameters for urea in the tetragonal lattice and the estradiol complex*

	Tetragonal		Orthorhombic complex			
	Eigenvalues	Direction of eigenvectors	Eigenvalues	Direction cosines of eigenvectors		
T_1	0·202 Å	a+b	0·174 Å	−0·5371	0·7465	0·3928
T_2	0·188	a−b	0·217	−0·8420	−0·4461	−0·3035
T_3	0·141	c	0·182	−0·0512	−0·4937	0·8681
ω_1	13·13°	c	8·15°	−0·1624	0·0015	−0·9867
ω_2	6·08	a+b	10·72	−0·2214	0·9744	0·0379
ω_3	2·70	a−b	3·26	−0·9616	−0·2246	0·1579

UM00013228
NOVARTIS EXHIBIT 1517
Novartis v. Regents, IPR2023-01347
Page 1974 of 4460

independent motion of atoms not in closest packing contact with other molecules in the lattice. Similar analysis of the estradiol thermal motion in the urea complex suggested that in this case the molecule does not behave as a rigid body. When the 17 atoms of the steroid nucleus were included in rigid-body calculations (Schomaker & Trueblood, 1968), the root-mean-square difference between the observed U_{ij}'s and the U_{ij}'s calculated from T and ω was found to be 0·009 Å^2. Although the librational motion about axes perpendicular to the general plane of the steroid (ω_2 = 1·4°) and parallel to the length of the steroid (ω_1 = 3·7°) were similar to those observed in the structures cited above, libration about the third axis [ω_3, Fig. 5(*a*)] was calculated as $(-5{\cdot}26)^{1/2}$. This suggests that the molecule is not a rigid body but flaps in the center where molecular packing is least dense.

The thermal motion of urea in its tetragonal crystalline form has been thoroughly studied (Caron & Donohue, 1964). In the tetragonal structure, the principal axes of T and ω are fixed in the directions **a**+**b**, **a**−**b**, and **c** by symmetry requirements. Despite the lack of space-group-imposed symmetry, the librational motion of urea in the orthorhombic complex is similar to that in the tetragonal structure. The magnitudes and directional cosines of T and ω for the urea molecules in the two crystals are compared in Table 7. The r.m.s. difference between the observed U_{ij}'s and the U_{ij}'s calculated from T and ω in the complex is 0·001 Å^2. Translational motion in the complex is nearly isotropic, and the principal axes are not coincident with either the cell sides or the axes of inertia of the molecule. The axis about which there is least librational is nearly coincident in the two structures and is perpendicular to the plane of the molecule. The other librational axes in the tetragonal structure are parallel and perpendicular to the carbon–oxygen double bond. In the complex, these axes are rotated 20° from this orientation [Fig. 5(*b*)]. The coordinates of the unweighted centroid are x=0·2451, y=−0·0059, z=0·1389.

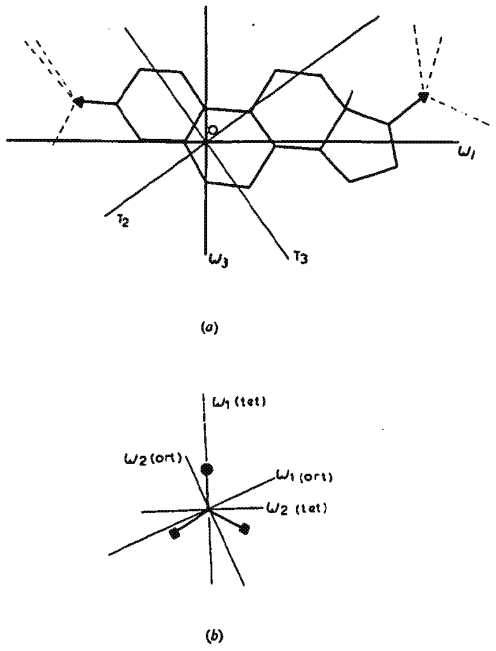


Fig. 5. (*a*) The principal axes of T and ω in the estradiol nucleus viewed parallel to the axis about which there is least rotation (ω_2). (*b*) The principal axes of libration of the urea molecule in the tetragonal lattice, and in the estradiol complex viewed parallel to the axis of least librational freedom (ω_3).

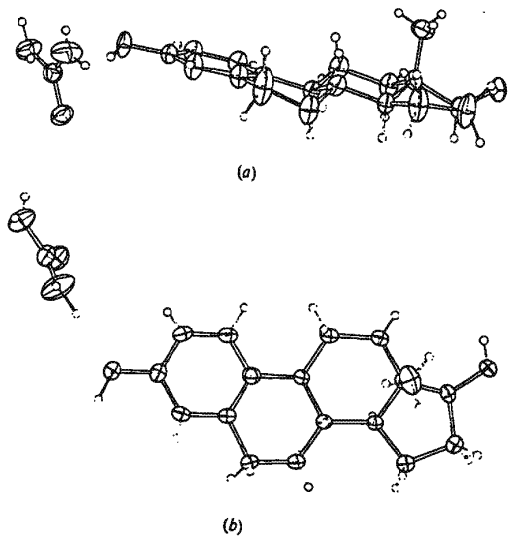


Fig. 4. Perspective views of estradiol, showing 50% probability thermal vibrational ellipsoids (*a*) rotated 77° about the C(13)–C(10) vector and (*b*) parallel to the cross product of the vectors C(13)–C(10) and C(12)–C(14).

Molecular packing and hydrogen bonding

The spatial arrangement of molecules can best be described as a partitioned packing system, with alternate layers of steroid and urea molecules. The planes of the steroid molecules are roughly perpendicular to the planes of the urea molecules, as shown in Fig. 6. The characteristic pattern observed in estrogen crystal structures is an arrangement of infinite chains of steroid molecules, hydrogen-bonded head to tail. This pattern is retained in the complex, with the additional feature that all bonding to lateral chains is *via* the urea molecules. The only intermolecular contacts of less than 2·7 Å are listed in Table 8. The absence of contacts of less than 2·5 Å distance (with the exception of those hydrogen atoms involved in hydrogen bonding) is due to the rigid hydrogen-bonding arrangement. Distor-

UM00013229
NOVARTIS EXHIBIT 1517
Novartis v. Regents, IPR2023-01347
Page 1975 of 4460

tions of hydrogen positions due to packing forces are probably at a minimum.

Table 8. *Intermolecular distances less than 2·7 Å between hydrogen atoms*

Contact	Position*	Distance
H(1)——H(14)	4/1̄10	2·54 Å
H(2)——H	1/01̄0	2·65
H(6β) —H(18*C*)	4/1̄01	2·57
H(7α)—H(11α)	4/1̄00	2·64
H(7β) —H(18*B*)	4/1̄01	2·62
H(11α)—H(15α)	1/01̄0	2·51
H(N*B*1)-H(017)	3/000	2·324
H(017)—H(03)	3/1̄10	2·317

* Equivalent position nomenclature: the symbol 4/1̄10 is taken to mean that the second atom mentioned in the contact is in the molecule at equivalent position 4, translated 1̄, 1, and 0 unit cells in the a, b, and c directions, respectively. The equivalent positions are 1=(x, y, z); 2=($\frac{1}{2}-x$, $-y$, $\frac{1}{2}+z$); 3=($\frac{1}{2}+x$, $\frac{1}{2}-y$, $-z$); 4=($-x$, $\frac{1}{2}+y$, $\frac{1}{2}-z$).

Fig. 7 illustrates the hydrogen-bonding system viewed parallel to the *a* axis, and Table 9 summarizes the geometry of the hydrogen bonds. All hydrogen bonds have acceptable geometries. The longest hydrogen bond (3·151 Å) has the most favorable N–H···O angle (173°), while the smallest N–H···O angle occurs in conjunction with a shorter N···O distance of 3·039 Å. The 2·85 Å, N···O (carbonyl) bond is very strong, when compared to the average N–H···O bond of 3·01 Å observed in the tetragonal urea structure. The other N–H···O (hydroxyl) bonds in this structure are of a length and geometry comparable to the N–H···O (water) hydrogen bonds observed in arginine hydrochloride monohydrate (Dow, Jensen, Mazumdar, Srinivasan & Ramachandran, 1970), as shown in Table 9. The only hydrogen bond between urea molecules forms infinite chains extending in the direction of the *c* axis. Each urea molecule is hydrogen-bonded to four different estradiol molecules, resulting

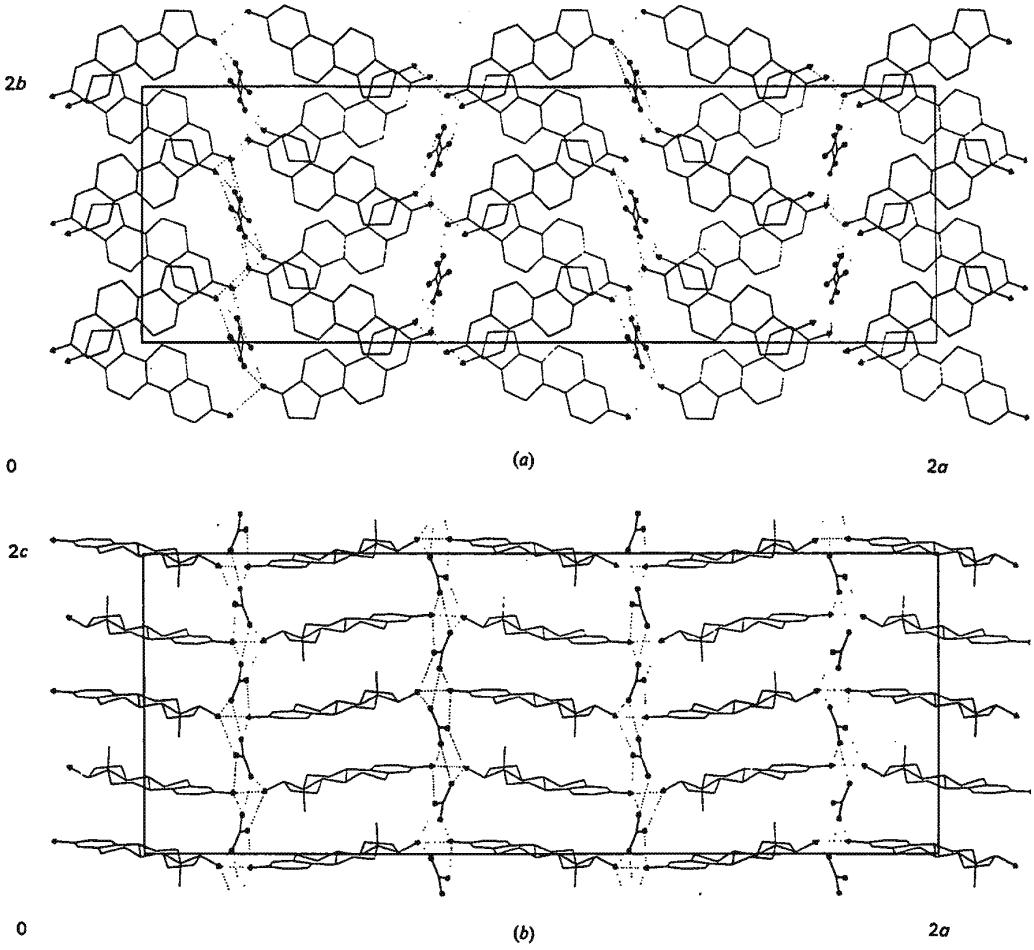


Fig. 6. Projection of four unit cells (*a*) onto the (001) plane and (*b*) onto the (010) plane.

UM00013230
NOVARTIS EXHIBIT 1517
Novartis v. Regents, IPR2023-01347
Page 1976 of 4460

Table 9. (*a*) *Summary of the geometry of the hydrogen bonding in estradiol.urea, and* (*b*) *selected hydrogen bonds in arginine hydrochloride monohydrate*

	Hydrogen bond X-H···Y	X-H	Distance H···Y	Distance X···Y	Angle X-H···Y
(*a*)	O(3)—H ·····O(17)	0·93	1·78 Å	2·679 Å	161°
	O(17)-H ·····O(19)	0·85	1·81	2·652	170
	N(*A*) -H(*A*1)···O(3)	0·83	2·39	3·039	138
	N(*A*) -H(*A*2)···O(17)	0·83	2·31	3·151	173
	N(*B*) -H(*B*1)···O(3)	0·96	2·23	3·034	156
	N(*B*) -H(*B*2)···O(19)	0·66	2·20	2·854	169
(*b*)	N(8)—H(31) ···O(3)	0·79	2·26	3·03	164
	N(8)—H(32) ···O(3)	0·83	2·06	2·88	169
	N(4)—H(14) ···O(6)	0·87	2·11	2·97	169
	N(4)—H(15) ···O(6)	0·88	2·03	2·90	167

in a strong interlocking of the steroid chains. At first glance, the alternate layers of steroid and urea molecules suggest similarities to the urea clathrate structures (Smith, 1950; Schlenk, 1951). However, the urea's primary interaction is to bind the steroid's chains together, rather than to surround or isolate the steroid molecules.

The author wishes to thank Dr Dorita A. Norton, Research Director of the Medical Foundation, for her enthusiastic support of this project. The author is also indebted to Dr Chaim Eger whose chemical knowledge of complex formation resulted in the preparation of the estradiol.urea complex. Invaluable technical assistance was given by Miss Mary Greiner who prepared the single crystals of the complex, Mrs Catherine DeVine who collected the X-ray diffraction data, and by Miss Melda Tugac and Miss Phyllis Strong who helped to prepare the Figures and Tables included in this report. This research was supported in part by U.S. Public Health Grant No. CA 10906-02 from the National Cancer Institute.

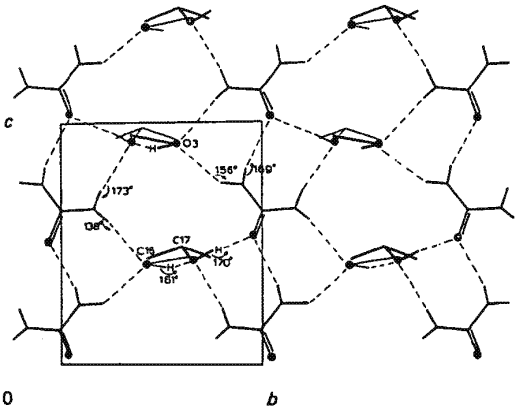


Fig. 7. Hydrogen-bonding in a plane perpendicular to the *a* axis in estradiol.urea (1:1).

References

ALTONA, G., GEISE, H. J. & ROMERS, C. (1968). *Tetrahedron*, **24**, 13.

BONHAM, R. A. & BARTELL, L. S. (1959). *J. Amer. Chem. Soc.* **81**, 3491.

BUSETTA, B. & HOSPITAL, M. (1969). *C. R. Acad. Sci. Paris*, **268**, 1300.

CARON, A. & DONOHUE, J. (1964). *Acta Cryst.* **17**, 544.

CODY, V., DEJARNETTE, F., DUAX, W. L. & NORTON, D. A. (1971). *Acta Cryst.* B**27**, 2458.

COOPER, A. & NORTON, D. A. (1968). *Acta Cryst.* B**24**, 811.

COOPER, A., NORTON, D. A. & HAUPTMAN, H. (1969). *Acta Cryst.* B**25**, 814.

DOW, J., JENSEN, C. H., MAZUMDAR, S. K., SRINIVASAN, R. & RAMACHANDRAN, G. N. (1970). *Acta Cryst.* B**26**, 1662.

DUAX, W. L., WEEKS, C. M. & HAUPTMAN, H. (1972). *Acta Cryst.* B**28**, 1857.

International Tables for X-ray Crystallography. (1962). Vol. III, Table 3.31A. Birmingham: Kynoch Press.

JOHNSON, C. K. (1965). *ORTEP*, Report ORNL-3794, Oak Ridge National Laboratory, Oak Ridge, Tennessee.

KLYNE, W. & PRELOG, V. (1960). *Experientia*, **16**, 521.

LIDE, D. R. (1962). *Tetrahedron*, **17**, 125.

NORTON, D. A., KARTHA, G. & LU, C. T. (1964). *Acta Cryst.* **17**, 77.

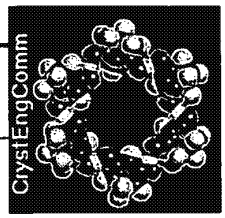
SCHLENK, W. VON (1951). *Liebigs Ann.* 572.

SCHOMAKER, V. & TRUEBLOOD, K. N. (1968). *Acta Cryst.* **23**, 1049.

SMITH, A. E. (1950). *J. Chem. Phys.* **18**, 150.

UM00013231
NOVARTIS EXHIBIT 1517
Novartis v. Regents, IPR2023-01347
Page 1977 of 4460

Crystal and co-crystal: a second opinion



Letter

Jack D. Dunitz

Organic Chemistry Laboratory, Swiss Federal Institute of Technology, ETH-Hönggerberg, CH-8093 Zurich, Switzerland. E-mail: dunitz@org.chem.ethz.ch

Received 2nd December 2003, Accepted 3rd December 2003
First published as an Advance Article on the web 8th December 2003

With his essay "Crystal and co-crystal"[1] Gautam Desiraju provokes a discussion about the use of the term *co-crystal* to describe what he prefers to call *molecular complex*. Although one can sympathize with some of Desiraju's objections to *co-crystal*, its popularity has good reasons; the word provides a succinct though possibly inelegant definition of what it is intended to describe, a crystal containing two or more components together†. Thus *co-crystal* encompasses molecular compounds, molecular complexes, solvates, inclusion compounds, channel compounds, clathrates, and possibly a few other types of multi-component crystals. Desiraju asks: in a co-crystal what is co- to what? We might just as well ask: in co-education what is co- to what? One of the uses of the prefix co- is to indicate togetherness, and that is its function in *co-crystal*. We must all agree that the hyphen is essential: *co-crystal*, but under no circumstances *cocrystal*.

Even if the term *co-crystal* is not perfect, its flaws seem to be less serious than those of other options. The trouble with terms such as *molecular compound* or *molecular complex* or even *intermolecular complex* is that they have long been used in chemistry in a rather broad sense, not necessarily connected with the crystalline state. Thus, these terms are applied to systems—they could be solids, liquids or even gases—in which the constituent molecules are considered to be more strongly associated than in a simple mixture. Such systems have been taken to include everything from weak van der Waals complexes to charge-transfer complexes to coordination complexes, all these "complexes" regarded as being held together by interactions other than straightforward covalent or ionic bonds.

That old classic, Glasstone's *Textbook of Physical Chemistry*,[2] offers a definition of what he termed *lattice compounds*: "Substances of this type, formed between definite stoichiometric amounts of two molecular species, which owe their stability to packing in the crystal lattice, and not to ordinary valency forces, are termed lattice compounds." Change *two* to *two or more* and we have a definition of what we are looking for. Unfortunately, crystallographers do not even agree about the meaning of *lattice*; some take it to be the translation group, the set of translations that acts on a unit of pattern to produce a periodic array, some take it to mean the periodic array itself, and some take it to indicate a general structural type, *e.g.*, the sodium chloride lattice. Therefore, I do not give *lattice compound* much of a chance, especially as it has lain dormant for more than sixty years. In my opinion it will be difficult to displace *co-crystal* as the term to describe a crystal containing more than a single component. We might as well stick to it.

References

1 G. R. Desiraju, *CrystEngComm*, 2003, **5**, 466.
2 S. Glasstone, *Textbook of Physical Chemistry*, McMillan, London, 1940, p. 389.

† According to this definition, a crystalline racemate consisting of non-interconverting enantiomers, *e.g.* D,L-alanine, should be classified as a co-crystal, but we may defer to established usage in such cases.

 DOI: 10.1039/b315687g

This journal is © The Royal Society of Chemistry 2003

UM00013232
NOVARTIS EXHIBIT 1517
Novartis v. Regents, IPR2023-01347
Page 1978 of 4460

New Light on an Old Story: The Solid-State Transformation of Ammonium Cyanate into Urea

Jack D. Dunitz,*[†] Kenneth D. M. Harris,*[‡] Roy L. Johnston,[‡] Benson M. Kariuki,[‡] Elizabeth J. MacLean,[§] Katerina Psallidas,[‡] W. Bernd Schweizer,[†] and Rik R. Tykwinski*[⊥]

Organic Chemistry Laboratory
Swiss Federal Institute of Technology
ETH-Zentrum, CH-8092 Zürich, Switzerland
School of Chemistry, University of Birmingham
Edgbaston, Birmingham B15 2TT, United Kingdom
Daresbury Laboratory, Warrington
Cheshire WA4 4AD, United Kingdom
Department of Chemistry, University of Alberta
Edmonton, Alberta T6G 2G2, Canada

Received September 15, 1998

According to a long held tradition, organic chemistry started in 1828 when Friedrich Wöhler heated ammonium cyanate to obtain urea. Even the Encyclopaedia Britannica[1] states: "Wöhler's classical experiment (1828) was the thermal conversion of ammonium cyanate into urea

$$NH_4{\cdot}NCO \xrightarrow{HEAT} H_2N{\cdot}CO{\cdot}NH_2$$

From this experiment Wöhler concluded that heat had transformed ammonium cyanate into urea."

If this account were true, the above reaction would qualify as the very first solid-state chemical reaction. In fact, however, Wöhler did not obtain urea by heating ammonium cyanate. His 1828 paper[2] makes it quite clear that he was actually trying to prepare ammonium cyanate, first by combining cyanic acid with ammonia in solution, then by the reaction of silver cyanate with ammonium chloride solution, and then again by reacting lead cyanate with ammonia. All of these reactions led not to the desired product ammonium cyanate but to a crystallizable white substance that Wöhler was able to identify as urea.[3] It was only two years later that Liebig and Wöhler[4] succeeded in preparing ammonium cyanate as a fluffy, white powder by the direct union of dry ammonia and cyanic acid. In a sealed vessel under ammonia, the powder could be kept essentially unchanged; open to the atmosphere, it transformed in 2 days into urea.

The transformation of ammonium cyanate into urea thus takes place both in solution and in the solid state. It has been studied by many authors for more than a century.[5] Much information about the rate and equilibrium in solution has been accumulated, but details of the reaction in the solid state are sparse. The careful study of Walker and Wood a century ago[6] was necessarily restricted by the limited choice of methods then available, and little seems to have been done in this area since then. Thus, even the crystal structure of ammonium cyanate has been unknown until now. We therefore decided to take up the study of this reaction anew—to prepare solid ammonium cyanate, determine its crystal structure, and obtain information by modern methods about its transformation to urea. This paper reports our first explorations in this area.

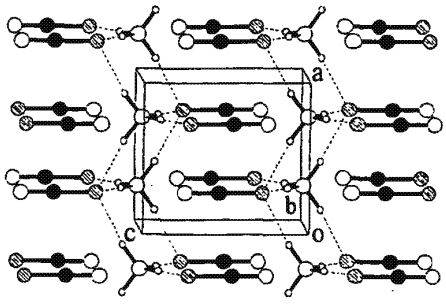


Figure 1. Crystal structure of ammonium cyanate viewed almost along the *b*-axis [N, large open circles; H, small open circles; C, filled circles; O, shaded circles]. The dashed lines represent hydrogen bonds (H···O, 2.07 Å; N−H···O, 177°; N−H, 0.98 Å).

Ammonium cyanate was synthesized by ion exchange between tetraethylammonium cyanate and ammonium thiocyanate with use of a modified version of the procedure described by Dieck et al.[7,8] The sample was collected as a microcrystalline powder, from which we have been unable to obtain single crystals. The powder X-ray diffraction pattern[9] was indexed in terms of a tetragonal unit cell: $a = b = 5.15$ Å, $c = 5.56$ Å, space group $P4/n$. With two formula units NH_4NCO per unit cell, the linear NCO^- anions must lie along 4-fold axes and the N atom of the ammonium cation must sit on a site of $\bar{4}$ symmetry. Rietveld refinement with the GSAS program package,[12] with standard geometric restraints applied to bond lengths and isotropic displacement parameters refined for all atoms (assuming a common value for all non-hydrogen atoms), led to the structure shown in Figure 1. The parameters listed in Table 1 give an excellent fit to the powder diffraction profile (Figure 2).

Each NH_4^+ cation is surrounded by eight NCO^- anions (see Figure 1). The local geometry around the NH_4^+ cation is that of a slightly distorted cube, with O and N atoms at alternate corners. Each H atom engages in a nearly linear N−H···O hydrogen bond (H···O, 2.07 Å; N−H···O, 177°). There are no analogous N−H···N interactions. Although the two ends of the NCO^- anion have similar scattering power, the assignment of the O and N atoms is readily made on bond distance criteria (C−O, 1.278 Å; C−N, 1.172 Å) corresponding to the valence bond description

* To whom correspondence should be addressed.
† Swiss Federal Institute of Technology.
‡ University of Birmingham.
§ Daresbury Laboratory.
⊥ University of Alberta.

(1) Encyclopaedia Britannica, article on CHEMISTRY, Benton, Chicago, 1964.
(2) Wöhler, F. *Pogg. Ann.* **1828**, *12*, 253.
(3) Many authors have drawn attention to the incorrectness of the traditional textbook account. For a recent contribution to the subject see: Cohen, P. S.; Cohen, S. M. *J. Chem. Educ.* **1996**, *73*, 883.
(4) v Liebig, J.; Wöhler, F. *Ann. Phys. Leipzig, Ser. 2* **1830**, *20*, 369.
(5) See chapter on ammonium (iso)cyanate in Gmelin and also the following review: Shorter, J. *Chem. Soc. Rev.* **1978**, *7*, 1.
(6) Walker, J.; Wood, J. K. *J. Chem. Soc.* **1900**, *77*, 21.
(7) Dieck, R. L.; Peterson, E. J.; Galliart, A.; Brown, T. M.; Moeller, T. *Inorg. Synth.* **1976**, *16*, 131.
(8) The ion exchange reaction was conducted under normal laboratory conditions in standard glassware and kept under a nitrogen atmosphere rather than a drybox (as described in ref 7). Furthermore, prior to drying in vacuo, the filtered solid was washed twice with ether to remove traces of acetonitrile. In earlier attempts to crystallize ammonium cyanate from dioxane solution we obtained single crystals of a 1:1 urea:dioxane cocrystal (monoclinic, a = 6.751 Å, b = 4.547 Å, c = 12.634 Å, β = 95.145°, space group $P2/c$, Z = 2), the structure of which will be reported elsewhere.
(9) The powder X-ray diffraction pattern of a ground sample was recorded at 22 °C in transmission mode on a Siemens D5000 diffractometer, using Ge-monochromated Cu $K\alpha_1$ radiation and a linear position-sensitive detector covering 8° in 2θ. The total data range was $3° \le 2\theta \le 90°$, measured in 0.02° steps, and collected over 12 h. The diffractogram was indexed by using the program TREOR[10] on the basis of the first 20 observable reflections. Tetragonal cell dimensions reported previously[11] [$a = b = 3.64$ Å, $c = 5.58$ Å] correspond to a sub-cell.
(10) Werner, P.-E.; Eriksson, L.; Westdahl, M. *J. Appl. Crystallogr.* **1985**, *18*, 360.
(11) Waddington, T. C. *J. Chem. Soc.* **1959**, 2499.
(12) Larson, A. C.; Von Dreele, R. B. Los Alamos Lab Report No. LA-UR-86-748, 1987.

10.1021/ja983285c CCC: $15.00 © 1998 American Chemical Society
Published on Web 12/04/1998

UM00013233
NOVARTIS EXHIBIT 1517
Novartis v. Regents, IPR2023-01347
Page 1979 of 4460

Table 1. Fractional Coordinates for the Crystal Structure of Ammonium Cyanate at Ambient Temperature [*P4/n*; $a = b = 5.1431(1)$ Å, $c = 5.5552(2)$ Å; Origin at $\bar{1}$]

atom	*x*	*y*	*z*	U_{iso}/Å^2
N(1)	0.25	0.75	0	0.02(1)
H(5)	0.245(1)	0.908(1)	0.100(1)	0.03(1)
O(2)	0.25	0.25	0.296(1)	0.02(1)
C(3)	0.25	0.25	0.526(1)	0.02(1)
N(4)	0.25	0.25	0.737(1)	0.02(1)

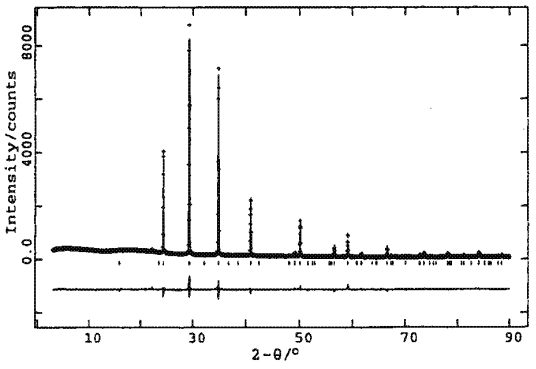


Figure 2. Experimental (+ marks), calculated (solid line), and difference (bottom) powder diffraction profiles for the Rietveld refinement of ammonium cyanate ($R_{wp} = 6.4\%$ and $R_p = 4.7\%$). Reflection positions are marked.

N≡C−O$^-$. Reorientation of the NH_4^+ cation to point the N−H bonds toward the other four corners of the cube (to form N−H···N interactions) gives significantly worse agreement with the powder diffraction data. In contrast to the observed preference for N−H···O hydrogen bonding in ammonium cyanate, cyanic acid exists overwhelmingly as H−NCO rather than NCO−H.[13,14]

The preference for N−H···O rather than N−H···N hydrogen bonding in the crystal is corroborated by our results of periodic Hartree−Fock calculations (basis set 6-31G**) using the CRYSTAL95 program.[16] The experimental structure was found to be more stable (by about 10 kcal mol^{-1}) than the alternative structure with inverted orientation of the NH_4^+ cation.

We have made a preliminary study of the solid-state transformation to urea at 50 °C by in situ synchrotron X-ray powder diffraction[17] (Figure 3). In the course of about 6 h, microcrystalline

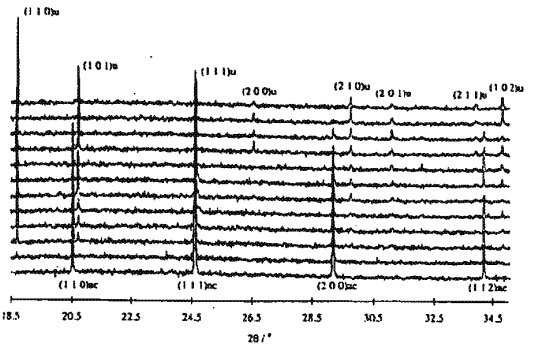


Figure 3. Synchrotron X-ray powder diffractograms ($\lambda = 1.300$ Å, calibrated against Si standard) recorded for ammonium cyanate at 50 °C as a function of time (bottom to top, with recording time per diffractogram ca. 30 min). Selected peaks characteristic of ammonium cyanate (subscript ac) and urea (subscript u) are marked.

ammonium cyanate transforms completely to microcrystalline urea. There is no evidence for any crystalline intermediate phase during the transformation, and no significant amounts of amorphous material are produced. The loss of starting material is approximately zeroth order, the rate constant increasing with temperature. On melting, the reaction goes almost instantly to completion.

Indeed, differential scanning calorimetry shows that a strongly exothermic process, accompanied by melting, occurs between 80 and 90 °C, depending on the scanning rate.[18] Thermogravimetric analysis shows loss of volatile material (presumably ammonia) in this region. The sudden rate increase on melting suggests that the solid-state reaction is not topochemical.[19−21] In any case, according to the standard mechanism involving initial proton transfer from NH_4^+ to the N of NCO$^-$, dynamic orientational disorder of the cation would seem to be a prerequisite for the onset of the chemical reaction in the crystal. Further in situ powder diffraction and solid-state NMR studies are under way to clarify these issues.

Acknowledgment. We are grateful to the following for financial support: EPSRC (postdoctoral fellowship to B.M.K.), CCLRC (award of beam-time at Daresbury Laboratory), Glaxo Wellcome plc (studentship to K.P.), and the University of Alberta (Gen-Science Endowment to R.R.T.).

JA983285C

(13) Belson, D. J.; Strachan, A. N. *Chem. Soc. Rev.* **1982**, *11*, 41.
(14) According to our MO calculations at the Hartree−Fock limit (basis set 6-31G**) using the SPARTAN program[15] on the molecules NCOH and HNCO, the latter is more stable by 23 kcal mol^{-1}.
(15) SPARTAN, Wave function Inc., Irvine, CA, USA (SGI Version 4.0.4 GL).
(16) Dovesi, R.; Saunders, V. R.; Roetti, C.; Causà, M.; Harrison, N. M.; Orlando, R.; Aprà, E. *CRYSTAL95 User's Manual*; University of Torino: Torino, Italy, 1996.
(17) A sample of ammonium cyanate was gently ground, loaded into a capillary (0.5 mm diameter), and mounted on the high-resolution powder diffractometer on Station 2.3 at the Synchrotron Radiation Source (Daresbury Laboratory). Powder X-ray diffraction data ($\lambda = 1.300$ Å) were recorded at 50 °C in 30 min scans over the range $18.5° \leq 2\theta \leq 40°$ in steps of 0.015°.
(18) The heat of reaction has been estimated[6] as 4.9 kcal mol^{-1}.
(19) Kohlschütter, V. *Z. Anorg. Chem.* **1919**, *105*, 1.
(20) Cohen, M. D.; Schmidt, G. M. J. *J. Chem. Soc.* **1964**, 1996.
(21) Thomas, J. M. *Philos. Trans. R. Soc.* **1974**, *277*, 251.

UM00013234
NOVARTIS EXHIBIT 1517
Novartis v. Regents, IPR2023-01347
Page 1980 of 4460

J|A|C|S
COMMUNICATIONS

Published on Web 07/23/2003

Thermally Programmable Gas Storage and Release in Single Crystals of an Organic van der Waals Host

Gary D. Enright, Konstantin A. Udachin, Igor L. Moudrakovski, and John A. Ripmeester*

Steacie Institute for Molecular Sciences, National Research Council of Canada, 100 Sussex Drive, Ottawa, Ontario, Canada, K1A 0R6

Received March 14, 2003; E-mail: John.Ripmeester@NRC.CA

The synthesis of frameworks for storage, processing, and controlled release of molecular species is a much-researched topic today. Many such frameworks have been assembled via directional bonds of various strengths, for example, covalent, H-bonding, and metal-coordination, yielding frameworks of varying degree of robustness.[1-3] As well, recently there has been a keen interest in frameworks that transform under some sort of external stimuli to take on different functions, these sometimes being referred to as smart, responsive, or third generation materials.[4,5] Few simple van der Waals solids have shown a propensity for this kind of application,[6] although such solids often are flexible, suggesting that there should be a dimension of response possible.[4,5,7] Crystalline van der Waals solids that can change function cyclically via a relatively low energy pathway clearly have the potential for applications. Herein, we report examples of process control in *p-tert*-butylcalix[4]arene (tBC) where guests can be loaded into or released from single crystals by controlling guest concentration and temperature.

p-tert-Butylcalix[4]arene (tBC) is an extremely versatile inclusion host, with several guest-directed structural motifs.[8] By far, the most common are the 1:1 (*P4/n*) and 2:1 (*P4/nnc*) tetragonal crystal forms, obtained by recrystallization of the host material from solvents consisting of small guests (benzene, toluene, pentane) in the first instance, and from somewhat larger guests (hexane, *p*-xylene) in the second. Guest-free forms are obtained by heating inclusion compounds above ~150 °C, yielding either a dense, self-included form or a low-density $P2_1/n$ form (**1**), depending on the conditions.[7,9] The low-density form in fact can be converted to the *P4/n* 1:1 compound by exposing the material to guest liquid.[7]

Single crystals of guest-free **1** can also be converted into a new family of 1:1 guest−host materials where the host lattice does not change; that is it remains $P2_1/n$. When a single crystal of **1** is heated at temperatures between room temperature and 140 °C in a sealed tube under ~20 atm of xenon, the Xe guest filled at least half of the cavities, the single crystal remaining intact and the crystal structure of the product (**2**) remaining the same (Figure 1) as that for the empty form. These crystals were stable at room temperature for a period of at least days. Structural information for **1** and **2** is given in the Supporting Information.

The accessibility of crystal form **1** with respect to the loading and release of small guest molecules was tested for NO, air, SO_2, and Xe by sealing the gas and host material into a Pyrex tube to achieve pressures of 10−20 atm. Release of the gases as a function of temperature from the products was checked with TGA (Figure 2a) for Xe also under isothermal conditions at 100 °C (Figure 2b), the weight losses varying between 4% and 10%. The larger guests are retained quite tenaciously considering that the bulk guest materials are well above their boiling points. The isothermal plot for Xe shows that the rate of guest release becomes slower with increasing length of time, suggesting that the process is thermally activated with the interior guests traveling a longer diffusional path length than those near the surface of the particles. Xe NMR

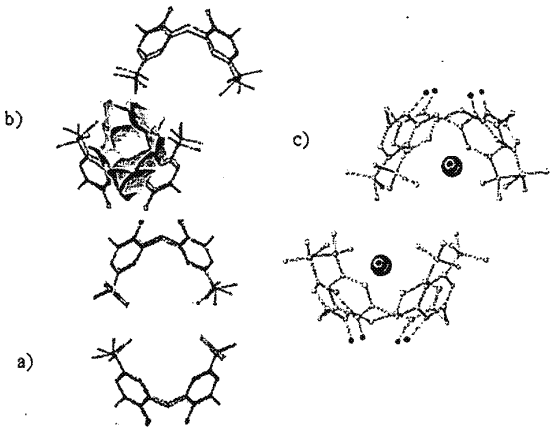


Figure 1. Crystal structure of the empty host (**1**) and the inclusion compound with xenon (**2**); (a) empty calixarenes (**1**), view along *a* axis; (b) empty calixarenes (**1**), view along *c* axis; the shading shows the van der Waals surface inside the cavity; (c) compound with Xe (**2**), view along *a* axis.

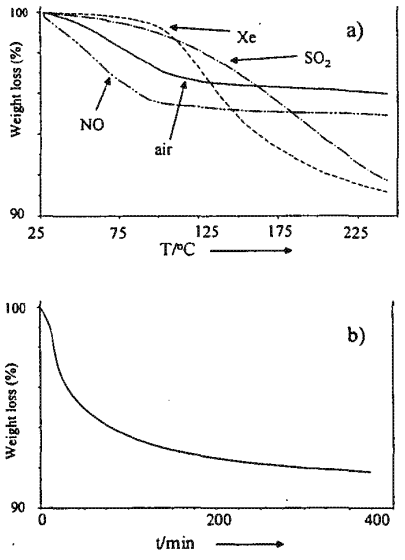


Figure 2. Thermogravimetric analysis of *p-tert*-butylcalix[4]arene guest host compounds; (a) temperature scans for Air, NO, Xe, SO_2; (b) isothermal run at 100 °C for the Xe compound.

10.1021/ja0351701 CCC: $25.00 © 2003 American Chemical Society

UM00013235
NOVARTIS EXHIBIT 1517
Novartis v. Regents, IPR2023-01347
Page 1981 of 4460

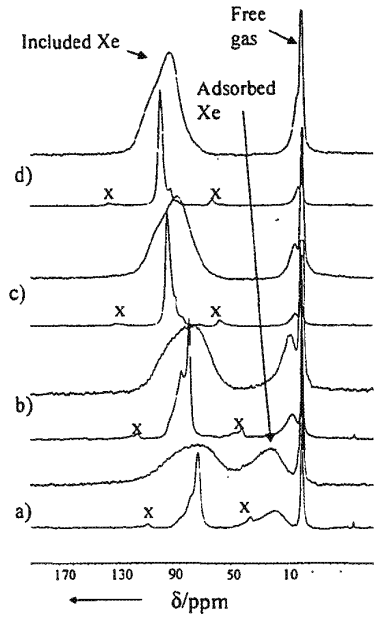


Figure 3. ^{129}Xe NMR spectra recorded under continuous flow conditions with hyperpolarized xenon at different temperatures: (a) 25 °C, (b) 60 °C, (c) 80 °C, (d) 100 °C. Both static-sample spectra as well as those obtained under magic angle spinning conditions are shown. Effective Xe gas pressure is 7 Torr; X marks spinning sidebands.

spectroscopy, using hyperpolarized xenon produced in a continuous flow system system,[10] lends itself well as an in-situ probe of the temperature-dependent access to the guest sites in **1**.[11] Figure 3 shows a set of ^{129}Xe spectra for **1** in contact with a flowing gas mixture (98% He, 1% N_2, 1% Xe) containing HP Xe (partial pressure 7 Torr) as a function of temperature under both static and spinning conditions.

The room-temperature spectrum shows resonances at 0, ~20, and 75 ppm which can be assigned to free xenon gas, Xe interacting with the outside surface, and xenon interacting with host cavities, respectively. The width and shape of the 20 ppm line suggest that considerable exchange occurs. As the temperature increases, the latter line shifts toward that of the free gas, as the rate of exchange with xenon in the free gas also increases. The isotropic low field line always shows some fine structure. We attribute this to the presence of a phase change that takes place for the empty lattice at ~90 °C.[9b]

Loading of the host will change the transition temperature, and nonuniform loading will give a range of such transition temperatures. The largest change in the spectrum comes between 60 and 80 °C, where the strongest isotropic component shifts from the high field to the low field side of the complex peak, so it is likely that the bulk of the sample transforms in this temperature range. At the highest temperature, the Xe powder pattern has an isotropic chemical shift of ~105 ppm which corresponds to Xe inside the calixarene cavities. So, as the temperature is increased from room temperature to 100 °C, the Xe atom locations change from a good fraction being external to the host cavities to being almost completely included. The spectra confirm that passage in and out of the crystal by flowing xenon gas is rather difficult at room temperature and much easier at 100 °C. We also note that the Xe powder pattern is quite different from that obtained previously for the mixed Xe/nitrobenzene calix compound, the larger chemical shift confirming that the cavity is much smaller in **2** than in the known versions of the 1:1 compound.[12] The observation of reversible functional behavior involving the release or adsorption of guest species makes the material suitable for applications such as the release of packaged reagents (SO_2, HCl) or the controlled release of biologically active species (NO). Storage of guest molecules, including low-boiling gases, can be accomplished by loading at about room temperature under a high guest pressure, followed by storing at a suitable temperature. Controlled release can then be accomplished by thermal programming. Another application is molecular sieving, as it was noted that even at room temperature compound **1** takes up components from air. Studies of selective adsorption for possible gas separations are currently in progress. It is clear that the collective weak forces in van der Waals hosts are remarkably strong in retaining highly volatile guests;[6,13] yet they can be responsive to external conditions so that cavity hosts should be considered for possible applications, a role primarily considered for the many novel open channel systems recently reported.[1-3]

Supporting Information Available: Crystallographic data of **1**, **2**, and further experimental details (PDF). This material is available free of charge via the Internet at http://pubs.acs.org.

References

(1) Eddaoudi, M.; Kim, J.; Rosi, N.; Vodak, D.; Wachter, J.; O'Keeffe, M.; Yaghi, O. M. *Science* **2002**, *295*, 469.
(2) Uemura, K.; Kitagawa, S.; Kondo, M.; Fukui, K.; Kitaura, R.; Chang, H.; Mizutani, T. *Chem.-Eur. J.* **2002**, 3586.
(3) (a) Tanaka, T.; Endo, K.; Aoyama, Y. *Chem. Lett.* **2000**, *12*, 1424. (b) Abrahams, B. F.; Jackson, P. A.; Robson, R. *Angew. Chem., Int. Ed.* **1998**, *37*, 2656. (c) Kondo, M.; Shimamura, M.; Noro, S.; Minakoshi, S.; Asami, A.; Seki, K.; Kitagawa, S. *Chem. Mater.* **2000**, *12*, 1288. (d) Min, K. S.; Suh, M. P. *J. Am. Chem. Soc.* **2000**, *122*, 6834. (e) Tabares, L. C.; Navarro, J. A. R.; Salas, J. M. *J. Am. Chem. Soc.* **2001**, *123*, 383. (f) Holman, K. T.; Pivovar, A. M.; Swift, J. A.; Ward, M. D. *Acc. Chem. Res.* **2001**, *34*, 107. (g) Soldatov, D. V.; Ripmeester, J. A. *Chem.-Eur. J.* **2001**, *7*, 2979.
(4) Kitagawa, S.; Kondo, M. *Bull. Chem. Soc. Jpn.* **1998**, *71*, 1739.
(5) (a) Soldatov, D. V.; Ripmeester, J. A.; Shergina, S. I.; Sokolov, I. E.; Zanina, A. S.; Gromilov, S. A.; Dyadin, Y. A. *J. Am. Chem. Soc.* **1999**, *121*, 4179. (b) Soldatov, D. V.; Grachev, E. V.; Ripmeester, J. A. *Cryst. Growth Des.* **2002**, *2*, 401.
(6) Atwood, J. L.; Barbour, L. J.; Jerga, A. *Science* **2002**, *296*, 2367.
(7) Atwood, J. L.; Barbour, L. J.; Jerga, A.; Schottel, B. L. *Science* **2002**, *298*, 1000.
(8) (a) Andreetti, G. D.; Ungaro, R.; Pochini, A. *Chem. Commun.* **1979**, 1005. (b) Ungaro, R.; Pochini, A.; Andreetti, G. D.; Domiano, P. J. *J. Chem. Soc., Perkin Trans. 2* **1985**, 197. (c) Brouwer, E. B.; Udachin, K. A.; Enright, G. D.; Ratcliffe, C. I.; Ripmeester, J. A. *Chem. Commun.* **1998**, 587. (d) Udachin, K. A.; Brouwer, E. B.; Enright, G. D.; Ripmeester, J. A. *J. Supramol. Chem.* **2001**, *1*, 97.
(9) (a) Brouwer, E. B.; Udachin, K. A.; Enright, G. D.; Ripmeester, J. A.; Ooms, K. J. *Chem. Commun.* **2001**, 565. (b) Brouwer, E. B.; Enright, G. D.; Udachin, K. A.; Lang, S.; Ooms, K. J.; Halchuk, P. A.; Ripmeester, J. A. *Chem. Commun.* **2003**, 1416.
(10) Moudrakovski, I. L.; Nossov, A.; Lang, S.; Breeze, S.; Ratcliffe, C. I.; Simard, B.; Santyr, G.; Ripmeester, J. A. *Chem. Mater.* **2000**, *12*, 1181.
(11) Nossov, A. V.; Soldatov, D. V.; Ripmeester, J. A. *J. Am. Chem. Soc.* **2001**, *123*, 3563.
(12) Brouwer, E. B.; Enright, G. D.; Ripmeester, J. A. *Chem. Commun.* **1997**, 939.
(13) Blum, Z.; Hyde, S. T.; Ninham, B. W. *J. Phys. Chem.* **1993**, *97*, 661.

JA0351701

UM00013236
NOVARTIS EXHIBIT 1517
Novartis v. Regents, IPR2023-01347
Page 1982 of 4460

Acta Cryst. (1976). B32, 2180

The X-ray Crystal Structure of the Molecular Complex 8-Bromo-9-ethyladenine–5-Allyl-5-isobutylbarbituric Acid

BY RICHARD H. EPSTEIN, ALICE V. ZEIGER, CAMILLA CROCKER AND DONALD VOET

Department of Chemistry and the Laboratory for Research on the Structure of Matter, University of Pennsylvania, Philadelphia, Pennsylvania 19174, *U.S.A.*

(*Received* 29 *August* 1975; *accepted* 30 *January* 1976)

Crystals of the hydrogen-bonded 1:1 complex 8-bromo-9-ethyladenine–5-allyl-5-isobutylbarbituric acid, $C_{18}H_{24}BrN_7O_3$, have the space group $P2_1/c$ with the unit-cell parameters $a=13{\cdot}732$ (3), $b=25{\cdot}685$ (19), $c=15{\cdot}132$ (4) Å and $\beta=123{\cdot}56$ (1)°, with eight complexes per unit cell. Intensity data were measured with an automated diffractometer using graphite-monochromated Cu $K\alpha$ radiation. The structure was solved by the heavy-atom technique and was refined by full-matrix least-squares procedures to a final discrepancy index of $R=0{\cdot}129$ based on the 2318 observed unique reflections. Both of the unlike adenines and one of the barbiturates associate through Watson–Crick-type base pairing to form six-molecule-long hydrogen-bonded ribbons of heterocycles. These ribbons terminate at both ends with adenine residues whose amino groups participate in only one of the two hydrogen bonds they have the potential to form. The second barbiturate does not participate in base-pairing interactions but rather makes a single hydrogen bond to the N(3) atom of each of the unlike adenines. This barbiturate ring is inclined by over 60° to the planes of the adenine rings. There is no precedent among the 36 published crystal structures containing base pairs for either of these hydrogen-bonding anomalies. Hence this structure constitutes further evidence that barbiturates are poor hydrogen-bond acceptors. The crystal structure assumes a complicated pattern in which layers containing the base-paired ring molecules alternate with regions containing the non-base-paired barbiturate rings together with the hydrocarbon substituents to the rings. These latter regions are quite loosely packed. This accounts for the observed disorder of the hydrocarbon substituents to the barbiturates and hence the relatively large discrepancy index of the refined structure.

Introduction

Adenine–barbiturate complexes were first studied by Kyogoku, Lord & Rich (1968). They reported that in $CHCl_3$ solution the association constants of these hydrogen-bonded complexes, as determined by IR measurements, were an order of magnitude greater than those of the closely analogous adenine–uracil complexes. This conclusion prompted several crystallographic studies of adenine–barbiturate complexes in an effort to elucidate the structural basis of their high binding strength. The N–H···O hydrogen bonds in these crystal structures (Kim & Rich, 1968; Voet & Rich, 1972; Voet, 1972), in which the oxygen atom was that of a barbiturate carbonyl group and the NH group was from adenine, were often found to be extremely long and are therefore, presumably, weak (Nakamoto, Margoshes & Rundle, 1955). In the complex 9-ethyladenine–parabanic acid–oxaluric acid monohydrate (Shieh & Voet, 1975), the parabanic acid molecule, which is chemically related to the barbiturates, appears to avoid all hydrogen-bonding acceptor interactions. These studies suggest that the conjugation of several carbonyl groups drastically reduces their hydrogen-bonding acceptor affinities (Voet, 1972; Shieh & Voet, 1975). A similar conclusion was reached by Gartland & Craven (1974) in their survey of N–H···O hydrogen bonds in which the oxygen atom belonged to a barbiturate with nonpolar C(5) substituents and the N–H group belonged to some other type of molecule.

The present study was initiated in order to further elucidate the hydrogen-bonding properties of crystalline adenine–barbiturate complexes. A bromine atom substituted at the 8-position of an adenine residue sterically prevents the formation of a Hoogsteen complex. Hence it was expected that the structure of the title complex would resemble that of the complex phenobarbital–(8-bromo-9-ethyladenine)$_2$ (Kim & Rich, 1968). It will be seen below that these expectations were, in part, borne out but that there are several unique features in the structure that further emphasize that carbonyl groups on barbiturates are poor hydrogen-bond acceptors.

Experimental

Colorless tabular crystals of 8-bromo-9-ethyladenine–5-allyl-5-isobutylbarbituric acid (*A*.*B*) were grown by the slow evaporation of a 50% aqueous ethanol solution of 8-bromo-9-ethyladenine (Cyclo Chemical) and 5-allyl-5-isobutylbarbituric acid (butalbital, a gift of Sandoz Pharmaceuticals) in equimolar ratio. The ultraviolet absorption spectrum of an aqueous solution of a washed crystal suggested that the crystals contained 8-bromo-9-ethyladenine and 5-allyl-5-iso-

UM00013237
NOVARTIS EXHIBIT 1517
Novartis v. Regents, IPR2023-01347
Page 1983 of 4460

butylbarbituric acid in approximately equimolar amounts.

Systematic absences of the $0k0$ reflections for k odd and of the $h0l$ reflections for l odd in the Weissenberg and precession photographs of a crystal of *A*.*B* indicate that its space group is $P2_1/c$. All subsequent X-ray measurements were made with a Picker FACS-I diffractometer equipped with a pyrolytic graphite monochromator and employing Cu $K\alpha$ radiation (λ= 1·5418 Å). The parameters of the unit cell, as determined from the angular positions of 12 reflections, are presented in Table 1.

Table 1. *Crystal data for 8-bromo-9-ethyladenine-5-allyl-5-isobutylbarbituric acid*

$C_{18}H_{24}BrN_7O_3$	V=4447·49 Å^3
F.W. 466·35	d_{obs}=1·400 g cm^{-3}
a=13·732 (3) Å	d_{calc}=1·393
b=25·685 (19)	μ(Cu $K\alpha$)=3·08 mm^{-1}
c=15·132 (4)	F(000)=2112
β=123·56 (1)°	
Space group $P2_1/c$	
Z=8	

The crystal density (Table 1), as determined by flotation in a mixture of cyclohexane and CCl_4 is in good agreement with the calculated density for the unit cell containing eight molecules each of 8-bromo-9-ethyladenine and 5-allyl-5-isobutylbarbituric acid.

The X-ray diffraction data were measured to the limit 2θ=125° using the θ–2θ scan mode, a scan rate of 1° min^{-1}, and a scan width of 1·2°. Stationary background counts of 20 s duration each were taken at both limits of each scan.

Structure determination and refinement

The measured intensities, I, were corrected for Lorentz and polarization effects. No absorption corrections were made. Standard deviations, $\sigma(I)$, were calculated (Stout & Jensen, 1968) assuming an instrumental instability factor of 0·03. Of the 5236 measured unique reflections, 2318 had $I>2·33\sigma(I)$ and hence were considered observed. The great majority of the 2918 unobserved reflections occurred at high Bragg angles as is expected for a disordered structure (see below).

The two unique bromine atoms in the structure were located by analysis of the Patterson map. The discrepancy index at this point was R=0·499. The remaining 56 unique non-hydrogen atoms in the structure were located using the heavy-atom technique as modified by Woolfson (1956) in a series of successive electron density maps. The side groups of the barbiturates were quite poorly resolved in these maps and hence were located with considerable difficulty.

The structure was refined by the full-matrix least-squares method in which the quantity minimized was $\sum w(|F_o|-|F_c|)^2$. Here the summation is over the 2318 observed reflections and $w=1/\sigma^2(I)=1/\sigma^2(F_o)$. The atomic scattering factors were taken from Cromer & Waber (1965). The overall scale factor together with all atomic positional and isotropic thermal parameters was refined to convergence. This was followed by a similar procedure in which the anisotropic thermal parameters were varied but in which the refinements were carried out on half the unique structure at a time, due to limitations of the computer memory. The agreement indices are presented in Table 2 for both the isotropic and the anisotropic refinement models.* The hypothesis that only the isotropic refinement of this structure is significant is strongly rejected at the 0·005 confidence level by the R-ratio test (Hamilton, 1965). The final parameter shifts were of the order of their estimated standard deviations for the atoms of the barbiturate side groups and somewhat less than this for the other atoms of the structure.

Table 2. *Agreement indices*

	Anisotropic observed data	Aniso-tropic* all data	Isotropic observed data
$R=\frac{\sum\|\|F_o\|-F_c\|}{\sum\|F_o\|}$	0·129	0·203	0·226
$R_w=\left[\frac{\sum w(\|F_o\|-\|F_c\|)^2}{\sum w\|F_o\|^2}\right]^{1/2}$	0·153	0·181	0·235
Goodness of fit: $\left[\frac{\sum w(\|F_o\|-\|F_c\|)^2}{(m-n)}\right]^{1/2}$	2·002	–	2·861
Number of observations, m	2318	5236	2318
Number of parameters, n	523	523	233

* The refinement model is based on the 2318 observed reflections only.

The final atomic parameters of the structure are presented in Table 3. The difference Fourier map did not reveal the presence of any hydrogen atoms. However it contained considerable positive and negative density in the vicinity of the hydrocarbon substituents to the rings. This, together with the large agreement indices of the refined structure, the distorted geometry of the hydrocarbon residues (see below), and the large and sometimes unrealistic thermal parameters and standard deviations of their component atoms, clearly indicates that these side groups are disordered in some manner. Several unsuccessful attempts were made to fit the data to various models in which the barbiturate side groups were statistically disordered. Least-squares refinements of these models invariably caused the various overlapping and fractionally weighted side groups to coalesce into a structure much like that de-

* A list of structure factors has been deposited with the British Library Lending Division as Supplementary Publication No. SUP 31660 (28 pp., 1 microfiche). Copies may be obtained through The Executive Secretary, International Union of Crystallography, 13 White Friars, Chester CH1 1NZ, England.

UM00013238
NOVARTIS EXHIBIT 1517
Novartis v. Regents, IPR2023-01347
Page 1984 of 4460

scribed by the final parameters. These models caused little variation in the agreement indices. Hence it appears that the atoms of the hydrocarbon substituents are continuously disordered about the positions indicated by the final parameters.

The molecular structures

The molecular configuration of an asymmetric unit of the complex together with the atomic numbering system used in this report is illustrated in Fig. 1. The covalent bond distances and angles of the structure are presented in Fig. 2. These data indicate that the covalent bonding parameters of the adenine and the barbiturate residues are in reasonable agreement with the corresponding averages of similar structures (Voet & Rich, 1970) although there are regions in these rings that appear to be somewhat distorted. Fig. 2 also shows that the hydrocarbon substituents to the rings all exhibit considerable distortion. These distortions are un-

Table 3. *Positional and thermal parameters for the complex 8-bromo-9-ethyladenine–5-allyl-5-isobutylbarbituric acid*

The positional parameters are expressed as fractions of unit-cell edges. The anisotropic temperature factors have the functional form $T=\exp[-(h^2\beta_{11}+k^2\beta_{22}+l^2\beta_{33}+2hk\beta_{12}+2hl\beta_{13}+2kl\beta_{23})\times 10^{-3}]$. Standard deviations as determined from the variance-covariance matrix of the final cycles of least-squares refinement are given in parentheses and refer to the least significant digits of their corresponding parameters.

8-Bromo-9-ethyladenine 1 (*A*1)

	x	y	z	β_{11}	β_{22}	β_{33}	β_{12}	β_{13}	β_{23}
N(1)	0·6902 (18)	0·4457 (10)	1·2422 (18)	4 (2)	2 (1)	8 (2)	−1 (1)	3 (2)	−1 (1)
C(2)	0·5969 (23)	0·4282 (13)	1·2491 (24)	7 (3)	3 (1)	8 (3)	0 (1)	6 (3)	−1 (1)
N(3)	0·5967 (18)	0·4315 (10)	1·3381 (21)	3 (2)	3 (1)	8 (2)	−1 (1)	4 (2)	−1 (1)
C(4)	0·6931 (24)	0·4508 (11)	1·4238 (27)	6 (3)	1 (1)	8 (3)	1 (1)	6 (3)	1 (1)
C(5)	0·7925 (23)	0·4673 (11)	1·4242 (26)	5 (3)	1 (1)	7 (3)	0 (1)	5 (3)	0 (1)
C(6)	0·7875 (23)	0·4631 (12)	1·3323 (25)	6 (3)	1 (1)	8 (3)	−1 (1)	5 (3)	−1 (1)
N(7)	0·8773 (17)	0·4867 (10)	1·5239 (18)	5 (2)	3 (1)	5 (2)	−2 (1)	3 (2)	−1 (1)
C(8)	0·8321 (23)	0·4801 (13)	1·5811 (20)	7 (3)	3 (1)	3 (2)	−1 (1)	1 (2)	−2 (1)
N(9)	0·7179 (17)	0·4579 (10)	1·5224 (18)	4 (2)	2 (1)	4 (2)	−1 (1)	2 (2)	−2 (1)
N(6)	0·8806 (16)	0·4758 (9)	1·3241 (15)	7 (2)	2 (1)	7 (2)	−2 (1)	6 (2)	−1 (1)
Br	0·9072 (3)	0·4944 (2)	1·7204 (3)	9 (0)	5 (0)	8 (0)	−3 (0)	6 (0)	−2 (0)
C(1′)	0·6501 (22)	0·4404 (16)	1·5693 (22)	5 (3)	4 (1)	5 (3)	−3 (2)	5 (2)	−3 (2)
C(2′)	0·6646 (32)	0·3872 (15)	1·6027 (32)	20 (5)	1 (1)	22 (5)	0 (2)	16 (4)	1 (2)

8-Bromo-9-ethyladenine 2 (*A*2)

	x	y	z	β_{11}	β_{22}	β_{33}	β_{12}	β_{13}	β_{23}
N(1)	0·2860 (17)	0·4096 (10)	0·6775 (20)	6 (2)	2 (1)	8 (2)	0 (1)	4 (2)	1 (1)
C(2)	0·2807 (22)	0·4045 (13)	0·5873 (27)	5 (2)	2 (1)	8 (3)	0 (1)	0 (2)	−2 (1)
N(3)	0·1859 (25)	0·3822 (10)	0·4992 (23)	15 (3)	2 (1)	17 (3)	0 (1)	14 (3)	0 (1)
C(4)	0·0946 (25)	0·3689 (13)	0·5105 (27)	11 (3)	2 (1)	9 (3)	0 (1)	6 (3)	0 (1)
C(5)	0·0994 (19)	0·3776 (11)	0·6005 (22)	3 (2)	2 (1)	8 (3)	0 (1)	2 (2)	0 (1)
C(6)	0·2042 (23)	0·3990 (13)	0·6929 (23)	10 (3)	3 (1)	6 (3)	1 (1)	5 (2)	1 (1)
N(7)	−0·0046 (22)	0·3591 (11)	0·5870 (25)	9 (2)	2 (1)	15 (3)	1 (1)	8 (2)	1 (1)
C(8)	−0·0619 (23)	0·3438 (14)	0·4882 (31)	6 (2)	3 (1)	12 (3)	−2 (1)	2 (3)	−3 (2)
N(9)	−0·0144 (19)	0·3485 (11)	0·4292 (24)	6 (2)	4 (1)	18 (4)	−3 (1)	9 (3)	−4 (1)
N(6)	0·2157 (18)	0·4019 (11)	0·7832 (20)	9 (2)	3 (1)	12 (2)	0 (1)	6 (2)	0 (1)
Br	−0·2189 (3)	0·3200 (2)	0·4220 (4)	9 (0)	5 (0)	16 (0)	−2 (0)	7 (0)	−1 (0)
C(1′)	−0·0778 (24)	0·3378 (14)	0·2995 (26)	9 (3)	2 (1)	15 (3)	0 (1)	7 (2)	−1 (1)
C(2′)	−0·0608 (26)	0·2917 (17)	0·3004 (28)	10 (3)	3 (1)	12 (4)	−1 (1)	3 (3)	−3 (2)

5-Allyl-5-isobutylbarbituric acid 1 (*B*1)

	x	y	z	β_{11}	β_{22}	β_{33}	β_{12}	β_{13}	β_{23}
N(1)	0·6493 (20)	0·4444 (11)	1·0398 (18)	3 (2)	3 (1)	6 (2)	−1 (1)	2 (2)	−2 (1)
C(2)	0·5415 (36)	0·4404 (15)	0·9544 (34)	16 (5)	3 (1)	13 (5)	0 (2)	13 (5)	−1 (2)
N(3)	0·5193 (18)	0·4421 (11)	0·8554 (20)	6 (2)	3 (1)	6 (2)	0 (1)	3 (2)	0 (1)
C(4)	0·6025 (38)	0·4485 (16)	0·8371 (33)	19 (6)	3 (1)	11 (4)	2 (2)	12 (5)	2 (2)
C(5)	0·7349 (32)	0·4546 (24)	0·9270 (25)	6 (4)	8 (2)	0 (3)	−2 (2)	1 (3)	−1 (2)
C(6)	0·7384 (29)	0·4519 (14)	1·0251 (29)	7 (3)	3 (1)	7 (3)	−1 (2)	2 (3)	−2 (2)
O(2)	0·4612 (14)	0·4346 (9)	0·9661 (13)	5 (2)	5 (1)	5 (2)	0 (1)	3 (1)	0 (1)
O(4)	0·5777 (15)	0·4468 (11)	0·7451 (18)	6 (2)	5 (1)	8 (2)	0 (1)	4 (2)	0 (1)
O(6)	0·8365 (17)	0·4568 (10)	1·1123 (16)	7 (2)	5 (1)	6 (2)	0 (1)	4 (2)	0 (1)
C(1′)	0·8075 (46)	0·4311 (42)	0·9142 (36)	12 (6)	11 (4)	8 (4)	5 (4)	6 (4)	0 (4)
C(2′)	0·7695 (57)	0·3703 (37)	0·9274 (72)	13 (7)	6 (3)	36 (11)	4 (4)	5 (7)	−7 (5)
C(3′)	0·6846 (54)	0·3349 (20)	0·8776 (66)	30 (10)	2 (1)	54 (14)	0 (3)	28 (10)	1 (3)
C(4′)	0·8496 (75)	0·3369 (35)	0·9322 (90)	39 (15)	7 (3)	84 (23)	−2 (6)	15 (15)	2 (6)
C(5′)	0·7850 (55)	0·5153 (36)	0·9111 (40)	23 (8)	10 (3)	12 (5)	−7 (5)	15 (6)	−2 (4)
C(6′)	0·7213 (40)	0·5458 (28)	0·9117 (59)	9 (5)	5 (2)	22 (8)	0 (2)	2 (5)	−4 (3)
C(7′)	0·7895 (62)	0·5797 (28)	0·9840 (42)	37 (11)	9 (3)	14 (6)	−1 (4)	13 (7)	−1 (3)

UM00013239
NOVARTIS EXHIBIT 1517
Novartis v. Regents, IPR2023-01347
Page 1985 of 4460

Table 3 (*cont.*)

5-Allyl-5-isobutylbarbituric acid 2 (*B*2)

	x	*y*	*z*	β_{11}	β_{22}	β_{33}	β_{12}	β_{13}	β_{23}
N(1)	0·2825 (17)	0·3428 (12)	0·3781 (20)	7 (2)	1 (1)	13 (3)	−1 (1)	6 (2)	−1 (1)
C(2)	0·3529(26)	0·3800 (16)	0·3738 (28)	6 (3)	3 (1)	12 (3)	−2 (1)	5 (2)	0 (2)
N(3)	0·4271 (17)	0·3573 (12)	0·3418 (16)	6 (2)	2 (1)	9 (2)	−2 (1)	6 (2)	−3 (1)
C(4)	0·4408 (25)	0·3090 (14)	0·3323 (23)	12 (3)	1 (1)	10 (3)	−2 (1)	7 (3)	−1 (1)
C(5)	0·3605 (28)	0·2633 (13)	0·3341 (30)	13 (3)	1 (1)	15 (4)	−1 (1)	10 (3)	0 (1)
C(6)	0·2745 (27)	0·2951 (19)	0·3597 (28)	7 (3)	3 (1)	16 (4)	2 (2)	9 (3)	3 (2)
O(2)	0·3512 (18)	0·4236 (11)	0·3908 (20)	10 (2)	3 (1)	16 (3)	−2 (1)	9 (2)	−1 (1)
O(4)	0·5117 (17)	0·2938 (9)	0·3137 (16)	12 (2)	4 (1)	16 (2)	−2 (1)	12 (2)	−3 (1)
O(6)	0·2094 (20)	0·2607 (10)	0·3619 (22)	16 (3)	3 (1)	27 (3)	−3 (1)	17 (3)	−1 (1)
C(1')	0·4300 (30)	0·2225 (17)	0·4114 (33)	10 (3)	4 (1)	17 (5)	0 (2)	10 (3)	0 (2)
C(2')	0·5305 (39)	0·2454 (21)	0·5292 (31)	15 (6)	6 (2)	10 (4)	2 (2)	6 (4)	3 (2)
C(3')	0·5952 (54)	0·2003 (27)	0·5929 (40)	34 (10)	9 (2)	13 (5)	7 (4)	5 (6)	1 (3)
C(4')	0·4845 (43)	0·2640 (27)	0·5833 (36)	21 (7)	11 (3)	14 (4)	−2 (3)	8 (4)	2 (3)
C(5')	0·2898 (34)	0·2408 (19)	0·2265 (35)	14 (4)	5 (1)	14 (4)	−6 (2)	8 (3)	−7 (2)
C(6')	0·2080 (43)	0·2808 (23)	0·1311 (46)	16 (5)	6 (2)	10 (5)	−2 (3)	2 (5)	−4 (3)
C(7')	0·1476 (65)	0·2713 (30)	0·0650 (53)	47 (11)	7 (2)	18 (8)	0 (4)	−18 (8)	−7 (4)

doubtedly artifacts of the refinement process attributable to the disorder in the crystal structure.

Both adenine rings and both barbiturate rings are planar within experimental error as can be seen from the planarity data in Table 4. The two hydrocarbon side groups on each of the barbiturates, together with the barbiturate atom C(5), can be considered to be a 6-methyl-1-heptene molecule that is disubstituted at its 4 position. On both barbiturates, this hydrocarbon chain assumes a conformation that is nearly fully extended in the direction normal to the plane of its attached barbiturate ring.

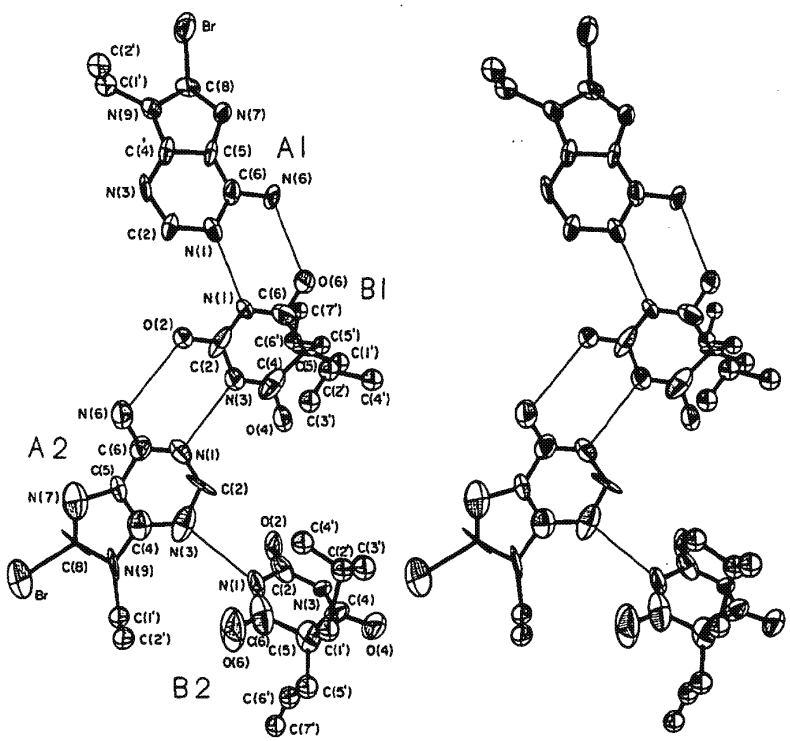


Fig. 1. A stereographic view of an asymmetric unit of the crystalline complex 8-bromo-9-ethyladenine–5-allyl-5-isobutylbarbituric acid. All atoms but those of the hydrocarbon side groups are illustrated as thermal ellipsoids at the 50% probability level. The atoms of the hydrocarbon side groups are shown as spheres of an arbitrary radius for the sake of clarity. Hydrogen bonds are represented by thin lines.

UM00013240
NOVARTIS EXHIBIT 1517
Novartis v. Regents, IPR2023-01347
Page 1986 of 4460

Table 4. *Deviations of atoms from the least-squares plane through the indicated atoms*

Adenine atom	Deviation for molecule *A*1 (Å)[a]	Deviation for molecule *A*2 (Å)[b]
N(1)	−0·03	0·02
C(2)	0·01	−0·02
N(3)	0·00	0·02
C(4)	0·00	0·02
C(5)	0·02	−0·03
C(6)	0·03	−0·01
N(7)	−0·02	0·01
C(8)	0·00	0·01
N(9)	0·01	−0·02
N(6)	0·10*	0·11*
Br	0·07*	−0·10*
C(1′)	0·18*	−0·20*
R.m.s. deviation	0·02	0·02

Barbiturate atom	Deviation for molecule *B*1 (Å)[c]	Deviation for molecule *B*2 (Å)[d]
N(1)	0·02	0·03
C(2)	0·05	0·01
N(3)	−0·04	−0·09
C(4)	−0·06	0·01
C(5)	0·02	0·02
C(6)	−0·02	−0·02
O(2)	0·07	0·03
O(4)	−0·07	0·03
O(6)	0·03	−0·02
R.m.s. deviation	0·05	0·04

* Atoms not included in calculating the least-squares plane.

(*a*), (*b*), (*c*), (*d*) refer to equations of least-squares planes: (*a*) $4{\cdot}0955x-23{\cdot}6069y+0{\cdot}7525z=-7{\cdot}4837$; (*b*) $3{\cdot}6248x-23{\cdot}5484y+1{\cdot}5700z=-7{\cdot}5625$; (*c*) $1{\cdot}6952x-25{\cdot}3789y+0{\cdot}1266z=-10{\cdot}1930$; (*d*) $2{\cdot}2864x-3{\cdot}6605y+10{\cdot}9103z=3{\cdot}4882$ Å.

The intermolecular associations

The crystal structure of *A.B* can be considered to be formed from a hierarchy of structural motifs. These motifs, some of which have quite unusual features, will be described in the order of their increasing complexity.

Both unique adenine molecules and barbiturate molecule *B*1 associate by hydrogen bonding to form extended ribbons of planar rings with the sequence *A*2–*B*1–*A*1–*A*1*–*B*1*–*A*2* (where the asterisks indicate the centrosymmetrically related molecules). This is illustrated in Fig. 3. Within these ribbons adenines *A*1 and *A*2 are each hydrogen-bonded to barbiturate *B*1 by a Watson–Crick-type association. In addition, adenine *A*1 forms a hydrogen-bonded cyclic dimer (*i.e.* molecules joined by two or more hydrogen bonds so as to form one or more rings) with a centrosymmetrically related adenine molecule, *A*1*, in a manner quite common for hydrogen-bonded adenine pairs (Voet & Rich, 1970; Voet, 1972). However, adenine *A*2 forms only one of the two hydrogen bonds that it has the potential to form [there is no possible acceptor group for such a second hydrogen bond that is within 4·0 Å of atom *A*2N(6)]. Failure to form a full complement of hydrogen bonds is rare in crystal structures in general and is without precedent among the 36 published crystal structures of base pairs (Voet & Rich, 1970; Sobell, 1971; Hsu & Craven, 1974).

The foregoing ribbon of hydrogen-bonded heterocyclic molecules has the form of an undulating plane. The mean planes of the two centrosymmetrically related (and hence parallel) adenine *A*1 molecules that form a cyclic dimer are 0·30 Å apart. The dihedral angles between the mean plane of barbiturate group *B*1 and those of adenine rings *A*1 and *A*2 are 14 and 15°, respectively. It is interesting to note that the dihedral angles between base-paired adenine and uracil rings are rarely greater than 10° (Voet & Rich, 1970) whereas those between base-paired adenine and barbiturate rings are all observed to be greater than 10° (Kim & Rich, 1968; Voet & Rich, 1972; Voet, 1972). The reasons for this phenomenon are not readily apparent.

Barbiturate molecule *B*2 does not join in the formation of hydrogen-bonded cyclic dimers. Rather it forms two single N–H···N hydrogen bonds in which atoms N(3) of both adenine residues *A*1 and *A*2 are the acceptor groups. Translationally related (by $z=1$) hydrogen-bonded ribbons of molecules of the previously described sort are thereby joined into planar strips that extend infinitely along the z direction. This structural feature can be seen in Fig. 3 and is schematically represented in Fig. 4(*a*).

The parameters describing the hydrogen bonds interconnecting this assemblage of molecules are all within the normal ranges for such interactions. The two N–H···O hydrogen bonds in the structure are both somewhat longer than the average for such interactions in agreement with the N–H···O distances reported in other crystal structures containing uracil or barbiturate residues in complex with adenine derivatives (Voet, 1972; Gartland & Craven, 1974).

Barbiturate *B*2 is more nearly perpendicular than parallel to the previously described ribbon of hydrogen-bonded molecules. The dihedral angles between the mean plane of barbiturate *B*2 and those of adenines *A*1 and *A*2 are 64 and 62°, respectively. This structural feature is also without precedent among the known crystal structures of base pairs (Voet & Rich, 1970; Sobell, 1971; Hsu & Craven, 1974).

Neighboring planar strips that are related by the translation (1,0,1) associate vertically in an overlapping manner much like that of shingles on a roof. A two to three-ply mat of hydrogen-bonded and stacked molecules is thereby formed that extends infinitely in the x and z directions and which is 7–11 Å thick along y. Such mats are centered at $y=0$ and $\frac{1}{2}$ according to the twofold screw symmetry of the unit cell. This assemblage of molecules is schematically illustrated in Fig. 4(*b*).

Within these mats of molecules adjacent parallel ribbons of hydrogen-bonded molecules associate vertically to form two to three-layered stacks of parallel

UM00013241
NOVARTIS EXHIBIT 1517
Novartis v. Regents, IPR2023-01347
Page 1987 of 4460

planar rings. This is illustrated in Fig. 5. Here it is seen that although these stacked ribbons lie directly over one another, their intermolecular interactions are largely characterized by a lack of overlap between neighboring rings. Such associations are typical of stacking interactions among purines and pyrimidines. The greatest amount of ring overlap in the structure is found in the stacking interactions between adenine rings *A*1 and *A*2. The relative orientation of the adenine rings in this interaction is almost identical to that found in the stacking interaction between two crystallographically non-equivalent 8-bromo-9-ethyladenine molecules in the crystal structure of the hydrogen-bonded complex phenobarbital–(8-bromo-9-ethyladenine)$_2$ (Kim & Rich, 1968) [see Fig. 11(*e*) of Bugg, Thomas, Rao & Sundaralingam, 1971]. The most intimate contact in this interaction is between the bromine atom of adenine *A*2 and the pyrimidine ring of adenine *A*1. The closest *A*2Br$\cdots$*A*1 ring contacts, *A*2Br$\cdots$*A*1N(3) $[x-1,y,z-1]$ and *A*2Br$\cdots$*A*1C(4) $[x-1,y,z-1]$ are 3·56 and 3·58 Å, respectively. The closest contact between light atoms in this stack, that between atom *A*2C(6) and *A*1N(6)$[1-x,1-y,2-z]$, is 3·38 Å. These distances are all near their respective minimal van der Waals contacts.

The rather large spaces between the above described mats of heterocycles are filled by the rings of barbiturates *B*2 and by the hydrocarbon substituents to the heterocycles as is indicated schematically in Fig. 4(*b*). However, these spaces are not efficiently filled as is suggested by the rather low density of the crystal (Table 1; other crystalline complexes of base pairs with elemental compositions similar to that of the present complex are generally reported to have densities in the range 1·5–1·7 g cm^{-3}). Indeed, barbiturate ring *B*2 makes no intermolecular contacts less than 4·0 Å, except for the regions about the two hydrogen bonds that it forms with adenines *A*1 and *A*2. This inefficient packing accounts for the disorder of the hydrocarbon substituents to the barbiturates. A similar phenomenon

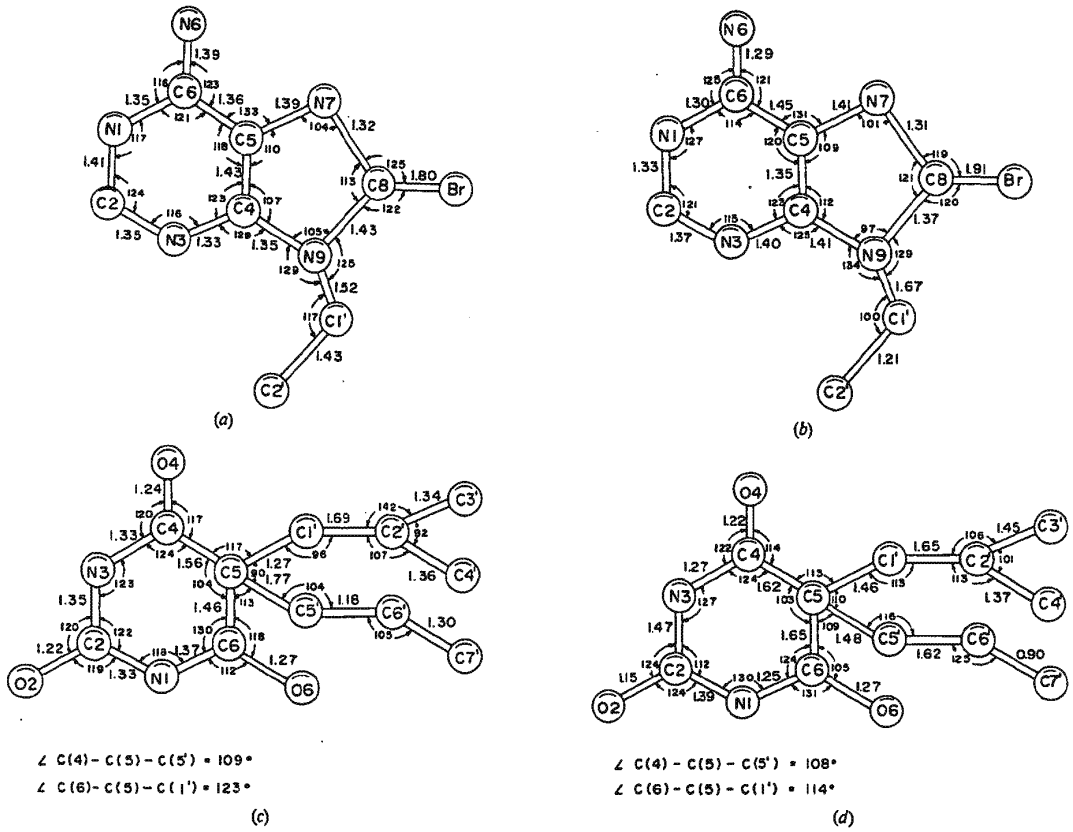


Fig. 2. The covalent bond distances (Å) and angles (°) of (*a*) 8-bromo-9-ethyladenine 1, (*b*) 8-bromo-9-ethyladenine 2, (*c*) 5-allyl-5-isobutylbarbituric acid 1 and (*d*) 5-allyl-5-isobutylbarbituric acid 2. The average standard deviations of these quantities are 0·04 Å and 3°, respectively, for ring distances and angles and are 0·08 Å and 5°, respectively, for distances and angles involving the hydrocarbon side groups.

UM00013242
NOVARTIS EXHIBIT 1517
Novartis v. Regents, IPR2023-01347
Page 1988 of 4460

has been described by Smit & Kanters (1974) in the crystal structure of 5-ethyl-5-(1,3-dimethylbutyl)barbituric acid. Despite the looseness of the crystal structure of *A.B* there is no indication that it incorporates any solvent of crystallization.

Both unique bromine atoms make closer than van der Waals contacts with oxygen atoms of neighboring barbiturate rings. The $A2\mathrm{Br}\cdots B2\mathrm{O}(4)[x-1,y,z]$ and the $A1\mathrm{Br}\cdots B1\mathrm{O}(6)[2-x,1-y,3-z]$ distances are 3·18 and 3·24 Å, respectively (the latter transformation relates the two halves of the hydrogen-bonded ribbon of heterocycles). The Br···O minimal van der Waals contact is 3·35 Å (Pauling, 1960). The C–Br···O angles associated with these close contacts are 173 and 132° for $A2\mathrm{C}(8)$–$A2\mathrm{Br}$–$B2\mathrm{O}(4)[x-1,y,z]$ and $A1\mathrm{C}(8)$–$A1\mathrm{Br}$–$B1\mathrm{O}(6)[2-x,1-y,3-z]$, respectively. The near linearity of the former angle suggests that the close $A2\mathrm{Br}\cdots B2\mathrm{O}(4)[x-1,y,z]$ contact is an association of the type that Hassel (1970) described as a charge-transfer interaction. The poor linearity of the latter Br···O interaction together with the relatively large errors in the bond distances suggest that the close $A1\mathrm{Br}\cdots B1\mathrm{O}(6)[2-x,1-y,3-z]$ contact can be attributed to the packing requirements necessary to maintain the integrity of the hydrogen-bonded ribbon of ring molecules. There are no other notably close interatomic contacts within the crystal structure.

Discussion

The most striking feature of the present structure is the nearly perpendicular disposition of barbiturate rings *B*2 with respect to the ribbons of base-paired molecules. Consideration of the 36 reported crystal structures containing base pairs (Voet & Rich, 1970; Sobell, 1971) leads to the expectation that all of the bases in a crystalline complex of stoichiometry $(A.B)_2$ will associate to form endless ribbons of hydrogen-bonded heterocycles in which the repeating motif is $\cdots A2\,.\,B2\,.\,A1\,.\,B1\cdots$. In the structure of *A.B* all of the hetero base-pairing

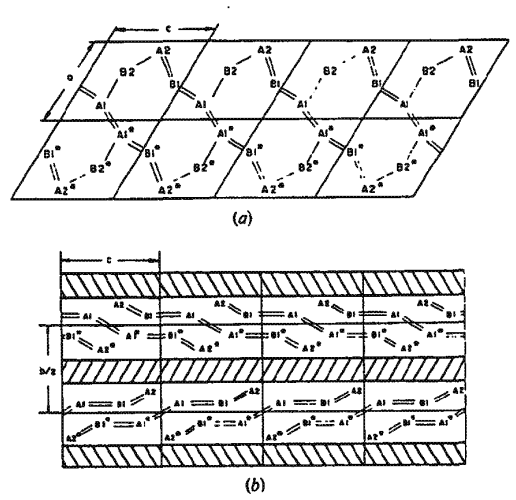


Fig. 4. Schematic drawings indicating the packing of the molecules of the complex *A.B* into its crystal structure. (*a*) View along the *b* axis illustrating the pattern of association of a hydrogen-bonded layer of heterocycles. (*b*) View along the *a* axis indicating the vertical packing mode of the hydrogen-bonded layers of heterocycles. Hydrogen bonds are represented by thin lines. The regions of the crystal structure containing the hydrocarbon side groups together with the rings of barbiturates *B*2 are represented by hatched areas.

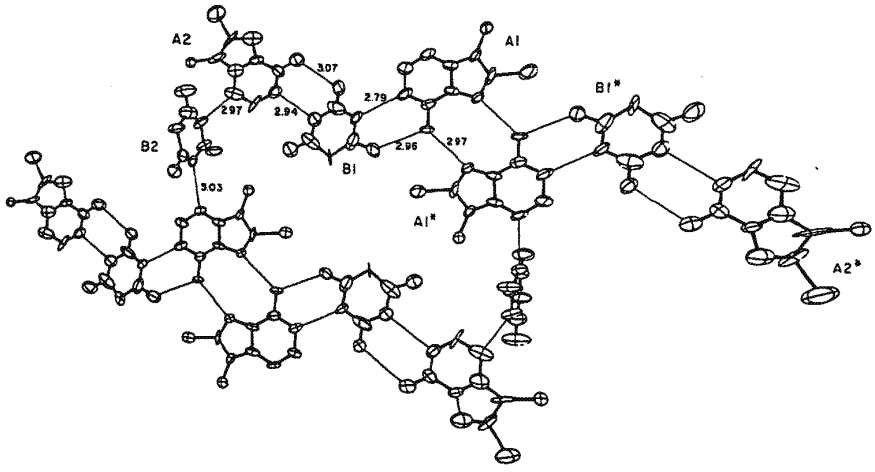


Fig. 3. A perspective drawing illustrating the hydrogen-bonding interactions in the crystalline complex 8-bromo-9-ethyladenine–5-allyl-5-isobutylbarbituric acid. All atoms are shown but atoms C(1′) of the adenine residues are illustrated as thermal ellipsoids at the 50% probability level. Atoms C(1′) of the adenine residues are represented by spheres of arbitrary radii. The other atoms of the hydrocarbon side groups have been omitted for the sake of clarity. Hydrogen bonds are represented by thin lines. The lengths of the unique hydrogen bonds are given in Å.

UM00013243
NOVARTIS EXHIBIT 1517
Novartis v. Regents, IPR2023-01347
Page 1989 of 4460

interactions must be of the Watson–Crick type because Hoogsteen pairing is prevented by steric interference with the 8-substituent bromine atoms of the adenine residues. Nevertheless model building studies using space filling (*CPK*) models indicate that there would be no obvious steric objection to the formation of any of several such Watson–Crick paired assemblies.

Previous structural studies of crystalline complexes of adenine derivatives with barbiturates (Voet, 1975) as well as those of other crystals incorporating barbiturates (Gartland & Craven, 1974) have shown that N–H···O hydrogen bonds, in which the acceptor is a barbiturate carbonyl group, tend to be abnormally long. Several of those hydrogen bonds are so long (3·3–3·4 Å) as to be essentially non-existent (Hamilton & Ibers, 1968). In other crystal structures containing barbiturates or barbiturate derivatives (Shieh & Voet, 1975; Bolton, 1964) the barbiturates do not participate as hydrogen-bonding acceptors. This information is consistent with the hypothesis that barbiturates are poor hydrogen-bonding acceptors (Voet, 1972; Gartland & Craven, 1974; Voet, 1975).

The prominent structural features of the present complex are also consistent with the above hypothesis. Only two of the possible twelve unique hydrogen-bond acceptor sites on the barbiturates participate in hydrogen bonding. In contrast, all six such sites on the adenine residues do so with the exception of atom *A*2N(7). However, the hydrogen-bonding capabilities of this latter position are significantly restricted due to the previously described steric interference with Hoogsteen pair formation.

In previously reported structures in which barbiturates or their derivatives have formed extremely long hydrogen bonds (Voet, 1972; Voet & Rich, 1972) or do not participate in hydrogen-bond formation (Shieh & Voet, 1975; Bolton, 1964), the barbiturates associate through dipole–dipole interactions between carbonyl groups. On the basis of these structures it could be argued that the hydrogen-bond acceptor capabilities of the barbiturates are not necessarily weak but that they are dominated by the presumably strong dipole–dipole interactions in which the barbiturates take part. However in the present structure, barbiturate *B*2, the molecule that accepts no hydrogen bonds, interacts quite loosely with its surrounding milieu. Hence this argument becomes considerably less convincing.

The experimental data concerning adenine–barbiturate complexes appear contradictory. Solution studies have shown that the association constants of adenine–barbiturate complexes are an order of magnitude greater than those of adenine–uracil complexes (Kyogoku, Lord & Rich, 1968). Yet crystallographic studies clearly indicate that N–H···O hydrogen bonds in which the acceptor group forms part of a barbiturate ring are significantly weaker than those in which the acceptor group is from a uracil derivative.

The simple electrostatic theory of hydrogen bonding leads to the expectation that the strong dipole moments generated by barbiturate carbonyl groups would render their affinity for hydrogen-bond formation particularly great. However, CNDO/2 molecular orbital calculations on 5,5-diethylbarbituric acid (Voet, 1972) suggest that the dipole moments of barbiturate carbonyl groups are no greater than those of uracil derivatives. Present day theory has not satisfactorily explained the barbiturates' observed lack of hydrogen-bond acceptor affinity nor has it accounted for the strength of the adenine–barbiturate association in a manner that is consistent with crystallographic observations. It remains for future studies, both theoretical and experimental, to resolve this apparent paradox.

This work was supported, in part, by NIH Grant No. GM 18632 and by NSF Grant No. DMR72-03025.

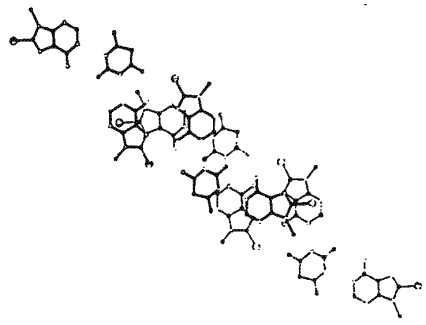


Fig. 5. A projection of two consecutive parallel ribbons of base-paired molecules onto the least-squares plane of adenine ring *A*1. This illustrates the ring stacking relationships within the crystal structure of *A.B.* Atoms are represented as circles of arbitrary radii with carbons as filled circles, nitrogen atoms as unfilled circles, oxygen atoms as shaded circles and bromine atoms as larger shaded circles.

References

Bolton, W. (1964). *Acta Cryst.* **17**, 147–152.

Bugg, C. E., Thomas, J. M., Rao, S. T. & Sundaralingam, M. (1971). *Biopolymers*, **10**, 175–219.

Cromer, D. T. & Waber, J. T. (1965). *Acta Cryst.* **18**, 104–109.

Gartland, G. L. & Craven, B. M. (1974). *Acta Cryst.* B**30**, 980–987.

Hamilton, W. C. (1965). *Acta Cryst.* **18**, 502–510.

Hamilton, W. C. & Ibers, J. A. (1968). *Hydrogen Bonding in Solids*. New York: Benjamin.

Hassel, O. (1970). *Science*, **170**, 497–502.

Hsu, I. -N. & Craven, B. M. (1974). *Acta Cryst.* B**30**, 988–993.

Kim, S. -H. & Rich, A. (1968). *Proc. Natl. Acad. Sci. U. S.* **60**, 402–408.

Kyogoku, Y., Lord, R. C. & Rich, A. (1968). *Nature, Lond.* **218**, 69–72.

Nakamoto, K., Margoshes, M. & Rundle, R. E. (1955). *J. Amer. Chem. Soc.* **77**, 6480–6486.

Pauling, L. (1960). *The Nature of the Chemical Bond*, 3rd ed., pp. 257–264. Ithaca: Cornell Univ. Press.

UM00013244
NOVARTIS EXHIBIT 1517
Novartis v. Regents, IPR2023-01347
Page 1990 of 4460

SHIEH, H. -S. & VOET, D. (1975). *Acta Cryst.* B31, 2192–2201.
SMIT, P. H. & KANTERS, J. A. (1974). *Acta Cryst.* B30, 784–790.
SOBELL, H. M. (1971). *The Purines, Theory and Experiment* (*The Jerusalem Symposia on Quantum Chemistry and Biochemistry* IV), edited by E. D. BERGMAN & B. PULLMAN, pp. 124–148. New York: Academic Press.
STOUT, G. H. & JENSEN, L. H. (1968). *X-ray Structure Determination*, pp. 456–458. New York: Macmillan.
VOET, D. (1972). *J. Amer. Chem. Soc.* 94, 8213–8222.
VOET, D. (1975). *Quantum and Molecular Pharmacology* (*The Jerusalem Symposia on Quantum Chemistry and Biochemistry* VII), edited by E. D. BERGMAN & B. PULLMAN, pp. 429–439. Dordrecht, Holland: Reidel Publishing Co.
VOET, D. & RICH, A. (1970). *Progr. Nucl. Acid. Res. Mol. Biol.* 10, 183–265.
VOET, D. & RICH, A. (1972). *J. Amer. Chem. Soc.* 94, 5888–5891.
WOOLFSON, M. M. (1956). *Acta Cryst.* 9, 804–810.

Acta Cryst. (1976). B32, 2188

A Neutron-Diffraction Study of the 1:1 Molecular Complex of 7,7,8,8-Tetracyanoquinodimethane with *p*-Terphenyl*

BY G. C. LISENSKY,† C. K. JOHNSON AND H. A. LEVY‡
Chemistry Division, Oak Ridge National Laboratory, Oak Ridge, Tennessee 37830, *U.S.A.*

(*Received* 10 *October* 1975; *accepted* 24 *January* 1976)

The 1:1 complex between 7,7,8,8-tetracyanoquinodimethane (TCNQ) and deuterated *p*-terphenyl forms dark red crystals, space group $P\bar{1}$, with one molecule of each component in the unit cell of dimensions $a = 8{\cdot}0189$ (5), $b = 8{\cdot}8927$ (5), $c = 8{\cdot}0264$ (5) Å, and $\alpha = 96{\cdot}413$ (3), $\beta = 95{\cdot}861$ (9), $\gamma = 102{\cdot}800$ (7)°. The structure was solved by fitting the transform of terphenyl-d to neutron-diffraction intensity data and was refined by least-squares methods, using 2614 unique reflections, to a final discrepancy index $R(F^2)$ of 0·042. All bond distances were determined to a precision of $\leq 0{\cdot}002$ Å. The structure consists of stacks in which TCNQ and terphenyl molecules alternate on centers of symmetry along the *a* axis. *p*-Terphenyl is an overcrowded molecule showing in-plane and out-of-plane deviations from the idealized planar conformation, the largest of which is a 12° torsion between the center and each end ring. The resultant distances between overcrowded deuterium atoms, 1·972 (2) and 1·985 (2) Å, are still less than the sum of van der Waals radii. An unusual pattern of incomplete deuteration was noted.

Introduction

Two main structure types of molecular complexes with TCNQ have been observed. In 'segregated stack' structures, approximately parallel molecules of the same kind occur in infinite stacks, while in 'mixed-stack' structures, molecules of two kinds alternate. Some charge-transfer complexes with TCNQ are good organic electrical conductors; although the segregated-stack arrangement seems to characterize the best conductors, mixed-stack structure determinations help to provide further understanding of TCNQ behavior.§ The structures of a number of mixed-stack charge-transfer complexes of TCNQ and planar aromatic compounds have been determined and are listed in Table 5.

The *p*-terphenyl complex with TCNQ has two features which are different from those with other planar aromatic compounds whose structures have been determined. The *p*-terphenyl molecule is longer than the TCNQ, so that there are several ways the two could overlap. The present structure determination shows that viewed perpendicular to the TCNQ plane the quinonoid *exo* double bonds center over the middle ring of terphenyl (see Fig. 1). Secondly, *p*-terphenyl in a planar conformation is an overcrowded molecule because the distance between the *ortho* bay§ hydrogen atoms is less than the sum of van der Waals radii. Rietveld, Maslen & Clews (1970) found that in crystals of *p*-terphenyl the molecule departs only slightly from planarity and the overcrowding is relieved by in-plane deformations. Baudour (1972) concluded that the planarity, however, did not necessarily correspond to the equilibrium configura-

* Research sponsored by the U. S. Energy Research and Development administration under contract with Union Carbide Corporation.
† Oak Ridge Associated Universities research participant from Earlham College, Richmond, Indiana 47374.
‡ Author to whom correspondence should be addressed.
§ The present compound is an insulator: the conductivity at room temperature is less than 4×10^{-11} ohm^{-1} cm^{-1}.

§ We suggest the descriptive term '*ortho* bay' to designate a pair of positions on separate rings each *ortho* to and lying on the same side of the bond between the rings. Jones & Sowden (1975) have employed the term 'bay' in a similar connection.

UM00013245
NOVARTIS EXHIBIT 1517
Novartis v. Regents, IPR2023-01347
Page 1991 of 4460

suitable for such exploitation, e.g., for selective oxidation of hydrocarbons.

Concluding Remarks

It should be encouraging, for organic chemists and chemical engineers alike, to know that enzymes can work not only in water but also in organic solvents. The still-existing prejudice against enzymes as practical catalysts will be lessened further by the forthcoming greater availability of a wider variety of enzymes at a lower cost, brought about by modern biotechnology. Moreover, protein engineering, particularly redesigning enzymes by site-directed mutagenesis,[90] has an exciting potential of altering the enzymatic properties at will, e.g., broadening substrate specificity,[91] as well as enhancing enzyme action in organic media.[92]

The ever intensifying search for novel biologically active compounds inevitably results in increasingly complex molecules, often containing stereocenters and existing as distinct structural isomers. Usually, one of the enantiomers or isomers has a higher biological activity than others. Consequently, there is mounting pressure on the manufacturers of pharmaceuticals and agricultural chemicals to produce only the desired stereoisomer, which would enhance the compound's benefit-to-harm ratio. As a result, the need for simple and scalable asymmetric conversions will grow. Hopefully, this Account demonstrates that enzymatic catalysis in organic solvents provides a useful methodology toward that aim.

I am grateful to David Volkin and Paul Burke for their help in the preparation of this manuscript and to the National Institutes of Health for financial support (Grant GM39794).

(90) Fersht, A. R.; et al. *Angew. Chem., Int. Ed. Engl.* **1984**, *23*, 467–473. Knowles, J. R. *Science* **1987**, *236*, 1252–1258.
(91) Bone, R.; Silen, J. L.; Agard, D. A. *Nature* **1989**, *339*, 191–195.
(92) Arnold, F. H. *Protein Eng.* **1988**, *2*, 21–25.

Encoding and Decoding Hydrogen-Bond Patterns of Organic Compounds

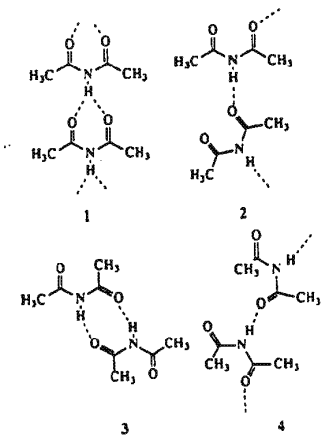
MARGARET C. ETTER

Department of Chemistry, University of Minnesota, Minneapolis, Minnesota 55455

Received June 20, 1989 (Revised Manuscript Received January 31, 1990)

Are hydrogen-bond patterns predictable? Benzoic acids form cyclic dimers. Salicylic acid has an intramolecular hydrogen bond. These hydrogen-bond patterns seem obvious because they satisfy the chemical criteria of pairing a somewhat acidic hydrogen with an electronegative atom, and because spectroscopic and crystallographic studies have confirmed our chemical intuition about how and when hydrogen bonds should form in these and in similar frequently studied structures.[1] But what about other, less studied, yet simple compounds like diacetamide? Diacetamide has two proton acceptors, one proton donor, and three possible conformers each of which could form two- or three-centered hydrogen-bonded chains or dimers. Four of the hydrogen-bond possibilities are shown. Patterns 1 and 3 are found in the two polymorphs of diacetamide.[2]

Besides these patterns, diacetamide also cocrystallizes with many other hydrogen-bonding molecules.[3] The inherent complexities in making such predictions are apparent in the intricate hydrogen-bond pattern observed for diacetamide and acetamide,[4] shown below. It certainly is not obvious that the cyclic pattern shown



1 2 3 4

Margaret C. Etter, a native of Wilmington, DE, obtained her B.A. in chemistry from the University of Pennsylvania, an M.Sc. from the University of Delaware, and her Ph.D. in organic chemistry from the University of Minnesota in 1974 under the direction of J. Z. Gougoutas. After seven years as a solid-state chemist and crystallographer at the 3M Company in St. Paul, MN, she returned to the University of Minnesota to do postdoctoral work with R. G. Bryant in solid-state NMR spectroscopy. She is currently an Associate Professor of Chemistry at the University of Minnesota, where her work on solid-state organic chemistry involves interdisciplinary studies of structures and properties of small-molecule organic solids, with special interests in hydrogen-bond interactions and crystal growth. She was recently awarded an Alfred P. Sloan Fellowship.

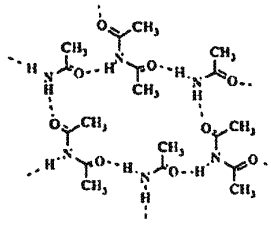
(1) The idea that some hydrogen-bond patterns are obvious and can be used to prepare aggregate patterns with predictable structures has been demonstrated by several different groups. (a) Ducharme, Y.; Wuest, J. D. *J. Org. Chem.* **1988**, *53*, 5789–5791. (b) Chang, S. K.; Hamilton, A. D. *J. Am. Chem. Soc.* **1988**, *110*, 1318–1319. (c) Askew, B.; Ballester, P.; Buhr, C.; Jeong, K. S.; Jones, S.; Parris, K.; Williams, K.; Rebek, J., Jr. *J. Am. Chem. Soc.* **1989**, *111*, 1082–1090, (d) Stadler, R. *Prog. Colloid Polym. Sci.* **1987**, *75*, 140–145.
(2) (a) Kuroda, Y.; Taira, Z.; Uno, T.; Osaki, K. *Cryst. Struct. Commun.* **1975**, *4*, 321–324. (b) Kuroda, Y.; Taira, Z.; Uno, T.; Osaki, K. *Ibid.* **1975**, *4*, 325–328.
(3) Etter, M. C.; Reutzel, S., unpublished results.

0001-4842/90/0123-0120$02.50/0 © 1990 American Chemical Society

UM00013246
NOVARTIS EXHIBIT 1517
Novartis v. Regents, IPR2023-01347
Page 1992 of 4460

is the most likely aggregate pattern.

Diacetamide-Acetamide (1:1) Cocrystal



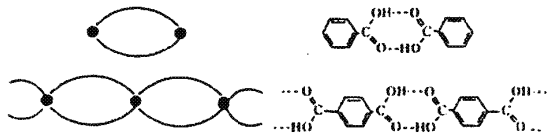
In the solid state, hydrogen-bond patterns are usually well defined and often involve infinite chains or arrays. Dimer patterns may be preferred in dilute solutions, and chains preferred in concentrated solutions or melts. Solvents with high dielectrics might favor more polar conformers. Such considerations pose additional difficulties for making empirical predictions of hydrogen-bond patterns. Theoretical methods have proven useful in addressing some of these problems.[5]

In this Account it is shown that empirical hydrogen-bond rules useful for determining preferred modes of hydrogen bonding can be developed by using the vast resource of data on intermolecular contacts found in the Cambridge Crystallographic Database.[6] Different functional-group classes show clear preferences for specific hydrogen-bond patterns in their crystal structures, despite the presence of other unpredictable and nonspecific lattice forces. These preferences can be framed as empirical "rules", which are most useful for predicting complete hydrogen-bond patterns of systems with a limited number of functional groups, or for predicting hydrogen-bond patterns of subsets of more complex systems. The rules are to be used as indicators of hydrogen-bond preferences of a particular functional group, whether in the solid state or in solution, in the absence of other competing forces.

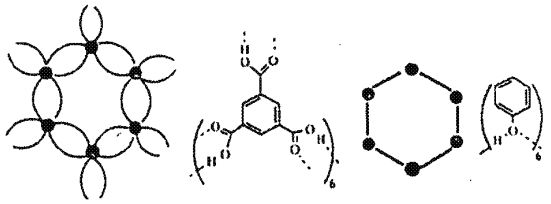
One of the challenges in determining hydrogen-bond preferences from crystal structures is to find a useful way to define a hydrogen-bond pattern. Frequently there are multiple intertwined hydrogen-bond patterns present in a single crystal structure, and similarities between complex patterns of chemically different systems may be completely lost without a consistent and analytically straightforward way to define the patterns. For example, a phenol–DMSO pair could be represented graphically by two points (the molecules) and one line (the hydrogen bond). The pattern is finite, and many other molecules can be imagined that fit this pattern:



Monocarboxylic acid dimers can be represented similarly, showing a finite dimeric graph with two hydrogen bonds per molecule. The infinite repeating dimer pattern is representative of the hydrogen-bond pattern of a dicarboxylic acid, such as terephthalic acid:



Other patterns can be constructed at will and molecules designed to fit the patterns. Conversely, similarities between subsets of hydrogen-bond patterns of known structures are readily recognized from their graphs. For example, trimesic acid (1,3,5–benzenetricarboxylic acid), left, and a cyclic hexameric phenol, right, would have a common hexagonal pattern. Other subsets of the trimesic acid structure match those of benzoic acid, and of terephthalic acid.



Assigning graph sets to particular hydrogen-bond patterns is the encoding process discussed in this Account. Development of empirical hydrogen-bond rules, based on the frequency of occurrence of specific graph sets within a functional group class, and based on observations about stereoelectronic hydrogen-bond preferences and hydrogen-bond selectivity, is the decoding process.

Hydrogen Bonds

The criteria for identifying hydrogen bonds must be established in order to define a hydrogen-bond pattern. Typically, criteria for defining hydrogen bonds are based on physical[7] and geometric properties.[8] Useful summaries of these criteria are given in recent reviews,[9] and comprehensive analyses are also available.[10] Most of these methods, however, focus on the three or four atoms involved in a hydrogen bond rather than on the consequences of such contacts for the rest of the atoms and molecules in the system. Now, with the luxury of a large data base of crystal structures of organic compounds,[6] the function of hydrogen bonds in aggregate structures can be evaluated, and the behavior of parts of a molecule or of many molecules in relation to their hydrogen bonds can be studied. The collective behavior of hydrogen bonds in many different related structures

(4) Matias, P. M.; Jeffrey, G. A.; Ruble, J. R. *Acta Crystallogr.* 1988, *B44*, 516–522.
(5) Ab initio calculations: (a) Jorgensen, W. L. *Acc. Chem. Res.*, in press, (b) Dory, M.; Delhalle, J.; Fripiat, J. G.; Andre, J.-M. *Int. J. Quantum Chem., Quantum Biol. Symp.* 1987, *14*, 85–103. Semiempirical calculations: (c) Radom, L.; Riggs, N. V. *Aust. J. Chem.* 1980, *33*, 2337–2342. (d) Vinson, L. K.; Dannenberg, J. J. *J. Am. Chem. Soc.* 1989, *111*, 2777–2781. Molecular mechanics calculations: (e) Dauber, P.; Hagler, A. T. *Acc. Chem. Res.* 1980, *13*, 105–112 and references therein.
(6) Allen, F. H.; Bellard, S.; Brice, M. D.; Cartwright, B. A.; Doubleday, A.; Higgs, H.; Hummelink, T.; Hummelink-Peters, B. G.; Kennard, O.; Motherwell, W. D. S.; Rodgers, J. R.; Watson, D. G. *Acta Crystallogr.* 1979, *B35*, 2331–2339.
(7) (a) Arnett, E. M. *Prog. Phys. Org. Chem.* 1963, *1*, 223–403. (b) Arnett, E. M.; Mitchell, E. J.; Murty, T. S. S. R. *J. Am. Chem. Soc.* 1974, *96*, 3875–3891.
(8) Taylor, R.; Kennard, O. *Acc. Chem. Res.* 1984, *17*, 320–326.
(9) (a) Kroon, J.; Kanters, J. A.; van Duijneveldt van de Rijdt, J. G. C. M.; Duijneveldt, F. B.; Vliegenthart, J. A. *J. Mol. Struct.* 1975, *24*, 109–129. (b) Brown, I. D. *Acta Crystallogr.* 1976, *A32*, 24–31. (c) Ceccarelli, C.; Jeffrey, G. A.; Taylor, R. *J. Mol. Struct.* 1981, *70*, 255–271. (d) Taylor, R.; Kennard, O.; Versichel, W. *J. Am. Chem. Soc.* 1984, *106*, 244–248. (e) Donohue, J. *Structural Chemistry and Molecular Biology*; Rich, A., Davidson, N., Eds.; W. H. Freeman: San Francisco, 1968; pp 443–465. (f) Joesten, M. D. *J. Chem. Educ.* 1982, *59*, 362–366.
(10) Schuster, P., Zundel, G., Sandorfy, C., Eds. *The Hydrogen Bond*; North-Holland: Amsterdam, 1976; Vols. I–III.

UM00013247
NOVARTIS EXHIBIT 1517
Novartis v. Regents, IPR2023-01347
Page 1993 of 4460

is the focus of this study. Our operative definition of hydrogen bonds is taken from Pauling's early definition of chemical bonds, which emphasizes the *organizational consequences* of bonds:[11]

> A hydrogen bond is an interaction that directs the association of a covalently bound hydrogen atom with one or more other atoms, groups of atoms, or molecules into an aggregate structure that is sufficiently stable to make it convenient for the chemist to consider it as an independent chemical species.

X-ray crystallography has made it convenient to consider hydrogen-bonded aggregates as independent species. The range of energies implied for hydrogen bonds defined in this way is yet to be determined. The range will probably extend down to less than 1 kcal/mol, but those very weak interactions will be included only when they have resulted in recognizable and recurring aggregate patterns.

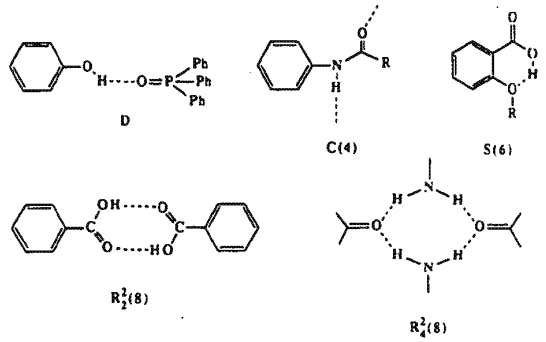
Graph Sets

The purpose of graph-set assignments is to define the morphology of hydrogen-bonded arrays. Kuleshova and Zorkii[12] were the first to apply graph theory[13] to organic crystal structures, while Wells[14] and Hamilton and Ibers[15] had developed accounting schemes for hydrogen bonds, which were precursors of the graph-set concept used here. In our method, real molecules rather than points are used as nodes, and hydrogen bonds are differentiated by the type of donors and acceptors that are present rather than being represented as just abstract lines.[16]

The process of assigning a graph set begins with identification of the number of different types of hydrogen bonds, as defined by the nature of the donors and acceptors in a hydrogen bond, that are present in the structure of interest. The set of molecules that are hydrogen bonded to one another by repetition of just one of these types of hydrogen bonds is called a motif and is characterized by one of four designators that indicate whether the motif is infinite or finite, and cyclic or not. For motifs generated from intermolecular hydrogen bonds, these designators are **C** (chain), **R** (ring), and **D** (dimer or other finite set), while **S** denotes an intramolecular hydrogen bond. The number of donors (**d**) and acceptors (**a**) used in each motif are assigned as subscripts and superscripts, respectively, and the size or degree of the motif (corresponding to the number of atoms in the repeat unit) is indicated in parentheses.

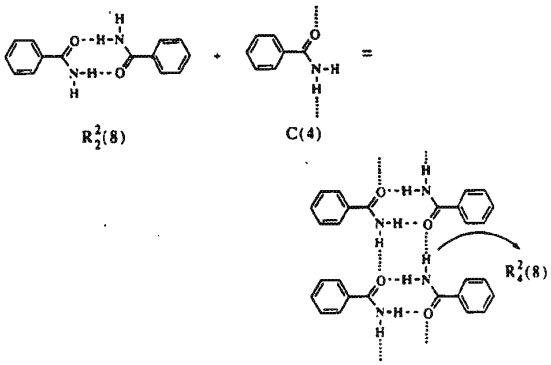
(11) Pauling, L. *The Nature of the Chemical Bond*, 3rd ed.; Cornell University Press: New York, 1960; p 6.
(12) (a) Kuleshova, L. N.; Zorky, P. M. *Acta Crystallogr.* **1980**, *B36*, 2113–2115. (b) Zorky, P. M.; Kuleshova, L. N. *Zh. Strukt. Khim.* **1980**, *22*, 153–156.
(13) (a) Harary, F. *Graph Theory and Theoretical Physics*; Academic Press: New York, 1967. (b) Merrifield, R. E.; Simmons, H. E. *Topological Methods in Chemistry*; John Wiley and Sons, Inc.: New York, 1989.
(14) Wells, A. F. *Structural Inorganic Chemistry*; Clarendon Press: Oxford, 1962; pp 294–315.
(15) Hamilton, W. C.; Ibers, J. A. *Hydrogen Bonding in Solids*; W. A. Benjamin, Inc.: New York, 1968; pp 19–21.
(16) (a) Etter, M. C.; Bernstein, J. B.; MacDonald, J. M. *Acta Crystallogr., Sect. B*, in press. (b) Etter, M. C. *Isr. J. Chem.* **1985**, *25*, 312–319. (Graph-set notation was introduced in this paper. Some of the designations have been changed in the present Account to be more consistent with other work in the field.)

Chart I
Graph-Set Assignments for Representative Hydrogen-Bond Motifs



Thus a benzoic acid dimer is a motif with graph set $\mathbf{R}_2^2(8)$, and a phenol hydrogen-bond chain has graph set C(2). Examples are given in Chart I.

One of the most useful aspects of this methodology involves differentiating between motifs containing only one type of hydrogen bond, and networks, $\mathbf{N}_i$, containing two or more types of hydrogen bonds. For example, a primary amide has two motifs corresponding to a cyclic dimer $\mathbf{R}_2^2(8)$ and a chain C(4). Combination of the two motifs generates a new $\mathbf{R}_4^2(8)$ pattern, shown below, containing two kinds of hydrogen bonds. In some cases the nature of an implied pattern like this one is important to the properties or structures of the compounds being studied, so it is helpful to specify it independently.



Graph-set assignments, thus, are done in stages. The first stage involves assigning all the motifs. Higher order networks resulting from combinations of the motifs may be assigned or not, as dictated by the chemical problem at hand. For very complex patterns, higher and higher order networks, involving three, four, or more different combinations of hydrogen bonds, can be identified systematically in this manner. Details of the process of making graph-set assignments have been published elsewhere.[16]

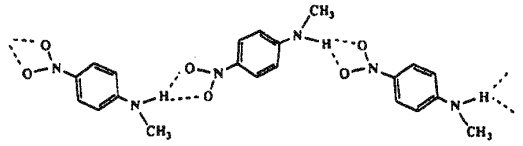
Using Graph Sets

By assigning graph sets to a series of crystal structures that contain one type of functional group, preferred patterns of hydrogen bonding may be seen. Leiserowitz found that most primary amides had the preferred hydrogen-bond motifs involving cyclic dimers and chains, $\mathbf{C(4)R}_2^2(8)$.[17] Special relationships between

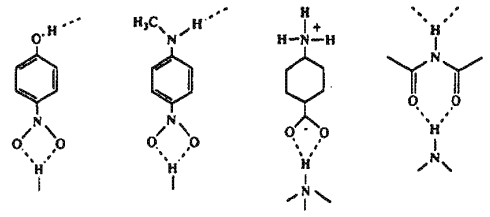
UM00013248
NOVARTIS EXHIBIT 1517
Novartis v. Regents, IPR2023-01347
Page 1994 of 4460

different amides and between amides and other kinds of molecules become evident upon comparison of their graph sets. The orthorhombic form of acetamide, for example, has an anomalous hydrogen-bond pattern, reflected in its unusual graph set, $C(4)R_1^1(12)$.[18] Most carboxylic acids have graph sets that match one of the primary amide motifs, $R_2^2(8)$, while secondary amides have the same graph set as the other primary amide motif, C(4).

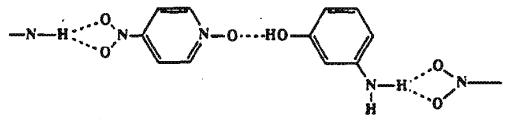
A study of all known crystal structures of small-molecule nitroaniline compounds showed that nitroanilines prefer a motif involving one amino proton associating with both oxygens of a nitro group,[19] as shown below. This pattern was observed even when bond lengths from nitro oxygens to the nearest amino hydrogens were longer than the sum of van der Waals radii. In several of the papers cited in the literature, it was stated that these interactions were not hydrogen bonds. Nevertheless, we found that the same aggregate pattern was present in all cases except those with unusual steric hindrance around the amino or nitro groups.



The hydrogen-bonding relationships derived for nitroanilines are useful for understanding the hydrogen-bonding properties of other molecules as well. For example, the OH group and the NH group in *p*-nitrophenol and *N*-methyl-*p*-nitroaniline both have a single proton donor that associates with a nitro group in a graph set $R_1^2(4)$. Chemically different functional groups having the same graph set are isographic. Recognition of isographic relationships between functional groups is a very useful and time-saving feature of this method since it allows the graph sets for one class of compounds to be transferred to another. Isographic functional groups usually have the same number of proton donors and acceptors, as shown.



The concept of isographic relationships also provides a powerful design tool for constructing cocrystals. In the nitroaniline examples above, the proton donors and acceptors were on the same molecule, but they should hydrogen bond to one another in the same way even if they are on different molecules. This principle is illustrated in the cocrystal structure of *p*-nitropyridine *N*-oxide and *m*-aminophenol, where the *N*-oxide and OH groups form a strong hydrogen bond to one another. The dimer is analogous to *m*-nitroaniline since the pair of molecules has a nitro group and an amino group oriented meta to one another. In this cocrystal, acentric chains form as a result of the expected intermolecular nitroaniline hydrogen bonding. The entire bulk cocrystal is acentric,[20] as is *m*-nitroaniline.[21]



Graph sets can also be used to understand polymorphic relationships. Iminodiacetic acid, $^-O_2CCH_2NH_2^+CH_2CO_2H$, is zwitterionic and exists in three polymorphic modifications. Two previous attempts had been made in the literature to compare and analyze the hydrogen-bond patterns in these structures.[22] The analyses involved comparing bond lengths and bond angles, symmetry relationships between neighboring hydrogen-bonded molecules, and identification of some of the ring patterns. Nevertheless, little insight was gained into similarities that existed between these structures or into the relative stabilities of the crystals. One of the previous authors, J. Bernstein, recently used the graph-set method to reanalyze these patterns. Similarities in the motifs were observed immediately. Five motifs occurred in different combinations in the three polymorphs. Two of the polymorphs had the same first-order network but differed in their second-order network, as shown.[23]

polymorph 1: $N_1 = C(5)R_2^2(10)C(8)$ $N_2 = R_2^2(14)$

polymorph 2: $N_1 = C(5)R_2^2(10)C(8)$ $N_2 = R_4^2(8)$

polymorph 3: $N_1 = C(5)C(5)C(8)$

Hydrogen-Bond Rules

Empirical hydrogen-bond rules (Table I) are a way to use correlations that exist between functional groups and hydrogen-bond patterns, with graph sets being one type of correlation. Graph sets deal with the connectivity or configuration of a set of hydrogen-bonded molecules, analogous to the primary structure of a macromolecule. Other stereoelectronic or structural factors affecting the primary, secondary, and even tertiary structures provide the other hydrogen-bond rules.[24]

The first three rules listed in Table I apply in general to functional groups in neutral organic molecules. To apply the first rule, which was originally put forth by

(17) (a) Carboxylic acids: Leiserowitz, L. *Acta Crystallogr.* 1976, *B32*, 775–802. (b) Primary amides: Leiserowitz, L.; Schmidt, G. M. J. *J. Chem. Soc. A* 1969, 2372–2382. (c) Secondary amides: Leiserowitz, L.; Tuval, M. *Acta Crystallogr.* 1978, *B34*, 1230–1247. (d) From refs 17a–c, four simple hydrogen-bond rules are evident: carboxylic acids prefer to form cyclic hydrogen-bonded dimers ($R_2^2(8)$); a few carboxylic acids form hydrogen-bonded chains (C(4)); acyclic secondary amides form only chains (C(4)); primary amides form cyclic dimers which are hydrogen-bonded together to form chains ($C(4)R_2^2(8)$). Additional specific rules may be further deduced from these papers.

(18) Hamilton, W. C. *Acta Crystallogr.* 1965, *18*, 866–870.

(19) Panunto, T. W.; Urbańczyk-Lipkowska, Z.; Johnson, R. B.; Etter, M. C. *J. Am. Chem. Soc.* 1987, *109*, 7786–7797.

(20) Lechat, J. R.; de Almeida Santos, R. H.; Bueno, W. A. *Acta Crystallogr.* 1981, *B37*, 1468–1470.

(21) Shapski, A. C.; Stevenson, J. L. *J. Chem. Soc., Perkin Trans. 2* 1973, 1197–1200.

(22) (a) Bernstein, J. *Acta Crystallogr.* 1979, *B35*, 360–366. (b) Boman, C.-E. Herbertsson, H.; Oskarsson, A. *Acta Crystallogr.* 1974, *B30*, 378–382.

(23) Bernstein, J.; Etter, M. C.; MacDonald, J. M. *J. Chem. Soc., Perkin Trans. 2*, in press.

(24) The idea of secondary structure in sets of small molecules is discussed in the following: (a) Leiserowitz, L.; Hagler, A. T. *Proc. R. Soc. London* 1983, *A388*, 133–175. Stereoelectronic effects in hydrogen bonding are discussed in the following: (b) Glusker, J. P.; Murray-Rust, P. *J. Am. Chem. Soc.* 1984, *106*, 1018–1025.

UM00013249
NOVARTIS EXHIBIT 1517
Novartis v. Regents, IPR2023-01347
Page 1995 of 4460

Table I
Hydrogen-Bond Rules for Organic Compounds

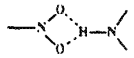
A. General Rules

1. All good proton donors and acceptors are used in hydrogen bonding.
2. Six-membered-ring intramolecular hydrogen bonds form in preference to intermolecular hydrogen bonds.
3. The best proton donors and acceptors remaining after intramolecular hydrogen-bond formation form intermolecular hydrogen bonds to one another.

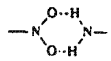
B. Additional Rules for Specific Classes of Functional Groups

Nitroanilines[19]

4. Amino protons will hydrogen bond to nitro groups.
5. One or more intermolecular amino–nitro hydrogen bonds will form.
6. The aggregate patterns formed from intermolecular hydrogen bonds between substituents in meta and para positions will be acentric.
7. The amino–nitro interaction is usually a three-center hydrogen bond, $R_1^2(4)$.

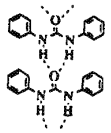


8. Ortho-substituted primary nitroanilines usually form two-center intermolecular hydrogen bonds, rather than three-center, with graph set $R_2^2(6)$.

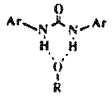


Diarylureas[28b]

4. The NH hydrogens prefer to adopt an anti relationship to the carbonyl group and to form three-center bonds to urea carbonyl groups, $C(4)[R_2^1(6)]$.



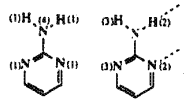
5. Cocrystals form in $R_2^1(6)$ patterns when there are strong meta-substituted electron-withdrawing substituents, like NO_2 groups, on the aryl rings, and when the guest molecules have acceptor groups that are stronger than the internally hydrogen bonded urea carbonyl oxygen.



6. When cocrystals form, the NH protons form three-center bonds to acceptor groups, $R_2^1(6)$.
7. Nitro groups of *m*-nitro-substituted diarylureas are not usually used as hydrogen-bond acceptors for urea NH hydrogens in the presence of guest molecules with good hydrogen-bond acceptors.

Carboxylic Acid Cocrystals with 2-Aminopyrimidine[27]

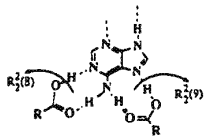
4. Both NH protons and both ring nitrogens are used in hydrogen bonds.
5. 2-Aminopyrimidine (2AP) prefers to form hydrogen bonds to acids rather than to itself.
6. 2AP forms cyclic $R_2^2(8)$ patterns with acids and with itself.
7. The two NH protons need not form hydrogen bonds to identical groups. Likewise for the ring nitrogens.
8. A ranking of proton-accepting ability consistent with these structures is N1 > N3 > acid carbonyl > N2, or N4, where the numbered pyrimidine atoms are those indicated in the monomeric and hydrogen-bonded structures.



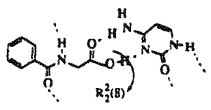
9. Proton donor ranking is acid OH > NH(1) > NH(3) > NH(2).

Nucleotide Base (NB) Cocrystals[38]

4. Adenine (A) and cytosine (C) form cocrystals with many acidic organic compounds, but thymine and uracil do not.
5. Cocrystals of A or of C with carboxylic acids give patterns with $R_2^2(8)$ or $R_2^2(9)$ graph sets.



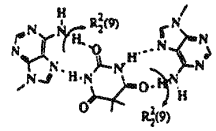
6. Neutral *N*-acylamino acids complex with A or C in $R_2^2(8)$ patterns.



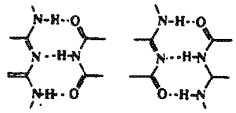
UM00013250
NOVARTIS EXHIBIT 1517
Novartis v. Regents, IPR2023-01347
Page 1996 of 4460

Table I (Continued)

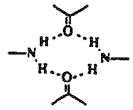
7. Cyclic alternant –C(O)–NH– groups complex with A and C with preferred graph set $R_2^2(9)R_2^2(9)$.



8. Three-centered hydrogen-bond contacts are frequently found with $N_1 = R_2^2(8)$ and $N_2 = R_3^2(12)$.

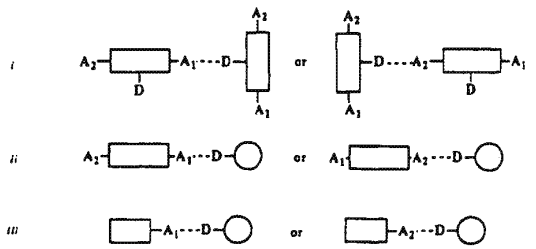


9. A common motif for NB complexes involves two primary amines and two carbonyl groups in an $R_4^2(8)$ or $C_2^1(4)$ pattern.



Donohue,[25] "good proton donors" and "good proton acceptors" have to be defined. We have found, not unexpectedly, that proton donors such as those in carboxylic acids, amides, ureas, anilines, imides, and phenols are nearly always used in hydrogen bonding in a crystal structure. Less acidic protons such as those in acetylenes, aldehydes, or activated aromatic and aliphatic compounds may be used in hydrogen bonding when there are extra proton acceptors available after all the more acidic protons have found an acceptor. Proton acceptors are typically acid and amide carbonyl groups, sulfoxides, phosphoryls, nitroxides, and amine nitrogens.

Solid-state acceptor and donor properties of molecules can be ranked by using the schemes shown below. Each scheme presents a different experimental technique for testing the competition between formation of $A_1\cdots D$ vs $A_2\cdots D$. In the first case, the two acceptor groups and the donor are on the same molecule. Two different crystal structures result from the two different hydrogen-bond choices. In the second case, the donor is on a guest molecule and the two possible hydrogen-bond contacts give rise to two different cocrystal structures. In the third case, the donor guest molecule selectively hydrogen bonds to one of the two acceptor molecules in a mixed solution. The chemical composition of cocrystals formed in scheme iii will actually be different. By changing the A groups in these experiments, relative acceptor strengths can be ranked.



The second rule derives from competition studies where we find that an intramolecular hydrogen bond is more difficult to break than a comparable intermolecular hydrogen bond formed between similar donors and acceptors. We have also observed that six-membered-ring intramolecular hydrogen bonds usually occur in crystal structures in preference to intermolecular hydrogen bonds when donor and acceptor groups are positioned to allow such an interaction. There are exceptions to this rule, but they are rare.[26] Intramolecular hydrogen bonds in five- and seven-membered rings are also common, but we do not have data at this point about competition between these bonds and intermolecular hydrogen bonds.

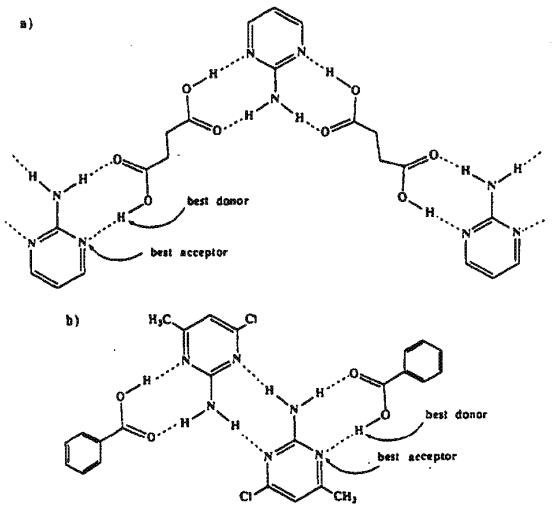


Figure 1. Hydrogen-bond patterns of 2-aminopyrimidine (2AP) and carboxylic acids. (a) This pattern shows the use of all good proton donors and acceptors, selectivity of the best proton donor (carboxylic acid proton) for the best proton acceptor (pyrimidine ring nitrogen), and formation of $R_2^2(8)$ ring motifs.[27] (b) Cocrystals (1:1) of the 4-chloro-6-methyl derivative of 2AP and benzoic acid have been made, but the crystal structure is unknown.[39] A proposed hydrogen-bond pattern, consistent with the known stoichiometry, and based on the rules from Table I, is shown.

The third rule is illustrated by 2-aminopyrimidine–carboxylic acid cocrystals. In these structures (Figure 1), the best donors (acid OH) are paired with the best acceptors (ring N).[27] When substituents are present

(25) Donohue, J. *J. Phys. Chem.* **1952**, *56*, 502–510.

(26) Etter, M. C.; Urbańczyk-Lipkowska, Z.; Fish, P. A.; Panunto, T. W.; Baures, P. W. *J. Crystallogr. Spectrosc. Res.* **1988**, *18*, 311–325.

(27) Etter, M. C.; Adsmond, D. A. *J. Chem. Soc., Chem. Commun.*, in press.

UM00013251
NOVARTIS EXHIBIT 1517
Novartis v. Regents, IPR2023-01347
Page 1997 of 4460

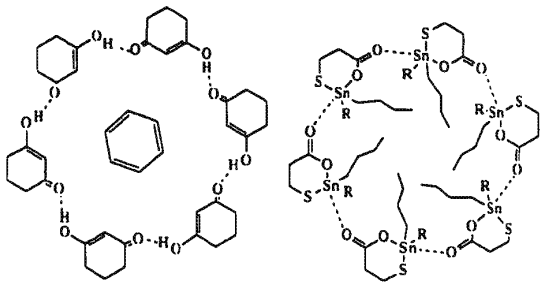
on the pyrimidine ring, the relative accepting strengths of the two ring nitrogens change in a predictable way, changing the aggregate hydrogen-bond patterns but still reflecting association of the best acceptor and the best donor. Examples of this rule have also been demonstrated for carboxylic acid hetero dimers, urea cocrystals, and triphenylphosphine oxide complexes.[28]

Specific hydrogen-bond rules, in addition to the three general rules given above, can be derived for other functional-group classes. Some examples are given in Table I. Others are available in the literature.[17d,29] Graph-set frequency for the functional group of interest is monitored from sets of crystal structures to see if preferences are apparent, while perturbations of hydrogen-bond patterns by competing functional groups give information about selectivity. These observations constitute the specific hydrogen-bonding rules. The rules should evolve as new structures become available, but we have found that the most important relationships are usually seen from the first 10 or so structures in a series.

Other Weak Intermolecular Interactions and Competition with Hydrogen Bonds

Hydrogen bonds are not the only type of intermolecular interactions that are useful for directing molecular self-assembly. Lithium–oxygen chelation is a well-known example of such an interaction.[30] Other intermolecular interactions that occur in organic systems may also be candidates for "intermolecular syntheses" when they are sufficiently strong and sufficiently directional to give rise to recognizable and reproducible molecular assemblies.

Two directed intermolecular interactions that are about as strong as hydrogen bonds are S···O[31] and Sn···O bonds. A striking example of the use of the latter interaction as a hydrogen-bond surrogate involves the two structures shown below.[32,33]



Ionic interactions are considerably stronger than hydrogen bonds, and they usually dominate a packing pattern;[34] nevertheless, hydrogen bonds may still be useful as organizing forces even in the presence of ionic interactions.[35] Very weak electrostatic attractions sometimes give predictable association patterns, as shown by Burgi and Dunitz.[36] Van der Waals interactions, charge-transfer interactions, and halogen–halogen interactions have also been used.[37]

Graph-set analysis and the protocol presented here for developing hydrogen-bond rules provide a framework for studying hydrogen-bond-directed aggregation, with the long-range goal of learning how hydrogen bonds compete with and cooperate with other forces that determine aggregate structures. Hopefully in the future these results can be coupled with theoretical studies in order to gain a better understanding of why particular patterns are preferred.

I am particularly grateful to Prof. Joel Bernstein, Ben Gurion University of the Negev, for his enthusiasm and helpful comments about the work and the manuscript. I also thank the students in my research group for the many hours spent developing and testing graph sets. Financial support from the NIH (GM 42148-01), NSF (CHE8600383-02), and Office of Naval Research is gratefully acknowledged.

(28) (a) Etter, M. C.; Baures, P. W. *J. Am. Chem. Soc.* **1988**, *110*, 639–640. (b) Etter, M. C.; Panunto, T. W. *J. Am. Chem. Soc.* **1988**, *110*, 5896–5897. (c) Etter, M. C.; Frankenbach, G. M. *Chem. Mater.* **1989**, *1*, 10–11.

(29) (a) Carbohydrates: Jeffrey, G. A.; Takagi, S. *Acc. Chem. Res.* **1978**, *11*, 264–270. (b) Amino acids: Jeffrey, G. A. In *Structure and Biological Activity*; Griffin, J. F., Duax, W. L., Eds.; Elsevier Science Publ.: New York, 1982; pp 135–150.

(30) Setzer, W. N.; Schleyer, P. v. R. *Adv. Organomet. Chem.* **1985**, *24*, 353–451.

(31) (a) Kálmán, A.; Parkanyi, L. *Acta Crystallogr., Sect. B* **1980**, *36*, 2372–2378. (b) Rosenfield, R. E., Jr.; Parthasarathy, R. J.; Dunitz, J. D. *J. Am. Chem. Soc.* **1977**, *99*, 4860–4862.

(32) Etter, M. C.; Urbańczyk-Lipkowska, Z.; Jahn, D. A.; Frye, J. S. *J. Am. Chem. Soc.* **1986**, *108*, 5871–5876.

(33) Lockhart, T. *Organometallics* **1988**, *7*, 1438–1443.

(34) Fagan, P. J.; Ward, M. D.; Calabrese, J. C. *J. Am. Chem. Soc.* **1989**, *111*, 1698–1719.

(35) Day, V. W.; Klemperer, W. G.; Maltbie, D. J. *J. Am. Chem. Soc.* **1987**, *109*, 2991–3002.

(36) Burgi, H. B.; Dunitz, J. D. *Acc. Chem. Res.* **1983**, *16*, 153–161.

(37) (a) Charge transfer: Torrance, J. B. *Acc. Chem. Res.* **1979**, *12*, 79–86. (b) Halogen–halogen: Desiraju, G.; Sarma, J. A. R. P. *Acc. Chem. Res.* **1986**, *19*, 222. (c) Van der Waals: Salemme, F. R.; Genieser, L.; Finzel, B. C.; Helmer, R. M.; Wendoloski, J. J. *J. Cryst. Growth* **1988**, *90*, 273–282. (d) Griffin, J. F.; Smith, G. D. *Structure and Expression*, Vol. I from *From Proteins to Ribosomes*; Sarma, R. H., Sarma, M. H., Eds.; Adenine Press: New York, 1988; pp 129–147.

(38) Structural data taken from the following: Tamura, C.; Sato, S.; Hata, T. *Bull. Chem. Soc. Jpn.* **1973**, *46*, 2388–2394 and references therein.

(39) Etter, M. C.; Adsmond, D. A., unpublished results.

UM00013252
NOVARTIS EXHIBIT 1517
Novartis v. Regents, IPR2023-01347
Page 1998 of 4460

Concluding remarks

The pressure-induced structural transformation of CHD involves, apart from other effects, the interchange of donor and acceptor sites by the enolic H atoms in the hydrogen bonds. The structure, despite its close similarities with antiferroelectric crystals, is ordered in the high-pressure phase, also retaining its low-pressure symmetry. It is possible that the crystals have a domain structure in both low- and high-pressure phases. The proposed mechanism of the transformation strongly suggests an important role of electrostatic interactions in the transformation and in the jump of the enolic H atom to its other site in the OH···O bond. This mechanism also affords an explanation of the phase transition observed in CPD and of the exceptional stability of MCPD at high pressures; however, several points still need to be confirmed and further studies are being carried out on the CHD crystals.

The author is grateful to Professor Z. Kałuski for encouragement, to Dr R. J. Nelmes for his invitation to use the high-pressure and X-ray facilities of the Physics Department, University of Edinburgh, to Professor M. C. Etter of the Department of Chemistry, University of Minnesota, for stimulating discussions and providing the 1,3-cyclohexanedione samples crystallized from 2-pentanone, and to Dr J. Koput (Adam Mickiewicz University) for his expertise in the MNDO calculations. This study was partly supported by the British Council and by the Polish Academy of Sciences, Project CPBP, 01.12.

References

ALLMANN, R. (1977). In *Homoatomic Rings, Chains and Macromolecules of Main Group Elements*, edited by A. RHEINGOLD. Amsterdam: Elsevier.
DEWAR, M. J. S. & THIEL, W. (1977). *J. Am. Chem. Soc.* **99**, 4899–4907.
DREMIN, A. N. & BABARE, L. V. (1984). *J. Phys. (Paris) Colloq.* C8, 177–186.
DUPONT, L., LAMOTTE, J., CAMPSTEYN, H. & VERMEIRE, M. (1978). *Acta Cryst.* B34, 1304–1310.
ETTER, M. C., URBAŃCZYK-LIPKOWSKA, Z., JAHN, D. A. & FRYE, J. S. (1986). *J. Am. Chem. Soc.* **108**, 5871–5876.
FINGER, L. W. & KING, H. E. JR (1978). *Am. Mineral.* **63**, 337–342.
KATRUSIAK, A. (1989). *Acta Cryst.* C45, 1897–1899.
KATRUSIAK, A. (1990*a*). *Acta Cryst.* C46. In the press.
KATRUSIAK, A. (1990*b*). *J. Appl. Cryst.* **23**. Submitted.
KATRUSIAK, A. (1990*c*). *Acta Cryst.* B46. Submitted.
KATRUSIAK, A. (1990*d*). *Acta Cryst.* B46. In preparation.
KATRUSIAK, A. & NELMES, R. J. (1986). *J. Phys. C*, **19**, L765–L772.
KING, H. E. JR (1981). *High-Pressure Crystallography with a CAD-4*. Enraf–Nonius, Delft, The Netherlands.
MERRILL, L. & BASSETT, W. A. (1974). *Rev. Sci. Instrum.* **45**, 290–294.
MOTHERWELL, W. D. (1976). *PLUTO*. Program for plotting molecular and crystal structures. Univ. of Cambridge, England.
NICOL, M. & YIN, G. Z. (1984). *J. Phys. (Paris) Colloq.* C8, 163–172.
PIERMARINI, G. J., BLOCK, S., BARNETT, J. D. & FORMAN, R. A. (1975). *J. Appl. Phys.* **46**, 2774–2780.
SAMARA, G. A. & SEMMINGSEN, D. (1979). *J. Chem. Phys.* **71**, 1401–1407.
SAPRIEL, J. (1975). *Phys. Rev. B*, **12**, 5128–5139.
SEMMINGSEN, D. (1974). *Acta Chem. Scand. Ser. B*, **28**, 169–174.
SHELDRICK, G. (1976). *SHELX76*. Program for crystal structure determination. Univ. of Cambridge, England.
SINGH, I. & CALVO, C. (1975). *Can. J. Chem.* **53**, 1046–1050.
TUN, Z., NELMES, R. J. & MCINTYRE, G. J. (1987). *J. Phys. C*, **20**, 5667–5675.

Acta Cryst. (1990). B46, 256–262

Graph-Set Analysis of Hydrogen-Bond Patterns in Organic Crystals

BY MARGARET C. ETTER* AND JOHN C. MACDONALD

Department of Chemistry, University of Minnesota, Minneapolis, MN 55455, USA

AND JOEL BERNSTEIN

Ben-Gurion University of the Negev, Beer Sheva, Israel

(*Received* 17 *August* 1989; *accepted* 15 *November* 1989)

Abstract

A method is presented based on graph theory for categorizing hydrogen-bond motifs in such a way that complex hydrogen-bond patterns can be disentangled, or decoded, systematically and consistently. This method is based on viewing hydrogen-bond patterns topologically as if they were intertwined nets with molecules as the nodes and hydrogen bonds as the lines. Surprisingly, very few parameters are needed to define the hydrogen-bond motifs comprising these networks. The methods for making these assignments, and examples of their chemical utility are given.

* Alfred P. Sloan Foundation Fellow, 1989–1991.

0108-7681/90/020256-07$03.00

© 1990 International Union of Crystallography

UM00013253
NOVARTIS EXHIBIT 1517
Novartis v. Regents, IPR2023-01347
Page 1999 of 4460

Introduction

Since hydrogen bonds were first proposed, efforts to characterize them, measure them, and understand them have proliferated (Latimer & Rodebush, 1920; Schuster, Zundel & Sandorfy, 1976; Joesten & Schaad, 1974). As it became obvious that these interactions occurred in many kinds of materials, and were important for determining the properties and activities of most biochemicals, hydrogen-bond classifications were developed; the most successful of these relate to their spectroscopic and chemical properties (Taylor & Kennard, 1984; Murray-Rust & Glusker, 1984; Emsley, 1980). Wells (1962) was one of the first to recognize the importance of hydrogen-bond patterns, independent of the geometry or of spectroscopic or thermal properties of the bonds. This perspective provided new insights into the role of hydrogen bonds in controlling the structures of ensembles of molecules. The consequences of repetitive hydrogen-bond interactions throughout a crystal structure or throughout a self-assembled aggregate structure had not previously been addressed. In other words, this topological point of view allowed one to characterize subsets of crystal structures or arrays, namely, the hydrogen-bonded subset.

Wells proposed a classification scheme for describing hydrogen-bond structures in inorganic compounds based on consideration of molecules as single points with hydrogen bonds as lines emanating from these points. Hamilton & Ibers (1968) developed this idea further, characterizing hydrogen-bonded networks with two numbers (N, M), the number of hydrogen bonds per point (N), and the number of molecules to which a point is hydrogen bonded (M). Kuleshova & Zorky (1980) recognized that these early classification schemes were actually an application of graph theory, a mathematical formalism for analyzing graphs and networks (Harary, 1967). This theory has been used for many different chemical applications, such as analysis of stereochemical topology (Walba, 1987), development of synthetic strategies (Fujita, 1988*a*) and coding of reaction pathways (Fujita, 1988*b*). Kuleshova & Zorky developed Wells' idea and applied graph theory to hydrogen-bond patterns in organic crystal structures. They identified finite sets, chains, layers and frameworks of hydrogen-bonded molecules, and they made initial surveys of the crystallographic literature to determine whether certain graph sets occurred more frequently than others. They also studied a set of hydrogen-bonded polymorphs and found that about half of them had the same graph set for both polymorphs (Zorky & Kuleshova, 1980).

The graph-set method presented here uses a molecular version of graph-set representations of hydrogen-bond patterns where functional groups and molecular structure are used explicitly. Graph theory has been adapted here rather freely to preserve a strong chemical component. The derivation from single points to molecules as the basic unit of a graph is important in order to represent hydrogen-bond patterns of organic molecules where different functional groups on a single molecule contribute in different ways to the hydrogen-bond network. Attempts are made to make the method applicable to as many different kinds of systems as possible within the constraints of keeping the notation and the process simple. Arrays that are easiest to handle using the graph-set method involve typical neutral organic molecules with a low density of hydrogen bonds, as opposed to structures like urea or oxalic acid which have high hydrogen-bond densities.

Graph sets, as presented here, are descriptions like the organic chemist's empirical formula or the crystallographer's space group. They tell how many donors and acceptors are used in a hydrogen-bond pattern and what the nature of the pattern is, yet they also highlight common features of molecular aggregates that are not addressed by empirical formulae or by the symmetry considerations of space groups. To analyze a hydrogen-bond pattern, the criteria for identifying hydrogen bonds must be established by the investigator. For the present purpose we find it useful to consider the collective behavior of molecules as they self assemble by interactions between hydrogen-bond donors and hydrogen-bond acceptors, without setting arbitrary limits on hydrogen-bond lengths or energies. The topologies of the patterns are considered rather than their particular geometries.

Operational definitions are given here and the process of assigning graph sets is explained.* Examples of how to apply graph sets to problems of decoding and comparing hydrogen-bond patterns are given at the end of this article.

Graph-set definitions

The set of molecules to be analyzed is called an *array*. Some or all of the molecules in the array are

* Several of the concepts developed here have a direct analogy with graph-theoretical concepts, while others have a more distant relation. To clarify these relations, the equivalencies are given, with the first term being the one used here, and the second italicized term being the one used by graph theoreticians (Harary, 1967): hydrogen bonds/*lines*; molecules/*points*; array/*graph*; motif/*spanning walk*; the superscript character *a* used in the notation/*indegree of a directed graph*; subscript character, *d*/*outdegree of a directed graph*. The most important difference between the two methods is that mathematical graphs involve points and lines having no structural properties. The points used in our method are molecules whose structure is implicit in the graph-set assignments. Likewise, we differentiate between different kinds of hydrogen bonds, but in mathematical graph sets all lines are identical.

UM00013254
NOVARTIS EXHIBIT 1517
Novartis v. Regents, IPR2023-01347
Page 2000 of 4460

associated through hydrogen bonds. This array need not be in a crystal structure, but regularly repeating sets such as those found in crystal structures are particularly suitable for graph-set assignments. The geometry of a hydrogen bond is not critical in these analyses, so even a hand-drawn picture of a hypothetical set of molecules is sufficient for making graph-set assignments.

A *network* is a subset of an array in which each molecule in the network is connected to every other molecule by at least one hydrogen-bonded pathway. A network contains any number of different kinds of hydrogen bonds. Our challenge is to define the morphology of this network.

A *motif* is a special type of network. *It is a hydrogen-bonded set in which only one type of hydrogen bond is present.* A hydrogen-bond type is defined by the chemical nature of the proton donor and acceptor used in the hydrogen bond. Thus, a hydrogen bond between a phenol and a nitro group would be a different type from a hydrogen bond between a phenol and a ketone. A motif is constructed by identifying all occurrences of one of these types of hydrogen bonds throughout the network. The subset of molecules that becomes hydrogen-bonded together by this operation is called a motif. The ability to single out one type of hydrogen-bond pattern at a time is one of the most useful features of this graph-set method.

Graph sets are assigned first to motifs, and then to networks. Frequently only one or a few motifs need to be assigned to answer questions about preferred aggregate patterns. This level of analysis is easy to learn, and to remember. The process of making the assignments is what is important here. It allows one to see clearly how multiple hydrogen-bond patterns are interrelated and to focus on the chemistry of particular sets of molecules.

A graph set is specified using the pattern designator (G), its degree (r), and the number of donors (d) and acceptors (a), as shown:

$$G_d^a(r).$$

G is a descriptor referring to the pattern of hydrogen bonding. It has four different assignments based on whether hydrogen bonds are inter- or intramolecular: S, C, R and D. S (standing for self) denotes an intramolecular hydrogen bond. Different patterns of intramolecular hydrogen bonds are not specified with this notation. A method for specifying particular intramolecular hydrogen bonds in cyclic peptide structures has been developed and may be useful for other types of molecules as well (Karle, 1981). For intermolecular bonds, C refers to hydrogen-bonded chains that are infinite, R refers to rings. A typical ring pattern is a cyclic carboxylic acid dimer. D refers to noncyclic dimers and other finite hydrogen-bonded sets, such as a phenol hydrogen-bonded to acetone.

The parameter r refers to the degree, being either the number of atoms in a ring or the repeat length of a chain. For a ring, in an S or R set, the degree is defined as the number of atoms in the ring, counted by traversing the ring in one direction along the shortest chain of covalent and hydrogen bonds until all the atoms in the ring have been counted once. For a chain, C, the degree is the repeat length of the monomer unit in the chain, *i.e.*, the number of atoms encountered by traversing the shortest pathway from the hydrogen atom of one hydrogen bond to the acceptor atom of the next. For D motifs the degree is the number of atoms in the entire length of the hydrogen-bonded set starting with the proton of the first hydrogen bond, proceeding along the shortest pathway, and ending with the acceptor atom in the last hydrogen bond of the set. If there is only one hydrogen bond in the motif, then the degree of the D pattern is 2. Since this pattern occurs so frequently, $r = 2$ is considered the default degree value for a D pattern and it is not specified. The parameters d and a refer to the number of different kinds of donors (d) and acceptors (a) used in the hydrogen-bond pattern. When all the molecules in a set are the same, d and a will be the number of participating donors and acceptors per molecule. When the set is composed of different kinds of molecules, d and a will be the sum of the participating donors and acceptors from all the different molecules. The default value for d and a is 1.

Assigning graph sets to motifs

First, identify the different types of hydrogen bonds in the array of interest. One motif will be generated for each type of hydrogen bond.

Second, rank the hydrogen bonds by chemical priority. This step is necessary so hydrogen-bond patterns can be reconstructed from graph sets [prioritization can be performed consistently by using the Cahn–Ingold–Prelog rules (IUPAC, 1970) which have been extended here to include hydrogen bonds (see *Appendix*)]. If hydrogen bonds are encountered that are not covered by application of these rules, they should be enumerated arbitrarily before proceeding further.

Third, generate a motif, selecting the highest priority hydrogen bond, H(1), and finding all occurrences of this bond in the array. To identify a motif choose one molecule as the starting point and identify all molecules that are attached to it by H(1). Then proceed from each of these molecules to all others bonded to them by H(1), *etc.* until a molecule is encountered which has no additional attached molecules, or until it is obvious that the set is infinite.

UM00013255
NOVARTIS EXHIBIT 1517
Novartis v. Regents, IPR2023-01347
Page 2001 of 4460

The process is like gluing certain molecules in an array together [with H(1) glue], then pulling one molecule out of the array to see which additional molecules come with it, and whether they form an infinite (*C*) or a finite (*S*, *R* or *D*) set. *This step is the essential decoding step in the procedure.*

Fourth, assign a graph set to the motif. A straightforward example is given as example (I) in Table 1, with graph set *D*. Example (II) is an infinite chain, with degree 7. Its complete graph set is *C*(7) (*A* stands for proton acceptor and *D*H for proton donor). In some cases H(1) occurs in a ring as well as in a chain. In these cases, the ring may be indicated as a subset, given in brackets. For (III), the complete graph set is $C_1^2(8)[R_1^2(4)]$. If the hydrogen atom of a single hydrogen bond occurs in two of the *same* rings at the same time, then the graph set assigned to one of the patterns is doubled. For (IV) (Table 1) the graph set is $2R_1^2(4)$.

Fifth, repeat steps three and four until graph sets have been assigned to all hydrogen-bond types.

Assigning graph sets to first-order networks

A first order network, N_1, is just a sequential listing of the graph sets that correspond to each motif in the network, where M_1 is the motif containing the highest priority hydrogen bond:

$$N_1 = M_j \cdots M_3 M_2 M_1.$$

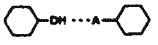
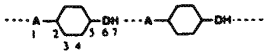
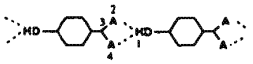
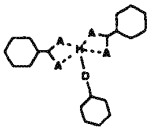
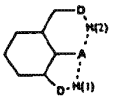
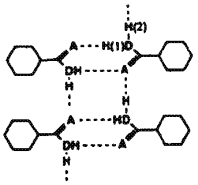
In examples (I)–(III) above, where there was only one kind of hydrogen bond in each example, their first-order networks consist of only one motif, M_1. In example (V), Table 1, there are two different kinds of hydrogen bonds in the pattern, so two motifs are needed to represent N_1. Since the highest priority hydrogen bond is *S*(5) and the second highest priority one is *S*(6), $N_1 = S(6)S(5)$.

Assigning graph sets to higher-order networks

Although all the information about individual hydrogen-bond contributors is given in the motifs, other hydrogen-bond patterns may be present in the structure, and in some cases it may be useful to identify them. These other patterns arise from combinations of two or more different types of hydrogen bonds (recalling that motifs contain only one kind of hydrogen bond). Higher-order networks, N_i, are assigned by adding sequentially one new graph set per network. The lowest degree pattern is given the highest priority, as for motifs, and is assigned first. The lowest degree pattern will usually contain only two different kinds of proton donors, but it could contain more. If there are still two new patterns with the same priority (*e.g.*, two different kinds of chains with $r = 6$) then the ranking is specified by the user.

Table 1. *Examples of graph-set assignments*

The hexagons are meant to represent any organic ligand. This specific form is given so the degrees of the patterns can be assigned in this table. If the organic ligands were other kinds of groups, then the degrees of some of the patterns would change.

(I)		$N_1 = D$
(II)		$N_1 = C(7)$
(III)		$N_1 = C_1^2(8)[R_1^2(4)]$
(IV)		$N_1 = 2R_1^2(4)$
(V)		$N_1 = S(6)S(5)$ $N_2 = S_2^1(9)$
(VI)		$N_1 = C(4)R_2^2(8)$ $N_2 = R_2^2(8)$

There is a simple procedure for finding higher-order networks. Search for that pattern (of any graph-set type) that has the smallest number of atoms in its repeat unit, yet contains two or more different kinds of proton donors. In searching for chains, start with H(1) for example, and proceed along a hydrogen bond and along the continuing atom chain until reaching H(2). Then find a pathway that returns to H(1) in another molecule without including any other H atoms. If this sequence propagates itself then it is accepted as a chain. The procedure is applied to all the pairwise combinations of the individual proton donors, and thereafter to triplet combinations, *etc.*

Rings are readily identified by a similar procedure. A ring of second order or above must contain at least two types of hydrogen bonds. Hence start again with H(1), proceed along its hydrogen bond and along its intramolecular atomic chain to H(2). The smallest ring possible would then include a second H(1), and a second H(2), returning in a cycle to the starting H(1). Again, proceeding through all pairwise combinatorial possibilities higher-order rings can be identified. Rings with more than two types of hydrogen bonds in them are assigned as even higher networks, with ring size (or degree) determining their respective priorities.

UM00013256
NOVARTIS EXHIBIT 1517
Novartis v. Regents, IPR2023-01347
Page 2002 of 4460

Higher-order networks arise by combination of motifs from two different kinds of hydrogen bonds. In example (VI), Table 1, one kind of hydrogen bond gives rise to a ring and another kind of hydrogen bond gives rise to chains. The first-order network for (VI) is $C(4)R_2^2(8)$. When the dimer is repeated by a chain, several new networks are created. The highest priority one is a new eight-membered ring between the original dimers. Thus, $N(2)$ is $R_4^2(8)$. Graph sets can be assigned to even higher-order networks in the same way as demonstrated for N_2.

Troubleshooting

Most, but not all, hydrogen-bond patterns of small molecules can be assigned with the method outlined above. For some compounds, there may be complicating circumstances that make the assignments intractable. For hydrogen-bond patterns that are very difficult to visualize or to decode a useful approach is to assign just part of the pattern to a graph set. In some cases an optional notation using O superscript and O subscript can be used to resolve difficulties:

$$[G_d^a(r)]_o^o$$

An example where optional fields are useful is in comparison of Watson–Crick, Hoogsteen and reverse Hoogsteen hydrogen-bond patterns (Hoogsteen, 1959, 1963; Saenger, 1984). The graph set of the Watson–Crick pattern is characteristic, but the graph sets of the other two types are identical to one another even though their hydrogen-bond patterns are not. An optional field identifying which oxygen atom is used in the hydrogen-bond pattern resolves this ambiguity allowing each of the three hydrogen-bond types to have a unique and useful graph set, as shown in Fig. 1.

Applications of graph sets

The use of graph sets for designing new materials, deconvoluting crystal structure data, and comparing and contrasting sets of molecules has been demonstrated (Etter, 1989; Bernstein, Etter & MacDonald, 1989). This approach views hydrogen-bonded sets of molecules as distinct chemical species that can be studied independently. The molecular sets are conceptually like macromolecules. A particular graph set may be common to many kinds of molecules. Such sets are isographic as well as isoentropic since the number of intermolecular hydrogen-bond connections are the same for all sets of molecules with the same graph set. For example, *N*-methyl-4-nitroaniline (VII) and 4-nitrophenol (VIII) are isographic (Panunto, Urbañczyk-Lipkowska, Johnson & Etter, 1987) even though the proton-donating ability of a phenol ($pK_a = 9{\cdot}9$) is much greater than that of an aniline ($pK_a = 27$), Fig. 2.

Similarly, the graph sets of three polymorphs of iminodiacetic acid (IX) have been analyzed. Despite the extraordinary complexity of the intermeshed hydrogen-bond patterns in these structures, and despite the fact that the molecules are zwitterions (the graph-set method was developed here primarily for use with neutral organic molecules), the similarities and differences in the graph sets of the three polymorphs provides an explicit basis for comparison and insight into the chemical similarities and differences of the polymorphs (Bernstein *et al.*, 1989), Fig. 3.

Since hydrogen bonds are generally weak interactions, most hydrogen-bonded assemblies have been studied in the solid state where they are stable enough for spectroscopic and chemical investigations. The occurrence of certain hydrogen-bond motifs throughout a series of compounds, *e.g.*,

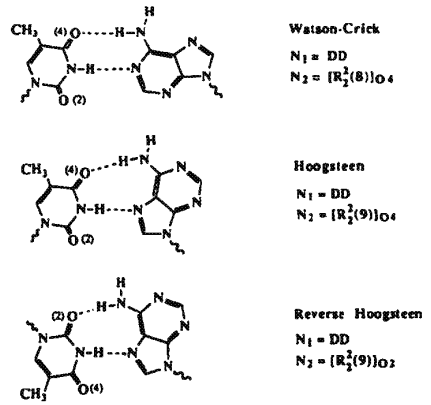
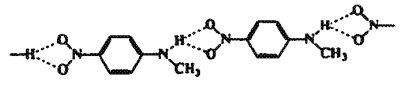
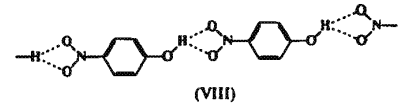


Fig. 1. An example of the use of optional fields (brackets with sub/superscripts) to explicitly define hydrogen-bond patterns. In these examples the ambiguity about O2 or O4 as the hydrogen-bond acceptor has been resolved with the use of optional fields.



(VII)



(VIII)

Fig. 2. Isographic hydrogen-bond patterns of a secondary aniline and a phenol. Both sets of molecules have the same first- and second-order graph sets: $N_1 = R_1^2(4)$ and $N_2 = C_1^2(8)$.

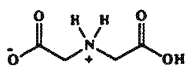
UM00013257
NOVARTIS EXHIBIT 1517
Novartis v. Regents, IPR2023-01347
Page 2003 of 4460

$C(4)R_2^2(8)$ for primary amides, or $R_2^2(8)$ for carboxylic acids, suggests that these patterns may be present in solution and may be controlling the structure of crystal nucleation sites. Even though the hydrogen-bond aggregates would be transient in solution, and may even be present in very low concentrations, at the instant when nucleation begins these structures must be forming. It is unlikely that other crystal-packing forces, which vary almost randomly throughout a series of compounds, could by chance direct all primary amides into the same hydrogen-bond pattern. Rather, it is more likely that crystal-packing forces influence the observed geometry of the hydrogen bonds, but do not determine their connectivity patterns. Preferred hydrogen-bond modes derived from crystal structures may be useful for determining the preferred modes of association of the individual functional groups on complex multi-functional molecules like biopolymers. Hopefully, graph-set analysis will aid in transferring information about molecular recognition properties of molecules from the solid state to solution and mobile phases, and will provide a unifying methodology for describing hydrogen-bonded sets of molecules.

APPENDIX

Assigning hydrogen-bond priorities

The Cahn–Ingold–Prelog (CIP) rules deal specifically with priorities of groups attached to a carbon atom. We propose here that the same protocol be used for assigning priorities to hydrogen bonds based first on the priorities of the hydrogen atoms in the hydrogen bonds, secondly on the acceptor atoms, and finally on other hydrogen-bond criteria (IUPAC, 1970). Often the CIP rules can be applied unchanged to hydrogen bonds. For example, a hydrogen atom attached to an oxygen would be higher priority than one attached to a nitrogen since the oxygen has higher atomic number.



Iminodiacetic acid zwitterion (IX)

Polymorph 1:	N_1 = C(5)R_2^2(10)C(8)	$N_2 = R_2^2(14)$
Polymorph 2:	N_1 = C(5)R_2^2(10)C(8)	$N_2 = R_4^2(8)$
Polymorph 3:	N_1 = C(5)C(5)C(8)	

Fig. 3. Graph-set assignments for the three polymorphs of (IX). All three polymorphs have C(5)C(8) in common in their first-order networks N_1. Polymorphs 1 and 2 differ in their second-order networks N_2.

When CIP rules are not directly applicable they can be extended as follows with the highest priority rules listed first:

1. Primary amides – the *cis* hydrogen atom is higher priority than the *trans* hydrogen atom.

2. Primary amines – the hydrogen atom on the highest priority side of the molecule is given highest priority.

3. In a carboxylic acid, the hydrogen atom with *cis* geometry is higher priority than one with *trans* geometry.

4. A hydrogen atom in an intermolecular hydrogen bond has priority over one in an intramolecular hydrogen bond.

5. The CIP priorities of acceptor atoms in hydrogen bonds are used to determine priorities of the hydrogen atoms when two hydrogen atoms are identical by all other criteria above.

6. When the acceptor and donor atoms in two hydrogen bonds are identical, then the following criteria apply:

(*a*) Lone pairs of electrons are treated as acceptors. The highest priority lone pair is on the highest priority side of a molecule.

(*b*) A hydrogen atom in a two-center bond is higher priority than one in a single bond. Likewise, hydrogens in multicenter bonds have even higher priorities.

(*c*) A hydrogen atom in a short hydrogen bond has a precedence over one in a longer bond.

Financial support from NIH (GM 42148-01) and the Petroleum Research Fund of the American Chemical Society to MCE is gratefully acknowledged.

References

BERNSTEIN, J., ETTER, M. C. & MACDONALD, J. C. (1989). *J. Chem. Soc. Perkin Trans.* 2. In the press.

EMSLEY, J. (1980). *Chem. Soc. Rev.* **9**, 91–124.

ETTER, M. C. (1989). *Acc. Chem. Res.* In the press.

FUJITA, S. J. (1988*a*). *J. Chem. Inf. Comput. Sci.* **28**, 128–137.

FUJITA, S. J. (1988*b*). *J. Chem. Inf. Comput. Sci.* **28**, 137–142.

HAMILTON, W. C. & IBERS, J. A. (1968). *Hydrogen Bonding in Solids*, pp. 19–21. New York: W. A. Benjamin.

HARARY, F. (1967). *Graph Theory and Theoretical Physics*. New York: Academic Press.

HOOGSTEEN, K. (1959). *Acta Cryst.* **12**, 822–823.

HOOGSTEEN, K. (1963). *Acta Cryst.* **16**, 907–916.

IUPAC (1970). *J. Org. Chem.* **35**, 2849–2867.

JOESTEN, M. D. & SCHAAD, L. J. (1974). *Hydrogen Bonding*. New York: Marcel Dekker.

KARLE, I. (1981). *The Peptides*, Vol. 4, edited by E. GROSS & J. MEIENHOFER, pp. 1–54. New York: Academic Press.

KULESHOVA, L. N. & ZORKY, P. M. (1980). *Acta Cryst.* **B36**, 2113–2115.

LATIMER, W. M. & RODEBUSH, W. H. (1920). *J. Am. Chem. Soc.* **42**, 1419–1433.

MURRAY-RUST, P. & GLUSKER, J. P. (1984). *J. Am. Chem. Soc.* **106**, 1018–1025.

UM00013258
NOVARTIS EXHIBIT 1517
Novartis v. Regents, IPR2023-01347
Page 2004 of 4460

PANUNTO, T. W., URBAŃCZYK-LIPKOWSKA, Z., JOHNSON, R. & ETTER, M. C. (1987). *J. Am. Chem. Soc.* **109**, 7786–7797.
SAENGER, W. (1984). *Principles of Nucleic Acid Structure*, ch. 6. New York: Springer-Verlag.
SCHUSTER, P., ZUNDEL, G. & SANDORFY, C. (1976). *The Hydrogen Bond*, Vols. I–III. Amsterdam: North-Holland.
TAYLOR, R. & KENNARD, O. (1984). *Acc. Chem. Res.* **17**, 320–326.
WALBA, D. M. (1987). *Graph Theory and Topology in Chemistry, Studies in Physical and Theoretical Chemistry*, Vol. 51, edited by R. B. KING & D. H. ROUVRAY, pp. 23–42. Amsterdam: Elsevier.
WELLS, A. F. (1962). *Structural Inorganic Chemistry*, pp. 294–315. Oxford: Clarendon Press.
ZORKY, P. M. & KULESHOVA, L. N. (1980). *Zh. Strukt. Khim.* **22**, 153–156.

Acta Cryst. (1990). B**46**, 262–266

Structure of a Low-Temperature Polymorph of Chenodeoxycholic Acid, $C_{24}H_{40}O_4$, Determined with Synchrotron Radiation

BY P. J. RIZKALLAH

Department of Chemistry, Liverpool University, PO Box 147, Liverpool L69 3BX, England, and SERC Daresbury Laboratory, Warrington WA4 4AD, England

MARJORIE M. HARDING

Department of Chemistry, Liverpool University, PO Box 147, Liverpool L69 3BX, England

P. F. LINDLEY

Department of Crystallography, Birkbeck College, Malet Street, London WC1E 7HX, England

AND A. AIGNER AND A. BAUER

Diamalt Aktiengesellschaft, Werk Raubling, Postfach 1151, D-8201 Raubling, Federal Republic of Germany

(*Received* 21 *July* 1989; *accepted* 17 *October* 1989)

Abstract

The low-temperature polymorph of chenodeoxycholic acid ($3\alpha,7\alpha$-dihydroxy-5β-cholanic acid) forms very fine needle-shaped crystals (30–60 μm cross-section), containing a variable solvent content. The crystal and molecular structure has been solved using synchrotron radiation in conjunction with an area detector. $M_r = 392{\cdot}6$ (excluding solvent), hexagonal, space group $P6_5$, $a = 22{\cdot}250\ (5)$, $c = 10{\cdot}255\ (2)$ Å, $Z = 6$, $V = 4396{\cdot}7$ Å^3, $F(000) = 1296$, $D_m = 1{\cdot}12\ (6)$ g cm^{-3} (flotation in bromobenzene/toluene), $D_x = 0{\cdot}89$ g cm^{-3} for $C_{24}H_{40}O_4$ without solvent of crystallization, D_x (max.) $= 1{\cdot}17$ g cm^{-3} for $C_{24}H_{40}O_4.C_6H_5Br$, $\lambda = 1{\cdot}5418$ Å for unit-cell determination, $\lambda = 0{\cdot}895$ Å for intensity measurements, $\mu = 1{\cdot}09$ cm^{-1}, m.p. = 388–390 K, $T = 291\ (1)$ K. The structure refined to $R = 0{\cdot}11$ for 578 reflections with $|F_o| > 2\sigma(F)$. The molecular conformation is similar to that of the high-melting-point (438–439 K) form, but the molecular packing is far more open. All the oxygen atoms are involved in intermolecular hydrogen bonding. The crystal structure contains wide cylindrical channels, parallel to **c**, sufficient to accommodate molecules with van der Waals diameters up to 8·0 Å.

0108-7681/90/020262-05$03.00

© 1990 International Union of Crystallography

Introduction

Chenodeoxycholic acid, $3\alpha,7\alpha$-dihydroxy-5β-cholanic acid (CDCA), $C_{24}H_{40}O_4$, is a bile acid which is an efficacious agent for inducing dissolution of cholesterol gallstones (see, for example, Hofmann & Paumgartner, 1975). The cholanic bile acids form a number of mixed crystals which may be sub-divided into two categories, choleic acids and 'canal' complexes. The choleic acids contain highly stable complexes of host (bile acid) and guest (second organic molecule) which may, indeed, be stable outside the crystalline state. The crystal structures of the canal complexes contain channels or 'canals' which contain the guest molecules. The host–guest interactions in these complexes are usually less specific than for the choleic acids and can have non-integral coordination numbers. The canals can be either hydrophilic whereby they readily accommodate guest molecules with polar substituents, or hydrophobic where the guest molecules tend to be apolar. Although several canal complexes involving deoxycholic acid, DCA, have been reported, very few where the host molecule is another bile acid have been characterized. Polymorphism of CDCA has been reported (Giuseppetti & Paciotti, 1978), and the high-temperature

UM00013259
NOVARTIS EXHIBIT 1517
Novartis v. Regents, IPR2023-01347
Page 2005 of 4460

Hydrogen Bond Directed Cocrystallization and Molecular Recognition Properties of Acyclic Imides

Margaret C. Etter* and Susan M. Reutzel

Contribution from the Department of Chemistry, University of Minnesota, Minneapolis, Minnesota 55455. *Received September 28, 1990*

Abstract: The cocrystallization behavior of acyclic imides is studied as a way to map out the hydrogen bond directed molecular recognition properties of a class of small biochemically related molecules under conditions where there is no preorganized cavity controlling the recognition events. Cocrystallization of over 80 imide–guest pairs was examined by solution and solid-state cocrystallization methods. The crystal structures of nine host–guest pairs are reported. The hydrogen bond patterns of 16 other cocrystal pairs were characterized by noncrystallographic means. Common hydrogen bond patterns and hydrogen bond selectivity properties were analyzed and are presented in the form of a set of hydrogen bond rules. Diacetamide was found to be a versatile cocrystallizing agent, forming 10 different cocrystal pairs. Imides that have a cis–trans conformation in their homomeric forms retain that conformation in their cocrystal structures. Imides that have a trans–trans conformation in their homomeric structures do not usually form cocrystals. Three imide cocrystal hydrogen types were observed repeatedly, with the most common pattern involving cyclic imide dimers with pendant hydrogen-bonded guests or cyclic heteromeric patterns having bivalent contacts between the imide and guest species. Guest molecules that successfully formed cocrystals covered a wide range of chemical types, including phenols, acids, amides, phosphine oxides, pyridines, imidazoles, and ureas.

Introduction

The use of cocrystallization as a way to study the molecular recognition properties of a single host molecule or of a class of related host molecules has been demonstrated.[1-3] When a strong intermolecular interaction, such as a hydrogen bond, drives the self-assembly of host and guest molecules, the number, orientation, and type of hydrogen-bonding functional groups on these molecules can be varied as a way to manipulate their aggregation patterns. This approach is particularly useful, and particularly informative, when all or nearly all steric constraints to aggregation have been removed. In other words, these systems have no preorganized cavities for trapping guest molecules; nevertheless, host–guest selectivity and predictable aggregation patterns are observed. While the role of hydrogen bonds in contributing extra stabilization to host–guest pairs with preorganized host cavities or clefts has been well-documented,[4] the directing and selectivity properties of the hydrogen bonds themselves have been all but ignored in host–guest systems.[5] In homomeric systems, the importance of hydrogen bond motifs has long been recognized,[6,7] and hydrogen bond selectivity in multifunctional homomeric crystals has also been shown.[8,9]

In this paper, molecular complexes of imides are prepared, showing that hydrogen bond selectivity criteria can be applied to heteromeric as well as to homomeric systems. Common features of their hydrogen bond aggregate structures are formulated as a set of rules, intended to be used as synthetic guidelines for designing new aggregate structures. Chemical rationale for the observed hydrogen bond selectivity properties and for the observed cocrystal stoichiometries are discussed in relation to the molecular recognition properties of imides.

Experimental Section

General Methods. Melting points were determined on a Fischer–Johns apparatus and are uncorrected. Infrared spectra were recorded on a Nicolet 5DXB FTIR spectrometer from Nujol mulls and are reported (cm^{-1}). ^1H and ^{13}C NMR spectra were recorded on IBM NR200AF and Varian VXR-300 spectrometers, respectively, and chemical shifts are reported in parts per million (δ) from Me_4Si. ^{13}C and ^{31}P CP/MAS NMR spectra were recorded on an IBM NR100AF spectrometer operating at a carbon frequency of 25.178 MHz and a phosphorus frequency of 40.55 MHz and with a Doty solid-state probe. ^{13}C chemical shifts are reported (δ) relative to *p*-di-*tert*-butylbenzene (CH_3 δ 31.0). ^{31}P chemical shifts are reported (δ) relative to triphenylphosphine oxide (δ 27.9). Spectroscopic-grade solvents were used for all recrystallizations. Deuterated solvents were obtained from Aldrich Chemical Co. Diacetamide (**1**) and other imide guest compounds were purchased from Aldrich and used without purification.

* Alfred P. Sloan Fellow, 1989–1991.

***N*-Acetylbenzamide (2).** *N*-Acetylbenzamide was obtained from an acid-catalyzed condensation of benzamide and acetic anhydride.[9]

2α. Recrystallization from acetone gives colorless blocks: mp 117–119 °C (lit.[10] mp 117 °C); IR (Nujol) 3270, 1745, 1740, 1680, 1520, 1490, 1470, 1370, 1270, 1220, and 700 cm^{-1}; ^{13}C CP/MAS NMR (25 MHz) δ 24.3, 25.4, 127.1, 129.1, 132.3, 162.7, 170.1, and 176.5.

2β. Recrystallization from ethanol gives colorless plates: mp 118–120 °C; IR (Nujol) 3270, 1740, 1680, 1510, 1490, 1470, 1370, 1280, 1220, and 700 cm^{-1}; ^{13}C CP/MAS NMR (25 MHz) δ 22.7, 129.4, 133.8, 164.3, 168.5, and 174.5; ^1H NMR (200 MHz, $CDCl_3$) δ 2.60 (s, 3 H), 7.48–7.61 (m, 3 H, *J* values include 7.1 and 1.8 Hz), 7.81 (dd, 2 H, *J* = 6.8 and 1.7 Hz), and 8.4 (b s, 1 H); ^{13}C NMR (75 MHz, $CDCl_3$) δ 25.6, 127.8, 128.8, 132.5, 133.1, 165.5, and 173.1.

***N*-Propionylbenzamide (3).** To a stirred solution of 5.0 g (41 mmol) of benzamide in 20 mL of acetonitrile was added dropwise 3.6 mL (41 mmol) of propionyl chloride in 5 mL of acetonitrile over 30 min. After the solution was refluxed for 6 h, it was poured over 100 mL of ice and warmed to room temperature. The product was filtered, washed, and recrystallized from diethyl ether to give **3** (2.5 g, 34%) as a white, crystalline solid: mp 95–98 °C (lit.[11] mp 98 °C); IR (Nujol) 3290, 1710,

(1) Etter, M. C.; Baures, P. W. *J. Am. Chem. Soc.* **1988**, *110*, 639–640.
(2) Etter, M. C.; Urbańczyk-Lipkowska, Z.; Zia-Ebrahimi, M.; Panunto, T. W. *J. Am. Chem. Soc.* **1990**, *112*, 8415–8426.
(3) Etter, M. C.; Adsmond, D. A. *J. Chem. Soc., Chem. Commun.* **1990**, *8*, 589–591.
(4) (a) Rebek, J., Jr.; Askew, B.; Ballester, P.; Costero, A. *J. Am. Chem. Soc.* **1988**, *110*, 923–927. (b) Rebek, J., Jr.; Askew, B.; Ballester, P.; Buhr, C.; Jones, S.; Nemeth, D.; Williams, K. *J. Am. Chem. Soc.* **1987**, *109*, 5033–5035. (c) Rebek, J., Jr. *Pure Appl. Chem.* **1989**, *61*, 1517–1522. (d) Askew, B.; Ballester, P.; Buhr, C.; Jeong, K. S.; Jones, S.; Parris, K.; Williams, K.; Rebek, J., Jr. *J. Am. Chem. Soc.* **1989**, *111*, 1082–1090. (e) Rebek, J., Jr.; Askew, B.; Islam, N.; Killoran, M.; Nemeth, D.; Wolak, R. *J. Am. Chem. Soc.* **1985**, *107*, 6736–6738. (f) Rebek, J., Jr.; Nemeth, D. *J. Am. Chem. Soc.* **1985**, *107*, 6738–6739. (g) Rebek, J., Jr. *Science* **1987**, *235*, 1478–1484. (h) Zimmerman, S. C.; Wu, W. *J. Am. Chem. Soc.* **1989**, *111*, 8054–8055. (i) Chang, S.-K.; Hamilton, A. D. *J. Am. Chem. Soc.* **1988**, *110*, 1318–1319. (j) Kelly, T. R.; Maguire, M. P. *J. Am. Chem. Soc.* **1987**, *109*, 6549–6551. (k) Bell, T. W.; Liu, J. *J. Am. Chem. Soc.* **1988**, *110*, 3673–3674. (l) Sheridan, R. E.; Whitlock, H. W., Jr. *J. Am. Chem. Soc.* **1986**, *108*, 7120–7121.
(5) (a) Weber, E.; Csöregh, I.; Stensland, B.; Czugler, M. *J. Am. Chem. Soc.* **1984**, *106*, 3297–3306. (b) Weber, E.; Hecker, M.; Csöregh, I.; Czugler, M. *J. Am. Chem. Soc.* **1989**, *111*, 7866–7872. (c) Toda, F. *Top. Curr. Chem.* **1987**, *140*, 43–69. (d) Hart, H.; Lin, L.-T. W.; Ward, D. L. *J. Am. Chem. Soc.* **1984**, *106*, 4043–4045. (e) Hart, H.; Lin, L.-T. W.; Goldberg, I. *Mol. Cryst. Liq. Cryst.* **1986**, *137*, 277–286. (f) Goldberg, I.; Lin, L.-T. W.; Hart, H. *J. Inclus. Phenom.* **1984**, *2*, 377–389. (g) Seto, C. T.; Whitesides, G. M. *J. Am. Chem. Soc.*, in press.
(6) Leiserowitz, L.; Schmidt, G. M. J. *J. Chem. Soc. A* **1969**, 2372–2382.
(7) (a) Leiserowitz, L. *Acta Crystallogr.* **1976**, *B32*, 775–802. (b) Leiserowitz, L.; Tuval, M. *Acta Crystallogr.* **1978**, *B34*, 1230–1247.
(8) Etter, M. C. *Acc. Chem. Res.* **1990**, *23*, 120–126.
(9) Baburao, K.; Costello, A. M.; Petterson, R. C.; Sander, G. E. *J. Chem. Soc. C* **1968**, 2779–2781.
(10) Tóth, G. *Acta Chim. Acad. Sci. Hung.* **1970**, *1*, 101–109.
(11) Dunn, P.; Parkes, E. A.; Polya, J. B. *Rec. Trav. Chim.* **1952**, *71*, 676–683.

0002-7863/91/1513-2586$02.50/0 © 1991 American Chemical Society

UM00013260
NOVARTIS EXHIBIT 1517
Novartis v. Regents, IPR2023-01347
Page 2006 of 4460

1680, 1500, 1470, 1370, 1240, 1210, 1080, and 710 cm^{-1}; ^1H NMR (200 MHz, $CDCl_3$) δ 1.22 (t, 3 H, J = 7.3 Hz), 3.03 (q, 2 H, J = 7.3 Hz), 7.46–7.61 (m, 3 H, J values include 7.2 Hz), 7.84 (dd, 2 H, J = 7.0 Hz), and 8.61 (b s, 1 H); ^{13}C NMR (75 MHz, $CDCl_3$) δ 31.1, 127.9, 128.6, 132.6, 132.9, 165.4, and 176.7; ^{13}C CP/MAS NMR (25 MHz) δ 7.3, 31.8, 128.8, 131.0, 162.9, 170.0, 175.8, and 183.6.

***N*-Butyrylbenzamide (4).** To a stirred solution of 5.0 g (41 mmol) of benzamide in 20 mL of acetonitrile was added dropwise 4.3 mL (41 mmol) of *n*-butyryl chloride over 30 min. After the solution was refluxed for 3 h, it was poured over 100 mL of ice and warmed to room temperature. The product was filtered, washed, and recrystallized from toluene to give 4 (3.5 g, 44%) as a white crystalline solid: mp 103–104 °C (lit.[11] mp 104 °C); IR (Nujol) 3290, 1710, 1680, 1670, 1600, 1580, 1510, 1470, 1380, 1320, 1240, and 1190 cm^{-1}; ^1H NMR (200 MHz, $CDCl_3$) δ 1.03 (t, 3 H, J = 7.4 Hz), 1.74 (sext, 2 H, J = 7.4 Hz), 2.99 (t, 2 H, J = 7.4 Hz), 7.50–7.65 (m, 3 H, J = 1.5, 7.5, 7.6, and 7.0 Hz), 7.85 (dd, 2 H, J = 6.9 and 1.6 Hz), and 8.7 (b s, 1 H); ^{13}C NMR (50 MHz, $CDCl_3$) δ 13.7, 17.6, 39.6, 128.1, 128.8, 133.0, 166.0, and 177.2; ^{13}C CP/MAS NMR (25 MHz) δ 12.4, 14.2, 40.3, 127.4, 130.1, 133.8, 161.0, 167.9, 175.3, and 182.1.

Dibenzamide (5). Dibenzamide was obtained from a base-catalyzed condensation of benzamide and benzoyl chloride.[12] Recrystallization from diethyl ether gives colorless needles: mp 144–145 °C (lit.[12] mp 144 °C); IR (Nujol) 3240, 1700, 1500, 1230, and 710 cm^{-1}; ^1H NMR (200 MHz, $CDCl_3$) δ 7.44–7.62 (m, 6 H, J = 7.5 Hz), 7.86 (dd, 4 H, J = 6.9 and 1.6 Hz), and 9.0 (b s, 1 H); ^{13}C NMR (75 MHz, $CDCl_3$) δ 127.9, 128.9, 133.1, 133.3, and 166.2; ^{13}C CP/MAS NMR (25 MHz) δ 129.7, 132.5, 134.4, 168.0, and 174.

Other Imides. Six other imides, dipropionamide (6), *N*-acetylpropionamide (7), diisobutyramide (8), *N*-(cyclohexylcarbonyl)cyclohexylamide (9), *N*-(phenylacetyl)phenylacetamide (10), and *N*-isobutyrylbenzamide (11), were synthesized. Details of their syntheses and product analyses are available in the supplementary material.

General Methods for the Preparation of Imide Cocrystals. Imide cocrystals can be obtained by solution, solid-state, or melt techniques.

Method A (solution): Equimolar amounts of the imides and guest molecules are dissolved in a mutually miscible solvent(s) and are allowed to recrystallize slowly at room temperature. When possible, the crystals are removed from solution as soon as they are formed and before the solvent has completely evaporated. Alternately, cocrystals are obtained after all of the solvent(s) has evaporated.

Method B (solid state): Equimolar amounts of the imides and guest molecules are ground together in a Wig-L-Bug dental amalgamator for 10 min. Conversion of the starting materials to the cocrystal in the solid state approaches 100%.

Method C (melt): Equimolar amounts of the imides and guest molecules are melted together and cooled to room temperature.

Cocrystals prepared by all methods were characterized by physical and spectroscopic methods. In all cases where two or more methods were used for one system, the same solid-state phases were obtained from the different methods.

Diacetamide (1)–4-nitrophenol (1:1) cocrystal (12): methods A and B; colorless, irregular (1:1 toluene–$CHCl_3$); mp 75–77 °C; IR (Nujol) 3160, 1720, 1680, 1590, 1510, 1500, 1460, 1370, 1330, 1290, 1270, 1240, 1170, 1110, 1030, 860, 750, 650, and 630 cm^{-1}; ^1H NMR (200 MHz, $CDCl_3$) δ 2.32 (s, 6 H), 6.34 (b s, 1 H), 6.91 (dd, 2 H, J = 9.1 and 2.1 Hz), 8.16 (dd, 2 H, 9.1 and 2.2 Hz), and 8.2 (b s, 1 H); ^{13}C CP/MAS NMR (25 MHz) δ 25.6, 115.4, 126.2, 137.6, 141.7, 163.6, 173.5, and 177.

***N*-Butyrylbenzamide (4)–4-nitrophenol (1:1) cocrystal (13):** methods A and B; colorless prisms (toluene); mp 94–95 °C; IR (Nujol) 3290, 3250, 1710, 1670, 1600, 1520, 1500, 1470, 1340, 1310, 1280, 1260, 1230, 1180, 1160, 1110, and 710 cm^{-1}; ^1H NMR (200 MHz, $(CD_3)_2CO$) δ 0.97 (t, 3 H, J = 7.3 Hz), 1.68 (sext, 2 H, J = 7.3 and 7.4 Hz), 2.84 (t, 2 H, J = 7.3 Hz), 7.02 (d, 2 H, J = 9.2 Hz), 7.49–7.64 (m, 3 H, J = 7.6, 1.6, 7.2, and 7.0 Hz), 7.99 (dd, 2 H, J = 6.9 and 1.6 Hz), 8.16 (dd, 2 H, J = 9.1 Hz), and 9.9 (b s, 1 H); ^{13}C CP/MAS NMR (25 MHz) δ 12.5, 15.9, 41.0, 115.4, 128.1, 135.1, 141.7, 162.0, 169.9, 175.2, and 182.7.

Diacetamide (1)–hydroquinone (2:1) cocrystal (14): methods A and B; colorless plates (1:1 toluene–ethanol); mp 77–79 °C; IR (Nujol) 3450, 3270, 3250, 3210, 3180, 1730, 1690, 1520, 1510, 1470, 1370, 1300, 1250, 1230, 1200, 1030, 840, and 760 cm^{-1}; ^1H NMR (200 MHz, $(CD_3)_2CO$) δ 2.20 (s, 12 H), 6.66 (s, 4 H), 7.67 (s, 2 H), and 9.6 (b s, 1 H); ^{13}C CP/MAS NMR (25 MHz) δ 25.0, 114.9, 149.4, 168.2, 174.5, and 181.6.

***N*-Butyrylbenzamide (4)–hydroquinone (2:1) cocrystal (15):** methods A and B; colorless plates (1:1 toluene–acetone); mp 120–121 °C; IR (Nujol) 3370, 3290, 1700, 1670, 1520, 1470, 1310, 1250, 1210, 1190, and 700 cm^{-1}; ^1H NMR (200 MHz, $(CD_3)_2CO$) δ 0.97 (t, 6 H, J = 7.4 Hz), 1.68 (sext, 4 H, J = 7.3 and 7.3 Hz), 2.84 (t, 4 H, J = 7.3 Hz), 6.66 (s, 4 H), 7.48–7.67 (m, 8 H, J = 7.4 and 1.6 Hz), 7.99 (dd, 4 H, J = 7.0 and 1.4 Hz), and 9.9 (b s, 2 H); ^{13}C CP/MAS NMR (25 MHz) δ 12.7, 16.1, 40.4, 115.0, 116.4, 128.9, 133.4, 150.0, 164.1, 171.1, 175.5, and 182.4.

Diacetamide (1)–4-hydroxybenzoic acid (1:1) cocrystal (16): methods A and B; colorless blocks (ethyl acetate); mp 126–128 °C; IR (Nujol) 3140, 1770, 1720, 1680, 1650, 1610, 1590, 1300, 1290, 1250, 1230, 1160, and 1030 cm^{-1}; ^1H NMR (200 MHz, $(CD_3)_2CO$) δ 2.21 (s, 6 H), 6.92 (dd, 2 H, J = 8.9 and 2.0 Hz), 7.91 (dd, 2 H, J = 8.7 and 2.0 Hz), and 9.7 (b s, 1 H); ^{13}C CP/MAS NMR (25 MHz) δ 25.6, 116.0, 116.5, 120.0, 132.7, 162.0, 170.5, 174.5, and 179.4.

Diacetamide (1)–4-hydroxybenzamide (1:1) cocrystal (17): methods A and B; colorless prisms (acetonitrile); mp 124–127 °C; IR (Nujol) 3470, 3350, 3230, 3120, 1720, 1680, 1640, 1620, 1580, 1540, 1520, 1400, 1290, 1240, and 1030 cm^{-1}; ^1H NMR (200 MHz, $(CD_3)_2CO$) δ 2.20 (s, 3 H), 6.4 (b s, 1 H), 6.87 (dd, 2 H, J = 8.7 and 1.9 Hz), 7.3 (b s, 1 H), 7.83 (dd, 2 H, J = 8.7 and 1.9 Hz); ^{13}C CP/MAS NMR (25 MHz) δ 25.0, 114.9, 120.7, 129.6, 162.2, 167.7, and 173.7.

***N*-Acetylbenzamide (2)–triphenylphosphine oxide (1:1) cocrystal (18):** methods A and B; colorless prisms (1:1 toluene–acetone); mp 122–123 °C; IR (Nujol) 3090, 3050, 1710, 1690, 1670, 1510, 1480, 1460, 1440, 1370, 1280, 1260, 1190, 1180, 1120, 1070, 1020, 720, 710, 700, 690, and 680 cm^{-1}; ^1H NMR (200 MHz, $(CD_3)_2CO$) δ 2.45 (s, 3 H), 7.52–7.75 (m, 18 H), 8.00 (dd, 2 H, J = 6.8 and 1.7 Hz), and 10.0 (b s, 1 H); ^{13}C CP/MAS NMR (25 MHz) δ 25.3, 127.8, 132.6, 165.2, 171.8, and 178.4; ^{31}P CP/MAS NMR (40 MHz) δ 29.8.

***N*-Propionylbenzamide (3)–triphenylphosphine oxide (1:1) cocrystal (19):** methods A and B; colorless prisms (1:1 toluene–acetone); mp 103–105 °C; IR (Nujol) 3093, 3058, 1710, 1683, 1460, 1436, 1369, 1259, 1202, 1188, 1120, 722, 707, and 695 cm^{-1}; ^1H NMR (200 MHz, $(CD_3)_2CO$) δ 1.12 (t, 3 H, J = 7.4 Hz), 2.88 (q, 2 H, J = 7.4 Hz), 7.53–7.75 (m, 18 H), 8.00 (d, 2 H, J = 6.9 Hz), and 9.9 (b s, 1 H); ^{13}C CP/MAS NMR (25 MHz) δ 10.5, 31.6, 127.5, 131.4, 164.4, 170.6, 175.3, and 182.3; ^{31}P CP/MAS NMR (40 MHz) δ 35.8.

Dibenzamide (5)–triphenylphosphine oxide (1:1) cocrystal (20): methods A and B; colorless prisms (1:1 toluene–acetone); mp 120–122 °C; IR (Nujol) 3210, 3140, 3060, 1730, 1510, 1480, 1470, 1440, 1230, 1180, 1120, 710, and 700 cm^{-1}; ^1H NMR (200 MHz, $(CD_3)_2CO$) δ 7.48–7.73 (m, 21 H), 7.99 (dd, 4 H, J = 7.0 and 1.1 Hz), and 10.4 (b s, 1 H); ^{13}C CP/MAS NMR (25 MHz) δ 128.7, 132.4, 162.9, 166.8, 170.6, and 173.0; ^{31}P CP/MAS NMR (40 MHz) δ 26.0.

***N*-Propionylbenzamide (3)–4-nitrophenol (1:1) cocrystal (21):** methods A and B; colorless rods (1:1 ethanol–toluene); mp 85–87 °C; IR (Nujol) 3240, 3160, 1710, 1680, 1620, 1600, 1500, 1490, 1460, 1340, 1290, 1270, 1240, 1210, 1110, and 710 cm^{-1}; ^1H NMR (200 MHz, $(CD_3)_2CO$) δ 1.12 (t, 3 H, J = 7.4 Hz), 2.90 (q, 2 H, J = 7.4 Hz), 7.02 (d, 2 H, 9.2 Hz), 7.48–7.67 (m, 3 H, J values include 8.1 Hz), 8.00 (d, 2 H, J = 8.4 and 6.8 Hz), 8.16 (d, 2 H, J = 9.2 Hz), and 9.9 (b s, 1 H); ^{13}C CP/MAS NMR (25 MHz) δ 7.5, 32.2, 114.8, 139.5, 162.2, 167.4, 176.9, and 183.4.

Diacetamide (1)–4-cyanophenol (1:1) cocrystal (22): methods A and C; colorless blocks (1:1 toluene–acetone); mp 53–54 °C; IR (Nujol) 3160, 2220, 1680, 1660, 1610, 1590, 1510, 1490, 1280, 1250, 1170, 1030, 840, and 700 cm^{-1}; ^1H NMR (200 MHz, $(CD_3)_2CO$) δ 2.21 (s, 6 H), 2.53 (b s, 1 H), 7.00 (dd, 2 H, J = 2.0 and 8.7 Hz), 7.61 (dd, 2 H, J = 2.0 and 8.9 Hz), and 9.5 (b s, 1 H); ^{13}C CP/MAS NMR (25 MHz) δ 25.4, 98.3, 114.3, 134.3, 134.8, 160.6, and 173.5.

***N*-Butyrylbenzamide (4)–4-bromophenol (1:1) cocrystal (23):** methods A and B; colorless needles (1:1 toluene–acetone); mp 75–76 °C; IR (Nujol) 3350, 3300, 1700, 1680, 1670, 1590, 1490, 1470, 1430, 1310, 1250, 1220, 1190, 830, and 700 cm^{-1}; ^1H NMR (200 MHz, $(CD_3)_2CO$) δ 0.97 (t, 3 H, J = 7.4 Hz), 1.68 (sext, 2 H, J = 7.4 Hz), 2.84 (t, 2 H, J = 7.3 Hz), 6.80 (dd, 2 H, J = 9.0 and 2.3 Hz), 7.33 (dd, 2 H, J = 9.0 and 2.3 Hz), 7.48–7.63 (m, 3 H, J values include 7.1 Hz), 7.99 (d, 2 H, J = 7.0 Hz), 8.61 (b s, 1 H), and 9.9 (b s, 1 H); ^{13}C CP/MAS NMR (25 MHz) δ 13.6, 41.2, 117.8, 129.2, 157.0, 164.5, 171.0, 175.4, and 182.7.

***N*-Propionylbenzamide (3)–4-bromophenol (1:1) cocrystal (24):** methods A and B; colorless prisms (1:1 toluene–acetone); mp 52–53 °C; IR (Nujol) 3290, 1700, 1680, 1590, 1510, 1490, 1470, 1430, 1370, 1270, 1260, 1200, 1070, 810, and 710 cm^{-1}; ^1H NMR (200 MHz) δ 1.12 (t, 3 H, J = 7.3 Hz), 2.88 (q, 2 H, J = 7.3 Hz), 6.80 (dd, 2 H, J = 8.8 and 2.1 Hz), 7.33 (dd, 2 H, J = 8.8 and 2.1 Hz), 7.49–7.64 (m, 3 H, J values include 7.5, 7.0, and 1.6 Hz), 7.99 (dd, 2 H, J = 7.0 and 1.7 Hz), 8.6 (b s, 1 H), and 9.9 (b s, 1 H); ^{13}C CP/MAS NMR (25 MHz) δ 7.6, 31.0, 117.2, 131.0, 155.3, 165.2, 171.8, 176.8, and 182.7.

***N*-Butyrylbenzamide (4)–4-chlorophenol (1:1) cocrystal (25):** methods A and B; colorless needles (1:1 toluene–acetone); mp 64–67 °C; IR

(12) (a) Titherley, A. W. *J. Chem. Soc.* **1904**, *85*, 1673–1691. (b) Mizrahi, V.; Niven, M. L. *S. Afr. J. Chem.* **1983**, *36* (4), 137–142.

UM00013261
NOVARTIS EXHIBIT 1517
Novartis v. Regents, IPR2023-01347
Page 2007 of 4460

Table I. Summary of Imide–Guest Cocrystallization Experiments

Imide–Guest Pairs That Form Cocrystals

imide	guests	imide	guests
diacetamide (1)	b, g, j, k, m, q, s, u, v, hh	*N*-propionylbenzamide (3)	b, e, m, kk
diacetamide (1)[a]	a, e, f, y, bb–dd	*N*-butyrylbenzamide (4)	b, e, f, m
N-acetylbenzamide (2)	kk	dibenzamide (5)	kk

Imide–Guest Pairs That Do Not Form Cocrystals

imide	guests	imide	guests
diacetamide (1)	c, d, h, l, o, p, r, t, w, z, aa, ee–gg, ii–kk	dipropionamide (6)	k, m
N-acetylbenzamide (2)	b, k, m, w, x, cc	*N*-acetylpropionamide (7)	kk
N-propionylbenzamide (3)	gg, i–l, q, y, bb, cc	diisobutyramide (8)	kk
N-butyrylbenzamide (4)	g, i–l, q, y, hh, kk	*N*-(cyclohexylcarbonyl)cyclohexylamide (9)	kk
dibenzamide (5)	b, k, n, u, hh	*N*-(phenylacetyl)phenylacetamide (10)	kk
		N-isobutyrylbenzamide (11)	kk

Codes for Guest Molecules

a	phenol	n	perfluorophenol	z	2-amino-5-bromopyridine
b	hydroquinone	o	benzoic acid	aa	2-amino-5-nitropyridine
c	4-acetamidophenol	p	4-aminobenzoic acid	bb	2-aminopyridine
d	4-aminophenol	q	3,4-dinitrobenzoic acid	cc	imidazole
e	4-bromophenol	r	3,5-dinitrobenzoic acid	dd	4-methylimidazole
f	4-chlorophenol	s	4-(methylamino)benzoic acid	ee	4-nitroimidazole
g	4-cyanophenol	t	4-nitrobenzoic acid	ff	4-phenylimidazole
h	2,4-dinitrophenol	u	acetamide	gg	carbanilide
i	4-hydroxyacetophenone	v	benzamide	hh	1,3-dimethylurea
j	4-hydroxybenzamide	w	*N*-methylbenzamide	ii	adenine
k	4-hydroxybenzoic acid	x	*N*-phenylacetamide	jj	*N*-methyl-4-nitroaniline
l	methyl 4-hydroxybenzoate	y	2-hydroxypyridine	kk	triphenylphosphine oxide
m	4-nitrophenol				

[a] These host–guest pairs form cocrystals that are liquids at room temperature.

(Nujol) 3360, 3240, 3160, 1710, 1670, 1600, 1590, 1490, 1470, 1430, 1350, 1310, 1260, 1250, 1220, 1160, 1090, 830, 720, and 640 cm^{-1}; ^1H NMR (200 MHz, $(CD_3)_2CO$) δ 0.98 (t, 3 H, J = 7.3 Hz), 1.67 (sext, 2 H, J = 7.3 Hz), 2.85 (t, 2 H, J = 7.2 Hz), 6.84 (dd, 2 H, J = 2.3 and 6.6 Hz), 7.19 (dd, 2 H, J = 2.2 and 6.7 Hz), 7.49–7.67 (m, 3 H, J = 7.5, 7.0, and 1.5 Hz), and 7.99 (dd, 2 H, J = 1.6 and 7.0 Hz); ^{13}C CP/MAS NMR (25 MHz) δ 16.1, 40.9, 119.8, 128.8, 155.0, 164.3, 174.5, and 179.9.

***N*-Propionylbenzamide (3)–hydroquinone (2:1) cocrystal (26)**: methods A and B; colorless plates (1:1 toluene–ethyl acetate); mp 104–106 °C; IR (Nujol) 3430, 3290, 1700, 1680, 1520, 1460, 1370, 1250, 1210, 1200, 1190, 1080, 900, 820, 760, and 710 cm^{-1}; ^1H NMR (200 MHz, $(CD_3)_2CO$) δ 1.12 (t, 6 H, J = 7.4 Hz), 2.88 (q, 4 H, J = 7.3 Hz), 6.66 (s, 4 H), 7.49–7.67 (m, 8 H, J = 2.0 and 7.0 Hz), 7.99 (dd, 4 H, J = 2.0 and 6.8 Hz), and 9.8 (b s, 2 H); ^{13}C CP/MAS NMR (25 MHz) δ 5.5, 30.3, 113.6, 128.3, 132.4, 148.4, 161.6, 168.1, 175.8, and 182.9.

Diacetamide (1)–acetamide (1:1) cocrystal (27): method B; mp 59–62 °C; IR (Nujol) 3300, 3240, 3120, 1730, 1690, 1660, 1630, 1530, 1380, 1290, 1240, 1130, and 1040 cm^{-1}; ^{13}C CP/MAS NMR (25 MHz) δ 20.9, 23.6, 26.0, 170.6, 174.9, and 180.2.

Diacetamide (1)–benzamide (1:1) cocrystal (28): method B; mp 64–67 °C; IR (Nujol) 3460, 3350, 3280, 3240, 3130, 1740, 1680, 1640, 1610, 1570, 1530, 1460, 1450, 1410, 1380, 1290, 1250, 1220, 1020, and 720 cm^{-1}; ^{13}C CP/MAS NMR (25 MHz) δ 24.2, 128.3, 131.6, 169.9, 174.7, and 180.3.

Diacetamide (1)–4-(methylamino)benzoic acid (1:1) cocrystal (29): methods A and B; yellow rods (ethyl acetate); mp 132–134 °C; IR (Nujol) 3400, 3370, 3150, 2660, 2540, 1700, 1660, 1600, 1540, 1520, 1510, 1420, 1320, 1290, 1280, 1230, and 1180 cm^{-1}; ^1H NMR (200 MHz, $(CD_3)_2CO$) δ 2.20 (s, 6 H), 5.8 (b s, 2 H), 6.62 (dd, 2 H, J = 8.9 and 1.9 Hz), and 7.81 (dd, 2 H, J = 8.9 and 2.0 Hz); ^{13}C CP/MAS NMR (25 MHz) δ 24.3, 34.7, 106.9, 108.5, 114.0, 130.9, 133.3, 151.1, 160.6, 168.7, 172.8, and 179.2.

Diacetamide (1)–3,4-dinitrobenzoic acid (1:1) cocrystal (30): method B; mp 74–78 °C; IR (Nujol) 3300, 3250, 3200, 3150, 3120, 1740, 1720, 1560, 1530, 1390, 1370, 1350, 1260, 1210, 1150, and 1110 cm^{-1}; ^1H NMR (200 MHz, $(CD_3)_2CO$) δ 2.20 (s, 6 H), 8.32 (d, 1 H, J = 8.2 Hz), 8.58 (dd, 1 H, J = 9.9 and 2 Hz), 8.67 (d, 1 H, J = 1.5 Hz), and 9.6 (b s, 1 H); ^{13}C CP/MAS NMR (25 MHz) δ 25.1, 124.8, 128.9, 133.3, 138.8, 139.3, 144.6, 147.3, 163.3, 171.2, 172.6, 178.0, and 179.2.

Diacetamide (1)–1,3-dimethylurea (1:1) cocrystal (31): methods A, B, and C; colorless flakes ($CHCl_3$); mp 55–58 °C; IR (Nujol) 3400, 3360, 3250, 3170, 1760, 1660, 1610, 1570, 1530, 1500, 1460, 1380, 1370, 1270, 1190, and 1170 cm^{-1}; ^1H NMR (200 MHz, $CDCl_3$) δ 2.30 (s, 6 H), 2.77 (d, 6 H, J = 4.9 Hz), 4.43 (b s, 2 H), and 8.6 (b s, 1 H); ^{13}C CP/MAS NMR (25 MHz) δ 24.6, 32.5, 153.9, 163.4, 169.4, and 175.6.

Imide Cocrystals That Are Neat Liquids at Room Temperature. Seven 1:1 cocrystals of diacetamide and other organic guest donors and acceptors that melt below room temperature have been prepared as described previously. These host–guest pairs are indicated in Table I.

The formation of hydrogen bonded heteromers in the neat liquids was confirmed by the presence of new peaks in their IR spectra. The occurrence of melting points of the host–guest pairs at 10–80 °C below that of either of the components or below room temperature was used as supporting evidence for cocrystal formation, although in some cases lowered melting points may simply be due to eutectic formation. The structures of the hydrogen bonded aggregates in the neat liquids were not explored in detail.

Imide–Guest Pairs That Do Not Form Cocrystals. Many attempts at cocrystallizing imides with a variety of hydrogen bond donor and acceptor guests were not successful by either solution or solid-state methods. The imide–guest pairs that did not form cocrystals are shown in Table I. Spectroscopic and physical methods were used to show that separate phases of each component were present in the solid-state products of these imide–guest mixtures.

Crystallographic Literature Search. A Cambridge Crystallographic Data Base Search (Version 4.3) for acyclic imides and their complexes was carried out.[13] From the connectivity search of C–CO–NH–CO–C, 23 structures were obtained. Of these, 13 were uncomplexed imides, 9 were imide cocrystals with group I or II metal halides, and 1 was an imide cocrystal with an organic guest. The search algorithm and bibliographic citations retrieved from the search are included in the supplementary material.

Crystal Structure Determinations for Compounds 12–20. Data were collected on an Enraf-Nonius CAD4 diffractometer with graphite monochromated Mo Kα radiation (λ = 0.71069) using the ω–2θ scan technique. Lattice parameters were obtained from least-squares analysis of 25 reflections. Structures were solved by direct methods with MITHRIL[14] and DIRDIF.[15] All non-hydrogen atoms were refined anisotropically. All NH and OH protons were refined isotropically. The acetyl hydrogen atoms were refined isotropically as a group. The other hydrogen atoms included in the structure factor calculations were placed in idealized positions (d_{C-H} = 0.95 Å) with assigned isotropic thermal parameters (B = 1.2B of bonded atoms). The experimental details for the X-ray analysis of nine imide cocrystals are listed in Table II. The

(13) *Cambridge Structural Database*; Cambridge Crystallographic Data Centre, University Chemical Laboratory: Cambridge, England, June 1990 update; Version 4.3 (Vax).
(14) Gilmore, C. J. *J. Appl. Crystallogr.* **1984**, *17*, 42–46.
(15) Beurskens, P. T. Technical Report, University of Nijmegen: The Netherlands, 1984; Vol. 1.

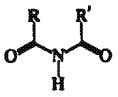
UM00013262
NOVARTIS EXHIBIT 1517
Novartis v. Regents, IPR2023-01347
Page 2008 of 4460

last line in the table gives the graph set for each structure. The graph set is a representation of the topology of hydrogen-bonded sets of molecules in the crystal.[16] Descriptions of how these assignments were made and of how to use graph sets to analyze acyclic imide patterns will be given in a future paper.

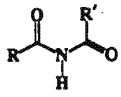
Results

The cocrystallization of acyclic imides with hydrogen bond donor and acceptor guest molecules was explored to test solid-state selectivity preferences of hydrogen-bonding groups. As we have done with ureas and nitroanilines previously, we wanted to see if a set of hydrogen bond rules useful for designing new imide aggregate structures could be developed. When cocrystal pairs were designed, intramolecular hydrogen bonding interactions that would compete with intermolecular hydrogen bonding were avoided by using imides that had no competitive hydrogen bonding functional groups, besides CO–NH–CO, and by using guest molecules with no near-neighbor hydrogen bond donor and acceptor groups. Over 80 host–guest pairs were evaluated, including 11 aromatic and/or aliphatic acyclic imides, and a variety of hydrogen bond guest molecules was attempted. Cocrystalline solids formed for 25 of these host–guest pairs. Successful guest molecules included phenols, carboxylic acids, amides, phosphine oxides, and ureas. The crystal structures of single crystals of nine imide cocrystals are presented. The hydrogen bond patterns of homomeric imide crystals and of their heteromeric cocrystals are compared geometrically and topologically.

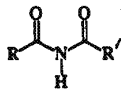
Crystallographic Studies of Acyclic Imides. Acyclic imides have three planar conformations, cis–cis (cc), cis–trans (ct), and trans–trans (tt), differentiated by the relative orientations of the carbonyl groups to the central NH bond. The cc conformer has



cis-cis (cc)



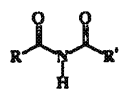
cis-trans (ct)



trans-trans (tt)

the highest energy due to steric overcrowding between R and R′. This conformer has not been observed in solution or in the solid state for any known acyclic imides. The ct conformer is the most stable form and is observed in solution for all simple acyclic imides (11 examples) except dipivalamide.[17] The tt conformer is destabilized by ~4 kJ/mol relative to the ct conformer by the electrostatic repulsion between the two imide carbonyl groups; nevertheless, it is frequently observed in the solid state.[18]

Diacetamide (**1**), the simplest of the acyclic imides, crystallizes in two polymorphic forms: α, the stable form, containing molecules with the ct conformation, and β, the metastable form containing molecules with the tt conformation.[19,20] When **1** is complexed with organic molecules, the ct conformation is retained. The only conditions under which **1** forms its tt conformer in a cocrystal are when it is complexed with group I or II metal halides.[21] Three other examples of simple, acyclic imides, *N*-acetylbenzamide (**2**α), *N*-propionylbenzamide (**3**), and *N*-butyrylbenzamide (**4**), were also found to crystallize in the ct conformation. These imides are unsymmetrical and have two possible ct conformations, only one of which is found in their crystal structures.[22] The same ct conformation, with the acyl carbonyl group syn and the benzoyl carbonyl group anti with respect to the NH, is also present in their complexes. Another polymorph of *N*-acetylbenzamide (**2**β) and imides **5**–**11** crystallize in the tt conformation. The tt conformation of dibenzamide (**5**) is retained in its complexes.



	R	R′	conformer in crystals		R	R′	conformer in crystals
1α,β	Me	Me	ct, tt	**7**	Me	Et	tt
2α,β	Me	Ph	ct, tt	**8**	*i*-Pr	*i*-Pr	tt
3	Et	Ph	ct	**9**	Cy	Cy	tt
4	Pr	Ph	ct	**10**	Bn	Bn	tt
5	Ph	Ph	tt	**11**	*i*-Pr	Ph	tt
6	Et	Et	tt				

Crystallographic Studies of Acyclic Imide Cocrystals. X-ray crystal structure analyses of cocrystals of the previous imides were performed when suitable single crystals could be obtained and definitive characterization of the hydrogen bond patterns was needed. Comparative hydrogen bond geometries and selected intra- and intermolecular bond lengths are given in Table III.

The ct conformations of **1** and **4** are retained in their cocrystal structures, **12**–**15**. These cocrystals, shown in Figures 1 and 2, consist of planar imide molecules that form centrosymmetric dimers, like those found in plain diacetamide (α form), linked by NH···O hydrogen bonds to the cis imide carbonyl groups. Except for the trans carbonyl and adjacent C–N bond lengths, the bond lengths and angles of diacetamide and *N*-butyrylbenzamide are very similar in their homomeric structures and in their cocrystals, **12**, **13**, and **15**. The anti lone pairs of electrons of the trans imide carbonyls are hydrogen bonded in the cocrystals **12**, **13**, and **15** to the –OH groups of *p*-nitrophenol or hydroquinone. The –OH groups of hydroquinone hydrogen bond to the syn lone pair of electrons in **14**, however. An unexpected increase of 0.008 Å for the cis carbonyl bond length and decrease of 0.009 Å for the adjacent C–N bond length occurs in this cocrystal. The phenol molecules are coplanar with the imide dimers in each of these cocrystals.

Planar ct molecules of **1** form imide–acid and imide–amide heterodimers in **16** and **17** in contrast to the imide···imide dimers in **1**, **3**, **4**, and **12**–**15**. The heterodimers, which are shown in Figure 3a,b, are linked into chains by OH···O hydrogen bonds between the trans carbonyl group and the phenolic hydroxyl group of the guest. An additional hydrogen bond between the anti lone pair of electrons of the cis imide carbonyl group and the trans NH of the amide relates two hydrogen-bonded chains by a pseudoinversion center in **17**.

The ct conformation of *N*-acetylbenzamide (**2**), *N*-propionylbenzamide (**3**), and the tt conformation of dibenzamide (**5**) are retained in their respective triphenylphosphine oxide (TPPO) cocrystal structures, **18**–**20** (Figure 4a–c). The imide fragments are not quite planar in **18**–**20** as indicated by the C–N–C–O torsion angles of 166.0 and 6.8°, 170.5 and 6.6°, and 21.3 and 13.4°, respectively. The phosphoryl oxygen, rather than the imide carbonyl groups, is the sole hydrogen bond acceptor in these cocrystals. The P=O bond length increases up to 0.010 Å as a consequence of complexation with **5** but does not change significantly upon complexation with **2** or **3**.[23] The imides adapt to the bulky guest molecule by twisting their phenyl groups from the plane of the imide π systems by 29.4° in **18**, 22.1° in **19**, and 15.4 and 28.5° in **20**. This conformational adaptation is similar to those observed in diarylureas when they complex with TPPO.[2]

The imide carbonyl bond lengths increase by 0.004–0.017 Å when hydrogen bonded to guest donors, as in **12**–**17**. The cor-

(16) The notation used in graph set analysis is $G^d_a(r)$. The pattern designator, G, is assigned as S, intramolecular (or self), D, a noncyclic finite pattern (e.g., a dimer), R, a cyclic finite pattern (ring), or C, an infinite pattern (chain). The parameters *a* and *d* refer to the number of acceptors and donors participating in the hydrogen bond, respectively. The degree or "size" of the pattern (*r*) is given in parentheses. For a detailed discussion of graph set analysis, see: Etter, M. C.; MacDonald, J. C.; Bernstein, J. *Acta Crystallogr.* 1990, *B46*, 256–262.

(17) (a) Noe, E.; Raban, M. *J. Am. Chem. Soc.* 1975, *97*, 5811–5820. (b) Hvoslef, J.; Tracy, M. L.; Nash, C. P. *Acta Crystallogr.* 1986, *C42*, 353–360.

(18) Radom, L.; Riggs, N. V. *Aust. J. Chem.* 1980, *33*, 2337–2342.

(19) Matias, P. M.; Jeffrey, G. A.; Ruble, J. R. *Acta Crystallogr.* 1988, *B44*, 516–522.

(20) Kuroda, Y.; Taira, Z.; Uno, T.; Osaki, K. *Cryst. Struct. Commun.* 1975, *4*, 321–324.

(21) Gentile, P. S.; Shankoff, T. A. *J. Inorg. Nucl. Chem.* 1965, *27*, 2301–2309.

(22) Etter, M. C.; Britton, D.; Reutzel, S. M. *Acta Crystallogr.* 1990, *C46*, in press.

(23) (a) Brock, C. P.; Schweizer, W. B.; Dunitz, J. D. *J. Am. Chem. Soc.* 1985, *107*, 6964–6970. (b) Spek, A. L. *Acta Crystallogr.* 1987, *C43*, 1233–1235.

UM00013263
NOVARTIS EXHIBIT 1517
Novartis v. Regents, IPR2023-01347
Page 2009 of 4460

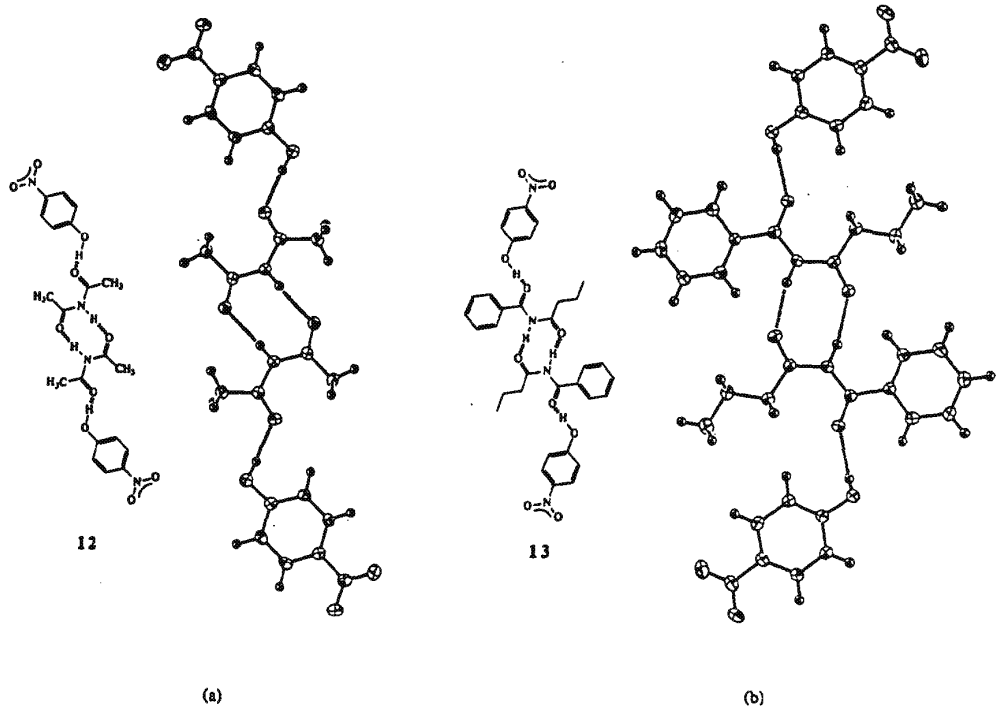


Figure 1. Tetrameric cocrystal hydrogen bond pattern formed by appending nitrophenols to the trans carbonyl groups of (a) diacetamide dimers, and (b) *N*-butyrylbenzamide dimers.

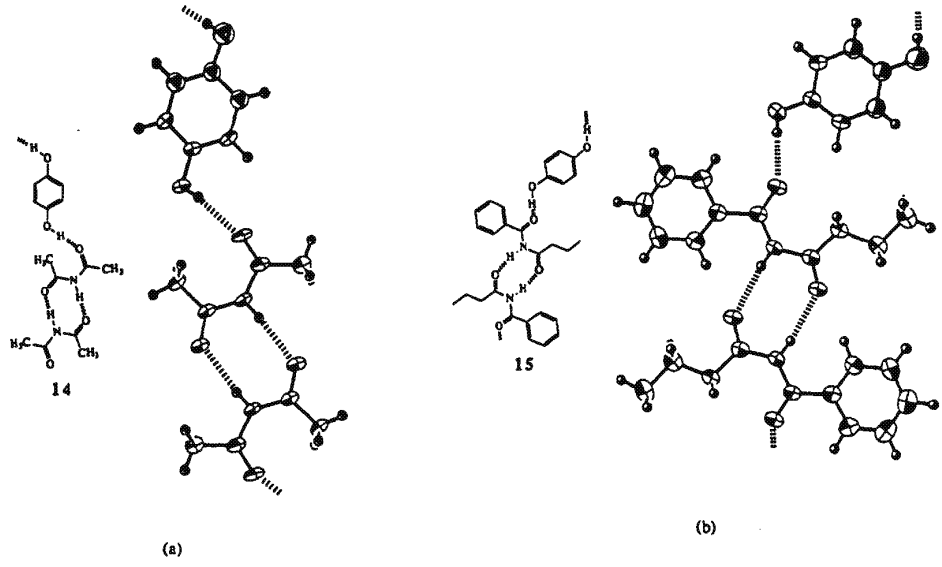


Figure 2. Infinite polymeric cocrystal hydrogen bond chains formed by appending bifunctional hydroquinone molecules to (a) diacetamide dimers, and (b) *N*-butyrylbenzamide dimers.

responding C–N bond lengths decrease by 0.004–0.021 Å. These structural changes are analogous to those caused by hydrogen bonding in amides.[24] The most important structural effect of the complexation of **2**, **3**, or **5** with TPPO is to cause the carbonyl groups to lose the hydrogen bonds that are present in their homomeric structures. As a result, these carbonyl bond lengths should decrease and the adjacent C–N bond lengths should increase relative to their values in their homomeric crystal forms. For **18** and **20**, the carbonyl bond lengths do decrease (by 0.007 Å in **18** and by 0.056 and 0.064 Å in **20**) and the C–N bond lengths do increase (by 0.009 Å in **18** and by 0.005 and 0.012 Å in **20**) upon complexation with TPPO. In **19**, however, no significant bond length differences were observed for imide molecules in their homomeric or cocrystal structures.

(24) (a) Jeffrey, G. A.; Ruble, J. R.; McMullan, R. K.; DeFrees, D. J.; Binkley, J. S.; Pople, J. A. *Acta Crystallogr.* **1980**, *B36*, 2292–2299. (b) Jeffrey, G. A.; Ruble, J. R.; McMullan, R. K.; DeFrees, D. J.; Pople, J. A. *Acta Crystallogr.* **1981**, *B37*, 1885–1890. (c) Stevens, E. D. *Acta Crystallogr.* **1978**, *B34*, 544–551.

UM00013264
NOVARTIS EXHIBIT 1517
Novartis v. Regents, IPR2023-01347
Page 2010 of 4460

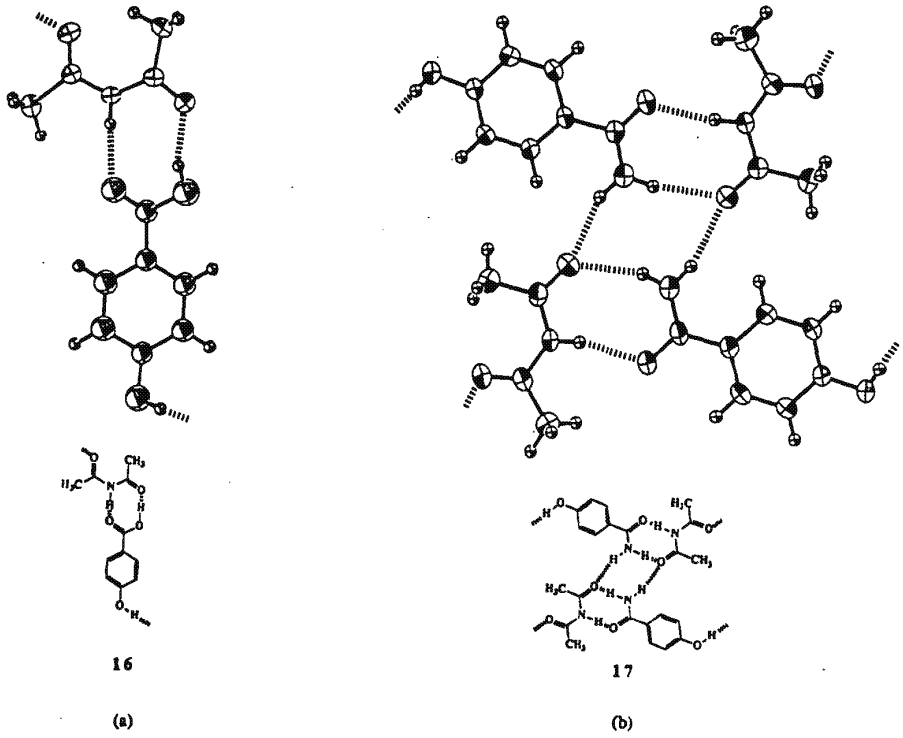


Figure 3. Diacetamide heterodimers formed by replacing a diacetamide molecule in a homodimer with a better hydrogen bond donor such as (a) benzoic acid or acceptor such as (b) benzamide.

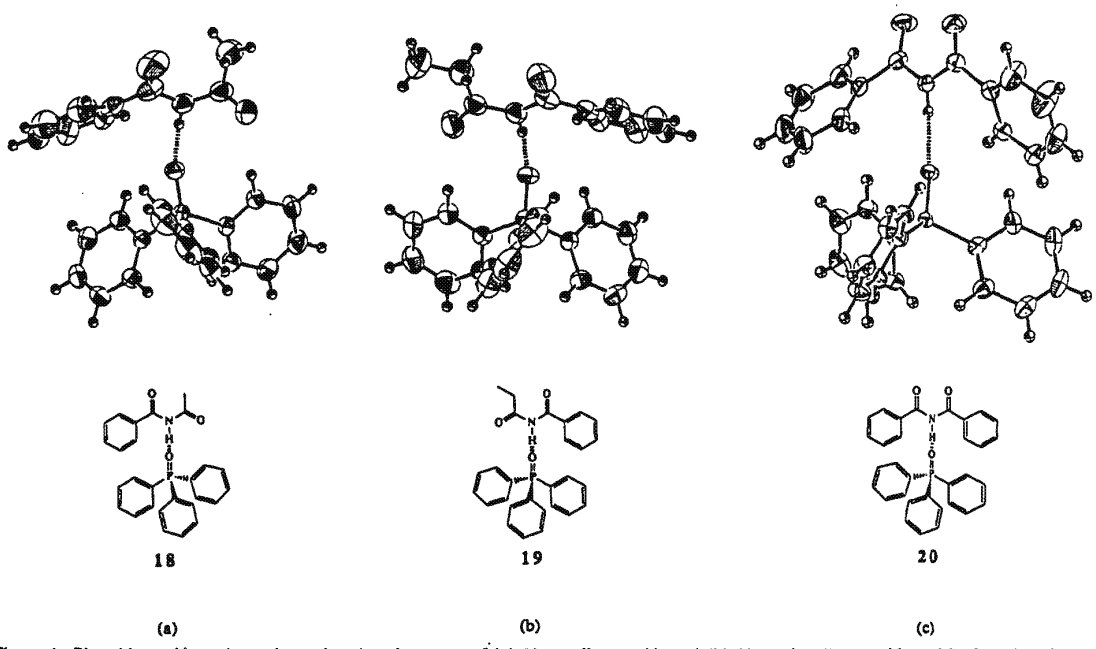


Figure 4. Phosphine oxide replaces the acyl carbonyl oxygens of (a) *N*-acetylbenzamide and (b) *N*-propionylbenzamide and both carbonyl oxygens of (c) dibenzamide as the hydrogen bond acceptor to the imide NH.

Noncrystallographic Methods for Characterizing Cocrystals. The experimental challenge in characterizing cocrystals is to determine whether the solid-state material obtained from a crystallization experiment is homogeneous or not, whether it contains any cocrystalline materials, and what the composition of the cocrystalline phase is. When nice single crystals make up the solid phase, then microscopy is a good indicator of overall homogeneity. A single crystal can often be extracted for further analysis of composition. New crystal forms may be observed even if they are not cocrystals. For example, polymorphs or solvates

UM00013265
NOVARTIS EXHIBIT 1517
Novartis v. Regents, IPR2023-01347
Page 2011 of 4460

Table II. Crystallographic Data for 12–20

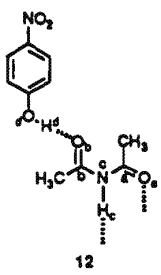
compd	12	13	14	15	16	17	18	19	20
formula	$C_{10}H_{12}N_2O_5$	$C_{17}H_{18}N_2O_5$	$C_{14}H_{20}N_2O_6$	$C_{28}H_{32}N_2O_6$	$C_{11}H_{14}N_2O_4$	$C_{11}H_{13}NO_5$	$C_{27}H_{24}NO_3P$	$C_{28}H_{26}NO_3P$	$C_{32}H_{26}NO_3P$
fw	240.22	330.34	312.32	492.57	238.24	239.23	441.47	455.49	503.54
space group	$P\bar{1}$	$P\bar{1}$	$P\bar{1}$	$P\bar{1}$	$P2_1/n$	$P\bar{1}$	$P\bar{1}$	$P\bar{1}$	$P2_1/c$
a (Å)	7.296 (4)	7.895 (8)	5.095 (6)	5.454 (3)	12.853 (7)	5.202 (2)	9.981 (5)	10.027 (3)	14.864 (4)
b (Å)	8.097 (2)	8.319 (3)	8.062 (5)	11.064 (7)	13.490 (3)	8.569 (4)	11.040 (7)	11.008 (4)	9.012 (1)
c (Å)	11.001 (7)	12.614 (7)	9.977 (4)	12.219 (3)	13.884 (2)	13.561 (2)	11.865 (3)	12.505 (4)	20.904 (7)
α (deg)	110.930 (4)	77.19 (4)	83.50 (4)	113.80 (2)		74.83 (2)	102.55 (4)	104.51 (3)	
β (deg)	107.460 (4)	89.10 (6)	88.82 (6)	96.38 (3)	101.49 (4)	87.39 (2)	101.80 (3)	99.91 (3)	109.97 (2)
γ (deg)	95.850 (3)	88.32 (5)	71.29 (7)	101.24 (5)		86.12 (3)	108.38 (5)	109.33 (3)	
V (Å^3)	562.9 (8)	807 (2)	386 (1)	647 (1)	2359 (2)	581.9 (7)	1156 (2)	1211 (2)	2632 (2)
Z	2	2	1	1	8	2	2	2	4
d_{calc} (g/cm^3)	1.417	1.359	1.345	1.265	1.341	1.365	1.268	1.249	1.271
crystl size (mm)	0.45 × 0.50 × 0.60	0.45 × 0.35 × 0.25	0.60 × 0.45 × 0.30	0.60 × 0.50 × 0.50	0.60 × 0.30 × 0.50	0.60 × 0.50 × 0.50	0.60 × 0.30 × 0.25	0.55 × 0.50 × 0.35	0.60 × 0.50 × 0.30
μ(Mo Kα) (cm^{-1})	1.08	0.95	0.99	0.83	0.97	1.02	1.41	1.37	1.33
T (°C)	−85 (1)	−64 (1)	24 (1)	24 (1)	23 (1)	24 (1)	23 (1)	22 (1)	−60 (1)
no. unique data total	2713	3877	1517	2275	5334	2800	4509	4246	5368
no. data used	2074	2436	1153	1598	2587	1715	3407	2691	3493
R^a	0.049	0.060	0.061	0.050	0.056	0.067	0.047	0.042	0.052
R_w[b]	0.065	0.077	0.079	0.068	0.065	0.099	0.056	0.052	0.070
$2\theta_{max}$ (deg)	55.9	56	51.9	49.9	53.9	55.9	52.1	49.9	51.9
range of hkl	$-7 \le h \le 9$ $-10 \le k \le 10$ $-14 \le l \le 13$	$0 \le h \le 10$ $-10 \le k \le 10$ $-16 \le l \le 16$	$0 \le h \le 4$ $-8 \le k \le 9$ $-12 \le l \le 12$	$-6 \le h \le 3$ $-13 \le k \le 12$ $-13 \le l \le 14$	$0 \le h \le 16$ $0 \le k \le 16$ $-17 \le l \le 17$	$-5 \le h \le 6$ $-11 \le k \le 11$ $-17 \le l \le 17$	$0 \le h \le 12$ $-13 \le k \le 12$ $-14 \le l \le 13$	$0 \le h \le 11$ $-13 \le k \le 12$ $-14 \le l \le 14$	$0 \le h \le 18$ $-11 \le k \le 10$ $-25 \le l \le 24$
$(\text{shift/error})_{max}$	0.02	0.04	0.01	0.01	0.07	0.10	0.05	0.04	0.01
largest peak (e$^-$/Å^3)	0.26	0.37	0.31	0.20	0.26	0.28	0.44	0.28	0.27
graph set	$N_1 = R_2^2(8)D$	$N_1 = R_2^2(8)D$	$N_1 = R_2^2(8)D$ $N_2 = C_4^4(17)$	$N_1 = R_2^2(8)D$ $N_2 = C_4^4(17)$	$N_1 = DDD$ $N_2 = R_2^2(8)$	$N_1 = DDD$ $N_2 = R_2^2(8)$ $N_3 = R_4^2(8)$	$N_1 = D$	$N_1 = D$	$N_1 = D$

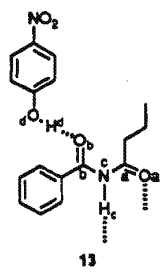
[a] $R = \sum||F_o| - |F_c||/\sum|F_o|$. [b] $R_w = [(\sum w(|F_o| - |F_c|)^2/\sum wF_o^2)]^{1/2}$; $w = 4F_o^2/\sigma^2(F_o^2)$.

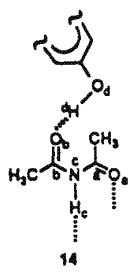
UM00013266

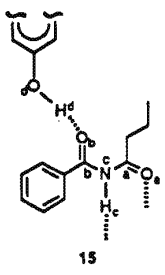
NOVARTIS EXHIBIT 1517
Novartis v. Regents, IPR2023-01347
Page 2012 of 4460

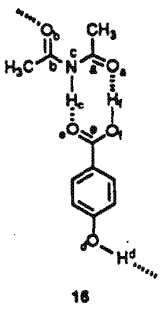
Table III. Hydrogen Bond Geometries and Selected Intra- and Intermolecular Bond Lengths for **12–20**

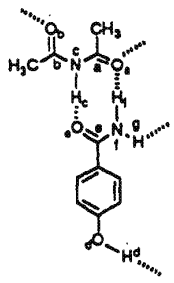

12

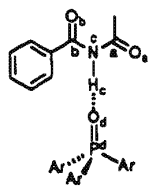

13

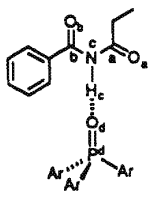

14

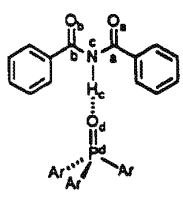

15


16


17


18


19


20

	12	**13**	**14**	**15**	**16**	**17**		**18**	**19**	**20**
$C_a{=}O_a$ (Å)	1.223 (2)	1.218 (3)	1.231 (3)	1.216 (3)	1.217 (3)	1.217 (4)	1.221 (4)	1.207 (3)	1.216 (3)	1.205 (4)
$C_b{=}O_b$ (Å)	1.225 (2)	1.228 (3)	1.215 (3)	1.217 (3)	1.221 (3)	1.217 (4)	1.219 (4)	1.214 (3)	1.222 (3)	1.209 (4)
$C_e{=}O_e$ (Å)					1.209 (3)	1.238 (4)	1.237 (3)			
$P_d{=}O_d$ (Å)								1.480 (2)	1.483 (2)	1.493 (2)
$C_a{-}N_c{-}C_b$ (deg)	130.1 (1)	129.6 (2)	130.7 (2)	129.7 (2)	129.6 (2)	129.3 (3)	129.2 (3)	128.7 (3)	128.7 (3)	123.9 (3)
$N_c{-}C_a{-}O_a$ (deg)	117.7 (1)	116.9 (2)	117.6 (2)	117.1 (2)	118.2 (2)	117.9 (3)	118.1 (3)	122.0 (3)	118.6 (3)	121.9 (3)
$N_c{-}C_b{-}O_b$ (deg)	122.8 (2)	120.9 (2)	123.6 (2)	120.8 (2)	122.4 (2)	122.4 (3)	122.4 (3)	118.8 (2)	122.7 (3)	123.2 (3)
$N_c{\cdots}O_{a,d,\text{or}e}$ (Å)	2.912 (2)	2.973 (3)	2.952 (4)	3.012 (3)	2.842 (3)	2.871 (4)	2.878 (4)	2.839 (3)	2.836 (3)	2.897 (3)
$H_c{\cdots}O_{a,d,\text{or}e}$ (Å)	2.08 (2)	2.08 (3)	2.12 (4)	2.17 (3)	2.00 (4)	2.014	2.034	2.02 (3)	1.96 (3)	2.03 (4)
$N_c{-}H_c{\cdots}O$ (deg)	174.0 (1)	161.5 (1)	176 (3)	167.5 (1)	175.3 (1)	173.0 (1)	166.4 (1)	171 (3)	172 (3)	164.4 (1)
$O_d{\cdots}O_b$ (Å)	2.690 (2)	2.685 (3)	2.832 (4)	2.777 (3)	2.703 (3)	2.730 (4)	2.728 (4)			
$H_d{\cdots}O_b$ Å	1.85 (3)	2.04 (4)	2.14 (4)	2.02 (3)	1.97 (6)	2.04 (1)	1.99 (1)			
$O_d{-}H_d{\cdots}O_b$ (deg)	173.9 (1)	176.0 (1)	165 (3)	170.6 (1)	140.5 (1)	171.1 (1)	172.2 (1)			
$O_a{\cdots}O_f$ (Å)					2.715 (3)					
$O_a{\cdots}N_f$ (Å)						3.007 (4)	2.974 (5)			
$H_f{\cdots}O_a$ (Å)					1.93 (6)	2.133	2.179			
$O_f{-}H_f{\cdots}O_a$ (deg)					149.2 (1)					
$N_f{-}H_f{\cdots}O_a$ (deg)						166.0 (1)	145.8 (1)			
$N_f{-}H_g{\cdots}O_a$ (deg)						159.6 (1)	157.5 (1)			

of the reagents might form or even just a new crystal morphology of one of the starting materials could form. The problem when working with single crystals is to know whether they are representative of the bulk material. If large single crystals are not evident, then the problem is more difficult. All analyses necessarily involve many particles, some of which might be cocrystals. It is not the purpose of this paper to describe the general analytical strategies for studying organic solids, rather to show a few examples of how noncrystallographic analytical methods were used to solve the problem of characterizing imide cocrystals.

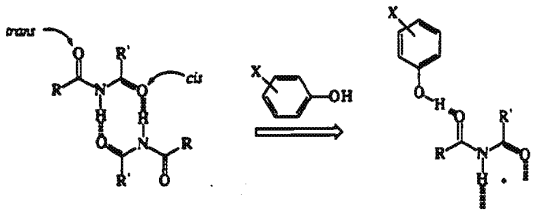
Cocrystals **21–31** have been prepared and characterized by chemical and spectroscopic means other than by crystallography. Except for **28** and **31**, we were able to determine their hydrogen bond patterns unambiguously. The proposed hydrogen bond aggregates of most of the cocrystals for which X-ray crystal structure analyses have not been done are based on spectroscopic evidence and are shown in Figure 5.

Characterization of the chemical composition of the cocrystals and their hydrogen bond patterns was based on melting point analysis, solid-state IR, solution-state ^1H and ^{13}C NMR, ^{13}C and ^{31}P CP/MAS NMR, and X-ray powder diffraction. Solid-state NMR was particularly useful in characterizing the imide cocrystals.[25] Since carbonyl carbon chemical shifts are sensitive to hydrogen bonding, complexation could be monitored by comparing the carbonyl ^{13}C shifts of the cocrystal relative to those of the host imide in the solid state.[26] Solid-state IR proved to be a particularly reliable tool for discriminating between possible imide conformers.[27] The other techniques were used for supporting evidence of cocrystal formation.

The crystal structures of **12–15** showed that the cis imide carbonyl groups were hydrogen bonded in both their homomeric as well as their cocrystal forms, but that the trans imide carbonyl groups were hydrogen bonded only in their cocrystal phases. Thus, one would expect complexation to cause large downfield NMR shifts for the trans carbonyl carbons but small or no shifts for the cis carbonyl carbons. When **1**, **3**, and **4** are complexed with para-substituted phenols, usually only one of their two NMR carbonyl carbon resonances shifted downfield (by 2–5 ppm), so those peaks were assigned to the trans imide carbonyl carbons.

(25) Details of the ^{13}C CP/MAS NMR characterization of the imide cocrystals will be reported in a future report.
(26) Etter, M. C.; Hoye, R. C.; Vojta, G. M. *Cryst. Rev.* **1988**, *1*, 281–338.
(27) Uno, T.; Machida, K. *Bull. Chem. Soc. Jpn.* **1961**, *34*, 551–556.

UM00013267
NOVARTIS EXHIBIT 1517
Novartis v. Regents, IPR2023-01347
Page 2013 of 4460



Homomeric Form *Cocrystal Form*

The remaining carbonyl peaks that did not move were attributed to the cis carbonyl carbons. In **14**, no significant change in either of the carbonyl carbon chemical shifts occurred. Solid-state NMR was not sensitive enough to detect the weak OH···O hydrogen bond. The O···O hydrogen bond length in **14** (2.832 (4) Å) is longer than that usually observed in the imide–phenol complexes (2.685–2.730 Å). Other ct amide cocrystals with phenols substituted with Br, Cl, NO_2, or OH (**21–26**) showed the usual spectral shifts relative to their host imides, so it is proposed that these structures have the patterns shown in Figure 5.

Interpretation of the solid-state NMR spectra of cocrystals of **1** with carboxylic acids and amides was sometimes complicated by overlapping carbonyl peaks of the hosts and guests. In most cases, a downfield shift (2–3 ppm) of one of the imide carbonyls was observed, although characterization of the precise hydrogen bond patterns was not possible from this data alone.

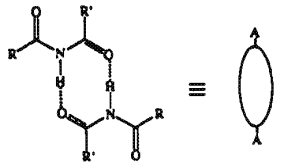
Solid-state NMR provided critical information for characterizing the 1:1 cocrystal between **1** and 3,4-dinitrobenzoic acid (**30**) (Figure 6).[25] Upon complexation with 3,4-dinitrobenzoic acid, the trans carbonyl carbon peak of **1** shifted 3 ppm downfield, while the cis carbonyl carbon peak did not move. Both imide carbonyl groups therefore must be hydrogen bonded in the cocrystal. Simultaneously, the carboxyl carbon peak of 3,4-dinitrobenzoic acid shifted 7 ppm upfield compared to its position in its own crystal structure (where it is a hydrogen bonded dimer),[28] clearly indicating that the carbonyl group is no longer hydrogen bonded in the cocrystal. The proposed hydrogen bond aggregate that accounts for these chemical shift changes is shown in Figure 5. This pattern is analogous to those of **12**, **13**, and **21–25**.

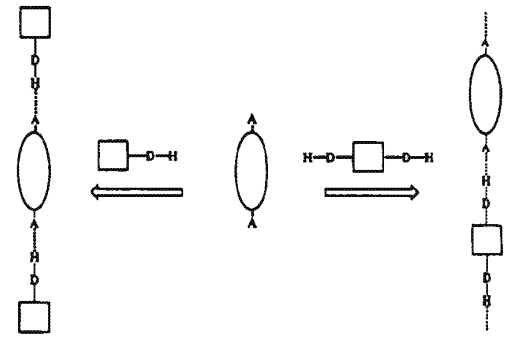
Evidence for the structure of the hydyrogen bonded aggregate in the dibenzamide–TPPO complex (**20**) was also provided by ^{13}C CP/MAS NMR. The carbonyl carbon chemical shifts in the cocrystal were 2 and 5 ppm upfield, respectively, compared to their homomeric structures, indicating that they were probably no longer hydrogen bonded. The presence of two peaks also indicated that the carbonyls are no longer crystallographically equivalent. This interpretation was subsequently confirmed by the X-ray crystal structure of **20**.

By comparing the relative intensities of the coupled symmetric and asymmetric amide C=O bands of the imides, which are usually in the ratio of ~50:1, IR spectroscopy was used to determine which imide conformer was present in the cocrystals.[27] The relative band intensities in **2α** and **3** remained unchanged upon complexing TPPO, indicating that the ct imide conformation was retained in **18** and **19**, respectively (Figure 4). This hypothesis was later confirmed by X-ray crystallography. The ct conformation of **2** and **3** is observed despite possible electrostatic repulsion between the acetyl oxygen and the near-neighbor phosphoryl oxygen.

Hydrogen Bond Patterns of Acyclic Imides and Their Cocrystals. The simple ct imides **1–4** form cyclic hydrogen bonded dimers. In this aggregate, one of the carbonyl groups is not used in hydrogen bonding. This dimer behaves like a bifunctional acceptor, shown schematically, in its cocrystallization properties.

We proposed that the non-hydrogen-bonded carbonyl groups of these dimers would be available to serve as sites for hydrogen bonding to proton donor guests, such as phenols. Indeed, not only was it possible to form such cocrystals, but their aggregate patterns could be controlled by choosing guest molecules with appropriate numbers and orientations of proton donor groups. Heteromeric tetramers or infinite chains were prepared according to the scheme shown below where A is the imide carbonyl acceptor and –DH is a guest proton donor.





heteromeric tetramer *imide-imide dimer* *heteromeric infinite chain*

Finite hydrogen-bonded aggregates were prepared by cocrystallizing monophenols with the ct imide dimers of **1**, **3**, and **4**. Seven 1:1 cocrystals of this type, including **12** and **13** (Figure 1a,b), were prepared. The OH···O hydrogen bonds between the trans imide carbonyl groups and the phenolic OH's are the driving force for cocrystal formation. Infinite hydrogen-bonded chains were formed by linking imide dimers of **1**, **3**, and **4** with diphenols, analogous to the preparation of copolymers using two difunctional reagents. Three 2:1 cocrystals, including **14** and **15** (Figure 2a,b), have been prepared with this type of hydrogen bond pattern.

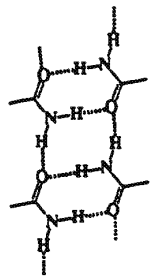
N-Acetylbenzamide (**2**) exists as cyclic hydrogen-bonded dimers in its α polymorph but does not behave like the other ct imides toward proton donor guests. Under the standard conditions (methods A and B) used for obtaining cocrystals, the tt polymorph, β, is obtained rather than cocrystals with phenols. These results indicate that the cocrystallization properties of **2** are dictated by the tt polymorph, β, rather than the ct polymorph, α.

The 1:1 cocrystals between imides **1**, **3**, and **4** and para-substituted phenols form with phenols that have NO_2, Br, Cl, or CN groups as substituents. These substituents are weak acceptors and do not compete with imide carbonyl groups for the available hydrogen bond donors in the cocrystals. When the para-substituents are carboxylic acids or amides, however, the hydrogen-bonded aggregates change dramatically as these functional groups provide competitive hydrogen-bonding sites. Cyclic eight-membered ring heterodimers form in preference to the imide dimers discussed previously when **1** is crystallized with a primary amide or an acid, as in **16** and **17** (Figure 3a,b). Imide···guest heterodimers are linked into chains by OH···O hydrogen bonds between carbonyl groups and phenolic hydrogens. When an amide replaces an acid group, as in **17**, an additional hydrogen bond donor is added to the system. It is accommodated in the same way as the extra hydrogen in homomeric primary amide structures by bonding as the second hydrogen bond donor to the anti lone pairs of electrons of a neighboring carbonyl group.[6] The tetramers resulting from these interactions in **17** are linked into infinite chains by the phenol –OH groups bonding to the unused diacetamide carbonyl groups (O(1)).

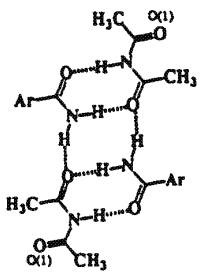
The complexing behavior of ct imides is distinctly different toward various classes of proton donors. Whereas **1** forms co-

(28) 3,4-Dinitrobenzoic acid crystallizes as hydrogen-bonded dimers as determined by solid-state IR spectroscopy. For determination of hydrogen-bonded chain vs dimers by solid-state IR, see: Walborsky, H. M.; Barash, L.; Young, A. E.; Impastato, F. J. *J. Am. Chem. Soc.* **1961**, *83*, 2517–2525.

UM00013268
NOVARTIS EXHIBIT 1517
Novartis v. Regents, IPR2023-01347
Page 2014 of 4460



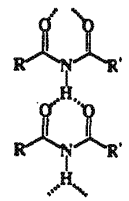
primary amide chains



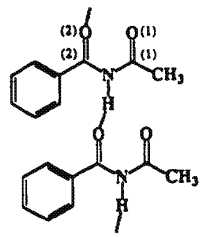
diacetamide - amide tetramers

crystals with many different classes of proton donors, **3** and **4** form cocrystals only with phenol donors. It is also difficult to cocrystallize the ct imides **1**, **2α**, **3**, and **4** with most acceptors. Two examples, however, are the 1:1 complexes of **2** and **3** with TPPO, **18** and **19**, respectively (Figure 4a,b). The NH groups of **2** and **3** preferentially form hydrogen bonds to the phosphoryl oxygen of TPPO rather than to their own carbonyl groups, thus preventing the formation of the cyclic dimers found in their homomeric structures **2α** and **3**, respectively. The other ct imides, **1** and **4**, do not complex with TPPO.

The complexing behavior of tt imides reflects both the conformational and hydrogen bonding preferences of these imides. Imides that adopt the tt conformation in their homomeric crystal forms almost always form infinite chains linked by bifurcated hydrogen bonds. The only acyclic imide that has the tt con-

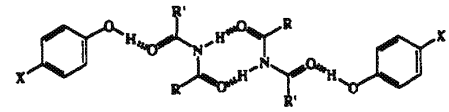


formation and does not form bifurcated hydrogen-bonded chains is **2β**. It forms chains linked by NH···O hydrogen bonds to only the benzoyl carbonyl groups. The acetyl carbonyl oxygen atom is 3.069 Å from the nearest intermolecular NH hydrogen atom. The imide moiety (–CO–NH–CO–) is nonplanar as indicated by the O(1)–C(1)–N–C(2) and O(2)–C(2)–N–C(1) torsion angles of 11.1 (3) and 13.9 (3)°, respectively.

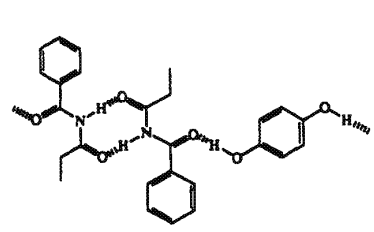


Imides adopting the tt conformation did not form cocrystals with hydrogen bond donor guests, such as phenols, carboxylic acids or amides, but a few of them did complex the best hydrogen bond acceptors. As previously mentioned, TPPO is a guest hydrogen bond acceptor for **2**, which is tt in the β form, in cocrystal **18** (Figure 4a). TPPO is also a guest acceptor to **5** in its cocrystal **20** (Figure 4c). These cocrystals of tt imides are rare since we found that neither tt diacylamines nor tt acylbenzamides with bulky acyl groups would complex TPPO.

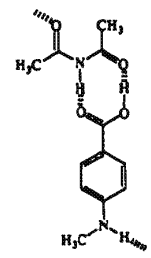
Cocrystallization Process. Both solid-state and solution cocrystallizations of all the host–guest pairs were attempted. Cocrystals were not always obtained by both methods. Solid-state grinding afforded cocrystals of **28** and **30** when their solution-state



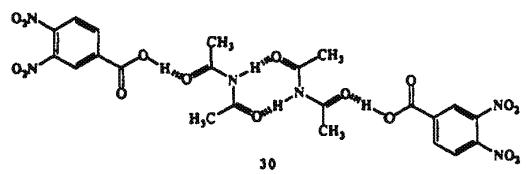
Cmnd	R	R'	X
21	Et	Ph	NO_2
22	Me	Me	CN
23	Pr	Ph	Br
24	Et	Ph	Br
25	Pr	Ph	Cl



26



29



30

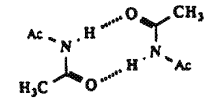
Figure 5. Proposed hydrogen-bonded aggregates for **21–26**, **29**, and **30** on the basis of chemical and spectroscopic data.

cocrystallizations were unsuccessful. The inability to isolate cocrystals from solution when they could be readily obtained in the solid state is frequently due to different solubilities of the components, so the solid-state grinding method proved to be the best indicator of potential cocrystal formation.

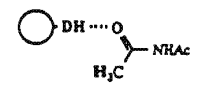
Typically, from one to three common solvents or solvent pairs were used in the recrystallization experiments. Some cocrystals that were expected to form on the basis of previous successful cocrystallizations of related host–guest pairs did not form by either solid-state grinding or solution recrystallizations. In such cases, evaporation rates, temperature, light vs darkness, and additional solvents were tested. These changes did not result in cocrystal formation, so for most of the host–guest pairs only the standard methods (methods A and B in Experimental Section) were used.

Discussion

The cocrystallization properties of acyclic imides depend on which conformation they adopt in their homomeric crystal forms. The cis–trans and trans–trans conformers found in imide crystal structures have their own unique hydrogen bond properties. The cis–trans forms behave like a combination of two independent functional groups: a primary amide (forming dimers) and a tertiary amide (acting as an acceptor only).



"Primary amide-like" portion



"Tertiary amide-like" portion

(◯–DH is a guest donor)

Cis-trans Imides

UM00013269
NOVARTIS EXHIBIT 1517
Novartis v. Regents, IPR2023-01347
Page 2015 of 4460

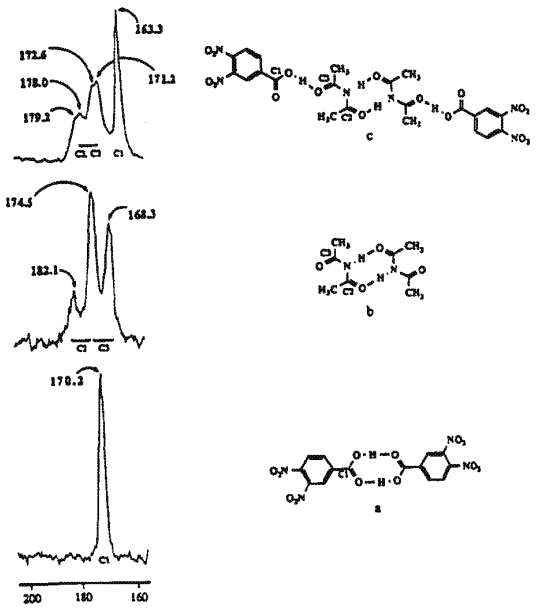
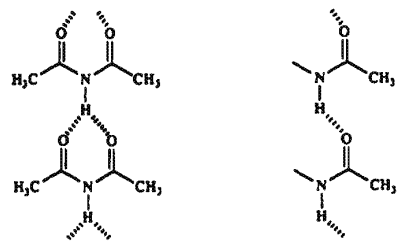


Figure 6. Carbonyl region of ^{13}C CP/MAS solid-state NMR spectra (25 MHz). The imide carbonyl peaks are split into asymmetric doublets due to the adjacent quadrupolar ^{14}N atoms. (a) 3,4-Dinitrobenzoic acid spectrum showing a single peak for the carbonyl carbon (C(1)) in a hydrogen bond pair. (b) Diacetamide spectrum (polymorph Iα) showing two partially overlapping doublets due to the carbonyl carbons in a hydrogen-bonded carbonyl group (C(2), 7 ppm downfield) and in a free carbonyl group (C(3)). (c) Diacetamide–acid cocrystal showing that both carbonyl carbons of diacetamide have nearly the same chemical shift (C(2), C(3) both 3–4 ppm downfield), so they are now both hydrogen-bonded, while the acid carbonyl peak (distinguishable as a singlet) has moved upfield since it is no longer hydrogen bonded in the cocrystal.

In trans–trans imides, the two carbonyl groups usually act like a bidentate ligand that complexes a proton donor. This pattern is like that of secondary amides with an additional acceptor ligand:



Trans-trans Imides *Secondary Amides*

The cocrystallization process can be viewed as a competition between homomeric aggregation and heteromeric aggregation. Consideration of how a hydrogen bond guest could compete with and displace the hydrogen bond pattern of the homomeric ct or tt forms prior to crystal nucleation is a useful way to predict imide cocrystallization patterns. If the imide aggregates with itself in a ct conformation, it will then have an unused carbonyl group as a site for complexation to proton donor guest molecules (cocrystals of this type are referred to as type I complexes). If the guest donor is itself capable of forming eight-membered ring hydrogen bonded chains, e.g., a primary amide or a carboxylic acid, then an alternative complexation mechanism would be to form the type II heterodimer cocrystal. The hydrogen bonded chains formed by tt imides that aggregate with themselves could be perturbed by guest molecules to give either type III or IV cocrystals (Figure 7).

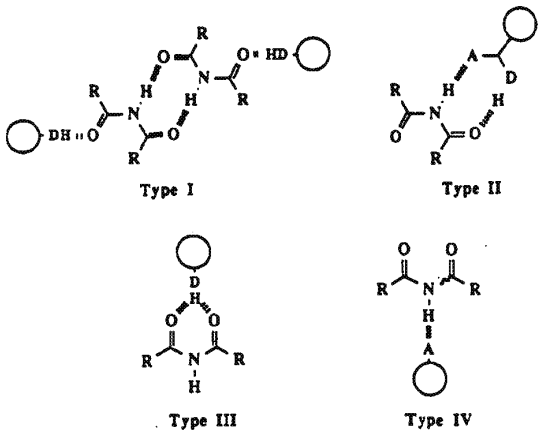


Figure 7. Acyclic imide cocrystal types. Types I and II are observed most frequently. Type III is surprisingly uncommon, indicating how difficult it is to disrupt hydrogen bond chains of tt imides. Type IV is observed only for TPPO complexes.

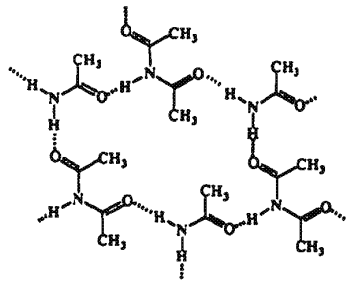
Type I Complexes (12–15, 21–26, 30). These cocrystals are observed most frequently for diacetamide or aryl–alkyl imides with phenols or carboxylic acids of high acidity. The imides that form type I cocrystals are found in the same ct conformation in their own homomeric crystal structures.

Type II Complexes (16,17,29). These cocrystals form when a strong carboxylic acid or a primary amide is used as a guest molecule. In these cases, the host and guest molecules are both capable of forming stable hydrogen bonded dimers. The driving force for cocrystallization in these cases may be that the heteromeric pairing involves a stronger hydrogen bond than those formed in the respective homomeric dimers.

Type III Complexes. The imide carbonyl groups have been used to chelate group I and II metal ions, but no organic donor molecules have been found to give a type III structure.

Type IV Complexes (18–20). These cocrystals were very difficult to form, occurring only in three cases where an exceptionally strong proton acceptor (TPPO) was used. Attempts were made unsuccessfully to cocrystallize TPPO with seven other imides. In light of our previous use of TPPO as a general cocrystallizing agent for proton donors,[1] these findings were unexpected. One implication is that the cost of breaking two imide NH···O=C bonds is too large to be compensated for by a strong NH···O=P bond.

Exceptions (27). The crystal structure of **27** has been reported previously.[19] In this structure, diacetamide and acetamide form hydrogen-bonded chains similar to those formed by secondary amides. The hydrogen-bonded chains are cross-linked by hydrogen bonds between the cis amide NH and the anti lone pair of electrons of the cis imide carbonyl group. This pattern has the expected features that diacetamide is in its ct conformation and all carbonyl groups and –NH hydrogens are used in the hydrogen bond patterns. What is unexpected is that neither diacetamide nor acetamide participate in any eight-membered ring hydrogen bond patterns in this structure.

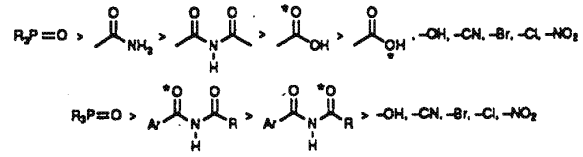


27

UM00013270
NOVARTIS EXHIBIT 1517
Novartis v. Regents, IPR2023-01347
Page 2016 of 4460

Table IV. Hydrogen Bond Rules for Acyclic Imides and Their Cocrystals

1 All alkyl and aryl acyclic imides that adopt the trans–trans conformation (8 in paper, 13 studied to date) form chains, usually involving bifurcated hydrogen bonds.
2 All alkyl and aryl acyclic imides that adopt the cis–trans conformation form eight-membered hydrogen-bonded ring dimers in their homomeric structures and in their cocrystals.
3 Hydrogen bond patterns form as if the best hydrogen bond donor paired with the best hydrogen bond acceptor first and subsequent hydrogen bonds were formed according to their relative donating and accepting abilities.
4 The imide donor and both acceptors are used in their cocrystals when possible.
5 Relative accepting abilities of imide groups and other functional groups present in imide crystals or cocrystals:



Hydrogen Bond Rules and Relative Proton-Donating and -Accepting Abilities. There are certain features common to hydrogen bond patterns in organic crystals in general and other features that are specific to different functional group classes.[8] We have found it useful, with a large number of crystal and cocrystal structures of one class of functional groups, to summarize their hydrogen bond patterns according to their topology and to their functional group selectivity. In the best cases, these summaries, or hydrogen bond rules, can be used as predictors of hydrogen bond patterns for new structures and as guidelines for designing new cocrystals and host–guest pairs.

The imide series presented here is the largest database we have yet analyzed. From just a handful of imide homomeric structures from the literature, an iterative process of predicting new structures based on that small database, preparing those compounds and their cocrystals, determining their structures, and then modifying the rules as dictated by the new data was followed. Certain hydrogen bond properties emerged repeatedly and became very useful for predicting new structures. These properties are listed in Table IV as hydrogen bond rules for acyclic imides and their cocrystals.

One of the most remarkable features of these rules is that the hydrogen bond connectivity patterns are based on functional group analysis only, as if *the crystal nucleation and growth processes do not perturb the preferred hydrogen bond connectivity patterns.* An example of this phenomenon is the ranking of relative accepting abilities of the various proton-accepting functional groups in the imide series (rule 5, Table IV). This ranking was derived from the empirically determined connectivity patterns in the crystal structures of **12–20** and in the proposed hydrogen bond patterns of **21–26**, **29**, and **30**. The rankings derive from assigning the best acceptor as either the only one that is used in the presence of other acceptors or the one that is bonded to the most acidic proton donor in a structure with several donors. For example, in **16** the calculated pK_a's are $-CO_2H$ (4.57), $-OH$ (9.23), and $-NH$ (11.8).[29] Thus, the best acceptor is assigned to the one bonded to the carboxylic acid hydrogen. Using this criterion, the best acceptor is the imide carbonyl group. This method has pitfalls since pK_a is not a direct measure of hydrogen bond abilities when comparing different kinds of functional groups and when working in nonaqueous media. Nevertheless, it is the best indicator of hydrogen bonding ability available, in lieu of α and β rankings determined by solvatochromatic measurements.[30] When pK_a differences are small and when there are multiple competing groups (i.e., more than two or three), then we expect these rankings will not be strictly observed in the solid state. Other cases where they may not be observed is when steric interference prevents the preferred contact from forming or when other intermolecular interactioins that are stronger than hydrogen bonds are present (e.g., ionic interactions). For example, 2,4-dinitrophenol does not complex with **1** in the usual type I pattern, presumably due to interference by the ortho nitro group.

Cocrystallization Phenomenon. The prior discussion has referred to observed hydrogen bond patterns in homomeric imides and their cocrystals, but many proposed cocrystal pairs could not be prepared at all. Diacetamide is an exception. It is a very versatile cocrystallizing agent, forming cocrystals from solution or in the solid state with many proton-donor and -acceptor guests.

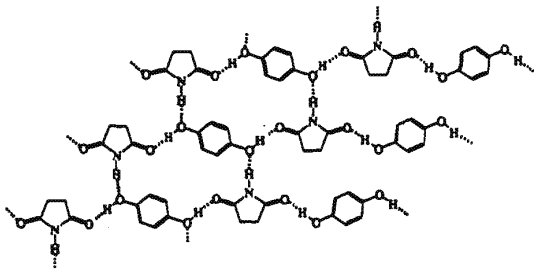
Simply choosing a proton-donor host and an acceptor guest that can form a stronger hydrogen bond to one another than to themselves is not a sufficient condition for predicting when cocrystals will form. For example, 4-nitrobenzoic acid does not cocrystallize with diacetamide even though 3,4-dinitrobenzoic acid does (**30**). Other forces must be operating that prevent the cocrystallization of this host–guest pair. The inability of most imides to complex TPPO, thus forming strong NH···O=P hydrogen bonds, further demonstrates that optimizing donor and acceptor strengths does not necessarily result in cocrystal formation.

The cocrystallization process represents a balancing of all the forces impinging on a molecule in solution as well as in the solid state. Since most of the imide cocrystals that form do so either in the absence or presence of solvent, the solvent effects alone are not dictating which pairs of molecules will cocrystallize. Once cocrystals have formed, however, the heteromeric hydrogen bond rules presented previously can be used to predict their hydrogen bond patterns.

Use of Acyclic Imide Hydrogen Bond Rules in Biochemical Systems. We have shown how preferred imide hydrogen bond patterns are related to those of primary, secondary, and tertiary amides. It is also tempting to apply imide hydrogen bond rules to chemical homologues and analogues such as cyclic imides, uracils, and barbiturates and to investigate host–guest interactions of imide-type functional groups in DNA, protein, or enzyme receptor sites.[31] For small-molecule analogues, such as cyclic imides, the relationship between their hydrogen bond properties and those of acyclic imides is, however, not obvious. Despite the chemical homology of these classes of compounds, the fact that cyclic imides can adopt only the cc conformer but that acyclic imides prefer the tt conformer (occasionally ct is found, but never cc), is more important to their molecular recognition properties than are their chemical similarities. For example, succinimide forms typical hydrogen bonded dimers in its homomeric crystals,[32] but forms an unusual 1:1 cocrystal with hydroquinone.[33] By comparison, **14** and **15** (Figure 2a,b) form 2:1 cocrystals with

(29) Perrin, D. D.; Dempsey, B.; Serjeant, E. P. *pK_a Prediction for Organic Acids and Bases*; Chapman and Hall: London and New York, 1981.
(30) (a) Taft, R. W.; Kamlet, M. J. *J. Am. Chem. Soc.* **1976**, *98*, 2886–2894. (b) Kamlet, M. J.; Taft, R. W. *J. Am. Chem. Soc.* **1976**, *98*, 377–383. (c) Kamlet, M. J.; Abboud, J.-L. M.; Abraham, M. H.; Taft, R. W. *J. Org. Chem.* **1983**, *48*, 2877–2887.
(31) (a) Seeman, N. C.; Rosenberg, J. M.; Rich, A. *Proc. Nat. Acad. Sci. U.S.A.* **1976**, *73*, 804–808. (b) Pabo, C. O.; Sauer, R. T. *Annu. Rev. Biochem.* **1984**, *53*, 293–321. (c) Feibush, B.; Figueroa, A.; Charles, R.; Onan, K. D.; Feibush, P.; Karger, B. L. *J. Am. Chem. Soc.* **1986**, *108*, 3310–3318. (d) Buchet, R.; Sandorfy, C. *J. Phys. Chem.* **1984**, *88*, 3274–3282. (e) Kyogoku, Y.; Lord, R. C.; Rich, A. *Nature* **1968**, *218*, 69–72. (f) Voet, D.; Rich, A. *J. Am. Chem. Soc.* **1972**, *94*, 5888–5891. (g) Yu, N.-T.; Kyogoku, Y. *Biochim. Biophys. Acta* **1973**, *331*, 21–26.
(32) Mason, R. *Acta Crystallogr.* **1956**, *9*, 405–410.
(33) Unpublished results.

UM00013271
NOVARTIS EXHIBIT 1517
Novartis v. Regents, IPR2023-01347
Page 2017 of 4460



1:1 Cocrystal of a Cyclic Imide and Hydroquinone

hydroquinone. Thus, the hydrogen bond patterns of the cyclic or acyclic imide–hydroquinone complexes are completely different. We are currently studying the relationships between cyclic and acyclic imide cocrystal patterns and plan in the future to relate these systems to uracils.

Conclusions

The use of hydrogen bond interactions to direct selective molecular recognition processes of acyclic imides has been demonstrated by studying their cocrystallization properties. Acyclic imides retain their native conformation (as found in homomeric crystals) when interacting with guest molecules during the cocrystallization process. Host–guest pairs self-assemble in the absence of preorganized cavities according to relative hydrogen bond donating and accepting abilities of the functional groups that are present as well as according to the number and orientation of such groups. These results show that cocrystallization experiments provide a useful way to map out the molecular recognition properties of a class of molecules and to test for hydrogen bond selectivity in weakly associated, multifunctional systems.

Acknowledgment. We gratefully acknowledge Prof. Doyle Britton, Department of Chemistry, University of Minnesota, for his crystallographic assistance and the NIH (GM 42148-01) for financial support.

Supplementary Material Available: Positional parameters, anisotropic thermal parameters, intra- and intermolecular bond lengths and angles, and unit cell drawings for seven crystal structures (149 pages); tables of observed and calculated structure factors (147 pages). Ordering information is given on any current masthead page.

Use of Aza-Cope Rearrangement–Mannich Cyclization Reactions To Achieve a General Entry to *Melodinus* and *Aspidosperma* Alkaloids. Stereocontrolled Total Syntheses of (±)-Deoxoapodine, (±)-Meloscine, and (±)-Epimeloscine and a Formal Synthesis of (±)-1-Acetylaspidoalbidine

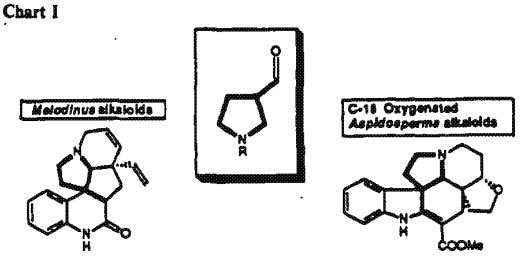
Larry E. Overman,* Graeme M. Robertson, and Albert J. Robichaud

Contribution from the Department of Chemistry, University of California, Irvine, California 92717. *Received June 29, 1990*

Abstract: The first total syntheses of the structurally unusual pentacyclic *Melodinus* alkaloids (±)-meloscine (**1**) and (±)-epimeloscine (**2**) and the hexacyclic *Aspidosperma* alkaloid (±)-deoxoapodine (**4**) are reported. The syntheses proceed via a highly functionalized common tetracyclic intermediate **7**, which is accessed (with complete stereocontrol) by the title rearrangement of pyrindinol **10**. These syntheses provide excellent examples of the power of tandem aza-Cope rearrangement–Mannich cyclization reactions as the key element of stereocontrolled alkaloid synthesis design.

In recent years we have developed a fundamentally new approach to alkaloid synthesis in which the facile [3,3]-sigmatropic rearrangement of iminium cations is combined with an intramolecular Mannich cyclization.[1] In the simplest case, a homoallylic amine with alkoxyl or hydroxyl substitution at the allylic site is allowed to react with an aldehyde or ketone in the presence of an equivalent or less of acid to yield a substituted 3-acylpyrrolidine product (eq 1).[2] If the starting amino alcohol is cyclic, the aza-Cope rearrangement–Mannich cyclization reaction affords a pyrrolidine annulated product in which the initial ring is expanded by one carbon. This latter transformation has been employed to provide a variety of cis fused hydroindoles, cyclopenta[*b*]pyrrolidines, and cyclohepta[*b*]pyrrolidines (eq 2)[3] as well as complex alkaloids of the *Dendrobatid*,[4] *Amaryllidaceae*,[5] and *Aspidosperma*[6] families.

Chart I



(1) Part 21 in the series *Synthesis Applications of Cationic Aza-Cope Rearrangements*. For a brief review, see: Overman, L. E.; Ricca, D. J. In *Comprehensive Organic Synthesis*; Trost, B. M., Fleming, I., Heathcock, C. H., Eds.; Pergamon: Oxford, in press.

(2) See, inter alia: (a) Overman, L. E.; Mendelson, L.; Jacobsen, E. J. *J. Am. Chem. Soc.* **1983**, *105*, 6629. (b) Overman, L. E.; Jacobsen, E. J.; Doedens, R. J. *J. Org. Chem.* **1983**, *48*, 3393. (c) Overman, L. E.; Okazaki, M. E.; Jacobsen, E. J. *J. Org. Chem.* **1985**, *50*, 2403.

(3) Overman, L. E.; Kakimoto, M.-a.; Okazaki, M. E.; Meier, G. *J. Am. Chem. Soc.* **1983**, *105*, 6622. Overman, L. E.; Kakimoto, M.-a. *J. Am. Chem. Soc.* **1979**, *101*, 1310.

(4) Overman, L. E.; Fukaya, C. *J. Am. Chem. Soc.* **1980**, *102*, 1454.

(5) Overman, L. E.; Sugai, S. *Helv. Chim. Acta* **1985**, *68*, 745.

0002-7863/91/1513-2598$02.50/0 © 1991 American Chemical Society

UM00013272
NOVARTIS EXHIBIT 1517
Novartis v. Regents, IPR2023-01347
Page 2018 of 4460

is a decided falloff in $\bar{M}_n$ at 350–450 °C.[21] The soot spectra reported here thus represent the volatile components (tar) present in the soot.

The spectrum for the soot from a diesel engine (Figure 3b) shows the presence of the unburnt fuel (m/z 150–250 range) superimposed on a broader envelope of peaks at every mass up to about 600 amu. Apparently, this soot was formed under the conditions that do not defunctionalize the original hydrocarbon structures completely. In the case of the soot from the detonation of RDX–TNT composite (Figure 3c), we can find substantial intensity of peaks at odd masses corresponding to nitrogen-containing compounds. Two series of prominent peaks are evident in this spectrum: (i) due to benzonitrile (m/z 103) and its benzologues at m/z 153 and 203 and (ii) due to naphthalene (m/z 128) and its benzologues at m/z 178 (phenanthrene) and 228. Weaker peaks due to alkylated homologues (e.g. at m/z 117 due to methylbenzonitrile) are present. In preliminary work, we have also examined soots from combustion of polymers such as polyurethane, polystyrene, and polyoxazoline. These soots give spectra with features characterized by oligomeric species but, again, no peaks corresponding to fullerenes were observed.

In summary, the lack of peaks due to C_{60} and C_{70} in the FI mass spectra of most of the common soots is in concert with the conclusion of Frenklach and Ebert[20b] that pyrolysis and combustion of organic materials does not generally lead to soots with fullerene structures.

Acknowledgment. We are grateful to Dr. L. Ebert for encouraging us to examine this question. We thank Dr. P. R. Solomon for the sample of the butane pyrolysis soot and Dr. R. Greiner for the soot from RDX–TNT detonation. This work was supported by SRI's IR&D Fund.

(21) Ross, D. S.; Hirschon, A. *Am. Chem. Soc., Div. Fuel Chem., Prepr. Pap.* **1990**, *35*, 37–45.

FEATURE ARTICLE

Hydrogen Bonds as Design Elements in Organic Chemistry

Margaret C. Etter

Department of Chemistry, University of Minnesota, Minneapolis, Minnesota 55455 *(Received: October 2, 1990; In Final Form: December 26, 1990)*

This work involves the use of crystal chemistry and crystallographic data base analyses as a way to study hydrogen-bond directed molecular recognition properties of organic molecules. By using the solid phase rather than solution, our studies are not limited to tightly bound dimeric species but encompass aggregate structures with multiple molecules, intricate interlinked patterns, and both strong and weak (often *very* weak) intermolecular interactions. The point of view taken here is to analyze the consequences of directed and selective hydrogen-bond interactions on sets of molecules rather than focusing on the energy or geometry of individual hydrogen-bond interactions. The "consequences" are to a solid-state chemist what a new synthesis is to a solution chemist, i.e., the formation of new chemical species. Methods for deriving hydrogen-bond rules from large sets of crystal structures are presented here. Ways to prepare organic cocrystals and to use cocrystallization to probe the forces involved in aggregation phenomena are discussed, and examples are given of how molecular aggregation can impart unexpected new properties to organic compounds.

Covalent bonds are the primary design elements in organic molecules. They are stable enough to be detected and directional enough to have predictable structural consequences and occur frequently enough to be of practical interest. Hydrogen bonds play a similar role in organic materials, yet they have escaped attempts at systematization of this role; hence, their use as a tool for carrying out "intermolecular syntheses" has been nearly neglected.[1] The products of these intermolecular syntheses are hydrogen-bonded molecular aggregates, defined by connectivity patterns arising from hydrogen bonds. These aggregates could form in solution, at interfaces, or in the solid state.

Recently, considerable effort has been devoted to the study of molecular association in solution, especially for cases where the aggregate pattern that is formed involves only two species (usually called a host and a guest), where association or binding constants are very high (10^4 M^{-1} or greater) and where the aggregates are stabilized primarily by topological features such as preorganized cavities.[2] Such systems are important as small molecule models of enzyme activity. Our work addresses the general class of molecular aggregates, including species with weak association constants as well as species with multiple molecules per aggregate structure. Such species are extremely difficult to study in solution, but they are as easy to study in the solid state as are dimers with high solution binding constants. Our work has focused on the role of hydrogen bonds in the absence of preorganized cavities specifically so we could evaluate the independent contributions (such as selectivity or topology) of hydrogen-bonding groups to the structures of aggregates.

(1) A few notable exceptions include: (a) Ducharme, Y.; Wuest, J. D. *J. Org. Chem.* **1988**, *53*, 5789–5791. (b) Weber, E.; Hecker, M.; Csöregh, I. *J. Am. Chem. Soc.* **1989**, *111*, 7866–7872. (c) Hart, H.; Lin, L.-T. W.; Ward, D. L. *J. Am. Chem. Soc.* **1984**, *106*, 4043–4045. (d) Zerkowski, J. A.; Seto, C. T.; Wierda, D. A.; Whitesides, G. M. *J. Am. Chem. Soc.* **1990**, *112*, 9025–9026.

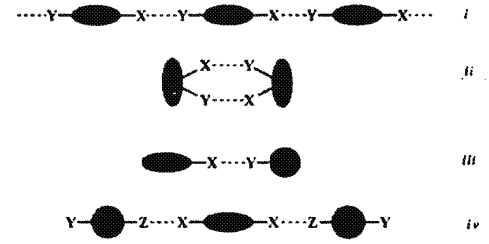
(2) (a) Rebek, J., Jr. *Angew. Chem.* **1990**, *102*, 261. (b) Blake, J. F.; Jorgensen, W. L. *J. Am. Chem. Soc.* **1990**, *112*, 7278–7286. (c) Diederich, F. *Angew. Chem., Int. Ed. Engl.* **1988**, *27*, 362–386. (d) Friedrichsen, B. P.; Powell, D. R.; Whitlock, H. W. *J. Am. Chem. Soc.* **1990**, *112*, 8931–8941. (e) Hamilton, A. D.; Pant, N.; Muehldorf, A. *Pure Appl. Chem.* **1988**, *60*, 533–538. (f) Zimmerman, S. C.; Wu, W. *J. Am. Chem. Soc.* **1989**, *111*, 8054–8055. (g) Kelly, T. R.; Maguire, M. P. *J. Am. Chem. Soc.* **1987**, *109*, 6549–6551. (h) Bell, T. W.; Liu, J. *J. Am. Chem. Soc.* **1988**, *110*, 3673–3674.

0022-3654/91/2095-4601$02.50/0 © 1991 American Chemical Society

UM00013273
NOVARTIS EXHIBIT 1517
Novartis v. Regents, IPR2023-01347
Page 2019 of 4460

We have also shown that hydrogen-bonded molecular aggregates can have unexpected properties as a result of the collective behavior of these weakly bound molecules. The chemical and physical properties of collective sets of small molecules acting in concert at the surface of or within membranes or near active sites on proteins or on DNA have not been addressed, in part because there have not been tools for either asking or answering these questions effectively. Our crystal chemical approach to such questions offers a way to study such problems and provides information about the role of particular intermolecular effects that occur in weakly bound aggregates as well as in tightly bound host–guest complexes.

The strategy of the present work is to focus on the organizational consequences of hydrogen bonds in organic crystals, where the structures of molecular aggregates can be characterized readily. Ideal systems will be sets of neutral molecules with sterically accessible hydrogen-bonding groups where the hydrogen-bond interactions are perturbed minimally by competing steric or ionic interactions. Such systems are represented schematically in i–iv,



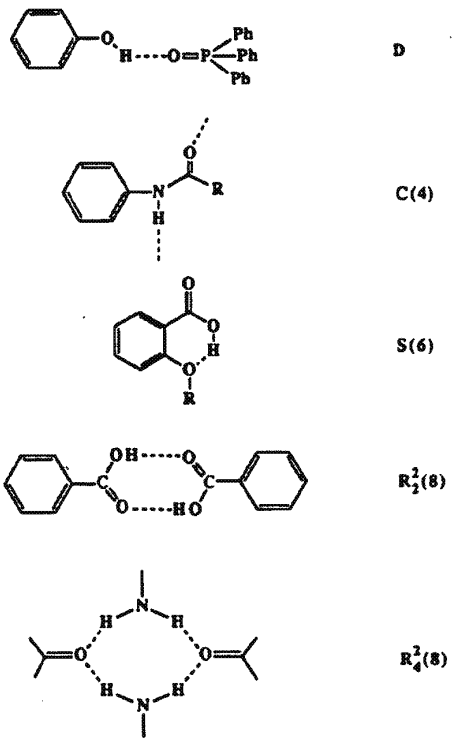
showing -X···Y- as a hydrogen-bond interaction and different types of molecular aggregate patterns arising from different numbers and orientations of substituents. Note that iii and iv represent cocrystal patterns.

From a series of structures that have competitive hydrogen-bonding functional groups, as for iv, where Z is a better hydrogen-bond acceptor than Y, selectivity properties of individual functional groups can be determined, and correlations between hydrogen-bond types and aggregate patterns can be made. Competition between hydrogen bonds and other intermolecular interactions can be systematically introduced and evaluated once the intrinsic organizational properties of the hydrogen-bonding functional groups are established.

Our approach to systematizing the use of hydrogen bonds is to analyze crystallographic information from small molecule crystal structures, available through the Cambridge Structural Database (CSD),[3] to determine if there are hydrogen-bond preferences for individual functional groups (preferences in terms of selectivity and preferences in terms of the patterns of molecular aggregates generated by these hydrogen bonds) and then to design organic crystals and cocrystals based on these hydrogen-bond preferences. We have found that cocrystal formation involving hydrogen-bonded host and guest molecules is a remarkably versatile tool for testing hydrogen-bond selectivity. Most of the cocrystals can be prepared either by crystallization from a solvent containing the two reagents or by grinding the two components together in the solid state. Usually the same crystal structures are obtained from the two different methods, indicating that hydrogen-bond connectivity patterns are not idiosyncratic or determined by nonspecific and unmanageable solvent effects or crystallization conditions. These effects are similar to those of solvent, concentration, or temperature in an intramolecular synthesis. They may dictate whether a particular experiment works, but the variability they introduce does not usually preclude the development of useful synthetic methods.

Methods for characterizing hydrogen-bond patterns of small organic molecules, for developing hydrogen-bond rules, and for determining hydrogen-bond selectivity preferences of common functional groups will be presented here. Since the solid-state cocrystallization technique is not generally known and since it provides a remarkably easy way to modify the solid-state properties of an organic compound, a short descriptive section about solid-state cocrystallization is included. Diarylureas and their crystal and cocrystal patterns are discussed as examples of how to use the principles developed here to study molecular recognition properties.

CHART I



Hydrogen-Bond Pattern Recognition in Molecular Aggregates

Hydrogen-bond patterns frequently involve many types of hydrogen bonds with multiple intertwined hydrogen-bond networks. Comparing two or more such patterns, which might even be composed of different kinds of molecules, is a formidable pattern-recognition problem that is usually done, if at all, by visual inspection of stereoviews of crystallographic unit cells. There has been no consistency in what features of the patterns are reported or even detected. Comparing the hydrogen-bond patterns of thousands or possibly tens of thousands of structures from the CSD by visual inspection is a completely unrealistic undertaking. As a step toward simplifying the problem and structuring it so it will be amenable to automatic search methods, a topological decoding scheme is presented that facilitates comparison of hydrogen-bond patterns. This method involves decomposing hydrogen-bond networks into graph sets which are based on the number of proton donors (subscripts) and acceptors (superscripts) used in the motif, on whether the hydrogen bonds are intra- (S) or intermolecular, and in the latter case on whether the intermolecular motifs are finite (R or D) or infinite (C). The size or degree of a pattern, based on the number of atoms in a hydrogen-bonded ring, for example, is shown in parentheses following the graph set descriptor. The details of this procedure have been published elsewhere;[4] examples are given in Chart I.

The process for assigning patterns is illustrated in the *p*-nitroaniline figure, Figure 1a, where three motifs from the crystal structure are highlighted. Patterns A and B contain hydrogen-

(3) Allen, F. H.; Bellard, S.; Brice, M. D.; Cartwright, B. A.; Doubleday, A.; Higgs, H.; Hummelink, T.; Hummelink-Peters, B. G.; Kennard, O.; Motherwell, W. D. S.; Rodgers, J. R.; Watson, D. G. *Acta Crystallogr., Sect. B: Struct. Sci.* **1979**, *B35*, 2331–2339.

UM00013274
NOVARTIS EXHIBIT 1517
Novartis v. Regents, IPR2023-01347
Page 2020 of 4460

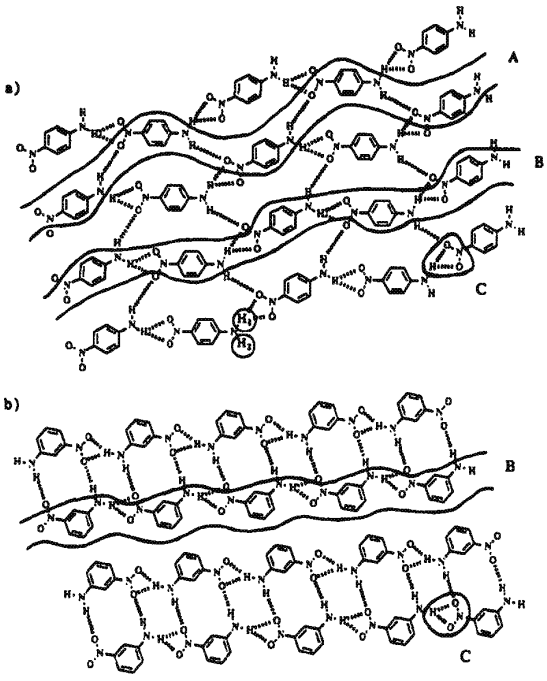


Figure 1. Hydrogen-bond patterns for (a) *p*-nitroaniline and (b) *m*-nitroaniline. It is evident that patterns B and C are present in both structures.

bonded aggregates made from interactions between either H_1 or H_2 and a single nitro oxygen. Similarities between these aggregate structures and those of *m*-nitroaniline, Figure 1b, are immediately evident.

The presence of aggregate patterns can also be used, like bond-length or wavelength criteria, as an indicator of, not proof of, hydrogen bonds. When all the structures in a series show the same molecular aggregate patterns, i.e., when their graph sets are the same, then the whole set of structures is classified as hydrogen-bonded. When this procedure was used to study nitroaniline compounds it was found that subsets of the *p*-nitroaniline pattern, in particular, pattern C, had the same graph set as those found in 21 of the 28 structures investigated[5] (six of the seven that differed had competing intramolecular hydrogen bonds). These patterns were present even though they had very long –NH---O distances (N---O = 3.250 Å; the sum of the van der Waal's radii is 3.20 or 3.14 Å depending on the reference source used: N = 1.70 and O = 1.50 Å[6] or 1.60 and 1.54 Å[7]). The $-N(H)\cdots O_2N$ bond lengths for the other compounds had a reasonably uniform distribution from 2.93 to 3.22 Å. There is no reason based on crystallographic evidence to categorize the slightly longer contacts as being qualitatively different kinds of interactions from the shorter contacts. Their organizational properties are topologically like those of shorter hydrogen bonds. It is these topological similarities that are within the purview of crystallography and that are the basis for designing "intermolecular syntheses".

The graph set method does provide a way to evaluate how molecular aggregate patterns differ as a function of artificially imposed hydrogen-bond cutoff lengths, or included angles, or other measurable parameters. In other words, it can be used to test the consequences of having different definitions of hydrogen bonds. If van der Waals cutoff distances alone had been used as the defining criteria in the nitroaniline study, then similarities between

Polymorph	Motifs	Networks
1	$C(5)R_3^3(10)C(8)$	$R_4^4(14)$
2	$C(5)R_2^2(10)C(8)$	$R_4^4(8)$
3	C(5)C(5)C(8)	

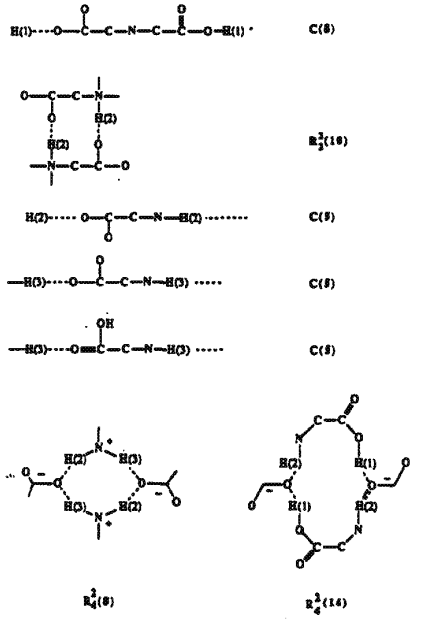


Figure 2. Graph set assignments for three polymorphs of iminodiacetic acid showing that polymorph 3 differs from 1 and 2 in the presence of a second C(5) motif, whereas 1 and 2 are differentiated only when combinations of different kinds of hydrogen bonds are considered. Their networks consist of rings of different sizes.[8] In the crystal structure, some of the amino and carboxyl groups are charged, whereas others are neutral, as indicated.

the aggregate patterns of *m*- and *p*-nitroaniline would have been lost.

The nitroaniline analysis presented above dealt only with motifs, since the hydrogen-bond patterns contained just one type of hydrogen bond. *Networks* containing all the combinatorial possibilities of hydrogen bonds formed from two different kinds of hydrogen bonds, or from three different kinds, etc., can also be assigned sequentially. In this manner, complex hydrogen-bond patterns can be described explicitly and pattern similarities become readily recognized as common motifs or combinations of motifs. For example, IMDA, $^-O_2CCH_2NH_2{}^+CH_2CO_2H$, has three different hydrogen-bond donors in the molecule and it exists in three polymorphic forms.[8] It is a straightforward process to compare the hydrogen-bond patterns of these polymorphs by using graph sets, as shown in Figure 2.[9] Two of the polymorphs (1 and 2) have identical sets of motifs, $C(5)R_2^2(10)C(8)$, indicating that the connectivity patterns generated by each individual hydrogen donor by itself, independent of any other donor in the system, are the same in these structures. In the third polymorph two of the connectivity patterns match those of 1 and 2 but the third motif is a chain instead of a ring (C(5) instead of $R_2^2(10)$). Polymorphs 1 and 2 are differentiable when the hydrogen-bond patterns that contain two different kinds of hydrogen bonds simultaneously are considered. Polymorph 1 has a 14-membered ring with two donors

(4) Etter, M. C.; MacDonald, J. C.; Bernstein, J. *Acta Crystallogr., Sect. B: Struct. Sci.* **1990**, *B46*, 256–262.
(5) Panunto, T. W.; Urbańczyk-Lipkowska, Z.; Johnson, R.; Etter, M. C. *J. Am. Chem. Soc.* **1987**, *109*, 7786–7797.
(6) Bondi, A. *J. Phys. Chem.* **1964**, *68*, 441–451.
(7) Nyburg, S. C.; Faerman, C. H. *Acta Crystallogr., Sect. B: Struct. Sci.* **1985**, *B41*, 274–279.
(8) Bernstein, J. *Acta Crystallogr., Sect. B: Struct. Sci.* **1979**, *B35*, 360–366.

UM00013275
NOVARTIS EXHIBIT 1517
Novartis v. Regents, IPR2023-01347
Page 2021 of 4460

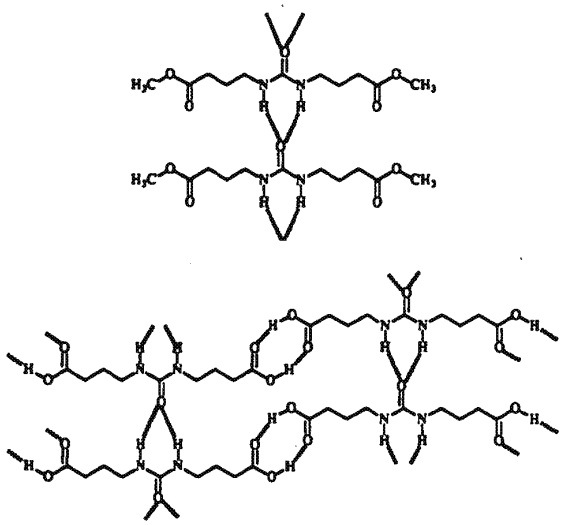


Figure 3. Hydrogen-bond pattern of a disubstituted urea retained even in the presence of a second hydrogen-bonding functional group.[13] These structures illustrate that hydrogen-bond patterns are functional-group dependent and can be used for designing new materials containing their preferred motifs.

and two acceptors per ring, while polymorph 2 has an eight-membered ring with four donors and two acceptors per ring.

Hydrogen-Bond Rules

The use of graph sets as a tool for analyzing hydrogen-bond patterns of large numbers of structures allows one to determine graph set distributions corresponding to a class of molecules containing one particular functional group, and conversely functional group distributions corresponding to all structures with a particular graph set. Hydrogen-bond rules reflect these relationships and provide useful information about preferred connectivity patterns, hydrogen-bond selectivity, and stereoelectronic properties of hydrogen bonds for a particular functional group or for sets of functional groups. There are three very useful rules of thumb that apply to organic hydrogen-bonded structures. The first rule was developed by Donohue during the early days of crystallography when there was only a handful of organic crystal structures known. He observed that *all acidic hydrogens available in a molecule will be used in hydrogen bonding in the crystal structure of that compound.*[10] This is still the most useful of all the hydrogen-bond rules. A second rule, complementary to the first one, is that *all good acceptors will be used in hydrogen bonding when there are available hydrogen-bond donors.*[11] This rule is not followed as rigorously as the first one, but it is a useful corollary nonetheless. The third rule, frequently observed in our work on cocrystal design, is that *the best hydrogen-bond donor and the best hydrogen-bond acceptor will preferentially form hydrogen bonds to one another.*[12]

These rules reflect energetically favorable kinds of intermolecular association. What is not intuitively obvious is that crystal packing patterns also reflect these simple rules so frequently. A lovely example of this effect is seen in the urylene and substituted urylene structures studied by Fowler et al. (Figure 3).[13] The urea portions of the molecules have a bidentate chain pattern whether or not the carboxylic acid substituents are present. Conversely, the typical carboxylic acid dimer pairs which are found in most acid structures are preserved in the acid-substituted urylenes. In this example, each functional group retains its preferred hydrogen-bond pattern in the presence of the other functional group

(9) Bernstein, J.; Etter, M. C.; MacDonald, J. C. *J. Chem. Soc., Perkin Trans. 2* **1990**, 695–698.
(10) Donohue, J. *J. Phys. Chem.* **1952**, *56*, 502–510.
(11) Etter, M. C. *J. Am. Chem. Soc.* **1982**, *104*, 1095–1096.
(12) Etter, M. C. *Acc. Chem. Res.* **1990**, *23*, 120–126.

TABLE I: Hydrogen-Bond Rules

General Rules

(1) all good proton donors and acceptors are used in hydrogen bonding
(2) if six-membered ring intramolecular hydrogen bonds can form, they will usually do so in preference to forming intermolecular hydrogen bonds
(3) the best proton donors and acceptors remaining after intramolecular hydrogen-bond formation form intermolecular hydrogen bonds to one another

Additional Rules for Nitroanilines

(4) amino protons will hydrogen bond to nitro groups, if no better proton acceptors are present
(5) one or more intermolecular amino-nitro hydrogen bonds will form
(6) the aggregate patterns formed from intermolecular hydrogen bonds between substituents in meta and para positions will be acentric
(7) the amino–nitro interaction is usually a three-center hydrogen bond, $R_1^2(4)$

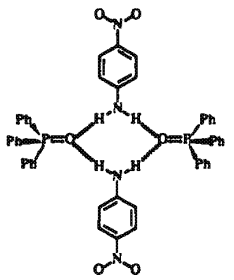


(8) ortho-substituted primary nitroanilines usually form two-center intermolecular hydrogen bonds with graph set $R_2^2(6)$ rather than three center



and in a variety of different packing patterns and space groups.

Expected or typical hydrogen-bond patterns may not occur for a variety of reasons, including the presence of multiple competitive hydrogen-bond sites, steric overcrowding, or competing dipolar and ionic forces. Part of the purpose of our work is to evaluate how hydrogen-bond patterns adjust to the presence of such perturbations. An extreme example would be the introduction of a hydrogen-bonding guest molecule that competes with and displaces intermolecular hydrogen bonds between host molecules to give a cocrystal. This approach was used to design nitroaniline cocrystals. Hydrogen-bond rules for homomeric nitroanilines were determined from data obtained using the Cambridge Data Base (Table I). Molecules that are better acceptors than the nitro group, such as triphenylphosphine oxide, were introduced as guest molecules during crystallization of *p*-nitroaniline to specifically perturb the –NH---O_2N– interaction. A cocrystal with the aniline hydrogens bonding to the phosphine oxide oxygen atom was obtained:[14]



An alternative cocrystal system could be prepared by using hydrogen bonds instead of σ bonds to link the nitro and aniline groups together. For example, a nitro-substituted benzoic acid and an amino-substituted benzoic acid form cocrystals of heteromeric dimers. The acids bond to one another to provide the σ-bond like link, while the nitro and aniline –NH groups remain to link these dimers into polymer chains according to the nitroaniline hydrogen-bond rules. Several examples of these structures are given in Table II.

Nitroanilines are of interest as organic nonlinear optical materials since they are polarizable and since the electron-donating

(13) Zhao, X.; Chang, Y.-L.; Fowler, F. W.; Lauher, J. W. *J. Am. Chem. Soc.* **1990**, *112*, 6627–6634.

UM00013276
NOVARTIS EXHIBIT 1517
Novartis v. Regents, IPR2023-01347
Page 2022 of 4460

TABLE II: Cocrystals of Nitroaniline Analogues



no.	O_2N—◯—A[a]	HD—◯—NRH	SG[b]	ref
1	4-nitropyridine *N*-oxide	4-aminophenol	*Cc*	47
2	4-nitropyridine *N*-oxide	4-aminobenzoic acid	$P2_12_12_1$	48
3	4-aminobenzoic acid	3,5-dinitrobenzoic acid	*Fdd*2	19
4	4-aminobenzoic acid	4-chloro-3,5-dinitro-benzoic acid	–	49
5	4-aminobenzoic acid	3,5-dinitrosalicylic acid	–	49
6	4-aminobenzoic acid	4-methyl-3,5-dinitro-benzoic acid	–	49
7	4-aminobenzamide	3,5-dinitrobenzoic acid	$P2_1/c$	49
8	4-aminobenzamide	3,5-dinitrobenzoic acid	$P2_1/c$	49
9	3,5-dinitrobenzamide	4-aminobenzoic acid	–	49
10	4-aminobenzamide	3,5-dinitrobenzamide	–	49

[a] A is a hydrogen-bond acceptor and –DH is a hydrogen-bond donor. [b] The space group is given for those systems where single crystals were obtained. A dash in this column indicates that cocrystal phases were obtained and were characterized by noncrystallographic means.

and -accepting properties of the –NH and $-NO_2$ groups contribute to large molecular hyperpolarizabilities.[15] Two of the early entries into the field of organic NLO compounds were *m*-nitroaniline and 2-methyl-*p*-nitroaniline.[16] Many related compounds have been prepared since then, and questions about the role of hydrogen bonds in producing good NLO materials have been addressed.[17] One of the necessary conditions for second-order nonlinear optical properties is that the bulk material have no center of symmetry. This property is very hard to control, especially since more than 74% of all organic crystals crystallize in centric space groups. Since nitroanilines were found to form chain structures, it is obvious that each nitroaniline aggregate is acentric. Neighboring molecules in a hydrogen-bonded chain must align so their dipole moments are head-to-tail, unlike dipolar stabilized aggregates where the dipole moments can be arranged in a centric manner. Despite the common occurrence of non-hydrogen-bonding dipolar groups in organic molecules, close-packing of bulky irregularly shaped organic molecules is usually a more important directing force than dipolar stabilization.[18] In hydrogen-bonded structures, however, sets of related structures frequently have the same hydrogen-bond patterns regardless of steric irregularities. Their structures look as if the hydrogen bonds had formed first and then were retained during crystallization:



H-Bond Stabilization

(acentric)

Thus, nitroanilines can become acentric by way of hydrogen-bond directed association. In an effort to capitalize on this self-organization principle, we sought to design an acentric two-dimensional aggregate using the cocrystal design ideas presented above. Acentric heteromeric 2-D networks were formed by using multiple nitro groups and –NH donors in appropriate orientations. The nitroaniline cocrystal shown in Figure 4 is such an example. The best donor in the structure is the acid hydrogen of 3,5-dinitrobenzoic acid, and the best acceptor is the carbonyl group of 4-aminobenzoic acid. Interactions between these groups promote heterodimer formation. The remaining nitro and amino groups form hydrogen bonds to one another to generate the acentric array. In this particular case the final bulk structure was also found to

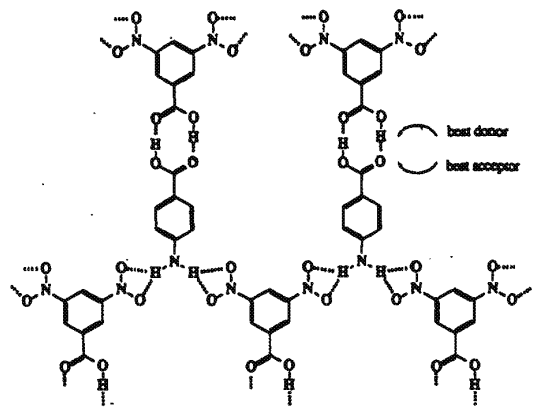


Figure 4. Polar hydrogen-bonded cocrystal composed of carboxylic acid heterodimers linked into a polar array by nitroaniline hydrogen bonds.[19] The nitro and aniline groups have the same kinds of hydrogen-bond patterns as those found in homomeric nitroanilines.[5]

be acentric, although the nature of the interplanar interactions is not clear.[19]

In the simplest hydrogen-bonded crystals, composed of small molecules with a limited number of hydrogen-bonding groups and no other strong intermolecular interactions, stereoelectronic preferences may be critical in determining the packing mode and even the chemical and physical properties of a system. The 1,3-cyclohexanedione system is well suited to such a study since it has only one proton donor and one good proton acceptor. Four stereochemically unique modes of association arise from two different planar conformations of the –OH group, and the choice of syn vs anti lone pairs of electrons as their acceptor sites (Figure 5). Structure A has been observed for dimedone (5,5-dimethyl-1,3-cyclohexanedione),[20] structure B for 1,3-cyclohexanedione (CHD),[21] and structure C (with a molecule of benzene trapped in the cyclamer cavity) for both 1,3-cyclohexanedione and 5-methyl-1,3-cyclohexanedione.[22] The cyclamer structures are like crown ethers with hydrogen-bonded rather than σ-bonded backbones. When crystallized from solutions of mixed benzene and toluene, 1,3-cyclohexanedione has the ability to selectively trap molecules of benzene in the cyclamer cavities. Solutions of as little as 30% benzene yielded crystals of the cyclamer containing only benzene (structure C), though solutions with less than that gave only crystals of the unsolvated structure B. The ability of CHD to separate benzene from toluene was completely unexpected and unpredictable since the monomer has no apparent complexing ability, though this property is reasonable in light of its crystal structures. Even vapor-phase osmometry indicates that the preferred aggregate form in benzene solution is the same as that in toluene and is a dimer rather than a cyclic hexamer (~20% dimer, 72% monomer, in benzene, 39 °C, 0.025 M). Besides the observation that sets of associated molecules can adopt the properties of macromolecules, these crystals illustrate that stereoelectronic ordering can direct molecular self-assembly.

Solid-State Preparation of Cocrystals

The cocrystals discussed above can be made by evaporating solutions containing stoichiometric mole ratios of the components. We have found that almost all of them can also be prepared *simply by grinding the two solid reagents together*. Depending on the rate and vigor of grinding, particle size, and vapor pressures of the reagents, a complete conversion to the new hydrogen-bonded

(14) Etter, M. C.; Huang, K.-S. *New Materials for Nonlinear Optics*; ACS Symposium Series, in press.
(15) Williams, D. J. *Angew. Chem., Int. Ed. Engl.* **1984**, *23*, 690–703.
(16) (a) (i) Shapski, A. C.; Stevenson, J. L. *J. Chem. Soc., Perkin Trans. 2* **1973**, 1197–1200. (ii) Ploug-Sorensen, G.; Andersen, E. K. *Acta Crystallogr., Sect. C: Cryst. Struct. Commun.* **1986**, *C42*, 1813–1815. (b) Lipscomb, G. F.; Garito, A. F.; Narang, R. S. *J. Chem. Phys.* **1981**, *75*, 1509–1526.
(17) Zyss, J.; Nicoud, J. F.; Coquillay, M. *J. Chem. Phys.* **1984**, *81*, 4160–4167. (b) Zyss, J.; Berthier, G. *J. Chem. Phys.* **1982**, *77*, 3635–3653.
(18) (a) Whitesell, J. K.; Davis, R. E.; Saunders, L. L.; Wilson, R. J.; Feagins, J. P. *J. Am. Chem. Soc.*, in press. (b) Gavezzotti, A. *J. Phys. Chem.* **1990**, *94*, 4319–4325.
(19) Etter, M. C.; Frankenbach, G. M. *Chem. Mater.* **1989**, *1*, 10.
(20) (a) Semmingsen, D. *Acta Chem. Scan.* **1974**, *B28*, 169–174. (b) Singh, I.; Calvo, C. *Can. J. Chem.* **1975**, *53*, 1046–1050.
(21) Etter, M. C.; Urbańczyk-Lipkowska, Z.; Jahn, D. A.; Frye, J. S. *J. Am. Chem. Soc.* **1986**, *108*, 5871–5876.

UM00013277
NOVARTIS EXHIBIT 1517
Novartis v. Regents, IPR2023-01347
Page 2023 of 4460

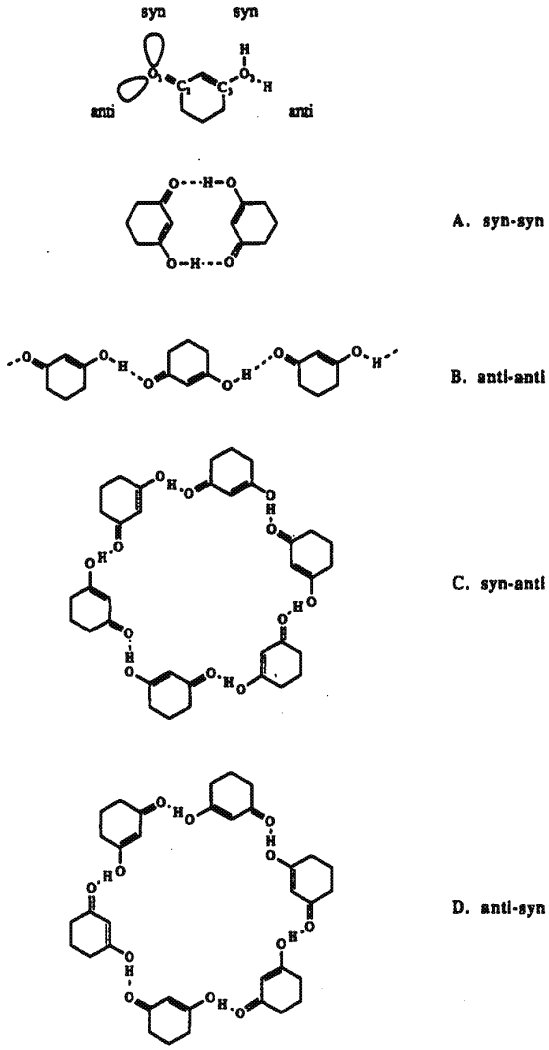


Figure 5. Four stereoelectronically different hydrogen-bond patterns of 1,3-cyclohexanedione are shown. Structures A–C have been found for differently substituted cyclohexanedione structures.[20-22] Crown-ether-like type C structures occur with molecules of benzene included in their cavities.

cocrystal phase can be accomplished in the solid state. More often than not, the phase that is obtained is identical with that obtained from solution crystal growth, implying that *solvent is not necessary* to direct molecules with strong directional intermolecular interactions into their preferred crystal form. Solvation and desolvation mechanisms certainly are important in controlling rates of formation and stabilities of aggregates in solution, and they can determine as well which of the several polymorphs is preferred. Solvent also promotes mobility, so different species can diffuse together more readily to initiate and propagate crystal nucleation. To our surprise, however, diffusion of small molecules through solids can take place rapidly at room temperature and at temperatures well below the melting point of either component or of their eutectics. Elevated temperatures promote these reactions, as does continuous grinding to free clean surfaces for reaction. The details of these mechanisms are not understood, although there are precedents for solid-state cocrystallization.[23] The one consistent feature in the solid-state cocrystallization we have carried out is that cocrystallizations are most likely to be successful when the two components form stronger hydrogen bonds to one another than to themselves.

(22) Etter, M. C.; Parker, D. L.; Ruberu, S. R.; Panunto, T. W.; Britton, D. *J. Inclusion Phenom. Mol. Recognit. Chem.* **1990**, *8*, 395–407.

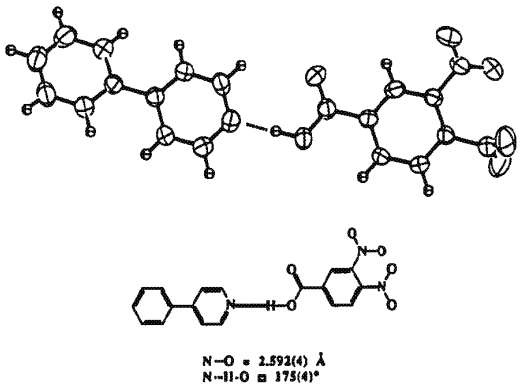
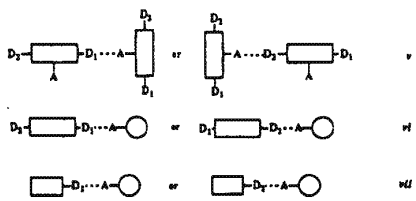


Figure 6. ORTEP pattern showing the strongly hydrogen-bonded pyridine---acid dimer found in cocrystals formed selectively in the presence of a second weaker acid, *p*-(dimethylamino)benzoic acid.

Hydrogen-Bond Selectivity

Determining relative hydrogen-bonding abilities of organic functional groups has been a subject of intensive research for decades. Most of these studies have been based on measurements of solution association constants under equilibrium conditions[24] or microwave studies of molecules with competitive intramolecular hydrogen bonds.[25] While it is difficult to model or measure the detailed thermodynamic and kinetic contributions to formation of a particular crystal structure, one can determine whether or not functional groups show consistent selectivity patterns in the solid state and can compare observed solid-state selectivities to solution and gas-phase selectivities. The degree to which the solid-state patterns match solution patterns is indicative of the degree to which equilibrium hydrogen-bond strengths determine association patterns in the solid state and in ordered media.

Our methods for ranking solid-state hydrogen-bond preferences are based on functional group competitions in homomeric crystals or heteromeric cocrystals. The procedure involves analyzing which donors are selected by a limited number of acceptors or vice versa during crystallization. Three general schemes are shown in v–vii,



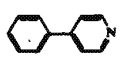
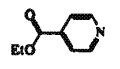
where $-D_i$ are hydrogen-bond donors and $-A$ is a hydrogen-bond acceptor. The choices that the donor group has for bonding to an acceptor in each different type of experiment are indicated. Scheme v is a crystallization of a homomeric system where there are two donors and only one acceptor on each molecule. Scheme vi is a cocrystallization containing two components, a molecule with two different donors, and a second molecule with one acceptor. Scheme vii is also a cocrystallization. This experiment

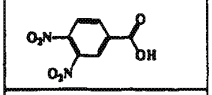
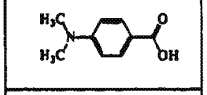
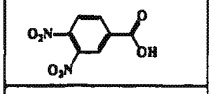
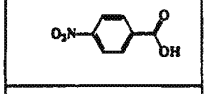
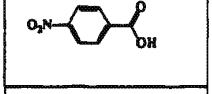
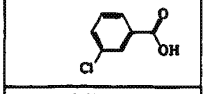
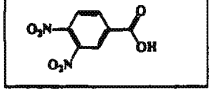
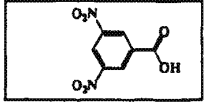
(23) (a) Rastogi, R. P.; Bassi, P. S.; Chadha, S. L. *J. Phys. Chem.* **1963**, *67*, 2569–2573. (b) Rastogi, R. P.; Singh, N. B. *J. Phys. Chem.* **1966**, *70*, 3315–3324. (c) Rastogi, R. P.; Singh, N. B. *J. Phys. Chem.* **1968**, *72*, 4446–4449. (d) (i) Patil, A. O.; Pennington, W. T.; Desiraju, G. R.; Curtin, D. Y.; Paul, I. C. *Mol. Cryst. Liq. Cryst.* **1986**, *134*, 279–304. (ii) Patil, A. O.; Curtin, D. Y.; Paul, I. C. *J. Am. Chem. Soc.* **1984**, *106*, 348–353.

(24) Abraham, M. H.; Duce, P. P.; Prior, D. V.; Barratt, D. G.; Morris, J. J.; Taylor, P. J. *J. Chem. Soc., Perkin Trans. 2* **1989**, 1355–1375.

UM00013278
NOVARTIS EXHIBIT 1517
Novartis v. Regents, IPR2023-01347
Page 2024 of 4460

TABLE III: Selectivity in Cocrystallization of Pyridines with Mixtures of Carboxylic Acids

Pyridines in Cocrystal	
	

Acid in Cocrystal	ΔpKa	Uncomplexed Acid
	2.35	
	0.74	
	0.41	
	0.04	

involves three different molecules, with the acceptor selecting one of two donor molecules during cocrystallization.

An example of the third scheme is the cocrystallization of pyridines with pairs of carboxylic acids. We have found that 4-phenylpyridine and ethyl isonicotinate are both capable of completely separating the acid of lower pK_a value from the one with the higher pK_a by cocrystallization (Table III). Neutral hydrogen-bonded cocrystals form with a single hydrogen bond between the acid –OH group and the nitrogen of the pyridine component (Figure 6).[26]

We were surprised to find that even acids with very similar pK_a values, such as 3,4-dinitro- and 3,5-dinitrobenzoic acids, could still be cleanly separated by this technique. The implications are that the strength of the hydrogen bond in solution, to the extent that pK_a reflects this parameter, has determined which species will nucleate crystal growth. Experiments are underway now to test this hypothesis by detecting and comparing aggregates formed in solution with those observed in the solid state.

Cocrystal selectivity can be used to monitor subtle changes in proton-accepting abilities that arise from intramolecular substituent effects. Carboxylic acids readily cocrystallize with 2-aminopyrimidines (2AP) to form either 2:1 or 1:1 complexes.[27] Interestingly, the preferred pattern is not a function just of the stoichiometries of the starting reagents. Sometimes the 1:1 pattern is preferred even if the solution or solid-state mixture that is used as the starting material is a 2:1 mixture. Phase diagrams of several of these systems have shown that both patterns may be possible for a particular combination of acid and pyrimidine, with one of them being the kinetically favored product. The phase diagram for 2-aminopyrimidine and succinic acid is shown in Figure 7. This phase diagram is unusual since a metastable 2:1 cocrystal phase is evident to the right of the diagram. We have not been able to make a sample of pure 2:1 cocrystal since it is always contaminated with the 1:1 phase. Also the 2:1 phase will revert even in the solid state (with heating and grinding, over a period of days) to give a mixture of the 1:1 phase and excess 2-aminopyrimidine.[27]

(25) (a) Legon, A. C.; Millen, D. J. *Acc. Chem. Res.* **1987**, *20*, 39–46. (b) Wilson, E. B.; Smith, Z. *Acc. Chem. Res.* **1985**, *20*, 257–262.
(26) Etter, M. C.; MacDonald, J. C., unpublished results.
(27) Etter, M. C.; Adamond, D. *J. Chem. Soc., Chem. Commun.* **1990**, *8*, 589–591.

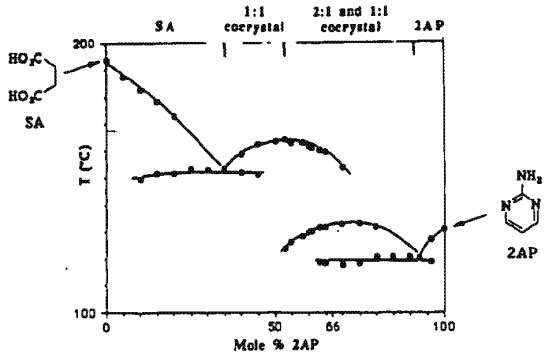
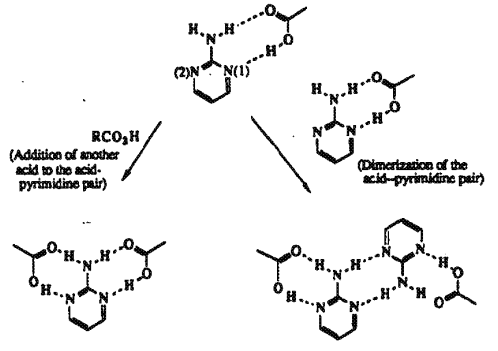


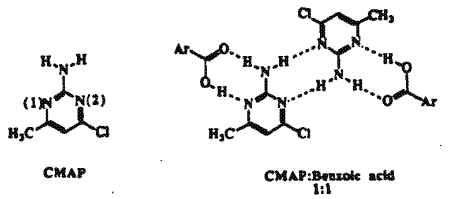
Figure 7. Nonequilibrium phase diagram for 2-aminopyrimidine and succinic acid indicating that the 2:1 cocrystal composition is unstable relative to 1:1. This result is consistent with our observation that solid-state grinding of the two components in concentrations of 50–80% 2AP frequently yields pure 1:1 cocrystals, but 2:1 cocrystals are always contaminated with the 1:1 phase.

In the 1:1 hydrogen-bond pattern, pattern B, the pyrimidine ring nitrogens have become inequivalent. One explanation for



the inequivalence is to consider the crystallization process as a series of steps, each one involving addition of another molecule to a preformed aggregate. The first complexation step might consist of one acid bonding to 2AP, causing the accepting ability of the as-yet unbonded N(2) ring nitrogen to decrease due to conjugative effects. Reduced accepting ability would make this nitrogen a less attractive site for further acid hydrogen bonding, so rather than pick up an additional acid molecule to form pattern A, it associates with another dimer to give pattern B. A-type patterns have been observed for many cocrystals of 2-aminopyrimidine with small difunctional acids like succinic acid.[27]

B-type patterns are more likely to occur for unsymmetrically substituted 2-aminopyrimidines with acids. For example, in 2-amino-4-chloro-6-methylpyrimidine (CMAP), a neighboring



methyl group (an electron-donating group) should increase the electron density on N(1), and the chlorine atom should decrease it on N(2). It is predicted that cocrystallization with a carboxylic acid should proceed by preferentially binding to the N(1) side of the molecule, thus reducing the accepting ability of N(2) even further. The B-type pattern should have the acid groups only at the N(1) sites while the pyrimidine···pyrimidine interactions should occur only on the N(2) side of the molecule. Subsequent

UM00013279
NOVARTIS EXHIBIT 1517
Novartis v. Regents, IPR2023-01347
Page 2025 of 4460

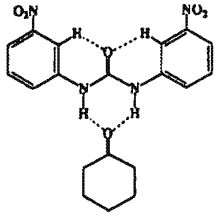
crystallographic analyses of cocrystals of CMAP with benzoic acid and of CMAP with glutaric acid have confirmed these predictions.[28]

While these studies give only relative rankings, not quantitative rankings (e.g., N(1) is a better acceptor than N(2), but it is not known how much better), they are generally consistent with the quantitative rankings that Taft et al. have developed from solution solvatochromic studies.[29] The study of multiple equilibrating aggregate species in solution is an extremely difficult problem since multiply hydrogen-bonded species involving three or more molecules will be present in low concentrations in the presence of the more dominant dimers. Solid-state measurements provide a convenient way to rank the relative hydrogen-bonding abilities of multiply bonded functional groups, allowing a free carbonyl, a once hydrogen-bonded carbonyl, and a twice hydrogen-bonded carbonyl, for example, to be ranked independently.

Diarylureas as a Model System for the Study of Hydrogen-Bond Directed Host–Guest Complexation

Bis(*m*-nitrophenyl)urea (BmNU) is a host molecule that adapts its conformation and its hydrogen-bonding properties to the presence of proton-accepting guest molecules. Guests usually bind to both –NH protons of the urea. Unlike crown ethers, or specially designed rigid acceptor molecules,[30] there is no preorganized pocket in BmNU for trapping acceptors and promoting strong binding interactions. Our interest is not in optimizing binding constants but rather in determining how selective the binding process can be even when there are no preorganized binding sites. There are two features of this chemistry that are noteworthy. One is that BmNU, unlike virtually all other known neutral proton donor molecules, behaves primarily as a proton donor, a property that is even more remarkable given the presence of a strong accepting group (the urea carbonyl) in the molecule.[31] Also, other closely related analogues of BmNU show very limited or no complexation ability. Both of these features appear to arise from an unusual weak intramolecular property of the host, which was evident only by inspection of a large number of crystal structures and by the use of selective cocrystallization studies.

When BmNU is cocrystallized with small molecules containing strong acceptors such as phosphoryl or sulfoxide groups or with molecules that are much weaker acceptors such as ketones, ethers, and nitro compounds, it forms 1:1 cocrystals with the following typical hydrogen-bond pattern:



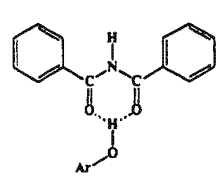
BmNU : Cyclohexanone

The common features of these cocrystals are that the urea carbonyl is not hydrogen bonded by any intermolecular hydrogen bonds, both –NH protons are used in hydrogen bonding, the conformation of the molecule places the m-nitro groups syn to the carbonyl group, and the torsion angles of the phenyl rings relative to the urea groups are close to zero. If the nitro groups are replaced with –H, $-CH_3$, $-OCH_3$, or if the nitro groups are moved to the para positions, the derivatives are no longer good complexing agents. It is difficult to form cocrystals with these compounds at all, and the only cocrystals that have been isolated are for the $-CH_3$ and p-NO_2 derivatives with the strongest acceptor guest, triphenylphosphine oxide. In most instances these urea hosts separate as pure phases during cocrystallization attempts.

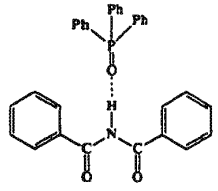
The clue to the special complexation properties of BmNU appears to be that the ability of the urea carbonyl group to form intermolecular hydrogen bonds has been reduced to nearly zero by the presence of the m-nitro groups.[32] The origin of this effect is not clear, but the consistent planarity of the urea molecule in its cocrystals compared to the nonplanar structure of BmNU and other diaryl ureas in their homomeric crystals and the fact that nitro groups are good electron-withdrawing groups suggest that there may be special stabilizing interactions between the aromatic ring hydrogen atoms and the carbonyl group of the BmNU molecules. To test this idea, $-CF_3$ groups were substituted for the $-NO_2$ groups to give a derivative that readily formed cocrystals with the two strongest acceptors (triphenylphosphine oxide and dimethyl sulfoxide) only.

The significance of intramolecular —CH---O═C hydrogen bonds to the special cocrystallization properties of BmNU has been further supported by ab initio self-consistent field molecular orbital analysis of these structures.[33] It was found that the calculated atomic charge of the aromatic –CH hydrogen adjacent to the $-NO_2$ group in BmNU is larger than the analogous charge in diphenylurea (+0.130 vs +0.095). The negative charges on the urea oxygens are about the same in both structures (–0.295 in BmNU vs –0.305 in diphenylurea). Analyses of surface electrostatic potentials of these ureas by Politzer et al.[33] also provide new insight into selectivity questions. Diphenylurea has a surprisingly extended negative surface potential on the carbonyl side of the molecule. It extends over the carbonyl group as well as over the near-neighbor –CH hydrogens. The possibility that self-association rather than cocrystallization is promoted by this property implies that the cocrystallization differences between BmNU and diphenylurea are amplified due to differences in their self-association abilities.

We have recently begun a study of imide cocrystallization properties since they appear at first glance to be complementary to the ureas.[34] They could in principle serve as bidentate acceptors, just as the ureas have served as bidentate hydrogen-bond donors. Thus, we sought hydrogen-bond-donating molecules, such as phenols, which could donate one proton to both of the imide carbonyl groups. To our surprise, diphenylimide does not easily form cocrystals with any proton donors; rather, it prefers to act as a proton donor itself and bind to triphenylphosphine oxide through a hydrogen bond with the –NH hydrogen. It prefers to leave its two carbonyl groups free rather than leave an –NH hydrogen free.



Postulated Imide Analog of a Urea Cocrystal

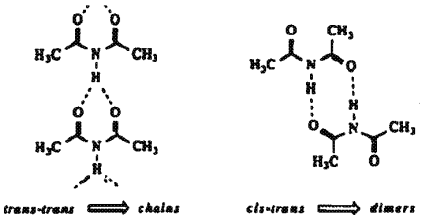


Observed Benzimide Cocrystal

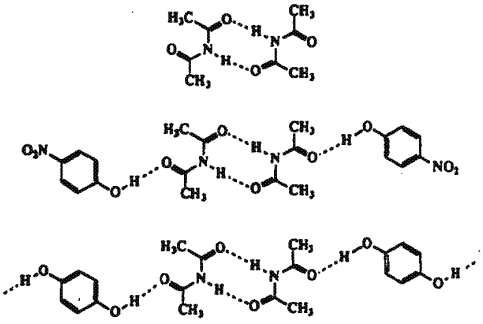
Diacetamide, the simplest imide in the set, proved to be a very versatile cocrystallizing agent, in contrast to diphenyl imide. It crystallizes in two crystal forms.[35] The metastable form has a trans-trans conformation and forms hydrogen-bonded chains, as expected. The cis-trans conformation forms diacetamide dimers leaving one carbonyl group unbonded.

(28) Etter, M. C.; Adamond, D., unpublished results.
(29) Kamlet, M. J.; Abboud, J.-L. M.; Abraham, M. H.; Taft, R. W. *J. Org. Chem.* **1983**, *48*, 2877–2887.
(30) Cram, D. J.; Trueblood, K. N. In *Host–Guest Chemistry, Macrocycles*; Vögtle, F., Weber, E., Eds.; Springer-Verlag: New York, 1985; pp 125–188.
(31) Etter, M. C.; Panunto, T. W. *J. Am. Chem. Soc.* **1988**, *110*, 5896–5897.
(32) Etter, M. C.; Urbańczyk-Lipkowska, Z.; Zia-Ebrahimi, M.; Panunto, T. W. *J. Am. Chem. Soc.* **1990**, *112*, 8415–8426.
(33) Murray, J. S.; Grice, M. E.; Politzer, P. *J. Mol. Eng.*, in press.
(34) Etter, M. C.; Reutzel, S. M. *J. Am. Chem. Soc.*, in press.
(35) (a) Kuroda, Y.; Taira, A.; Uno, T.; Osaki, K. *Cryst. Struct. Commun.* **1975**, *4*, 321–324. (b) Matias, P. M.; Jeffrey, G. A.; Ruble, J. R. *Acta Crystallogr., Sect. B: Struct. Sci.* **1988**, *B44*, 516–522.

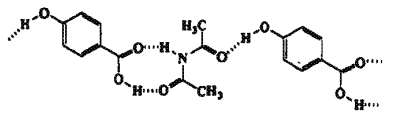
UM00013280
NOVARTIS EXHIBIT 1517
Novartis v. Regents, IPR2023-01347
Page 2026 of 4460



Diacetamide forms cocrystals with many different proton donors, including carboxylic acids, phenols, amides, and ureas. The hydrogen-bond patterns in these structures are varied and are currently being investigated. One pattern that has emerged is that diacetamide cocrystallizes with phenols by preserving the stable dimer pattern shown above for the cis-trans conformation, while using its lone carbonyl group as an appendage for attaching to phenol –OH groups. Thus diacetamide can be converted from a dimer into a complex with four molecules and into an infinite hydrogen-bonded chain by cocrystallizing with *p*-nitrophenol or with hydroquinone, respectively:



The pattern shown below, from the crystal structure of diacetamide with *p*-hydroxybenzoic acid, shows that the diacetamide dimer is not preserved here, but that a heterodimer is formed instead. Clearly, there are many challenges awaiting crystal chemists!



Weak Hydrogen-Bond Interactions as Design Elements in Organic Crystals

It is not unreasonable to consider that strong hydrogen-bond interactions can direct molecular aggregation in organic crystals since only one or a few specific intermolecular contacts provide a large proportion of the stabilization energy of the crystals.[36] When are hydrogen bonds or other less well-defined intermolecular contacts also able to control the organization of molecules in a crystal? The answer depends not only on the enthalpic properties arising from a particular kind of interaction but also on all the processes that contribute to crystal nucleation, which, we propose, are very similar to those that contribute to any form of molecular association. It is important to recognize that crystals obtained in the lab may not be the lowest free energy forms, even if they are the only forms that are isolable. Polymorphism is ubiquitous among organic compounds.[37] Metastable crystal forms are often easy to obtain and are often indefinitely stable once they have been isolated. Another important point is that the hydrogen-bond aggregate found in a crystal is not necessarily the most stable aggregate pattern. Once nucleation of one crystal type occurs, all the solution equilibria can be displaced to favor the aggregate being trapped in the fastest growing nuclei. For example, in the scheme shown below, even if crystal form 1 were the most stable

(36) Dauber, P.; Hagler, A. T. *Acc. Chem. Res.* **1980**, *13*, 105–112.

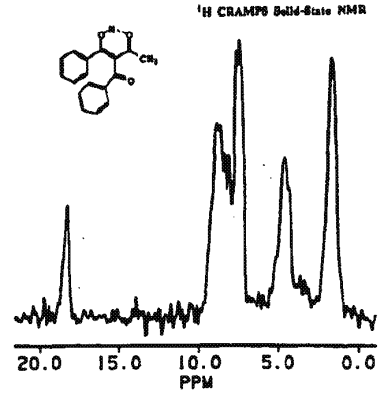
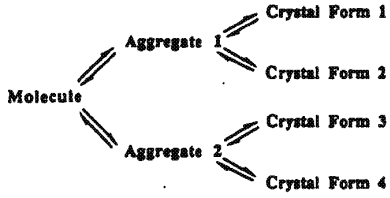


Figure 8. ¹H CRAMPS solid-state NMR spectrum of acetyldibenzoylmethane showing the unusual highly shielded resonance at 5.0 ppm due to a close intermolecular CH---π interaction.

form, crystal form 3 might be the only one obtained if aggregate 2 nucleated crystal growth faster than aggregate 1 did.



Sometimes multiple polymorphic forms are all nucleated in the same solution and mixtures of polymorphs crystallize simultaneously.[38] More often only a single crystal type is isolated, and it is not always the most stable form.

It may be that very weak intermolecular interactions have a disproportionately large effect on the crystal growth process compared to their interaction energies.[39] Weak interactions like –OH---π or –CH---π contacts do appear in crystal structures.[40-42] They may be just chance occurrences. They might even be repulsive interactions. Crystallographic data cannot answer those questions directly, but they can show that these interactions are present and that the structures appear to have been organized as though that interaction was the determining factor in establishing connectivity patterns during the aggregation and nucleation process.

During the course of investigating the tautomeric properties of β-diketomethanes in the solid state, we found that one of our samples, 2-methyl-1,3-diphenylpropanedione, had an unusual ¹H solid-state NMR spectrum.[41] There was a strong well-resolved peak at about 5 ppm, a region of the spectrum where very few hydrogen resonances occur. In solution, there was no peak in that region. We had previously solved the crystal structure of this compound and had not noticed any inter- or intramolecular interactions that looked unusual. The solid-state NMR results prompted us to reinvestigate the crystal structure, and we found that there was a close contact between an aromatic –CH hydrogen of one molecule and the aromatic ring in a neighboring molecule (2.73 Å, displaced by 0.27 Å from the hexad axis). Such effects are postulated as being important stabilizing interactions for side-chain phenyl rings of amino acids in proteins.[42] Analogous

(37) Haleblian, J. K. *J. Pharm. Sci.* **1975**, *64*, 1269–1288.
(38) Etter, M. C.; Kress, R. B.; Bernstein, J.; Cash, D. J. *J. Am. Chem. Soc.* **1984**, *106*, 6921–6927.
(39) Desiraju, G. R.; Murty, B. N.; Kishan, K. V. R. *Chem. Mater.* **1990**, *2*, 447–449.
(40) (a) Traetteberg, M.; Bakken, P.; Seip, R.; Lüttke, W.; Knieriem, B. *Acta Chem. Scand.* **1988**, *A42*, 584–593. (b) Nakatsu, K.; Yoshioka, H.; Kunimoto, K. *Acta Crystallogr., Sect. B: Struct. Sci.* **1978**, *B34*, 2357–2359 and references therein.
(41) Etter, M. C.; Vojta, G. M.; Bronnimann, C. E. *J. Magn. Reson.*, in press.

UM00013281
NOVARTIS EXHIBIT 1517
Novartis v. Regents, IPR2023-01347
Page 2027 of 4460

intramolecular –CH···π interactions have been known and studied by solution NMR spectroscopy for many years.[43] A close –CH···π interaction is known to cause the hydrogen to become highly shielded with a resultant upfield shift in its resonance position, which is precisely the effect we found in our solid-state NMR spectrum (Figure 8).

These results do not prove that this interaction is a stabilizing one or even that it is decisive in controlling the packing pattern. There are, however, no other intermolecular interactions in the crystal structure that are even suggestive of hydrogen bonds, charge-transfer interactions, or other stabilizing interactions besides van der Waals' contacts. This crystal structure and its solid-state NMR pattern show that –CH···π interactions may be important in organizing sets of molecules in crystal structures. It alerts crystallographers and theoreticians to be aware that such interactions may be important determinants in controlling molecular aggregation and that the possibility of such weak interactions should not be overlooked in interpreting known crystal structures or in designing new ones.

Conclusions

Intermolecular hydrogen-bond interactions have enormous potential as design tools in both solution and solid-state chemistry. The procedures presented here, where hydrogen bonds are thought of as synthetic tools similar to σ bonds in classical organic chemistry, should be helpful in studying a wide range of chemical problems. Structure–property relations in pharmaceutical, electrooptical, and energetic solid-state materials might be studied by correlating graph sets of hydrogen-bonded or otherwise strongly associated sets of molecules with one or more of their solid-state properties. Cocrystallization and the study of cocrystal structures holds promise for modeling molecular recognition events taking place in nonrigid media. Postulated structures of small molecule host–guest complexes in solution might be observable in cocrystal forms even if they are not present in very high concentrations in solution.[44] Site-specific recognition in protein–DNA complexes[45] or interchain association in polymeric matrices[46] might also be amenable to cocrystallization of components of these systems. Hydrogen-bond rules developed with small molecule studies are functional-group specific and as such should be useful as initial models of the independent role of hydrogen-bonding functional groups in complex systems.

Acknowledgment. A special thank you to Diana Parker, a graduate student at the University of Minnesota (UM), for technical and scientific assistance with preparation of this paper, to Professor Doyle Britton, (UM), for providing expert crystallographic assistance, and to Professor Jim Loehlin, Wellesley College, for helpful discussions about graph sets. Acknowledgment is made to the donors of the Petroleum Research Fund, administered by the American Chemical Society, and to NIH (GM42148-01), NSF (CHE8600383-02), and ONR (N00014-89-K-1301) for partial support of this research.

(42) Burley, S. K.; Petsko, G. A. *Science* **1985**, *229*, 23–28.

(43) Bovey, F. A. *Nuclear Magnetic Resonance Spectroscopy*; Academic: New York, 1969; pp 64–71.
(44) Rebek, J. *Science* **1987**, *235*, 1478–1484.
(45) Jordan, S. R.; Pabo, C. O. *Science* **1988**, *242*, 893–907.
(46) Stadler, R. *Prog. Colloid Polym. Sci.* **1987**, *75*, 140–145.
(47) Lechat, J. R.; de A. Santos, R. H.; Bueno, W. A. *Acta Crystallogr., Sect. B: Struct. Sci.* **1981**, *B37*, 1468.
(48) Lechat, J. R., private communication.
(49) Etter, M. C.; Frankenbach, G. M., unpublished results.

ARTICLES

Excitation of IF($B^3\Pi(0^+)$) by Metastable O_2. 1. Studies Involving IF(X,v)

S. J. Davis* and A. M. Woodward

Physical Sciences Inc., 20 New England Business Center, Andover, Massachusetts 01810
(Received: June 12, 1990; In Final Form: December 14, 1990)

A mechanistic study of the energy transfer from singlet molecular oxygen $O_2(a^1\Delta, b^2\Sigma)$ to the $B^3\Pi(0^+)$ state of iodine monofluoride is reported. Chemiluminescence and laser-induced fluorescence techniques were used to probe various aspects of this reaction scheme. By using several precursor reactions as the source of the IF(X), we have shown that vibrationally excited IF(X,$v \geq 9$) is an active participant in the excitation of IF(B) by $O_2(^1\Delta)$.

1. Introduction

The excitation of the lower lying triplet states ($A^1\Pi_1$, $B^3\Pi_0$) of the halogens and interhalogens via energy transfer from metastable collision partners has been the subject of numerous studies over the past two decades. A pioneering study was completed by Arnold, Finlayson, and Ogryzlo,[1] who reported that I_2 was both electronically excited and dissociated in the presence of electronically excited $O_2(a^1\Delta, b^1\Sigma)$. Later, Derwent and Thrush[2,3] completed a series of detailed experiments that showed that the $B^3\Pi(0_u^+)$ state in I_2 was excited when molecular iodine was reacted with $O_2(^1\Delta, ^1\Sigma)$. They also observed that the I_2 was dissociated by the O_2, and as a result of this study, Derwent and Thrush correctly predicted that the near resonant energy transfer from $O_2(^1\Delta)$ to the atomic iodine $^2P_{1/2}$ state could produce an atomic iodine electronic transition laser operating on the $^2P_{1/2} \rightarrow {}^2P_{3/2}$ transition at 1.315 μm. This pioneering study was the basis

(1) Arnold, S. J.; Finlayson, N.; Ogryzlo, E. A. *J. Chem. Phys.* **1966**, *44*, 2529.
(2) Derwent, R. G.; Thrush, B. A. *Trans. Faraday Soc.* **1971**, *67*, 2036.
(3) Derwent, R. G.; Thrush, B. A. *Chem. Phys. Lett.* **1971**, *9*, 591.

0022-3654/91/2095-4610$02.50/0 © 1991 American Chemical Society

UM00013282
NOVARTIS EXHIBIT 1517
Novartis v. Regents, IPR2023-01347
Page 2028 of 4460

Acta Cryst. (1999). B55, 1099–1108

Volumetric measure of isostructurality

László Fábián and Alajos Kálmán*

Institute of Chemistry, Chemical Research Center of the Hungarian Academy of Sciences, Budapest, PO Box 17, H-1525 Hungary. E-mail: akalman@cric.chemres.hu

(*Received 23 April 1999; accepted 5 July 1999*)

Abstract

The numerical descriptors of isostructurality are critically reviewed and to overcome their limitations a new volumetric measure is proposed. It is defined as the percentage ratio of the overlapping volume of molecules in the analyzed structures to the average of the corresponding molecular volumes. For the calculation of this index a numerical approach is presented, which is also capable of treating disordered structures. The use of isostructurality calculations is demonstrated using a series of examples. Homologous 9-alkylthiophenanthrenes are used as simple illustrations of the necessity and applicability of the new descriptor. The structural changes in the inclusion compounds of 5-methoxysulfadiazine with chloroform, dioxane and tetrahydrofuran are analyzed and rationalized with the aid of isostructurality indices. The diverse relationships among a series of helical tubuland diols cocrystallized with simple phenols are also characterized. The modifications in molecular and crystal structures are correlated with the calculated degree of isostructurality.

1. Introduction

The similarities observed among the crystal packings of several related steroid structures (Kálmán *et al.*, 1991, 1992) prompted us to rationalize the isostructurality of organic crystals in general (Kálmán *et al.*, 1993). From the examples allocated in the current literature it became obvious that a given packing motif may *tolerate* small changes in the molecular structure without a visible effect on the already established close packing. These changes included atomic replacements and minor alterations in substitution and/or epimerization. The tolerance may be ascribed to the presence of *ca* 30% free space in close-packed structures. (Note that the packing coefficients of organic crystals are typically in the range 0.6–0.7.)

Since 1993 isostructurality has proved to be much more frequent than it was expected to be (Kálmán & Párkányi, 1997). In particular, associate crystals tend to be isostructural. Different guest molecules may be incorporated into a host lattice without substantially changing its structure. With the increasing number of known examples (predominantly binary systems) the study of isostructurality is becoming a useful tool in the deeper understanding of close-packing principles.

This, however, requires numerical descriptors to quantify the degree of similarity. In this paper we propose a new measure of isostructurality which can also handle supramolecular (binary, ternary) systems. Since crystal packing, at the first approximation, is based on the self-complementarity of molecular volumes, a measure based on the overlap of the volumes of molecules should provide physically meaningful data. Such an index also enables one to describe cases where a straightforward atom–atom correspondence cannot be established.

2. Descriptors of packing similarity

2.1. *Unit-cell similarity*

A basic prerequisite of isostructurality is the similarity of unit cells. According to Kálmán *et al.* (1993) they can be compared using

$$\Pi = [(a+b+c)/(a'+b'+c')] - 1 \qquad (a+b+c > a'+b'+c'), \tag{1}$$

where a, b, c and a', b', c' are the orthogonalized† unit-cell parameters of the related crystals. For similar unit cells $\Pi \simeq 0$. Unfortunately, the calculated values of Π depend on the orthogonalization scheme applied and thus only results obtained by the same method are comparable. As the first calculations were carried out on orthorhombic structures, this problem occurred only recently with the need to calculate a uniquely defined Π for triclinic structures. To provide a scheme that treats the axes equally, we adapted the symmetric orthogonalization method of Löwdin (1950) developed originally for the transformation of quantum chemical basis functions (see *Appendix*). All the Π values reported in this paper were determined using this orthogonalization procedure.

A more sophisticated way of comparing unit cells was proposed by Rutherford (1997). The difference in cell size is described by the mean elongation (ϵ), while the

† Orthogonalization in space groups with fixed cell angles is not necessary.

© 1999 International Union of Crystallography
Printed in Great Britain – all rights reserved

UM00013283
NOVARTIS EXHIBIT 1517
Novartis v. Regents, IPR2023-01347
Page 2029 of 4460

so-called asphericity index (A) accounts for the shape distortion. The definition of ϵ is

$$\epsilon = (V'/V)^{1/3} - 1 \qquad (V' > V), \tag{2}$$

where V and V' are the volumes of the respective unit cells. The asphericity index is defined as

$$A = (2/3)\Big[1 - \sum_{j>i}\{[(1+\epsilon)M_i - 1] \times [(1+\epsilon)M_j - 1]/3\epsilon^2\}\Big]^{1/2}, \tag{3}$$

where M_i's are the principal axes of matrix **M**, which gives the pure shear component of the transformation between the two crystallographic coordinate systems. (For more details and the derivation of the asphericity index see Rutherford, 1997, and references therein.) The closer the relationship between the structures, the closer ϵ and A are to 0. Thus, the product ϵA may also be used as a unified unit-cell similarity descriptor.

2.2. *Comparing the position of molecules in the unit cell*

Naturally, isostructurality involves not only similar unit cells, but also a similar internal arrangement of molecules. In the case of closely related molecules this means that the common atoms of the two structures are located approximately at the same coordinates. This relationship is expressed by the *isostructurality index* of Kálmán *et al.* (1993)

$$I_i(n) = \left[1 - \left(\sum \Delta R_i^2/n\right)^{1/2}\right] \times 100\%, \tag{4}$$

where ΔR_i values are the differences between the orthogonalized coordinates (Dunitz, 1979) of n identical heavy atoms in the related structures. The molecules, of course, have to be transformed to the same asymmetric unit and origin choice. This descriptor has proved to be very informative on the similarity between several steroid crystal structures, organometallic compounds of $Ph_3X{-}X'Me_3$ composition (where X, X' = Si, Ge, Sn) *etc.*, but as more complex examples have been encountered, its limits have to be taken into account:

(i) It should not be forgotten that I_i given as a percentage may even assume a *negative* value, which is impractical. Namely, the average of the coordinate differences in (4) is not limited to the crystallographic unit length (1 Å). In the beginning (Kálmán *et al.*, 1991, 1992), all the related structures investigated showed a high degree of isostructurality with low $\Pi \leq 0.010$, and I_i calculations only fitted molecules in the asymmetric units chosen to be the closest to the origin. Thus, $\langle \Delta R_i \rangle$ has never exceeded 1 Å and from such values normalized to the crystallographic unit length I_i could be calculated as a percentage with relatively high positive values.

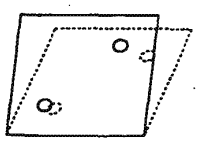


Fig. 1. The effect of unit-cell dissimilarity on the distance of equivalent points in different asymmetric units. Points with coordinates $(\frac{1}{4}, \frac{1}{4})$ and $(\frac{3}{4}, \frac{3}{4})$ are shown.

Table 1. *Isostructurality indices calculated for 9-ethylthiophenanthrene (I), 9-propylthiophenanthrene (II) and 9-butylthiophenanthrene (III)*

Structures	Π	$I_i(17)$ (%)	$I_i(17 \times 4)$ (%)	I_v (%)	$[I_v^{max}]$ (%)
(I)–(II)	0.022	42.8	50.7	84.6	[96.1]
(II)–(III)	0.049	24.3	−33.9	65.6	[96.9]
(I)–(III)	0.073	−18.4	−61.8	57.2	[93.0]

However, with the extension of studies on isostructurality (Kálmán & Párkányi, 1997), misfits in the superposition of 'swelling/shrinking' unit cells are increasing. Therefore, it is very likely that $\langle \Delta R_i \rangle$ becomes greater than 1 Å, especially if the calculations are extended over the full unit cells, which is unavoidable for heteromolecular systems. In such cases, as shown by a two-dimensional sketch of overlapping oblique unit cells (Fig. 1), the points with coordinates $(\frac{1}{4}, \frac{1}{4})$ are much closer to each other than those at $(\frac{3}{4}, \frac{3}{4})$. In general, the ΔR_i distance between equivalent points in two unit cells increases with their distance from the common origin, fixed either at (0, 0, 0) or even at $(\frac{1}{2}, \frac{1}{2}, \frac{1}{2})$. Of course, with increasing Π values (≥ 0.01), $I_i(n)$, but especially $I_i(n \times Z)$, where Z is the number of asymmetric units, may assume high negative values. This phenomenon is well demonstrated by the homologous series of 9-alkylthiophenanthrenes (Table 1, §4.1).

(ii) More complicated alterations to the molecule than a simple substitution exclude the changed part from the comparison since there are no common atoms there. For the same reason different guest molecules associated with the same host cannot be compared either.

(iii) In some instances, owing to small internal rotations, in the crystals not the corresponding atoms of the respective molecules are the nearest to each other. This can lead to large individual ΔR's that cannot be justified by differences in the space occupied by the molecules compared.

(iv) Although the increasing number of H atoms seems to stabilize the formation of isostructural pairs (Go & Bhandary, 1989), they are to be excluded from I_i calculations because of the limited accuracy of their coordinates.

The above experiences led us to redefine one of the conditions of isostructurality. Not the atomic coordinates (as stated earlier), but the *volumes* occupied in the unit cell should be closely related in isostructural pairs. (Obviously, it is still possible to compare certain parts of

UM00013284
NOVARTIS EXHIBIT 1517
Novartis v. Regents, IPR2023-01347
Page 2030 of 4460

a structure, *e.g.* one can state that host molecules are more isostructural in a given inclusion compound than guest molecules.) This viewpoint is expressed in a new *volumetric isostructurality index*

$$I_v = 2V_\cap/(V_1 + V_2) \times 100\%, \qquad (5)$$

where V_1 and V_2 are the volumes of the compared fragments and $V_\cap$ is the intersection of these volumes. As $(V_1 + V_2)/2$ is the average volume, I_v may also be expressed as the ratio of volume overlap to the average volume.

The calculation is performed on a whole unit cell to avoid the problem raised by unit-cell dissimilarity (Kálmán & Párkányi, 1997). Thus, an *averaging* is implicitly performed over the asymmetric units and the results depend on the degree of unit-cell similarity. Most I_i indices reported in this paper were *also* calculated for the whole unit cell. To emphasize this difference from the original definition we use the notation $I_i(n \times Z)$.

For identical structures we obtain $I_v = 100\%$, while with no overlap $I_v = 0\%$ is obtained. When $V_1 \neq V_2$, the theoretical maximum of I_v is

$$I_v^{max} = (2\min\{V_1, V_2\})/(V_1 + V_2) \times 100\%, \qquad (6)$$

since $V_\cap$ cannot be greater than the smaller of the overlapping volumes.

3. Calculation of I_v

Since the analytical calculation of $V_\cap$ requires the application of extremely complicated formulae, no straightforward calculation of the novel isostructurality index (5) can be performed. To circumvent this problem we developed a numerical algorithm to calculate I_v.†

The basic idea of the calculation originates from the method of Gavezzotti (1983) to compute molecular volumes. In his algorithm the molecule is enclosed in a box of known volume and a large number of evenly distributed random points is generated in the box. The ratio of the molecular volume to the volume of the box is equal to the portion of points falling within the molecule‡ to the total number of points generated. Our method introduces only slight modifications to the above procedure to handle the intersection of two structures. Since guest molecules are frequently disordered in inclusion compounds, this algorithm is also extended to the capability of working with disordered structures.

3.1. *Input*

First, to make the structures comparable, occasionally some transformations must be performed. This may include symmetry transformations and unit-cell origin shifts. It is also possible to compare structures of different space groups by transforming both to a space group with lower symmetry. Of course, in this case more symmetry or pseudo-symmetry related molecules are compared. Then symmetry equivalent molecules are generated to fill the unit-cell box ($x, y, z \in [0; 1]$).§

From such a prepared pair of data files the program reads the unit-cell parameters, and the fractional coordinates and occupancies of each atom. Both coordinate sets are orthogonalized and the van der Waals radii of the corresponding elements are assigned to the atoms. The I_v results also depend on the arbitrary choice of orthogonalization method. For simplicity we used the standardized routine (Dunitz, 1979) which takes X parallel to crystal a, Y in the ab plane and Z perpendicular to X and Y.

3.2. *Basic scheme of the calculation*

(i) To define a common bounding box around both structures, the maximum and minimum x, y and z coordinates are determined.

(ii) Three counters N_1, N_2 and $N_\cap$ are initialized to zero for the calculation of V_1, V_2 and $V_\cap$, respectively.

(iii) A random point is generated within the bounding box. If the point is closer to any of the atoms of molecule 1 and/or 2 than its van der Waals radius then the corresponding counter is incremented. If it is close to atoms of both molecules the counter assigned to $V_\cap$ is also increased by one. This step is repeated several times to obtain a good sampling of the bounding box (1000 points $Å^{-3}$).

(iv) V_1, V_2 and $V_\cap$ are calculated using the formula

$$V_i = V_{box} \times (N_i/N) \qquad (i = 1, 2, \cap), \qquad (7)$$

where N_i is the respective counter and N is the total number of random points generated. The volumetric isostructurality index is then calculated by applying (5).

3.3. *Treatment of disorder*

A distinct advantage of this numerical approach is that it is easily extendable to handle disordered structures as well. This capability is most useful for the analysis of disordered guest regions. The key of such an extension is a modification of the increments added to the counters in step (iii) of the above algorithm. Namely, values that represent the *probability* of the point being occupied are used rather than incrementing the counters Ni by one.

† The *C* program which calculates I_v for two *SHELX* files is available from the authors.

‡ A point is considered to be within the molecule if it is closer to any of its nuclei than the van der Waals radius of the corresponding atom.

§ It is more adequate to transform molecules as a whole to preclude the occurrence of physically meaningless unbound fragments. Hence, some atomic coordinates may overstep the [0; 1] interval.

UM00013285
NOVARTIS EXHIBIT 1517
Novartis v. Regents, IPR2023-01347
Page 2031 of 4460

The structure is divided into disordered parts (*PART* instructions in a *SHELX* file). Of course, the non-disordered part of the structure is treated with full occupancy. Depending on the position of the random point concerning the respective structure, the following increments are added to N_1 and N_2:

(i) The corresponding counter is not incremented if the point is not within the van der Waals radius of any atom in the structure investigated.

(ii) If the point is close to only one atom then the counter is incremented by the site occupation factor of this atom.

(iii) If the point is close to more atoms forming the same disordered moiety then the common site occupation factor of these atoms, *i.e.* the occupancy of the disordered part, is added to the respective counter.

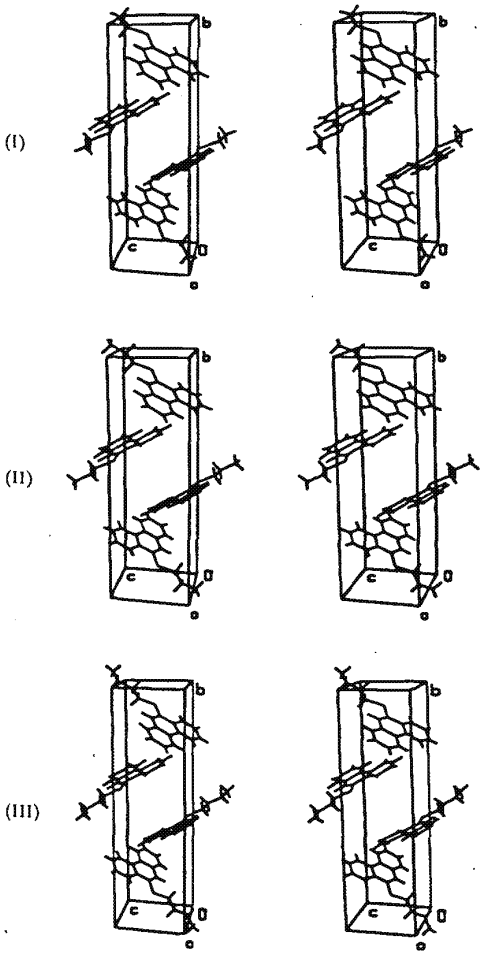


Fig. 2. Crystal packing of 9-ethylthiophenanthrene (I), 9-propylthiophenanthrene (II) and 9-butylthiophenanthrene (III).

(iv) If the point is simultaneously close to atoms that belong to different disordered parts then the counter is incremented by the sum of the occupancies of each disordered moiety involved. However, when this point is close to both non-disordered and disordered atoms, an increment greater than one is obtained. This value evidently has to be reset to one.

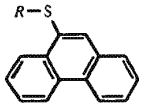
The increment of $N_\cap$ is the product of the two values obtained for N_1 and N_2, *i.e.* it is equal to the probability of the selected random point being occupied in *both* structures coincidently.

4. Results

As a benchmark of the new descriptor, I_v values were calculated for several isostructural crystal pairs (Table 2). Structures that could not sufficiently be described using I_i were selected from the literature. We compare the results obtained applying (4) and (5) and show how the latter extends the possible scope of isostructurality studies.

4.1. *Isostructurality of homologous 9-alkylthiophenanthrenes*

The homologous alkylthiophenanthrene structures were reported by Kansikas & Sipila (1997) with group *R* being ethyl (I), *n*-propyl (II) and *n*-butyl (III), respectively. All three crystallize in space group $P2_1/c$ with similar lattice parameters and molecular arrangements (Table 2, Fig. 2).



(I)–(III)

Index I_i was calculated for the 17 common heavy atoms within an asymmetric unit and for the 17 × 4 common heavy atoms in the unit cell, but I_v only for the four corresponding molecules (Table 1). In general, the use of a whole unit cell rather than a single molecule diminishes I_i. Therefore, it may be surprising that $I_i(17)$ for the pair (I)–(II) is smaller than $I_i(17 \times 4)$. In fact, it is not assured that the molecules closest to the origin overlap the most since the cell parameter and the fractional coordinate differences may compensate in other asymmetric units and thus lead to a better fit.

Apparently, I_i and I_v indices change in a parallel manner. The former, which is based on atomic coordinates (4), is much more sensitive than the latter, calculated from molecular volumes (5). Despite the visible close-packing similarity, negative I_i's are obtained, whereas the I_v scale remains reasonable. (One should bear in mind that the statistical nature of the calculation accounts for a *ca* ±0.2% uncertainty shown by the I_v indices.)

UM00013286
NOVARTIS EXHIBIT 1517
Novartis v. Regents, IPR2023-01347
Page 2032 of 4460

Table 2. *Space groups, unit-cell parameters and packing coefficients of the structures analyzed*

Structure	Space group	*a*	*b*	*c*	*β*	p.c.
(I)	$P2_1/c$	9.054	20.644	6.659	98.10	0.69
(II)	$P2_1/c$	9.067	21.123	7.007	99.12	0.70
(III)	$P2_1/c$	9.010	23.124	6.888	97.81	0.69
(IV)	$P2_1/c$	8.403	7.489	14.025	97.18	0.69
(V)	$P2_1/c$	8.473	7.437	13.952	94.51	0.71
(VI)	$P2_1/c$	12.282	13.920	10.068	99.51	0.68
(VII)	$P2_1/c$	12.279	13.938	10.037	99.55	0.67
(VIII*a*)	$P2_1/c$	8.129	19.077	11.256	101.56	0.68
(VIII*b*)	$P2_1/c$	8.020	19.187	11.175	98.89	0.69
(VIII*c*)	$P2_1/c$	8.056	19.500	11.252	98.72	0.69
(IX*d*)	$P2_1/c$	6.927	12.696	19.286	94.82	0.66
(X*d*)	$P2_1/c$	6.875	13.244	19.878	97.56	0.68
(X*e*)	$P2_1/c$	6.871	13.255	20.021	96.64	0.69
(X*f*)	$P2_1/c$	6.896	13.145	20.598	97.21	0.68
(XI*g*)	$P2_1/c$	6.908	13.754	19.561	102.90	0.66

An interesting conclusion can be drawn from the comparison of I_v and I_v^{max} values. Although the relative change in the molecular volumes between (I) and (II) is larger than between (II) and (III), the former pair shows a closer relationship in the crystal phase. Thus, the more similar molecular volumes do not necessarily lead to more similar crystal packings.

As indicated by the packing coefficients (p.c. in Table 2), the first methylene group added to *R* in (II) tightens its packing. The second, however, diminishes it again, which means that molecules are *necessarily* displaced in (III) to avoid possible strains induced by the longer chain. Also, this displacement is properly reflected by the smaller (II)–(III) isostructurality index compared with I_v^{max}.

4.2. *Test calculations on non-isostructural crystals*

Obviously, the theoretical minimum of $I_v = 0$ is never obtained in a calculation, since there is always some overlap even between unrelated structures. To estimate a reasonable lower limit of the I_v index, test calculations were performed on crystal pairs retrieved from the Cambridge Crystallographic Database (Allen & Kennard, 1993) possessing similar unit cells with the same space group, but showing no other structural relationship.

As an example, acetyl benzoyl peroxide (IV) (Karch *et al.*, 1975) and 2,6-dimethoxy-1,4-oxathiane 4,4-dioxide (V) (Estrada & López-Castro, 1991) are presented. Despite the similarity of their unit cells (Table 2, $\Pi = 0.001$) and an I_v^{max} of 99.4%, the volumetric isostructurality index for these structures is only 22.6%. Similarly, the unit cells of 6-phenyl-4-oxa-8,9-10,11-dibenzotricyclo[5,4,0,$0^{1,6}$]undeca-2,8,10-triene-5-one (VI) (van Arendonk *et al.*, 1978) and *rel*-(1*R*,4*R*,9*R*)-1-acetyl-9-(*t*-butylthio)-9-cyano-1,4-dihydro-1,4-ethanonaphthalene (VII) (Döpp *et al.*, 1989) are almost the same ($\Pi = 0.004$) and $I_v^{max} = 99.1\%$. Nevertheless, I_v is only 30.2%.

From these examples it is apparent that volumetric isostructurality indices of ~50% still indicate pronounced structural resemblance, whereas around 30% they can be obtained from randomly overlapping structures.

4.3. *Inclusion compounds of 5-methoxysulfadiazine*

The inclusion properties of 5-methoxysulfadiazine (VIII) were studied by Caira & Mohamed (1993). The solvates formed with chloroform (VIII*a*), tetrahydrofuran (VIII*b*) and 1,4-dioxane (VIII*c*) are isostructural. The different guest molecules are incorporated into an almost unaltered host lattice (Fig. 3).

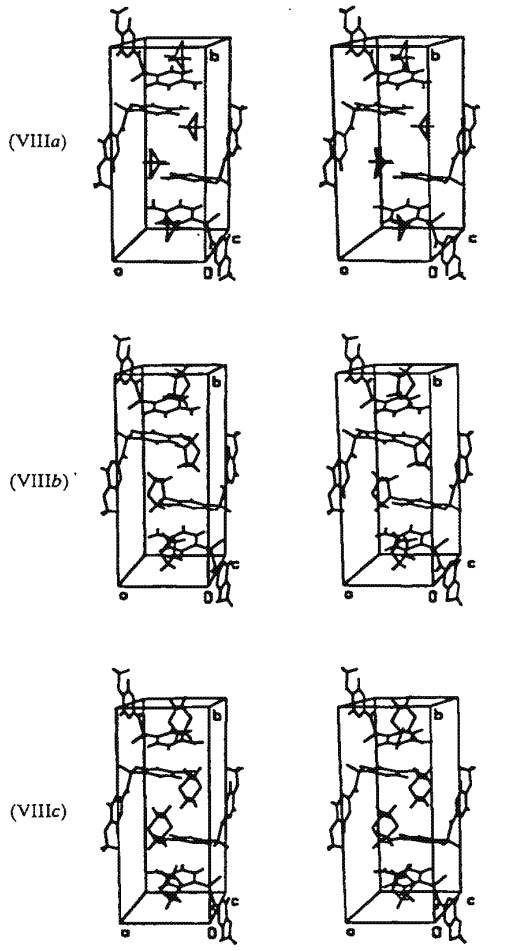


Fig. 3. Stereoview of inclusion compounds of 5-methoxysulfadiazine with chloroform (VIII*a*), tetrahydrofuran (VIII*b*) and dioxane (VIII*c*).

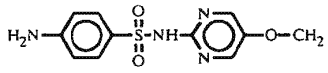
UM00013287
NOVARTIS EXHIBIT 1517
Novartis v. Regents, IPR2023-01347
Page 2033 of 4460

Table 3. *Isostructurality of inclusion compounds of 5-methoxysulfadiazine with chloroform (VIIIa), tetrahydrofuran (VIIIb) and 1,4-dioxane (VIIIc)*

I_i can be calculated only for the 19 heavy atoms of the host molecules.

Structures	Π	$I_i(19 \times 4)$ (%)	I_v^{host} (%)	I_v^{guest} (%)	I_v (%)
(VIII*b*)–(VIII*c*)	0.011	71.0	90.6	86.5 [95.6]	89.7 [98.6]
(VIII*a*)–(VIII*b*)	0.001	70.1	91.0	77.1 [96.2]	87.7 [99.4]
(VIII*a*)–(VIII*c*)	0.010	59.3	87.6	75.3 [91.7]	84.8 [97.9]

Interestingly, the chemically unrelated solvent ($CHCl_3$) also gives the same packing as the cyclic ethers, although its looser fit is emphasized by disorder. The host molecule itself and its clathrate with acetylsalicylyc acid (Caira, 1994) are not isostructural either with these associates or each other.



(VIII)

The study of these isostructural inclusion compounds (Kálmán & Párkányi, 1997) was limited to the inspection of host molecules by the restrictions implicit in the definition of I_i. In contrast, the descriptor I_v allows for the comparison of regions occupied by such dissimilar molecules as dioxane and tetrahydrofuran, as well as for a systematic treatment of disorder shown by chloroform.

As expected, the highest I_v value is obtained for the associates with dioxane and tetrahydrofuran (Table 3). In accordance with the similar solvent volumes (VIII)–chloroform is closer to the tetrahydrofuran solvate. However, the sequence of I_i indices computed for the host molecules differs from the sequence of I_v^{host} values, suggesting that such small differences between isostructurality indices are of limited significance.

Neglecting these minor deviations, I_v and I_v^{host} values move together with I_v^{max}. On the other hand, I_v^{guest} for the (VIII*a*)–(VIII*b*) pair is small compared with the corresponding maximum value. This shows that in spite of the similar volumes, chloroform and tetrahydrofuran, owing to their different shapes, cannot occupy the same volume. The smaller change in I_v^{host} shows that the host structure damps guest alteration effects.

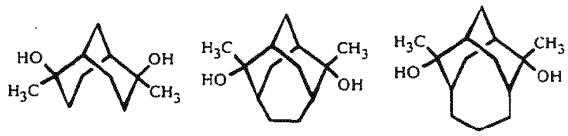
The relationship $I_v^{host} > I_v^{guest}$ corresponds to loosely bound guest molecules *versus* a relatively rigid hydrogen-bonded host lattice. One may anticipate that the comparison of full and partitioned isostructurality indices can give a general hint on the stiffness of those fragments with respect to packing forces.

4.4. *Cocrystalline compounds of tubuland diols*

The helical tubuland diols (IX), (X) and (XI) were cocrystallized with simple phenols by Ung *et al.* (1994). The resulting cocrystals provide an outstandingly good subject of our examinations through the variation of both host and guest molecules (*d*: *p*-chlorophenol, *e*: *p*-hydroxythiophenol, *f*: *p*-methoxyphenol and *g*: phenol).

Table 4. *Isostructurality of cocrystals of (X) with p-chlorophenol (Xd), p-hydroxythiophenol (Xe) and p-methoxyphenol (Xf)*

	Π	I_v (%)	I_v^{host} (%)	I_v^{guest} (%)
(X*d*)–(X*e*)	0.004	92.5 [99.3]	92.7	91.1 [97.9]
(X*e*)–(X*f*)	0.012	86.7 [99.3]	87.7	83.7 [97.6]
(X*d*)–(X*f*)	0.010	83.0 [98.6]	83.8	79.6 [95.5]



(IX) (X) (XI)

The compounds of 2,7-dimethyltricyclo[4.3.1.$1^{3,8}$]-undecane-*syn*-2,*syn*-7- diol (X) with *p*-chlorophenol (X*d*), *p*-hydroxythiophenol (X*e*) and *p*-methoxyphenol (X*f*) equally crystallize in space group $P2_1/c$, assuming 1:1 host:guest ratio (Table 2).

The volumes of the solvent molecules increase in the order (X*d*), (X*e*) and (X*f*). In terms of I_v^{max}, (X*e*) is midway between the others (Table 4). Contrasting the similar maximum values, the isostructurality indices for the (X*d*)–(X*e*) and (X*e*)–(X*f*) pairs differ significantly. Here, a similar situation is encountered again as with the phenanthrene thioethers [(I), (II) and (III)]. A small increase in the guest volume ($d \rightarrow e$) is tolerated by the crystal without a major displacement of the molecules, whereas an even larger molecule does not fit in the same space (X*f*) and thus the packing distorts more (see also the packing coefficients in Table 2).

The I_v^{guest} indices calculated for only the heavy atoms would be approximately 5% smaller for (X*f*), showing that the volume of H atoms cannot be disregarded in the volume of the methoxy group. (Usually, omitting H atoms leads to only 1–2% difference in the resulting I_v.)

In these binary crystals host molecules are more isostructural than guest molecules, but the differences between their respective isostructurality indices are much smaller than in the solvates of (VIII). While guest molecules are located in open channels in (VIII*a*), (VIII*b*) and (VIII*c*), in the inclusions of host (X) they form separate molecular layers (Fig. 4). The layers are interconnected by → (host → host → guest) → hydrogen-bond chains, hence the guest molecules are also held tightly in these crystals.

The 2,6-dimethylbicyclo[3.3.1]nonane-*exo*-2,*exo*-6-diol *p*-chlorophenol cocrystal (IX*d*) was also reported to be isostructural with (X*d*)–(X*f*) (Fig. 5). In principle, this structure can be obtained from (X*d*) by removing a linking dimethylene group from the host molecule. In

UM00013288
NOVARTIS EXHIBIT 1517
Novartis v. Regents, IPR2023-01347
Page 2034 of 4460

practice, the molecule turns around and the single carbon linkage moves into the position of the missing atoms, while its original place remains unoccupied by the host. This *ca* 180° rotation is accompanied by a significant translation of the molecules. The relatively small isostructurality indices (Table 5) also emphasize how much the structure is rearranged. Nevertheless, the packing arrangement and the hydrogen-bonding network are unaltered.

Surprisingly, (IX*d*) is more similar to (X*e*) than to (X*d*). The effects of host and guest changes are probably better compensated in the former case. It also seems to be reasonable that the need of a different host for being complementary to the same guest leads to an increased displacement. This may also explain the low I_v^{host} value obtained for (IX*d*) and (X*d*).

Table 5. *Isostructurality of the p-chlorophenol associate of (IX) with cocrystals of (X) and p-chlorophenol (Xd), p-hydroxythiophenol (Xe) and p-methoxyphenol (Xf)*

	Π	I_v (%)	I_v^{host} (%)	I_v^{guest} (%)
(IX*d*)–(X*d*)	0.027	72.7 [95.4]	69.1 [93.4]	76.2 [99.3]
(IX*d*)–(X*e*)	0.031	74.8 [94.7]	72.1 [93.2]	77.1 [97.2]
(IX*d*)–(X*f*)	0.044	71.9 [94.0]	71.4 [93.6]	69.3 [94.9]

The structure of (IX*d*) is clearly the farthest from (X*f*). While the larger *p*-methoxyphenol guest expands the cell compared with (X*d*), replacement of the host with (IX) shrinks it. The combined effect of these opposite changes gives rise to a further decrease of isostructurality.

Even smaller isostructurality indices were obtained between the inclusions of (X) and the phenol solvate of 2,8-dimethyltricyclo[5.3.1.1^{3,9}]dodecane-*syn*-2,*syn*-8-diol (XI*g*). The host molecule (XI) can be formed by adding a CH_2 group to (X), whereas phenol is smaller than any of the guests of (X). Thus, one would predict that some 'guest regions' of (X*d*)–(X*f*) are occupied by the enlarged host in (XI*g*) and that host molecules are simultaneously shifted towards the released guest space. Indeed, the overall isostructurality index I_v is greater than either I_v^{host} or I_v^{guest} for all three pairs, proving the validity of this assumption (Table 6).

The (X*d*)–(X*f*) *versus* (XI*g*) I_v values decrease as the size of the guest molecule increases in the order (X*d*), (X*e*) and (X*f*). A careful observation of the crystal structure (Fig. 6) reveals that the elongated ring protrudes towards the *para* hydrogen of the phenol molecules. Increasing the size of the *para* substituent of the guest molecule in (X) cocrystals thus repels the host molecule further away from its position in (XI*g*).

The Π descriptor of unit-cell similarity gives misleading results for (XI*g*), because the more than 0.5 Å lengthening of axis *b* is compensated by a similar shortening of axis *c*. The more complicated description of Rutherford (1997) would presumably reflect the dissimilarity of cells.

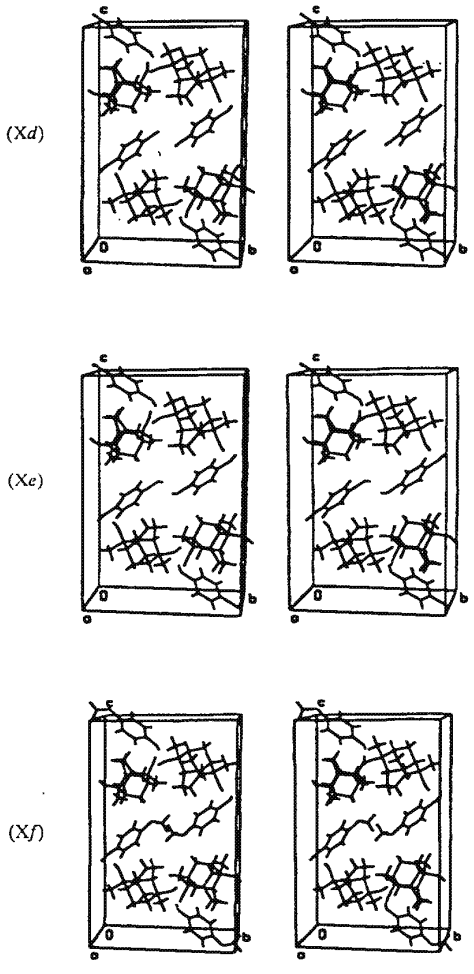


Fig. 4. Cocrystalline compounds of 2,7-dimethyltricyclo[4.3.1.1^{3,8}]undecane-*syn*-2,*syn*-7-diol (X) with *p*-chlorophenol (X*d*), *p*-hydroxythiophenol (X*e*) and *p*-methoxyphenol (X*f*).

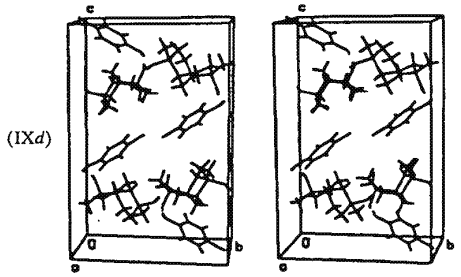


Fig. 5. Structure of the cocrystals of 2,6-dimethylbicyclo[3.3.1]nonane-*exo*-2,*exo*-6-diol with *p*-chlorophenol (IX*d*).

UM00013289
NOVARTIS EXHIBIT 1517
Novartis v. Regents, IPR2023-01347
Page 2035 of 4460

Table 6. *Isostructurality of the phenol solvate of (XI) with (X), p-chlorophenol (Xd), p-hydroxythiophenol (Xe), p-methoxyphenol (Xf), and with (IX), p-chlorophenol (IXd) cocrystalline compounds*

	Π	I_v (%)	I_v^{host} (%)	I_v^{guest} (%)
(XIg)–(X*d*)	0.003	70.0 [99.8]	69.2 [96.5]	64.5 [92.4]
(XIg)–(X*f*)	0.013	61.8 [98.7]	61.5 [96.2]	51.2 [88.0]
(XIg)–(X*e*)	< 0.001	65.9 [99.3]	65.1 [96.6]	58.7 [90.4]
(XIg)–(IX*d*)	0.031	54.3 [95.3]	49.7 [89.9]	55.3 [93.0]

The difference between structures (IX*d*) and (XI*g*) is so large that I_v drops to 54.3%. This rather low value indicates the borderline between isostructurality and homostructurality (Kálmán *et al.*, 1993). Although the sum of host and guest volumes is similar ($I_v^{max} = 95.3\%$), as is the relative arrangement of molecules, the condition of molecular *isometricity* is poorly satisfied. The relatively small packing coefficient of 0.66 for both structures also suggests that they can be considered as distortions of the more ideal binary packing of (X) in opposite directions.

Ung *et al.* (1994) reported on other cocrystalline compounds of (IX) and (X) which are expected to be either isostructural or homostructural with those discussed above on the basis of their X-ray powder patterns. In the 2:1 clathrate of (IX) with hydroquinone the guest molecule occupies the place of two phenol molecules without altering the packing motif. The *c* axis, however, shortens from ~20 to ~16 Å, thus the resulting structure is only homostructural with the others. A detailed description of the factors determining these structures, which is beyond the scope of this paper, has already been given (Ung *et al.*, 1994).

5. Conclusions

The limitations of the isostructurality index I_i (4) lead us to introduce a new measure of isostructurality I_v (5), which is based on the overlap of molecular volumes. This new descriptor extends the scope of isostructurality studies to the analysis of weakly isostructural, non-orthogonal, heteromolecular and disordered structures also. The results of such an investigation provide useful data for interpreting the close-packing rules.

The results for 9-alkylthiophenanthrenes show that a stepwise homologous extension of a molecule can either result in an increase of the packing coefficient or displacement of molecules. The former is achieved by inserting the newly added atoms to the space unoccupied by the smaller molecules. If there is no more room for new atoms then molecules are displaced relative to each other, but the isostructurality may still be retained.

In heteromolecular crystals the roles of host and guest changes were studied using volumetric isostructurality indices. From I_v values information was extracted on the stiffness of intermolecular interactions and on the degree and structural consequences of alterations in host–guest complementarity.

Presumably, isostructurality calculations accompanied by a careful structural interpretation of the results may become a useful tool in understanding the factors determining a series of related crystal structures.

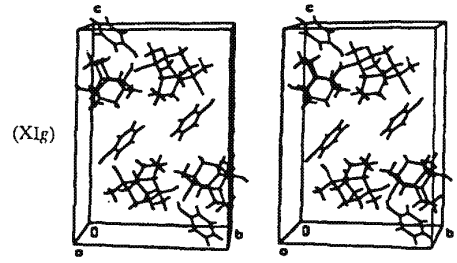


Fig. 6. Crystal structure of 2,8-dimethyltricyclo[5.3.1.1^{3,9}]dodecane-*syn*-2,*syn*-8-diol phenol solvate (XI*g*).

APPENDIX A
The application of Löwdin orthogonalization for crystal structures

The symmetric orthogonalization method (Löwdin, 1950) is well known among quantum chemists and is usually described in textbooks of quantum chemistry (*e.g.* Szabo & Ostlund, 1982). It transforms a set of non-orthogonal, *i.e.* overlapping set of vectors $\{\mathbf{a}_i\}$ to an orthonormal vector set $\{\mathbf{x}_i\}$ that fulfills the equations:

$$\mathbf{x}_i \cdot \mathbf{x}_j = \delta_{ij},$$
$$\sum_i |\mathbf{x}_i - \mathbf{a}_i|^2 \rightarrow \min. \qquad (8)$$

To apply this procedure for cell axes let us define $\{\mathbf{a}_i\}$ as the set of unit cell translation vectors. Let us form the metric tensor $\mathbf{S}$, where $S_{ij} = \mathbf{a}_i \cdot \mathbf{a}_j$. The orthogonal directions (vectors of unit length) that are closest to the directions of the original vectors can then be obtained as

$$\mathbf{x}_i = \sum_j (\mathbf{S}^{-1/2})_{ji} \mathbf{a}_j, \qquad (9)$$

where $\mathbf{S}^{-1/2}$ is the matrix for which $\mathbf{S}^{-1/2} \cdot \mathbf{S}^{-1/2} = \mathbf{S}^{-1}$, *i.e.* its square equals to the inverse of $\mathbf{S}$. The orthogonalized cell axis lengths are calculated as the dot product of the original vectors and the corresponding orthonormal ones, *i.e.* as the projection of the original axes to the orthogonal directions.

$$a_i^{orth} = \mathbf{x}_i \cdot \mathbf{a}_i = \left(\sum_j (\mathbf{S}^{-1/2})_{ji} \mathbf{a}_j \right) \cdot \mathbf{a}_i$$
$$= \sum_j (\mathbf{S}^{-1/2})_{ji} S_{ji} \qquad (10)$$

UM00013290
NOVARTIS EXHIBIT 1517
Novartis v. Regents, IPR2023-01347
Page 2036 of 4460

Unfortunately, the eigenvectors and eigenvalues of **S** are needed for the calculation of $\mathbf{S}^{-1/2}$ and we were unable to derive a formula to obtain them from the unit-cell parameters. Thus, the calculation can only be performed numerically, *e.g.* with the aid of a computer algebra package.†

To illustrate the application of this method in the calculation of Π, we describe the Löwdin orthogonalization of the cell parameters of (I) (Table 2).

$$a = 9.054\ \text{Å} \quad b = 20.644\ \text{Å} \quad c = 6.659\ \text{Å}$$
$$\alpha = 90° \quad \beta = 98.10° \quad \gamma = 90°$$

In this case the metric tensor can be calculated as:

$$\mathbf{S} = \begin{pmatrix} a^2 & ab\cos\gamma & ac\cos\beta \\ ab\cos\gamma & b^2 & bc\cos\alpha \\ ac\cos\beta & bc\cos\alpha & c^2 \end{pmatrix} = \begin{pmatrix} 81.975 & 0 & -8.495 \\ 0 & 426.175 & 0 \\ -8.495 & 0 & 44.342 \end{pmatrix}$$

In order to calculate the $-1/2$ power of **S**, we write it as a product of three matrices (eigenvalue decomposition)

$$\mathbf{S} = \mathbf{U}\mathbf{D}\mathbf{U}^T = \begin{pmatrix} 0.978 & 0 & 0.210 \\ 0 & 1 & 0 \\ -0.210 & 0 & 0.978 \end{pmatrix} \times \begin{pmatrix} 83.804 & 0 & 0 \\ 0 & 426.175 & 0 \\ 0 & 0 & 42.514 \end{pmatrix} \times \begin{pmatrix} 0.978 & 0 & -0.210 \\ 0 & 1 & 0 \\ 0.210 & 0 & 0.978 \end{pmatrix},$$

where **D** has the eigenvalues of **S** in its diagonals, whereas **U** contains the eigenvectors of **S** as column vectors.

The $-1/2$ power of **D** is obtained by taking the square root of the reciprocal of the diagonal elements.

† A utility to perform this calculation in the *MuPAD* computer algebra system, which is free for non-commercial users (http://www.mupad.de), is available from the authors on request. An orthogonalization program is also available as C++ source code or as Linux/i386 or SGI IRIX executable.

$$\mathbf{D}^{-1/2} = \begin{pmatrix} 1/(83.804)^{1/2} & 0 & 0 \\ 0 & 1/(426.175)^{1/2} & 0 \\ 0 & 0 & 1/(42.514)^{1/2} \end{pmatrix} = \begin{pmatrix} 0.1092 & 0 & 0 \\ 0 & 0.04844 & 0 \\ 0 & 0 & 0.1534 \end{pmatrix}$$

$\mathbf{S}^{-1/2}$ can now be determined as

$$\mathbf{S}^{-1/2} = \mathbf{U}\mathbf{D}^{-1/2}\mathbf{U}^T = \begin{pmatrix} 0.978 & 0 & 0.210 \\ 0 & 1 & 0 \\ -0.210 & 0 & 0.978 \end{pmatrix} \times \begin{pmatrix} 0.1092 & 0 & 0 \\ 0 & 0.04844 & 0 \\ 0 & 0 & 0.1534 \end{pmatrix} \times \begin{pmatrix} 0.978 & 0 & -0.210 \\ 0 & 1 & 0 \\ 0.210 & 0 & 0.978 \end{pmatrix} = \begin{pmatrix} 0.1112 & 0 & 0.0091 \\ 0 & 0.04844 & 0 \\ 0.0091 & 0 & 0.1514 \end{pmatrix}.$$

Finally, the orthogonalized axes are calculated according to (10).

$$a^{orth} = \sum_{j=1}^{3} (\mathbf{S}^{-1/2})_{j1} S_{j1} = 0.1112 \times 81.975 + 0 \times 0 + 0.0091 \times (-8.495) = 9.038$$

$$b^{orth} = \sum_{j=1}^{3} (\mathbf{S}^{-1/2})_{j2} S_{j2} = 0 \times 0 + 0.04844 \times 426.175 + 0 \times 0 = 20.644$$

$$c^{orth} = \sum_{j=1}^{3} (\mathbf{S}^{-1/2})_{j3} S_{j3} = 0.0091 \times (-8.495) + 0 \times 0 + 0.1514 \times 44.342 = 6.636$$

The authors thank Mr Gy. Argay for his help. This work was supported by the Hungarian Research Fund (Grant No. OTKA T023212) and the Hungarian Academy of Sciences (AKP Grant No. 96/2–671 2,4/24).

UM00013291
NOVARTIS EXHIBIT 1517
Novartis v. Regents, IPR2023-01347
Page 2037 of 4460

References

Allen, F. H. & Kennard, R. (1993). *Chem. Des. Autom. News*, **8**, 31–37.

Arendonk, R. J. F. M. van, Laarhoven, W. H. & Prick, P. A. J. (1978). *Recl Trav. Chim. Pays-Bas*, **97**, 197–201.

Caira, M. R. (1994). *J. Chem. Cryst.* **24**, 695–701.

Caira, M. R. & Mohamed, R. (1993). *Supramol. Chem.* **2**, 201–207.

Döpp, D., Memarian, H. R., Krüger, C. & Raabe, E. (1989). *Chem. Ber.* **122**, 585–588.

Dunitz, J. D. (1979). *X-ray Analysis and the Structure of Organic Molecules*, pp. 235–240. London: Cornell University Press.

Estrada, M. D. & López-Castro, A. (1991). *Acta Cryst.* C**47**, 1030–1032.

Gavezzotti, A. (1983). *J. Am. Chem. Soc.* **105**, 5220–5225.

Go, K. & Bhandary, K. K. (1989). *Acta Cryst.* B**45**, 306–312.

Kálmán, A., Argay, Gy., Scharfenberg-Pfeiffer, D., Höhne, E. & Ribár, B. (1991). *Acta Cryst.* B**47**, 68–77.

Kálmán, A., Argay, Gy., Zivanov-Stakić, D., Vladimirov, S. & Ribár, B. (1992). *Acta Cryst.* B**48**, 812–819.

Kálmán, A. & Párkányi, L. (1997). *Advances in Molecular Structure Research*, edited by M. Hargittai and I. Hargittai, Vol. 3, pp. 189–226. Greenwich, CT: JAI Press.

Kálmán, A., Párkányi, L. & Argay, Gy. (1993). *Acta Cryst.* B**49**, 1039–1049.

Kansikas, J. & Sipila, K. (1997). *Acta Cryst.* C**53**, 1127–1131.

Karch, N. J., Koh, E. T., Whistel, B. L. & McBride, J. M. (1975). *J. Am. Chem. Soc.* **97**, 6729–6743.

Löwdin, P.-O. (1950). *J. Chem. Phys.* **18**, 365–375.

Rutherford, J. S. (1997). *Acta Chim. Hung.* **134**, 395–405.

Szabo, A. & Ostlund, N. S. (1982). *Modern Quantum Chemistry: Introduction to Advanced Electronic Structure Theory*, pp. 142–144. New York: Macmillan.

Ung, A. T., Bishop, R., Craig, D. C., Dance, I. G. & Scudder, M. L. (1994). *Chem. Mater.* **6**, 1269–1281.

UM00013292

NOVARTIS EXHIBIT 1517
Novartis v. Regents, IPR2023-01347
Page 2038 of 4460

Acta Cryst. (1973). B29, 2549

The Crystal and Molecular Structure of 5-Fluorouracil

BY LAWRENCE FALLON III

Department of Materials Science, University of Virginia, Charlottesville, Virginia 22901, *U.S.A.*

(*Received* 11 *May* 1973; *accepted* 14 *June* 1973)

5-Fluorouracil ($C_4H_3FN_2O_2$) is triclinic, space group $P\bar{1}$, with $a=9{\cdot}22$ (3), $b=12{\cdot}66$ (3), $c=12{\cdot}67$ (3) Å, $\alpha=89{\cdot}7$ (3), $\beta=43{\cdot}9$ (3), $\gamma=98{\cdot}6$ (3)°, $Z=8$. Intensities were measured with an automated diffractometer and Mo $K\alpha$ radiation. Patterson and symbolic addition methods failed to yield a complete solution, but gave a partial structure which was used to supply initial phases to the tangent formula. The complete structure was thus determined in space group $P1$. Least-squares refinement in space group $P\bar{1}$ gave a final R_w of 0·054 and R of 0·092. The unit cell contains two molecular layers, each with four molecules. Structural features of interest include several pseudo-centers of symmetry and several different stacking interactions.

Introduction

The properties of purine and pyrimidine bases are determined to a great extent by their hydrogen and π-bonding systems. Several analog purine and pyrimidine bases have been developed which resemble structurally the natural bases. They alter the base hydrogen and π-bonding characteristics, however, and greatly affect the properties of the nucleic acids containing them. These analog bases have been observed to have inhibitory and mutagenic effects upon the growth of certain tumors. Of the pyrimidine analogs, 5-fluorouracil (FU) is probably the most widely used, and is of great interest in clinical and experimental cancer chemotherapy. The exact mechanism of the inhibitory and mutagenic action of FU is not known, but it is thought to involve (*a*) an inhibition of DNA synthesis, (*b*) an inhibition of the formation of ribosomes, and (*c*) a faulty information transfer within the cell caused by the replacement of uracil by FU in mRNA (Mandel, 1969).

FU bears a close resemblance to uracil (see Fig. 1). Since structural differences, especially differences in stacking interactions, are thought to be important in the activity of halogenated pyrimidines, it is of interest to examine the molecular structure of FU for comparison with the structures of related systems.

Experimental measurements

A crystalline powder of FU (2,4-dioxo-5-fluoropyrimidine) was obtained from the Sigma Chemical Company. This powder quickly dissolves in hot water and, upon evaporation, forms large crystals of FU which are stable transparent prisms showing a pronounced cleavage plane. A crystal approximately 0·1 × 0·2 × 0·4 mm was selected.

Precession, Weissenberg, and rotation photographs were taken at room temperature (~22 °C) with Cu $K\alpha$ radiation. The diffraction symmetry observed from the photographs is $\bar{1}$, and a measured unit cell is $a=9{\cdot}22$ (3), $b=12{\cdot}66$ (3), $c=8{\cdot}79$ (3) Å, $\alpha=80{\cdot}2$ (3), $\beta=90{\cdot}8$ (3), $\gamma=98{\cdot}6$ (3)°, $V=998$ Å^3.

The density measured by pycnometry at room temperature (23·5 °C) was 1·728 g cm^{-3} which may be compared with a calculated value of 1·731 g cm^{-3} for $Z=8$. A piezoelectric test was inconclusive. Because of the large Z, however, the space group was assumed to be $P\bar{1}$ with 4 molecules in the asymmetric unit. Intensities were measured for the equivalent of the asymmetric half of the copper sphere with a Picker four-circle card-controlled diffractometer and Mo $K\alpha$ radiation. Symmetric 2θ scans were used with a rate of 1°/min and a scan width of 2°. Background intensities were counted at each scan limit for 1 min. The net intensity was set equal to the scan count minus the sum of the background counts. Monochromatic radiation was obtained by reflecting the primary beam from 002 of a graphite crystal. During the data collection, the intensities of three standard reflections were measured after each group of fifty data reflections. 4366 independent reflections were measured. A standard error σ_I was calculated for each intensity from

$$\sigma_I=\sqrt{(s+b_1+b_2)}$$

where s is the scan count, and b_1 and b_2 are the two background counts. If an intensity was observed to be less than $2\sigma_I/3$, the reflection was typed as unobserved and assigned the value of $2\sigma_I/3$. 1122 observed and 3244 unobserved reflections were obtained. The Lorentz–polarization correction, adapted for the geometry of the monochromator, was calculated with computer program *DATRDN* of the X-RAY System (1972) of crystallographic computer programs. No absorption correction was made.

Computer program *NORNSF* from the X-RAY System (1972) was used to calculate a set of normalized structure factors. The atomic scattering factors were taken from *International Tables for X-ray Crystallography* (1968). The Wilson plot gave $B=3{\cdot}779$ Å^2 and $K=1{\cdot}1880$. The statistical averages calculated from

UM00013293
NOVARTIS EXHIBIT 1517
Novartis v. Regents, IPR2023-01347
Page 2039 of 4460

the normalized structure factors are listed in Table 1, and yield additional evidence for the space group $P\bar{1}$. The magnitudes of the normalized structure factors show a hypercentric distribution corresponding to the presence of one or more pseudo-centers of symmetry.

Table 1. *Statistical properties of normalized structure factors*

	Experimental	Theoretical Centric	Theoretical Acentric
$\langle\|E\|\rangle$	0·685	0·798	0·886
$\langle\|E\|^2\rangle$	1·000	1·000	1·000
$\langle\|E^2-1\|\rangle$	1·187	0·968	0·736
$\langle\|E^2-1\|^2\rangle$	5·492	2·000	1·000

Structure determination and refinement

In the calculated Patterson map obvious planar features were present. These layers were inclined with respect to the planes of calculation. The unit cell was transformed for greater ease of analysis by the matrix [100/010/101]. The planar layers are then perpendicular to **a*** and parallel to the *bc* plane.

The transformed unit cell used from this point throughout the structure determination has the following parameters: $a=9{\cdot}22$ (3), $b=12{\cdot}66$ (3), $c=12{\cdot}67$ (3) Å, $\alpha=89{\cdot}7$ (3), $\beta=43{\cdot}9$ (3), $\gamma=98{\cdot}6$ (3)°. One of the major features in the Patterson map is a very large peak at (0·477, 0·216, 0·483), indicating that there are a large number of atoms in one layer related by this vector to atoms in the next. Several figures, roughly the expected shape of FU molecules, were observed in the map, but

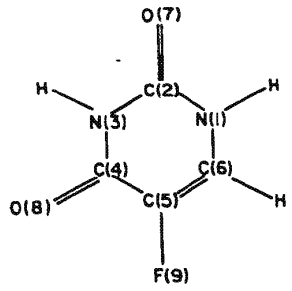


Fig. 1. The chemical structure and numbering system of 5-fluorouracil.

Table 2. *Final atomic coordinates* ($\times 10^4$) *and thermal parameters* ($\times 10^6$)

Thermal parameters listed are coefficients in the temperature factor expression

$$\exp[-2\pi^2(U_{11}h^2a^{*2}+U_{22}k^2b^{*2}+U_{33}l^2c^{*2}+2U_{12}hka^*b^*\cos\gamma^*+2U_{13}hla^*c^*\cos\beta^*+2U_{23}klb^*c^*\cos\alpha^*)].$$

	$x(\sigma)$	$y(\sigma)$	$z(\sigma)$	U_{11}	U_{22}	U_{33}	U_{12}	U_{13}	U_{23}
N(1,1)	2001 (18)	1047 (8)	4717 (13)	50418	45112	35163	7095.	−35201	−8089
C(1,2)	2255 (23)	1482 (12)	3559 (16)	39527	37833	37835	1642	−27595	484
N(1,3)	2306 (17)	2587 (8)	3450 (12)	45952	26448	43926	11720	−35650	−9775
C(1,4)	2152 (23)	3290 (11)	4349 (18)	26267	52310	30936	6067	−17665	−16020
C(1,5)	1972 (23)	2748 (12)	5473 (16)	41886	74185	24433	17180	−25338	−14247
C(1,6)	1859 (23)	1678 (11)	5675 (16)	31463	33463	45413	−3772	−23815	1971
O(1,7)	2369 (16)	918 (6)	2753 (10)	102834	31180	57977	22008	−69201	−14175
O(1,8)	2234 (16)	4268 (6)	4145 (11)	81545	25418	54516	11902	−54447	−3895
F(1,9)	1875 (12)	3428 (5)	6344 (8)	69885	44375	40358	14967	−44138	−5922
N(2,1)	2773 (19)	707 (8)	334 (13)	49206	23521	41030	3721	−34905	−4959
C(2,2)	2840 (24)	9687 (10)	9917 (18)	47517	61746	60526	5148	−44625	−14596
N(2,3)	2774 (18)	9569 (8)	8862 (13)	43070	37315	38681	3439	−33843	4872
C(2,4)	2583 (23)	387 (10)	8259 (17)	35418	17405	41776	−54	−28918	−7749
C(2,5)	2436 (22)	1433 (10)	8828 (16)	29153	43134	26899	−6669	−18433	5158
C(2,6)	2566 (22)	1563 (8)	9814 (16)	14327	26090	32752	−2273	−11909	9222
O(2,7)	2887 (16)	8919 (7)	476 (11)	91528	37303	61244	30130	−66789	−15456
O(2,8)	2428 (16)	225 (6)	7363 (11)	61421	26496	52527	3114	−47955	−1456
F(2,9)	2172 (12)	2213 (5)	8297 (8)	60992	36481	51400	10395	−40802	−1577
N(3,1)	2700 (18)	6737 (7)	763 (12)	38482	29589	32901	7792	−29113	−5893
C(3,2)	2720 (24)	6357 (12)	1772 (17)	20094	28977	44800	6108	−12507	−4605
N(3,3)	2482 (17)	5225 (8)	2039 (12)	38232	25579	55898	12046	−35093	−19043
C(3,4)	2324 (22)	4515 (11)	1259 (15)	27466	51170	9759	−4700	−7598	10082
C(3,5)	2241 (23)	5021 (10)	262 (16)	49644	79118	19124	3793	−26334	−3100
C(3,6)	2435 (24)	6114 (11)	33 (16)	51991	34174	32032	1878	−30479	−5879
O(3,7)	2886 (15)	6935 (6)	2481 (10)	75207	24301	48568	7302	−52808	−2872
O(3,8)	2220 (15)	3535 (6)	1463 (10)	61070	45722	43918	12991	−45002	−4828
F(3,9)	2041 (14)	4303 (5)	9573 (9)	123350	43818	74652	10719	−83557	−8533
N(4,1)	2780 (18)	7135 (7)	4704 (12)	35382	28728	20691	9950	−13882	−7784
C(4,2)	2596 (24)	8110 (11)	5205 (17)	16898	88371	12642	4179	−4295	−1487
N(4,3)	2654 (16)	8245 (8)	6283 (11)	36474	48489	15110	15531	−19672	2376
C(4,4)	2794 (24)	7432 (11)	6956 (18)	30182	20580	64874	2747	−32195	−11548
C(4,5)	3057 (23)	6438 (10)	6264 (18)	40803	43572	50883	23864	−30107	−12403
C(4,6)	2998 (22)	6251 (9)	5257 (16)	34084	52978	42820	16066	−28987	−4113
O(4,7)	2451 (15)	8912 (6)	4724 (10)	52997	40775	37220	5515	−35778	−1541
O(4,8)	2842 (17)	7623 (6)	7847 (11)	67268	32038	38083	10057	−41080	−12063
F(4,9)	3271 (13)	5643 (5)	6829 (9)	90480	23721	70009	11268	−67179	−2093

UM00013294
NOVARTIS EXHIBIT 1517
Novartis v. Regents, IPR2023-01347
Page 2040 of 4460

Patterson methods failed to give a complete solution.

Symbolic addition was next attempted. However, a correct structure was not found in any of the possible *E*-maps. The failure of symbolic addition will be the subject of a future paper.

A considerable amount of information had thus far been accumulated about the structure of FU, even though Patterson and symbolic addition methods did not give the complete structure. Drs Jerome and Isabella Karle suggested to the author that the tangent formula (Karle & Hauptman, 1956) is useful in such situations. Structure factors were calculated with one FU molecule in an orientation consistent with images in the Patterson map and previous *E*-maps. The position of this molecule was unknown with respect to the origin (that is, with respect to a center of symmetry). Space group $P1$ was then chosen as appropriate, and an arbitrary origin was assigned (Karle & Karle, 1971). The calculated phases from the partial structure were accepted if the corresponding $|E|$ was greater than 2·5 and if the calculated structure factor $|F_c|$ was greater than the quantity $0{\cdot}125F_o$. Of the 137 phases corresponding to reflections whose $|E|$ calculated greater than 2·5, 77 were accepted. With the computer program *TANGEN* from the X-RAY System (1972) the tangent formula generated a total of 318 phases for the normalized structure factors greater than 1·8. If the initial 77 phases were allowed to refine during these calculations, the resultant *E*-map was unintelligible. If the initially accepted phases were held constant throughout, and only the others allowed to refine, the *E*-map then calculated showed the molecule corresponding to the initial partial structure. Also visible was a second molecule, identical in orientation with the first, but translated from it by a vector corresponding to the very large peak in the Patterson map. Structure factors were then calculated with these two molecules. Of the 200 $|E|$'s greater than 2·2, the $|F_c|$ of 105 reflections calculated greater than $0{\cdot}250\ F_o$, and thus were accepted. These were used to generate a total of 429 phases in four cycles of tangent refinement, to an $|E|$ threshold of 1·6. If the 105 initially accepted phases were held constant for the entire four cycles, the *E*-maps calculated showed only the two molecules used to start the phasing. However, when these 105 phases were held fixed for only two cycles and allowed to refine with all the phases for the final two cycles, the *E*-map then contained the whole structure. All the atoms were present as strong peaks in the map. There were very few false peaks and for the most part these were small. The centers of symmetry were easily found in the structure. The atomic coordinates were then translated so that space group $P\bar{1}$ could be used in least-squares refinement.

The coordinates of the 36 atoms in the asymmetric unit were read from the *E*-map and, after translation, were used as input to the least-squares program, *CRYLSQ* from the X-RAY System (1972). All atoms were initially assigned isotropic temperature factors of 3·0 Å^2. The scale factor calculated by *NORMSF*, $K=1{\cdot}1880$, was also used initially. The first few cycles of least-squares refinement used only the 876 largest reflections. No corrections were made for anomalous dispersion or extinction. Before the first cycle, R, calculated from $R=\sum||F_o|-|F_c||/\sum|F_o|$, was 0·348. Six cycles reduced it to 0·111. A difference synthesis indicated that anisotropic refinement was necessary. After two cycles R was reduced to 0·080. The full data set was used in further refinement cycles. Each structure factor was weighted by $w=1/\sigma_F{}^2$ where

$$\sigma_F=\left(|F_o|^2+\frac{\sigma(I)}{\mathrm{Lp}}\right)^{1/2}-|F_o|\,.$$

R_w was calculated with the observed reflections from $R_w=\sum w(|F_o|-|F_c|)^2/\sum w|F_o|^2$.

After two more cycles of anisotropic refinement R_w dropped to 0·068. The 3244 unobserved reflections contributed to the parameter shifts only if they calculated greater than their observed value. It was decided that the structure had refined enough to attempt to find the hydrogen atoms. A difference synthesis showed no features with a peak height greater than 0·75 e Å^{-3}. Peaks were located which corresponded to likely positions for all the hydrogen atoms except one. After 4 cycles of least squares, it became obvious that the hydrogen atoms were moving to geometrically unfavorable positions. These atoms were then removed from the refinement. Because $||F_o|-|F_c||$ was excessively large, 14 reflections were removed. This left 1109 observed and 3243 unobserved reflections. After two more

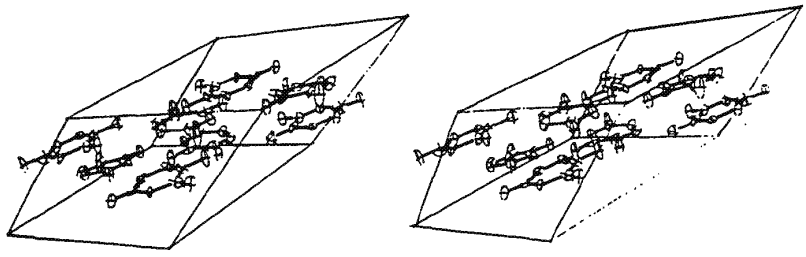


Fig. 2. Stereoscopic view of unit cell. Atoms are represented by thermal ellipsoids drawn to 50% probability.

UM00013295
NOVARTIS EXHIBIT 1517
Novartis v. Regents, IPR2023-01347
Page 2041 of 4460

cycles with the 36 atoms of the asymmetric unit refining anisotropically, R_w fell to a final value of 0·054. The final value of R was 0·092. During the last cycle of least-squares calculations the average shift per error was 0·683 and the largest was 8·203. Final atomic parameters with their standard deviations are listed in Table 2. The final scale factor is $K = 1·26$ (6). Atoms are designated by symbols of the form $A(m,n)$ where

Table 3. *Observed and calculated structure factors*

Columns are h, $10F_o$, $10F_c$. Unobserved reflections are marked by *.



UM00013296
NOVARTIS EXHIBIT 1517
Novartis v. Regents, IPR2023-01347
Page 2042 of 4460

Table 3 (*cont.*)



A is the atom type, *m* refers to the number of the molecule in the asymmetric unit, and *n* refers to the atom position within a molecule as shown in Fig. 1. Observed and calculated structure factors after the last refinement cycle are given in Table 3.

Discussion of the structure

A stereoscopic view of the contents of the unit cell, drawn by computer program *ORTEP* (Johnson, 1965), is shown in Fig. 2. Atoms are represented by thermal

UM00013297
NOVARTIS EXHIBIT 1517
Novartis v. Regents, IPR2023-01347
Page 2043 of 4460

ellipsoids drawn to 50% probability. Bond lengths and angles, listed in Table 4, are similar to FU molecular dimensions determined earlier (Kim & Rich, 1967; Voet & Rich, 1969).

The structural information earlier deduced from the Patterson map and the reflection statistics is indeed present: the two layers in the unit cell are identical and are translated with respect to one another by a non-lattice translation vector corresponding to the very large peak in the Patterson map; and each layer contains several pseudo-centers of symmetry (Fig. 3). The molecules within each layer are arranged in a way that suggests a fourfold rotation axis in projection. This symmetry is destroyed in three dimensions when the layers stack upon each other.

Hydrogen bonds are drawn as dashed lines in Fig. 3. The molecules in each layer are hydrogen bonded to one another using all probable bonding sites. The lengths of these bonds (Table 5) are similar to those observed in other structures of this type.

The molecules are hydrogen bonded in a ring around the apparent fourfold axis within each layer. This kind of pattern has been observed in several other structures involving purines and pyrimidines. Hydrogen bonding in uracil (Parry, 1954) is different from this scheme,

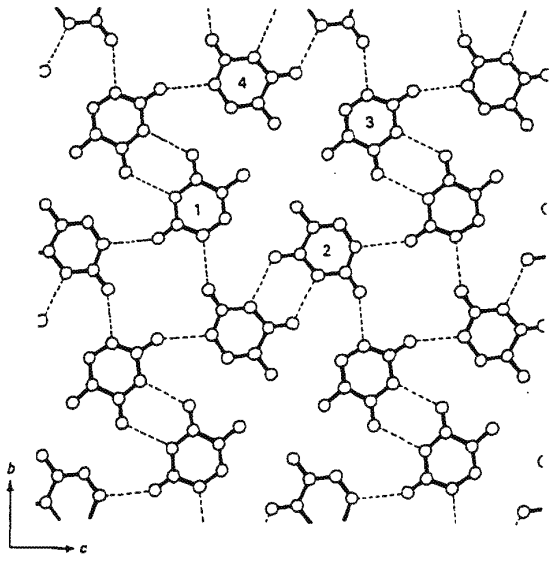


Fig. 3. View of one molecular layer. This drawing contains the equivalent of nearly four unit cells.

Table 4. *Bond lengths and angles*

Atoms are labeled as shown in Fig. 1.

Central atom	Atom 1	Atom 3	Molecule 1	Molecule 2	Molecule 3	Molecule 4
N(1)	C(2)		1·40 (3)	1·39 (2)	1·38 (3)	1·37 (2)
	C(6)		1·39 (3)	1·37 (3)	1·35 (3)	1·43 (3)
	C(2)	C(6)	122 (1)	124 (2)	125 (1)	122 (2)
C(2)	N(1)		1·40 (3)	1·39 (2)	1·38 (3)	1·37 (2)
	N(3)		1·40 (2)	1·39 (4)	1·42 (2)	1·42 (3)
	O(7)		1·20 (3)	1·23 (3)	1·24 (3)	1·26 (3)
	N(1)	N(3)	116 (2)	116 (2)	117 (2)	119 (1)
	N(1)	O(7)	121 (2)	123 (2)	124 (1)	124 (2)
	N(3)	O(7)	123 (2)	121 (2)	118 (2)	118 (1)
N(3)	C(2)		1·40 (2)	1·39 (4)	1·42 (2)	1·42 (3)
	C(4)		1·39 (3)	1·39 (3)	1·41 (3)	1·41 (3)
	C(2)	C(4)	127 (2)	124 (1)	122 (2)	125 (1)
C(4)	N(3)		1·39 (3)	1·39 (3)	1·41 (3)	1·41 (3)
	C(5)		1·46 (4)	1·49 (2)	1·47 (3)	1·49 (2)
	O(8)		1·24 (2)	1·26 (3)	1·24 (2)	1·19 (3)
	N(3)	C(5)	112 (1)	115 (2)	115 (1)	110 (2)
	N(3)	O(8)	122 (2)	122 (1)	120 (2)	120 (1)
	C(5)	O(8)	126 (2)	123 (2)	125 (2)	129 (2)
C(5)	C(4)		1·46 (4)	1·49 (2)	1·47 (3)	1·49 (2)
	C(6)		1·35 (2)	1·35 (4)	1·37 (2)	1·34 (4)
	F(9)		1·36 (2)	1·34 (2)	1·34 (2)	1·35 (3)
	C(4)	C(6)	125 (2)	121 (2)	122 (2)	128 (2)
	C(4)	F(9)	113 (1)	116 (2)	113 (1)	112 (2)
	C(6)	F(9)	122 (2)	123 (1)	125 (2)	120 (1)
C(6)	N(1)		1·39 (3)	1·37 (3)	1·35 (3)	1·43 (3)
	C(5)		1·35 (2)	1·35 (4)	1·37 (2)	1·34 (4)
	N(1)	C(5)	118 (2)	119 (1)	118 (2)	116 (1)
O(7)	C(2)		1·20 (3)	1·23 (3)	1·24 (3)	1·26 (3)
O(8)	C(4)		1·24 (2)	1·26 (3)	1·24 (2)	1·19 (3)
F(9)	C(5)		1·36 (2)	1·34 (2)	1·34 (2)	1·35 (3)

UM00013298
NOVARTIS EXHIBIT 1517
Novartis v. Regents, IPR2023-01347
Page 2044 of 4460

Table 5. *Hydrogen-bond lengths*

N(1,1)···O(4,7)	2·80 (2) Å
N(1,3)···O(3,8)	2·84 (3)
N(2,1)···O(1,7)	2·83 (3)
N(2,3)···O(4,8)	2·77 (2)
N(3,1)···O(2,7)	2·75 (1)
N(3,3)···O(1,8)	2·77 (3)
N(4,1)···O(3,7)	2·76 (3)
N(4,3)···O(2,8)	2·82 (2)

however. In uracil, one oxygen atom forms two hydrogen bonds to nitrogen atoms in neighboring molecules while the other forms no hydrogen bonds at all.

Unfortunately, hydrogen-bonding data on the other halogenated uracils are not yet available.

Another interesting feature of the FU structure, also shown in Fig. 3, is the localization of several fluorine atoms in the same area. Such a highly electronegative concentration is somewhat unusual. These fluorine-to-fluorine distances are given in Table 6.

Table 6. *Fluorine-to-fluorine distances for atoms within the same layer*

F(1,9)···F(2,9)	3·11 (2) Å
F(2,9)···F(3,9)	3·08 (1)
F(3,9)···F(4,9)	3·15 (2)
F(4,9)···F(1,9)	3·16 (1)

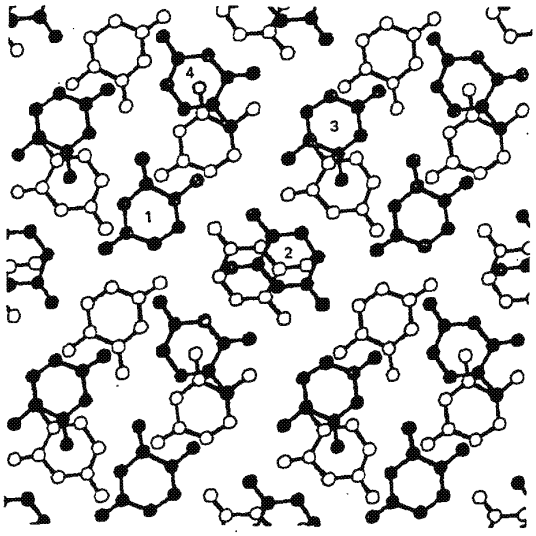


Fig. 4. Projection of molecular layer at $x\sim-\frac{1}{4}$ and layer at $x\sim\frac{1}{4}$ onto (100). Black circles represent atoms in layer at $x\sim\frac{1}{4}$.

The overlap of molecular layers is shown in two views. In Fig. 4 the molecular layer at $x\sim\frac{1}{4}$ is illustrated with the layer at $x\sim-\frac{1}{4}$. Fig. 5 shows the layer at $x\sim\frac{3}{4}$ with the layer at $x\sim\frac{1}{4}$. Several types of stacking interaction are visible. In general, there is very little actual base overlap. This is typical of halogenated analogs (Bugg, Thomas, Sundaralingam & Rao, 1971). The fluorine atoms in molecules 1, 2 and 4 interact with ring atoms of type N(1) or C(5) in bases above or below them. This is also typical of halogenated analog structures. The fluorine atom in molecule 3, however, does not appear to interact with any atoms in layers above or below it, and it has no approaches less than 3·5 Å in these layers. In many cases, there are polar groups (C=O) positioned over parallel rings, but in no case does the uracil-type stacking interaction occur (Parry, 1954). This interaction involves the positioning of an N–H group over the ring of an adjacent base.

Several of the closest interlayer distances are listed in Table 7. Of special interest here are the fluorine–nitrogen distances. The distance between atom F(1,9) in the layer at $x\sim\frac{1}{4}$ and atom N(3,1) in the layer at $x\sim-\frac{1}{4}$ is especially small (2·96 Å), and suggests a strong interaction. It is possible that these fluorine–nitrogen interactions cause a disordering of several of the hydrogen-atom positions resulting in difficulty in the refinement of some of the hydrogen positional parameters.

It is unfortunate that quantitative data on the stacking of 5-chloro-, 5-bromo-, and 5-iodo-uracil are not yet available, since the comparisons would be interesting. From preliminary results by Freeman, Chastain & Bugg (1970), we know that chloro- and bromo-uracil are nearly isostructural and stack so that the halogen has close contact with an atom of the ring of a parallel base. They have also reported that iodouracil stacking is like non-halogenated pyrimidine derivatives; that is, with a polar group overlapping an adjacent base. A comparison of the various stacking patterns in the FU structure seems to indicate that FU stacking patterns, themselves, are not as specific as we might have believed earlier, but that certain characteristic interactions do occur.

Conclusion

It is believed that halogenated pyrimidine derivatives effect base-stacking interactions in ways that may cause changes in possible hydrogen-bonding geometry. For example, in some cases normal Watson–Crick base pairing could be destroyed. These altered interactions

Table 7. *Interlayer distances*

Atom 1 at $x\sim\frac{1}{4}$	Atom 2 at $x\sim\frac{1}{4}$	Distance (Å)	Atom 1 at $x\sim\frac{1}{4}$	Atom 2 at $x\sim-\frac{1}{4}$	Distance (Å)
F(1,9)	C(4,5)	3·21 (2)	F(1,9)	N(3,1)	2·96 (1)
F(1,9)	F(4,9)	3·16 (1)	F(1,9)	C(3,2)	3·09 (2)
F(2,9)	N(4,1)	3·18 (1)	F(2,9)	N(2,3)	3·46 (1)
F(4,9)	C(1,4)	3·27 (2)	F(4,9)	C(3,5)	3·44 (2)

Distances less than 3·3 Å and which involve fluorine atoms are listed. Two distances greater than 3·3 Å are listed since they are the only approaches that the fluorine atoms make in that direction. Atom F(3,9) makes no interlayer approaches less than 3·5 Å.

UM00013299
NOVARTIS EXHIBIT 1517
Novartis v. Regents, IPR2023-01347
Page 2045 of 4460

could be connected with activity of FU in some situations, for example when FU is substituted into RNA. The variety of stacking interactions observed in the FU structure demonstrates that a particular stacking geometry seems to be affected by a number of external constraints. The matter is therefore not simple, and it is difficult to generalize about the stacking geometry of FU in other environments. Interactions as strong as those observed between fluorine atoms and nitrogen atoms of adjacent pyrimidine rings have no counterpart in naturally occuring purine or pyrimidine bases. These kinds of interaction should be investigated further, since they are liable to recur in various environments and could be connected with the mutagenic action of FU.

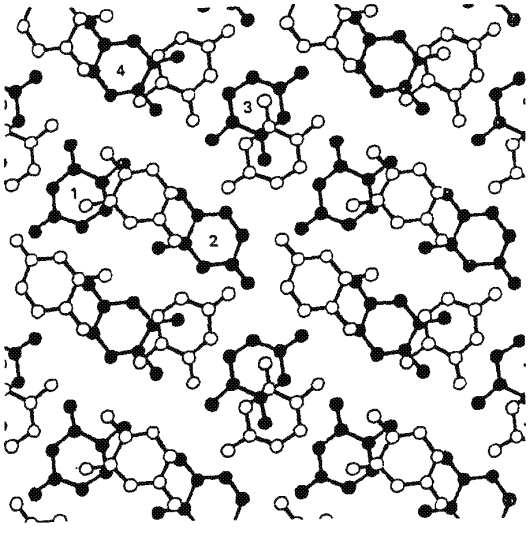


Fig. 5. Projection of molecular layer at $x \sim \frac{1}{4}$ and layer at $x \sim \frac{1}{4}$ onto (100). Black circles represent atoms in layer at $x \sim \frac{1}{4}$.

The author is indebted to Dr Fredrik A. Muller and to Dr Roger Hanscom for their suggestions and assistance. Additional advice which proved critical in yielding a solution to this problem was given by Drs Jerome and Isabella Karle. Support of the research program by USPHS Research Grant DE 02111 from the National Institute of Dental Research, National Institutes of Health, Bethesda, Maryland is also gratefully acknowledged.

References

BUGG, C. E., THOMAS, J. M., SUNDARALINGAM, M. & RAO, S. T. (1971). *Biopolymers*, **10**, 175–219.
FREEMAN, G. R., CHASTAIN, B. & BUGG, C. E. (1970). Amer. Cryst. Assoc. Meeting Program and Abstracts. Paper B7, p. 26.
International Tables for X-ray Crystallography. (1968). Vol. III, pp. 201–209. Birmingham: Kynoch Press.
JOHNSON, C. K. (1965). *ORTEP*. Report ORNL–3794, Oak Ridge National Laboratory, Oak Ridge, Tennessee.
KARLE, J. & HAUPTMAN, H. (1956). *Acta Cryst.* **9**, 635–651.
KARLE, I. L. & KARLE, J. (1971). *Acta Cryst.* **B27**, 1891–1898.
KIM, SUNG-HOU & RICH, A. (1967). *Science*, **158**, 1046–1048.
MANDEL, H. G. (1969). *Prog. Mol. Subcell. Biol.* **1**, 82–135.
PARRY, G. S. (1954). *Acta Cryst.* **7**, 313–320.
VOET, D. & RICH, A. (1969). *J. Amer. Chem. Soc.* **91**, 3069–3075.
X-ray System (1972). Technical Report TR–192 of the Computer Scince Center, Univ. of Maryland. Version of June, 1972.

Acta Cryst. (1973). B**29**, 2556

The Crystal Structure of $KIBr_2.H_2O$

BY STUART SOLED AND GENE B. CARPENTER

Metcalf Chemical Laboratories, Brown University, Providence, Rhode Island 02912, *U.S.A.*

(*Received* 9 *June* 1973; *accepted* 11 *June* 1973)

Crystals of potassium dibromoiodide monohydrate, $KIBr_2.H_2O$, are orthorhombic, space group *Pnnm*, with $a = 12{\cdot}183$ (5), $b = 13{\cdot}046$ (5), $c = 4{\cdot}390$ (3) Å, $Z = 4$. All atoms lie on mirror planes. The structure was refined from diffractometer data by least-squares methods to $R = 5{\cdot}8\%$. The structure consists of nearly linear chains of halogen atoms extending infinitely along **b**. The two independent IBr_2^- anions are linear and symmetrical, both with I–Br bond lengths of 2·71 Å. The closest O···Br distance is 3·60 Å, indicative of weak hydrogen bonding.

Introduction

Wells, Wheeler & Penfield (1892) were the first to report preparing 'potassium dibromoiodide'. Later, Cremer & Duncan (1932) proved by measurements of dissociation pressures that both hydrated and anhydrous versions of the compound exist. Although single-crystal X-ray studies of compounds containing triiodide

UM00013300
NOVARTIS EXHIBIT 1517
Novartis v. Regents, IPR2023-01347
Page 2046 of 4460

(14) Å, $\beta = 96.16\ (7)°$, $V = 3525$ Å^3, and $Z = 4$. The measured density was 1.585 g/cm^3, yielding a measured formula weight of 841.2. The calculated formula weight of $[Ph_4As^+]$ III′ is 817.3.

Preparation of IV. In a typical reaction, $[Et_3BH]Li$ (6 mmol) was added to $Fe(CO)_5$ (5 mmol) in 20 mL of hexane at 0 °C and stirred for 10 min. Commercial BH_3·THF (10 mmol) was added over a period of several minutes, causing the color of the reaction solution to change from pale yellow to dark brown. After the solution was stirred at 0 °C for 1.5 h, the solvent was removed at room temperature, leaving a brown solid residue. This was acidified with H_3PO_4 (25 mL, 40% aqueous), and the neutral ferraborane and hydrocarbyl products were extracted with hexane (3 × 25 mL), yielding a brown–green solution. Subsequent extractions contained mainly $Fe_3(CO)_{12}$. The orange ferraborane IV was separated from the product mixture as the third fraction by column chromatography (hexane) carried out at −40 °C: MS, m/e P$^+$ 450 (−9CO), $^{56}Fe_2{}^{12}C_{10}{}^{16}O_9{}^{11}B^1H_7$ measd 449.823, calcd 449.823; IR ν_{CO} (hexane, cm^{-1}) 2095 m, 2064 sh, 2057 vs, 2044 s, 2037 vs, 2025 vs, 2015 s, 2006 m, 1982 m; ^{1}H NMR (CD_2Cl_2, −80 °C) δ 1.03 (s, 3 H), −14.6 (br, 3 H), −24.0 (s, 1 H); ^{11}B NMR (hexane, 20 °C) δ 22.1 (quintet, $J_{BH} = 40$ Hz).[34]

Preparation of IV′. Deprotonation of IV was carried out by stirring a hexane solution (20 mL) of the neutral ferraborane with a solution of Ph_4AsCl (or PPNCl) in methanol. The hexane layer was rapidly decolorized, and the methanol layer became deep red. After the methanol layer was separated, the methanol was removed and the residue extracted with ether. Removal of the ether yielded the final product: IR ν_{CO} (THF, cm^{-1}) 2045 m, 2000 vs, 1978 vs, 1956 vs, 1935 m; ^{1}H NMR ($CD_3C(O)CD_3$, 20 °C) δ 7.87 (m, 20 H), Ph_4As^+ 1.09 (s, 3 H), −12.9 (br, 3 H); ^{11}B NMR ($CD_3C(O)CD_3$, 20 °C) δ 29.3 (br q, $J_{BH} = 53$ Hz).

(34) Significant amounts of the ethyl derivative are formed as well, but little III is observed.

Acknowledgment. The support of the National Science Foundation under Grant CHE 8408251 and the Petroleum Research Fund, administered by the American Chemical Society, is gratefully acknowledged. We thank Reynaldo Barreto for the UV–vis spectrum and Grant B. Jacobsen and Fung-E. Hong for assistance with the preparative work and NMR studies.

Registry No. III, 92055-43-1; III′, 101810-38-2; III$[Ph_4As^+]$, 101810-39-3; IV, 101834-61-1; IV′$[Ph_4As^+]$, 101810-41-7; $[(CO)_4FeC(O)CH_3]Na$, 64867-63-6; $[(CO)_4FeC(O)CH_3]PPN$, 36464-58-1; $Fe(CO)_5$, 13463-40-6; $[Et_3BH]Li$, 22560-16-3; BH_3·THF, 14044-65-6.

Supplementary Material Available: Listing of observed and calculated structure factor amplitudes, thermal parameters, and the packing diagram (10 pages). Ordering information is given on any current masthead page.

Chiral Separation of Heterocyclic Drugs by HPLC: Solute–Stationary Phase Base-Pair Interactions

Binyamin Feibush,*† Alvaro Figueroa, Rosita Charles,‡ Kay D. Onan, Pnina Feibush, and Barry L. Karger*

Contribution from the Barnett Institute and Department of Chemistry, Northeastern University, Boston, Massachusetts 02115. *Received October 28, 1985*

Abstract: Hydrogen bonding between a chromatographic stationary phase and several classes of drug molecules has been explored as a means to effect HPLC chiral separation. *N,N′*-2,6-Pyridinediylbis[alkanamides] have been shown by NMR and X-ray diffraction to be complementary to the drug classes of interest and to form a highly specific triple hydrogen bond complex. A derivative of optically active *N,N′*-2,6-pyridinediylbis[(*S*)-2-phenylbutanamide] was bonded to silica gel and used in an HPLC column to separate racemic mixtures of barbiturates (**1**), glutarimides (**3**), and hydantoins (**4**). Mechanistic models of chiral resolution are suggested for these three classes of drugs. No chiral separation was effected for succinimides (**5**). Methylation of an imido nitrogen of these drugs resulted in disruption of the complementarity; therefore, such *N*-methyl derivatives were unretained by the column. This type of bonded phase would appear to offer high potential for separation of closely related species.

Hydrogen bonds are one of the key factors through which a biological system "recognizes" another system on a molecular level. For example the well-known double helix structure of double-stranded DNA is formed by hydrogen bonding between complementary pairs of purine and pyrimidine bases on the two polynucleotide strands. Pairs of these heterocyclic bases can form a hydrogen bonded complex only if there is an appropriate juxtaposition of acid/base character and if complementary functionalities are coplanar and in the correct orientation.

Broad classes of drugs have structural similarities to the bases found in nucleic acids. For example, as shown in Figure 1, glutarimides, barbiturates, succinimides, and hydantoins have similarities to uracil and thymine. These drugs form associates with adenine similar to those found in the base pairs of adenine–thymine and adenine–uracil.[1] Such associations with adenine and its derivatives have been suggested to be in part the basis of the pharmacological activity of these drugs.[2] In addition, IR studies have shown that barbiturates can displace derivatives of uracil or thymine from associates with 9-ethyladenine; however, no pairing of the barbiturates was detected with the other bases.[1] In similar studies, the glutarimides, hydantoins, and succinimides were demonstrated to complex with adenine and not with the other bases.[3] Recent studies employing IR, near IR, and proton NMR have further explored the displacement of thymine from adenine by barbiturates.[4] Such interactions have been proposed to be important in anaesthesia.[5]

The use of hydrogen bonding associates for achievement of separation in chromatography is well established, in both gas chromatography[6,7] and liquid chromatography.[8,9] Moreover,

† Supelco Inc., Bellefonte, PA.
‡ Department of Organic Chemistry, Weizmann Institute of Science, Rehovot, Israel.

(1) Kyogoku, Y.; Lord, R. C.; Rich, A. *Nature (London)* **1968**, *218*, 69–72.
(2) Bush, M. T. *Physiological Pharmacology*; Academic: New York, 1963; Vol. I, p 185–218.
(3) Yu, N. T.; Kyogoku, Y. *Biochim. Biophys. Acta* **1973**, *331*, 21–26.
(4) Buchet, R.; Sandorfy, C. *J. Phys. Chem.* **1984**, *88*, 3274–3288.
(5) Buchet, R.; Sandorfy, C. *J. Phys. Chem.* **1983**, *87*, 275–280.
(6) Gil-Av, E.; Feibush, B.; Charles, R. *Tetrahedron Lett.* **1966**, 1009–1015.

0002-7863/86/1508-3310$01.50/0 © 1986 American Chemical Society

UM00013301
NOVARTIS EXHIBIT 1517
Novartis v. Regents, IPR2023-01347
Page 2047 of 4460

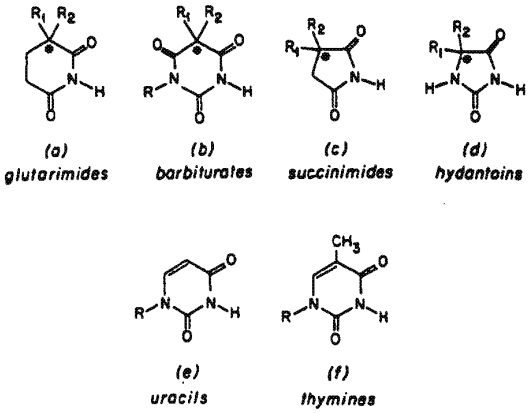


Figure 1. General structure of classes of heterocyclic compounds of pharmacological interest examined in this work, as well as the structure of bases thymine and uracil.

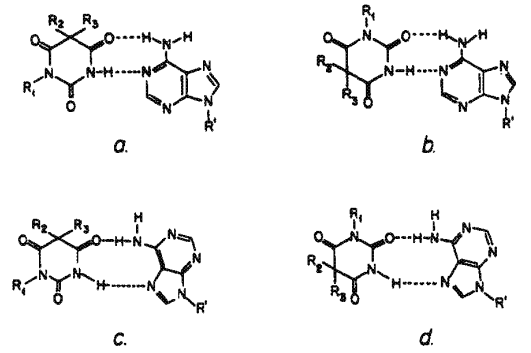


Figure 2. Four different pairing modes between 9-alkyladenine and a barbiturate.

differential hydrogen bond association of enantiomers is a well-established principle of chiral recognition.[10,11] The classes of drugs in Figure 1 have in general not been resolved as optical isomers in this manner; however, work using a polymerized chiral substituted acrylamide has been presented,[12] and enantiomers of hydantoins and succinimides have been resolved on charge-transfer chiral stationary phases.[13] In addition, no functional groups exist on these drugs to allow simple formation of diastereomeric derivatives for separation although some attempts have been carried out;[14] hence, specially designed chiral phases must be developed for separation. The purpose of this paper is to explore the possibility of using the specificity of hydrogen bonding in the HPLC chiral separation of the broad classes of drugs listed in Figure 1.

Hydrogen bond formation between the drugs and an adenine derivative leads to four possible pairing modes, each with two hydrogen bonds, as shown in Figure 2. Two of these modes, parts a and b, involve Watson–Crick pairing wherein N(1) and the C(6) amino group of adenine interact with the barbiturate. Parts c and d illustrate Hoogsteen[15] pairing, where N(7) and the C(6) amino group of adenine hydrogen bond to the barbiturate.

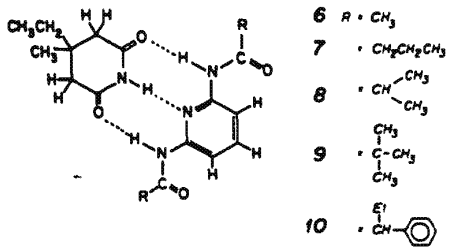


Figure 3. The triple hydrogen bonded complex formed between bemegride (**3e**) and compounds **6–10**.

In solution, all four structures can exist simultaneously, with their relative distribution depending on the various substituents of the drug and the adenine derivative. Given these four competitive possibilities, it can be postulated that the contribution of the complex between a chiral derivative of adenine and the drugs having the highest enantioselectivity might be diminished in favor of complexes of lower selectivity. In this latter case, hydrogen bonding without chiral recognition could occur, leading to a lack of enantiomer separation.

The above argument led us to seek a more specific complementary base in order to increase the possibility of chiral recognition. In particular, we decided to consider the possibility of formation of triple hydrogen bonds between molecules of the drugs in Figure 1 and complementary bases, predicated on the pairing of guanine with cytosine.[16] We selected for base pairing derivatives of *N,N'*-2,6-pyridinediylbis[alkanamide], where the possibility of a triple hydrogen bond exists (see Figure 3). When identical substitution occurs at the two amides only one hydrogen bond complex can form, thus maximizing the possibility of chiral recognition.

An optically active bonded phase attached to silica gel has been synthesized, and chiral recognition has been achieved. The basis of separation in terms of steric interactions of groups attached to the chiral centers of the base pairs is presented. The use of such tailor-made groups provides specificity not only for chiral separation but also for specific structural elements required for association to take place.

Results and Discussion

The design of a base capable of forming a hydrogen bond complex with the drugs shown in Figure 1 requires careful consideration of several factors. In order to achieve the greatest possible specificity, it is desirable first to produce the maximum number of hydrogen bonds between the base pairs, second to produce only one possible base pair structure, and third to bring the centers of chirality of each species in close proximity while still allowing hydrogen bonding to occur.

As discussed in the Introduction, we selected for base pairing derivatives of *N,N'*-2,6-pyridinediylbis[alkanamide] with which a triple hydrogen bond could, in principle, form with an imido functionality, e.g., with bemegride (**3e**) (Figure 3). The *N,N'*-2,6-pyridinediylbis[alkanamide] structure offers the possibility of introducing asymmetry through the R groups for chiral recognition, e.g., solute **10**. Moreover, when identical alkanamide groups are present the molecule possesses a C_2 axis of symmetry; the result is the formation of only one complex. The trans conformation of the amide group aids in the formation of the hydrogen bonds by removing the carbonyl groups from the zone of association; it also forces the chiral centers toward the solute as in Figure 3.

We will first demonstrate that the triple hydrogen bond does indeed form. We synthesized the series of *N,N'*-2,6-pyridinediylbis[alkanamides] listed in Figure 3 and tested for hydrogen bonding using **3e** as a model solute.

(7) Schurig, V. *Angew. Chem., Int. Ed. Engl.* **1984**, *23*, 747–765.
(8) Facklam, Ch.; Pracejus, H.; Oehme, G.; Much, H. *J. Chromatogr.* **1983**, *257*, 118–121.
(9) Oi, N.; Kithara, H. *J. Chromatogr.* **1984**, *285*, 198–202.
(10) Beitler, U.; Feibush, B. *J. Chromatogr.* **1976**, *123*, 149–166.
(11) Dobashi, Y.; Hara, S. *J. Am. Chem. Soc.* **1985**, *107*, 3406–3411.
(12) Blaschke, G. *Angew. Chem., Int. Ed. Engl.* **1980**, *19*, 13–24.
(13) Pirkle, W. H.; Finn, J. M.; Schriner, J. L.; Hamper, B. C. *J. Am. Chem. Soc.* **1981**, *103*, 3964–3966.
(14) Pirkle, W. H., private communication.
(15) Hoogsteen K. *Acta Crystallogr.* **1959**, *12*, 822.
(16) Arnott, S.; Dover, S. D.; Wonacott, A. J. *Acta Crystallogr., Sect. B: Struct. Crystallogr. Cryst. Chem.* **1969**, *B25*, 2192–2206.

UM00013302
NOVARTIS EXHIBIT 1517
Novartis v. Regents, IPR2023-01347
Page 2048 of 4460

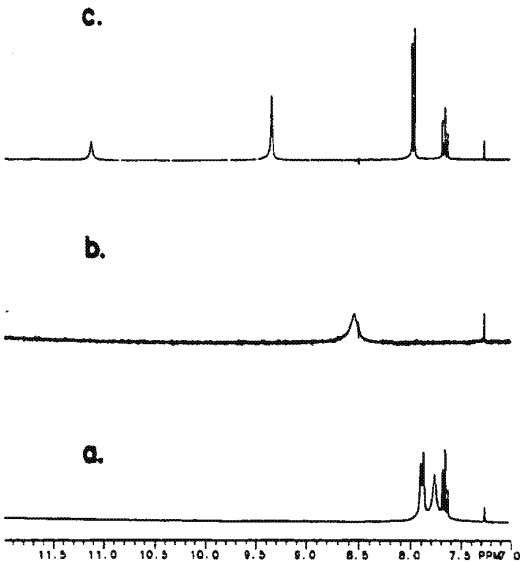


Figure 4. Chemical shifts of the protons participating in the formation of the triple hydrogen bonded complex. Conditions: 0.20 M deuterochloroform solution, 19.5 ±0.5 °C. (a) Spectrum of *N,N'*-2,6-pyridinediylbis[butanamide] (7), δ 7.75 (2 NH); (b) spectrum of bemegride (3e), δ 8.57 (NH); (c) the 1:1 mixtures 3e:7, δ 9.38 (2 NH), 11.15 (NH).

NMR spectra for 1:1 mixtures of 3e with each of the *N,N'*-2,6-pyridinediylbis[alkanamide] were measured. Figure 4 illustrates typical results in $CDCl_3$ for *N,N'*-2,6-pyridinediylbis[butanamide] (7) (Figure 4a), for 3e (Figure 4b), and for a 1:1 mixture of 3e and 7 (Figure 4c). In the mixture, shifts greater than 2 ppm were observed for signals of protons that participate in the hydrogen bonding. Thus, $\delta_{NH} = 8.57$ in 3e and 11.15 in a mixture of 1:1 3e:7, while $\delta_{2(NH)} = 7.75$ in 7 and 9.38 in a mixture of 1:1 3e:7.

Similar deshielding of the 2 NH protons of 6, 8, and 10 and the NH proton of 3e was observed in the respective 1:1 mixtures. These results are as expected for hydrogen bond formation.[17] Moreover, the simultaneous downfield shift of the three protons involved in the hydrogen bonding strongly supports the model of the formation of a triple hydrogen bond complex between 3e and 6, 7, 8, and 10. Note that 10 has a chiral center that will be used to advantage for chiral recognition.

In the case of a 1:1 mixture of 3e and 9 no significant downfield shift was observed. Thus, $\delta_{2(NH)} = 7.76$ in 9 and 7.85 in the 1:1 mixture of 3e:9, while $\delta_{NH} = 8.57$ in 3e and 8.85 in the 1:1 mixture of 3e:9. The triple hydrogen bond does not appear to form in this case. The structural difference between 9 and the other ligands, 6, 7, 8, and 10, is in the two carbons adjacent to the amide groups. These α carbons are tertiary in 9 and either primary or secondary in the others. Evidently, these carbons must be substituted with at least one hydrogen each in order for base-pair complexation to take place.

In order to investigate further the complex formed between 3e and 7, crystals of a 1:1 complex of these species were grown and an X-ray analysis was conducted. The X-ray study unambiguously defines the 1:1 complex of 3e with 7 to be held together by three hydrogen bonds. A perspective view of this complex is shown in Figure 5. The lengths of the hydrogen bonds in the complex 3e:7 (N···N 3.089 (3), O···N 2.943 (4), 2.942 (4) Å) are within the normal range of these types (N···N, N···O) of hydrogen bonds. They are, however, in each case longer than those found in

(17) Silverstein, R. M.; Bassler, G. C.; Morrill, T. C. *Spectrometric Identification of Organic Compounds*, 4th ed.; Wiley: New York, 1982; p 194.

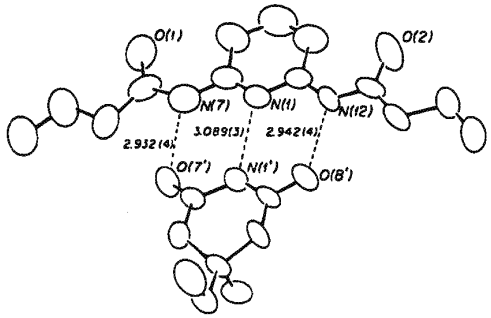


Figure 5. ORTEP drawing of non-hydrogen atoms of the complex 3e:7 with thermal ellipsoids drawn at the 50% probability level. Hydrogen bonds are denoted by dashed lines.

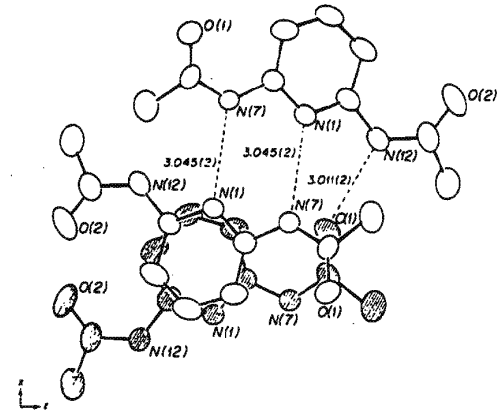


Figure 6. ORTEP drawing of a partial packing arrangement of 6 with thermal ellipsoids drawn at the 50% probability level. Hydrogen bonds are denoted by dashed lines and the lower molecule is cross-hatched for clarity.

guanylyl-3',5'-cytidine (GpC) salts,[18-20] though the estimated standard deviations for the distances in the GpC molecules are ca. 10 times those in this study. In the Na^{+} [16] and Ca^{2+} [17] structures of GpC, as well as in earlier studies of cytosine–guanine base pairs,[21] the N···O separations are shorter than the N···N separations, as they are in complex 3e:7.

The butanamide portion of the complex is approximately planar, with each butanamide chain adopting an extended, all anti conformation. The extent of the planarity of the molecule was examined by calculation of the deviation of each atom of the butanamide chains from the mean plane of the pyridine ring. The maximum deviations are ±0.16 Å except for O(2), which lies 0.28 Å from the plane. The thermal parameters for the butanamide atoms are rather large, and reference to Figure 5 shows the thermal ellipsoids to be quite elongated in the direction perpendicular to the plane of the molecule.

The glutarimide molecule adopts a symmetrical sofa conformation with C(4) lying 0.64 Å out of the plane of C(1')–C(3'), C(5')–O(8') and the larger (ethyl) substituent adopting the equatorial position. This conformation is the normal one for glutarimide molecules that are substituted at the C(4) position.[22-26]

(18) Rosenberg, J. M.; Seeman, N. C.; Day, R. O.; Rich, A. *J. Mol. Biol.* 1976, *104*, 145–167.
(19) Hingerty, B.; Sumramanian, E.; Stillman, S. D.; Sato, T.; Broyde, S. B.; Langridge, R. *Acta Crystallogr., Sect. B: Struct. Crystallogr. Cryst. Chem.* 1976, *B32*, 2998–3013.
(20) Aggarwal, A.; Islam, S. A.; Kuroda, R.; Sanderson, M. R.; Neidle, S.; Berman, H. M. *Acta Crystallogr., Sect. B: Struct. Sci.* 1983, *B39*, 98–104.
(21) Voet, D.; Rich, A. M. In *Progress in Nucleic Acid Research and Molecular Biology*; Davidson, J. N., Cohn, W. E., Ed.; Academic Press: New York, 1970; pp 183–265.

UM00013303
NOVARTIS EXHIBIT 1517
Novartis v. Regents, IPR2023-01347
Page 2049 of 4460

Table I. Unit Cell Dimensions and Other Experimental Parameters Used in X-ray Diffraction Studies of Compound **6** and the Base Pair **3e**:**7**

parameter	6[a]	3e:7[b]
formula wt, amu	193.2	404.5
cryst dimen, mm	0.20 × 0.25 × 0.40	0.30 × 0.30 × 0.75
a, Å	10.624 (2)	13.110 (2)
b, Å	7.827 (1)	23.415 (3)
c, Å	22.927 (3)	7.422 (1)
β, deg	90.0	100.38 (1)
space group	*Pbcn*	$P2_1/n$
Z	8	4
d_{calcd}, g cm^{-3}	1.346	1.199
μ, cm^{-1}	8.26	6.91
min scan speed, 2θ, deg min^{-1}	4.0	2.0
no. unique reflects meas	1775	3806
no. reflectns with $I \geq 2\sigma(I)$	1272	2639
$R(I \geq 2\sigma(I))$	0.050	0.076

[a] *N,N'*-2,6-pyridinediylbis[acetamide]. [b] Complex between bemegride and *N,N'*-2,6-pyridinediylbis[butanamide].

The C–N–C–C (3.4 (3), 5.5 (3)°) and O–C–N–C (−176.2 (4), 179.5 (4)°) angles in this moiety demonstrate the near planarity of the portion of the molecule that is complementary to the attachment site on **7**.

The complexes pack as discrete, hydrogen bonded units associated only by van der Waals forces; that is, the butanamide carbonyl groups do not participate in hydrogen bonding. Molecules pack in planar arrays in the z^* direction with essentially no overlap (save unit translation). Projection onto the a,b plane shows the molecules to lie in a herringbone pattern.

In order to establish that the parameters for **7** had not been distorted by the complexation of the drug molecule, the self-association of a similar ligand, *N,N'*-2,6-pyridinediylbis[acetamide] (**6**) was studied. A partial view of the packing of the molecule is shown in Figure 6. A comparison of the bond lengths, valency angles, and torsion angles in **6** with those found in the butanamide portion of the complex shows that these parameters do not differ even though the molecules exist in quite dissimilar environments.

The molecules of **6** are held together by extensive hydrogen bonding, each molecule fulfilling its capabilities by interaction with three other molecules. Oxygen O(2) does not participate and consequently its thermal ellipsoid is much larger than that of O(1). The molecules are joined via one amido group and the pyridine nitrogen as rather loosely held cyclic dimers (N···N 3.045 (2) Å) about a center of symmetry. The second amido group interacts, again rather weakly (N···O 3.011 (2) Å), with O(1) of a different symmetry-related molecule. In the y direction the molecules are tilted 12.3° with respect to one another. There is a virtually complete overlap of the pyridine rings, albeit with a rotation of ca. 150° about this axis (see Figure 6). The center-to-center separation of these rings is 3.92 Å and the closest approach is 3.41 Å. Layers of these stacks are linked by the hydrogen bonds in the x direction. The molecules associated by NH···N hydrogen bonds are tilted at 49° with respect to one another.

In summary, the X-ray crystal structures show the ligands to exist in planar, extended conformations with trans amide linkages and demonstrate a triple hydrogen bond when the glutarimide bemegride is complexed with **7**.

Chromatographic Separation of Chiral Species. The previous section has established the formation of hydrogen bonds between the classes of heterocyclic drugs listed in Figure 1 and 2,6-pyridinediylbis[alkanamides] in nonpolar solvents. We next synthesized bonded phase **19**, the optically active isomer of a homologue of compound **10**, which was previously shown to form base pairs with **3e**. Figure 7 illustrates the bonded phase in combination with a barbiturate *S*-**1a**. Figure 8 provides a scheme for the synthesis of the silane to be bonded to the silica gel, and specific details can be found in the Experimental Section. Identical substitution of the amides, as noted previously, will yield a single complex, thereby maximizing chiral recognition. An 11-carbon spacer was placed between the silicon atom and the active ligand in order to enhance accessibility of the active site and thus hydrogen bond formation.

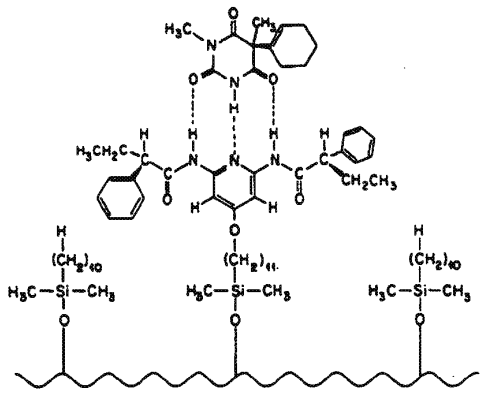


Figure 7. Structure of the complex between stationary phase **19** and the barbiturate *S*-**1a**.

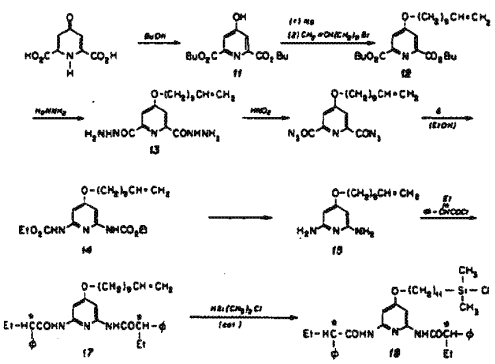


Figure 8. Synthetic scheme of the ligand **18**.

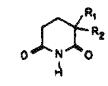
The long leash permits, in addition to the high accessibility of site, the removal of the bulky ligand from the silica gel surface and thus a relatively higher bonded phase coverage. The optical purity, determined as described in the Experimental Section, was found to be 93.4%. A second, end-capping step was performed with decyldimethylchlorosilane in order to reduce the number of unreacted silanol groups on the silica gel surface that could potentially be available for competitive hydrogen bonding with the heterocyclic drugs. The coverage by the end-capping groups was 2 μmol/m^2, yielding a total bonded phase loading of 3 μmol/m^2. Prior to bonding, the silica gel had been acid washed to remove metal impurities from the surface that could interfere with the formation of the hydrogen bond associate between the drug and active ligand.[27]

After the column was packed, it was operated at 25 °C in the normal-phase mode with a mobile phase of 2.5% 2-propanol in 1,2-dichloroethane. Table II presents results of retention and relative retention for six-membered heterocyclic compounds—barbiturates and glutarimides—and Table III for five-membered

(22) Allen, F. H.; Trotter, J. *J. Chem. Soc. B* **1971**, 1073–1079.
(23) Sayers, J.; Schindler, D.; Sundaralingam, M. *J. Am. Chem. Soc.* **1977**, *99*, 3848–3850.
(24) Onan, K. D.; Prakash Rao, H. S.; Parry, R. J. *Acta Crystallogr., Sect. C: Cryst. Struct. Commun.* **1985**, *C41*, 428–432.
(25) Bocelli, G.; Grenier-Loustalot, M. F. *Acta Crystallogr., Sect. B: Struct. Crystallogr. Cryst. Chem.* **1981**, *B37*, 1302–1304.
(26) Koch, M. H. J. *Acta Crystallogr., Sect. B: Struct. Crystallogr. Cryst. Chem.* **1973**, *B29*, 369–371.
(27) Tanaka, N.; Karger, B. L., submitted.

UM00013304
NOVARTIS EXHIBIT 1517
Novartis v. Regents, IPR2023-01347
Page 2050 of 4460

Table II. Chromatographic Characteristics of Six-Membered Heterocyclic Compounds (Mobile phase: 2.5% 2-propanol in 1,2-dichloroethane, T = 25 °C)

General Structure		R_1	R_2	R_3	F[b]	k_1'[c]	α[d]
A. Barbiturates[a]	(1a)	$-CH_3$	$-CH_3$		R	3.03	1.14
	(1b)	$-C_4H_9$	$-CH_3$		-	3.35	1.16
	(1c)	$-CH_3$	$-C_2H_5$		-	2.30	[e]
	(1d)	$-CH_3$	$-CH_2CH{=}CH_2$	$-\underset{CH_3}{CH}-C{\equiv}CC_2H_5$	-	2.69	1.11
	(1e)	$-C_2H_5$	$-CH_3$	$-N(CH_3)_2$	R	2.45	1.14
	(1f)	$-CH_3$	$-C_2H_5$	$-N(CH_3)_2$	R	2.17	1.10
	(1g)	$-CH_3$	$-C_3H_7$	$-N(CH_3)_2$	R	2.28	1.06
	(1h)		$-C_2H_5$		-	3.42	1.11
	(1i)	$-C_2H_5$	$-C_3H_7$		R	2.90	1.10
	(2)		$-CH_3$		-	4.26	1.07
B. Glutarimides[a]	(3a)	$-C_2H_5$			-	3.50	1.07
	(3b)	$-C_2H_5$			S	3.06	1.11
	(3c)	$-C_2H_5$			-	4.84	
	(3d)	$-C_2H_5$			S	5.74	1.05
	(3e)	$-CH_3$	$-C_2H_5$		-	3.23	

[a] Common names: **1a**, hexobarbital; **1c**, mephobarbital; **1d**,methohexital; **3a**, glutethimide; **3b**, N-TFA of aminoglutathimide; **3e**, bemegride. [b] F is the absolute configuration of first eluting enantiomer. [c] k' is the capacity factor of the first eluting enantiomer, $(t_r - t_0)/t_0$, where t_r is the retention time and t_0 is the unretained time. [d] $\alpha = k_2'/k_1'$, separation factor. [e] No separation observed. [f] An achiral compound.

Table III. Chromatographic Characteristics of Five-Membered Heterocyclic Compounds (Mobile phase: 2.5% 2-propanol in 1,2-dichloroethane, T = 25 °C)

General Structure		R_1	R_2	R_3	k_1'[b]	α[c]
A. Hydantoins[a]	(4a)	-H			2.44	[d]
	(4b)	-H	$-CH_3$		2.10	1.16
	(4c)	-H	$-C_2H_5$		2.27	1.16
	(4d)	$-CH_3$	-H	-H	1.85	[e]
	(4e)	$-CH_3$	$-C_2H_5$		0	[d]
B. Succinimides[a]	(5a)	-H	$-CH_3$		1.02	[d]
	(5b)	-H	$-C_2H_5$		1.38	[d]
	(5c)	-H	$-CH_3$	$-C_2H_5$	1.22	[d]
	(5d)	-H	$-CH_3$		1.24	[d]
	(5e)	$-CH_3$	-H		0	[d]
	(5f)	$-CH_3$	$-CH_3$		0	[d]

[a] Common names: **4e**, mephenytoin, **5c**, ethosuximide, **5e**, phensuximide, **5f**, methsuximide. [b] k_1' is the capacity factor of the first eluting enantiomer, $(t_r - t_0)/t_0$, where t_r is the retention time and t_0 is the unretained time. [c] $\alpha = k_2'/k_1'$, separation factor. [d] No separation observed. [e] An achiral compound.

heterocyclic compounds—hydantoins and succinimides. Chiral recognition is observed for three of the four classes of drugs, with only the succinimides yielding no separation.

As can be observed, relative retention (α) values up to 1.16 were obtained. Even though higher values are desirable, a factor of this magnitude is sufficient for base line separation with high-efficiency HPLC. This is illustrated in Figure 9, which shows the separation of various species including some pharmacologically

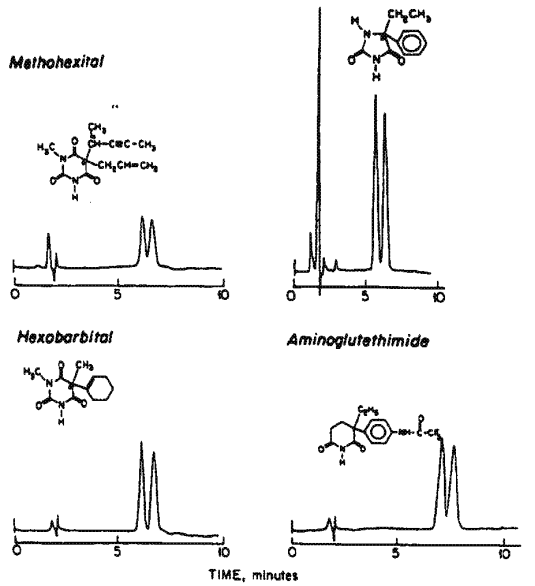


Figure 9. Chromatograms of the enantiomeric separations of methohexital (**1d**), hexobarbital (**1a**), N-TFA of aminoglutethimide **3b**, and the hydantoin **4c** on stationary phase **19**. Column, 15-cm length × 4.6-mm i.d.; mobile phase, 2.5% 2-propanol in 1,2-dichloroethane; 1.0 mL/min; 25 °C.

Table IV. Solute Enthalpy Differences between Specific Mobile Phases and the Chiral Stationary Phase[a]

	$-\Delta H$, kcal/mol	
solutes	X = 0%	X = 2.5%
barbiturate **1a**	7.68	5.23
1b		5.29
1c		5.03
1d		5.48
1h		5.45
1j		5.34
glutarimide **3a**	7.21	6.14
3b		6.87
hydantoin **4a**		5.96
4b	7.13	4.04
4c		3.43
4d		2.55
succinimide **5a**	6.73	3.76

[a] Mobile phase: X% 2-propanol in 1,2-dichloroethane.

important drugs. Presumably, improvements in the prototype bonded phase, through an understanding of the structural parameters controlling separation, will yield enhanced separation factors.

It is interesting to note that compounds **4e**, **5e**, and **5f** experience no retention and thus no separation. In the three examples the heterocyclic nitrogen flanked by the two carbonyls is substituted by a methyl group that blocks formation of the complex. The triple hydrogen bond is precluded, thereby leading to no retention for the methylated species. The high specificity inherent in the triple hydrogen bond creates a type of "affinity" site for specific binding of complementary structural units. Work is continuing on this approach to high specificity, particularly with methylated bases of nucleic acids.

The fact that methyl substitution on the heterocyclic nitrogen reduces retention to zero suggests that the major cause of retention for the drugs tested in Tables II and III is indeed hydrogen bond association. This conclusion can be reinforced by an examination of enthalpies of retention. Table IV presents $-\Delta H$ values for a number of solutes determined from van't Hoff plots of log k' vs. $1/T$. With 1,2-dichloroethane as mobile phase, $-\Delta H$ values lie

UM00013305
NOVARTIS EXHIBIT 1517
Novartis v. Regents, IPR2023-01347
Page 2051 of 4460

between approximately 7 and 8 kcal/mol. Interestingly, in chloroform the complexation enthalpy for 1-cyclohexyluracil:9-ethyladenine, a double hydrogen bond associate, was found to be 6.2 and 4.0–4.3 kcal/mol for their self-associates.[28]

When 2.5% 2-propanol was added to the mobile phase, all $-\Delta H$ values decrease due to the solvation of the drug in the bulk solvent and the competition of the 2-propanol for the bonded stationary phase. The barbiturates studied all have $-\Delta H$ values between 5 and 5.5 kcal/mol, whereas the glutarimides are somewhat higher at 6.3 kcal/mol. However, the five-membered hydantoins and succinimides now lie between 2.5 and 4 kcal/mol. Hence, smaller k' values are found for the solutes in Table III relative to Table II.

It is further observed in Table II that the *R* enantiomer elutes first for all the barbiturates for which an optically pure standard was available. This elution order can be rationalized with reference to Figure 7. Consider first the conformation of the bonded ligand when the hydrogen bond associate forms.

From the NMR studies it was noted that the carbon adjacent to the amide carbonyl in *N,N'*-2,6-pyridinediylbis[alkanamide] must possess at least one hydrogen for complex formation. This result suggests that free rotation about the (C=O)–CH(Et)Ph bond is restricted during complex formation and that the rotamer with the hydrogen substituent directed toward the solute molecule is preferred. This in turn requires the other two substituents at this site, Et and Ph, to lie above and below the plane of the complex (see Figure 7). This conformational stabilization and the resultant spatial orientation of the substituents are necessary for chiral recognition to occur, as described below.

Consider next the association of a barbiturate with the ligand. It is known that the heterocyclic ring is planar[29,30] and thus the three points of attachment can be coplanar with the active site of the bonded phase (see X-ray results). In the case of the *S* isomer of compound **1a**, shown in Figure 7, the bulky 1-cyclohexenyl group will now lie above and the methyl group below the plane of the complex. The *S* isomer can be expected to form the more stable hydrogen bond associate with the bonded ligand, since the larger 1-cyclohexenyl substituent is proximate to the smaller ethyl group of the ligand. On the other hand, in the *R* isomer the cyclohexenyl substituent is closer to the larger phenyl group. Similarly, for all other barbiturates where the elution order is known, the enantiomer that has its larger substituent in closer proximity to the phenyl group of the bonded ligand elutes first. Thus, the complex embodying less steric interaction between the substituents would appear to be the more stable.

That the steric difference between R_2 and R_3 is important for selectivity is demonstrated by a comparison of the α values of compounds **1e**, **1f**, and **1g**. Here, the larger substituent, R_3, is dimethylamino, while R_2 is methyl, ethyl, or propyl, respectively. The separation factor, α, decreases with a decrease in the size difference of R_2 and R_3 ($1.14 > 1.10 > 1.06$). Additionally, the only barbiturate that was not resolved was **1c**, where the larger group is phenyl. This result may be a consequence of a π–π interaction between aromatic rings of the solute and the ligand offsetting the steric hindrance. Finally, compound **2** illustrates that an imine can substitute for a carbonyl to yield retention and chiral recognition. Imine groups are known to be hydrogen bond acceptors.[31]

The results for the glutarimides differ from those for the barbiturates in that the *S* isomer is found to elute first (see Table II). As observed in Figure 5 for **3e**, glutarimides generally exist in a sofa (1,2-diplanar) conformation with C(4) lying either above or below the ring plane.[22–26] The two conformers of each enantiomer of **3d** are shown in Figure 10. The more stable conformer

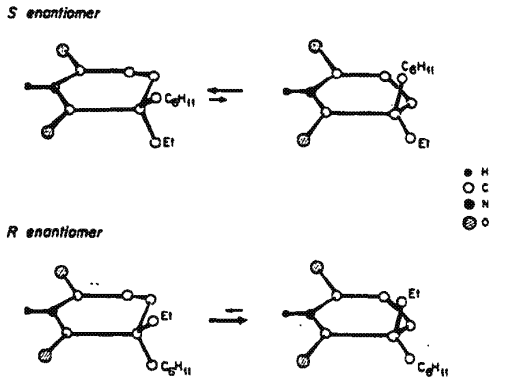


Figure 10. Sofa conformations of compound **3d**. In the predominant conformer of each enantiomer the cyclohexyl substituent is equatorial and the ethyl group is axial. The axial ethyl substituent lies below the plane for the *S* and above it for the *R* enantiomer.

is known to be the one in which the larger group occupies the equatorial position; therefore, for the *S* enantiomer, the smaller (ethyl) group lies below the plane in the axial position. This means that in the complex of the (*S*)-glutarimide with the *S* ligand, the axial ethyl group lies on the same side of the complex as does the phenyl (largest) group of the ligand. For this reason the complex with the *S*-glutarimide is less stable than that with the *R*-glutarimide and elutes first.

Turning next to hydantoins, it is known that the five-membered heterocyclic ring is planar.[32,33] Presumably, complexes analogous to that shown in Figure 7 may form having a chiral recognition mechanism similar to that of the barbiturates. Unfortunately, optically pure standards of the resolved hydantoins were not available. The fact that compound **4a** was not resolved may reflect the similar steric sizes of R_2 and R_3.

None of the succinimides tested in Table III showed chiral resolution. Even in 100% 1,2-dichlorethane, succinimides were not resolved, in spite of the increase in k'. While hydantoins and succinimides would be expected to exhibit similar structural features, e.g., O···O separations and O–C–N angles, there are electronic differences in the parent molecules due to the second heterocyclic nitrogen in the hydantoins. Examination of resonance structures suggests that there is greater negative charge localization on the carbonyl oxygens for hydantoins than for succinimides. These differences may make the hydantoins stronger Lewis bases, resulting in weaker complexation of the succinimides relative to the hydantoins. It is possible that there may be sufficient elongation of the hydrogen bonds in the complex that steric interactions between R_2 and R_3 of the drug with the bonded phase ligand is reduced to the point that chiral recognition is lost. However, more studies would be required, particularly X-ray structures of co-crystals, before more definitive statements could be made concerning the succinimides.

Conclusions

This work has shown that, in analogy to base pairing in nucleic acid chemistry, it is possible to design substrates for which hydrogen bond association with heterocyclic drugs can occur. By virtue of the coplanarity of the substrate and drug, a specific fit leading to strong binding can result. If this binding is disrupted (e.g., by methylation of nitrogen), complexation drops to zero. In addition, specific, multiple hydrogen bonding creates conformational stabilization in groups in proximity to the points of association. This stabilization allows chiral recognition to take place when groups of appropriate size differences are attached to the chiral centers.

(28) Kyogoku, Y.; Lord, R. C.; Rich, A. *J. Am. Chem. Soc.* **1967**, *89*, 496–504.
(29) Craven, B. M.; Vizzini, E. A. *Acta Crystallogr., Sect. B: Struct. Crystallogr. Cryst. Chem.* **1969**, *B25*, 1993–2009.
(30) Shimizu, N.; Nishigaki, S.; Nakai, Y.; Osaki, K. *Acta Crystallogr., Sect B: Struct. Crystallogr. Cryst. Chem.* **1982**, *B38*, 2309–2311.
(31) Noller, C. R. *Chemistry of Organic Compounds*, 2nd ed.; W. B. Saunders: Philadelphia, 1957; p 249.
(32) Cassady, R. E.; Hawkinson, S. W. *Acta Crystallogr., Sect B: Struct. Crystallogr. Cryst. Chem.* **1982**, *B38*, 1646–1647.
(33) Camerman, A.; Camerman, N. *Acta Crystallogr., Sect. B: Struct. Crystallogr. Cryst. Chem.* **1971**, *B27*, 2205–2211.

UM00013306
NOVARTIS EXHIBIT 1517
Novartis v. Regents, IPR2023-01347
Page 2052 of 4460

Experimental Section

Materials. The following derivatives of 2,4,6(1*H*,3*H*,5*H*)-pyrimidinetrione[barbiturates] were studied: 1-(1-cyclohexen-1-yl)-1,5-dimethyl (**1a**); 1-butyl-5-(1-cyclohexen-1-yl)-5-methyl (**1b**); 5-ethyl-1-methyl-5-phenyl (**1c**); 1-methyl-5-(1-methyl-2-pentynyl)-5-(2-propenyl) (**1d**); 5-(dimethylamino)-1-ethyl-5-methyl (**1e**); 5-(dimethylamino)-5-ethyl-1-methyl (**1f**); 5-(dimethylamino)-1-methyl-5-propyl (**1g**); 1-cyclohexyl-5-ethyl-5-(1-piperidinyl) (**1h**); 1-ethyl-5-(1-piperidinyl)-5-propyl (**1i**); 5-(1-cyclohexen-1-yl)-4,5-dihydro-4-imino-5-methyl-1-phenyl 2,6-(1*H*,3*H*)pyrimidinedione (**2**). Several derivatives of 2,6-piperidinedione [glutarimides] were studied: 3-ethyl-3-phenyl (**3a**); 3-ethyl-3-(4-(trifluoroacetamido)phenyl) (**3b**); 3-(1-cyclohexen-1-yl)-3-ethyl (**3c**); 3-cyclohexyl-3-ethyl (**3d**), 4-ethyl-4-methyl (**3e**). Derivatives of 2,4-imidazolidinedione [hydatoins] studied were 5-(4-methylphenyl)-5-phenyl (**4a**), 5-methyl-5-phenyl (**4b**), 5-ethyl-5-phenyl (**4c**), 1-methyl (**4d**), and 1-ethyl-3-methyl-5-phenyl (**4e**). Also studied were the following derivatives of 2,5-pyrrolidinedione [succinimides]: 3-methyl-3-phenyl (**5a**); 3-ethyl-3-phenyl (**5b**); 3-ethyl-3-methyl (**5c**); 3-(1-cyclohexen-1-yl)-3-methyl (**5d**); 1-methyl-3-phenyl (**5e**); 1,3-dimethyl-3-phenyl (**5f**). These compounds were obtained from the following sources. Prof. Dr. J. Knabe (Universitat des Saarlandes, Stadtwald, W. Germany) kindly provided *RS*-, *R*-, and *S*-**1a**; *RS*-**1b**; *RS*-, *R*-, and *S*-**1c**; *RS*-, *R*-, and *S*-**1e**; *RS*-, *R*-, and *S*-**1f**; *RS*-, *R*-, and *S*-**1g**; *RS*-, *R*-, and *S*-**1h**; *RS*-, *R*-, and *S*-**1i**; *RS*-**2**; *RS*-, *R*-, and *S*-**3c**; *RS*-, *R*-, and *S*-**3d**; *RS*-, *R*-, and *S*-**5a**; *RS*-, *R*-, and *S*-**5b**; *RS*-, *R*-, and *S*-**5c**; *RS*-, *R*-, and *S*-**5d**; *RS*- and *R*-**5f**. The United States Pharmacopeia kindly provides *RS*-**1a**, *RS*-**1c**, *RS*-**1d**, *RS*-**3a**, *RS*-**4e**, *RS*-**5c**, *RS*-**5e**, and *RS*-**5f**. The compounds **3e**, *RS*-**4a**, *RS*-**4b**, *RS*-**4c**, *RS*-**4d**, acetic anhydride, butyric anhydride, 1,4-dihydro-4-oxo-2,6-pyridinedicarboxylic acid (chelidamic acid), 18-crown-6, 2,6-diaminopyridine, hexachloroplatinic acid, isobutyryl chloride, *N*-methylmorpholine, (*RS*)-2-phenylbutyric acid, and pivaloyl chloride were obtained from Aldrich Chemical Co., Milwaukee, WI. (*S*)-2-Phenylbutyric acid (97% OP) was obtained from Norse Laboratories, Newbury Park, CA. Dimethylchlorosilane was bought from Petrarch Systems Inc., Bristol, PA. ω-Undecenyl bromide was obtained from Fairfield Chemical Co., Inc., Blythewood, SC. The free base of *RS*- and *S*-**3b** was kindly obtained from Dr. H. A. Salhanic (Harvard School of Public Health, Boston, MA). Silica gel for low-pressure column chromatography and TLC plates were purchased from Analtech (Newark, DE). The silica for bonded-phase was Supelcosil 100Å, 5 μm, 162 m^2/g (Supelco, Bellefonte, PA). All solvents were HPLC grade. Other chemicals were ACS reagent grade. Elemental analysis was performed by either Galbraith Laboratories Inc., Knoxville, TN, or Multichem Laboratories, Inc., Lowell, MA.

Equipment. ^1H NMR spectra were taken with either a T-60 or a XL-300 NMR spectrometer (Varian Associates, Palo Alto, CA), melting points (uncorrected) with the Thomas–Hoover Unit Melt (Arthur H. Thomas Co., Philadelphia, PA). The gas chromatograph was a Varian Model 1200 (Varian Associates, Palo Alto, CA). The liquid chromatograph was a Beckman instrument consisting of a 420 microprocessor controller, two Model 110A single-piston reciprocating pumps, a dynamically stirred gradient mixing chamber, a Model 210 sample injection valve, a Model 160 detector with an 18.5-μL analytical flow cell for UV detection at either 214, 254, or 280 nm (Beckman Instrument, Inc., Berkeley, CA), and a linear recorder Model 500 (Linear Instruments, Reno, NV). The chromatographic data were processed with a Nelson Analytical Model 2600 chromatography software package (Nelson Analytical, Cupertino, CA) used in conjunction with an IBM XT personal computer (IBM, Boca Raton, FL). Optical rotations were determined with a Perkin-Elmer Model 241 polarimeter (Perkin-Elmer, Norwalk CT). A pneumatic Haskel pump Model DSTV 122 (Haskel, Burbank, CA) was used to pack the column.

Synthesis. Preparation of *N*,*N*'-2,6-Pyridinediylbis[alkanamide] 6–10. A solution of 40 mmol of 2,6-diaminopyridine and 100 mmol of the respective carboxylic anhydride or the acyl chloride in 25 mL of dry pyridine was prepared and refluxed for 2 h. The reaction mixture was concentrated under reduced pressure and dissolved in ethyl acetate. The organic layer was extracted with water, 5% tartaric acid, and 5% sodium bicarbonate. The organic layer was then dried over sodium sulfate and filtered and the solvent was stripped off. The residue was purified by column chromatography on 10-fold silica gel, utilizing as a mobile phase toluene made increasingly polar with ethyl acetate. The final product was further purified by crystallization from toluene (yield 70–80%).

***N*,*N*'-2,6-Pyridinediylbis[acetamide] (6).** The product precipitated when the reaction mixture was poured in ethyl acetate. The precipitate was filtered, washed with ethyl acetate, and recrystallized from chloroform to yield a white crystalline material. Mp 205–206 °C (201.5 °C phase transition). Anal. Calcd for $C_9H_{11}N_3O_2$: C, 55.95; H, 5.74; N, 21.75. Found: C, 55.84, H, 5.75; N, 21.68. ^1H NMR ($CDCl_3$) δ 2.25 (s, 2 CH_3), 7.70 (s, 2NH), 7.60–8.10 (m, C_5H_3N).

***N*,*N*'-2,6-Pyridinediylbis[butanamide] (7).** The product was white crystals, mp 126–127 °C. Anal. Calcd for $C_{13}H_{19}N_3O_2$: C, 62.63; H, 7.68; N, 16.86. Found: C, 62.68; H, 7.53; N, 16.86. ^1H NMR ($CDCl_3$) δ 1.01 (t, 2 CH_3 J = 7.3 Hz), 1.76 (sextet, 2 CH_2, J = 7.3 Hz), 2.35 (t, 2 CH_2, J = 7.3 Hz), 7.75 (s, 2 NH), 7.69 (t, H-4-Py, J = 7.6 Hz), 7.90 (d, 2 (H-3-Py), J = 7.6 Hz).

***N*,*N*'-2,6-Pyridinediylbis[2-methylpropanamide] (8).** The product was white crystals, mp 142.5–143.5 °C. Anal. Calcd as for 7. Found: C, 62.73; H, 7.68; N, 16.81. ^1H NMR ($CDCl_3$) δ 1.26 (d, 4 CH_3, J = 6.8 Hz), 2.53 (septet, 2 CH, J = 6.8 Hz), 7.6 (s, 2 NH), 7.70 (t, H-4-Py, J = 7.7 Hz), 7.92 (d, 2 (H-3-Py), J = 7.7 Hz).

***N*,*N*'-2,6-Pyridinediylbis[2,2-dimethylpropanamide] (9).** The product was white crystals, mp 110–111 °C. Anal. Calcd for $C_{15}H_{23}N_3O_2$: C, 64.95; H, 8.36; N, 15.15. Found: C, 65.20; H, 8.49; N, 15.03. ^1H NMR ($CDCl_3$) δ 1.32 (s, 6 CH_3), 7.76 (s, 2 NH), 7.69 (t, H-Py, J = 8.1 Hz), 7.93 (d, 2 (H-3-Py), J = 8.1 Hz).

***N*,*N*'-2,6-Pyridinediylbis[2-phenylbutanamide] (10)** was prepared from *RS*-2-phenylbutyryl chloride. The crystalline material, a mixture of the meso and racemic forms, showed a double spot, R_f 0.45 and 0.49 (15% EtOAc/toluene), on a silica gel TLC plate. The melting point of such a mixture depends on the ratio of the optical isomers and therefore is not reported. Anal. Calcd for $C_{23}H_{27}N_3O_2$: C, 74.78; H, 6.78; N, 10.47. Found: C, 74.23; H, 6.77; N, 10.35. ^1H NMR ($CDCl_3$) δ 0.88 (t, 2 CH_3, J = 7.3 Hz), 1.82–2.19 (heptet, 2 CH_2, J = 7.0 Hz), 3.31 (t, 2 CH, J = 7.6 Hz), 7.28 (s, 2 C_6H_5), 7.31 (t, H-4-Py, J = 7.9 Hz), 7.61 (s, 2 NH), 7.88 (d, 2 (H-3-Py), J = 7.9 Hz).

Preparation of the Stationary Phase. The compounds **11–15** were prepared according to Markees et al.[34] with modifications. The intermediates **11–15** and compound **17** were purified by flash column chromatography as described in the preparation of **6–10**. Most of the compounds were viscous oils and their purities were verified by TLC and NMR spectrum. The steps for the synthesis of the bonded phase are shown in Figure 8.

Dibutyl 1,4-Dihydro-4-oxo-2,6-pyridinedicarboxylate (11). A 20% slurry of chelidamic acid (16.75 g) in 1-butanol containing 2% sulfuric acid was refluxed for 4 h. After cooling, the reaction mixture was filtered, most of the butanol removed from the filtrate under reduced pressure, and the residue dissolved in toluene and chromatographed: yield, 12.20 g (45%), viscous oil.

Dibutyl 4-(10-Undecenyloxy)-2,6-pyridinedicarboxylate (12). One equivalent of sodium (39.17 mmol) was dissolved in butanol and added to 11.61 g of compound **11**. The butanol was evaporated to dryness, the residue dispersed in toluene, 1.1 equiv of ω-undecenyl bromide added, and the mixture refluxed under nitrogen overnight in the presence of 18-crown-6 as catalyst. The reaction mixture was extracted with aqueous 10% sodium carbonate, followed by two water extractions. The residue of the organic layer was purified by chromatography, to yield 11.07 g (63%) of oil.

4-(10-Undecenyloxy)-2,6-pyridinedicarboxylic acid dihydrazide (13) was prepared according to a procedure described by Markees et al.[34] from compound **12**. The precipitate was filtered, washed with ether, and air-dried to yield 5.57 g (65%) of a crystalline white material, mp 140–142 °C.

Diethyl *N*,*N*'-[4-(10-Undecenyloxy)-2,6-pyridinediyl]bis[carbamate] (14). A suspension of 5.3 g of **13** in 110 mL of 9% aqueous hydrochloric acid was prepared, cooled to 10–15 °C, and stirred vigorously, and a solution of 4.0 g of sodium nitrite in 40 mL of water was added dropwise over 2 h. The waxy precipitate was filtered, washed with water to neutrality, and air-dried overnight. The crude diazide was dissolved in absolute ethanol and refluxed for 5 h. The reaction mixture was purified by chromatography to yield 2.6 g of a colorless solid (42%).

2,6-Diamino-4-(10-undecenyloxy)pyridine (15). Compound **14** (2.6 g) was dissolved in 50 mL of 95% ethanol containing 2.5 g of potassium hydroxide and refluxed for 3 h. Most of the alcohol was removed and the residue partitioned between ethyl acetate and water. The organic layer was washed with water, dried over sodium sulfate, and filtered, and the solvent was removed under vacuum to yield 1.45 g of **15** (85%). ^1H, NMR ($CDCl_3$) δ 1.32 (m, 7 CH_2, $W_{1/2}$ = 6 Hz), 1.6–2.4 (m, $CH_2C{=}C$), 3.82 (t, CH_2, J = 6 Hz), 4.22 (broad s, 2 NH_2, exchangable with D_2O), 4.7–5.2 (m, $CH_2{=}$), 5.38 (s, pyridino hydrogens), 5.4–6.2 (m, $CH{=}$).

(*S*)-2-Phenylbutyryl Chloride (16). A solution of 3.0 g of (*S*)-2-phenylbutyric acid [97% optically pure, $[\alpha]^{25}_D$ = +83.6° (neat)] in 55 mL of dry methylene chloride was prepared and cooled in an ice bath, and a solution of 10 mL of thionyl chloride in 20 mL of methylene chloride was added dropwise over 30 min. The solution was refluxed for 4 h and distilled: bp 97–98 °C (1.87 kPa); 2.67 g, 80%; $[\alpha]^{25}_D$ = +82.70

(34) Markees, D. G.; Dewey, V. C.; Kidder, G. W. *J. Med. Chem.* **1968**, *11*, 126–129.

UM00013307
NOVARTIS EXHIBIT 1517
Novartis v. Regents, IPR2023-01347
Page 2053 of 4460

(c = 2.7 in $EtCl_3$). A sample of the compound was converted to its *tert*-butylamido derivative and found to be 94.9% optically pure by GC (see section on optical purity of bonded phase).

N,N'-[4-(10-Undecenyloxy)-2,6-pyridinediyl]bis[(*S*)-2-phenylbutanamide] (17). A solution of 1 g of **15** and 0.9 mL of *N*-methylmorpholine in 40 mL of dry chloroform was prepared and cooled to −20 °C. A solution of 1.3 g of **16** in 10 mL of chloroform was added dropwise over 3 h and left at −15 °C overnight. The solvent was removed under reduced pressure and the residue was dissolved in ether, extracted with 5% tartaric acid and 5% sodium bicarbonate, dried over sodium sulfate, and filtered, and the solvent was stripped off. The residue (2 g) was chromatographed on 60 g of silica gel. Compound **17** (500 mg, 25%) was eluted with toluene and showed only the upper spot, R_f 0.61 (15% EtOAc/toluene), of the "doublet" on the TLC plate (see section optical purity of bonded phase). A second fraction, which eluted at 2% ethyl acetate in toluene (100 mg), contained the "double" spot, R_f 0.56 and 0.61 (15% EtOAc/toluene), with small amounts of other impurities. Rechromatographing this fraction on silica gel enriched the lower spot of the doublet, **17B**. Both separated compounds **17** and **17B**, showed the same NMR spectrum. Upper spot: mp 71.5–72.5 °C. Anal. Calcd for $C_{36}H_{47}N_3O_3$: C, 75.88; H, 8.32; N, 7.38. Found: C, 76.16; H, 8.33; N, 7.29. ^1H NMR ($CDCl_3$) δ 0.84 (t, 2 CH_3, J = 6 Hz), 1.28 (br s, 7 CH_2, $W_{1/2}$ = 6 Hz), 1.5–2.4 (m, 2 CH_2, 2 allylic), 3.22 (t, 2 PhCH, J = 7 Hz), 3.92 (t, CH_2O, J = 5.5 Hz), 4.8–5.3 (m, CH_2=), 5.4–6.1 (m, CH=), 7.12 (s, 2 C_6H_5), 7.42 (s, 2 pyridino protons), 7.58 (s, 2 NH).

A solution of 1.68 mmol of **17** was dissolved in 4 mL of dimethylchlorosilane, the solution heated to reflux, and a small crystal of platinic acid added. The reaction mixture was refluxed for 2 h. All volatiles were stripped off under high vacuum to obtain N,N'-[4-(11-(dimethylchlorosilyl)undecyloxy)-2,6-pyridinediyl]bis[2-(*S*)-phenylbutanamide] (**18**). The ^1H NMR spectrum showed the disappearance of the olefinic protons from **17** and the appearance of the dimethylsilyl protons.

Bonded Stationary Phase (19). Residue **18** was dissolved in 20 mL of dry pyridine, filtered through a 1-μm Millipore filter into 3.0 g of dried (200 °C, vacuum, overnight) Supelcosil. The slurry was gently homogenized and rotated for 5 h at room temperature. The mixture was then filtered and washed thoroughly with methylene chloride followed by methanol. The filtrates and washings were saved for further analysis (see below). The bonded silica was dried at 60 °C for 4 h at atmospheric pressure and 4 h under high vacuum. From carbon analysis (6.62%) the bonded ligand surface density was calculated to be 1.04 μmol/m^2. The bonded silica was dispersed again in pyridine containing dimethyldecylchlorosilane for 5 h, washed, and dried as before. Found (after C_{10} end-capping): C, 10.70. From the difference of the carbon content the density of the C_{10} ligand was estimated to be 2 μmol/m^2.

Characterization of the Washings from the Bonding. The volatiles of the previously combined filtrate and washings of **19** were removed under reduced pressure, the residue was dissolved in ethyl acetate, extracted with aqueous 5% tartaric acid followed by 5% sodium bicarbonate, and dried over sodium sulfate, and the solvent was removed under high vacuum. The residue (0.52 g) showed two main spots on a silica gel TLC plate, R_f 0.61 and 0.45 (15% EtOAc/toluene), and a tailing spot at R_f 0.35. The mixture was chromatographed on 10 g of silica gel to yield three purified compounds that were identified by NMR spectra. The first eluting material (320 mg), R_f 0.61, was found to be [4-(undecyloxy)-2,6-pyridinediyl]bis[(*S*)-2-phenylbutanamide] (**20**), a hydrogenated byproduct of **17**. ^1H NMR ($CDCl_3$) δ 0.82 (t, 3 CH_3, J = 6 Hz), 1.28 (br s, 9 CH_2), 1.50–2.40 (m, 2 CH_2), 3.33 (t, 2 PhCH, J = 7 Hz), 3.92 (t, CH_2O), 7.23 (s, 2 C_6H_5), 7.53 (s, 2 pyridino protons), 7.71 (br s, 2 amidic protons). The second, R_f 0.45, was found to be an oxy derivative of the silane [4-[11-(dimethylsilyl)undecyloxy]-2,6-pyridinediyl]bis[(*S*)-2-phenylbutanamide]. ^1H NMR ($CDCl_3$) δ 0.03 (s, 2 $SiCH_3$), 0.57 (br s, $SiCH_2$), 0.85 (t, 2 CH_3, J = 6 Hz), 1.28 (br s, 9 CH_2), 1.43–2.4 (m, 2 CH_2), 3.33 (t, PhCH, 7 Hz), 3.92 (t, CH_2O), 7.17 (s, 2 C_6H_5), 7.42 (s, 2 pyridino protons), 8.02 (br s, 2 amidic protons). A third compound (R_f 0.35), having an NMR spectrum similar to that of the second material, was isolated. From previous experience with TLC of analogous silane compounds,[35] it was assumed that the compound with R_f of 0.45 was disiloxane and that with R_f of 0.35 was a silanol derivative of **18**.

Optical Purity of the Bonded Phase. Compound **10**, which was prepared from racemic 2-phenylbutyric acid, was a mixture of the racemate (*RR* and *SS*) and the meso (*RS*) isomers and showed a double spot on a TLC plate, R_f 0.45 and 0.49 (15% EtOAc/toluene). When active compound **17** was purified by column chromatography, the last eluting fraction also contained a mixture showing a double spot, R_f 0.56 and 0.61 (15% EtOAc/toluene). This mixture was rechromatographed on silica gel to obtain a fraction containing predominantly the lower spot (fraction **17B**). The NMR spectrum of this sample was identical with that of active **17**, the first eluting compound. Moreover, compound **20** showed only one spot with the same R_f value as active **17**. If under the hydrosilylation conditions of active **17** or the bonding conditions of **18** partial racemization occurred, a meso form of **20** should be formed and the second spot of the doublet should appear, which was not the case.

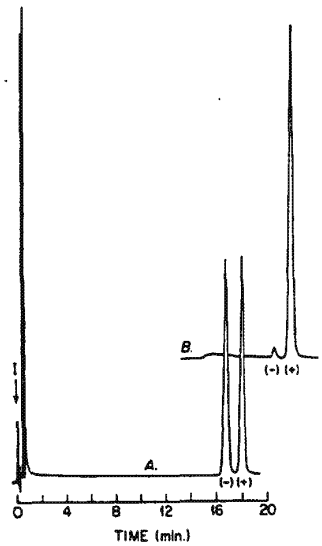


Figure 11. GC enantiomeric separation of *N*-(1,1-dimethylethyl)-2-phenylbutanamide: (A) racemic mixture; (B) obtained from the hydrolysis of **20**. Column, whisker-walled glass capillary column (8-m length × 0.35-mm i.d.) coated with *N*-((*R*)-1-naphthylethyl)dodecanamide. Conditions: temperature of the column, 140 °C; injector, 220 °C, detector, 240 °C; He, 1.5 mL/min.

The optical activity of 2-phenylbutyric acid obtained by hydrolysis of a pure active or a pure meso form of **10**, **17**, or **20** should be 100% or 0%, respectively. Compound **20** was hydrolyzed (20-h reflux in 75% trifluoroacetic acid) to produce 2-phenylbutyric acid. In addition, the sample that was predominantly the lower spot of **17** (fraction **17B**) was hydrolyzed spearately under similar conditions. After the volatiles of the hydrolysates were removed, each of the residues was dissolved in methylene chloride and the organic layer extracted with 5% sodium hydroxide. The aqueous layer was extracted with methylene chloride, acidified, and extracted back with methylene chloride. This last organic layer was dried over sodium sulfate and filtered, and the 2-phenylbutyric acid was converted to its *tert*-butylamide through the acyl chloride as for **17**. A TLC plate of the *tert*-butylamide product from **20** and from fraction **17B** showed a single spot for each product. Both had the same R_f value as pure *N*-(1,1-dimethylethyl)-2-phenylbutanamide. The optical purities of the products from **20** and from fraction **17B**, as determined by GC on a chiral stationary phase (see Figure 11), were 93.4% and 29.4%, respectively. Thus **20** was a mixture of 96.7% *SS* and 3.3% *RR* isomers, and fraction **17B** was predominantly *meso* **17**. The optical activity found in **17B** was due to incomplete purification of meso **17** from its optically active form (*SS*).

Packing of Column. The packing of the bonded phase into a 15 cm × 4.6 mm i.d. stainless steel column followed standard slurry procedures using a solution of 20% methanol in carbon tetrachloride as the slurry medium.

X-ray Diffraction. Crystals of complex **3e**:**7** suitable for diffraction were grown from a 0.02 M solution of **3e** and **7** in methylene chloride–heptane. The diacetyl compound **6** was barely soluble in methylene chloride. Its solubility increased with the addition of bemegride, but two types of crystals formed from slow evaporation of this mixture; one was the self-associated N,N'-2,6-pyridinediylbis[acetamide] and the other, hairlike crystals, was presumably bemegride. Data were collected at room temperature (21 °C) on a Syntex $P2_1$ automated diffractometer using Ni-filtered Cu Kα radiation (λ = 1.5418 Å). Cell dimensions were determined from least-squares refinement of several independently measured reflections well-separated in reciprocal space. The $\theta/2\theta$ scanning technique with variable scan rate was used to measure reflections of 2θ to 130°. Cell dimensions and other experimental parameters are given in Table I. Empirical absorption corrections were made for **6** using ψ scan data. Standard reflections for both **3e**:**7** and **6**, monitored

(35) unpublished results.

UM00013308
NOVARTIS EXHIBIT 1517
Novartis v. Regents, IPR2023-01347
Page 2054 of 4460

every 100 measurements, showed no diminution.

The structures were solved using MULTAN 80.[36] Non-hydrogen atoms were refined, first isotropically and subsequently anisotropically, by using full-matrix least squares using unique reflections with $I \geq 2\sigma(I)$. Hydrogen atoms for 6 were all refined isotropically. For 3e:7 all hydrogen atoms except those on C(10), C(11), C(16), C10′), and C(11′) were refined isotropically. Each unrefined hydrogen atom was assigned an isotropic temperature factor based on the thermal parameters of the carbon atom to which it is bonded. Some disorder was apparent at the end of each butanamide chain. Atomic scattering factors for non-hydrogen atoms were taken from ref 37, those for hydrogen atoms from ref 38. The function minimized was $\sum w(|F_o| - |F_c|)^2$, where the weights w, were determined as follows: $w^{1/2} = 1$ when $|F_o| \leq X$ and $w^{1/2} = X/|F_o| > X$. For 6 $X = 14.0$ and for 3e:7 $X = 9.0$.[39]

Acknowledgment. We acknowledge the National Science Foundation for support of this work under Grant No. CHE-7918536. We are especially grateful to Professor J. Knabe (Universitat des Saarlandes, Stadtwald, West Germany) for providing the optically active and racemic mixtures of many of the compounds used in this study. In addition, we thank Dr. K. Watabe (The Weizmann Institute of Science, Rehovot, Israel) for the determination of the optical purity of the chiral phase and the United States Pharmacopeia for the gift of some of the standard solutes. A.F. gratefully acknowledges the support of the Universidad del Valle (Colombia, South America) and Gillette, Inc. (Boston, MA) through their fellowship programs. B.F. thanks the Barnett Fund for Innovative Research for its support. Contribution No. 259 from the Barnett Institute.

Registry No. (*RS*)-**1a**, 7200-11-5; (*R*)-**1a**, 7245-06-9; (*S*)-**1a**, 7245-04-7; (*RS*)-**1b**, 64574-45-4; (*R*)-**1b**, 64625-35-0; (*S*)-**1b**, 64625-34-9; (*RS*)-**1c**, 2303-83-5; **1d**, 151-83-7; (*RS*)-**1e**, 101693-69-0; (*R*)-**1e**, 83128-88-5; (*S*)-**1e**, 83128-89-6; (*RS*)-**1f**, 83830-62-0; (*R*)-**1f**, 83128-90-9; (*S*)-**1f**, 83128-91-0; (*RS*)-**1g**, 101693-70-3; (*R*)-**1g**, 83128-92-1; (*S*)-**1g**, 83128-93-2; (*RS*)-**1h**, 101693-71-4; (*R*)-**1h**, 83128-76-1; (*S*)-**1h**, 83128-75-0; (*RS*)-**1i**, 83129-31-1; (*R*)-**1i**, 83541-58-6; (*S*)-**1i**, 101693-74-7; (*RS*)-**2**, 65934-66-9; (*R*)-**2**, 65981-70-6; (*S*)-**2**, 65981-69-3; (*RS*)-**3a**, 18389-24-7; (*R*)-**3a**, 17575-58-5; (*S*)-**3a**, 17575-59-6; (*RS*)-**3b**, 101630-91-5; (*R*)-**3b**, 101693-72-5; (*S*)-**3b**, 101693-75-8; (*RS*)-**3c**, 90355-50-3; (*RS*)-**3d**, 90355-75-2; (*R*)-**3d**, 90355-77-4; (*S*)-**3d**, 90355-76-3; **3e**, 64-65-3; (*RS*)-**4a**, 6322-50-5; (*RS*)-**4b**, 99571-24-1; (*R*)-**4b**, 101693-73-6; (*S*)-**4b**, 27539-12-4; (*RS*)-**4c**, 2216-93-5; (*R*)-**4c**, 65567-32-0; (*S*)-**4c**, 65567-34-2; **4d**, 616-04-6; (*RS*)-**4e**, 74007-05-9; (*RS*)-**5a**, 39122-09-3; (*RS*)-**5b**, 39122-12-8; (*RS*)-**5c**, 39122-18-4; (*RS*)-**5d**, 39122-15-1; (*RS*)-**5e**, 34367-67-4; (*RS*)-**5f**, 39122-21-9; **6**, 5441-02-1; **7**, 101630-92-6; **8**, 101630-93-7; **9**, 101630-94-8; (*meso*)-**10**, 101630-95-9; (*RS*)-**10**, 101630-96-0; **11**, 101630-97-1; **12**, 101630-98-2; **13**, 101630-99-3; **13** (diazide), 101631-00-9; **14**, 101631-01-0; **15**, 101631-02-1; **16**, 40473-35-6; (*meso*)-**17**, 101631-03-2; (*SS*)-**17**, 101693-76-9; **18**, 101631-04-3; (*RS*)-**20**, 101631-05-4; $CH_2{=}CH(CH_2)_8Br$, 7766-50-9; NH_2NH_2, 302-01-2; $HSiMe_2Cl$, 1066-35-9; (*S*)-EtCH(Ph)CO_2H, 4286-15-1; (±)-EtCH(Ph)CO_2H, 7782-29-8; 2,6-diaminopyridine, 141-86-6.

Supplementary Material Available: Tables of positional and thermal parameters, bond lengths, and valency angles and torsion angles for **6** and **3e:7**, all with their estimated standard deviations (12 pages). Ordering information is given on any current masthead page.

(36) Main, P.; Fiske, S. J.; Hall, S. E.; Lessinger, G.; Declercq, J. P.; Woolfson, M. M. MULTAN 80, Universities of York, England and Louvain, Belgium, 1980.
(37) Cromer, D. T.; Waber, J. T. *Acta Crystallogr.* **1965**, *18*, 104-109.
(38) Stewart, R. F.; Davidson, E. R.; Simpson, W. T. *J. Chem. Phys.* **1965**, *42*, 3175-3187.
(39) All calculations were carried out on a VAZ 11/780 computer. The least-squares refinement program was based on FMLS (Ganzel, P. L.; Sparks, R. A.; Trueblood, K. N.), UCLA, and modified by McPhail, A. T.; Duke University. Figures 5 and 6 were drawn with ORTEP, crystallographic illustration programs, Johnson, C. K., Oak Ridge, ORNL-3794.

Carbonylation of Titanocene Cyclobutenes. Synthesis and Characterization of a Titanocene–Vinylketene Complex

James D. Meinhart, Bernard D. Santarsiero, and Robert H. Grubbs*

Contribution No. 7164 from the Laboratories of Chemistry, California Institute of Technology, Pasadena, California 91125. *Received August 12, 1985*

Abstract: Carbonylation of several titanocene metallacyclobutene complexes yields the corresponding titanocene–vinylketene complex. The ketene complexes have been isolated as the trimethylphosphine adduct, one of which has been characterized by X-ray diffraction: $Cp_2Ti(C,O\text{-}\eta^2\text{-}OCC(C_6H_5)C(Si(CH_3)_3)CH_2)\cdot P(CH_3)_3$; space group $P2_1/c$; $Z = 4$; 6717 reflections; R_f 0.084, $I > 0$; $a = 9.625$ (2) Å, $b = 16.217$ (2) Å, $c = 16.917$ (4) Å; $\beta = 101.28$ (10)°; $V = 2589.5$ (9) Å^3. Mechanistic studies of the reaction by NMR indicate the presence of an intermediate acyl complex which has been isolated. The experimental evidence suggests that the insertion of carbon monoxide occurs into the less sterically encumbered sp^3 bond rather than the sp^2 bond of the metallacyclobutene. The rearrangement of the acyl complex to the vinylketene product may occur via a titanocene–cyclobutenone complex.

Mediation of complex organic transformations by organometallic catalysts and reagents is an important area of organic chemistry. The potential for both regio- and stereoselectivity in such reactions by the appropriate metal–ligand combinations, in addition to the ability of many organometallic systems to incorporate small organic molecules into larger more complex structures, has prompted a great deal of study in this area.[1] In particular, "Fischer" carbene complexes of Cr and Fe react with a variety of alkynes and carbon monoxide to form hydroquinones,[2] naphthols,[2] naphthoquinones,[3] or pyrones[4] and with imines to yield β-lactams.[5] The mechanistic details of these complex tranfor-

Table I. Titanocene–Vinylketene–Trimethylphosphine Complexes

compd	R	R′	yield, %
2a	Ph	Ph	82
2b	Ph	Me_2Si	92
2c	Ph	CH_3	80
2d	CH_3	CH_3	77
2e	CH_2CH_3	CH_2CH_3	70

(1) (a) Collman, J. P.; Hegedus, L. S. *Principles and Applications of Organotransition Metal Chemistry*; University Science Books: Mill Valley, CA, 1980.

(2) Dötz, K. H. *Pure Appl. Chem.* **1983**, *55*, 1689-1706.

0002-7863/86/1508-3318$01.50/0 © 1986 American Chemical Society

UM00013309
NOVARTIS EXHIBIT 1517
Novartis v. Regents, IPR2023-01347
Page 2055 of 4460

EUR. J. MED. CHEM. — CHIM. THER., 1934-19, N° 6, pp. 519-524

Fentanyl analogues 3. 2-(1,2,3,4-tetrahydro)-naphthyl substituted 4-anilidopiperidines (*)

E. KIM FIFER (1), W. MARVIN DAVIS (2), Ronald F. BORNE (1) (**)

(1) *Department of Medicinal Chemistry*
(2) *Department of Pharmacology, School of Pharmacy, University of Mississippi, University, MS 38677 U.S.A.*

(Received March 12, 1984, accepted September 4, 1984)

Summary. — The synthesis and analgetic properties of 2-(1,2,3,4-tetrahydro)-naphthyl analogues of fentanyl and 3-methylfentanyl are reported. The relation of the N-phenethyl group to the piperidine ring is discussed.

Résumé. — La synthèse et les propriétés analgésiques d'analogues (tétrahydro-1,2,3,4)-2-naphtyl du fentanyl et du méthyl-3 fentanyl sont rapportées. La conformation du groupe N-phénéthyl par rapport au cycle pipéridine est discutée.

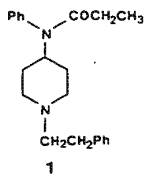
Zusammenfassung. — Synthese und analgetische Aktivität von 2-(1,2,3,4-Tetrahydro)-naphthylanalogen des Fentanyl und des 3-Methylfentanyl werden beschrieben. Die Konformation der N-Phenethylgruppe wird in Bezug zum Piperidinring diskutiert.

Key words : Fentanyl. — Analgetic. — Phenethyl. — Tetrahydronaphthyl. — Conformation.

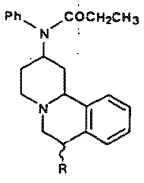
INTRODUCTION

Investigation of structure-activity relationships (SAR) of the 4-anilidopiperidine class of analgetics, represented by fentanyl **1**, has resulted in the discovery of numerous, potent morphine-like compounds (1). These studies have primarily focused on substitution of the various positions of the piperidine ring (2), along with variation of the N-phenyl (3), the N-acyl (4), and the N-phenethyl (2b, 5) groups. While much has been learned about the structural requirements of fentanyl for analgetic activity, relatively little is known about the effect of its conformation on activity. Casy (5) had previously suggested that the preferred conformation of fentanyl is that in which the piperidine ring assumes the chair form with an equatorial propanilido function. To test this hypothesis, the piperidine ring was restricted into a chair type conformation by incorporation into a tropane ring system (6). The β-3-(propanilido)-nortropane analogue assumed the predicted conformation and possessed activity not significantly different from that of fentanyl. In order to evaluate contributions of a piperidine boat conformation, 2-azabicyclo[2.2.2]octane analogues of fentanyl were prepared and evaluated (7). These analogues were much less active than either morphine or fentanyl. Attempts to restrict the conformational flexibility of the N-phenyl function by fusion to the piperidine ring (8) or by connection to the acyl moiety (9) have led to an abolition of activity. Likewise, connection of the acyl side chain to the 3-position of the piperidine ring to give perhydronaphthyridine analogues (10) resulted in a loss of activity.

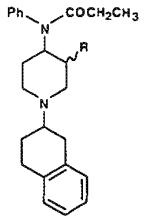
Conformational restriction of the phenethyl group may be perceived in the *cis*- and *trans*-isomers of the benzo[a]-quinolizidine **2a**, which may be viewed as *syn*-phenethyl-restricted analogues of fentanyl. Unfortunately, no analgetic studies were reported for **2a** (11). Substitution of a phenyl group in the 7-position of **2a** to give **2b** places phenyl groups in both *syn* and *anti*, extended conformations (12). However, the four diastereomers of *trans*-**2b** were reported to possess only modest analgetic activity. This may be considered consistent with previous reports that substitution at the 2-position of the piperidine ring leads to attenuation of activity (2 *a*). Because the most likely orientation of the phenethyl group would be expected to be an extended, antiperiplanar conformation, and because alkyl substitution



1



2a R=H
b R=Ph



3a R=H
b R=cis-CH_3
c R=trans-CH_3

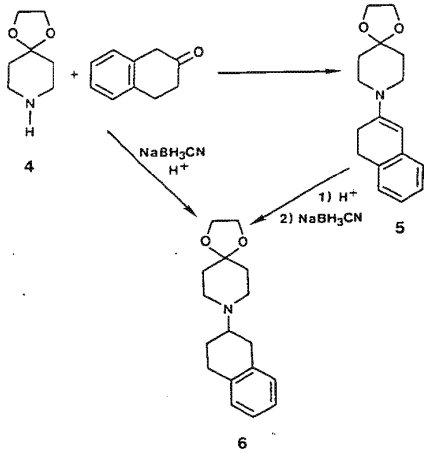
(*) Taken in part from the Ph. D. dissertation of E.K.F., University of Mississippi, University, MS 1983.
(**) Author to whom correspondence should be addressed.

UM00013310
NOVARTIS EXHIBIT 1517
Novartis v. Regents, IPR2023-01347
Page 2056 of 4460

of both the phenethyl side chain α- to the ring nitrogen and of the 3-position of the piperidine ring has been reported to enhance activity (2 *b*), **3a-c** were synthesized and pharmacologically evaluated.

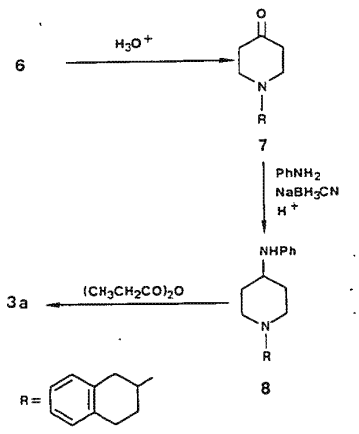
CHEMISTRY

Two methods of the preparation of **6** from ketal **4** and β-tetralone are illustrated in Scheme 1. The first involved



Scheme 1.

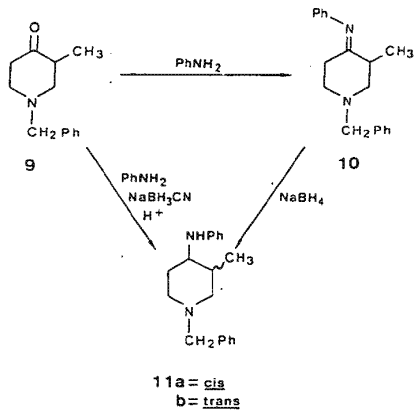
formation of the enamine **5**. The enamine was isolated, converted to its hydrochloride salt (iminium hydrochloride), and reduced to the amino ketal **6** with sodium cyanoborohydride (13). Alternatively, reductive amination of β-tetralone with **4** and sodium cyanoborohydride gave **6** in one step (13), although yields were much lower than for the two-step procedure. Ketal **6** was converted to the desired product **3a** as depicted in Scheme 2. Acid hydro-



Scheme 2.

lysis of the ketal to give **7**, followed by reductive amination with aniline and sodium cyanoborohydride afforded the anilino piperidine **8**. Finally, acylation of **8** with excess propionic anhydride gave the target fentanyl analogue **3a**.

Unlike the synthesis of **3a**, the preparation of **3b** and **3c** focused on the synthesis of the methylated piperidine ring and propanilido moieties, followed by coupling with the tetrahydronaphthyl substituent to give both **3b** and **3c**. The starting piperidone **9** was synthesized as previously reported (14), then converted to anil **10** by refluxing with aniline in xylene (Scheme 3). Reduction with sodium boro-



Scheme 3.

hydride afforded a mixture of the diastereomeric anilino piperidines **11a** and **11b**. Alternatively, **9** could be converted to **11** in one step by reductive amination with aniline and sodium cyanoborohydride as previously discussed. Flash chromatographic separation of the diastereomeric mixture produced by either procedure gave the two isomers in a 2:1 product ratio ; however, relative stereochemistry could not be determined due to overlap of peaks in the NMR spectra. Acylation of **11a** and **11b** with propionic anhydride afforded the 1-benzyl-3-methylnorfentanyl analogues **12a** and **12b** (Scheme 4), respectively, whose stereochemistry was assigned based on near first-order analysis of the proton NMR splitting pattern of the C-4 methine proton. Assuming the preferred chair conformation with an equatorial N-phenylpropanamide moiety, the *cis*-isomer **11a** exhibited a multiplet centered at δ 4.43 composed of a doublet (J = 12.0 Hz) of triplets (J = 4.5 Hz) while the *trans*-isomer **11b** exhibited a multiplet centered at δ 4.55 composed of a triplet (J = 10.8 Hz) of doublets (J = 4.4 Hz). Thus, the stereochemistry of compounds **11-13** prepared here is consistent with the work of Van Bever *et al.* (2 *b*) for the synthesis of analogues of 3-methylfentanyl in which the methyl group of the *cis*-isomer occupies the axial position, while it is equatorial in the *trans*-isomer. Consequently, the 2:1 ratio was *cis*:*trans* for the conversions of **9** to **11a-b**, which is comparable to that reported for the reduction of the carbamate analogue of **9** (2 *b*). The yield of the *trans*-isomer is greater in this case than when the 3-substituent

11a-l

3b-c

was a larger al
benzyl groups
methylnorfentan
Reductive amin
afforded the cor
fentanyl analogu

PHARMACOL

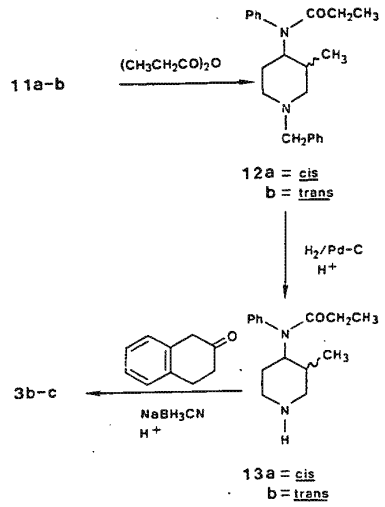
Compounds 3
analgetic activity
in mice using a
flick assay (15).

TABLE I. — *An*
1-[2-(1,2,3,4

Agonist	AD_{50} [a,b]
Fentanyl citrate	0.010 mg/k (0.007-0.01
3a-HCl	0.012 mg/k (0.006-0.02
3b-HCl	0.004 mg/k (0.001-0.01
3c-HCl	0.018 mg/k (0.006-0.05

[a] ICR Swiss male m
[b] (95 % confidence
[c] IC Swiss male mi
[d] Dose which gives
[e] Number in which a number tested.
[f] By the method of

UM00013311
NOVARTIS EXHIBIT 1517
Novartis v. Regents, IPR2023-01347
Page 2057 of 4460



Scheme 4.

was a larger aliphatic group (2 *c*). Hydrogenolysis of the benzyl groups of **12a** and **12b** gave the *cis*- and *trans*-3-methylnorfentanyl analogues **13a** and **13b**, respectively. Reductive amination of β-tetralone with **13a** and **13b** then afforded the corresponding 3-methyltetrahydronaphthylnorfentanyl analogues **3b** and **3c**.

PHARMACOLOGICAL RESULTS AND DISCUSSION

Compounds **3a-c** along with fentanyl were evaluated for analgetic activity and naloxone reversibility subcutaneously in mice using a modification of the d'Amour-Smith tail-flick assay (15). The results are presented in Table I, along

TABLE I. — *Analgesic activity and log P values of the isomeric 1-[2-(1,2,3,4-tetrahydro)naphthyl] analogues of fentanyl.*

Agonist	AD_{50} [ab]	Naloxone Antagonism: Agonist Dose [d]	Naloxone Antagonism: Results [e]	LD_{50} [bc]	Log P [f]
Fentanyl citrate	0.010 mg/kg (0.007-0.0018)	0.1 mg/kg	6/6	109.0 mg/kg (101.9-116.6)	2.63
3a·HCl	0.012 mg/kg (0.006-0.027)	0.1 mg/kg	6/6	44.8 mg/kg (38.6-52.0)	3.00
3b·HCl	0.004 mg/kg (0.001-0.008)	0.05 mg/kg	6/6	9.5 mg/kg (8.4-10.6)	3.00
3c·HCl	0.018 mg/kg (0.006-0.036)	0.1 mg/kg	6/6	77.0 mg/kg (60.5-98.1)	2.76

[a] ICR Swiss male mice, s.c., normal saline vehicle.
[b] (95 % confidence limits).
[c] IC Swiss male mice, i.p., normal saline vehicle.
[d] Dose which gives a 100 % response.
[e] Number in which analgesia was abolished by naloxone. HCl (4 mg/kg)/number tested.
[f] By the method of Baker (16) (uncorrected).

with log P values (uncorrected), as determined by the method of Baker (16). The analgesia produced was reversed by naloxone. The tetrahydronaphthyl analogues (**3a-c**) all exhibited the same pharmacological profile as fentanyl (17). In each case the mice appeared excitable, exhibiting an increase in motor activity, with circling. At doses which produce a greater than 100 % analgetic effect (> AD_{100}), the Straub-tail response was present. However, this response was absent at the AD_{50} level.

It is evident from the data in Table I that when the N-phenethyl substituent is restricted into an *anti*, extended or antiperiplanar conformation by incorporation into a tetrahydronaphthyl moiety (**3a-c**), analgetic activity is maintained or increased slightly.

Although Van Bever *et al.* (2 *b*) reported a slight increase in potency when an α-methyl group was incorporated into the N-phenethyl side chain, the corresponding tetrahydronaphthyl analogue **3a** showed no significant change in potency although the log P value was increased relative to fentanyl. Thus, any decrease in activity due to increased bulk or deviation from the preferred conformation is conceivably offset by a more favorable distribution into the CNS. The *cis*-3-methyl-isomer **3b** was found to be approximately three times as potent as fentanyl. The increase in potency of **3b** over fentanyl is analogous to that seen with *cis*-3-methylfentanyl (2 *b*). This increased potency is probably due to a more favorable interaction with the receptor rather than increased penetration into the CNS since there is no difference in log P values between **3a** and **3b**. The *trans*-3 methyl-isomer **3c** displays a slightly decreased activity relative to fentanyl. In this case the small increase in lipid solubility apparently does not offset the increased steric bulk.

Because the tetralin analogues **3a-c** could be considered as cyclized derivatives of the potent and toxic clandestine drug N-(α-methyl)phenethylfentanyl (« China White ») (18), acute toxicity studies were carried out by obtaining LD_{50} values. Results are presented in Table I. All three tetralin analogues were more acutely toxic than fentanyl with the most active analgetic (**3b**) being considerably more toxic than fentanyl or **3a** and **3c**. Loss of righting reflex occurred quickly (usually 2-6 minutes) after all four compounds. Lethality occurred, with few exceptions, in the first 20 minutes after injection, apparently consequent to respiratory failure. Excitatory signs (hyperreflexia, Straub tail, running or clonic jumps) were seen sporadically during onset with sublethal doses, and during the recovery phase. These were more prominent in the case of fentanyl than for the other compounds. When recovery occurred, there were no noticeable after-effects. Pronounced salivation was seen for occasional mice, mostly after administration of **3a**. The effects of stereochemistry on toxicity warrants further study.

The analgetic data indicate that the tetrahydronaphthyl group places the phenyl ring in a favorable conformation for interaction at the opiate receptor. It is thus suggested that the conformation of the phenethyl group of fentanyl and related 4-anilidopiperidine analgetics is, indeed, antiperiplanar when interacting with the opiate receptor. This

UM00013312
NOVARTIS EXHIBIT 1517
Novartis v. Regents, IPR2023-01347
Page 2058 of 4460

is supported by crystallographic studies of fentanyl and its analogues (19) which indicate that the phenethyl side chain is equatorial and extended (or antiperiplanar). Additionally, Dreiding models of **3a-c** indicate that the distance from the center of the aromatic ring to the basic nitrogen is approximately 5.2 Å, and that although the aromatic ring is antiperiplanar to the piperidine ring, it is locked into a conformation which is approximately 70° out of the plane of the piperidine ring as illustrated in Figure 1. X-Ray

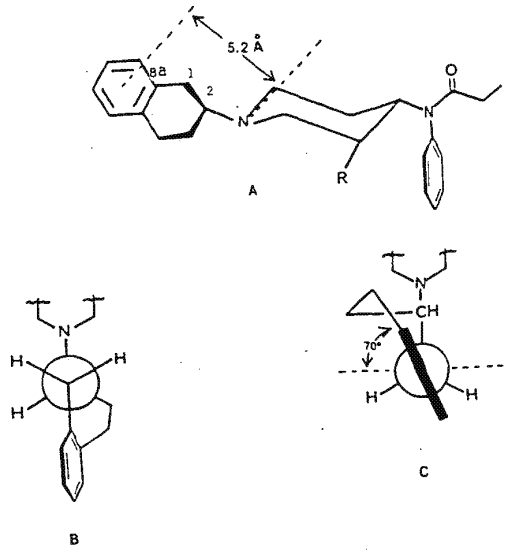


FIG. 1. — Geometry of the tetrahydronaphthyl fentanyl derivatives : A, the distance from the aromatic ring to the basic nitrogen ; B, the view down the C-1 to C-2 bond of the tetrahydronaphthyl moiety ; and C, the view down the C-1 to aromatic C-8a bond of the tetrahydronaphthyl moiety.

crystallographic data for **3b** support this latter conformation (20).

The results of this research provide evidence that an antiperiplanar phenethyl group is a requirement for interaction with the opiate receptor(s), and a more favorable interaction may result when the phenyl ring is skewed at 70° from the plane of the piperidine chair.

EXPERIMENTAL

All melting points were taken on a Thomas-Hoover Unimelt (uncorrected) or on a Mel-Temp apparatus. Infrared spectra were determined with a Perkin-Elmer Model 281B, a Perkin-Elmer Model 257, or a Beckman IR-33 spectrometer. Solution IR spectra were taken in matched sodium chloride cells of 0.197 mm (reference) and 0.214 mm (sample) widths. All ^1H NMR spectra were obtained on a Varian Model EM390 or a Jeolco Model C-60-HL spectrometer and all values are reported in ppm (δ) downfield from TMS. Thin-layer chromatography was performed on Macherey-Nagel silica gel G (0.25 mm) with fluorescent indicator. Column chromatography was performed on Macherey-Nagel silica gel 60 (0.05-0.2 mm), and flash chromatography was performed on Merck silica gel 60 (0.040-0.063 mm). High pressure liquid chromatographs were obtained on a Waters Associate HPLC unit equipped with a M-6000 pump, a Rheodyne 7161 injector, a Model 440 dual wavelength UV detector (254 nm and 280 nm), and a C_{18}-μBondapak reverse phase column. Mass spectra and GC/MS were recorded at an electron energy of 70 eV on a Finnigan 3200, MS/DS system. Kugelrohr distillation implies bulb to bulb distillation and reported temperatures are oven temperatures, not actual boiling points. Analyses indicated by elemental symbols were within ± 0.4 % of the theoretical values and were performed by either Galbraith Laboratories, Inc., Knoxville, TN, or Atlantic Microlab, Inc., Atlanta, GA.

1-[2-(1,2,3,4-Tetrahydro)naphthyl]-4-piperidone ethylene ketal **6**

Procedure A. A soln of 10.7 g (75 mmol) of 4-piperidone ethylene ketal **4**, 10.0 g (68 mmol) of β-tetralone, a few crystals of *p*-toluenesulfonic acid, and 100 mL of benzene was refluxed with azeotropic removal of water for 48 h. The solvent was removed *in vacuo* to give enamine **5** as an oil. This was used without further purification : IR ($CHCl_3$) 1613 cm^{-1} (enamine) ; ^1H NMR ($CDCl_3$) δ 1.74 (bt, 4, $-(RO)_2C-CH_2-$), 2.34 (m, 3), 2.85 (bt, 2), 3.37 (m, 3), 3.97 (s, 4, $-O-CH_2-CH_2O-$), 5.53 (s, 1, C=C-H), 7.00 (m, 4, ArH) ; m/e 207.9 (m^+), 127.7 (base).

The HCl salt of **5** was precipitated by bubbling HCl gas through a soln of 16.6 g (68 mmol) of **5** in 150 mL of anhyd tetrahydrofuran. A soln of 3.0 g (48 mmol) of sodium cyanoborohydride in 60 mL of MeOH was added and the mixture stirred for 4 h at room temp. The solvent was removed *in vacuo*, and the resulting solid was taken up in 200 mL of 0.1 *N* NaOH and extracted with Et_2O (4 × 100 mL). After drying over Na_2SO_4, the solvent was removed *in vacuo* to yield 10.0 g (54 % crude overall yield) of a dark oil which was converted to the oxalate salt and recrystallized from EtOH to yield 13.0 g (53 %) of white crystals : mp 185-186° C. The free base was regenerated for spectral purposes : ^1H NMR ($CDCl_3$) δ 1.77 (t, 4, $-CH_2C(OR)_2-$), 1.94-2.27 (m, 2, $ArCH_2CH_2-$), 2.65-3.00 (m, 9, $N-CH_2-$, and $ArCH_2CH-N$), 3.95 (s, 4, $-OCH_2-$), 7.09 (s, 4, ArH) ; m/e 273.2 (m^+, base). *Anal.* $C_{17}H_{23}NO_2.C_2H_2O_4$ (C, H, N).

Procedure B. To a soln of 6.9 g (47 mmol) of β-tetralone in 70 mL of MeOH was added a soln of **5** *N* HCl in MeOH (19 mL, 94 mmol), followed by 40 g (0.28 mol) of **4**, 2.1 g (33 mmol) of sodium cyanoborohydride, and 40 g of 3 A molecular sieves. The mixture was stirred for 5 days at room temp then filtered, cooled in an ice bath, made acidic with concd HCl, and concentrated *in vacuo* to give an orange oil. This was taken up in 150 mL of H_2O and extracted with Et_2O (3 × 60 ml). The aqueous phase was made basic with solid KOH, saturated with NaCl, and extracted with Et_2O (4 × 100 mL). The combined Et_2O layers were dried over Na_2SO_4 and concentrated *in vacuo* to give a green oil which was kugelrohr distilled (65° C/0.5 mm) to remove the excess starting ketal. The pot residue (3.65 g, 28 %) was converted to the hydrochloride salt and recrystallized from EtOH/Et_2O to give crystals : mp 213-215° C. The oxalate salt was prepared : mp 185-186° C (EtOH). The ^1H NMR spectrum of the free base was identical to the product of Procedure A.

1-[2-(1,2,3,4-Tetrahydro)naphthyl]-4-piperidone **7**

A soln of 4.2 g (15 mmol) of **6** in 80 mL of 10 % HCl was refluxed for 3 h, then extracted with 50 mL of Et_2O. The aqueous layer was cooled in an ice bath, made basic with solid Na_2CO_3, and extracted with Et_2O (4 × 60 mL). The combined Et_2O layers were dried over Na_2SO_4 and concentrated *in vacuo* to afford 3.4 g of a solid which was recrystallized from hexane to give 3.0 g (85 %) of tan crystals : mp 80-81.5° C ; IR (KBr) 1709 cm^{-1} (C=O) ; ^1H NMR ($CDCl_3$) δ 1.92-2.30 (m, 2, $ArCH_2CH_2-$), 2.48 (t, 4, $-CH_2-C=O$), 2.70-3.10 (m, 9, $-CH_2N-$, $Ar-CH_2CH-N-$), 7.13 (s, 4, ArH) ; m/e 228.8 (m^+), 129.8 (base). *Anal.* $C_{15}H_{19}NO$ (C, H, N).

4-Phenylamino-1-[2-(1,2,3,4-tetrahydro)naphthyl]piperidine **8**

To a soln of 3.0 g (13 mmol) of **7** in 30 mL of MeOH was added a 5 *N* soln of HCl in MeOH (6 mL, 26 mmol), followed by 7.3 g (78 mmol) of freshly distilled aniline, 500 mg (8 mmol) of sodium cyanoborohydride and 20 g of 3 A molecular sieves. Additional sodium

cyanoborohydride
at 48 h ; 100 mg at
mixture was filtered
HCl. The solvent v
50 mL of H_2O the
layer was cooled in
with NaCl, and ext
Na_2SO_4 and concer
by kugelrohr distill
chromatographed c
acetate with 0.05 %
was recrystallized fr
mp 83-85° C ; ^1H
(m, 3), 2.23-2.63 (m,
by NH), 3.44 (bs, 1,
m/e 306.1 (m^+), 212

N-[1-[2-(1,2,3,4-Tet
mide **3a**

A soln of 2.65 g
was stirred at reflu
stirred for 3 h with
with $CHCl_3$ (3 × 4
oil was taken up in
Na_2CO_3 soln. The
The aqueous fractio
with $CHCl_3$ (3 ×
in vacuo yielded an o
This resisted recryst
of silica gel 60 (Et
to give 1.3 g of a yell
mp 191.5-192.5° C.
Et_2O) : mp 272-27
purposes : mp 130-1
^1H NMR ($CDCl_3$) δ
and 12 Hz), 1.68-2.1
$-CH_2-CH_3$)], 2.19-3.1
C4-H), 7.03 (s, 6, Ar
Anal. $C_{24}H_{30}N_2O.C$

1-Benzyl-3-methyl-4-

Procedure A. A sc
aniline, a few crysta
was refluxed with az
of the solvent *in v*
distillation (55-60° C
phenyliminopiperidin
further purification
To a solution of 4
was added 5.8 g of
addition was comple
allowed to cool to r
the mixture was sti
about 140 mL *in va*
extracted with toluer
tration *in vacuo* a
gave **11a-b** as a yell
Thin-layer chromatc
spots R_f = 0.62 an
NH_4OH).

Separation of cis- a
11a-b

Flash chromatogra
and NH_4OH 0.05 %
vered pure product)
quently shown to be
(d, 3, CH_3), 1.50-1.8
CH_2, C4 H, NH D,
ArH). The oxalate s
to give white crysta
(base). *Anal.* $C_{19}H_{24}$

UM00013313
NOVARTIS EXHIBIT 1517
Novartis v. Regents, IPR2023-01347
Page 2059 of 4460

cyanoborohydride was added as the reaction progressed (200 mg at 48 h ; 100 mg at 72 h ; total = 800 mg, 13 mmol). After 5 days the mixture was filtered, cooled in an ice bath, and made acidic with concd HCl. The solvent was removed *in vacuo* and the residue taken up to 50 mL of H_2O then extracted with Et_2O (2 × 50 mL). The aqueous layer was cooled in an ice bath, made basic with solid KOH, saturated with NaCl, and extracted with Et_2O (4 × 40 mL). After drying over Na_2SO_4 and concentration *in vacuo*, the excess aniline was removed by kugelrohr distillation (50° C/0.1 mm). The dark residue was flash chromatographed on silica gel 60 (40 % petroleum ether in ethyl acetate with 0.05 % ammonium hydroxide). An oil was obtained which was recrystallized from hexane to give 2.1 g (53 %) of off-white needles : mp 83-85° C ; ^1H NMR ($CDCl_3$) δ 1.20-1.80 (m, 3), 1.87-2.23 (m, 3), 2.23-2.63 (m, 2), 2.63-3.10 (m, 7), 3.32 (tt, 1, ArNH-C*H*-, masked by NH), 3.44 (bs, 1, NH, D_2O exch), 6.61 (m, 3, ArH), 7.09 (s, 6, ArH) ; m/e 306.1 (m^+), 212.9 (base). *Anal.* $C_{21}H_{26}N_2$ (C, H, N).

N-{1-[2-(1,2,3,4-Tetrahydro)naphthyl]-4-piperidinyl}-N-phenylpropanamide **3a**

A soln of 2.65 g (9 mmol) of **8** in 40 mL of propionic anhydride was stirred at reflux for 16 h, allowed to cool to room temp, then stirred for 3 h with 40 mL of satd Na_2CO_3 . The mixture was extracted with $CHCl_3$ (3 × 40 mL). The $CHCl_3$ was removed *in vacuo*, and the oil was taken up in 50 mL of Et_2O and washed with 50 mL of 10 % Na_2CO_3 soln. The ether was extracted with 10 % HCl (3 × 30 mL). The aqueous fraction was made basic with solid Na_2CO_3 then extracted with $CHCl_3$ (3 × 40 mL) and dried over Na_2SO_4 . Concentration *in vacuo* yielded an oil (2.35 g, 75 % crude) which solidified on standing. This resisted recrystallization and was flash chromatographed on 70 g of silica gel 60 (EtOAc 33 % in petroleum ether in 0.2 % NH_4OH) to give 1.3 g of a yellow solid which formed an oxalate salt (EtOH/Et_2O): mp 191.5-192.5° C. The hydrochloride salt was also prepared (EtOH/Et_2O) : mp 272-274° C. The free base was regenerated for special purposes : mp 130-131.5° C ; IR ($CHCl_3$) 1636 cm^{-1} (C=O, amide) ; ^1H NMR ($CDCl_3$) δ 1.02 (t, 3, J = 7.5 Hz, -CH_3), 1.47 (btt, 3, J = 3.8 and 12 Hz), 1.68-2.19 [bs at 1.86 overlapping a q at 1.90 (J = 7.5 Hz, -CH_2-CH_3)], 2.19-3.15 (m, 9), 4.70 (tt, 1, J = 3.8 and 12 Hz, piperidine C4-H), 7.03 (s, 6, ArH), 7.36 (m, 3, ArH) ; m/e 362.2 (m^+), 82.5 (base). *Anal.* $C_{24}H_{30}N_2O.C_2H_2O_4$ (C, H, N).

1-Benzyl-3-methyl-4-phenylaminopiperidine **11a-b**

Procedure A. A soln of 35.0 g (0.17 mol) of **9**, 21.5 g (0.23 mol) of aniline, a few crystals of *p*-toluenesulfonic acid, and 300 mL of xylene was refluxed with azeotropic removal of water for 22 h. After removal of the solvent *in vacuo*, excess aniline was removed by kugelrohr distillation (55-60° C/0.2 mm) to leave 46.7 g of *1-benzyl-3-methyl-4-phenyliminopiperidine* **10** as an orange oil which was used without further purification : IR (neat) 1673 cm^{-1} (C=N-).

To a solution of 46.5 g (0.17 mol) of crude **10** in 125 mL of MeOH was added 5.8 g of sodium borohydride (0.15 mol) in portions. After addition was complete, the mixture was heated at 50° C for 17 h, then allowed to cool to room temp. Water (100 mL) was added slowly and the mixture was stirred at room temp for 2 h then concentrated to about 140 mL *in vacuo*. This was again diluted with 100 mL of H_2O, extracted with toluene (4 × 70 mL), and dried over $MgSO_4$. Concentration *in vacuo* and kugelrohr distillation (150-160° C/0.15 mm) gave **11a-b** as a yellow oil (42.6 g, 88 % overall yield based on **9**). Thin-layer chromatography of **11a-b** on silica gel G indicated two spots R_f = 0.62 and 0.46 (EtOAc/petroleum ether 1 : 1 with 0.05 % NH_4OH).

Separation of cis- and trans-1-Benzyl-3-methyl-4-phenylaminopiperidine **11a-b**

Flash chromatography of 5 g of **11a-b** on silica gel 60 (EtOAc 25 % and NH_4OH 0.05 % in petroleum ether) gave 2.2 g (66 % of the recovered pure product) of the isomer with R_f = 0.62 which was subsequently shown to be the *cis*-isomer (**11a**) : ^1H NMR ($CDCl_3$) δ 0.93 (d, 3, CH_3), 1.50-1.85 (m, 2), 1.85-2.75 (m, 5), 3.47 (m, 4, benzylic CH_2 , C4 H, NH D_2O exch), 6.49-6.84 (m, 3 ArH),. 7.04-7.50 (m, 7, ArH). The oxalate salt was prepared and recrystallized from EtOH to give white crystals : mp 176.5-177.5° C ; m/e 280.3 (m^+), 91.2 (base). *Anal.* $C_{19}H_{24}N_2.C_2H_2O_4$ (C, H, N).

In addition to a fraction containing both isomers, a fraction containing 1.25 g (34 % of the recovered pure product) of the isomer with R_f = 0.46 was isolated. This was subsequently shown to be the *trans*-isomer **11b** : ^1H NMR ($CDCl_3$) δ 0.93 (d, 3, CH_3), 1.17-2.20 (m, 5), 2.83 (bd, 3), 3.34 (bs, 1, D_2O exch, N-H), 6.40-6.74 (m, 3, ArH), 6.97-7.41 (m, 7, ArH). The oxalate salt was prepared and recrystallized from EtOH/Et_2O to give white crystals : mp 150-152° C ; m/e 280.3 (m^+), 91.2 (base). *Anal.* $C_{19}H_{24}N_2.C_2H_2O_4$ (C, H, N).

Procedure B. To a soln of 5.0 g (25 mmol) of **9** in 50 mL of MeOH was added a soln of 5 *N* HCl in MeOH (10 mL, 49 mmol), followed by 13.7 g (0.15 mol) of aniline, 0.93 g (15 mmol) of sodium cyanoborohydride, and 25 g of 3 A molecular sieves. After the mixture had stirred at room temp for 48 h, 0.4 g (6 mmol, total = 21 mmol) of sodium cyanoborohydride was added. After stirring an additional 24 h the mixture was filtered, cooled in an ice bath and made acidic with concd HCl. The solvent was removed *in vacuo*, the residue taken up in 150 mL of H_2O, and extracted with Et_2O (2 × 50 mL). The aqueous phase was cooled in an ice bath, made basic with solid KOH, saturated with NaCl, and extracted with Et_2O (4 × 60 mL). The combined ether extracts were dried over Na_2SO_4 , concentrated *in vacuo*, and kugelrohr distilled to give two fractions : aniline (50° C/0.2 mm) and 5.9 g (84 %) of a mixture of isomers (150° C/0.2 mm) which was identical to the mixture formed in Procedure A.

Cis-N-[3-Methyl-1-(phenylmethyl)-4-piperidinyl]-N-phenylpropanamide **12a**

A mixture of 2.8 g (10 mmol) of **11a** and 25 mL of propionic anhydride was refluxed for 4 h, cooled in an ice bath, and treated with 150 mL of 20 % NaOH. After stirring at room temp for 2 h, the mixture was extracted with Et_2O (4 × 40 mL), dried over Na_2SO_4 , and concentrated *in vacuo* to give 3.5 g of a dark oil. Conversion to the hydrochloride salt and recrystallization from EtOH/Et_2O gave 3.4 g (91 %) of white crystals : mp 202-203° C ; IR (KBr) 2613 cm^{-1} (amine HCl), 1623 cm^{-1} (C=O, amide) ; m/e 336.3 (m^+), 91.2 (base). A small portion was converted back to the free base : ^1H NMR ($CDCl_3$) δ 0.86-1.19 (t centered at 1.00, J = 7.5 Hz, -CH_2-CH_3 ; d centered at 1.12, 3, J = 6.5 Hz, -$CHCH_3$), 1.19-1.57 (m, 3), 1.94 (q, 2, J = 7.5 Hz, -CH_2CH_3) 2.06-2.39 (m, 1), 2.50-2.90 (m, 3), 3.38 (s, 2, $ArCH_2N$), 4.43 (dt, 1, J = 12 Hz and 4.5 Hz, $W_{1/2}$ = 22 Hz, C4 H), 6.92-7.42 (m, 10, ArH). *Anal.* $C_{22}H_{28}N_2O.HCl.1/2H_2O$ (C, H, N).

Trans-N-[3-Methyl-1-(phenylmethyl)-4-piperidinyl]-N-phenylpropanamide **12b**

A mixture of 7.0 g (25 mmol) of **11b** and 50 mL of propionic anhydride was heated at reflux for 3 h, cooled in an ice bath, and treated with 150 mL of 20 % NaOH. After stirring at room temp for 2 h the mixture was extracted with Et_2O (3 × 100 mL), dried over Na_2SO_4 , and concentrated *in vacuo* to a dark oil which was converted to the hydrochloride salt and recrystallized from EtOH/Et_2O to give 7.4 g (80 %) of crystals : mp 185-187° C ; IR (KBr) 2413 cm^{-1} (amine HCl), 1654 cm^{-1} (C=O, amide) ; m/e 336.3 (m^+), 91.2 (base). A small portion was converted back to the free base : ^1H NMR ($CDCl_3$) δ 0.84-1.14 (d centered at 0.98, 3, -$CHCH_3$, t, centered at 1.02, 3, CH_2-CH_3), 1.42-2.26 (m, 7), 2.87 (bd, 2), 3.44 (s, 2, $ArCH_2N$), 4.55 (td, 1, J = 10.8 Hz and 4.4 Hz, $W_{1/2}$ = 28 Hz, C4 H), 6.95-7.52 (m, 10, ArH). *Anal.* $C_{22}H_{28}N_2O$ (C, H, N).

Cis-N-(3-Methyl-4-piperidinyl)-N-phenylpropanamide **13a**

A soln of 14.6 g (39 mmol) of **12a**, 2 mL of concd HCl, and 150 mL of EtOH along with 1.5 g of 10 % Pd/C was hydrogenated (50 psi H_2) at 35° C for 21 h. After filtration and concentration *in vacuo*, the residue was taken up in 75 mL of H_2O, mixed with 75 mL of satd Na_2CO_3 soln, and extracted with $CHCl_3$ (3 × 50 mL). The combined $CHCl_3$ layers were washed with 100 mL of H_2O, dried over Na_2SO_4 , and concentrated *in vacuo* to an oil. Kugelrohr distillation gave 7.3 g (76 %) of a clear oil (125-130° C/0.1 mm) : ^1H NMR ($CDCl_3$) δ 0.87-1.17 (t centered at 1.01, 3, J = 7.5 Hz, -CH_2-CH_3 ; d centered at 1.05, 3, J = 7.5 Hz, -CH-CH_3), 1.17-1.47 (m, 2), 1.87 (bs, 1, NH, D_2O exch), 1.94 (q, 2, J = 7.5 Hz, CH_2-CH_3), 2.45-3.13 (m, 5), 4.55 (di, 1, C4 H), 6.95-7.53 (m, 5, ArH) ; m/e 246.2 (m^+), 97.1 (base).

UM00013314
NOVARTIS EXHIBIT 1517
Novartis v. Regents, IPR2023-01347
Page 2060 of 4460

The oxalate salt was prepared and recrystallized from EtOH/Et_2O to give white crystals : mp 155-156° C. *Anal.* $C_{15}H_{22}N_2O.C_2H_2O_4$ (C, H, N).

Trans-N-(3-Methyl-4-piperidinyl)-N-phenylpropanamide **13b**

A 7.2 g (19 mmol) sample of **12b** was mixed with 1.5 mL of concd HCl, 100 mL of EtOH, and 720 mg of 10 % Pd/C and treated according to the procedure described for the synthesis of **13a**. A dark oil was obtained which was kugelrohr distilled (105-112° C/0.05 mm) to give 3.64 g (77 %) of a clear oil which solidified on standing : mp 90.5-92° C ; ^1H NMR ($CDCl_3$) δ 0.90-1.14 (t centered at 1.01, 3, J = 7.5 Hz, CH_2CH_3 ; d centered at 1.04, 3, J = 7.5 Hz, -$CHCH_3$), 1.22-1.83 (m, 4, N-H, D_2O exch), 1.95 (q, 2, J = 7.5 Hz, -CH_2CH_3), 2.25-3.19 (m, 4), 4.58 (td, 1, C4 H), 7.14 (m, 2, ArH), 7.40 (m, 3, ArH) ; m/e 246.2 (m^+), 97.2 (base). *Anal.* $C_{15}H_{22}N_2O$ (C, H, N).

Cis-N-{3-Methyl-1-[2-(1,2,3,4-tetrahydro)naphthyl]-4-piperidinyl}-N-phenylpropanamide **3b**

To a soln of 6.4 g (26 mmol) of **13a** in 75 mL of MeOH was added 2.5 mL (12 mmol) of 5 *N* HCl in MeOH, followed by 7.6 g (52 mmol) of β-tetralone, 1.1 g (17 mmol) of sodium cyanoborohydride, and 30 g of 3 A molecular sieves. This was stirred at room temp under N_2 for 3.5 days then filtered, cooled in an ice bath and made acidic with concd HCl. The solvent was removed *in vacuo*, the residue taken up in 150 mL of H_2O, and extracted with Et_2O (2 × 50 mL). The aqueous phase was made basic with solid KOH, saturated with NaCl, and extracted with Et_2O (4 × 60 mL). After drying over Na_2SO_4, the solvent was removed *in vacuo* to give 5.9 g of an orange glassy oil. Conversion to the hydrochloride salt and recrystallization from EtOH/Et_2O gave 3.85 g (36 %) of off-white crystals : mp 244-246° C. The oxalate salt was prepared and recrystallized from EtOH/Et_2O to give needles : mp 206-207° C. The free base was regenerated : IR ($CHCl_3$), 1635 cm^{-1} (C=O, amide) ; ^1H NMR ($CDCl_3$) δ 0.89-1.19 (t centered at 1.00 overlapping a d centered at 1.10, 6, -CH_2CH_3 and -$CHCH_3$, J = 7.5 Hz and 6.5 Hz), 1.19-1.78 (m, 4), 1.95 (q, 2, -CH_2CH_3, J = 7.5 Hz), 2.15-2.96 (m, 10), 4.45 (dt, 1, C4 H, J = 12.0 Hz and 4.5 Hz), 7.03 (s, 5, ArH), 7.33 (m, 4, ArH) ; m/e 376.0 (m^+), 96.1 (base). *Anal.* $C_{25}H_{32}N_2O.C_2H_2O_4$ (C, H, N).

Trans-N-{3-Methyl-1-[2-(1,2,3,4-tetrahydro)naphthyl]-4-piperidinyl}-N-phenylpropanamide **3c**

To a soln of 3.5 g (14 mmol) of **13b** in 50 mL of MeOH was added 1.0 mL (5 mmol) of 5 *N* HCl in MeOH, followed by 4.15 g (28 mmol) of β-tetralone, 600 mg (9.5 mmol) of sodium cyanoborohydride, and 21 g of 3 A molecular sieves. This was stirred at room temp under N_2 for 3.5 days, and worked up in a manner analogous to that for **13b** to give 3.6 g of an orange oil. Conversion to the oxalate salt and recrystallization from EtOH/Et_2O gave 4.4 g (66 %) of white crystals : mp 148.5-150.5° C. A small portion was converted to the hydrochloride salt : mp 266.0-268.0° C. The free base was regenerated for spectral purposes : IR ($CHCl_3$) 1633 cm^{-1} (C=O, amide) ; ^1H NMR ($CDCl_3$) δ 0.90-1.20 (t centered at 1.03 overlapping a d centered at 1.09, 6, -CH_2CH_3 and -$CHCH_3$), 1.20-2.10 (m overlapping a q centered at 1.97, 8), 2.10-2.60 (m, 2), 2.60-3.12 (m, 6), 4.68 (td, 1, C4 H, J = 11.4 Hz and 4.5 Hz), 6.93-7.50 (m, 10, ArH) ; m/e 376.6 (m^+), 96.4 (base). *Anal.* $C_{25}H_{32}N_2O.C_2H_2O_4$.

PHARMACOLOGICAL EVALUATION

Analgetic activity was evaluated by a modification of the D'Amour-Smith tail-flick method (15), using male Swiss albino mice (Madison Colony, 20-40 g ; Harlan Industries, Inc., Cumberland, Indiana) and an analgesiometer as described by Bass and Vander Brook (21). All drugs were injected subcutaneously. Fentanyl citrate (Sublimaze, Janssen Pharmaceutica) was used as a positive control, and naloxone hydrochloride (Narcan8, Dupont) was used as a specific antagonist. All test compounds (as the hydrochloride or citrate salts) were injected as normal saline solutions in a volume of 0.1-0.3 mL. Median analgetic dose values (AD_{50}) or median lethal doses (LD_{50}) and their 95 % confidence limits were determined by the method of Litchfield and Wilcoxon (22). Intraperitoneal lethality data were obtained using standard procedures (23).

Acknowledgement. — The authors gratefully acknowledge the cooperation of Dr. John K. Baker in determining log P values, Dr. I. W. Waters for assistance in the analgetic assays, Dr. Cheryl Klein of Xavier University (LA) for X-ray crystallographic data, Ruth York and Barbara Arnold for typing this manuscript. This research was supported in part by the Research Institute of Pharmaceutical Sciences, School of Pharmacy, University of Mississippi. Additional support from the National Institute of General Medical Sciences National Research Service Award training grant program (E.K.F., No. GM 07099) is gratefully appreciated.

REFERENCES

(1) D. Lednicer, *in* « Central Analgetics », D. Lednicer, Ed., Wiley, New York, 1982, Chapter 4.
(2) (a) T. N. Riley, D. B. Hale and M. C. Wilson, *J. Pharm. Sci.*, 1973, **62**, 983 ; (b) W. F. M. Van Bever, C. J. E. Niemegeers and P. A. J. Janssen, *J. Med. Chem.*, 1974, **17**, 1047 ; (c) A. F. Casy and F. O. Ogungbamila, *Eur. J. Med. Chem.*, 1983, **18**, 56.
(3) (a) N. J. Harper and C. F. Chignell, *J. Med. Chem.*, 1964, **7**, 729 ; (b) S. Grossman, U. Moser and E. Mutschler, *Arch. Pharm.* (Weinheim), 1978, **311**, 1010.
(4) P. A. J. Janssen and C. A. M. Van der Eycken, *in* « Drugs Affecting the Central Nervous System », A. Burger, Ed., Marcel Dekker : New York, 1968, Vol. 2, Chapter 2.
(5) A. F. Casy, M. M. A. Hassan, A. B. Simmonds and D. Stanforth, *J. Pharm. Pharmacol.*, 1969, **21**, 434.
(6) T. N. Riley and J. R. Bagley, *J. Med. Chem.*, 1979, **22**, 1167.
(7) (a) S. J. Law, D. H. Lewis and R. F. Borne, *J. Heterocycl. Chem.*, 1978, **15**, 273 ; (b) R. F. Borne, S. J. Law, J. C. Kapeghian and L. W. Masten, *J. Pharm. Sci.*, 1980, **69**, 1104.
(8) J. G. Berger, F. Davidson and G. E. Langford, *J. Med. Chem.*, 1977, **20**, 600.
(9) W. Klein, W. Back and E. Mutschler, *Arch. Pharm.* (Weinheim), 1975, **308**, 910.
(10) R. F. Borne, E. K. Fifer and I. W. Waters, *J. Med. Chem.*, accepted.
(11) J. W. Van Dyke Jr., H. J. Havera, R. D. Johnson, H. Vidrio and A. Viveros, *J. Med. Chem.*, 1972, **15**, 91.
(12) B. E. Maryanoff, D. F. McComsey, R. J. Taylor Jr. and J. F. Gardocki, *J. Med. Chem.*, 1981, **24**, 79.
(13) R. F. Borch, M. D. Bernstein and H. D. Durst, *J. Amer. Chem. Soc.*, 1971, **93**, 2897.
(14) P. M. Carbateas and L. Grumbach, *J. Med. Pharm. Chem.*, 1962, **5**, 913.
(15) F. E. d'Amour and D. L. Smith, *J. Pharmacol. Exp. Ther.*, 1941, **72**, 74.
(16) J. K. Baker, *Anal. Chem.*, 1979, **51**, 1693.
(17) J. F. Gardocki and J. Yelnosky, *Toxicol. Appl. Pharmacol.*, 1964, **6**, 48.
(18) T. C. Kram, D. A. Cooper, A. C. Allen, *Anal. Chem.*, 1981, **53**, 1379A.
(19) C. de Ranter, O. Peeters and Y. Gelders, *Arch. Int. Physiol. Biochim*, 1979, **87**, 1031.
(20) C. L. Klein, personal communication.
(21) W. B. Bass and M. J. Vander Brook, *J. Amer. Pharm. Assoc.*, 1952, **41**, 569.
(22) J. T. Litchfield and F. Wilcoxon, *J. Pharmacol. Exp. Ther.*, 1949, **96**, 99.
(23) W. M. Davis, R. F. Borne, R. B. Hackett and I. W. Waters, *Life Sci.*, 1980, **26**, 2105.

UM00013315
NOVARTIS EXHIBIT 1517
Novartis v. Regents, IPR2023-01347
Page 2061 of 4460

This Page is Inserted by IFW Indexing and Scanning Operations and is not part of the Official Record

BEST AVAILABLE IMAGES

Defective images within this document are accurate representations of the original documents submitted by the applicant.

Defects in the images include but are not limited to the items checked:

- ☐ BLACK BORDERS
- ☐ IMAGE CUT OFF AT TOP, BOTTOM OR SIDES
- ☐ FADED TEXT OR DRAWING
- ☐ BLURRED OR ILLEGIBLE TEXT OR DRAWING
- ☐ SKEWED/SLANTED IMAGES
- ☐ COLOR OR BLACK AND WHITE PHOTOGRAPHS
- ☐ GRAY SCALE DOCUMENTS
- ☐ LINES OR MARKS ON ORIGINAL DOCUMENT
- ☐ REFERENCE(S) OR EXHIBIT(S) SUBMITTED ARE POOR QUALITY
- ☐ OTHER: _____

IMAGES ARE BEST AVAILABLE COPY.
As rescanning these documents will not correct the image problems checked, please do not report these problems to the IFW Image Problem Mailbox.

Pergamon

Crystal Engineering, Vol. 1, No. 1, pp. 109–118, 1998
Copyright © 1998 Elsevier Science Ltd
Printed in the USA. All rights reserved
0025-5408/98 $19.00 + .00

PII S0025-5408(98)00039-7

ENVIRONMENTALLY BENIGN SYNTHESIS USING CRYSTAL ENGINEERING: STERIC ACCOMMODATION IN NON-COVALENT DERIVATIVES OF HYDROQUINONES

B.M. Foxman[1], D.J. Guarrera[2], L.D. Taylor[2], D. VanEngen[3], and J.C. Warner[4]*

[1]Department of Chemistry, Brandeis University, Waltham, MA 02254 USA
[2]Polaroid Corporation, Media System Research Laboratories, Cambridge, MA 02139 USA
[3]Princeton University, Frick Chemical Labs, Princeton, NJ 08544 USA
[4]Department of Chemistry, University of Massachusetts Boston, 100 Morrissey Blvd., Boston, MA 02125 USA

(Refereed)
(Received November 13, 1997; Accepted February 2, 1998)

ABSTRACT

The solid state phase behavior of hydroquinone **1** with *bis*-(*N,N*-diethylamino)terephthalamide **2** and with *bis*-(*N,N*-dimethylamino)terephthalamide **3** has been investigated. Stoichiometric cocrystals have been prepared of the identified stable complexes. X-ray structure determinations of these cocrystals have been performed. The role of the alkyl side chains in the crystal packing geometry is discussed. © *1998 Elsevier Science Ltd*

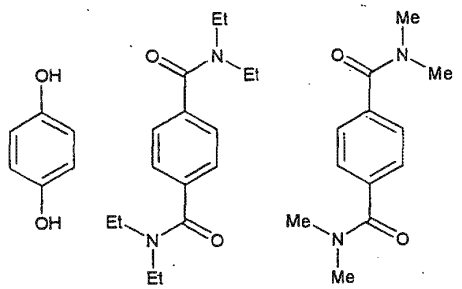
KEYWORDS: A. organic compounds, B. crystal growth, D. crystal structure, D. phase transition, D. thermodynamic properties

INTRODUCTION

Non-covalent derivatization [1] involves the designed incorporation of an auxiliary molecule within an organic crystalline lattice for the purpose of modifying the bulk physical properties of the original component. The synthetic organic chemist will typically generate a series of derivatives, by conventional covalent analog chemistry, of an interesting lead compound to optimize its performance in some particular application.

*To whom correspondence should be addressed.

UM00013317
NOVARTIS EXHIBIT 1517
Novartis v. Regents, IPR2023-01347
Page 2063 of 4460



1 2 3

FIG. 1
Hydroquinone 1, *bis*-(*N,N*-Diethyl)terephthalamide 2 and *bis*-(*N,N*-Dimethyl)terephthalamide 3.

Similarly, supramolecular derivatives can be constructed by using non-covalent interactions such as hydrogen bonding, π-stacking and lipophilic-lipophilic interactions. The new ordered structure can be viewed as a unique chemical entity distinct from either of its individual components. The extensive works of Cutin & Paul [2], Etter [3], Whitesides [4], Hamilton [5], and others have outlined methods for the construction and characterization of multimolecular systems.

The process of forming non-covalent derivatives can often be an environmentally benign alternative to conventional covalent derivatization. Assuming that the auxiliary molecules are themselves environmentally acceptable, the elimination of several solvent-requiring synthetic transformations may be bypassed by using this technique. The method of forming organic solid-state complexes can in many applications be performed under aqueous or solventless conditions [6].

This technique has been successfully applied in Polaroid's Instant Photographic systems [7]. The control of photographic developers within multi-layer thin film negative structures has been achieved by non-covalent derivatization. The incorporation of an auxiliary complexing reagent within the crystalline lattice of a substituted hydroquinone developer has provided improved diffusion control and redox stabilization. Photographic films with these modified non-covalent analogs demonstrate superior immediate images as well as a more stable product in response to time and storage conditions [8]. The manufacturing process itself has been made more environmentally benign by eliminating several solvent-using time-consuming synthetic steps that would be required using traditional covalent derivatives.

We have been extrapolating the general utility of this technique across a wide spectrum of technological applications. To do so, it is necessary for us to understand the processes available for designing, synthesizing and characterizing these assembled systems. Using the dialkyl amide–phenol hydrogen bond as the fundamental structural feature, we have been investigating a number of binary self-assembled systems. The first model system that we have studied is that of hydroquinone 1 with two different *bis*-(*N,N*-dialkyl)amides: *bis*-(*N,N*-diethyl)terephthalamide 2 and *bis*-(*N,N*-dimethyl)terephthalamide 3 (Fig. 1). The characterization of these binary systems by solid-state CP-MAS NMR and Differential Scanning

UM00013318
NOVARTIS EXHIBIT 1517
Novartis v. Regents, IPR2023-01347
Page 2064 of 4460

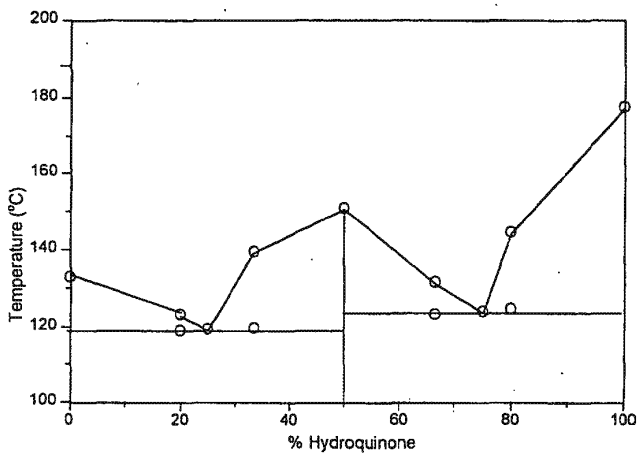


FIG. 2

Phase diagram for the hydroquinone-*bis*(*N*,*N*-diethyl)terephthalamide system. The eutectic compositions were not experimentally determined.

Calorimetry DSC has been reported previously [9]. These techniques allow for the determination of available stoichiometries of binary systems. This is achieved by the construction of phase diagrams.

Hydroquinone **1** and diethylterephthalamide **2** form a 1:1 solid state complex **4** as shown by the phase diagram (Fig. 2). This binary solid is a non-covalent derivative of hydroquinone.

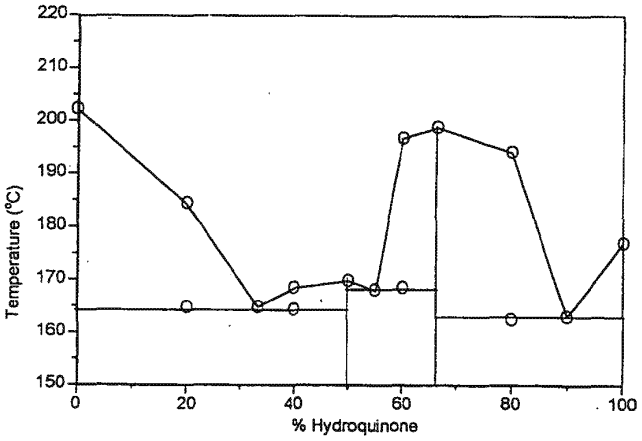


FIG. 3

Phase diagram for the hydroquinone-*bis*(*N*,*N*-dimethyl)terephthalamide system. The eutectic compositions were not experimentally determined.

UM00013319
NOVARTIS EXHIBIT 1517
Novartis v. Regents, IPR2023-01347
Page 2065 of 4460

TABLE 1
Crystallographic Data

Compound	4	5	6
CCDC deposit no.	CCDC-1290/4	CCDC-1290/5	CCDC-1290/6
Chemical Formula	$C_{22}H_{30}N_2O_4$	$C_{18}H_{22}N_2O_4$	$C_{24}H_{28}N_2O_6$
Formula weight	386.49	330.38	440.50
Space group	$P\bar{1}$	$P\bar{1}$	$P\bar{1}$
T, C	23	21	23
a, Å	7.4316(6)	7.237(4)	6.8911(6)
b, Å	7.7276(7)	9.992(6)	8.0086(6)
c, Å	10.0336(9)	13.070(8)	10.9160(10)
α, deg	71.194(7)	110.61(6)	74.723(6)
β, deg	89.596(7)	84.68(6)	86.737(6)
γ, deg	81.552(7)	103.49(6)	88.341(7)
V, Å^3	538.76(8)	860.2(21)	580.14(9)
Z	1	2	1
ρ_{calcd}, g cm^{-3}	1.191	1.276	1.261
λ, Å	1.54178	0.71073	1.54178
μ, mm^{-1}	0.626	0.085	0.712
R	0.060	0.053	0.062
R_w	0.079	0.053	0.070

The physical and chemical properties of this complexed material are unique. The melting point, solubility, and diffusivity, for example, are different and independent of either parent molecules **1** or **2**.

When the length of the alkyl chains in the dialkylterephthalamide **2** is reduced by one methylene unit, different phase behavior is observed. The phase diagram (Fig. 3) that can be constructed of the binary system of hydroquinone **1** and *bis*-(*N,N*-dimethyl)terephthalamide **3** shows that in addition to a 1:1 solid state complexed derivative of the two components **5**, there also exists a 2:1 solid state complexed derivative, **6**, that incorporates an additional molecular equivalent of hydroquinone **1**.

EXPERIMENTAL

Hydroquinone **1** was purchased from Aldrich Chemical and used without further purification. *Bis*(*N,N*-diethyl)terephthalamide **2** and *bis*(*N,N*-dimethyl)terephthalamide **3** were prepared from the condensation of terephthaloyl chloride and the appropriate amine. The products were purified by recrystallization from ethanol and confirmed by comparison to literature properties [10].

Structure Determination of 5. Routine operations were performed as described previously (Syntex $P2_1$ diffractometer at Brandeis University) [11]. The structure was refined by using anisotropic displacement parameters for N, O and C atoms; H atoms, except those attached to O, were fixed at calculated positions. Crystallographic data are presented in Table 1.

UM00013320
NOVARTIS EXHIBIT 1517
Novartis v. Regents, IPR2023-01347
Page 2066 of 4460

6

)C-1290/6
$H_{28}N_2O_6$
.50

)11(6)
)86(6)
)160(10)
723(6)
737(6)
341(7)
.14(9)

51
4178
12
62
70

unique. The melting
ndent of either parent

2 is reduced by one
m (Fig. 3) that can be
ethyl)terephthalamide
ıe two components **5**,
porates an additional

ut further purification.
nide **3** were prepared
amine. The products
mparison to literature

s described previously
ɜ was refined by using
except those attached
esented in Table 1.

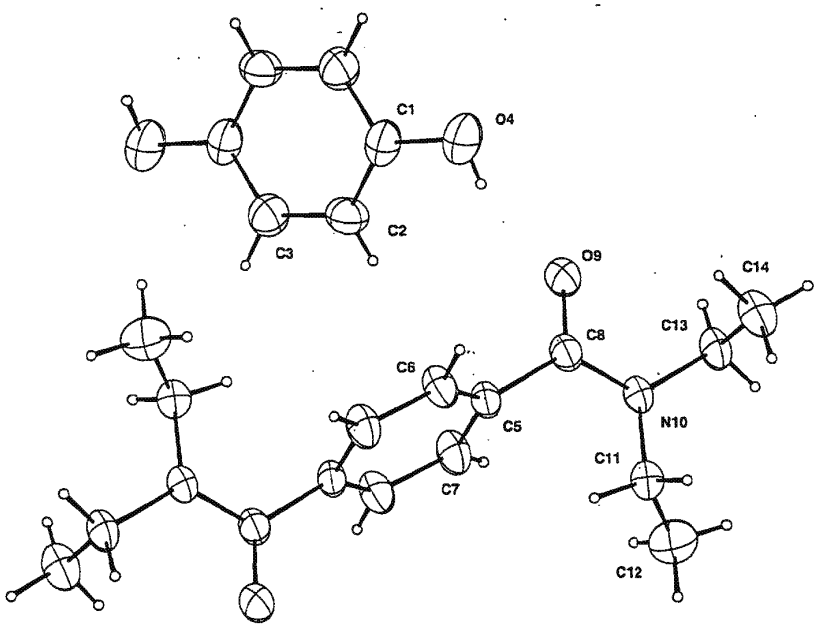


FIG. 4
Molecular structure of **4**, showing labeling scheme and 40% probability ellipsoids for atoms refined using anisotropic displacement parameters. The hydroquinone moiety crystallizes on a center of symmetry at (*0, ½, 0*), while the terephthalamide occupies a crystallographic center of symmetry at (*0, 0, ½*).

Structure Determination of 4 and 6. Routine operations were performed as described previously (Enraf-Nonius CAD4 diffractometer at Princeton University) [12,13]. The structures were refined by using anisotropic displacement parameters for N, O and C atoms; H atoms were fixed at calculated positions (for **4**, only ethyl H atoms were fixed). Crystallographic data are presented in Table 1.

RESULTS AND DISCUSSION

Inspection of the packing diagrams of these complexed systems allows some interesting rationalization for their differing phase behavior.

The molecular structure and labeling scheme of the 1:1 cocrystal **4** of hydroquinone **1** and *bis*-(*N,N*-diethyl)terephthalamide (**2**) is shown in Figure 4. The 1:1 assembly **4** may be viewed as extended hydrogen-bonded chains with alternating hydroquinone and terephthalamide subunits (Figs. 5 and 10a). The sole hydrogen bond which generates the chains (along with the centers of symmetry at **1** and **2**) is O4-H4···O9 [2.73 Å, 161°]. These chains are held together by non-covalent forces other than hydrogen bonding; inspection of the structure

UM00013321
NOVARTIS EXHIBIT 1517
Novartis v. Regents, IPR2023-01347
Page 2067 of 4460

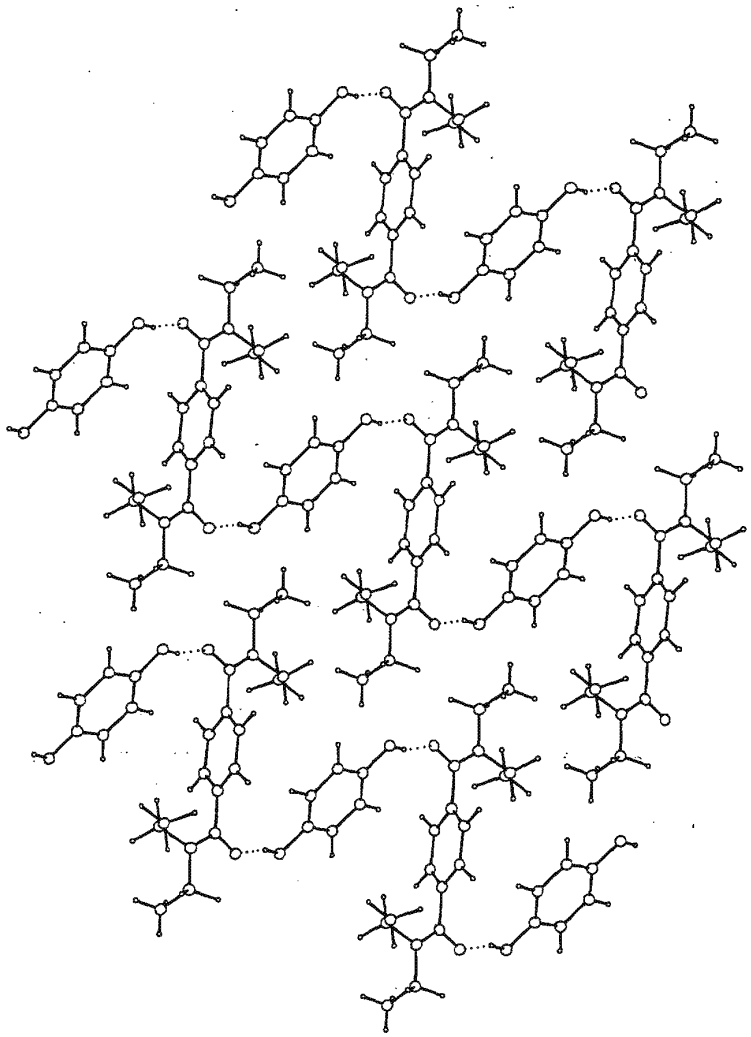
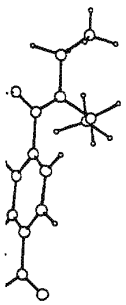


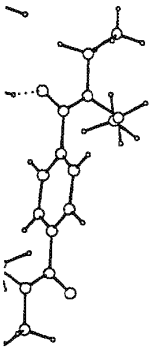
FIG. 5
Crystal packing diagram of 1:1 hydroquinone-*bis*(*N*,*N*-diethyl)terephthalamide **4**.

shows no evidence for significant C-H···O hydrogen bonds. It is interesting to note the absence of face-to-face π-stacking in this structure.

The molecular structure and labeling scheme of the 1:1 cocrystal **5** of hydroquinone **1** and *bis*-(*N*,*N*-dimethyl)terephthalamide **3** is shown in Figure 6. The 1:1 assembly **5** has no extended hydrogen-bond network. The packing of this system features a bilayer structure,

UM00013322
NOVARTIS EXHIBIT 1517
Novartis v. Regents, IPR2023-01347
Page 2068 of 4460





rephthalamide 4.

nteresting to note the

of hydroquinone 1 and
1 assembly 5 has no
es a bilayer structure,

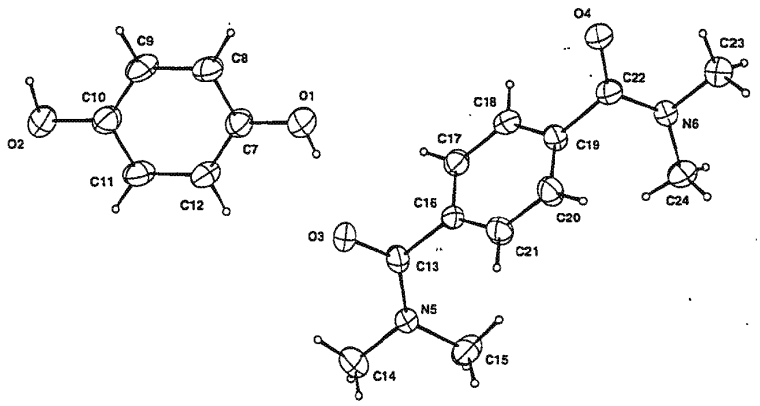


FIG. 6

Molecular structure of 5, showing labeling scheme and 40% probability ellipsoids for atoms refined using anisotropic displacement parameters.

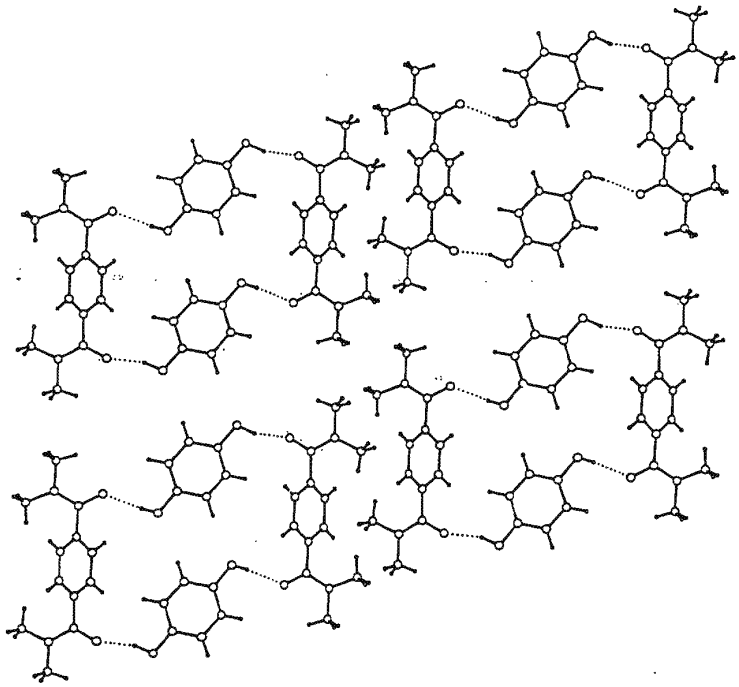


FIG. 7

Crystal packing diagram of 1:1 hydroquinone-*bis*(*N*,*N*-dimethyl)terephthalamide 5.

UM00013323
NOVARTIS EXHIBIT 1517
Novartis v. Regents, IPR2023-01347
Page 2069 of 4460

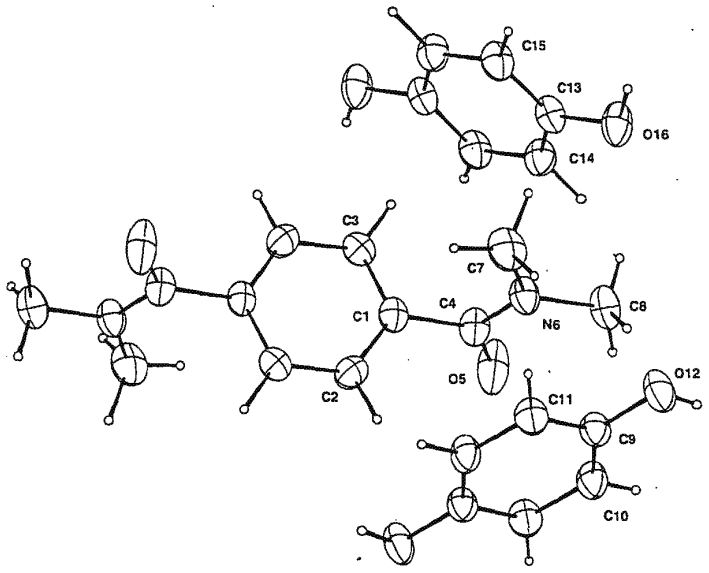


FIG. 8

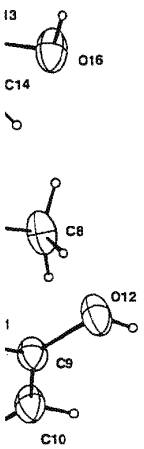
Molecular structure of **6**, showing labeling scheme and 40% probability ellipsoids for atoms refined using anisotropic displacement parameters. The upper hydroquinone moiety crystallizes on a center of symmetry at (*0, ½, 0*), the lower on a center of symmetry at (*½, 0, ½*), while the terephthalamide occupies a crystallographic center of symmetry at (*½, 0, 0*).

consisting of isolated hydrogen-bond tetramers containing two molecules of each of the individual components (Figs. 7 and 10b). The important hydrogen bonds which form the tetramer are O1-H1A···O3 [2.71 Å, 172°] and O2-H2A···O4 [(*1−x, 3−y, −z*), 2.69 Å, 163°].

The molecular structure and labeling scheme of the 2:1 cocrystal **6** of **1** and **3** is shown in Figure 8. The 2:1 assembly **6** is in some ways similar to **4**. The alternating chains of hydroquinone **1** and terephthalamide **3** are formed by phenol-amide hydrogen bonds, O16-H16···O5 [(*1+x, y, z*), 2.57 Å, 165°, Figs. 9 and 10c]. In addition to these hydrogen bond "polymeric" chains, an additional hydroquinone fills the voids generated by the absence of the methylene units in **4**. These intercalating hydroquinones may be viewed as "crosslinking" units of the alternating copolymeric chains. Alternatively, the terephthalamide **3** may be viewed as crosslinking the hydroquinone homopolymeric chains, which are generated by O12-H12···O16 [(*2−x, 1−y, 1−z*), 2.74 Å, 166°] hydrogen bonds.

The three non-covalent derivatives presented in this report represent the three possible hydrogen bonded motifs for hydrogen bonded systems. Extended chains, isolated rings and extended networks are each illustrated by assemblies **3**, **4** and **5**, respectively. The impact of these features on the thermodynamic and physical properties of these self-assembled systems is currently under investigation.

UM00013324
NOVARTIS EXHIBIT 1517
Novartis v. Regents, IPR2023-01347
Page 2070 of 4460



ɔability ellipsoids for
er hydroquinone moi-
a center of symmetry
.c center of symmetry

lecules of each of the
bonds which form the
-y, −z), 2.69 Å, 163°].
6 of **1** and **3** is shown
: alternating chains of
ıide hydrogen bonds,
ion to these hydrogen
ɔids generated by the
nones may be viewed
ernatively, the tereph-
ɔmopolymeric chains,
4 Å, 166°] hydrogen

sent the three possible
ains, isolated rings and
ectively. The impact of
self-assembled systems

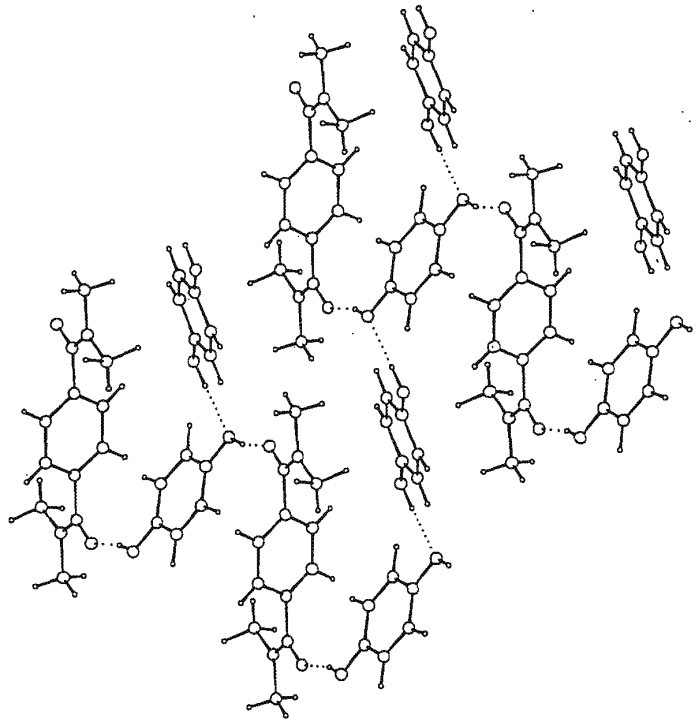


FIG. 9
Crystal packing diagram of 2:1 hydroquinone-*bis*(*N*,*N*-diethyl)terephthalamide **6**.

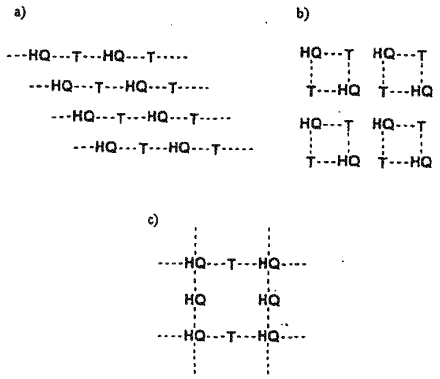


FIG. 10
Hydrogen bond assemblies *a*) extended chains, *b*) isolated rings, and *c*) extended networks.

UM00013325
NOVARTIS EXHIBIT 1517
Novartis v. Regents, IPR2023-01347
Page 2071 of 4460

ACKNOWLEDGMENTS

We wish to thank many members of the Polaroid Corporation for useful help and discussions as well as the E.P.A. [J.C.W., R825327], and the N.S.F. [B.M.F., DMR-9629994 and CHE-9305739] for financial support.

REFERENCES

1. J.C. Warner. *Green Chemistry: Frontiers in Benign Chemical Synthesis and Processing*, P.T. Anastas and T.C. Willi (eds.), Oxford University Press, 1998. In press.
2. A.O. Patil, D.Y. Curtin, and I.C. Paul, *J. Am. Chem. Soc.* **106**, 348 (1984); A.O. Patil, D.Y. Curtin, and I.C. Paul, *J. Am. Chem. Soc.* **106**, 4010 (1984); A.O. Patil, D.Y. Curtin, and I.C. Paul, *J. Chem. Soc., Perkin Trans* **2**, 557, (1986); A.O. Patil, D.Y. Curtin, and I.C. Paul, *J. Chem. Soc., Perkin Trans* **2**, 1687, (1986).
3. M.C. Etter and T.W. Panunto, *J. Am. Chem. Soc.* **110**, 5896 (1988); M.C. Etter, G.M. Frankenbach, and J. Bernstein, *Tetrahedron Lett.* **30**, 3617 (1989); M.C. Etter, *J. Phys. Chem.* **85**, 4601 (1991); M.C. Etter, *J. Am. Chem. Soc.* **113**, 2586 (113); M.C. Etter, *Acc. Chem. Res.* **23**, 120 (1990); M.C. Etter, S.M. Reutzel, and C.G. Choo, *J. Am. Chem. Soc.* **115**, 4411 (1994).
4. J.C. MacDonald and G.M. Whitesides, *Chem. Rev.* **94**, 2383 (1994); G.M. Whitesides, E.E. Simanek, J.P. Mathias, C.T. Seto, D.N. Chin, M. Mammen, and D. Gordon, *Acc. Chem. Res.* **28**, 37 (1995).
5. F. Garcia-Tellado, S.J. Geib, S. Goswami, and A.D. Hamilton, *J. Am. Chem. Soc.* **113**, 9265 (1991); S.J. Geib, S.C. Hirst, C. Vincent, and A.D. Hamilton, *J. Chem. Soc., Chem. Commun.* 1283 (1991).
6. D.J. Guarrera, L.D. Taylor, and J.C. Warner, *Proceedings of the 22nd NATAS Conference*, 496, 1993.
7. L.D. Taylor and J.C. Warner, US Patents 5,177,262 January 5 (1993); L.D. Taylor and J.C. Warner, US Patent 5,338,644 August 16 (1994).
8. D.J. Guarrera, E. Kingsley, L.D. Taylor, and J.C. Warner, *The Physics and Chemistry of Imaging Systems, Proceedings of the IS&T's 50th Annual Conference*, 537, 1997.
9. D.J. Guarrera, L.D. Taylor, and J.C. Warner, *Chem. Mat.* **6**, 1293 (1994).
10. Beilstein E IV 9 p. 3321. Syst.-Nr. 978/H 845; E III 4253.
11. B.M. Foxman, *Inorg. Chem.* **17**, 1932 (1978); B.M. Foxman and H. Mazurek, *Inorg. Chem.* **18**, 113 (1979); *MolEN, An Interactive Structure Solution Procedure*, Enraf-Nonius, Delft, The Netherlands, (1990); W.T. Robinson and G.M. Sheldrick. *Crystallographic Computing 4. Techniques and New Technologies*, N.W. Isaacs and M.R. Taylor (eds.), p. 366, International Union of Crystallography, Oxford University Press, Oxford, UK, 1988; R.A. Sparks and associates, *Operations Manual, Syntex XTL Structure Determination System*, Syntex Analytical Instruments, Cupertino, CA, (1976); D.J. Watkin, C.K. Prout and L.J. Pearce, *CAMERON*, Chemical Crystallography Laboratory, University of Oxford, Oxford, (1996).
12. G. Sheldrick, *SHELXTL-PLUS revision 4.11V, SHELXTL-PLUS users manual*, Siemens Analytical X-ray Inst. Inc., Madison WI, (1990).
13. A.V. Muehldorf, D. VanEngen, J.C. Warner, and A.D. Hamilton, *J. Am. Chem. Soc.* **110**, 6561 (1988).

UM00013326
NOVARTIS EXHIBIT 1517
Novartis v. Regents, IPR2023-01347
Page 2072 of 4460